MODELLING AND EXPERIMENTAL INVESTIGATION OF A MIXED-MODE NATURAL CONVECTION SOLAR CROP DRYER (MNCSCD)

FRANCIS KOFI FORSON, MSc., BSc., (Kumasi)

A thesis submitted in partial fulfilment for the degree of

Doctor of Philosophy

to De Montfort University, Leicester

Department of Mechanical and Manufacturing Engineering

Faculty of Computing Sciences and Engineering

May 1999

ABSTRACT OF THE RESEARCH

This thesis presents the experimental and theoretical investigation carried out on a typical Mixed-mode Natural Convection Solar Crop Dryer (MNCSCD) design. The ultimate aim of the study is to develop a simulation model to be used as an aid for future designs of such dryers.

Experiments were carried out on two MNCSCD's of similar construction: a small-scale model (laboratory) and a commercial-scale (field) version. The laboratory model, with a loading capacity of 3 kg of wet agricultural produce, was designed and constructed at De Montfort University, Leicester. The field model, an existing dryer in Ghana (designed previously by the author) with a capacity for 1000 to 1500 kg of wet agricultural produce, was basically similar to the laboratory one but with two air-heaters and two drying chambers joined back to back with no separating wall.

In all, thirteen tests- three under no load and ten under load conditions- were conducted on the laboratory dryer for three different configurations of a Single-Pass Double-Duct Solar Air-Heater type (SPDDSAH). Three tests under load conditions were also conducted on the field dryer. The two-set ups were adequately instrumented.

A mathematical model capable of predicting the performance of the MNCSCD was developed in parallel with the experimental work. The model is based on a one-dimensional steady-state operation of the system and comprises a set of coupled non-linear and partial differential equations, discretised using finite difference techniques. A computer code was written using FORTRAN 77 to solve the set of equations simulating the air-heating and drying processes. The simulation results were validated with experimental data from the two set-ups and the simulation model was subsequently fine tuned.

Parametric studies were conducted using the resulting simulation model to investigate the effect of a number of parameters on the performance of the system. Results obtained indicate that for the proposed system a significant improvement can be made by:

- maintaining the ratio of the drying bed cross-sectional area to the air-heater surface area of at least 1:1,
- increasing the volume of the drying chamber for a given drying surface area,
- increasing the thermal mass of the drying chamber,
- employing the ratio of the chimney exit air vent area to air-heater inlet vent area in the neighbourhood of 4:5,
- using the SPDDSAH with a length to width ratio ranging from 1:1 to 2:1 and a top to bottom air channel depth ratio between 1:1 and 7:2, and
- employing shorter external chimney.

The combined experimental and theoretical programme has provided a valuable insight into the usefulness of using the simulation model as an aid for achieving efficient designs of the MNCSCD in the future.

LIST OF CONTENTS

CHAPTER 6 Computer simulation: programs, results and discussion

CHAPTER 7 Conclusions and suggestions for further work

LIST OF TABLES

LIST OF FIGURES

In chapters one to four, the figures are presented within each relevant section, while in chapters five and six they are provided at the end of the relevant section.

LIST OF APPENDICES

NOMENCLATURE

Below is a partial listing of the symbols used throughout the thesis. Those symbols that are used infrequently or dropped out are defined locally. In some cases reference is made to the equations in which these symbols are used.

a'', b''	empirical constants in the Angstrom relation	
a_v	heat transfer area per unit volume of drying bed	1/m
A_{cs}	surface area of the crop bed for heat transfer and evaporation	m^2
A_{dc}	drying chamber cross-sectional area	m^2
A_c	primary collector or air-heater surface area	m^2
A_T	total surface area of primary and secondary collector areas	m^2
A_u	ratio of outside unwetted surface area to the evaporating surface of a wet product	
A_p	surface area of a drying bed	m^2
A_p	absorber plate area	m^2
B	breadth of drying chamber	m
C_{pl}	specific heat capacity of water	J/kg K
C_{pw}	specific heat capacity of water vapour	J/kg K
C_p	specific heat capacity	J/kg K
$C_{p,s}$	specific heat capacity of the sample	J/kg K
C_{pa}	specific heat capacity of air	J/kg K
C_c	specific heat of calorimeter	J/kg K
$C''m''$	equivalent heat capacity of the drying chamber	J/kg K
d_e	equivalent diameter of product particle	m
d_t	thickness of a material, drying bed thickness	m
$d_{h,i}$	hydraulic mean depth of an air-heater duct	m
D	diffusion coefficient	m^2/s
E_b	activation or binding energy for diffusion	kJ/kmol
f	friction factor	
f_v	mass transfer coefficient (equation 2.21)	(kg/s m^2).Pa
F_R	primary collector heat removal factor	
g	gravitational constant	m/s^2
Gr	Grashof number	
G_{sc}	solar constant	W/m^2
G_a	air-mass flux	$kg/s.m^2$
h'	vertical height of air column of the primary collector	ft
h	heat transfer coefficient	W/m^2
h_c	convective heat transfer coefficient	W/m^2 K
h_{cs}	surface heat transfer coefficient	W/m^2 K
h_{cv}	volumetric heat transfer coefficient	W/m^3 K
H	absolute humidity (Equation 2.126)	kg_w/kg_{air}
H_s^*	saturated absolute humidity	kg_w/kg_{air}
h_t	total heat transfer coefficient	W/m^2 K

h_{fg}	heat of vaporisation of free water	J/kg K
h_L	depth of a drying bed	m
$h_{r,\,pc}$	radiation heat transfer coefficient from an air-heater absorber plate to the cover	W/m^2 K
$h_{r,\,pb}$	radiation heat transfer coefficient from an air-heater absorber plate to the base plate	W/m^2 K
h_w	wind heat transfer coefficient	W/m^2 K
$h_{r,\,cs}$	radiant heat transfer from collector cover to the sky	W/m^2 K
H	Height of hot air column	m
$\overline{H}_d$	monthly average daily diffuse radiation on a horizontal plane	J/m^2
$\overline{H}_o$	extraterrestrial irradiance on a horizontal plane	W/m^2
$\overline{H}$	monthly average daily radiation on a horizontal plane	J/m^2
$\overline{H}_T$	monthly average daily radiation on a tilted plane	J/m^2
$\bar{I}_c$	energy incident on collector cover per unit area per unit time	W/m^2
$\bar{I}_c$	average hourly irradiation	J/m^2
JM	defined as (J - 1) in Appendix B on page 291	
k	thermal conductivity	
K	drying constant	1/s
$\overline{K}_T$	monthly average daily clearness index	
L	length of primary collector	m
L'	length	ft
L'_t	heat of evaporation of moisture from a product	J/kg K
$L_{t,\,wheat}$	heat of evaporation moisture from wheat	J/kg K
L'_t	heat of vaporisation of adsorbed product moisture	J/kg K
m	mass	kg
m_s	mass of a solid or product	kg
$\dot{m}$	air mass flow rate	kg/s
M	moisture content	decimal
M_e	equilibrium moisture content	decimal
M_c	critical moisture content	decimal
$M_{c,wb}$	moisture content (wet basis)	decimal
$M_{c,\,db}$	moisture content (dry basis)	decimal
$M_{f,\,db}$	final moisture content, dry basis	decimal
$M_{f,\,wb}$	final moisture content, wet basis	decimal
$M_{i,\,db}$	initial moisture content, dry basis	decimal
m_w	mass of water removed from a wet product	kg
MR	moisture content ratio of a product or material	decimal
n	hours of bright sunshine in a day	h
$\overline{n}$	monthly average daily hours of bright sunshine	h
$\overline{n}$	day of the year	
$\overline{N}$	maximum average of maximum possible hours of bright sunshine	h
N_d,	average drying time over a day	h
Nu	Nusselt number	
P	pressure, (N/m^2) or air-heater top to bottom channel depth ratio (no units)	

$P_{v,\,db}$	partial pressure of water vapour in moist air evaluated at T_{db}	N/m^2
P_{cL}	critical pressure of water (212 bar)	bar
P_s	vapour pressure of water at surface of wet material	N/m^2
P_v	partial pressure of water vapour in moist air	N/m^2
Pr	Prandtl number	
$\dot{q}_u$	useful energy per unit time per unit area	W/m^2
Q	air-heater length to width ratio	
$\dot{Q}$	energy transferred per unit time	W
$\dot{Q}_c$	energy transferred by convection	W
r_e	equivalent radius of a product particle	m
$\overline{R}$	monthly average of R	
R_b	ratio of beam radiation on a tilted plane to that measured on a horizontal plane	
R	ratio of total radiation on a tilted plane to that measured on a horizontal plane	
R_v	gas constant of water vapour	J/kg K
R	gas constant of dry air	J/kg K
Re	Reynolds number	
Ra	Rayleigh number	
R_o	universal gas constant	J/kmol K
$\overline{R}_b$	monthly average of R_b	
RH	relative humidity of air	%
s	depth of solar air-heater channel	m
s_p	spherecity of a particle	m
S	shrinkage (change in depth of a layer per unit depth of the layer)	
$\overline{S}_c$	monthly average absorbed solar radiation per unit area of collector	W/m^2
$\overline{S}_p$	monthly average absorbed solar radiation per unit area of collector	W/m^2
t	time	s
T_{cL}	critical temperature of water	K
T_{bL}	boiling point of water	K
T'_{abs}	absolute temperature	°R
T_{ch}	average temperature of air inside a chimney	K
T_{dp}	dew point temperature	K
$\overline{T}_f$	mean fluid temperature	K
$\overline{T}_f$	mean fluid temperature	K
T_s	sky temperature	K
T_p	average temperature of air-heater absorber plate	K
T_c	average temperature of air-heater cover plate	K
T_b	average temperature of air-heater base plate	K
$T_{f,1}$	mean temperature of heated air in top channel of a SPDDSAH	K
$T_{f,2}$	mean temperature of heated air in bottom channel of a SPDDSAH	K
T_{pt}	temperature of drying material or product	K

u	velocity	m/s
$U_{e,1}$	edge heat transfer coefficient of the top channel of a SPDDSAH	$W/m^2 K$
$U_{e,2}$	edge heat transfer coefficient of the bottom channel of a SPDDSAH	$W/m^2 K$
U_b	base plate heat transfer coefficient	$W/m^2 K$
U_L	overall heat transfer coefficient	$W/m^2 K$
V	volume	m^3
V_T	total volume of a wet product	m^3
W	width	m
W_T	mass of a wet material or product	kg
W_d	mass of dry matter content of a wet product or material	kg
W_m	mass of water content of a wet product or material	kg

Greek symbols

α_c	absorptance of collector cover	
α_p	absorptance of the air-heater absorber plate	
β	air-heater angle of tilt	degrees
β_v	coefficient of bulk shrinkage (equation 2.25)	kg_s/ kg_w
δ	declination	deg.
ΔT	difference in temperature	K
$\Delta\theta$	difference in temperature	°C
ε	bulk porosity	
ε_p	emittance of absorber plate	
ε_b	emittance of air-heater back or base plate	
ε_c	emittance of collector cover	
η_c	air-heater efficiency	%
η_d	drying efficiency	%
η_p	pick-up efficiency	%
θ	temperature of air (or angle between normal to collector surface and the incident radiation)	°C (deg)
θ_{pt}	temperature of product	°C
μ	dynamic viscosity	kg/s m
ν	kinematic viscosity	m^2/s
ρ_b	bulk density	kg/m^3
$\rho_{b,m}$	bulk density of a material	kg/m^3
$\rho_{b,wb}$	bulk density of a material (wet basis)	kg/m^3
$\rho_{b,dd}$	dry bulk density of a dry product	kg/m^3
ρ_s	density of solid material	kg/m^3
ρ_{pr}	density of the product	kg/m^3
ρ_w	density of water	kg/m^3
ρ'	density of material	lb/ft^3

σ	Stefan-Boltzman constant	
τ_c	transmittance of collector cover	
$(\overline{\tau\alpha})_e$	transmittance-absorptance product	
ϕ	latitude	deg
ω_s''	sunset (or sunrise) hour angle on a tilted plane	deg.
ω_s	sunset (or sunrise) hour angle on horizontal plane	h
ω	hour angle	deg
θ_a'	temperature of air	°F

Subscripts

amb	ambient
db	dry bulb
d.b	dry basis
dp	dew point
in	inlet
out	outlet
w.b	wet basis
wb	wet bulb

Others

$\frac{dM}{dt}$	moisture removal rate	kg_w/kg_s s
$\frac{dP}{dx}$	vapour pressure gradient	N/m^3
$\frac{dW}{dt}$	water removal rate	kg_w/s
$\frac{\partial M}{\partial t}$	drying rate	kg_w/kg_s s

PAGE NUMBERING AS ORIGINAL

ACKNOWLEDGEMENTS

The author wishes to express his appreciation to Dr M. A. A. Nazha, his supervisor, for continued support and guidance during the research, and to Mr Paul Dean and Mr Bob Burdett, technicians at the department of Mechanical & Manufacturing Engineering, De Montfort University- Leicester, for helping in the construction of the laboratory model of the dryer.

Thanks are due to the following personnel for their assistance during the testing programme and in the execution of the computer simulation model: Mr. Edwin Adjei, University of Science and Technology, Ghana; Dr H. Rajakaruna, Mr Narindra Karia and Mr Andy Rylott, all of De Montfort University, Leicester.

My deepest gratitude goes to: the Association of Commonwealth Universities, The British Council, The Government of Ghana for the financial support; and to The University of Science and Technology, Ghana for granting me a study leave.

Thanks are also due my wife, Mrs Georgina Forson, and family for the continued moral support and words of encouragement offered throughout the study period and testing moments at De Montfort University, Leicester.

Last but not the least, I thank God, for the wisdom, direction and protection offered me.

May 1999 **FRANCIS KOFI FORSON**

CHAPTER ONE

INTRODUCTION

1.1 Background

With the growing world population the provision of adequate food supply has assumed vital importance. The total population of the world in mid-1994 was estimated at 5,630 million, compared with 3,019 million in 1960 and 2,070 million in 1930 (Anon., 1994). By the end of the century, it is projected that the world population will increase to 6,158 million (Whitakker's Almanac, 1997). In the developing countries, where two-thirds of the world's population live, about 800 million people are chronically undernourished (Diouf, 1993). Although this figure is projected to drop to 730 million in 2010, it still represents an appalling level of suffering and wasted human potential. To cope with current and future demand of adequate food supply, three lines of action have been emphasised (Karel *et al*, 1975): (1) reducing future demand by reducing population growth, (2) augmenting food supply by expanding production, and (3) reducing food losses between harvesting and consumption. The third line of action has an added advantage in the fact that it provides for now as well as for future. It requires the provision of processes or preservation techniques that optimise the factors of cost, nutritional quality, environmental impact, and consumption of resources and energy.

Thermal drying has been, and is, the most common method of preserving and increasing the marketability of agricultural products world-wide. Mechanical dryers are widely used for crop drying and are capable of providing high quality products with minimum post-harvest losses. However, these dryers have high initial and running costs and in addition they require a source of fuel other than solar energy for heating the drying air and for providing motive power to drive the equipment accessories such as fans and motors. The ever-increasing price, and possible depletion globally, of fossil fuel and/or the absence of electricity in most farming communities in developing countries present barriers to their adoption by rural farmers. Mechanical thermal drying is an energy-intensive operation (Keey, 1978), and ways of reducing the use of heat energy required have constantly been sought. To exemplify the above, the capacity and energy consumption pattern for selected mechanical thermal dryers are presented in Table 1.1 Besides these limitations, from the

environmental point of view, potentially the most serious threat to the wider application of mechanical dryers is that of climate change, caused by atmospheric pollution from the burning of fossil fuels. The above scenario suggests that the development of a crop drying system that uses a cost-effective and a sustainable energy source for rural application will be useful.

Table 1.1: Capacity and energy consumption pattern for selected mechanical dryers.

Dryer type	Typical evaporation capacity (kg H_2O/h.m^2 or kg H_2O/h.m^3)	Typical energy consumption (kJ/kg H_2O evaporated)
Tunnel dryer	-	5500 - 6000
Band dryer	-	4000 - 6000
Impingement dryer	50	5000 - 7000
Rotary dryer	30 - 80	4600 - 9200
Fluid bed	-	4000 - 6000
Flash dryer	5 - 100	4500 - 6000
Spray dryer	1 - 30	4500 - 11,500
Drum dryer (for pastes)	6 - 20	3200 - 6500

Source: Mujumdar and Menon, 1995.

Traditionally, the open sun-drying has been used in most tropical and warm countries for drying agricultural and other products since time immemorial. This method remains to a large extent the predominant method for drying agricultural products in Ghana. The method entails spreading the crop thinly on bare ground or on a raised platform in the sun. The product is stirred and turned over periodically to ensure adequate exposure to the incident solar radiation. Solar energy incident on the crop vaporises its water content, and ambient air picks this moisture up and carries it away. Unfortunately, the tropics are characterised by hot damp climates and therefore the relative humidity of the ambient air is high. Hence, the moisture carrying capacity of the ambient air is low leading to slow rates of drying by the traditional sun-drying technique. In Ghana, this inefficient traditional drying technique is used by the rural and commercial farmers to dry about 90 % of the total agricultural produce (Dapaah, 1991). Though the traditional method of drying crops is cheap and environmentally friendly (no generation of pollutants or emissions); yet it is labour intensive, and requires a large area of land to dry a relatively small quantity of crop. In addition, the method provides no control over the drying process and no crop protection against unexpected rain and/or strong wind. Furthermore, the crop being dried is often subject to contamination by dirt and infestation by insects, rodents, moulds, pests, etc. All

these problems result in a poor quality dried product and in post-harvest losses (for example, in Ghana the figure can be as high as 20 to 30 %). The economic consequences to the farmer and to the country arising from these losses can be substantial.

Solar-energy drying in enclosed structures, an elaboration of the traditional sun-drying method, provides an efficient system of using the solar energy reaching the earth's surface. It is also an attractive way of lowering post-harvest losses associated with traditional drying method. Bassey *et al*, (1986) describe several successful attempts at developing solar dryers in Africa for drying commodities such as timber, rice, onions, vegetables, maize, pyrethrum, and fish. The designs described include: cabinet dryers, mixed-mode dryers with and without chimneys, indirect dryers with and without chimneys and through-flow dryers. Results obtained from comparative tests, (both predictive and physical experiments), on these dryers suggested that the performance of the mixed-mode crop-dryer was potentially most effective (Zaman and Bala, 1989; Garba *et al*, 1990). The mixed-mode solar crop dryer appears to be particularly promising in tropical areas where climatic conditions favour sun drying of agricultural products. Results (Forson *et al*, 1996) from preliminary studies on two commercial-scale mixed mode solar crop dryers at Agona-Asafo in Ghana are quite encouraging, and on the whole user-acceptability has been good. The dryers are in use presently and, subject to their performance, similar dryers could be introduced in other parts of the country. For future large scale application, possible changes in the current design are desirable to improve their overall efficiency.

The ever increasing price of fossil fuels coupled with their potentially diminishing availability, and public concern about environmental protection focuses interest in using the power of the sun as the energy source for the drying of agricultural products. Furthermore, solar energy represents a totally non-polluting inexhaustible energy resource that can be used economically to supply the world's energy needs for all time.

Ghana lies in the tropics between $4^{\circ}\ 45'$ N and $11^{\circ}\ 11'$ N parallels of latitude. The annual average solar radiation received in different parts of the country ranges from 15.84 - 20.16 MJ/m^2-day (4.4 to 5.6 kWh/m^2-day). Mean annual sunshine duration is in the range of 1800 to 2820 hours, with very little seasonal variation. These conditions make the use of solar energy for drying crops particularly attractive.

Forson (1993), designed and evaluated a prototype mixed-mode natural convection solar crop dryer (MNCSCD) for drying maize that served as the basis for the construction of two commercial solar crop dryers for drying pepper, at Agona-Asafo in the central region of Ghana. Experimental results from tests on these two dryers alone may not fully reflect the performance of such dryers under varied geographical sites. To fully investigate the effect of design variables on the system performance would involve studying the implications of a number of different configurations under varied operating conditions. In order to achieve an optimal design, data from long-term extensive experimentation on several designs operating under different climatic conditions is required. This exercise will be time consuming and costly for the prototype development of the dryer. The alternative is to perform experiments on small-scale models. The resulting information, however, must be extrapolated to full scale. The specific rules for doing this are in most cases unavailable. Furthermore, the small-scale model cannot simulate all the features of the full-scale system. Alternatively, a mathematical model of the physical system can be developed and used for investigating the effect of changes in the design and operating conditions on performance at a relatively low cost. Simulation models, as noted by Diamante and Munro (1991a), are needed in the development of dryer designs and in the operation of drying systems.

A simulation study is a powerful tool for system design, for study of new systems, and for understanding how existing systems function and how they can be improved. Simulation studies on the MNCSCD can give the same kind of thermal performance information as can be obtained from physical experiments. They are also relatively quick and inexpensive, and can be used to provide information on the effects of variable changes on system performance by a series of experiments. Another advantage of a theoretical study is its ability to simulate ideal conditions. On the other hand, even a carefully executed experiment can barely approximate the idealisation. Nevertheless, there are limits to what can be done with simulation studies since there is uncertainty about the extent to which the predicted results will agree with reality. It is therefore important that predicted results from a simulation study are compared with a carefully selected experimental data.

Hall (1980) contends that the solution to a mathematical model of a physical system is practically useless until it has been tested by comparing the predicted output with experimentally determined data. Therefore, carefully executed physical experiments are

essential. Such physical experiments will reveal if the theory is adequate and where difficulties lie in the design and the operation of the MNCSCD. At best, a judicious combination of numerical simulation and physical experiment will lead to a better understanding of how the system works, and a better knowledge of what difficulties can be expected and what can be done about them, and what logical steps should be taken to improve on existing designs. Once the theoretical results have been verified with results from carefully chosen physical experimental data and the validity of the model established, an optimal design can be achieved with confidence using the simulation methods (within the limits imposed by the assumptions on which the mathematical model was based).

It is intended in this study to develop an integrated computer code, to aid in the design and performance prediction of a MNCSCD, and to validate the model against experimental data. Figure 1.1 illustrates the schematic diagram of a conceptual design of such a solar drying system.

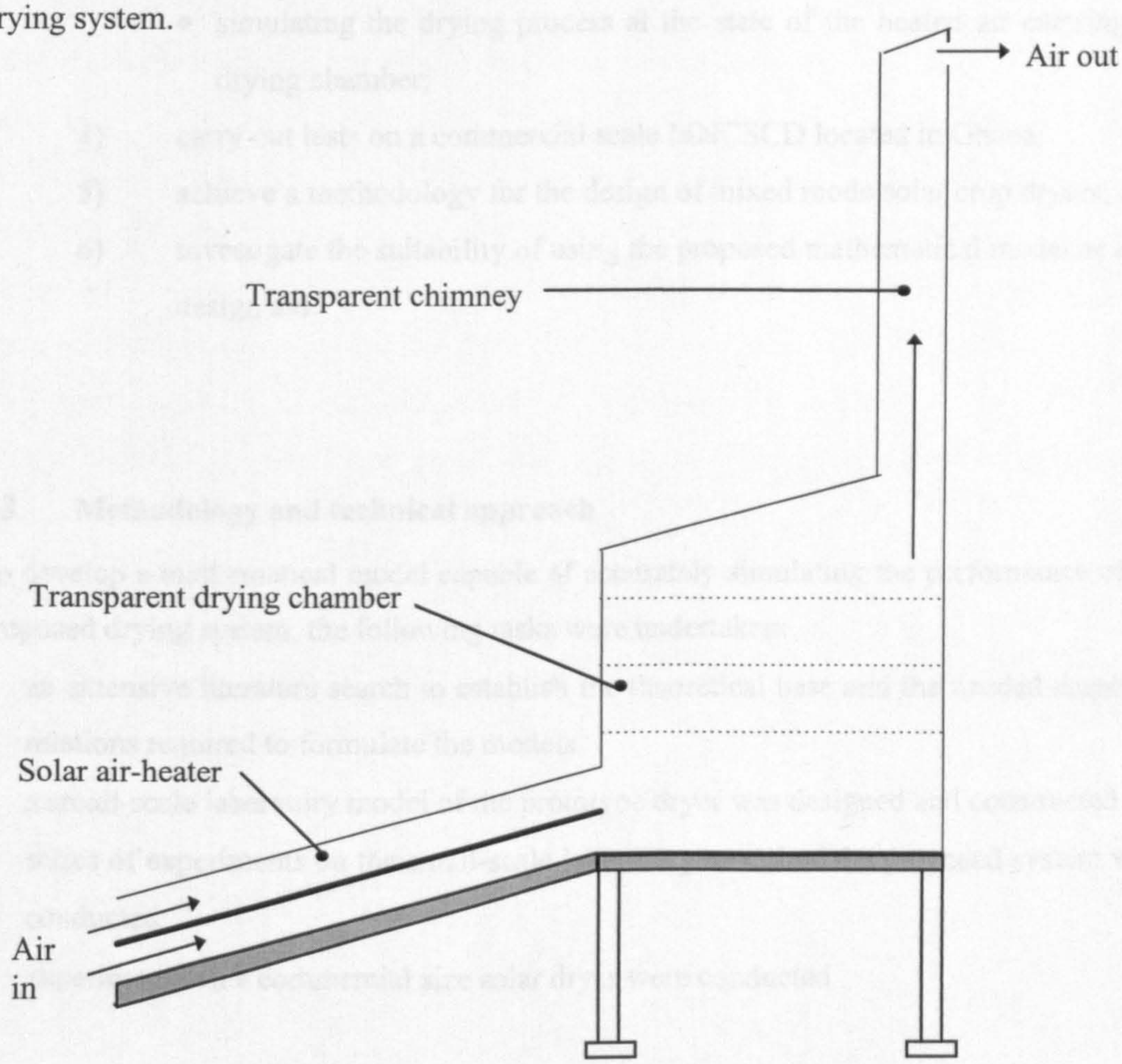

Figure 1.1: Schematic illustration of a mixed-mode natural convection solar crop dryer

1.2 Objectives of the study

The aim of this research is to develop a computer code for the design and performance prediction of MNCSCD's. The specific objectives are to:

1) design, construct and test a small-scale laboratory model. The main purpose of the experimentation is to verify some portions of the theories and assumptions that are used in developing the simulation procedure.
2) develop an integrated mathematical model for the proposed system which involves principally incorporating the design model, the solar air-heating model, and the drying model.
3) evaluate the overall performance of the proposed system by carrying out appropriate numerical predictions including:
   - determining the air-heater configuration for optimising performance;
   - determining the drying chamber dimensions for a given load;
   - simulating the drying process at the state of the heated air entering the drying chamber;
4) carry out tests on a commercial scale MNCSCD located in Ghana;
5) achieve a methodology for the design of mixed mode solar crop dryers; and
6) investigate the suitability of using the proposed mathematical model as a design aid.

1.3 Methodology and technical approach

To develop a mathematical model capable of accurately simulating the performance of the proposed drying system, the following tasks were undertaken:

- an extensive literature search to establish the theoretical base and the needed empirical relations required to formulate the models
- a small-scale laboratory model of the prototype dryer was designed and constructed
- series of experiments on the small-scale laboratory model of the proposed system were conducted
- experiments on a commercial size solar dryer were conducted

- the computer code developed was run simulating the performance of the dryer operating under varied conditions
- the predicted results were compared with the experimental data and the model was finely tuned and validated.

1.4 Organisation of the report

This thesis is organised in seven main chapters. Chapter 1, the introductory chapter, provides the socio-economic- and technical background information. It outlines the objectives of the study and the methodology adopted in solving the problem at stake. A summary of the organisation of the report is also provided in chapter 1. Chapter 2 provides a literature review related to the fundamentals of crop drying, the theoretical and experimental studies on solar crop drying, and crop drying simulation techniques. The state of the art regarding the design and simulation studies on solar crop drying is also presented. The description of the commercial-scale and laboratory dryers, and the experimental set-ups and procedures are presented in Chapter 3. The mathematical model developed for the design and predictions of the performance of the proposed dryer configuration is provided in Chapter 4. In Chapter 5 the results and discussion of all the tests, both in the laboratory and the field studies are presented, while the simulation results are presented and discussed in Chapter 6. This chapter also includes a comparison of the predicted and experimental results. Chapter 7 presents the conclusions and suggestions for further work.

CHAPTER TWO

LITERATURE REVIEW

2.0 Introduction

As noted by Kerkhof (1994), from a viewpoint of quantitative understanding, drying processes have the following special difficulties:

- the physical processes are highly non-linear
- they involve quite complicated exchange and interactive heat and mass transfer processes
- the rate of drying depends on drying conditions, and may change within the course of drying.

With these difficulties in focus, a thorough review of the fundamentals of drying theory is undertaken in this chapter in order to identify the type of information required to successfully design and model a drying system. This will not only help in the design of new dryers but will also improve the operation of existing equipment and aid in the selection of dryers for future projects. The chapter provides an overview of the physical, transport and thermodynamic properties of the wet product along with the psychrometric properties of the drying medium required as input parameters for developing a drying process model. The review also includes the theoretical and numerical models currently available for analysing crop drying processes in the conventional and solar crop-dryers.

2.1 Fundamentals of drying.

Drying, generally, refers to the thermal methods of removing liquid from a solid by means of evaporation. In agricultural work, Henderson and Perry (1976), Hall (1980), and Howe, (1980), among others, refer to drying as the removal of moisture from a product until its moisture content is in equilibrium with atmospheric air or to such a moisture content that decrease in quality from moulds, enzymic action, and insects is negligible. In the view of

Bakker-Arkema *et al* (1978), the objective of a crop drying process is to decrease the product moisture to a safe level for storage without badly affecting its quality.

When a wet product is subjected to thermal drying, two fundamental processes occur simultaneously (Hall, 1980; Porter *et al*, 1973): (1) heat is transferred from the surrounding environment to evaporate the surface moisture; (2) mass is transferred as liquid or vapour from within the material and as a vapour from the surface by evaporation due to process 1.

Process 1 involves the removal of water as vapour from the product surface. The rate at which this process proceeds depends on the external conditions of temperature, pressure, humidity, velocity and direction of airflow, retention time, the area of exposed surface, the method of supporting the product during drying, and the product reorientation during drying. Process 2 involves the movement of moisture internally within the solid; it is a function of the physical characteristics of the product, its temperature, and its moisture content.

In a drying operation either of these two processes may be a limiting factor governing the rate of drying, although they both proceed simultaneously throughout the drying cycle.

The rate at which drying is accomplished is governed by the rate at which the two processes proceed. Energy transfer as heat from the surrounding environment to the wet product during drying can occur as a result of; convection, conduction, radiation and/or dielectric heating. In most cases heat is transferred to the surface of the wet product and then into the interior. However, in dielectric, radio-frequency, or microwave drying, energy is supplied to generate heat internally within the product and flows to the exterior surfaces.

Classification of dryers

The various methods of drying may be classified into three categories: (a) traditional or sun-drying method, (b) conventional drying method, and (c) solar drying technology. The principal factors that define the nature of dryers are (Keey, 1978):

i) the manner whereby moist material receives heat,

ii) the pressure and temperature of operation, and

iii) the way in which the material is supported in the dryer.

Depending on temperature ranges, drying can be divided into three categories: low temperature drying, high temperature drying and freeze drying.

Low temperature drying is defined as a slow drying process, usually performed at temperatures between 30 and 50° C, with ambient air or air heated only a few degrees above the ambient (Ezekwe, 1993). In the low temperature drying systems the moisture content of the product is usually brought in equilibrium with the drying air by constant ventilation. Such drying systems tolerate intermittent or variable heat input. Low temperature drying enables the crop to be dried in bulk and in batches and is most suited for long-term storage systems, thus they are referred to as bulk dryers (Mclean, 1980). Important decisions that accompany low temperature drying include the depth of heaping of the crops, the suitability of the drying air conditions (i.e. its temperature and humidity), the volume of the system that needs ventilation and distribution of air through the crop mass.

High temperature drying is a fast drying process and it is usually employed when crops require a short exposure to the drying air. In high temperature dryers, the average temperature of the drying air is normally above 50° C (Ezekwe, 1993).

In freeze drying the material to be dried is first frozen and then placed in a high vacuum chamber connected to a very low temperature condenser or chemical desiccant. Most freeze-dried operations are performed between -10 and -40° C under low pressures. It is an expensive, slow operation, but it has definite advantages for heat sensitive materials.

Depending on relative directions of the flow of the crop mass and air, dryers are usually classified into batch dryers or continuous-flow dryers (Bakker-Arkema *et al*, 1978; Hall, 1980; Brooker *et al*, 1974). The continuous flow dryers are classified by the relative direction of flow of the crop mass and the heated air during drying. These dryers can be cross flow, concurrent flow or counter flow. Continuous-flow drying processes require equipment for the input of wet products and removal of the dry products at a rate consistent with the drying capacity of the unit.

In batch dryers, the product is dried in an enclosed chamber on a fixed bed, with low to medium air-flow rates, about 0.13-0.27 m^3/s per m^3 of crop, at medium drying air temperatures ranging from 37.8 to 49° C (Hall, 1980). In the case of particulate wet products they are placed on a tray or on tiers of trays. The operating principle of such dryers is to force large quantities of heated air through the crop mass in order to obtain fast drying. Batch dryers are used when different types of material are to be dried and where the production rate is small (under 200 kg/h) or seasonal and the low permissible heating temperature requires a long hold-up for internal diffusion of heat or moisture (Porter *et al*, 1973 and Karel *et al*, 1975). Included in the batch drying processes are ambient air, low-temperature, layer, column, batch-in-bin and solar drying systems (Bakker-Arkema *et al*, 1978). Batch dryers are most suitable for natural convection drying system because of the expected low self induced air-flow rates which could traverse the shallow depth of crop. In these dryers, drying takes place in a zone which advances slowly through the bed of material in the direction of air flow. A characteristic feature of batch dryers is the gradient in moisture content which develops across the bed during drying. Either mechanical or manual stirring devices, are normally used in an attempt to alleviate the problem of uneven drying in batch dryers. Brooker *et al*, (1974) pointed out that, trends in experimental data established by Frus (1968) and other researchers show that, when stirring is employed in batch drying vertical moisture gradient is reduced and air flow rate is increased by about 10 %.

2.2 Periods of drying

When a wet product is dried experimentally, data are usually obtained relating to moisture content and time. These data are plotted as moisture content M, either on dry or wet basis, versus time, t. A typical experimental drying curve is shown in fig. 2.1(a). This curve represents the general case when a wet product loses moisture first by evaporation from a surface saturated with water, followed in turn by a period of evaporation from a partially saturated surface of gradually decreasing area, and finally when water evaporates from the interior of the product.

Although fig. 2.1(a) indicates that the drying rate is subject to variation with time or moisture content, this variation can be better illustrated by graphically differentiating the curve and plotting $^{dM}/_{dt}$ versus M, as shown in fig. 2.1(b), or as $^{dM}/_{dt}$ versus *t*, as shown in fig. 2.1(c). These rate curves show that the drying process is not a smooth, continuous one in which a single mechanism is in control throughout.

The portion AB represents a warming-up period. Section BC on each curve represents the constant-rate period. The curve portion CD of figs. 2.1(a) and 2.1(b) is termed the falling-rate period, and is typified by a continuously changing rate throughout the remainder of the drying cycle. The moisture content at which the wet product demonstrates a change from constant rate drying to falling rate drying is called the critical moisture content. Point C, where the constant rate ends and the drying rate begins to fall, is termed the critical moisture content.

2.2.1 Constant rate period.

In this period, drying proceeds by diffusion of vapour from the saturated surface of the material across a stagnant-air film into the environment. Moisture movement within the solid is rapid enough to maintain a saturated condition at the surface, and the rate of drying is controlled by the rate of heat transfer to the surface. The rate of mass transfer is in equilibrium with the rate of heat transfer, and therefore the temperature of the saturated surface remains constant, if the external conditions are constant (Daly, 1992). The mechanism of moisture removal in this period is independent of the nature of the product (Porter *et al*, 1973).

If heat is transferred solely by convection, and in the absence of other heat effects, the surface temperature of the wet product approaches the wet-bulb temperature of the drying air. However, when heat is transferred by radiation, conduction or a combination of these and convection, the temperature of the saturated surface is between the wet-bulb

(a) Moisture content vs. time

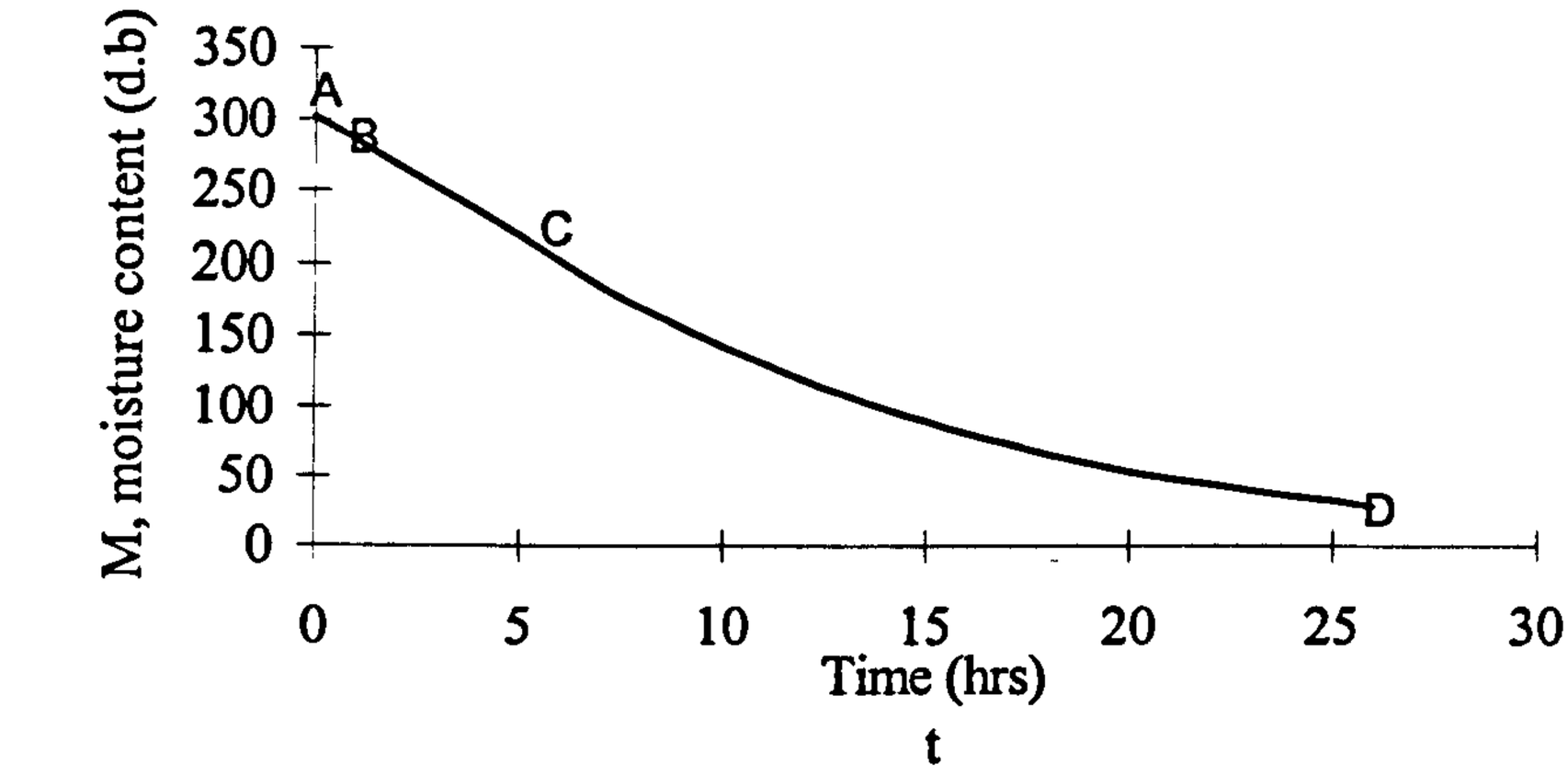

(b) Drying rate vs. moisture content

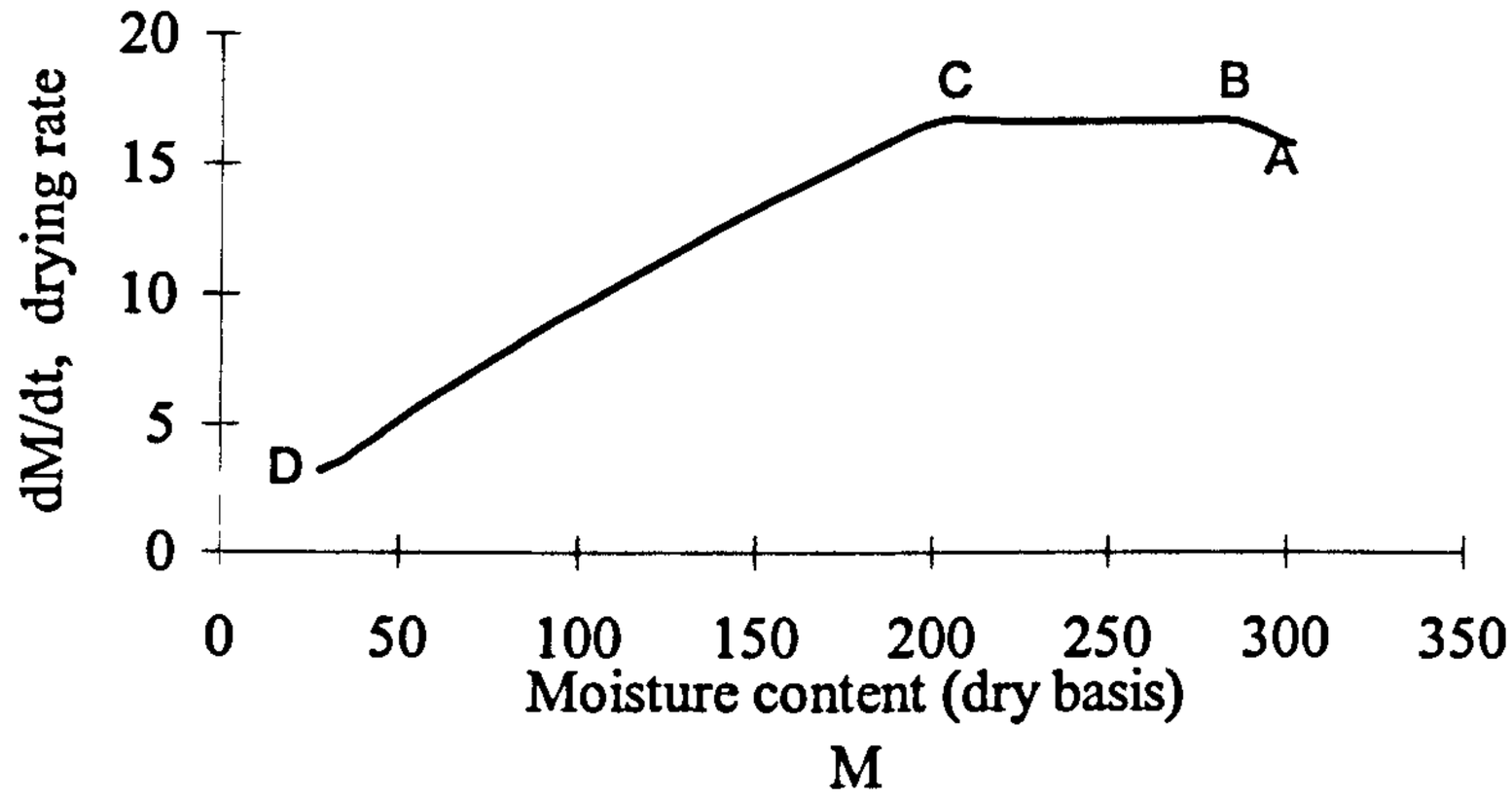

(c) Drying rate vs. time

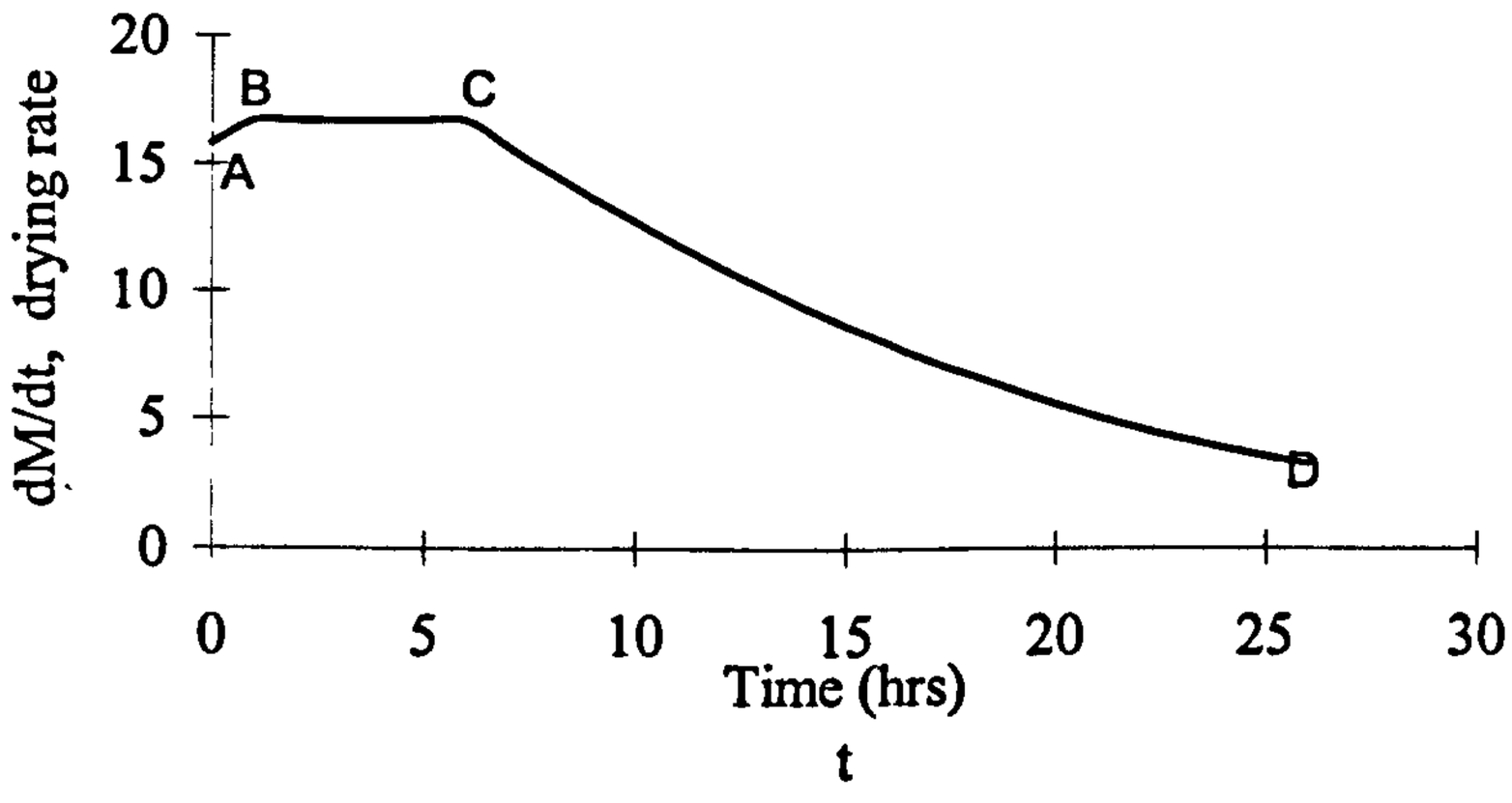

Figure 2.1: Periods of drying

temperature and the boiling point of water (Porter *et al*, 1973). Radiation is effective in increasing drying in the constant rate by augmenting the convection heat transfer and raising the surface temperature of the product above the wet-bulb temperature, in the order of about 5 to 10 K.

When the heat for evaporation in the constant-rate period is supplied by heated air or gas, an equilibrium is established between the rate of heat transfer to the material and the rate of vapour removal from the surface. The driving force of moisture movement and the internal factors of crop resistance to flow, during the constant rate period, is represented by equation (2.1) (Porter *et al*, 1973; Henderson and Perry, 1976; Hall, 1980):

$$\frac{dW}{dt} = -f_v A\left(P_s - P_{v,wb}\right) = -\frac{h_t A(T_{s'} - T_{wb})}{h_{fg}} \qquad (2.1)$$

where dW/dt = drying rate, kg water/s; f_v = mass-transfer coefficient, kg/s m^2 Pa; A = area for heat transfer and evaporation, m^2; P_s = vapour pressure of water in the product and is evaluated at the corresponding surface temperature of the product, Pa; $P_{v,wb}$ = partial pressure of water vapour in the air, Pa; h_t = total heat transfer coefficient, W/m^2 K, $T_{s'}$ = the surface temperature of the material, K; T_{wb} = air wet-bulb temperature, K and h_{fg} = latent heat of evaporation evaluated at the surface temperature of the material, J/kg.

When h_t is the coefficient of heat transfer by convection only, then $T_{s'}$ under equilibrium conditions is taken as the wet-bulb temperature of the inlet air, and P_s as the vapour pressure at this temperature. If heat is also supplied by radiation, then h_t is the total of the heat transfer coefficients by the two different modes and $T_{s'}$ becomes higher than the wet-bulb temperature. In batch drying in trays, heat arrives at the evaporation surface from the tray walls by conduction through the wet materials. The total heat transfer under the combined modes of heat transfer is given by Porter *et al*, (1973) as:

$$h_t = (h_c + h_r)\left[1 + \frac{A_w}{1 + d_t(h_c + h_r)/k_{ws}}\right] \qquad (2.2)$$

where h_t is the total heat-transfer coefficient; A_u is defined as the ratio of the outside unwetted surface to the evaporating-surface area; d_t is the depth of the material in the tray; k_{ws} is the thermal conductivity of the wet material.

The magnitude of drying achieved in the constant rate-period depends upon three external variables (Porter *et al*, 1973).: (1) the heat- or mass-transfer coefficient, (2) the area of wet product exposed to the drying medium, and (3) the difference in temperature or humidity between the air stream and the wet surface of the product.

For drying calculations, it has been suggested (Porter *et al*, 1973) that it is convenient to express equation (2.1) in terms of the decrease in the moisture content rather than the amount of water evaporated. For evaporation from a tray of wet product, assuming no change in volume during drying, equation (2.1) becomes:

$$\frac{dM}{dt} = -\frac{h_t}{\rho_p d_t h_{fg}}(T_{wb} - T_s) \tag{2.3}$$

where dM/dt = drying rate, kg water/(s) (kg dry product); ρ_p = bulk density of the dry product (kg/m^3); d_t = thickness of the bed, (m). For through-circulation drying, a similar equation is written of the form

$$\frac{dM}{dt} = -\frac{h_t a}{\rho_p h_{fg}}(T_{wb} - T_s) \tag{2.4}$$

where a = heat transfer area per unit volume of the bed (1/m); other symbols are the same as defined for equation (2.3). In practice, the volume of the wet product decreases as the drying progresses and therefore equation (2.3) or its modified form, equation (2.4) is not totally correct.

2.2.2 Falling-rate period.

The falling-rate period is entered into after the constant rate period. The moisture content at which the drying rate of a product changes from a constant rate to a falling rate (shown as point C in figs. 2.1(a) -(c)), is called the critical moisture content of the product. If the desired final moisture content is above the critical moisture content (for specified drying conditions), the whole drying process will occur under constant-rate conditions. It has been observed and proposed by several investigators that, if the initial moisture content is below the critical moisture content, the entire drying process will occur in the falling-rate period. This zone is, generally, divided into two zones: (1) the zone of unsaturated surface drying, and (2) the zone where internal moisture movement controls the drying process (Porter *et al*, 1973).

In the first period, the entire evaporating surface can no longer be maintained at saturated level by the moisture within the solid. The drying rate decreases for the unsaturated portion, and hence the rate for the total surface decreases. The drying rate depends on the factors affecting the diffusion of water vapour away from the evaporating surface and those affecting the rate of internal moisture movement. As drying proceeds, the plane of evaporation moves into the product, and the drying process enters into the second falling-rate period. Drying in the falling-rate period is therefore governed by external variables as well as the internal variables. In drying to low moisture contents, the falling-rate period predominates in determining the total drying time. This latter statement is supported by experimental evidence of Ayensu and Bondzie (1986). In drying 50 kg of cassava in a solar dryer from a moisture content of 75 % on wet basis to a final moisture content of 20 % (wet basis), they found that the constant-rate period proceeded for around 10 % of the total drying time (in fact 10 hours out a total drying time of 102 hours).

It has been recognised that individual cereal grain particles almost dry entirely within the falling-rate period because of the relatively low moisture contents of these at the time of harvest (Brooker *et al*, 1974). Igbeka *et al*, (1976) found that in drying of cassava and potato no constant-rate period was present; and the drying proceeded in the falling-rate period. Sherwood (1936) noted that in slow drying solids no constant-rate period appeared, and internal diffusion controlled the drying process from the start.

Studies of internal moisture movement indicate the possibility of several controlling mechanisms, the more significant ones being postulated as liquid or vapour diffusion, capillarity, and pressure gradients caused by shrinkage. According to Brenndorfer *et al*, (1987), the principal controlling mechanism that explains the migration of moisture from the interior of an agricultural product to the surface, and its subsequent evaporation from the surface, is diffusion. The general equation for diffusion of liquid through a porous solid according to Sherwood (1936) is given by Fick's law:

$$\frac{\partial M}{\partial t} = \nabla.(D\nabla M) \tag{2.5}$$

Equation 2.5 has been applied by several researchers (Becker and Sallans, 1955; Steffe and Singh, 1982; Suarez *et al*, 1980) to model the rate of moisture removal from wet products during the falling-rate period under the assumption that the functional dependencies of D are known or can be estimated.

The following relationship can also be used to describe the rate of drying in the falling-rate period (Sokhansanj and Jayas, 1995):

$$\frac{dM}{dt} = -KA\frac{dP}{dx} \tag{2.6}$$

where K is a moisture transfer (diffusion) coefficient, and dP/dx is the driving force for the moisture movement in terms of water vapour pressure gradient within the product. It must be emphasised that the choice between equations (2.5) and (2.6) to describe the rate of drying in the falling-rate period depends on whether concentration or vapour pressure gradient is considered as the potential for the moisture movement.

2.3 Drying: requirements for modelling and dryer design calculations

A mathematical model with which a dryer and its process parameters can be studied is of importance to prevent or minimise costly further prototype development. The model can be used to simulate the performance of existing or subsequent designs of a particular type

of dryer. In this section emphasis is on the presentation of significant parameters that influence the performance of a dryer or enter into dryer design calculations.

The following is a combined list of parameters that influence the performance of dryers, in particular solar dryers (Bakker-Arkema *et al*, 1978; Brenndorfer *et al*, 1987):

- Process air variables
    - airflow rate
    - drying air temperature
    - drying air humidity
- Product variables
    - throughput or batch size
    - initial and final moisture content
    - material sizes and size distribution
    - bulk density
    - shrinkage coefficient
    - maximum permissible drying air temperature
- Dimensional variables
    - drying chamber configuration
    - bed cross section and depth
    - area of the collector
    - air-heater configuration (length, width, and aspect ratio of the collector)
    - chimney configuration (height, cross-sectional, etc.,)
- Environmental variables
    - intensity of solar radiation
    - air temperature and relative humidity
- Transport and thermodynamic properties of the material
    - heat capacity
    - latent heat of evaporation of the material moisture
    - diffusion coefficient or drying rate constant
    - heat and mass transfer coefficients
    - equilibrium moisture content, and
    - thermal conductivity.

A comprehensive drying model must include all the aforementioned variables. It must also include the psychrometric and thermal properties of moist air. An information flow diagram for a drying model is shown in fig. 2.2. The part of the model that contains equations for heat and mass transfer phenomena is termed the *process model*, while the equations describing the dependence of drying conditions on transport properties form the *properties model*.

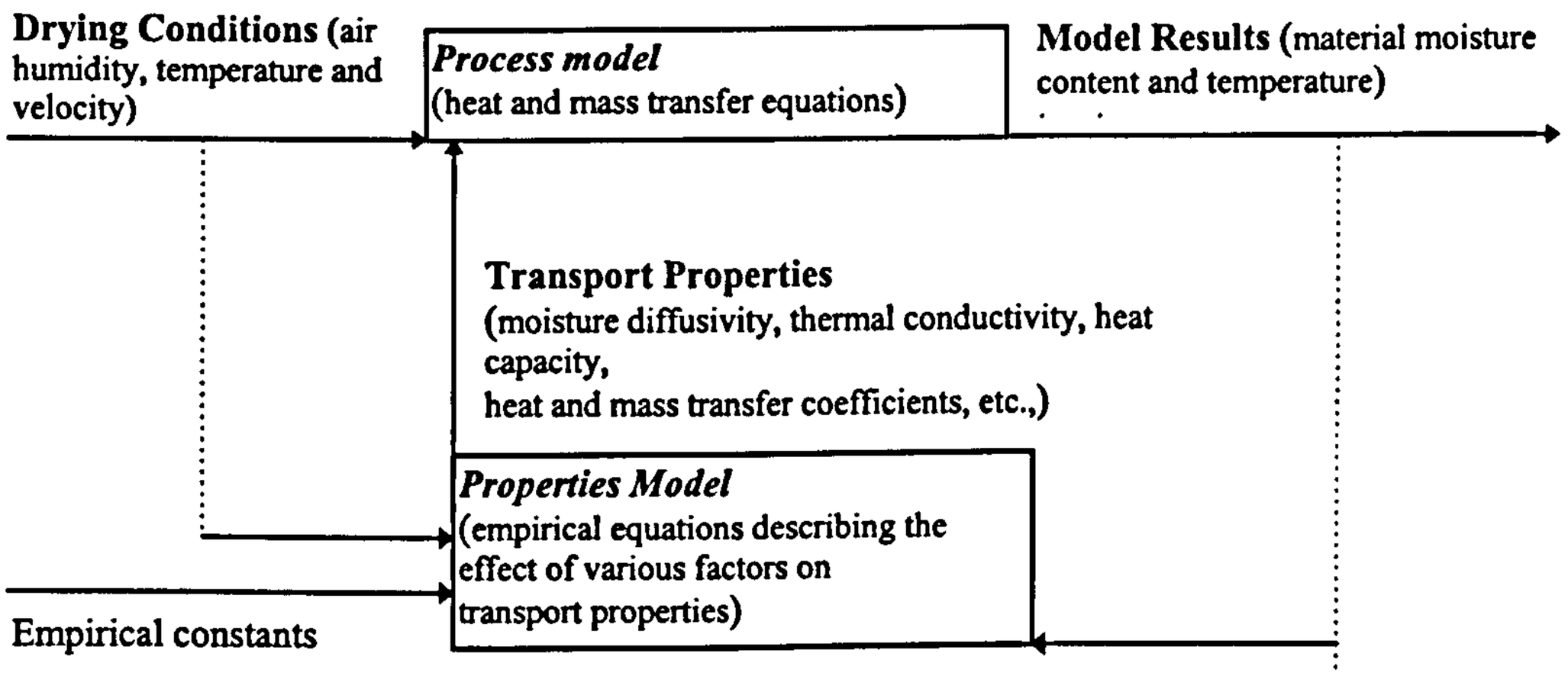

Figure 2.2: Drying model information flow diagram

2.4 Physical and thermal properties of wet products

2.4.1 Moisture content of agricultural products.

The moisture content of a wet product, $M_{c,wb}$, is usually defined as a fraction by mass on wet basis and is calculated by dividing the mass of water in the product by the total mass of the wet product as:

$$M_{c,wb} = \frac{W_m}{W_T} \tag{2.7}$$

where $M_{c,w.b}$, is moisture content fraction, wet basis; W_m, is the mass of moisture in the product; W_T, is the mass of the sample of wet product. This method of expressing the moisture content tends to give incorrect impression when applied to drying, since both the moisture content and the basis on which it is computed change as drying proceeds (Henderson and Perry, 1976). The moisture content on dry basis, is calculated by dividing the mass of water in the material by its dry matter content. The moisture content fraction on dry basis, $M_{c,d.b}$, is:

$$M_{c,d.b} = \frac{W_m}{W_d} = \frac{W_m}{W_T - W_m} \tag{2.8}$$

where, W_d is the mass of dry matter. The moisture content on dry basis is recommended (Porter *et al*, 1973) since the proportion of dry matter is constant at all moisture levels. The moisture content on a dry basis, $M_{c,d.b}$, and on wet basis, $M_{c,w.b}$, are related by equations (2.9) and (2.10) as follows:

$$M_{c,w.b} = \frac{M_{c,d.b}}{1 + M_{c,d.b}} \tag{2.9}$$

$$M_{c,d.b} = \frac{M_{c,w.b}}{1 - M_{c,w.b}} \tag{2.10}$$

Knowledge of the initial and final moisture content values, of a given crop, allows for the determination of the quantity of moisture to be removed to bring the crop to a safe level for storage.

The mass of water, m_w, to be removed from a given wet product to bring it to a safe level for storage is defined in terms of the initial and final moisture contents; it is given by the relations:

$$m_w = W_d\,(M_{i,d.b} - M_{f,d.b}) = W_T(M_{i,d.b} - M_{f,d.b})\,/\,(1 + M_{i,d.b}) \quad (2.11)$$

or

$$m_w = \frac{W_T\,(M_{i,w.b} - M_{f,w.b})}{(1 - M_{f,w.b)}}$$

The procedures for determining the moisture content of products are classified as primary and secondary methods by Henderson and Perry, (1976) or direct and indirect methods by Brooker *et al*, (1974) and Hall, (1980). The primary (or direct) procedures are such that the moisture in a sample is removed and the quantity is determined by weighing or measuring. The secondary (or indirect) procedures namely; electrical resistance methods, dielectric methods, chemical methods, hygrometric methods, neutron scattering method and the nuclear resonance-absorption method all involve the measurement of a property of the material including mechanical, electrical, or thermal property, which is related to moisture content and must be calibrated against a standard primary method. The two most common and useful primary procedures for determining moisture content are the vacuum oven and the air oven method (Brenndorfer *et al*, 1987). In the vacuum oven method, a given sample of a wet material is placed on a metal dish in a vacuum oven at 70° C and dried to constant weight. The ratio of the difference in the initial and final weights of the material to the original weight of the wet material, gives the moisture content fraction on wet basis. In the air oven method, a sample of the wet material of known weight is placed on a metal dish in an air oven at 105° C and dried to a constant weight. The moisture content fraction on wet basis is then evaluated as in the vacuum oven method.

2.4.2 Latent heat or heat of vaporisation.

The latent heat or heat of vaporisation of water (moisture) from a crop is defined as the energy required to vaporise moisture from the product. Its value is determined at the wet-bulb temperature of the air in contact with the surface of the crop (Daly, 1992). The energy required to vaporise water from a crop is dependent upon its moisture content, and its temperature. The lower the moisture content and the temperature, the higher the heat of vaporisation.

Othmer (1940), starting with the Clapeyron equation, developed the following relationship for calculating the heat of vaporisation of absorbed moisture from a product:

$$\frac{\log P_s'}{\log P_v} = \frac{L_t'}{h_{fg}} + q \tag{2.12}$$

where P_v and P_s' are vapour pressures and h_{fg} and L_t' are the heats of vaporisation of free water and of the adsorbed crop moisture, respectively. The constant q is product- and temperature- dependent.

Gallaher (1951) using published equilibrium moisture content data for wheat determined its latent heat of vaporisation. He developed Othmer plots for wheat by plotting the logarithm of the vapour pressure of the crop against the logarithm of the vapour pressure of water at the same temperature for each moisture content. The ratio of heat of vaporisation of moisture from the crop to the heat of vaporisation of free water was calculated from the slope of the line resulting from the plot. He also found that when the ratios of the heat of vaporisation of moisture from wheat to the heat of vaporisation free water were plotted against moisture content (dry basis), the resulting curve could be described by the following equation:

$$\frac{L_{t,\ wheat}}{h_{fg}} = 1 + 23\exp(-0.40\,M_{c,db}) \tag{2.13}$$

Equation 2.13 shows that the amount of heat required to vaporise water from wheat increases considerably as the moisture content of wheat decreases. Several researchers have used the Othmer plots to develop expressions similar to equation (2.13) for other crops: shelled corn (Strohman and Yoerger, 1967); soybeans (Alam and Shove, 1973); malt (Bala, 1983).

Henderson and Perry (1976) argue that the variation of the heat of vaporisation with moisture content of an agricultural crop is only significant for crops with moisture content below 6% (dry basis), however, it is noted that some variation exists between crops and the temperature. Exell (1980) suggests that over the range of conditions that occur in drying,

(rice drying in particular) the variation in the heat of vaporisation of water from grain will not exceed that of free water by about 10%. It is also reported in the literature (Mclean, 1980 and ASHRAE, 1989) that constant values can be used, as a fair approximation, and values of 2500 and 2560 kJ/kg of evaporated water have been suggested. Johnson and Dale (1954) argued that for calculations dealing with the moisture-time relation, as in most drying cases, it is not sufficient to assume a constant value for the heat of vaporisation. However, they suggested that for grains with moisture content (dry basis) less than 10%, the heat of vaporisation of water from the product could be estimated by increasing the value for free water by a factor of 15 to 20%.

The latent heat or heat of vaporisation has been observed to decrease steadily with temperature (Liley and Gambill, 1973). A known or calculated value of the heat of vaporisation of moisture from a wet product at a known temperature may be accurately extrapolated to other temperatures with the Watson's correlation (Reid *et al*, 1987):

$$L_{t,2} = L_{t,1}\left(\frac{1 - T_2/T_{cL}}{1 - T_1/T_{cL}}\right)^n \tag{2.14}$$

where n = 0.375 or 0.38 and T_c (= 647.3 K) is the critical temperature of water. A dimensionless equation which allows one to estimate the heat of evaporation at any temperature without the vapour-pressure data is given by Liley and Gambill (1973) as:

$$L_t = R_v T_{cL} T_{bL} \ln(P_{cL}) \frac{(T_{cL} - T)^{0.38}}{(T_{cL} - T_{bL})^{1.38}} \tag{2.15}$$

where,

T_{bL} is the boiling point of water, P_{cL} (221 bar) is the critical pressure of water, and R_v is the gas constant for water vapour. Equation 2.15 gives an average error of about 5%. However, if reliable data on vapour pressure and saturated liquid and vapour volumes are available, then the most reliable estimate of the heat of evaporation is obtained by using the exact Clayperon equation (Liley and Gambill, 1973).

In drying calculations, the amount of moisture removed from a wet product multiplied by the heat of vaporisation of moisture from the product yields the useful energy utilised in one batch of a drying process. Following from the above, the useful energy can be evaluated as the product of the average overall drying efficiency and the intensity of the solar radiation incident on the energy collection surfaces of the dryer.

2.4.3 Specific heat capacity.

Specific heat is simply referred to as the amount of heat needed to change the temperature of a unit mass by one degree. The specific heat at constant pressure is normally used for heat transfer problems during the drying of agricultural crops, since the pressure change is very small. The pressure dependence of specific heat is very little for solids and liquids until extremely high pressure is encountered. Specific heat is also a function of temperature; however, it has been established that at ordinary temperatures and over temperature intervals which are not too great, specific heat may be considered as a constant physical property.

Many articles have been reported on the determination of specific heat of agricultural crops. Most of this research involved determination of specific heat by the method of mixtures or by the method of differential scanning calorimetry (DSC). The DSC instrument is very expensive and is hardly used. The method of mixtures consists of adding a given quantity of a given crop to a known mass of water in a calorimeter. The equilibrium temperature, T_e attained by the calorimeter and its contents is then noted. At equilibrium, the heat lost by the crop is equated to the heat gained by the water and the calorimeter, from which relation the specific heat is calculated as:

$$C_{p,s}m_s(T_i - T_e) = m_w C_{p,w}(T_e - T_w) + m_c C_{p,c}(T_e - T_w) \qquad (2.16)$$

where the subscripts c, s and w refer to calorimeter, dry sample and water respectively, and T_i the initial temperature of the sample, T_w initial temperature of the calorimeter and water. The specific heat capacity of the wet sample is then expressed as:

$$C_p = C_{ps} + C_{pw} M_{db} \tag{2.17}$$

where C_{ps} is the specific heat of the dry matter, C_{pw} is the specific heat of water and M_d is the moisture content of the material on dry basis.

Siebel (1892) proposed that the specific heat of food materials might be estimated from the weighted sum of the specific heat of water and that of the solid matter. These equations have long been used and reported in the literature (ASHRAE, 1989 and Wallapapan *et al*, 1986) and they are given as:

$$C_p = 0.84 + 0.0335 M_{Wb}, \quad \text{(for values above freezing)} \tag{2.18}$$

$$C_p = 0.84 + 0.0126 M_{Wb}, \quad \text{(for values below freezing)} \tag{2.19}$$

where: C_p is the specific heat , kJ/kg K, and M_{Wb} is the moisture content, % wet basis.

Equations 2.18 and 2.19 are recommended by Wallapapan *et al*, (1986) for estimating specific heat only when data are lacking and there are no better alternative of determining the specific heat. It is reported by Choi and Okos (1986), that the equations proposed by Siebel are limited to food products with relatively high moisture content.

2.4.4 Bulk density.

Bulk density is one measure of quality. Chung and Converse (1971) observed that the relationship between weight and moisture content was curvilinear for both wheat and corn but dry bulk density was linearly dependent on moisture content. Vemuganti and Psoft (1980) observed that the weight of corn decreases with the increase in moisture content, whereas Matouk (1976) found that the bulk density of maize grain increases with the increase of moisture. Browne (1962) and Kazarian and Hall (1965) observed that the bulk density of wheat decreases with the increase of moisture content. Wratten *et al* (1969), and Morita and Singh, (1979) found that the bulk density of rough rice increases with the

increase of moisture content. Apart from rough rice, there seems to be no reported general trend in the variation of bulk density of common agricultural crops.

Three density measurement techniques (displacement method, air comparison pycnometer and by volumetric pycnometer) are listed in the literature (Choi and Okos, 1986). The displacement method is, however, the most common method and requires no sophisticated instrumentation. In this method, the sample is first weighed on a scale and then weighed in a known volume of water. The volume of the sample is calculated as the ratio of the weight of the displaced water (i.e. the second reading of the scale with the sample submerged minus the weight of the container and the water) to the density of water. The solid density of the sample is then obtained by the ratio of the weight of the sample to its volume as:

$$\rho_s = \frac{m_s}{V_s} \tag{2.20}$$

The bulk density ($\rho_b = m_s / V_T$) is the ratio of the mass of the product to the volume of the product including inter-particle and intra-particle air voids. The bulk density is related to the solid density according to the relation:

$$\rho_b = \rho_s(1 - \varepsilon) \tag{2.21}$$

where ε is the bulk porosity of the product which value ranges from 0.3 to 0.5 (Sokhansanj and Jayas, 1995).

The bulk density at any moisture content is related to the dry bulk density ($\rho_{b,\,dd}$) and the wet bulk density ($\rho_{b,\,wb}$) by the relation:

$$\rho_{b,m} = \rho_{b,\,dd} + \rho_{b,\,wb}\ M_d \tag{2.22}$$

2.4.5 Shrinkage.

The dimensions and volume of a solid diminish as the moisture is removed in the drying process. This phenomenon is called shrinkage in the process of drying. Luikov (1966) argued that for a majority of materials shrinkage takes place through the whole duration of the drying process. Simmonds *et al*, (1953b) showed that if the moisture content of a solid is less than 20% (dry basis) shrinkage can be neglected.

Wileman (1941) determined the shrinkage of seed corn in terms of both weight and volume during drying in the moisture content range 14.8 to 34.8%. He found the weight and volume shrinkage of the ear corn to be related linearly to the percentage of moisture removed from the grain during artificial drying of seed corn on the ear.

Spencer (1972) determined overall shrinkage of wheat for changes in bed mean moisture from the data of Clark and Lamond (1968). The following relationship was developed:

$$S = 0.85(M_{i,db} - M_{t,db}) \tag{2.23}$$

where S is the change in depth per unit depth, M_o is the initial moisture content, ratio (d.b) and $M_{d.b}$ is the moisture content, ratio, (d.b). He used the amount of bed shrinkage to alter the finite element width during the simulation of the deep bed drying of wheat.

Bala and Woods (1984) developed an equation for simulating shrinkage in the deep bed drying of malt. They hypothesised that the rate of change of the shrinkage of a malt bed with respect to the reduction in moisture content from initial moisture content is proportional to the difference between the maximum possible shrinkage and the actual shrinkage. They developed a relationship of the form:

$$S = 15.91[1 - e^{-0.0966(M_{w.o} - M_{w.b})}] \tag{2.24}$$

where S is the percentage shrinkage, M_{wo} is the initial moisture content, %, (w.b), $M_{w.b}$ is the moisture content at any given time, %, (w.b). Bala and Woods (1994) also used the amount of shrinkage to alter the finite element depth during the simulation of the deep-bed drying of malt in a solar dryer.

Based on numerous experiments on the drying of a variety of materials, it was established that the volume of a solid is a linear function of the mean moisture content (Luikov, 1966):

$$V = V_o(1 + \beta_v \overline{M}_{db}) \tag{2.25}$$

where V_o is the volume of the perfectly dry body for materials which shrink over the whole of the drying process or in the falling rate, β_v is the coefficient of bulk shrinkage equal to the relative reduction in volume with change in moisture content, i.e. $\beta_v = \frac{dv}{V_o\, d\overline{M}}$, and $\overline{M}_{db}$, is the moisture content fraction (d.b). For materials which shrink only during the first period the quantity V_o is nominal volume of the body, numerically equal to the size of the portion cut off by the straight line on the volume axis, constructed according to equation (2.25).

The coefficient of shrinkage can be determined in two ways:

a) From the slope of the straight line graph of V against $\overline{M}_d$, which is equal to $\beta_v V_o$.

b) From two values of V_1 and V_2 which correspond to the moisture contents $\overline{M}_{db1}$ and $\overline{M}_{db2}$, respectively, i.e. $\beta_v = \dfrac{(V_1 - V_2)/V_1}{(\overline{M}_{db1} - \overline{M}_{db2}) - \overline{M}_{db1}(V_1 - V_2)/V_1}$

2.4.6 Specific surface area of agricultural products.

The relationship between volumetric heat transfer coefficient h_{cv} and area heat transfer coefficient h_{cs} is

$$h_{cv} = a_v h_{cs} \tag{2.26}$$

and for a sphere $a_v = \frac{6(1-\varepsilon)}{d_e s_p}$, where ε is the void fraction and s_p is the sphericity which is defined as $s_p = \frac{\text{surface area of an equivalent spherical particle of the same volume}}{\text{surface area of a particle}}$

The void fraction can be determined by weighing a sample of the crop placed in a container of volume V_T before and after it is filled with water. The void fraction is equal to

$$\varepsilon = \frac{m_w / \rho_w}{V_T} \tag{2.27}$$

where m_w is the mass of water and ρ_w is the density of water. The solid density (ρ_s) of the material is then

$$\rho_s = \frac{m_s}{V_T(1-\varepsilon)} \tag{2.28}$$

The average particle diameter is the diameter of a spherical particle having the same volume and can be calculated from

$$d_e = \left(\frac{6m_s}{\pi \rho_s N}\right)^{1/3} \tag{2.29}$$

where N is the number of particles in the sample.

2.5 Transport properties in drying of wet products.

2.5.1 Equilibrium moisture content (EMC).

The moisture contained in a wet product exerts a vapour pressure to an extent depending upon the nature of the moisture, the nature of the product, and the temperature. When a hygroscopic material, for example a wet agricultural product, is exposed to continuous supply of fresh air at constant-temperature and constant-humidity it continues to lose moisture until the vapour pressure in the product is equal to the partial pressure of the vapour in the surrounding air. The product is then said to be in equilibrium, and the moisture content of the product is called the equilibrium moisture content under the prevailing drying conditions. The corresponding vapour pressure in the surrounding air at the same temperature (dry bulb temperature of the air) is called the equilibrium vapour pressure. The ratio of the equilibrium vapour pressure to the saturation vapour pressure of water at the same temperature is known as the equilibrium relative humidity. Further exposure of the product to this air for indefinitely long periods will not bring about any additional loss of moisture. However, the moisture content in the product could be reduced further by exposing it to air of lower relative humidity.

Determination of EMC values may be made under static and dynamic conditions, although the latter case is preferred. A simple static procedure is to place samples in ordinary laboratory desiccator containing sulphuric acid solutions of known concentrations which produce atmospheres of known relative humidity. The sample in each desiccator is weighed periodically until a constant weight is obtained. Moisture content at this final weight represents the equilibrium moisture content for the particular conditions.

The value of equilibrium moisture content, for many materials, depends on the direction in which the equilibrium is approached because it is relatively easier to add moisture to a dried product than to remove moisture from a wet product. For drying calculations the de-sorption values are preferred as opposed to adsorption values, since they give higher values.

Equilibrium moisture content can be measured dynamically by placing the sample in a U-tube through which a continuous flow of controlled-humidified air is drawn. Again the sample is weighed periodically until a constant weight is reached. Humidified air for this experiment can be obtained by bubbling dry air through a large volume of a saturated salt solution which produces a definite degree of saturation of the air.

In the absence of facilities for determining EMC values, a number of theoretical, semi-theoretical and empirical models have been proposed. Notwithstanding the extensive research efforts in this area, no theoretical EMC is yet capable of predicting accurately the moisture equilibrium contents of even cereal grains, the well researched field of study, over the full temperature and relative humidity ranges. A review of the frequently used EMC models is presented in this sub-section.

Smith (1947) suggested that static equilibrium moisture content expressed on wet basis provides an accurate correction to the isotherm equations for shrinking materials. He developed the following EMC equation:

$$M_{s,w} = M_b - g\ln(1 - RH) \tag{2.30}$$

where M_b is the bound moisture content and g is constant which depends on temperature. The Smith equation has been found to fit the experimental EMC de-sorption curves of cereal grains rather well in the region $0.5 \le RH \le 0.95$ (Becker and Sallans, 1956).

Henderson (1952) proposed the following semi-empirical model for predicting the static moisture equilibrium curves of biological products, including grains:

$$1 - RH = e^{-cT_{abs}M_e^n} \tag{2.31}$$

in which RH, the relative humidity is represented as a fraction; T, the absolute temperature, M_e, the static equilibrium moisture content, %, d.b.; and c and n are material-dependent constants. Henderson's equation, in the form described above, has been found to be inadequate for cereal grains (Brooker *et al*, 1974). A number of

empirically established modifications of the Henderson equation have been proposed. Day and Nelson (1965) modified Henderson's equation for calculating the EMC values for wheat as

$$1 - RH = \exp\left(-fM_e^{\,k}\right) \tag{2.32}$$

where,

$$f = \left(5.7336\times10^{-10}\right)\theta_F^{\,3.3718}$$

$$k = 14.863\,\theta_F^{\,-0.41733}$$

and θ_F is the temperature, °F.

Thompson (1967) modified the Henderson's equation for corn as:

$$1 - RH = \exp\left[-3.8195\times10^{-5.0}\,(T+50)\,M_e^{\,2.0}\right] \tag{2.33}$$

Strohman and Yoeger (1967) proposed the following equation to represent the relation between equilibrium relative humidity values of corn and static equilibrium moisture content, dry basis:

$$RH = \exp\left(a\exp\left\{b\,M_e\right\}\ln P_s + c\exp\left\{d\,M_e\right\}\right) \tag{2.34}$$

Equation (2.34) was found to be valid over the whole range of moisture content, relative humidity and temperature.

Data from drying of hygroscopic materials have also been fitted to an empirical relation of the form:

$$\ln\left(\frac{M_e}{p_o + p_1RH + p_2RH^2 + p_3RH^3}\right) = q_o + \left(q_1 + q_2RH + q_3RH^2 + q_4RH^3 + q_5RH^4\right)T_{abs} \tag{2.35}$$

Testing of expression (2.35) was performed for hygroscopic data of rice (Anon, 1962), coffee and corn (Teter and Citelly, 1970) and cassava (Roa, 1974). The results were found to be adequate for practical applications. The values of the constants p_i and q_i are listed in the literature (Roa, 1974).

An EMC equation based on the potential theory and a simplified equation of state was developed by Chung and Pfost (1967). The equation is of the form:

$$\ln(RH) = \frac{-A}{R_o\, T_{abs}} \exp(-BM_e) \tag{2.36}$$

where constants A and B are temperature-dependent and M_e is the static equilibrium moisture content, dry basis. The Chung and Pfost equation fits grain EMC data well over the 20 to 90% relative humidity range. The constants A and B can be calculated for shelled corn from the following relationships (Brooker *et al*, 1974)

$$\ln A = R_o\, T'_{abs} \left(1.544\times10^{-2} - 1.383\times10^{-5}\, T'_{abs}\right) \tag{2.37}$$

$$B = R_o\, T'_{abs} \left(3.211\times10^{-3} + 2.069\times10^{-5}\, T'_{abs}\right) \tag{2.38}$$

where T'_{abs} denotes the absolute temperature in $^{\circ}R$. Equation 2.36 is valid if $0.20 < RH < 0.90$.

Other EMC equations (BET, Harkins-Jura, Hasley, Kelvin, Langmuir, etc.) are available in the literature (Brooker *et al*, 1974). Pixton and Howe (1983) examined the suitability of using the following EMC equations for cereals and other products: (1) Smith equation, (2) Hasley equation, (3) Harkins and Jura equation, (4) BET (Brunaur, Emmet and Teller) equation, (5) Chung and Pfost equation, (6) Iglesias and Chirife equation, and (8) Henderson equation. They observed that the Chung and Pfost equation gave an excellent fit to the data relating moisture content and equilibrium relative humidity data of tapioca starch and found that it can be used to fit the relationship using only three points between

25 and 70% relative humidity. For field beans, dried peas, cereal derivatives other than flour, oilseeds and almonds, the Hasley relation was found to be the best.

It is interesting to note that depending on what parameters were known various researchers used one EMC relation or another or even modified existing models to apply to their work.

2.5.2 Moisture diffusivity.

Diffusion in solids during drying is a complex process involving several mechanisms including liquid and vapour diffusion, surface diffusion, hydrodynamic or bulk flow, and capillary flow (Marinos-Kouris and Maroulis, 1995). Combining all these phenomena into one, the effective diffusivity can be defined from Fick's law (see Equation 2.5).

There is no standard method for the experimental determination of diffusivity. Several methods for determining effective moisture diffusivity from drying data are presented in the literature (Choi and Okos, 1986; and Marinos-Kouris and Maroulis, 1995). Table 2.1 gives some literature values of the effective diffusivity of moisture in various materials.

Table 2.1: Effective moisture diffusivity in some materials

Material	Moisture content fraction (kg/kg d.b)	Temperature (^{o}C)	Diffusivity (m^2/s)
Alfafa stems	< 3.70	26	$2.6x10^{-12}$ - $2.6x10^{-9}$
Apple	0.12	60	$6.5x\ 10^{-12}$ - $1.2x10^{-10}$
	0.15 - 7.0	30 - 76	$1.2\ x10^{-10}$ - $2.6x10^{-10}$
Avocado		31 - 56	$1.1x\ 10^{-10}$ - $3.3x10^{-10}$
Beet	0.10 - 0.65	65	$1.54x10^{-9}$
Biscuit	0.10-0.65	20-100	$9.4x10^{-9}$ - $9.7x10^{-8}$
Bread	0.10 - 0.70	20 - 100	$2.5x10^{-9}$ - $5.5x10^{-7}$
Carrot	0.03 - 11.6	42 - 80	$9.0x10^{-10}$ - $3.3x10^{-9}$
Corn	0.05 - 0.23	40	$1.0x10^{-12}$ - $1.0x10^{-10}$
Corn	0.19 - 0.27	36 - 62	$7.2x10^{-11}$ - $3.3x10^{-10}$
Muffin	0.10 - 0.65	20 - 100	$8.4x10^{-10}$ - $1.5x10^{-7}$
Onion	0.05 - 18.7	47 - 81	$7.0x10^{-10}$ - $4.9x10^{-9}$
Fish muscle	0.05 - 0.30	30	$8.1x10^{-11}$ - $3.4x10^{-10}$
Pepper, green	0.04 - 16.2	47 - 81	$5.0x10^{-10}$ - $9.2x10^{-9}$
Pepperoni	0.19	12	$4.7x10^{-11}$ - $5.7x10^{-11}$

Table 2.1: continued.

Material	Moisture content fraction (kg/kg d.b)	Temperature (° C)	Diffusivity (m^2/s)
Pasta, semolina	0.01 - 0.25	40 - 125	$3.0x10^{-13}$ - $1.5x10^{-10}$
corn based	0.10 - 0.40	40 - 80	$5.0x10^{-11}$ - $9.2x10^{-9}$
Potato	0.60	54	$2.6x10^{-10}$
	<4.0	65	$4.0x10^{-10}$
	0.15 - 3.50	65	$1.7x10^{-9}$
	0.01 - 7.2	39 - 82	$5.0x10^{-11}$ - $2.7x10^{-9}$
Rice	0.18 - 0.36	60	$1.3x10^{-11}$ - $2.3x10^{-11}$
	0.28 - 0.64	40 - 56	$1.0x10^{-11}$ - $6.9x10^{-11}$
Soybeans, defatted	0.05	30	$2.0x10^{-12}$ - $5.4x10^{-12}$
Starch, gel	0.10 - 0.30	25	$1.0x10^{-12}$ - $2.3x10^{-11}$
	0.20 - 3.0	30 - 50	$1.0x10^{-10}$ - $1.2x10^{-9}$
	0.75	25 - 140	$1.0x10^{-10}$ - $1.5x10^{-9}$
granular	0.10 - 0.50	25 - 140	$5.0x10^{-10}$ - $3.0x10^{-9}$
Tapioca root	0.16 1.95	97	$9.0x10^{-10}$
Turkey	0.04	22	$8.0x10^{-15}$
Wheat	0.12 - 0.30	21 - 80	$6.9x10^{-12}$ - $2.8x10^{-10}$
	0.13 - 0.20	20	$3.3x10^{-10}$ - $3.7x10^{-9}$

Source: Marinos-Kouris and Maroulis, 1995

Moisture diffusivity for food materials have been found to depend on several factors including temperature, moisture content, shape of the material, and relative humidity of the surrounding medium. However, because of the problem with the measurement of the product temperature some authors have measured the air temperature instead of the product temperature (Igbeka *et al*, 1976). Husain *et al* (1972) suggested that for high moisture foods, the use of variable diffusivity in a model describing a drying process is appropriate, if shrinkage effect is neglected.

Pabis and Henderson (1961) expressed the dependence of diffusion coefficient at high moisture levels with temperature in terms of an Arrhenius-type expression:

$$D = D_o \exp(-E / RT_g) \tag{2.39}$$

where,

D_o (m^2 / s) is the Arrhenius factor, E (kJ / kmol) is the activation energy for diffusion at high moisture levels, R (kJ / kmol K) the gas constant, T_g (K) the temperature of the material.

Later, Hustrulid (1963) found that D is also a function of initial moisture content of seeds. Zaremba (1977), it is reported (Jayas *et al*, 1991), studied in detail the dependence of diffusion coefficient on temperature and moisture content. He found that the diffusion coefficient increases exponentially with an increase in temperature. Dependence of the diffusion coefficient on moisture content was described by a parabolic relationship which he found to be more pronounced with an increase in temperature. Pabis (1982) gave the following empirical equation to estimate the diffusion coefficient of grain kernel:

$$D(M,T) = D_0(T) + D_1(T)\,M + D_2(T)\,M^2 \tag{2.40}$$

where the coefficients $D_o(T)$, $D_1(T)$, and $D_2(T)$, can be defined by an exponential expression:

$$D_i(T) = \alpha_i \exp(\beta_i T_g) \tag{2.41}$$

where i = 0, 1 or 2.

Igbeka (1982) presented a mathematical representation of the variation of diffusivity of moisture during drying of cassava and potato. The relationship was based on his earlier experimental data. The relation is of the form:

$$D = -0.0274 - 5.74\times10^{-6}\,M + 5.98\times10^{-6}e^{M} + 0.0275e^{-1/T_a} + 2.23\times10^{-6}\,XR \tag{2.42}$$

where XR is the relative humidity indicator and it is 0 for $RH = 60\%$ and 1 if $RH = 10\%$, M is the moisture content fraction expressed on dry basis, and T_a is the absolute temperature of the drying air.

Effective moisture diffusivity of potato has also been expressed as a function of material moisture content and its temperature by Kiranoudis *et al*, (1993) in the form:

$$D = 2.94\times10^{-7}\exp(-1.58\times10^{3}/T)\exp(-6.72\times10^{-2}/M) \tag{2.43}$$

where, M is the moisture content fraction expressed on dry basis, and T is the absolute temperature of the drying air. From equations (2.42) and (2.43) it can be concluded that no single equation has been found to predict accurately the moisture diffusivity even for a single product. Moisture diffusivity relations are studied individually and the relation that best fits a given data set is chosen, however, their values generally depend on one or more of the following factors: material temperature, moisture content, and shape, and relative humidity of the drying medium.

For a naturally wet or fresh wheat grain, Jayas *et al* (1991) reported the following expressions for evaluating its diffusion coefficient:

$$D = 0.99 \times 10^{-11} M^{0.0062\theta_a + 0.0045} \exp[(-0.124\theta_a - 0.09)M + 0.064\theta_a] \qquad (2.44)$$

and for dry grains of wheat which have been artificially re-wetted the expression is:

$$D = 2.02 \times 10^{-11} M^{0.0062\theta_a + 0.0045} \exp[(-0.124\theta_a - 0.09)M + 0.064\theta_a] \qquad (2.45)$$

where D is in m^2/s and θ_a ($^\circ$C) is the temperature of the drying air.

From these equations, it follows that the value of the diffusion coefficient of rewetted wheat (at 20° C over 24 hours) was nearly twice that of the fresh grain. The increase in the diffusion coefficient as a result of rewetting of dry wheat has also been noted by Karczmarczyk (1990).

Xiong *et al* (1992) postulated that the decrease in the effective diffusivity at lower moisture contents is a result of a decrease in the availability of water molecules for diffusion. Their resulting expression relating the effective diffusivity and the proportional amount of free water is of the form:

$$D = D_o \exp(-E_b / RT_g) \frac{K \exp(-E_b / RT_g)}{1 + K \exp(-E_b / RT_g)} \qquad (2.46)$$

where E_b is the binding energy and is inversely related to the moisture content (Iglesias and Chirife, 1982), and K is an equilibrium constant. At higher moisture levels (> 70% wet basis) the binding energy is zero signifying that at these levels the effective moisture diffusivity is independent of moisture content.

2.5.3 Drying constant.

The drying constant depends on both material and air properties since it is phenomenological property representative of several transport phenomena. It is a function of the material moisture content, temperature, and thickness, as well as air humidity, temperature and velocity (Marinos-Kouris and Maroulis, 1995). The drying constant can be defined using the thin-layer equation (see equation 2.46). Lewis (1921) suggested that during the drying of porous hygroscopic materials in the falling-rate period, the rate of change in material moisture content is proportional to the instantaneous difference between material moisture content and the expected material moisture content when it comes into equilibrium with the drying air. If it is assumed that the material layer is thin enough or the air velocity is sufficiently high so that the conditions of the drying air (humidity, temperature) are kept constant throughout the drying of the material, the thin-layer equation has the following form:

$$\frac{dM}{dt} = -K(M - M_e) \tag{2.47}$$

where M (kg/kg) is the material moisture content (dry basis), M_e (kg/kg) the material moisture content in equilibrium with the drying air (dry basis), and t (s) is the time. The drying constant is estimated by fitting the thin-layer equation to experimental data. If the controlling mechanism of moisture removal during a drying process is diffusion then the drying constant can be determined as a function of moisture diffusivity. For slabs, for example, the following equation is valid:

$$K = \pi^2 D / L^2 \tag{2.48}$$

where D (m^2/s) is the effective diffusivity and L (m) is the thickness of the slab. In the drying of grains, Henderson and Pabis (1961) showed that the drying rate coefficient K can be related to the effective diffusion, D, and an equivalent grain radius, R, by:

$$K = D\frac{\pi^2}{R^2} \tag{2.49}$$

O'Callaghan (1954) observed that for wheat, in the temperature range 10-66° C, the drying constant is independent of the relative humidity of the drying air but is dependent on its temperature. He proposed the following equation:

$$K = A\exp(BT) \tag{2.50}$$

Henderson and Pabis (1961) proposed an Arrhenius-type equation to relate the thin-layer drying constant to drying air temperature.

$$K = p\exp(-q/T) \tag{2.51}$$

where p, q are material-dependant constants.

Van Rest and Isaacs (1968) and Chittenden and Hustrulid (1966) found that the value of the drying constant for shelled corn and other grains is dependent on moisture content as well as the drying air temperature. They found the effect of moisture content to be less than that of the drying air temperature.

Syarief *et al* (1984) observed that the drying constant of sunflower seeds is a function of the drying air temperature and its relative humidity according to the equation:

$$K = 5.16\times10^{-4}T^{1.8387} + 3.45\times10^{-5}RH^2 \tag{2.52}$$

Nellist (1974) observed during the drying of ryegrass seeds that the inclusion of moisture content and humidity in the form:

$$K = a\exp(bT + cH + dM_o) \tag{2.53}$$

improved the fit of the curve to the experimental data.

In the drying of green pepper, drying constant was observed to be a function of the material moisture content, temperature, and thickness, as well as air humidity, temperature and velocity of the form (Kiranoudis *et al*, 1992):

$$K = b_o M^{b_1} T^{b_2} d^{b_3} u^{b_4} \tag{2.54}$$

where, $b_o = 1.11\text{x } 10^{-8}$, $b_1 = 9.03 \text{ x } 10^{-2}$, $b_2 = 1.54$, $b_3 = -0.982$ and $b_4 = 0.293$.

2.5.4 Thermal conductivity.

Thermal conductivity, is a material property indicating the ease and speed with which heat is conducted through the material and, is defined as the proportionality constant in Fourier's law for steady-heat conduction as:

$$q = -k\,A\frac{dT}{dx} \tag{2.55}$$

According to Lof (1962) if products are dried in layers of sufficient depth; thermal conductivity must be high enough to allow heat conduction from one layer to another. If on the other hand thermal conductivity is very poor, circulation of heated air through the particles of the moist product would permit better heat transfer than direct radiation on the surface of relatively deep bed of particles. Since most agricultural products have relatively low thermal conductivity values, it follows from the observation of Lof (1962), that passing heated air through a bed of a product during drying will invariably increase the drying rate.

A compilation of thermal conductivity data for porous materials are available in the literature (Wallapapan *et al*, 1986; ASHRAE, 1989; and Mujumdar, 1995). Theoretically, models for predicting the effective thermal conductivity of porous materials are derived from the analysis of heat transfer processes through such materials. The thermal conductivity of a material is largely influenced by its moisture content and its temperature. For hygroscopic materials, models which are moisture content dependent in the form :

$$k_s = k_o + b\frac{M_{c,db}}{1 + M_{c,db}} \tag{2.56}$$

have been widely used. In equation (2.56), $M_{c,db}$ is the moisture content of the material expressed on dry basis. During drying, the amount of heat supplied to a wet product surface equals that which penetrates by conduction and that spent for moisture vaporisation. A better estimate of the thermal conductivity value is therefore of primary importance in drying models. The thermal conductivity of a bulk material filled with air can be estimated from the expression (Sokhansanj and Jayas, 1995):

$$k = k_g \nu_f + k_s(1 - \nu_f) \tag{2.57}$$

where ν_f is the void fraction, k_g is thermal conductivity of air, and k_s is the thermal conductivity of the material as given by equation (2.56).

2.5.5 Heat and mass transfer coefficients.

The rate of heat transfer between a solid surface and fluid may be defined as the proportionality factor in the Newton's law:

$$Q_c = h_c A \Delta T \tag{2.58}$$

where Q_c (W) is the rate of heat transfer by convection, h_c (W/m^2 K) is the convective heat transfer coefficient, A (m^2) heat transfer area, ΔT (K) is temperature difference between the solid surface and the fluid.

Two general methods are available for the determination of convective heat transfer coefficients from a crop bed: (1) dimensional analysis by correlating existing data (based on the film temperature), and (2) direct measurement of heat transfer coefficient by comparing temperature curves with Schumann's exact solution, based on the mean temperature of the sample.

Schumann (1929) made a significant contribution in the field of heat transfer by developing the following analysis for fluid and solid temperature distribution in a packed bed of crushed material:

$$\frac{\partial T_s}{\partial z} = T_a - T_s \tag{2.59}$$

$$\frac{\partial T_a}{\partial Y} = T_s - T_a \tag{2.60}$$

where $Y = k_2 x / v$, $z = k_1 (t - x / v)$, T_a = temperature of the fluid, T_s = temperature of the solid, x = distance traversed by the fluid in the bed, t = time, $k_2 = k / h_a f_{sp}$

$k_1 = k / h_s (1 - f_{sp})$, k = constant of heat transfer, h_s = heat capacity per unit volume of the solid, h_a = heat capacity per unit volume of the fluid, f_{sp} = free space per unit volume. He presented the following solution involving mathematical functions related to Bessel Function:

$$\frac{T_s}{T_o} = e^{-Y-Z} \sum_{n=1}^{\infty} Z^n M_n(YZ) \tag{2.61}$$

$$\frac{T_a}{T_o} = e^{-Y-Z} \sum_{n=0}^{\infty} Z^n M_n(YZ) \tag{2.62}$$

where $M_n(YZ) = \dfrac{d^n M_o(YZ)}{d(YZ)^n}$, $\qquad M_o(YZ) = I_o(2\sqrt{RT})$,

$I_o = (2\sqrt{YZ})$ and T_o = initial temperature of the fluid.

The numerical values of T_s / T_o and T_a/T_o were calculated from equations (2.61) and (2.62) for values of Y and Z ranging from 0 to 10 and the results presented graphically.

Furnas (1930) developed an interesting alternative numerical method of solution for the differential equations developed by Schumann and extended the temperature history curves for values up to 500. He also demonstrated the use of the computed temperature history curves to calculate the heat transfer coefficient from observed data on temperature history.

Colbourn (1933) made a significant contribution in the determination of heat transfer coefficient by proposing a general method to correlate the forced convection heat transfer data which involves plotting, against Reynolds number, a dimensionless group representing the experimentally measured data from which heat transfer coefficient would be determined, namely $\left[(T_1 - T_2)/\Delta T_m\right] S/A$ or its equivalent $h_{cs}/(c_{pa}G)$, multiplied by $(c_{pa}\mu/k)^{2/3}$. He called this dimensionless group the j-factor and by definition;

$$j_h = \frac{(T_1 - T_2)}{\Delta T_m}\frac{S}{A}\left(\frac{c_{pa}\mu}{k}\right)^{2/3} = \frac{h_{cs}}{c_{pa}G}\left(\frac{c_{pa}\mu}{k}\right)^{2/3} \qquad (2.63)$$

where j_h is the Colbourn j-factor for heat transfer, $(T_1 - T_2)$ is the temperature change, ΔT_m the mean temperature difference between the fluid and the surface, S is the cross-sectional area of air flow, A is the heat transfer area, c_{pa} is the specific heat of the fluid, μ is the viscosity of the fluid, k is the thermal conductivity of the fluid, h_{cs} is the surface heat transfer coefficient, and G is the mass-flux.

Gamson *et al* (1943) conducted a series of experiments on heat and mass transfer using spherical and cylindrical catalyst carrier pellets of diameters from 2.29 to 18.8 mm and cylinder heights 4.78 to 16.9 mm under conditions of constant drying rate, at temperatures from 26.7 to 71.1° C and at mass flux of air ranging from 0.54 to 3.12 kg/s.m^2. They found

a remarkable correlation of experimental data by plotting the heat transfer factor, j_h against modified Reynolds number, $d_e G/\mu$. For turbulent flow, 350 <Re < 4000

$$h_{cs} = 1.064\, c_{pa} G \left(\frac{d_e G}{\mu}\right)^{-0.41} \left(\frac{c_{pa}\mu}{k}\right)^{-2/3} \tag{2.64}$$

where Re = Reynolds number, and d_e, is the effective particle diameter, and $G = u\,\rho_a$.

It was observed that for all conditions of flow, turbulent, laminar or transition, the ratio of j_h to j_d remained constant and equivalent to 1.076.

Wilke and Hougen (1945) using a similar method of analysis proposed a correlation of an experimental data by plotting the mass transfer factor j_d , against the Reynolds number as follows:

$$j_d = 1.82\,\mathrm{Re}^{-0.51} \qquad \text{for } 40 < \mathrm{Re} \leq 350 \tag{2.65}$$

$$j_d = 0.989\ \mathrm{Re}^{-0.41} \qquad \text{for } \mathrm{Re} > 350 \tag{2.66}$$

For through-circulation drying where the gas flow is either upwards or downwards through a permeable bed of wet granular solids, the results of Gamson *et al* (1943) and Wilke and Hougen (1945) are applicable for evaluating the rates of adiabatic evaporation of water from packed beds of porous solids (Porter *et al*, 1973; Sokhansanj and Jayas, 1995).

Lof and Hawley (1948) following the measurement of the time-temperature relationship at the exit of a packed bed of granite gravels, determined the heat transfer coefficient by using the Schumann curves. They found that the results could be correlated by the equation

$$h_{cv} = 650\left(\frac{G}{d_e}\right)^{0.7} \tag{2.67}$$

Alanis *et al* (1977) measured the volumetric heat transfer coefficient of a rock pile by means of the transient method where a temperature step was applied to the bed, and the time-temperature relations obtained for fluid at different points in the pile were compared

with the theoretical curves computed by Schumann and Furnas. The following equation was developed for the volumetric heat transfer coefficient:

$$h_{cv} = 824\left(\frac{G}{d_e}\right)^{0.96} \tag{2.68}$$

where h_{cv} is the volumetric heat transfer coefficient in W/m^3 °C, G is the mass-flux in kg/s m^2, and d_e is the particle diameter in metres.

In the deep bed drying of malt, with an equivalent diameter of 4.57 mm, Bala and Woods (1984) performed nine experiments for air mass-flux values in the range 0.35 - 0.62 kg/sm^2 and air inlet temperatures of 50° to 70° C. Their experimental data was analysed by plotting temperature profiles at given time intervals in a dimensionless form and compared with the theoretical predictions by Schumann (1929). Their results were correlated by the equation:

$$h_{cv} = 49.32 \times 10^3 G^{0.6906} \tag{2.69}$$

where h_{cv} (W/m^3 K) and G (kg/s m^2).

Barker (1965) reviewed 244 papers on heat transfer in packed beds. He found that there was a general agreement amongst most investigators in the correlations presented in the literature. He observed that the agreement is generally by a multiplying factor of about 2 for Reynolds numbers ranging from 10 to 100,000. Bala (1983) obtained a similar result. Shewen *et al* (1978) extensively reviewed the available literature on the heat transfer in pack beds and subsequently recommended the Lof and Hawley (1948) equation.

The correlation obtained using the Culbourn approach generally predicts higher values of heat transfer coefficient in packed beds than those obtained using the Schumann analysis and therefore can over-predict the rate of moisture removal. As a factor of safety and from the design point of view, the correlation obtained by the Schumann analysis is to be preferred.

2.6 Psychrometry in relation to drying

As stated previously, two processes occur simultaneously during the thermal process of drying a wet product: heat transfer, to change the temperature of the wet product and to evaporate its surface moisture, and mass transfer of moisture to, and its subsequent evaporation from, the surface of the product to the surrounding medium. The drying medium is moist air, which is a binary mixture of dry air and water vapour. Relationships that can be used to model the inter-relationships between air and water vapour (i.e. psychrometric properties) are provided in the literature (Brooker *et al*, 1974 & 1978; Daly, 1992; and ASHRAE, 1993).

The water vapour saturation pressure for the temperature range of 0 to 200° C is given by (ASHRAE, 1993):

$$\ln(p_{ws}) = C_1 / T_{db} + C_2 + C_3 T_{db} + C_4 T_{db}^{\ 2} + C_5 T_{db}^{\ 3} + C_6 \ln(T_{db}) \qquad (2.70)$$

where $C_1 = -5.800\,220\,6 \times 10^3$, $C_2 = -5.5162560$, $C_3 = -4.864\,023\,9 \times 10^{-2}$, $C_4 = 4.176\,476\,8 \times 10^{-5}$, $C_5 = -1.445\,209\,3 \times 10^{-8}$, $C_6 = 6.545\,967\,3$ and T_{db} is the dry-bulb temperature.

or by (Brooker *et al*, 1974):

$$P_{ws} = R \exp\left(\frac{A + BT_{db} + CT_{db}^{\ 2} + DT_{db}^{\ 3} + ET_{db}^{\ 4}}{FT_{db} - GT_{db}^{\ 2}}\right) \qquad (2.71)$$

where,

P_{ws} = saturated water vapour pressure of the drying air, N/m^2

$R = 0.2210564925 \times 10^8$, $A = -0.274055258361 \times 10^5$, $B = 0.54189 \times 10^2$,

$C = -0.451370 \times 10^{-1}$, $D = 0.2153214 \times 10^{-4}$, $E = -0.462027 \times 10^{-8}$

$F = 0.241613 \times 10$, $G = 0.121547 \times 10^{-2}$

T_{db} = dry bulb temperature, K.

The absolute humidity of moist air (kg water vapour/kg dry air) in the temperature range of 255 K to 533 K is given by:

$$H = \frac{0.6219\, P_v}{P_{atm} - P_v} \tag{2.72}$$

where, P_v is the partial pressure of water vapour in the moist air sample which is evaluated from equation (2.70) or (2.71) by putting T_{db} equal to the wet bulb temperature of the surrounding air.

The saturated humidity, H_s , is the absolute humidity of moist air saturated with respect to water at the same temperature, T, and pressure, P. Its value is obtained from the equation (2.72) by putting $P_v = P_{vs,wb}$.

The wet-bulb temperature can estimated from the relationship below (ASHRAE, 1993)

$$\theta_{wb} = \frac{\left(2501(H_s - H_s^*) + \theta_{db}(1.805 H_s + 1)\right)}{\left(1 - 2.381 H_s^* + 4.186 H_s\right)} \tag{2.73}$$

where H_s^* is the humidity of moist air at saturation thermodynamic wet-bulb temperature, or from the following relationship given by Brooker *et al*, (1974)

$$T_{wb} = T_{db} - \frac{P_{vs,db} - P_{vs,wb}}{B} \tag{2.74}$$

where,

$$B = \frac{1006.9254\left(P_{vs,wb} - P_{atm}\right)\left(1 + 0.15577\, P_{vs,db}/P_{atm}\right)}{0.62194\, h_{fg,wb}} \tag{2.75}$$

and the latent heat of vaporisation of water vapour from moist air, h_{fg}, (J/kg) is calculated using one of the following relationships (Bakker-Arkema *et al*, 1978):

$$h_{fg} = 2502535.259 - 2385.764244\left(T - 338.72\right), \text{for} 273 \leq T \leq 339\,K \qquad (2.76)$$

$$h_{fg} = \left(7329155978000 - 15995964.08\,T^2\right)^{1/2}, \quad \text{for } 339 < T \leq 533\,K \qquad (2.77)$$

To evaluate the wet-bulb temperature by using either equation (2.73) or (2.74) requires a trial and error or a numerical solution method. The latent heat or heat of evaporation is evaluated at the wet-bulb temperature of the air in contact with the surface of the product (Daly, 1992). This statement assumes that at steady-state, the temperature of the wet surface of the material being dried is equal to the wet-bulb temperature of the air in contact with the surface of the product. However, in a mixed mode dryer since the surface temperature of the wet product is greater than the wet bulb temperature of the surrounding air, it is reasonable to assume a value of about 5 to 15K more than the wet bulb temperature as an initial guess.

The dew-point temperature, θ_d, of moist air with humidity H and pressure P is defined by (ASHRAE, 1993)

$$P_{ws}(t_d) = P_v = (pH)/(0.62198 + H) \qquad (2.78)$$

where, P_v is the water vapour partial pressure for the moist air sample and $P_{ws}(t_d)$ is the saturation vapour pressure at temperature θ_d. Alternatively, the dew-point temperature can be calculated from the following equation (ASHRAE, 1993)

$$\theta_d = a + b\alpha + c\alpha^2 + d\alpha^3 + e(P_w)^{0.1984} \qquad (2.79)$$

where, θ_d = dew point temperature, °C

α = $\ln(P_w)$

P_w = water vapour partial pressure, kPa

a = 6.54, b = 14.526, c = 0.7389, d = 0.09486 and e = 0.4569

The specific volume of moist air (m^3/kg. dry air) can be determined, by assuming ideal gas behaviour, by the following equation (ASHRAE, 1989):

$$\upsilon = \frac{R_a T}{P_{atm}}(1 + 1.608 H) \tag{2.80}$$

The density of moist air is evaluated as a reciprocal of the humid air specific volume from equation (2.80).

The relative humidity fraction is calculated from the following relation given by Daly (1992):

$$RH = \frac{1}{P_{vs,db}}\left\{P_{vs,wb} - 66.6\left(\frac{P_{atm}}{10{,}000}\right)(\theta_{db} - \theta_{wb})\right\} \tag{2.81}$$

or from the definition

$$RH = \frac{P_v}{P_{vs,\,db}} \tag{2.82}$$

where, θ_{db} and θ_{wb} are the dry-bulb and wet-bulb temperatures in $^{\circ}$C , $P_{vs,db}$ and $P_{vs,wb}$ are the saturation vapour pressure in Pa at θ_{db} and θ_{wb} respectively, and P_{atm} is the barometric pressure in Pa.

The specific enthalpy (or total heat) of moist air, per kilogram of dry air, is given by:

$$h = C_{p,a}\theta_{db} + C_{pw}H\theta_{db} + Hh_{fg} \tag{2.83}$$

where C_{pa} is the specific heat capacity of dry air and the other dependent variables are as previously defined.

2.7 Drying simulation

Ability to predict the rate at which a wet product dries in a given type of dryer can assist designers in developing similar dryers for maximum efficiency. Computer simulations can help researchers to understand the mechanisms and the processes involved in drying. Morey *et al* (1978) have shown that a comprehensive drying simulation model must include a thin-layer drying equation to predict the rate of moisture removal from the crop bed.

This section references the two methods of analysing the rate of drying of wet agricultural products. The first part considers the drying of the product as individual particles or in thin-layers and the next section considers the practical situation in which the products are dried in deep-beds. A review of mathematical expressions describing the drying rate of agricultural crops in thin-layers is presented. The use of these expressions in predicting the moisture loss from crops in conventional dryers is reviewed. The practical importance of thin-layer expressions, according to Bakker-Arkema *et al* (1978), is limited since agricultural crops, as they stated, are dried not as individual particles or in thin-layers; instead, crops are dried in either a stationary or a moving deep-bed. Nevertheless, the set of equations describing the drying of agricultural crops always include an expression that describes the rate of moisture removal from a thin-layer. Hence, in the second part of this section, the method of analysis of drying of a deep-bed of agricultural crops is reviewed.

2.7.1 Thin-layer drying equations.

A thin layer may be defined, contrary to a beep bed layer, as one in which there is no moisture gradient through the layer during drying. The thin-layer drying concept assumes that the ratio of the material volume to air is such that there is only a small change in temperature and relative humidity of the drying air when it exits the crop bed compared to its inlet conditions (ASHRAE, 1989). In crop drying, material depths of up to 200 mm are considered as thin-layers (Hall, 1975); but as pointed out by Henderson and Perry (1976), even depths as small as 25 mm provide evidence of moisture gradient and, thus may be considered as 'deep beds'.

The search for an accurate method of describing the drying rate of a thin-layer of material in a stream of air at constant temperature, velocity and absolute humidity (constant external drying conditions) has often been reported in the literature (Karel *et al,* 1975; Suarez *et al*, 1980; Igbeka, 1982; Hutchinson and Otten, 1983; and Chiang and Peterson, 1985).

Thin layer drying equations relate the rate of moisture loss to the drying conditions (drying air temperature, velocity and relative humidity) and the initial moisture content of the crop; they are based on empirical studies, or derived from theoretical or semi-theoretical considerations. In the theoretical approach, the equation is derived from either the diffusion equation or from simultaneous heat and mass transfer equations. In the semi-theoretical approach, approximated theoretical equations are used. In the empirical approach, experiments are conducted and empirical equations are developed to fit the experimental data. The main justification of the empirical equation is a satisfactory fit to experimental data (Zaman and Bala, 1989) and the subsequent benefit in describing thin-layer and deep bed drying of crops. The reasons for using theoretical equations are to give some physical explanation and understanding of the heat and mass transfer processes involved in drying of agricultural products. The approximated equations are simpler and take less computing time in comparison to the theoretical equations (Morey *et al*, 1978).

The following mechanisms have been proposed to account for moisture movement in capillary-porous solids such as agricultural crops (van Brakel, 1980; Brooker *et al*, 1974; Bakker-Arkema *et al*, 1978):

1) *liquid diffusion* due to moisture concentration gradient;
2) *vapour diffusion* due to partial vapour pressure gradient;
3) *capillary flow*, liquid movement due to surface forces ;
4) *surface diffusion,* liquid movement due to diffusion of moisture on the crop surfaces;
5) *thermal diffusion,* vapour movement due to temperature differences; and
6) *hydrodynamic flow or filtration,* liquid or vapour flow due to differences in total pressure.

Liquid diffusion, according to Igbeka (1982), is the most appropriate mechanism to describe the drying behaviour of cassava. Liquid and/or vapour diffusion have been assumed to be the primary mass transfer mechanism(s) in drying studies on cereal grains

and similar products (Hutchinson and Otten, 1983). The most widely investigated theoretical model in the thin-layer drying literature is the diffusion model, given by Fick's law (see equation 2.5).

The assumptions inherent in the diffusion model are as follows:

1) the primary mechanism for moisture transport is diffusion;
2) the principal driving force for mass transport is the internal moisture content gradient;
3) temperature within the kernel is assumed constant;
4) the resistance to moisture flow is uniformly distributed throughout the interior of the material; and
5) either vapour or liquid diffusion predominates. If both processes occur simultaneously, the diffusion coefficient must represent the combined effects of liquid and vapour diffusion.

Van Arsdel (1947) suggested that the diffusion equation could be used to describe the rate of moisture movement from a solid, if the potential for the moisture diffusion is represented by either concentration or vapour pressure gradient. Wang and Hall (1961) hypothesised that if the temperature distribution within a product being dried is assumed uniform, then the diffusion equation with concentration as the driving force is adequate in describing moisture movement from the product. Igbeka (1982) added that if resistance to moisture flow during drying is assumed to be uniformly distributed throughout the interior of the product, then the diffusion equation would be an appropriate model to describe moisture movement during drying of capillary porous materials. The selection of either moisture content gradient or vapour pressure gradient as the driving force for diffusion has been a subject of controversy. Babbitt (1949) and Bramhall (1979) maintain that vapour pressure gradient more consistently accounts for experimentally observed phenomena than does the concentration gradient. Babbitt explains that since vapour pressure is a function of moisture content and temperature, moisture transfer in response to a temperature gradient follows easily using the vapour pressure gradient as the driving force. Referring to this explanation, then under non-isothermal drying conditions as experienced in conventional dryers, it might be prudent to recognise vapour pressure gradient as the driving force for moisture diffusion rather than concentration gradient.

Waananen *et al*, (1993) presented a table summarising the mass transfer driving forces and the listed the various mechanisms used by previous researchers. In all they presented about 194 studies, out of which concentration gradient was applied as the sole driving force for moisture diffusion in about 67 % of the cases studied. The relationship between pressure gradient and moisture content gradient is not a linear function and therefore it would be simpler and easier to model a drying process using moisture gradient as the driving force for the diffusion process. In this way theoretical predictions of the moisture content of the drying product can be reliably compared with experimentally obtained results.

The exact solutions of the diffusion equation characterising moisture transfer in plane sheets, finite cylinders and spheres are listed by Young and Whitaker (1971a,b) and Crank (1975). The solution for a sphere, cylinder and the plane sheet commonly used for simulating moisture transfer in crops are respectively:

$$\frac{\overline{M} - M_e}{M_o - M_e} = \frac{6}{\Pi^2} \sum_{n=1}^{\infty} \frac{1}{n^2} \exp\left[-n^2 D \pi^2 t / r^2\right] \tag{2.84}$$

$$\frac{\overline{M} - M_e}{M_o - M_e} = \sum_{n=1}^{\infty} \frac{4}{a^2 \alpha_n^{\,2}} \exp(-D \alpha_n^{\,2} t) \tag{2.85}$$

$$\frac{\overline{M} - M_e}{M_o - M_e} = \frac{8}{\pi^2} \sum_{n=0}^{\infty} \frac{1}{(2n+1)^2} \exp\left[-(2n+1)^2 D \pi^2 t / z^2\right] \tag{2.86}$$

where the $\alpha_n's$ are the Bessel function roots of the first kind and order zero..

Solutions to the diffusion equations are restricted to conditions where the temperature, humidity, pressure, and velocity of the drying air are constant (Hougen *et al*, 1940). Referring to this statement, the assumption of a quasi-steady state analysis of the dynamic phenomena of drying could be justified. Agricultural crops , like wood, have water held in them in the form of bound and free water; thus diffusion equations can be applied for describing the variation in moisture content during drying, provided they agree with experimental data on moisture distribution during drying (Hougen *et al*, 1940).

Babbitt (1949) appears to be the first to apply diffusion equation to data for agricultural crops. He developed and applied the equation to the rate adsorption of water by wheat and to the rate of drying as well. Pabis and Henderson (1961) have shown that a three dimensional equation of internal diffusion with diffusion coefficient varying with time describes the drying curve very well for shelled yellow corn dried in a single kernel layer. They found that treating the grain as sphere gave satisfactory results.

Chinnan and Young (1977) considered peanut pods as composite spheres consisting of different materials where the inner core and the outer shell represented the kernel and hull respectively. They considered two mathematical models, one assuming moisture movement by vapour diffusion and the other by liquid diffusion. The liquid diffusion model was found to give a better fit with experimental data for thin layer drying than the vapour diffusion model in the falling rate period, though the vapour diffusion model gave a better fit over the total drying period, with a lower sum of squares of deviation between observed and predicted values, than the liquid diffusion model. Products modelled using a slab geometry include tapioca root (Chirife, 1971); apple (Roman *et al*, 1979); starchy food product (Igbeka 1982); and sugar beet root (Vaccarezza *et al*, 1974).

In addition to the exact solutions of equation (2.5), other relations or simplified solutions have frequently been employed in crop drying analyses. Lewis (1921) suggested that the rate of drying during the falling rate period is directly proportional to the difference between the actual moisture content of the material and the equilibrium moisture content, i.e :

$$\frac{dM}{dt} = -k(M - M_e) \tag{2.87}$$

After separating variables, equation (2.87) can be integrated to equation (2.88) or (2.89):

$$In\left(\frac{M - M_e}{M_o - M_e}\right) = -kt \tag{2.88}$$

$$\frac{M - M_e}{M_o - M_e} = \exp(-kt) \tag{2.89}$$

Equation 2.88 or 2.89 is commonly known as the exponential model. It was derived based on the approximated differential equation for diffusion on the following assumptions:

a) the resistance to moisture movement is concentrated in a layer at the surface of the material,

b) the initial moisture content of the material is not very high (less than 100 to 200 per cent on dry basis, depending on the material), since the drying rate no longer increases with moisture content but remains constant,

c) the material does not shrink greatly during drying , and

d) the drying coefficient , k , is a constant, though for a given material it varies with rate of diffusion and of surface evaporation and with its thickness.

It has been noted (ASHRAE, 1977) that equation (2.88) or (2.89) alone does not describe the usual drying process where grain is dried in a deep-bed because the drying air changes condition but does not necessarily reach moisture equilibrium with the crop. This notwithstanding, it has been widely used by a number of researchers.

Equation 2.87 was used by Ross and White (1972) to study differences in the drying characteristics of white and yellow corn. This equation was also used by Westerman *et al*, (1973) to study relative humidity effects on high temperature drying of corn; by Rodriguez-Arias (1956) to describe the thin-layer drying data of corn; by Hukill and Schmidt (1960) in their study of drying rates of fully exposed grain kernels; by White *et al*, (1981) in their study of drying behaviour of fully exposed popcorn; by O'Callaghan *et al*, (1971) in their simulation of agricultural dryer performance.

Henderson and Perry (1976) also reported that during the falling-rate drying period, the moisture removal rate (the drying rate) is inversely proportional to the moisture to be removed or the "free moisture" (M - M_e) as $\frac{dM}{dt} = -k(M - M_e)$, where M is the average moisture content of crop bed.

Sherwood (1936) contends that equation (2.87) should not be applied to the constant-rate drying period. If no constant rate period occurs, according to Sherwood, equation (2.87) will hold reasonably well, particularly when the drying curve is in the falling rate period. Sherwood (1936) noted that in certain slow-drying solids no constant rate period appeared, and internal liquid diffusion controlled the process from the start. The models of Lewis (1921) and Henderson and Pabis (1962) assumed that all the resistance to moisture flow was concentrated in a layer at the surface of the material. On the other hand, if it is assumed that the resistance to moisture flow is uniformly distributed throughout the interior of the material, then the fundamental diffusion equation would be an appropriate model describing the rate of moisture loss from an agricultural crop (Sherwood, 1936).

Hukill (1947) also observed that the rate of moisture loss is approximately proportional to the difference between the moisture content of the grain and the equilibrium moisture content (i.e. the amount of moisture available to be removed) for corn and sorghum. Thin-layer drying relations for cereal grains other than shelled corn have been proposed for barley (O'Callaghan *et al*, 1971), soybeans (Sabbah *et al*, 1976), rice (Walker, 1977), wheat (Watson and Bhargava, 1974; M'Ewen and O'Callaghan, 1954; Simmonds, Ward and M'Ewen, 1953a, b).

M'Ewen and O'Callaghan (1954) proposed the following exponential thin-layer drying equation for wheat in the temperature range 21° C -77° C:

$$\frac{\partial M}{\partial t} = -2.3m(M - M_e) \tag{2.90}$$

where m is an exponential function of temperature only and M_e has been correlated as a function of relative humidity and temperature of the drying air. They proposed that the value of the rate constant for wheat of normal size, approximately 3.3 mm in diameter (0.13 in diameter), is given in the temperature range 21° C to 77° C by

$$\log_{10} m = \frac{\theta_{a,F} - 159}{87} \tag{2.91}$$

where $\theta_{a,F}$ is the air dry bulb temperature, ° F.

In another study, Hall and Rodriguez-Arias (1958) plotted their data for shelled corn fully exposed to various drying conditions on semi-logarithmic graph paper using Equation (2.87). They reported that the plots yielded excellent straight lines over restricted regions of the curves with sharp changes in slopes occurring at regular intervals between the linear portions. They concluded that the drying rate constant vary in step-wise fashion occurring at intervals throughout the drying process. They reported that the drying rate constant increases as a function of temperature quadrupling in value as the temperature was increased from 4.5 to 60° C. They suggested that at temperatures above 37.8° C it would be sufficient to use equation (2.87) in the exponential form to characterise the drying rates. In another study, Ayensu and Bondzie (1986) observed that the drying curves of cassava leaves (initial moisture content 72%, wet basis), pepper (initial moisture content 68%, wet basis), cassava chips (initial moisture 75%, wet basis) and fish (initial moisture content 80%, wet basis) consisted of two distinct parts: the constant rate portion and the falling rate portion. They reported that the two distinct portions of each of the drying curves could be represented by equation (2.87), where k is the drying constant which can be evaluated differently for the constant period (as k_1) and for the falling rate period (as k_2). Equation (2.87) according to Ayensu and Bondzie can be applied to the constant and the falling rate periods respectively in the forms:

$$\frac{M - M_c}{M_o - M_c} = \exp(-k_1 t_c) \qquad \text{for the constant rate period} \tag{2.92}$$

$$\frac{M - M_e}{M_c - M_e} = \exp(-k_2 t_e) \qquad \text{for the falling rate period} \tag{2.93}$$

where M_c is the critical moisture content.

A modified form of the basic exponential drying equation, sometimes referred to as the Hustrulid & Flikke equation (Hustrulid and Flikke, 1959), has also been used by a number of researchers (Ross and White, 1972; Sharaf-Eldeen *et al*, 1980; White *et al*, 1981; Chiang and Petersen, 1985; Patil and Ward, 1989; Diamante and Munro, 1991b, 1994); it is of the form:

$$\frac{M - M_e}{M_o - M_e} = a\exp(-kt) \tag{2.94}$$

Equation (2.94) has been successfully used and validated for deep-bed solar air drying of rape seed by Patil and Ward (1989). Harvey *et al*, (1985) successfully fitted equation (2.94) to drying data obtained from the drying of sorrel, a high moisture crop, in a solar cabinet dryer from a moisture content of 90% (wet basis) to about 11 % in 4 days.

A simplified form of the Fick diffusion equation (SFFD) applicable to long drying times (Chirife and Cachero, 1970) is very similar to equation (2.93) and has the form:

$$\frac{M - M_e}{M_o - M_e} = a\exp(-\frac{\pi^2}{4}\frac{D}{L^2}t) \tag{2.95}$$

Equation (2.95) has been one of the most widely used equations in modelling drying rates of crops of high moisture content (Chirife and Cachero, 1970; Vaccarezza *et al*, 1974; Igbeka, 1982; Diamante and Munro, 1993).

An alternative approach to the analysis of thin-layer drying data has been to use purely empirical relationships. Very good fits of experimental data have been reported by researchers using purely empirical relationships (Hutchinson and Otten, 1983; Morey *et al*, 1978; Brooker *et al*, 1974). One equation that has been widely used in thin-layer studies of a variety of materials (Hutchinson and Otten, 1983) is Page equation.

Page (1949) (cited by Hall and Rodgriguez-Arias, 1958 and Van Rest and Isaacs, 1968), on the basis of his investigation on the basic drying rates of shelled corn at Purdue University, proposed an empirical equation for describing thin-layer drying of the form:

$$\frac{M - M_e}{M_o - M_e} = \exp(-kt^n) \tag{2.96}$$

where n is an experimental constant, and the value of the constant k was determined on the basis of time, t, expressed in half-response units. Page found that the constant n was a function of the relative humidity and obtained values of 0.60, 0.65 and 0.83 for relative humidity values of 35, 50 and 70% respectively, and 0.68 for k.

Other researchers (White *et al*, 1973; Misra and Brooker, 1980; Bala 1983; White, Bridges, Loewer and Ross, 1981; Li and Morey, 1984; Syarief *et al*, 1987; Diamante and Munro, 1991a, b; Janjai *et al*, 1994; Hutchinson and Otten, 1983; Agrawal and Singh, 1977; Wang and Singh, 1978; Overhults *et al*,1973) have also used Page equation to adequately fit and/or predict the thin-layer drying data of shelled corn, rough rice, malt, white beans and soybeans. In utilising Page equation, White *et al* (1973) expressed the time t in hours or actual time units and found both n and k to be functions of drying air temperature.

Misra and Brooker (1980) identified Page's equation as more promising for shelled corn. They gave an equation for k which is a function of drying air temperature and velocity and further described an equation for n as a function of drying air relative humidity and initial grain moisture. Their equation is valid for drying air temperature in the range of 2.5 to 70° C, drying air relative humidity ranging from 3 to 83%, drying air velocities from 0.025 to 2.33 m/s, and initial moistures of 18 to 60% (dry basis).

Li and Morey (1984) also obtained satisfactory fits for their drying data using equation (2.95) and found that within the limits of drying airflow rates and air relative humidity values used, k and n can be expressed as functions of air temperature and initial grain moisture only. Their equations for k and n apply to air temperatures ranging from 27 to 116° C, initial grain moistures in the range of 23 to 36% dry basis, airflow rates from 0.27 to 1.34 m/s, and air relative humidity ranging from 5 to 40%.

Bala (1983) fitted equation (2.96) to the thin-layer drying data of malt and found the exponent, n, of the equation to be a function of the drying air temperature and its relative humidity; but suggested that the contribution of the relative humidity term to the value could be ignored without a meaningful loss of accuracy.

Van Rest and Isaacs (1968) investigated exposed layer drying rates of shelled corn, wheat and oats for a variety of conditions. They found that the basic logarithmic model proved moderately adequate for wheat, but it failed to provide adequate fit for corn. They reported that the Page equation described the experimental data better than the logarithmic model for each of the crops. They tested also another empirical equation of the form:

$$\frac{M - M_e}{M_o - M_e} = p - q \log t \tag{2.97}$$

They found equation (2.97) to be more useful than the logarithmic model.

Flood *et al*, (1972) developed an empirical relation similar to Page's equation to describe the thin-layer drying of corn with natural air as the drying medium. They used actual time units for t and reported n to be constant (equal to 0.664) but k was described as a function of both drying air temperature and its relative humidity.

It was noted by Syarief *et al*, (1984) that the choice of the unit for time variable in the Page equation is very important. For example when t equals 1, no matter the time unit, t^n also equals 1 irrespective what the value of n. Often n is made a function of some parameter (eg. drying temperature, Syarief *et al*,1984) in developing a general model. Syarief *et al*, argued that since when t equals 1, n has no effect on t^n, the parameter would have no effect on the drying rate. They also observed that if the hour was chosen as the unit of time, unreliable prediction of the drying rate occurred in the middle of the drying period for many conditions. If the minute was chosen as the unit of time, the problem occurred at the beginning of the drying period and had little effect on the resulting model. For these reasons, Li and Morey, (1984) and Syarief *et al* (1984) recommend the unit of time in minutes when using the Page's model.

Troeger and Hukill (1971) developed the following empirical model for shelled corn

$$\frac{dM}{dt} = -k(M - M_e)^a \tag{2.98}$$

where, a is an arbitrary constant. They also observed that the use of three regions rather than a single region allows a good fit of the entire drying curve. They proposed a set of empirical drying equations for shelled corn in the temperature range of 32 to 71° C.

Equation (2.96) may be modified to include the dependence on sample thickness as a simplification of the Fick's diffusion equation to give the modified Page equation (Diamante and Munro, 1991b):

$$\frac{M - M_e}{M_o - M_e} = \exp(-k[t / L^2]^n) \qquad (2.99)$$

Diamante and Munro (1991b) studied the effect of air dry bulb temperature, air relative humidity, air velocity and sample thickness on the thin-layer drying of sweet potato slices in a conventional tunnel dryer. Each of equations (2.95)-(2.97) and (2.99) was fitted to their drying curves (M vs. t) for 29 experimental runs using linear regression analysis. They found that the modified Page equation best described the thin-layer drying of sweet potato slices from moisture content in the range 179 to 251% expressed on dry basis, down to a moisture content of 10% on dry basis. Diamante and Munro also found that the drying air temperature and the sample thickness were the major variables affecting the drying rate of sweet potato slices. They concluded that air humidity had a small effect on drying rates within the humidity range of 10-15%. The thickness of the sample has also been shown to influence the rate of drying in the studies of Igbeka (1982) and Chirife and Cachero (1970) for cassava or tapioca slices and Vaccarezza *et al* (1974) for sugar beet slices. The effect of air dry bulb temperature on drying is well documented in the literature (Igbeka, 1982; Hutchinson and Otten, 1983; Chiang and Petersen, 1985). Contrary to the observation of Diamante and Munro (1991b), several investigators have shown that air relative humidity below 20% has an insignificant effect on drying rates (White *et al*, 1973; Chiang and Petersen, 1985). It is revealing from the above studies that the effect of the air relative on the rate of drying cannot be ignored. A number of researchers have chosen to neglect the effect of air flow rates in the analysis of thin-layer drying data, citing the conclusion of Henderson and Pabis (1962) that resistance to moisture movement at the surface is negligible compared to internal resistance for turbulent flows, which occur in most conventional dryers. However, Islam and Flink (1982) pointed out that at air velocities of

2.5 m/s or less, the external mass transport resistance is significant and needs to be considered in the analysis of the drying data. The study of Diamante and Munro (1991b) showed this to be the case for air velocity within the range of 0.5-3.0 m/s. In natural convection solar dryers, air flow rates are relatively low enough for external mass transport resistance to be considered.

Thompson, Peart and Foster (1968) performed a series of thin-layer drying test at Purdue University in 1963. The main variable of their investigation in the tests conducted was the drying air temperature, however, other explanatory tests were performed to evaluate the effect of airflow rate and the product (corn) variety on drying rate. The tests were performed with corn at initial moisture contents of 19, 23, or 33% expressed on wet basis, for drying air flow rates of 20 and 60 cfm/ft^2 and at temperatures ranging from 49 to 171° C. They reported that the results of each drying test were analysed by fitting the experimental data to two thin-layer equations. The first was the simple exponential drying relation and second was a second-order exponential curve of the form:

$$t = A \ln MR + B (\ln MR)^2 \qquad (2.100)$$

They reported from the plots of the experimental data and those predicted using the simple exponential relation that the simple exponential relation did not adequately represent the experimental results. However, the plot of experimental drying results and those predicted by equation (2.100) showed a reasonable representation of the experimental results for the wide range of temperatures used. Thompson and Peart (1968) subsequently proposed equation (2.100) for predicting the drying rate of shelled corn in the temperature range of 49° C to 171° C, where, t = time in hours, θ_F = temperature in ° F, $A = -1.862 + 0.00488\theta_F$ and $B = 427.4 \exp(-0.033\theta_F)$. They assumed the Henderson (1955) equilibrium moisture content relation and hence developed by trial and error the following equation for shelled corn from the data by Rodriguez-Arias (1956) for a given air state point:

$$1 - RH = \exp\{-c(T+50) M_e^n\} \qquad (2.101)$$

They reported that the constants that represent the experimental results the best are : $c = 3.8195 \times 10^{-5}$, and $n = 2.0$. They found that the second order equation which involves time and natural logarithm of moisture ratio adequately represented drying characteristics of shelled corn.

Bunn *et al*, (1972) also proposed another empirical equation, simple in form, to describe the dynamic process of drying a variety of materials with high initial moisture content (100% d.b and above). The equation is of the form:

$$W = A\left[\frac{t + BC}{t + AB}\right] \tag{2.102}$$

By applying the initial and boundary conditions (when $t = 0$, $W = W_o$ and when $t = \infty$, $W = W_e$) and defining the time, t, when the weight ratio is equal to one-half as, $t_{1/2}$, the weight ratio in terms of half-life, equation (2.102) then becomes:

$$\frac{W - W_e}{W_o - W_e} = \frac{t_{1/2}}{t + t_{1/2}} \tag{2.103}$$

Equation (2.103), according to Bunn *et al*, was developed through many theoretical and empirical trials with weight-loss data from stalk-cut burley tobacco curing studies. They reported that the following form of the equation, in fact a re-arrangement, describes the weight-time relationship down to about 5 % moisture content (dry basis).

$$W = W_e + (W_o - W_e)\left[\frac{t_{1/2}}{t + t_{1/2}}\right] \tag{2.104}$$

They also indicated that their different sets of data were fitted to the Page's equation, as a way of comparison, and found that Bunn's equation fitted better than the Page's equation. No claims were made for the universality of equation (2.104) nor for its theoretical basis relative to the physical processes of drying. The relation between the parameter "$t_{1/2}$" and the drying conditions were, however, not provided.

Islam and Jindal (1981) developed a simulation model for predicting the drying in a deep bed of paddy consisting of thin layers of paddy in trays stacked upon each other. They used the second-order differential thin layer drying equation developed by Thompson *et al*, (1968) to calculate moisture changes in the layers. Their deep-bed simulation model was developed following the basic approach by Thompson *et al* (1968). The experimental results from the multi-layer drying tests were compared with the simulated results based on the model. They reported that predicted drying rates were higher than the experimental drying rates. They observed significant differences between the experimentally obtained and the predicted air temperatures in between the layers of the deep bed.

Glenn (1978) developed a semi-empirical approach to thin-layer modelling, by describing the kernel as made up of two distinct lumps, of the form:

$$\frac{M - M_e}{M_o - M_e} = A_o \exp(-k_o t) + A_1 \exp(-k_1 t) \qquad (2.105)$$

A thin-layer drying model of the form of Equation (2.105) was used by Keener *et al* (1978) to fit experimental grain drying data. They found that the double exponential thin layer drying relation provided prediction of the drying process over a wide range of conditions. Sharaf-Eldeen *et al*, (1979a) applied the general solution to the diffusion equation and developed a two term exponential thin layer drying equation of the form:

$$\frac{M - M_e}{M_o - M_e} = A \exp(-kt) + (1 - A) \exp(-Bkt) \qquad (2.106)$$

They assumed a constant diffusivity and observed that the two-term exponential model adequately describes the behaviour of fully exposed shelled corn, rough rice and soybeans. They also observed that Page equation gives a better description compared to the basic logarithmic model proposed by Lewis. Sharaf-Eldeen *et al* (1979b) found that a two-term exponential model adequately describes the drying behaviour of ear corn and shelled corn over the entire drying period. They indicated that the simple logarithmic model and its modified form fail to describe the drying behaviour for these products throughout the entire

drying period. They further observed that the predicted moisture ratios using Page's model were higher during the middle stages and lower during the early stages of drying compared to the observed moisture ratios.

Verma *et al* (1985) carried out an extensive experimental study in a vertical airflow dryer to evaluate the effects of the temperature, velocity and relative humidity of the drying air on the drying constants of steamed and unsteamed rough rice. Thirty-seven tests were conducted with unsteamed rice and thirty-five with steamed treated rice. Relative humidity varied from 3 to 60%, velocity from 0.025 to 0.50 $m^3/s.m^2$ and temperature from 35 to 95° C for unsteamed rice. In the case of steamed rice, the relative humidity varied from 10 to 58%, velocity from 0.05 to 0.50 $m^3/s.m^2$ and temperature from 30 to 75° C. They developed a two term exponential drying equation (an approximated form of the infinite series solution of the diffusion equation for a plane sheet) that describes the single layer drying of steamed and unsteamed rice of the form:

$$\frac{M - M_e}{M_\bullet - M_e} = A\exp(-kt) + F\exp(-gt) \qquad (2.107)$$

in which the drying the drying constant was expressed by an Arrhehius-type relation.
A number of researchers (Hustrulid and Flikke, 1959; Newman, 1931; Sharaf-Eldeen *et al* 1979b) have also pointed out that the second and subsequent terms of the series solution of the diffusion equation are negligible after extended drying.

Syarief *et al* (1984) also fitted the simple exponential, the Page's, the Thompson's and the double exponential thin-layer drying equations to the experimental data from the drying of sunflower seeds in thin layers. They found that the Page equation described moisture content reduction data somewhat better than the simple exponential equation. They reported that the double exponential equation gave the best fit to the drying data over the whole drying period. They indicated that the Thompson's model was incapable of describing the drying data in the first two hours of the drying period. Syarief *et al* (1984) concluded that a generalised thin-layer drying equation based on Page's equation with each of the empirical constants, k and n, expressed as a function of the drying air temperature provided the best prediction of the thin-layer drying rates of sunflower seeds.

Nellist (1976) fitted four alternative equations to the experimental data for ryeseeds. These equations were the single exponential equation, diffusion equation for a sphere, the equation of diffusion through an infinite plate and a two term exponential equation. The two term exponential equation gave the best fit but acceptable results were given by the series equation of diffusion through an infinite plane.

Wang and Singh (1978) applied the single exponential equation, the diffusion equation for a sphere, the Page equation and the Thompson's quadratic equation for single layer drying of rough rice. They observed that the diffusion model gave the worst fit and Thompson's equation was found to be the best.

Chhinnan (1984) designed and fabricated an experimental dryer for thin layer drying studies of pecans. Thin layer drying data was obtained for in-shell pecans for varying drying conditions. Four mathematical models were evaluated to fit the drying data, namely: the simple exponential model, the diffusion model, one term approximation of the infinite series solution of the diffusion model and the Page equation. The Page equation was found to be most suitable in describing drying characteristics of single layer of in-shell pecans and was recommended for bulk modelling studies. The exponent of the time, n was found to be a constant and equal to 0.6996. The basic exponential model was found to give the worst fit and diffusion model was found to give a better fit than the approximated diffusion model.

It must be emphasised that the unsatisfactory fit of the diffusion equation to most drying data is a result of inadequate information of the appropriate expressions for evaluating the diffusion coefficient for most agricultural crops. Many researchers as a result of this problem have solved the diffusion equation, assuming a constant diffusion coefficient.

2.7.2 Analysis of deep-bed drying.

The conditions of agricultural crops and of air change with position and time during deep bed drying processes (Boyce, 1965 and Thompson *et al*, 1968). Mathematical models have been used for studying low and high temperature deep-bed drying processes in the past. In these models, the drying phenomenon is analysed by calculating the drying of a thin layer of crop and then combining many thin layers to form the deep bed. The continuous drying process can be simulated by consecutively calculating the air and moisture changes that occur during short increments of time as the drying air passes from one layer to the next. Thus each layer is dried for a short time interval using exhaust air from the preceding layer. The process is repeated with consecutive short increments of time until a desired final moisture content of the crop bed is achieved.

The drying process is modelled using a set of mathematical formulations by considering energy and mass balances on a thin layer of crop located at an arbitrary position. These set of equations are complimented with equations describing the thin-layer drying and equilibrium property data of the products. A more detailed review of some of these efforts are available in the literature Brooker *et al*, (1974), Bakker-Arkema *et al* (1978), Sharp (1982), Parry (1985) and Cenkowski *et al*, (1993).

The models for simulation of deep bed drying are classified as (Cenkowski *et al*, 1993): non- equilibrium, equilibrium, or logarithmic type. The non-equilibrium and logarithmic models are applied in all crop drying theories. The equilibrium models are applied in the stationary bed theory only.

2.7.2.1 Non-equilibrium models.

The non-equilibrium drying models assume that there is no heat nor mass equilibrium between the drying air and the crop throughout the deep-bed. Based on this assumption a system of partial differential equations (PDE) is derived from the laws of heat and mass transfer, the mathematical theory of drying of single solid bodies, and the general crop drying theory to represent the crop drying model. The validity of such models is based on

the premise that the temperature difference between the drying air and the product being dried is high enough. The word 'high' is very relative but researchers have assumed for simplicity that the temperature of the air should be higher than the ambient temperature by about 5° C. It must be noted that one PDE crop drying model may generate many algebraic operational crop drying models depending on the method of solution and simplifying assumptions.

Four of the many non-equilibrium models applicable to situations in which the wet product is dried in a stationary bed are referenced in this section.

The non-equilibrium model derived by Bakker-Arkema *et al*, (1967) and also presented by Brooker *et al*, (1974) is based on a control volume isolated from a stationary crop bed (see fig. 2.3).

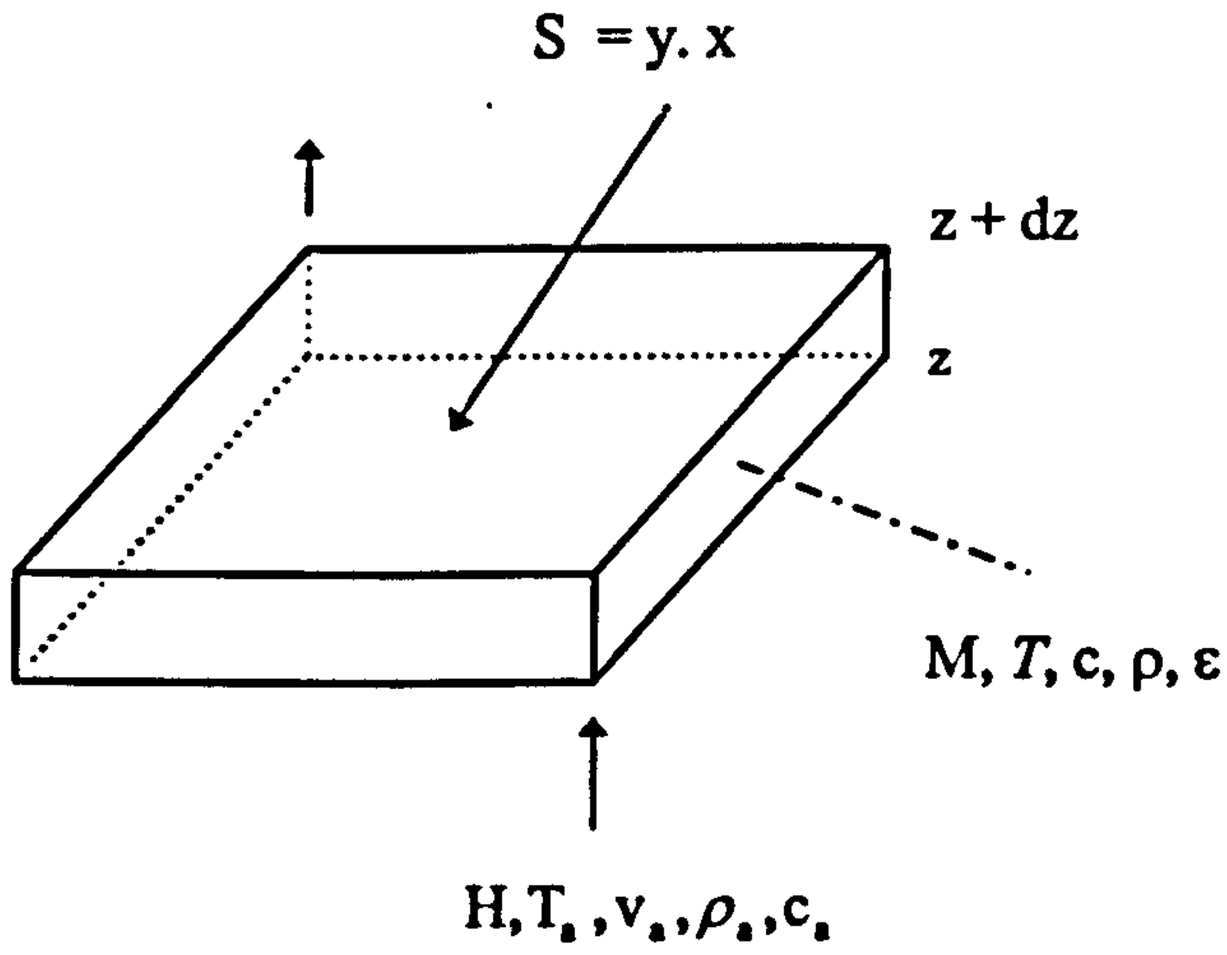

Figure 2.3: Control volume of a stationary bed of crop (Bakker-Arkema *et al*, 1967).

Their model is developed based on the following assumptions:

(i) volume shrinkage of a crop bed is negligible during drying,

(ii) temperature gradients within the individual kernels of grain are negligible,

(iii) conduction heat and mass transfer between crop particles is negligible,

(iv) airflow and grain flow are plug-type,

(v) changes in temperature and humidity over time are negligible when compared to air temperature and humidity changes over a thickness *dz* of the deep-bed in the direction of airflow,

(vi) bin walls are adiabatic with negligible heat capacity,

(vii) heat capacities of moist air and grain are constant over short periods, and

(viii) accurate thin-layer equation and moisture content equilibrium isotherms are known.

In practice a drying process is a non-stationary process, therefore, moisture content and temperature depend on position, z, and drying time, t, i.e. $M = M(z,t)$ and $\theta = \theta(z,t)$. According to assumption (ii), the temperature of the crop particle becomes the average temperature. For a quasi-steady solution, moisture content can be calculated or expressed as the average distribution of moisture within the crop bed.

When modelling the crop drying process in deep bed, the following unknowns are identified:

1. $M = M(z,t)$, the average moisture content of the crop bed,
2. $\vartheta = \vartheta(z,t)$, the average temperature of a product particle,
3. $H = H(z,t)$, the humidity of drying air in the bed, and
4. $T = T(z,t)$, the temperature of drying air in the bed.

Therefore, the model of crop drying process in a stationary bed must comprise of four differential equations which are: mass and energy balances of the crop and drying air and a drying rate equation of a thin-layer of the product. Bakker-Arkema *et al* (1967) and Brooker *et al*, (1974) presented the following set of differential equations for describing drying of grain in a stationary bed:

$$\frac{\partial H}{\partial z} = -\frac{\rho}{G_a}\frac{\partial M}{\partial t} \tag{2.108}$$

$$\frac{\partial T}{\partial z} = \frac{-ha}{G_a c_a + G_a c_v H}(T_a - T) \tag{2.109}$$

$$\frac{\partial \theta}{\partial t} = \frac{ha(T_a - T)}{\rho c + \rho c_w M} + \frac{h_v + c_v(T_a - T)}{\rho c + \rho c_w M} G_a \frac{\partial H}{\partial z} \tag{2.110}$$

$$\frac{\partial M}{\partial t} = \text{an appropriate thin layer equation.} \tag{2.111}$$

where: $G_a = v_a \rho_a$ is the air mass flow rate per unit area (air mass-flux).

Spencer (1969) presented a PDE grain drying model for a stationary deep-bed, but derived it based on premises different from the above model. He used the following assumptions in deriving his model:

(i) thermal properties of dry grain, moisture, and air are constant,

(ii) conduction heat transfer within the deep-bed is negligible,

(iii) the effect of condensation within the deep-bed is negligible, and

(iv) the problem is one dimensional.

The model also consists of four partial differential equations, and is based on an elemental volume of unit area and depth, *dz*.

$$v_a \frac{\partial \rho_v}{\partial z} + \varepsilon \frac{\partial \rho_v}{\partial t} = \rho(1-\varepsilon)\frac{\partial M}{\partial t} \tag{2.112}$$

$$c_a\left(G_a \frac{\partial T_a}{\partial z} + \varepsilon \rho_a \frac{\partial T_a}{\partial t}\right) = h(T - T_a) \tag{2.113}$$

$$\frac{\partial \theta}{\partial t} = \frac{h(T_a - T) + h_v(1-\varepsilon)\rho \dfrac{\partial M}{\partial t}}{(c + c_w M)(1-\varepsilon)\rho} \tag{2.114}$$

$$\frac{\partial M}{\partial t} = f(M, M_e, T, t, ...) \tag{2.115}$$

Sharp (1982) reviewed low temperature grain drying models for stationary beds. He presented a model based on an elemental bed of unit cross-sectional area with respect to airflow. By conducting the energy and mass balances, similar to Bakker-Arkema *et al*, (1967), he presented the following set of partial differential equations for describing drying of grain in a stationary bed:

$$G_a \frac{\partial H}{\partial z} = -\rho \frac{\partial M}{\partial t} - \varepsilon \rho_a \frac{\partial H}{\partial t} \tag{2.116}$$

$$G_a(c_a + c_v H)\frac{\partial T_a}{\partial z} = \rho c_v (T_a - T)\frac{\partial M}{\partial t} - h(T_a - T) - \rho_a \varepsilon (c_a + c_v H)\frac{\partial T_a}{\partial t} \tag{2.117}$$

$$\rho(c + c_w M)\frac{\partial T}{\partial t} = h(T_a - T) + h_v \rho \frac{\partial M}{\partial t} \tag{2.118}$$

$$\frac{\partial M}{\partial t} = -K(M - M_e) \tag{2.119}$$

Sharp suggested that the terms containing $\frac{\partial T_a}{\partial t}$ and $\frac{\partial H}{\partial t}$ in the above set of equations can be neglected, in which case the resulting set of equations will be very similar to the model of Bakker-Arkema *et al*, (1967).

A general mathematical model for grain drying for four basic grain drying systems: stationary deep-bed, cross-flow, concurrent-flow and counter-flow was presented by Laws and Parry (1983). They proposed a general PDE model by considering moist air and moist grain as a binary mixture. By assuming one-dimensional mass flow rates and constant densities for air and grain; and by neglecting conductive and radiative heating effects they obtained a generalised equation for a stationary bed of the form:

$$\frac{\partial \{u\}}{\partial t} + [A]\frac{\partial \{u\}}{\partial z} = \{b\} \tag{2.120}$$

2.7.2.2 Equilibrium models

The non-equilibrium models describe crop drying processes when high temperature air (up to 60° C) is used for drying. Such models are also applied to modelling grain drying using low temperatures (up to 5° C above the ambient air) and low airflow rates in a stationary bed. Under equilibrium conditions, the simplifying assumptions reduce the four equations in the partial differential equation model to two equations based on balances of moisture content in the grain and air humidity. For heat and mass equilibrium between the moist air and the grain throughout the stationary deep-bed, it is assumed that there is no resistance to heat and mass transfer within this bed. It is also assumed under equilibrium analysis that the air temperature is equal to the grain temperature. In equilibrium model analysis it is further assumed that under mass equilibrium M is equal to M_e (Cenkowski *et al*, 1993).

Thompson *et al*, (1968) developed an equilibrium grain model based on the empirical formula of the type

$$t = A \ln MR + B(\ln MR)^2 \qquad (2.121)$$

where MR is the moisture content ratio.

This drying model was modified by Bloome and Shove (1971) and again by Thompson (1972). Further development of this model and its validation was done by Morey *et al*, (1979), who found it suitable for predicting the moisture changes in a solar grain drying system. Ibrahim and Hansen (1984) used this model to simulate the solar drying of grain in an indirect crop dryer (i.e. a solar dryer in which the necessary amount of heat to evaporate the moisture from the surface of product is supplied by only the drying air). The fast speed of computation in using equilibrium models have been the main reason for the choice of such models for simulating drying processes.

2.7.2.3 Logarithmic models.

The logarithmic drying models are based on direct relationship between the rate of drying of a layer of grain in a deep bed, $\partial M/\partial t$, and the temperature gradient $\partial T_a/\partial z$ across this layer. This relationship can be derived from partial differential equations describing grain drying in a deep-bed presented by Sharp (1982). According to Cenkowski *et al*, (1993), these models have a low prediction accuracy yet most researchers still use them because of their simplicity.

The first logarithmic model for modelling grain drying was developed by Hukill (1954). Other such models were later developed and applied by many researchers (e.g. Barre *et al*, 1971, Barre and Hamdy 1974, Sabbah *et al*, 1979) mostly to low temperature drying in a stationary deep beds.

Assuming a unique relationship between the rate of moisture content change with time in deep bed drying, and the temperature change of air with respect to position, Hukill (1954)

developed an equation and a series of a dimensionless curves to predict the moisture content at any depth in a grain mass after a specified drying time as:

$$MR = \frac{M - M_e}{M_o - M_e} = \frac{2^D}{2^D + 2^Y - 1} \tag{2.122}$$

D = dimensionless depth factor

Y = dimensionless time.

One depth factor is defined as the depth of crop that contains, DM' of dry matter content given by

$$DM' = \frac{G'C_a(T_a - T_g)t_{1/2}}{vh_{fg}(M_{in} - M_e)} \tag{2.123}$$

where G' is the volumetric flow rate (m^3/s), and $t_{1/2}$ is the time for crop with a depth factor of zero to dry from a moisture ratio of 1.0 to a moisture ratio of 0.50. The depth factor of zero represents the drying of crop in a very thin layer. Also T_a and T_g represent the air temperature at inlet and outlet respectively. The dimensionless time, Y, is defined as

$$Y = t / t_{1/2} \tag{2.124}$$

where t is the drying time.

Equation (2.122) is referred to as the logarithmic model. Barre *et al* (1971) applied the modified form of Hukill's logarithmic model to cross-flow, low-temperature deep bed grain (ear corn) drying, and subsequently Barre and Hamdy (1974) employed the model to determine the optimal filling rates for in-storage drying of grain. Barre *et al* (1971) obtained quite good agreement between observed and predicted mean moisture contents for ear corn. Sabbah *et al* (1979) used a logarithmic model to simulate, forced-convection solar grain drying performance.

It may be concluded from the above that the equilibrium and logarithmic models are nothing but simplified variants of the partial differential equation models. It will therefore not be contentious if drying models are based non-equilibrium models.

2.8 Solar drying: an overview

A solar dryer is a device which uses solar energy as the heat source for the drying of food/agricultural products. The air flow through these dryers can be by means of either forced or natural convection. The heating of the material being dried could involve the passage of air pre-heated in a solar air-heater through the product, the exposure of product to the incident solar radiation directly or a combination of both. The material being dried is placed on a fixed (stationary) bed and is dried in batches. The total energy absorbed by the product over the drying period supplies the energy necessary for vaporisation of water from the product.

2.8.1 Classification of solar dryers

Solar dryers are classified according to the following criteria (Brenndorfer *et al*, 1987):

i) whether or not the drying product is exposed to radiation,

ii) the mode of air flow through the dryer, and

iii) the temperature of air entering the drying chamber.

These criteria are discussed in the next subsections.

2.8.1.1 Classification based on exposure of crop to direct solar radiation.

Based upon this criteria solar dryers can be termed either direct, indirect or mixed-mode dryers.

Direct type dryers refer to those systems in which the material to be dried is placed in shallow layers in an enclosure with a transparent cover or side panels. In these systems, part of the solar radiation may penetrate the material being dried and be absorbed within the product itself- generating heat in the interior of the product as well as its surface- thus enhancing thermal transfer. This heat causes evaporation of the moisture from the product. In addition, it allows the air inside the drying cabinet to expand, resulting in the removal of moisture by the movement of air. The solar absorptance of a product is an important factor in direct solar drying (radiation drying). Fortunately, most agricultural crops have

relatively high absorptance of between 0.67 and 0.90 (Arinze *et al*, 1979). The thermal conductivity of the crop is also important, particularly if the drying layer is deep enough to require heat conduction from particle to particle (Lõf, 1962). The examples of the direct type solar dryers are cabinet type dryer (fig. 2.4) and the tent dryer (fig. 2.5). Direct type dryers are usually employed for the drying of high moisture materials.

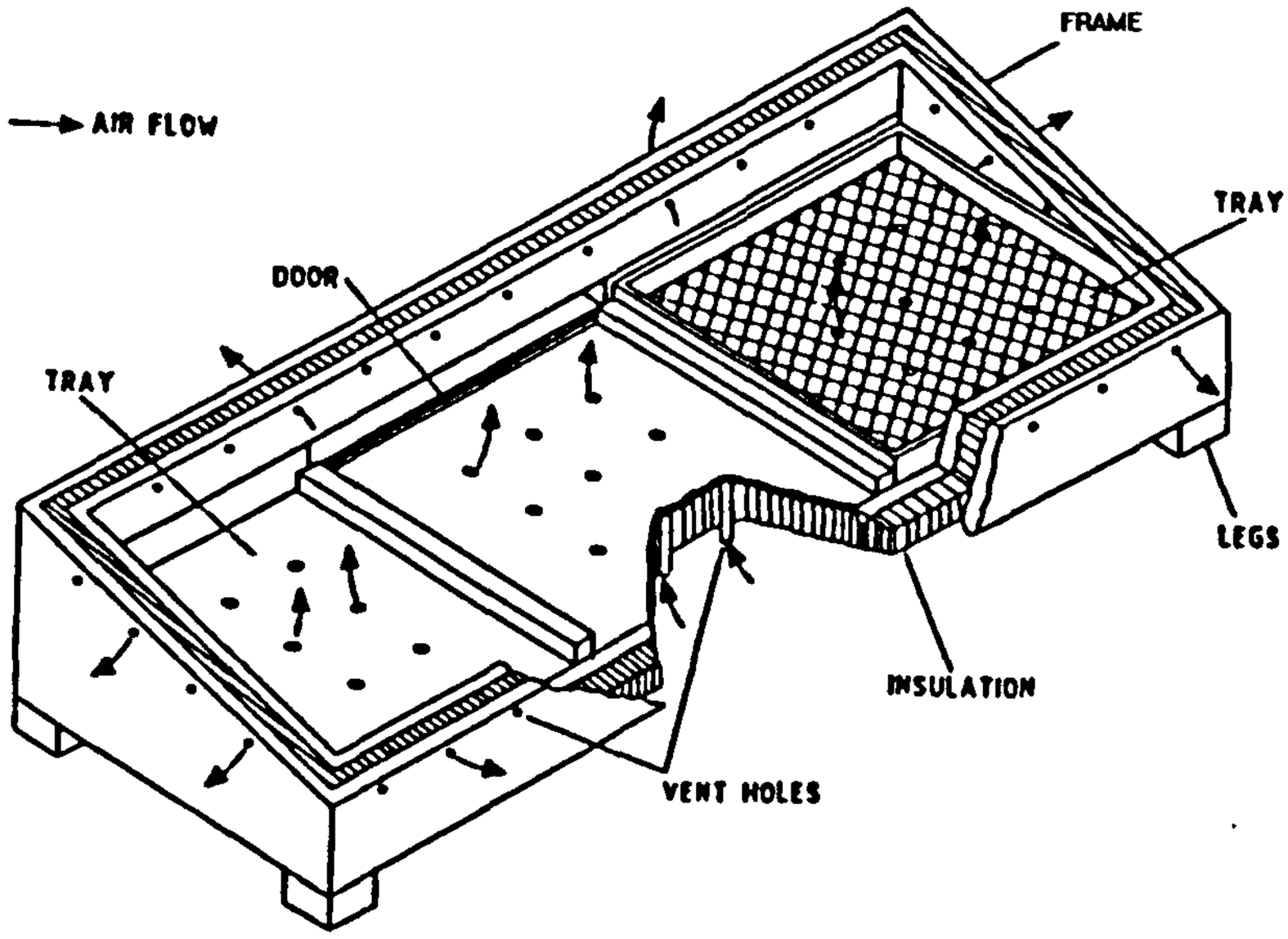

Figure 2.4: Natural convection solar energy cabinet-type dryer

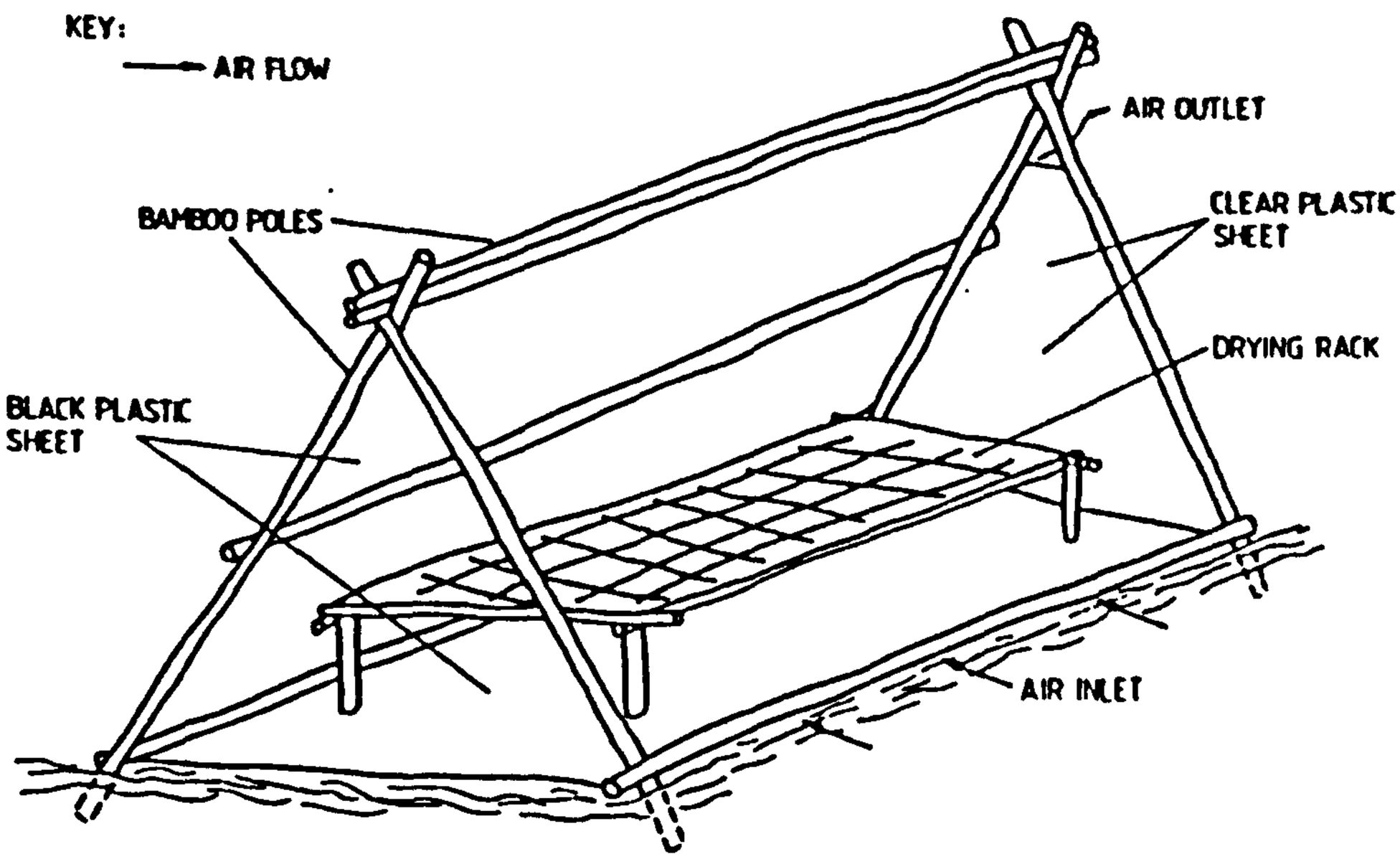

Figure 2.5: Natural convection solar energy tent-type dryer

In indirect-type solar dryers, the product is not exposed to the incident solar radiation. First, air is heated in a solar air-heater, and then channelled to the drying chamber (see fig. 2.6). The walls of the drying chamber are constructed of opaque material. Air flow is either by means of forced or natural convection. In these dryers, considerable manipulation of the material feed is necessary because the temperature of the air coming from the solar air-heater varies with time. Product re-orientation or stirring is necessary if uniform drying is to be achieved since the bottom layer will dry faster than the top layer.

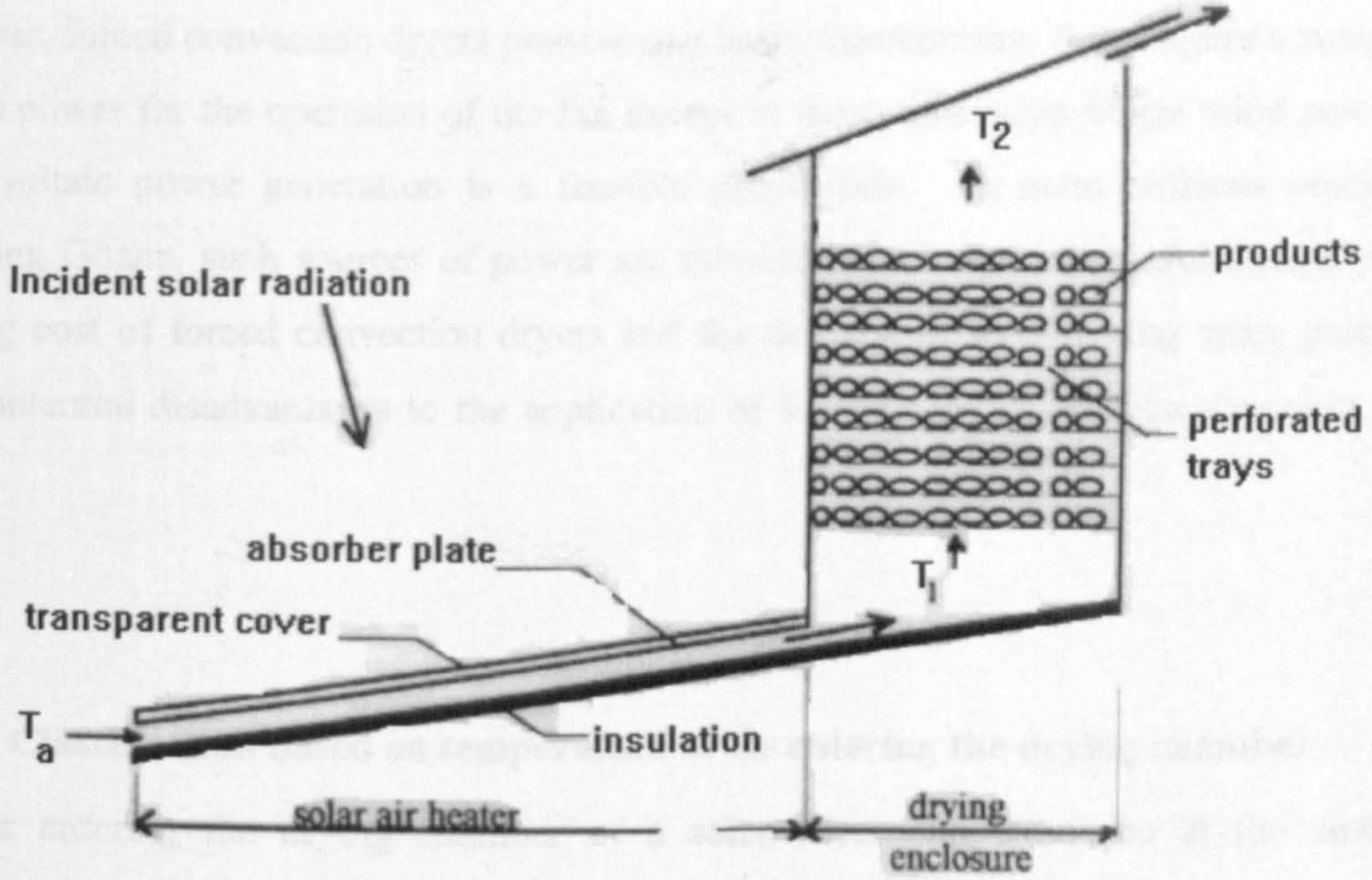

Figure 2.6: Natural convection solar energy indirect-type dryer

A mixed-mode dryer, as shown in fig. 1.1, combines the features of the direct-type and the indirect-type solar dryers: heat transfer to the crop is by means of a combination of the passage of solar pre-heated air in a solar-heater and by direct exposure to the incident solar radiation, hence the rate of drying could be greater than in both the direct and indirect dryers. In these dryers, since both the top and bottom layers of the material bed dry at almost equal rates very minimal amount of stirring of the drying material is required.

2.8.1.2 Classification based on the mode of air flow.

There are two possible modes of air flow, natural convection or forced convection. The former is reliant upon thermally induced density gradients for the flow of air through the dryer whereas for forced convection dryers the air flow is dependent upon pressure differentials generated by a fan. The latter is capable of providing a much greater air flow and therefore suitable for dryers with large throughputs. Another advantage of forced convection dryers is that air flow is independent of ambient climatic conditions and is easily and accurately controllable for most applications.

However, forced convection dryers possess one basic shortcoming; they require a source of motive power for the operation of the fan except in those rare cases where wind power or photo-voltaic power generation is a feasible proposition. In many African countries, including Ghana, such sources of power are unreliable and expensive. Additionally, the running cost of forced convection dryers and the difficulties in obtaining spare parts are other potential disadvantages to the application of forced convection solar dryers in rural areas.

2.8.1.3 Classification based on temperature of air entering the drying chamber.

The air entering the drying chamber of a solar dryer can either be at the ambient temperature or at some higher or elevated temperature; the elevation in temperature of the air being achieved by its passage through a solar collector (solar air-heater) prior to the drying chamber. Dryers that employ a separate solar collector and drying chamber have inherent tendency towards greater efficiency (Brenndorfer *et al*, 1987) as both units can be optimised for greater efficiency of their respective functions.

2.8.2 Hybrid dryers.

This term is used to denote those dryers in which energy from conventional sources is used in conjunction with solar energy for drying purposes. Such a system can be used in two ways. Firstly, solar heating can be the principal source of energy with additional heat, supplied by electricity, solid fuel etc. being used to maintain continuous drying. Secondly,

conventional energy sources could be used as the main means of heating the drying air and solar energy is used as a supplement heat source to reduce fuel costs. But in each of these applications a blower is required to supply air through the crop bed. The latter system has been extensively researched, in the drying of grains in the USA (Fraser and Muir, 1980; Pierce and Thompson, 1979; Morey *et al*, 1979; Petersen, 1973; Foster and Peart, 1976) and other places (Roa and Macedo, 1976; Trim *et al*, 1984). Such systems, like the forced convection solar dryers, cannot be easily adopted in the rural farming communities.

2.8.3 Natural convection (passive) solar-dryers.

In a passive solar dryer, solar energy is the main source of heat energy used in drying. Air is circulated through the crop mass by buoyancy forces or as a result of wind pressure, acting either singly or in combination. Three types of passive dryers have evolved, each maintaining the advantages and improving the effectiveness of traditional sun-drying methods. These are the direct, indirect and mixed-mode dryers. Zaman and Bala (1989) identified the mixed mode dryer as potentially most effective of these three types of natural convection solar dryers.

The basic components of natural convection solar dryers are: the air heating chamber, the drying chamber, and the chimney. In a direct mode dryer these components are integrated into a single unit but in the indirect and mixed mode dryers the components are separated. A discussion of the design considerations and constructional guides of the main components are given below.

2.8.3.1 Solar chimney: design considerations and construction

Natural ventilation relies on the presence of openings or chimneys in a ventilated structure. Changes in pressure over the surface of a structure, due to the effect of the structure and surrounding buildings on the local air flow patterns, leads to both driving and suction effects, while the temperature difference between the inside and outside of the structure leads to density variations and the stack effect. In practice both pressure- and temperature-driven natural ventilation infiltration air flows exist together (Douglas *et al*, 1995).

Proper design of chimneys, which enhance the buoyant flow is critical to the performance and overall design of natural convection solar crop dryers. In a solar chimney, forces which produce flow balance those that impede it. The buoyancy head required to operate the flow through the chimney is proportional to the difference between the mean air density within the chimney and the ambient air density, usually represented (Brenndorfer *et al*, 1987) as:-

$$\Delta P_b = g H_{ch} (\rho_a - \overline{\rho}_{ch}) \qquad (2.125)$$

The densities are related to temperature as well as to the absolute humidity (H) according to Sodha *et al*, (1987) as:

$$\rho = \rho_\bullet \left[\frac{1}{(1 + T/273)}\right](1 + H) \qquad (2.126)$$

Equation 2.125 suggests that if the air inside the chimney has the same temperature and humidity conditions and thus the same density as the ambient air, there would be no flow through the chimney. If, however, the mean air temperature inside the chimney is lower than the ambient air temperature, then there is no pressure head which encourages upward air flow. Thus, the main emphasis on chimney design is to minimise the rate at which the chimney air temperature cools to the ambient. The incorporation of a solar chimney may not necessarily improve the performance of a solar dryer as was observed in a study by Bassey (1994). Bassey suggested two ways of improving the performance of solar dryers: heating the air in a chimney attached to the dryer (using waste fuel), and reducing the air gap between an absorber placed inside the chimney and the outer transparent cover of the chimney. Daniels (1972) indicated that the use of thermal chimneys to improve the performance of solar dryers is possible, but they must be high enough to obtain sufficient difference in air pressure and large in cross section to prevent an undue resistance to the flow of air.

Othieno (1987) suggested that the rate of heat loss within the chimney should be considered in determining the optimum height of the chimney so as not to exceed the height at which the chimney air cools to the ambient temperature. Generally, the

temperature of the air leaving the crop mass is moist and its temperature could be close to that of the ambient air.

According to Ekechukwu (1987), the contribution of the buoyancy forces in natural circulation of air would be negligible, unless the air is heated subsequently above the stacked crop within the chimney. Oothuizen (1986) suggests that the incorporation of a chimney above the crop stack in natural convection circulation dryers will thus have little effect on the dryer performance unless the solar heating of the air within the chimney is significant. It was noted that since chimneys are usually vertical, heating of the solar chimney will usually be negligible except for dryers located far from the equator. As a result Oothuizen, assumed that the buoyancy forces occur effectively only in the collector and the drying chamber , if the chamber is transparent. This suggests that well designed transparent drying chambers can contribute to the buoyancy effects in natural convection solar dryers. It is also worth mentioning that for dryers located near the equator vertical chimneys receive diffuse radiation and for tropical locations the received diffuse components of solar radiation are fairly high. For such conditions chimneys can be efficiently designed such that the mean chimney air temperature remain well above that of the ambient air.

Ekechukwu and Norton (1997) contend that a recommended simple chimney should have black painted metal or wooden structure or a black painted material (to absorb radiation) within an external glazing. A chimney of similar in construction to that suggested by Ekechukwu and Norton was used by Puiggali *et al.*, (1985). Following from the recommendation of Ekechukwu and Norton (1997), it is reasonable to conclude that a transparent drying chamber will naturally aid the circulation of air for natural convection solar dryers.

Results from tests on the mixed-mode solar crop-dryer designed by Zambrano and Alvarado (1984) showed that the flow within a solar chimney can also be improved by slight geometrical modification (keeping the height constant). They showed that for a cylinder of a given height, using a chimney with the shape of an inverted truncated cone instead of a cylinder will increase the air velocity by a factor of 2 - 3.

For natural ventilation, Bruce (1978) suggests that, as a rule of thumb, the area of the inlet vent for fresh air entry should be twice the outlet for exhaust air.

2.8.3.2 Solar air heaters

A solar air-heater is simply a device to heat air by utilising solar energy. They are employed in many applications requiring low to moderate temperatures (below 60° C), such as crop drying and space heating. Various forms of solar air-heaters have been described in the literature and many studies, theoretical and experimental, have been carried out on their performance. The first extensive theoretical studies of some configuration of air heaters were conducted by Close (1963) and Whillier (1964). Selcuk (1977) critically reviewed the literature on solar air-heaters. It can be stated that the differences between the various forms of solar air-heaters arise from the differing constructions of the absorber, and in the path that the air takes when passing through the air-heater relative to the absorber (see fig. 2.7).

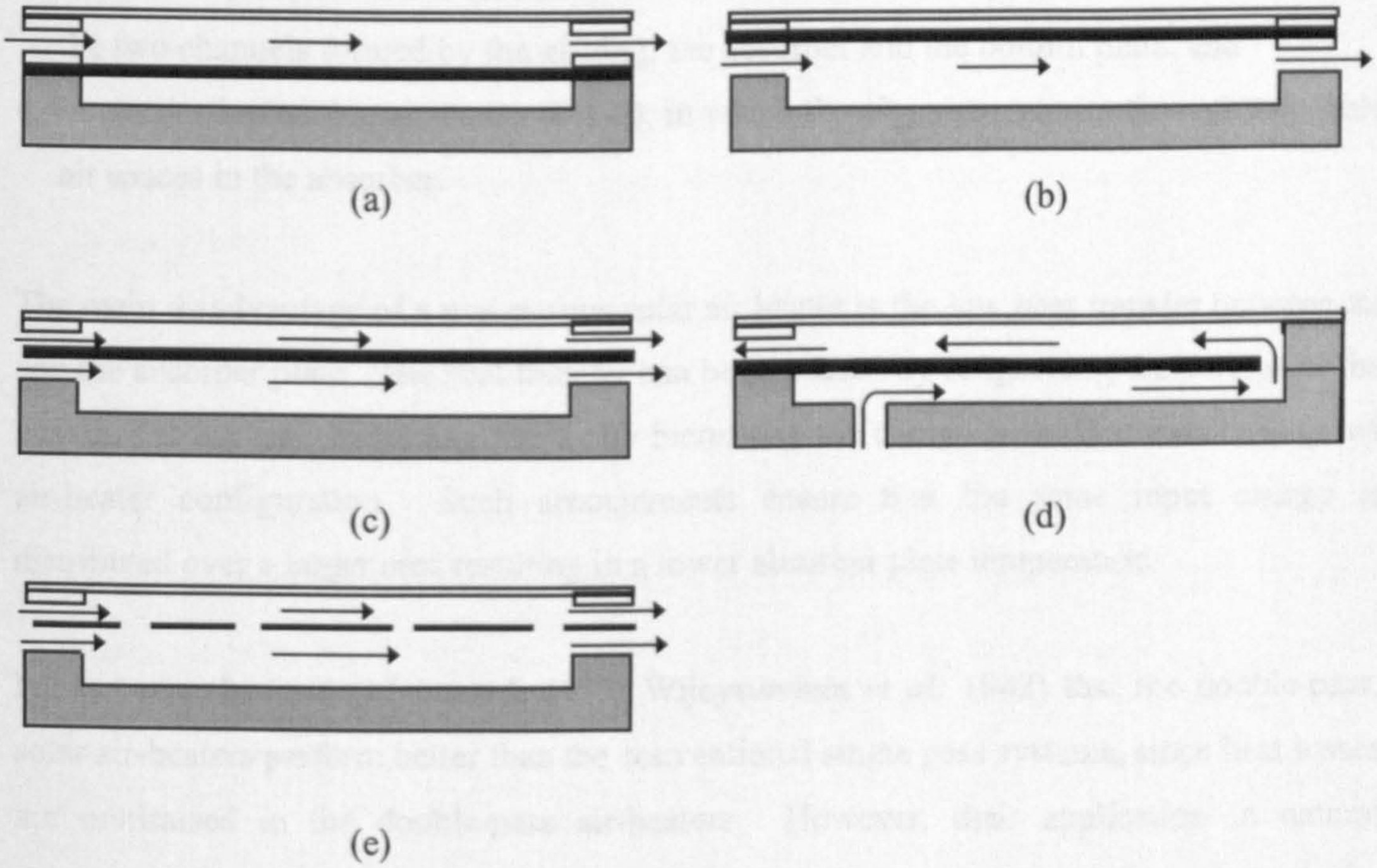

Figure 2.7: Schematic illustration of covered-type solar air-heaters: (a) Front pass, (b) Back pass, (c) Parallel pass, (d) Double pass, and (e) Parallel pass with porous absorber plate.

All designs of solar air heaters, so far, can be classified into two categories. The first type has a non-porous absorber (with or without an absorber cover), as in figs. 2.7(a)-(d) above, in which the air stream may flow above and/or behind the absorber plate. The second type has a porous absorber, as in fig. 2.7(e), in which air flows through the absorber. For applications which require temperature elevations of less than 40° C above ambient (as in crop drying), single-glazed solar air-heaters are adequate (Norton, 1992). Figure 2.7 illustrates the five principal types of the single-glazed covered-type solar air-heaters that can be incorporated into solar crop-dryers and these are:

a. the single-pass, front duct air-heater (**SPFDAH**); in which the air circulates between the absorber plate and the glazing,
b. the single-pass, rear duct air-heater (**SPRDAH**); in which the air stream is passed along the back of the absorber and in a gap formed between the absorber plate and the bottom plate, and there is stagnant air gap between the absorber plate and the glazing,
c. the single-pass, double-duct air-heater (**SPDDSAH**); in which air passes, in the same direction, through two channels formed between the glazing and the absorber plate and between the absorber plate and the bottom plate,
d. the double-pass, air-heater (**DPAH**); in which air flows in opposite directions through the two channels formed by the glazing, the absorber and the bottom plate, and
e. the porous/infiltrating air-heater (**PAH**); in which the air stream passes through available air spaces in the absorber.

The main disadvantage of a non-porous solar air heater is the low heat transfer between air and the absorber plate. The heat transfer can be increased by roughening the surface of the absorber at the rear, by adding fins or by increasing the energy collection area for a given air-heater configuration. Such arrangements ensure that the same input energy is distributed over a larger area resulting in a lower absorber plate temperature.

It has been observed (Mohamad, 1997; Wijeysundera *et al*, 1982) that the double-pass, solar air-heaters perform better than the conventional single pass systems, since heat losses are minimised in the double-pass air-heaters. However, their application in natural convection flow is limited since air needs to be forced through the two flow channels for efficient utilisation of the system. In addition for applications which require temperature elevations of less than 40° C above ambient (as in crop drying), single-glazed covered solar

air-heaters are adequate (Norton, 1992). Studies (Macedo and Altemani, 1978; Ong, 1982; Close, 1963) on the three types of single-pass, solar air-heaters employing a solid absorber have shown that the performance of the SPDDSAH is better than the SPFDSAH or the SPRDSAH.

Several studies have been conducted on SPDDSAH but issues regarding the best geometrical proportions are not conclusive. Following successive studies on solar air heaters at the University of Malaysia, it was reported that the determination of the optimum collector length will greatly aid in the design of future air heaters (Ong, 1982). For a SPDDSAH in which the flow is by forced convection, Pawar *et al*, (1994) recommend that for higher efficiencies the collector length should be in the order of 1.5 to 2.5 m . This recommendation is based on a fixed collector width of 1 m, suggesting that air-heaters having length to width ratios in the range 1.5 to 2.5 are ideal. However, for an SPDDSAH in which the flow is by natural convection, recommendations for optimal designs for specific applications are lacking. It is necessary to develop a mathematical model and perform detailed investigation using the model in order to determine the optimal design configuration of the system.

Mathematical models developed for predicting the useful energy gained by a flat-plate solar collector operating under steady-state or quasi-steady conditions are generally based on the equation:

$$q_u = F'[(\overline{\tau\alpha})_e I - U_L(\overline{T}_f - T_a)] \tag{2.127}$$

where F' and U_L are the collector efficiency factor and the collector heat-loss coefficient respectively, $\overline{T}_f$ is the local time-averaged fluid temperature and $(\overline{\tau\alpha})_e$ is the effective transmittance-absorptance product. Equation 2.127 is based on the assumption that the thermal capacitance of the air-heater is negligible. Three parameters [F' , $(\overline{\tau\alpha})_e$ and U_L] in equation (2.127) are needed to describe the thermal performance of a collector. Therefore, optimisation of the thermal performance must be exercised through changes in these three parameters. An examination of equation (2.127) suggests possible ways of increasing the amount of useful energy collected for a given solar radiation input. The

efficiency can be increased by increasing F', and $(\overline{\tau\alpha})_e$ and reducing U_L. Parker (1980) was the first to develop expressions for F' and U_L for a SPDDSAH but in arriving at the solution he made the following simplifying assumptions regarding the mass flow rate and the heat transfer coefficients:

a. the mass flow rates of air in the upper and lower channels of the heater are of the same magnitude, which may not necessarily be true,

b. the heat transfer coefficients between the absorber and the air has the same value in the top and the bottom channels of the collector, and

c. the heat transfer coefficients between air in the upper channel and the cover and between air in the lower channel and the bottom plate are equal.

Parker also defined the mean air temperature as the average of the temperatures in the two channels. He further introduced a fractional deviation *n:* the deviation of the temperature of air in each of the two channels from the mean. Parker (1981) noted that the assumption of equal values of n for the two channels would be valid, if all the assumptions are true; otherwise a better estimate of n should be sought since its value significantly influence the value of U_L.

The difficulty in obtaining the value of n, a value that changes along the direction of flow of the heated air was the basis for later work, looking for simplified expressions for F' and U_L. Boindi *et al* (1988) argued that hypothesising the same temperatures for air in the upper and lower channels, leads in general to results that vary only 2 to 3 % from the exact solution. Boindi *et al*, also derived expressions for F' and U_L by assuming equal temperatures of the air in the two channels.

The general expressions for the values of F' and U_L are related to the heat transfer parameters which are also dependent on the characteristics and operating surface temperatures of the absorber plate, the transparent cover and the base plate of the system.

In most studies aimed at predicting the thermal performance of solar air-haters, mathematical models based on equation (2.126) have been employed. Equation (2.126) is obtained by manipulating the basic set of the governing equations. To avoid the rigorous mathematical manipulations, some authors developed models based on the basic set of the

governing equations. Pawar *et al* (1994) developed a steady-state model, based on the latter approach, and provided analytical expressions for predicting the temperatures of the air in the upper and lower channels. Their model provides no means of estimating the air flow rates but uses given values; and it over-predicts the collector efficiency by 10 - 15%. However, the method used, by Pawar and his co-workers, in grouping the parameters in their resulting governing equations are adequate and can increase computational speed of a numerical solution.

Ong (1995a, 1995b) manipulated the governing equations and employed the matrix inversion technique to solve the resulting constitutive equations. In the Ong's model the mass flow is assumed. The model over-predicts the mean temperature of heated air near the inlet of the collector while that near the outlet of the collector is under-predicted. It is interesting to note that the models proposed by Pawar *et al*, and Ong are for situations in which the air flow through the heater is by forced convection and therefore the mass flow rate can easily be estimated. The mass flow rate affects the performance of a collector significantly and must be accounted for in the model.

2.8.3.3 Suggested approach for optimising the performance of a solar dryer.

For economic reasons, maximum drying rates are desired, though other factors, including product quality must be considered. The heat transfer and evaporation rates must be controlled to guarantee optimum drying rates. The control of the drying process in natural convection dryers offers a major problem. However, structural features that would guarantee that extreme conditions are not attained in the dryer could be incorporated into the design of natural convection solar dryers. One such approach, which regulates or promotes the necessary air flow of the drying air within the drying chamber for natural convection dryers, is the incorporation of a chimney (Ekechukwu,1987). Also excessive temperatures are to be avoided when drying certain crops and therefore heated air at a desired temperature must be channelled to the drying chamber. These problems call for a proper design of the air heating device and in addition the solar chimney.

2.8.4 Design of solar dryers

The design principles that have been developed for natural convection solar crop dryers can be classified under two main categories (Diamante and Munro, 1993):

i. the semi-explicit method, based on the chimney effect and complemented with psychrometric equations, and
ii. the implicit method, based on the chimney effect and using thin-layer equations.

In the semi-explicit method, the dimensions of the dryer are estimated based on the following design factors: the quantity of the product to be dried, the estimated drying time, the intensity of incident solar radiation for a given location, the initial and desired final moisture content of the product to be dried, the drying characteristics of the product and climatic conditions during the drying season.

Exell (1980) presented the design procedure based on the semi-explicit method for estimating the dimensions of a solar dryer in which air pre-heated in a solar collector is the sole source of heat for the drying process. The method is essentially a back calculation approach aimed at knowing the total volume of air needed for the drying and then fixing the grain bed depth accordingly. In this method the simple heat balance equation

$$m_w L_t = m_a C_s (T_i - T_f) \tag{2.128}$$

was used for estimating the mass of air required for drying a given quantity of wet agricultural product. Exell assumed the final conditions of the drying air escaping from the drying bed in an arbitrary manner. The method does not present a way of cross-checking the validity of the guessed values of the condition of the air leaving the drying bed. It is necessary, first to estimate realistically the drying taking place in a grain bed due to convective flow of the air, and then to compute the temperature and relative humidity of exit air. The latter is not entrenched in the design procedure presented by Exell. However, some commercial scale natural convection solar crop dryers have been designed based on Exell's approach by other researchers (Forson *et al*, 1996 and Iloeje *et al*, 1993) and are reported to be performing satisfactorily. A modification of the Exell's approach might be an ideal design procedure.

In the implicit method, as used by Ibrahim and Hansen (1984) and Steinfeld and Segal (1986), a mathematical model of the drying system for a given dryer geometry is first developed in which the dryer dimensions are made variables. Parametric studies are then conducted using the model. The theoretical results from the simulation runs can be presented in the form of charts, relating the various drying parameters. The design of a typical dryer can be effected using these charts. It is significant to note that, because a drying process involves complicated interactive factors, predictions from a theoretical model of the drying phenomenon cannot be considered absolutely reliable and experimental validation of the results is required.

The traditional techniques for designing dryers rely on a combination of pilot scale tests and experience with existing units to generate empirical rules for sizing dryers. While being adequate for designing dryers along tried and tested lines, the approach is limiting because these empirical rules will not apply to departures from designs. A design approach that brings in perception the two approaches outlined above would be beneficial.

2.9 Solar drying - mathematical and computer simulation studies

Models for simulating solar drying of different commodities can be found in the literature (Taylor and Wierd, 1985; Chirarattananon *et al*, 1988; Patil and Ward, 1989; Zaman and Bala, 1989; Garg and Sharma, 1990; Bala and Ziauddin, 1990; Harvey *et al*, 1985; Steinfeld and Segal, 1986; Elsayed, 1990; Ibrahim and Hansen, 1984). In all these studies a uniform thin layer of drying material is assumed and described either by a simple use of the psychrometric properties of air, or the fully exposed drying equations for the given material.

Bala and Woods (1994) contested and examined the validity of the assumption of a uniform, fully exposed layer drying. They presented a mathematical model based on the partial differential equation (PDE) model, to simulate the drying of rough rice in an indirect natural convection dryer. They described the temperature variation of the air along a single-pass, single-duct solar collector by a numerical solution. The drying of the grain was described by the introduction of a deep-bed solution procedure. The variation of the air temperature in the collector and across the drying bed were incorporated in the

prediction of the thermal buoyancy effect. They observed the product in the bottom layer of the bed to dry more rapidly while the top layers remained almost wet. They concluded that the assumption of a uniformly drying layer in crop drying analysis is not valid. Bala and Woods (1994) further examined the sensitivity of collector efficiency, dryer efficiency, overall drying efficiency, and moisture removal to a range of parameters. Their analysis showed that the overall dryer performance is most sensitive to bed depth followed by the collector length. Their simulation results were not verified experimentally, however, the appropriateness of a deep bed model was established. Although the layer may appear physically thin, low air flow rates give rise to a very slow moving drying front. Othieno (1987) reported similar experimental results during the natural convection solar drying of maize.

Ratti and Mujumdar (1997) applied a mathematical model developed by Ratti and Mujumdar (1995) for simulating the behaviour of a batch dryer to the deep-bed drying of carrots cubes in an indirect type solar dryer. In their model they correlated the solar collector exit air temperature data of Jayaraman *et al*, (1992) as a function of time of the day with a second order polynomial of the form:

$$T = -231.81 + 46.25 t_d - 1.77 t_d^2 \qquad (2.129)$$

where t_d is the hour of the day which was related to the process time, t, as:

$$t_d = t + 9.5 \qquad (2.130)$$

They reported that the dryer was simulated with a constant average inlet air humidity and air velocity for lack of information in Jayaraman *et al*, (1992). Their predicted and experimental values were in good agreement but they admitted that a better agreement would have been found if a natural convection model for heat transfer had been used. They simulated the drying rate for varied air flow rates and found air flow rate as an important factor affecting the drying time. Application of their model to even indirect type solar dryers is location specific and limited in its general applicability. In reality, the performance of a solar dryer is location- and time- dependent and therefore any

comprehensive model must include sub-programmes to model the following: the collector (air-heater) performance, the air flow rates and incident solar radiation prevailing at a given locality.

As far as the author is aware the studies of Bala and Woods (1994) and Ratti and Mujumdar (1997) are the only two studies reported in the literature for simulating crop drying in deep-beds. A selective review of recent studies in which agricultural products are assumed to dry uniformly in thin layers is presented below.

Zahed and Elsayed (1989) developed steady-state, mathematical model for simulating the drying process in a cabinet type solar dryer. The authors neglected the mass transfer process during drying and developed a model based on the heat transfer processes. The governing equations for the solid and air temperatures were derived by considering the energy balances for the air and solid in a control volume of thickness *dx*. The resultant equations were then put in dimensionless forms. The finite difference technique was used to solve the governing equations together with boundary conditions. The results obtained from their computer simulation were used to develop charts to be used as design aid. The computed results were not compared with experimental data and hence the validity of the model could not be assured. The model neglected the mass transfer of moisture and therefore could not fully predict the drying process explicitly.

Elsayed (1990) presented a mathematical model for predicting thin layer drying of agricultural products in a forced convection solar kiln. The rate of moisture transfer between the air and the material per unit area of the material surface was represented by an equation of the form:

$$\dot{m}''_{ev} = \rho_a f_w h_D (W_s^* - W_a) \qquad (2.131)$$

where, f_w $(= \dfrac{\overline{M} - \overline{M}_e}{\overline{M}_{cr} - \overline{M}_e})$ was defined as a weighing factor of value between zero and one. The value of the weighing factor (or the relative drying rate), according to Elsayed (1990), depends on the moisture content in the dried material and the kind of the material.

The other equations of the model were derived by considering the moisture balance of air inside the kiln and energy balances for the dried material, air in the kiln, and the glass cover of the drying chamber. Parametric studies were carried out with the model to examine the effects of the following parameters on the performance of the dryer: rate of absorbed solar energy in the dryer; rate of air flow through the kiln, volume of the material being dried; ambient air temperature, and humidity of the drying air. The results indicated that a combination of an increase in the air temperature and in the rate of absorbed solar radiation, lower air humidity, and lower initial airflow rate will increase the overall efficiency of the drying system. The predicted values were not compared with experimental data.

Zahed and Elsayed (1994) presented a thin-layer mathematical model for a naturally ventilated cabinet solar kiln. The model was a modification of previous models by the same authors (Zahed and Elsayed, 1989; and Elsayed, 1990). Unlike the earlier models, in which airflow rate and absorbed solar radiation were assumed constant, their new model included the basic models for estimating, the air flow rate, and the rate of solar radiation absorbed. They carried out a parametric study which looked at the effects of: thermal capacity of the kiln structure, the dimension of the chimney, and the kiln geometry on the dryer performance. The results of the study suggest that:

a. the effect of inertia of the kiln structure on the thermal performance of system is important and should not be ignored.
b. decreasing the ratio of the cross sectional area of the chimney to the area of the drying bed causes an increase in the product temperature however, the value should not be less than 0.001.
c. increasing the height of the hot air column beyond 10 m does not affect the performance of the dryer significantly.

Garg and Sharma (1990) reported results of drying studies in a mixed-mode natural convection solar crop dryer. They incorporated equation (2.89) into their mathematical model for predicting the drying rate of green peas and cauliflower. They assumed the drying constant, k, to be a function of temperature and humidity of the drying air and used an equation developed by Syarief *et al*, (1984) for calculating the value of k. They presented graphs showing the variation of the predicted and experimentally determined

values of the moisture contents of green peas and cauliflower as a function of the drying time. In each case there was a good fit between the simulated results to the experimental data.

Bala and Ziauddin (1990) presented a mathematical model for natural convection solar drying of rough rice. The drying rate equation of rough rice in the form of equation (2.87) was used for predicting the moisture changes in the grain bed. They compared the simulated average moisture content predicted by the model to the actual data obtained by Zaman (1986) and reported that the model over-predicted the average moisture contents. They attributed this mishap to the fact that the model did not consider the effect of solar radiation falling on the top of the bed. In another study on the performance of a cabinet type solar dryer, Zaman and Bala (1989) also reported higher drying rate at the top of the bed instead of the bottom. They also reported, without providing any justification, that the chimney height, grain depth and collector size are the most critical parameters controlling natural air flow through the grain bed.

Zaman and Bala (1989) successfully used the integral of equation (2.86) in the form:

$$\int_{m_i}^{m_{i+1}} \frac{dM}{M - M_e} = -k \int_{t}^{t+\Delta t} dt \tag{2.132}$$

for fitting curves to six sets of experimental data obtained from natural convection solar drying of rough rice in a mixed-mode type dryer, box-type dryer and open floor drying system. In the above fits they considered k firstly as fixed constant and secondly as a temperature-dependent constant of the form:

$$k = A \exp(-b/\theta_t) \tag{2.133}$$

They reported a better fit of equation (2.132) to the experimental data of the thin-layer drying (80 mm thick of grains for each drying system) of rough rice with k treated as a constant. A worse fitting was obtained when k was considered as an exponential function of the grain temperature, as indicated in equation (2.133). They reported that the change in

moisture content of the rough rice predicted by the equations were in good agreement with the observed values. The results of the study showed that the highest drying rate was attained in the mixed-mode dryer.

Ayensu and Bondzie (1986) observed that the drying curves of cassava leaves (initial moisture content 72%, wet basis), pepper (initial moisture content 68%, wet basis), cassava chips (initial moisture 75%, wet basis) and fish (initial moisture content 80%, wet basis) consisted of two distinct parts: the constant rate portion and the falling rate portion. They reported that the two distinct portions of each of the drying curves could be represented by equation (2.89) where k is the drying constant which can be evaluated for the constant period (as k_1) and the falling rate period (as k_2). They determined the values of k_1 and k_2 to be 0.031 s^{-1} and 0.016 s^{-1} respectively. Equation 2.89 according to Ayensu and Bondzie can be applied to the drying of cassava chips for the constant and falling rates respectively in the forms:

$$\frac{M - M_e}{M_o - M_e} = \exp(-k_1 t_e) \qquad \text{for the constant rate period} \tag{2.134}$$

$$\frac{M - M_e}{M_c - M_e} = \exp(-k_2 t_e) \qquad \text{for the falling rate period} \tag{2.135}$$

where M_c is equal to 55% on wet basis. The observation of Ayensu and Bondzie (1986) is not at variance with that of Igbeka *et al*, (1976) who found that in drying cassava (maximum initial moisture content 214% dry basis or 68% wet basis) and potato no constant rate period was present. The above observations reveal that above a certain minimum initial moisture content drying of crops can fall under two distinct drying rate periods- the constant- and the falling- rate periods.

Equation (2.94) has been successfully used and validated for deep-bed solar air drying of rape seed by Patil and Ward, (1989). Akyurt and Selcuk (1973) tried to fit equation (2.94) to their solar drying data obtained from a combined dryer (solar dryer supplemented with auxiliary heating systems for continuous operation). However, they did not elaborate on the extent of the accuracy of the fit.

Harvey *et al* (1985) successfully fitted equation (2.94) to drying data obtained from the drying of sorrel, a high moisture crop, in a solar cabinet dryer from a moisture content of 90% (wet basis) to about 11% in 4 days.

Steinfeld and Segal (1986) presented a mathematical model of the physical process of an indirect-solar fixed-bed thin-layer drying system. The mathematical formulation was based on conventional heat and mass transfer equations and complemented with an analysis of the drying process based on the Lewis analogy and the Equilibrium Moisture content concept. The model is not adequate for natural convection air heaters, where air flow rate is not an external parameter but a consequence of thermo-syphon effect. The model is not suitable for deep-bed drying, where bed-depth plays an important role in the calculation of the pressure drop across the bed. The model, like all previous models, assumes that the drying process is an adiabatic process and therefore takes no account of a situation in which the crop is dried by a combination of the effects of direct, and indirect solar absorption by the product. In addition, like all drying simulation models, the design of the dryer is not an explicit component of the model. A comprehensive model that explicitly integrates the dryer design with the air-heating model, the drying model, and the performance model of a natural convection solar crop dryer is desirable.

Selcuk *et al* (1974) presented a linearlised mathematical model for simulating the drying process of a forced convection mixed-mode dryer. The formulation of the drying model was based on quasi-steady state heat and mass transfer analysis. The computed or predicted results were compared with an experimental data obtained from a drying experiment. Equal quantities of grapes were placed on the three shelves (trays) inside the dying chamber. The top grapes on the top shelve were subjected to direct radiation while the grapes on the lower shelve were subjected to the hottest air. The results, the predicted and experimentally obtained values, indicated that the grapes on the top and the lower shelves dried faster than the grapes on the middle shelve. The model could predict the temperature of the crop bed, the air stream temperature and humidity ratio inside the drying chamber, but not the drying rate and hence not the drying time. The model consistently under-predicted the fruit bed temperature and over-predicted the air stream temperature and humidity ratio. Nevertheless, an agreement of $\pm 3^{\circ}$ C for temperatures and 6.2% for the humidity ratio were obtained. It can be inferred from the experimental observations that:

a. both solar radiation and hot air are driving potentials for drying, and
b. a drying model that assumes non uniform layer conditions can best predict the drying performance of natural convection dryers.

Roa and Macedo (1976) conducted an experiment where 600 kg of "carioca" dry beans were dried in a stationary bin (1 m in diameter., 1.2 m tall and a bed depth of 0.8 m), using heated air from a single-pass double duct solar collector (10 m long and 8 m). A centrifugal fan drew air through the 80 m^2 of simple plane collectors and forced it through the bin at an average air flux of 0.13 m^3/s against a static pressure of 215.7 N/m^2. The drying phenomena was analysed with a mathematical model based on the fundamental laws of heat and mass transfer, complemented with empirical equations describing both the thin layer drying and equilibrium property data for the beans. They simplified the drying model presented by Brooker *et al*, (1974). The following empirical thin layer equation was used:

$$\frac{\partial M}{\partial t} = -m\,q(M - M_e)(p_s - p_v)^n\, t^{q-1} \qquad (2.136)$$

where the equilibrium moisture content values M_e were calculated by the following empirical equation

$$M_e = \left(p_1\phi + p_2\phi^2 + p_3\phi^3 + p_4\phi^4\right)\exp\left[\left(q_0 + q_1\phi + q_2\phi^2 + q_3\phi^3\right)(T + 273)\right] \qquad (2.137)$$

The agreement between the predicted and experimentally determined values of the bean moisture content was reasonably accurate with a maximum error of 2.6%. Simulation results of drying with unheated air indicated that the net effect of the solar collection was to accelerate (in four times) the drying rates of grain located in the top of the bin.

2.9.1 Comparative or evaluation studies on alternative propositions.

With a view of evaluating the benefit of utilising a separate solar collector attached to a crop dryer, a study was undertaken in Canada. The study was carried out by Fraser and Muir (1980) to look at the possible savings in electrical energy that could result from adding a solar collector to a forced convection in-bin dryer that utilises ambient air as the drying medium. The drying process was simulated using the Thompson (1972) equilibrium model. The study revealed that the addition of solar collectors could reduce the electrical energy consumed by an average of 19-35% for the conditions considered.

In another comparative study, Pierce and Thompson (1979) compared the performance of solar grain dryers ventilated with either air pre-heated in a solar collector or by conventional heating system. The drying phenomenon in the solar-supplemented drying was analysed using the Thompson (1972) equilibrium model to predict the drying rate.

Morey *et al*, (1979) showed that supplementing a conventional dryer with heated air from a solar collector reduced the minimum air flow rate required for grain drying by 10 - 15% compared to a situation in which ambient air (unheated air) was used. The results of these studies suggest that the potential of the drying air in removing moisture from a product is enhanced with pre-heating.

Bala (1983) successfully fitted the simple exponential, the double exponential and the Page thin-layer drying equations to varied sets of experimental data obtained from the thin layer drying of malt. The double exponential equation, it was reported, gave the best fit to some of the experimental runs with a standard error of estimate value of 0.30 %; whereas the Page and the simple exponential equations fitted all the experimental runs with a mean standard error of estimate values of 0.46% (d.b) and 1.22% (d.b) respectively.

Diamante and Munro (1993) used an indirect natural convection solar dryer to study the drying of sweet potato slices. Sweet potato sliced to a thickness of 3 or 6 mm were spread evenly on a drying tray placed on the middle shelf of the drying chamber. The loading density was 5 kg/m^2. The solar drying experiments were carried out during the period of February to April 1986 at Baybay, Leyte, Philippines. Typical climatic conditions for the

period reported are ambient air temperature of 28-32° C during the day and about 80% relative humidity. The intensity of the incident solar radiation was not reported in the literature. Each of equations (2.94), (2.95), (2.96) and (2.99) was fitted to the solar drying curves. However, they simplified the moisture ratio to M/M_o instead of $(M - M_e)/(M_o - M_e)$ for lack of accurate M_e data for Philippines' sweet potato among other reasons. They reported that the simplified form of the diffusion equation could satisfactorily describe the solar drying process of sweet potato slices down to a moisture content of 20 % dry basis from initial value in the range of 160-180% dry basis with an r^2 value between 0.962 and 0.999.

The results of comparative studies by several researchers (Keener *et al*, 1978; Sharaf-Eldeen *et al*, 1979; Syarief *et al*, 1984; Nellist, 1976; Bala (1983); and Chhinnan, 1984) point to the conclusion that the inclusion of a series solution of the diffusion equation with significant number of terms in a drying model can describe the drying behaviour of agricultural products over a wide range of moisture contents. For a given product, the number of terms required would depend on the accuracy of the diffusion coefficient and the length of the drying time among other possible reasons.

2.10 Numerical solution techniques of drying models

From previous sections of this chapter, it is obvious that in order to describe a drying process by a heat and mass transfer simulation code generally, a system of two to four tightly coupled non-linear partial differential equations must be solved. To develop a computer code an appropriate discretisation technique should also be adopted to transform the underlying partial differential equations into a system of non-linear algebraic equations.

In general the popular techniques for achieving such transformations in computational fluid dynamics (CFD) include Finite Difference, Finite Volume or Finite Element Techniques with each method offering its own advantages and disadvantages. Regarding the numerical analysis of crop drying, the finite difference technique (Spencer, 1969; Brooker *et al*, 1974; Ingram, 1976; Douglas *et al*, 1994) and the finite element method (Misra and Young, 1978, 1979; Sokhansanj and Gustafson, 1980; Haghighi and Segerlind, 1988; Haghighi *et al*

1990; Sarker *et al*, 1994) are the most commonly used techniques. It is recommended that for simplified geometries and problems not involving stresses, the finite difference techniques are the preferred discretisation strategy since these techniques are straightforward to implement.

After the discretisation phase is completed, there is the decision of whether to solve the resulting discrete equations as a coupled or uncoupled set (Turner and Pierre 1995). In the uncoupled manner each variable is resolved individually at each point on the mesh. In the coupling approach, the coupling exists amongst the equations at each node of the mesh. The resulting matrix system becomes block structured since the number of variables represented for each node point on the mesh must be determined as a complete set. In this case block iterative schemes are used to resolve the matrix system (Turner and Pierre 1995).

It has been found in previous research (Pierre and Turner, 1995) that only the coupled method offers an efficient numerical resolution strategy which provides fast and realistic computation times for simulating a drying process. The disadvantage of this method is that it requires large amounts of computer storage to deal with the solution of the non-linear equations set. If computer memory is limited, then the uncoupled solution strategy may be preferred.

2.11 Summary and areas for research.

Notwithstanding all the advantages of mathematical modelling, the present crop drying simulations models, and in particular solar dryer simulation models, lack in several aspects. A catalogue of the areas requiring attention and further development is presented together with the author's conception of the possible solutions.

(1) Lack of a general and suitable thin-layer drying equation. None of the hitherto published drying rate equations characterise the drying process accurately over the full range of moisture contents varying from the initial moisture content, M_{in} to the desired equilibrium moisture content, M_e. Usually an arbitrary term is inserted in the thin-layer

drying equation so that a reasonable accuracy may be achieved when predicted values are compared with experimental data In most mathematical models it has been noted (Brooker *et al*, 1974) that the theoretical drying equation, based on diffusion theory, does not predict the drying processes accurately because of :

(i) the improper choice of boundary conditions, and

(ii) the incorrect assumption that diffusion coefficient is independent of moisture content.

Kumar and Sodha (1986) have also observed that the assumption that the diffusion coefficients are independent of the material moisture content leads to erroneous results when the drying process occurs over a wide moisture content range. Experimental evidence suggest or show that the drying rate is a function of the material moisture content and time. Following from the above observations, since most agricultural products dry over a wide range of moisture contents, the dependence of the diffusion coefficient with moisture content must be accounted for in drying models. The thin-layer drying rate equation is basically a simplification of the solution to the Fick's diffusion equation and therefore the author proposes to use the diffusion equation over the entire drying duration by treating the diffusion coefficient as a variable parameter which is dependent on the following factors: the product moisture content, the drying air relative humidity and its temperature, and the shape of the drying bed.

(2) Lack of a comprehensive mathematical model for simulating deep-bed drying of agricultural products in a mixed-mode natural convection dryer. It is also clear from the literature that the equilibrium and logarithmic models for simulating a deep-bed drying process are a simplification of the non-equilibrium model. The author proposes to develop a comprehensive integrated solar drying simulation model for a MNCSCD based on a non-equilibrium partial differential drying model for simulating the drying process. The simulation models developed for drying processes do not generally discuss the modelling of air-heating phenomenon and usually constant inlet air conditions are assumed. For natural convection solar-assisted dryers, it is essential to include theoretical modelling of solar air-heaters which should take into account the effect of varying meteorological parameters affecting the quality of the product. The proposed model will have sub-programmes for executing the following:

- estimating solar radiation available at a typical geographical location,

- estimating the moist air properties and the equilibrium moisture content of the agricultural product,
- predicting the thermal performance of the solar air-heating system for all possible locations and the effect of the changes in the configuration of the air-heater on the dryer performance,
- predicting the effect of the changes in design of the drying chamber configuration and the chimney dimension on the overall performance of the system.

(3) Radiation and shrinkage effects are ignored in most drying process models but these effects must be incorporated since they affect the drying rate significantly. When a high moisture content material is dried shrinkage effect is very prominent and therefore its effect cannot be ignored. Apart from convection, radiation is the other principal mode by means of which a product dried in a mixed-mode natural convection solar dryer is heated. Radiation is effective in increasing the product temperature which aids the diffusion of the moisture from within the product to its surface thereby increasing the drying rate. Radiation and shrinkage effects are therefore to be accounted for in drying models.

(4) As noted by Ayensu and Bondzie (1986), the constant rate period occurs over a relatively short interval compared to the total time drying time. In addition, in the drying of natural agricultural crops, the water content in the product occurs as bound water inside it with little free water on the surface; thus constant drying-rate will hardly occur. The diffusion equation can be applied by assuming varying diffusion coefficient over the whole drying period.

(5) Solar drying is a non-isothermal process, and therefore the author proposes to use concentration gradient as the driving force for water from the drying material.

(6) Agricultural products are dried in bulk or batches not as individual particles but instead in layers (thin or deep) or on tiers of trays in stationary or movable beds. The shape of the dryer bed must therefore be considered as the determinant in choosing either the slab, cylindrical or spherical shape in approximating the shape of the bulk of the material as required in the appropriate simplification to the diffusion equation.

CHAPTER THREE

EXPERIMENTAL SET-UPS: DESCRIPTION, INSTRUMENTS, MEASUREMENT TECHNIQUES, AND TESTS

3.0 Introduction.

Experimental data needed for the development and validation of the mathematical model was obtained using two experimental dryers of geometrically similar construction. These dryers were of the mixed-mode natural convection solar crop-dryer type (MNCSCD) and consisted of a small-scale laboratory model and a field or commercial-scale model. The laboratory model has a holding capacity for 3 kg of wet agricultural produce. The author designed this dryer and it was constructed at De Montfort University by the technicians of the Department of Mechanical Engineering. The commercial-scale model, which is capable of handling between 1000 kg and 1500 kg of various wet agricultural products, is located at Agona-Asafo in the central region of Ghana. The design and constructional details of the commercial-scale model of the MNCSCD were reported by Forson *et al*, (1996). The general descriptions of the laboratory and commercial-scale models used are provided in section 3.1. The description of the instruments and the measurements' techniques adopted during the experiments is presented in section 3.2. A summary of the test series is provided in section 3.3. A more detailed description of the design principles including sample calculations for the determination of the various dimensions of the laboratory model is outlined in Appendix A.

3.1 Description of experimental solar-dryer models

3.1.1 Laboratory or small-scale model

Figure 3.1 shows a pictorial view of the laboratory model of the MNCSCD and the solar simulator in operation. Three main components of the dryer can be identified: *an air-heater* (the primary collector), through which the drying air is heated as it flows over and under an absorber plate, heated in turn by direct absorption of incident radiation; *a drying*

Figure 3.1: Pictorial view of the laboratory model of the MNCSCD.

chamber, in which the crop to be dried is placed; and *a chimney*, through which the moist air flows and escapes into the surrounding. Ten infra-red lamps, 100 W each, arranged on a panel supported by means of four stands, (as shown in fig. 3.1) served to simulate the incident solar energy required for the drying operation.

The *air-heater* (also referred to as the primary collector) is of the **SPDDSAH** type. It makes use of a non-porous absorber plate, a galvanised steel sheet painted matt black and suspended between the top glass cover and the base plate, which divides the air duct of an overall depth of 75 mm into two channels (upper and lower channels). The effective area of the two air passages is 0.033 m^2. The primary collector has an aperture measuring 440 mm wide by 720 mm long. Air flows in the same direction on both sides of the absorber plate thus providing twice as much surface area for heat transfer to the air compared to the SPRDSAH or the SPFDSAH. The movable absorber plate of the air-

heater can be suspended at three possible positions, thus providing three geometrically similar air-heaters with the same length, width and overall depth but with varying upper and lower channel depths. The upper channel is covered with glass and the lower channel by plywood that serves as both the base plate and the bottom insulation of the air-heater. The top glass-cover (glazing), the absorber plate and the base plate are fixed in position in air-tight wooden side panels. In an attempt to simulate the performance of commercial model, and for maximum collection of solar energy on an all-year round basis, the primary collector is inclined at 6° to the horizontal, corresponding to the latitude of the test site in Ghana.

The *drying chamber* has a trapezoidal section but with a rectangular drying surface measuring 440 mm x 380 mm. It houses three removable extended metal-mesh trays, arranged vertically in line on guides that are spaced 100 mm apart with the lower tray at a height of 140 mm from the base of the drying chamber. The side walls and the roof (also referred to as the secondary collector) are glazed extensively. The secondary collector is also tilted at the same inclination as the air-heater. There is a door that provide access to the chamber for loading, unloading, and stirring of the crop.

The *chimney*, trapezoidal in section, runs along the entire breadth of the drying chamber to aid the natural circulation of air inside the whole assembly. The side walls of the chimney are glazed. The chimney is 620 mm high (above the uppermost side of the secondary collector), and it has an airflow area of about 0.039 m^2 (440 mm in width x 88 mm in breadth). An exit air vent of area 0.0132 m^2 (440 mm wide by 30 mm high) runs across the chimney width. The crops dried in such a dryer are heated from the top by the direct absorption of incident radiation, transmitted through the transparent roof and the sides of the drying chamber, and from below by air at an elevated temperature, pre-heated in the air-heater.

3.1.2 Field or commercial-scale model

Figure 3.2 shows a pictorial view of two commercial-scale sizes of the laboratory model joined back to back with a common drying-chamber. During the field test, the drying

chamber was partitioned into two parts with a transparent polyethylene sheet, along the central line of the drying chamber, resulting in two geometrically similar MNCSCD's. The field experiments were conducted on one of such dryers with the air-heater inlet vent of the other dryer closed. Except for the dimensions, the constructional features of the commercial-scale model are similar to that of the laboratory model.

Figure 3.2: Pictorial view of two commercial sizes of MNCSCD joined back to back.

A brief description of the experimental dryer set-up is given below:

The length of the air-heater, which is also of the SPDDSAH type, is 12.6 m and the width is 6.75 m. The overall depth of the air duct is 0.28 m but the absorber plate divides the air duct into two flow channels of equal depths and each with a duct of flow area of 0.85 m^2. The air-heaters are aligned in the North-South axis to receive solar radiation throughout the daylight. One of the two SPDDSAH's faces the South while the other is north facing. Each air-heater is tilted 6° to the horizontal, corresponding to the latitude of the site for maximum collection of incident solar radiation on an all year-round basis.

The transparent drying chamber measures 6.75 m by 4.0 m. The chamber houses three drying racks with gangways between them. Each drying rack has two shelves arranged vertically in line and spaced 0.50 m apart. The middle drying rack measures 3.60 m by 1.5 m while the two outer racks are each of dimensions 3.60 m long by 1.30 m wide. The first shelf is at a height of 1.25 m from the base of the drying chamber.

The chimney, which is about 620 mm high (above the uppermost point of the drying chamber), is of trapezoidal cross section and has an air channel of rectangular section of sides 6.75 m x 350 mm. The exit air vent is located along the rear side of the chimney and it measures 6.75 m wide by 100 mm high.

3.2 Instruments and measurement techniques

The laboratory and commercial-scale dryers were fully instrumented for measurements of air flow, temperature, relative humidity and weight loss of the drying material.

The instruments and the techniques used to measure the various quantifiable parameters during the experiments carried out on the two models described in section 3.1 are provided below.

3.2.1 Instrumentation of the laboratory set-up

Temperature measurement

The air, absorber plate, glazing and base plate temperatures of the air-heater were measured at hourly intervals with commercially available Nickel- Chromium/Nickel- Aluminium thermocouples (type K) suitable for temperatures ranging from 0 to 200° C. Eight thermocouples were bonded to the top and bottom surfaces of the glazing and the absorber plate at the middle and the outlet sections of the primary collector to measure their surface temperatures. Two more of the self-adhesive (type-K) thermocouples were also bonded to the inner surface of the base plate. The surface temperature of the outer surface of the base plate was measured at two locations with two ordinary mercury-in-glass thermometers. The mean air temperatures in the air-heater were measured along the centre-lines of the two

channels at the inlet and outlet sections with four thermocouple air probes. The mean absorber plate, glazing and base plate temperatures were each calculated in turn as an average of the measured values of top and bottom temperatures of each component at the two locations. The temperatures of the air inside the drying chamber was measured along its centre line with thermocouple probes at three locations: 140, 240 and 340 mm above the base of the drying chamber. One probe was also located in the lower section of the drying chamber to measure the plenum temperature. The air temperature at the entry to, and at the mid-section of, the chimney were measured along the centre-line using ordinary mercury-in-bulb thermometers with and accuracy of ± 0.1° C and a precision of ± 0.05° C. The temperature and relative humidity of the air exiting the chimney were taken with a hand-held thermo-hygrometer (relative humidity/temperature measuring instrument). The mean temperature of air inside the chimney was calculated using the values taken at the two locations. The ambient temperature was taken with the hand-held thermo-hygrometer (testo 610 from RS Components UK) with an accuracy of ± 0.2° C for temperatures in the range 0 to 70° C. These readings were taken at 0.6 m above the ground surface and just at the inlet to the collector.

The output terminals from eight thermocouples, measuring the top and bottom surface temperatures of the absorber plate and the air temperatures in both channels at the inlet and outlet sections of the air-heater, were connected to a thermocouple temperature logger: (calibrated with accuracy of ± 0.1° C and precision ± 0.02° C). The logger, (TC-08 from RS components) is equipped with a software for data logging and analysis. The picolog data logger collects sets of measurements from the 8 channels of an analogue to digital converter (ADC) and stores them on a disk. The output terminals from ten other type-K thermocouples measuring the temperatures of the cover plate, the base plate and air inside the drying chamber were connected to a Comark 6600 microprocessor scanning thermometer. Readings from the microprocessor thermometer, with an accuracy of ± 0.1° C, were taken every one hour. Figure 3.3 is a schematic diagram of the dryer showing the positions of temperature measuring sensors.

Air speed and relative humidity measurement.

The ambient air speed at inlet to the primary collector was measured parallel to the plane of the collector aperture at two points spaced 25 cm apart and each at a height of 30 mm above the aperture. The air speeds of the heated air at the outlets of the air-heater were measured along the centre-line of the air channels. Two thermal anemometers, for measuring air velocities in the range 0 to 2 m/s, were positioned at the inlet and outlet of the collector to measure the air speeds. The relative humidity of ambient air at inlet to the primary collector was taken manually at hourly intervals with a hand held relative humidity/temperature measuring instrument with an accuracy of ± 2% RH for the range 2 to 98% RH.

Incident radiation measurement

A pyranometer (Kipp and Zonen "Compensated Moll Thermopile", type CA 1 No. 754379) connected to a micro-galvanometer (type AL 4) readout was employed to measure the global radiation. The accuracy of the microva-galvanometer was ± 1% of the full-scale deflection. The intensity of energy incident on the plane of the primary and secondary collectors was measured at several points (56 locations) over the collector aperture. These readings (in mV) were averaged out to give the mean incident radiation on the collector surface. The mean incident radiation, in W/m^2, on the collector surface was computed from the manufacturer's formula in the form:

$$\overline{H}_T = \frac{(44.6 + r_\Omega)}{r_\Omega}\frac{V_v}{S_f} \qquad (3.1)$$

where r_Ω is the internal resistance of the microva-galvanometer in ohms, V_v is the scale voltage reading in milli-volts, and S_f is the thermopile sensitivity factor corresponding to the aperture of the instrument.

Measurement of crop weight loss

A weighing system was devised and designed to continuously monitor the weight loss of the samples without removing them from the drying chamber. It consisted of bonding four

120 ohms bonded resistance strain gauges with a gauge factor of 2.11 and connecting them in a Full-Wheatstone bridge circuit arrangement on a cantilever to increase its sensitivity. The cantilever was fixed to a rigid connecting member close to the roof of the drying chamber. The two strain gauges bonded to the top surface of the cantilever bar measured the tensile strains while the bottom two measured the compressive strains. The output terminals of the strain gauges were connected to a, Tinsley Telcon Ltd., microstrain digital indicator Type 5792 capable of reading a maximum of 1999 microstrains with a resolution of 1 microstrain. The instrument has an accuracy of ± (1% of reading + 5 μstrain) for gauge factors ranging from 1.95 to 2.15. The microstrain indicator has a balance control for setting the appropriate gauge factor and zero balance at the start of each experiment. An extended metallic-screen tray containing the material being dried is hanged in the drying chamber on a hanger connected to the cantilever bar. The total deflection of the cantilever and hence the strain corresponding to the weight of the material is indicated on the digital display indicator in microstrains. The system was calibrated by adding standard weights to the tray with air flowing through the drying chamber to take into account the buoyancy effect. A calibration curve was obtained relating the microstrain reading ($y_{\mu\varepsilon}$) to the weight of the sample (W) at any given time in the form:

$$y_{\mu\varepsilon} = 0.8988W - 1.270 \tag{3.2}$$

where W is the weight of the sample in grammes. Additionally an electronic weighing scale with an accuracy of ± 1 g and a resolution of 0.1 g was used in situations in which the crop samples were dried simultaneously on two or three tiers of drying shelves.

3.2.2 Instrumentation of the field model.

Temperature measurement.

The collector was instrumented with type K thermocouples for measuring the temperatures of the components of the air-heater; the absorber plate, the glazing, and the base plate, at three locations along the length of the air-heater. At each location, the top and the bottom temperatures of the components were taken. The temperatures of the air in the two flow

channels of the air-heater were measured at the inlet and outlet sections. The ambient air temperature was also measured with a type K thermocouple with the sensor placed at 1 m above the ground surface and positioned 8 m from the nearest edge of the collector in conformity with the British Standards (Anon, 1986). The plenum temperature was measured with a thermocouple.

It was difficult to locate thermocouple probes in the chimney wall in order to monitor the air temperature within the chimney because it could not be reached in the absence of a safe and reliable ladder.

Air speed and ambient relative humidity measurement.

The ambient air speed at inlet to the primary collector was measured parallel to the plane of the collector aperture at two points spaced 25 cm apart and each at a height of 30 mm above the aperture. The air speeds of the heated air at the outlets of the collector ducts were measured along the centre-line of each air channel. A thermal anemometer, suitable for measurement of air velocities within the range 0.02 to 5.0 m/s and at temperatures between -10 and 50° C, was used to measure the air speed at inlet to the air-heater and at outlet section of the lower channel at hourly intervals. Continuous monitoring of the air velocity at the outlet section of the upper channel of the air-heater was obtained using the Gill Propeller anemometer (from R.M Young Company, U.S.A) model 27106T.

The relative humidity at the inlet and outlet of the collector were taken manually at hourly intervals with a hand-held relative humidity/temperature measuring instrument with an accuracy of ± 2%RH for relative humidity values in the range 2 to 98%RH.

Incident solar radiation measurement

An LI-200SA LI-COR PYRANOMETER (from Campbell Scientific Incorporation, U.S.A.) located at middle of primary collector was used for measuring the incident global solar radiation on the collector. The LI-200SA outputs a low level voltage but the differential voltage measurement technique was employed for better noise rejection compared to the single-ended measurement.

Measurement of sample weight loss

It was not possible to devise a mechanism to continuously monitor the weight loss of the material being dried. An electronic weighing scale with an accuracy of ± 2 g and a resolution of 1 g was used for the weight measurement. Three sets of experiments were conducted but in the first experiment, the entire crop mass being dried was weighed only at the beginning and end of each day's operation. In test 3, the entire crop mass was weighed after every 3 hours and the weight noted, while in test 2 the weight of the material at the beginning of the first day and at the end of each day's operation was recorded.

Data Logging

In the instrumentation of the field model, except for the measurements taken manually all other readings were continuously monitored and logged out using a 21X Micrologger from Campbell Scientific Incorporation, U.S.A. The logger was programmed in the single channel mode to select an input to a channel every 10 minutes and recorded data integrated to give the hour-by-hour values.

3.3 An overview of the test series

Tests performed using both models of the MNCSCD described in section 3.1 can be classified broadly into two categories as: a) tests under no load conditions and, b) tests under load conditions. In each test under load conditions, cassava was used as the drying material. A loading density of between 6.3 and 19 kg/m^2 was employed in all the tests. The loading density was chosen in conformity with the recommended values of 5 to 15 kg/m^2 recorded in the literature for the drying of cassava chips (Roa, 1974). The cassava used for the laboratory tests was purchased from the Leicester Open Market in the evening prior to the day of the experiment.

3.3.1 Laboratory tests

In all, thirteen carefully planned tests were conducted using the same dryer model but with three configurations of the same SPDDSAH. The tests investigated the (i) temperature rise

in the chimney, (ii) mean temperature of the drying air at the exit of the air-heater (iii) temperature variation and mean temperature rise of air inside the drying chamber, (iv) mean operating temperatures of the components of the air-heater, (v) the flowrate of air entering the drying chamber, (vi) the drying rates of the material dried, and (vii) the overall performance of the dryer. The tests are grouped and discussed under six headings in order to highlight the main objective(s) of each test or set of tests.

(a) Tests to examine relative performance of the dryer under no load conditions

Three tests (Tests 1, 2 &3) were conducted with the primary aim of examining the relative performance of the three different configurations of the same SPDDSAH and the corresponding performance of the drying chamber and chimney under no load conditions. For every test, recordings were made for periods of at least three consecutive days with five to seven readings taken hourly per day. Test 1 was undertaken from 2 June 1997 to 4 June 1997. On each day, the experiment was conducted within the hours of 9:15 am to 4:45 pm. Test 2 was carried out from 9 June 1997 to 11 June 1997, while test 3 was performed between 20 June and 23 June 1997. All the experiments in test 2 were conducted between 10.30 am and 4.30 pm on each day, while the four experiments in test 3 were conducted from 9:15 am to 5:15 pm daily. A summary of the description of the three options of the SPDDSAH configuration used in each test including the dimensions of the top and the bottom channel depths is provided in Table 3.1.

Table 3.1: Summary of the test conditions for laboratory tests 1, 2 and 3.

Test Conditions	TEST 1	TEST 2	TEST 3
Position of absorber plate	Option A - absorber plate in top position	Option B - absorber plate in middle position	Option C - absorber plate in lower position
Air duct, top channel depth (mm)	20	39	58
Air duct, bottom channel depth (mm)	55	36	17

(b) Tests to examine the overall performance of the dryer for the three options of the air-heater configuration

Three tests (Tests 4, 5 and 6) were conducted under load conditions to examine the performance of the dryer for all the three air-heater configurations. Tests 4, 5 and 6 were carried out on options A, B and C of the air-heater configuration, respectively. The experiments were devised for the material moisture content to be monitored continuously for the same loading density. In each of these tests cassava was dried in a single tray at a height of 190 mm from the base of the drying chamber and drying proceeded till the desired moisture content was achieved or the experiment was terminated. In test 4, 1458.3 g of cassava was dried from an initial moisture content of 67% (wet basis) for 22 hours, after which the experiment was terminated. This test was undertaken from 11:40 am on 22 March 1998 to 09:40 am on 23 March 1998. Test 5 was conducted from 11:20 am on 28 March 1998 to 09:20 on 29 March 1998. In this experiment cassava with an initial weight of 1460 g and at moisture content of 66% was dried. Test 6 was performed from 11:20 am on 4 April 1998 to 09:20 am on 5 April 1998. Cassava at an initial weight of 1460.1 g and an initial moisture content of 67% was dried. In each of the above tests, the specified quantity of cassava was spread on a metal mesh tray on an area of about 0.16 m^2. The load was suspended on the cantilever system at a distance of 190 mm from the base of the drying chamber. The microstrain reading corresponding to the weight of the crop being dried was recorded at hourly intervals. To compare the performance of the solar dryer with that of 'natural sun-drying', in test 4 a control sample (122 g of cassava) was spread over an area of 0.043 m^2 on metal-mesh tray near the dryer at the same elevation as the sample in the drying chamber. The control sample was dried simultaneously under the same room conditions. The weight of the control sample was taken at hourly intervals by means of an electronic weighing scale.

(c) Tests to examine the effect of the thermal inertia of the dryer on the overall drying efficiency for three air-heater options

To examine the effect of the thermal inertia of the dryer on its performance, three experiments (Tests 7, 8 and 9) were performed on options A, B, and C of the air-heater configuration respectively. In this set of tests, the crop was dried during the day-time for at least four hours each day between 0900 and 1800 hours. At night the light source was

switched off. Each experiment was carried out until the desired moisture level was attained or the experiment was terminated. The microstrain readings corresponding to the weight of the crop being dried was recorded at hourly intervals and in addition the weight of the crop sample at the beginning and the end of each day of the experiment was recorded. This series of tests was also a way of investigating the nocturnal moisture re-absorption or de-sorption. In these tests, the samples were dried in tray suspended at a height of 190 mm from the base of the drying chamber.

Test 7 was conducted from 10.55 am on 21 September 1997 to 5.25 pm on 24 September 1997; on about 1425.6 grammes of cassava chips.

In test 8, 1023.3 grammes of cassava chips were spread on the same drying tray and dried from 10.07 am on 12 November 1997 till 4:55 pm on 14 November 1997.

Test 9 was commenced at 10:15 am on 18 August 1997 and stopped at 5:05 pm on 20 August 1997; 1116.7 g of cassava chips were dried in this test. The material dried in each of the above tests was spread on an area of 0.16 m^2 on a metal mesh tray located at a height of 190 mm from the base of the drying chamber.

(d) Test to investigate the effect of the position of the drying tray on drying progress for the SPDDSAH option C

This test (Test 10) was conducted from 10:15 am on 26 August 1998 to 28 August 1998. A drying tray of surface area 0.16 m^2 located at a height of 240 mm away from the base of the drying chamber was loaded with 1117 g of cassava at an initial moisture content of 67 % (wet basis). The drying was performed on daily basis. To compare the performance of the solar dryer with that of 'natural sun-drying', in test 10 a control sample (322.3 g of cassava) was spread over an area of 0.046 m^2 on a metal-mesh tray near the dryer and at the same height as the sample in the drying chamber. The control sample was dried simultaneously under the same room conditions. The weight of the control sample was taken at two hour interval on an electronic weighing scale. The experiment was started at 10:15 am on 26 August 1998 and terminated at 4:30 pm on 28 August 1998.

(e) Tests to investigate the optimal loading arrangement for SPDDSAH option C

In this series, two tests, namely tests 11 and 12, were conducted with the primary aim of investigating the optimal loading arrangement for the dryer. In test 11, about 1329.3 g of cassava at an initial moisture content of 65% (wet basis) was divided into three parts (423.7 g, 486.8 g and 418.8 g) and dried on the three drying shelves. About 423.7 g of cassava was placed on the top shelf, while 486.8 and 418.8 g of cassava were dried on the middle and bottom drying shelves respectively. The samples were placed vertically in line on the three shelves and spread over an area of 0.053 m^2 on each shelf. In test 12, about 664.6g and 664.7 g of cassava at an initial moisture content of 67% (wet basis) were dried on the top and bottom shelves respectively. Similar to test 11, the samples were placed vertically in line and spread to cover an area of 0.10 m^2. In test 11, drying commenced on 12:25 noon on 4 September 1998 on daily basis and proceeded till 4:16 pm on 8 September 1998. Test 12 was conducted from 9:15 am on 9 September 1998 on daily basis till 4:40 pm on 11 September 1998 when the experiment was terminated.

(f) Test to evaluate the performance of the dryer at the rated or design capacity

In this test (Test 13), a drying tray of surface area 0.16 m^2 was loaded with 3.0 kg of cassava at an initial moisture content of 68% (wet basis) and placed at a height of 340 mm away from the base of the drying chamber. To ensure adequate exposure of the entire crop mass to the incident radiation the crop mass was stirred twice in a day. This experiment was conducted with the absorber plate in the bottom position as in test 3. Test 13 was conducted from 9.39 am on 15 September 1998 to 4.47 pm on 17 September 1998.

3.3.2 Field tests

Three field tests were carried out, which are hereafter referred to as Tests 1, 2, and 3. These experiments were conducted from 2nd to 14th October 1997. Cassava was used as the drying material because it was readily available and less expensive at the time of the experiments. In all the tests, the dryer was loaded with cassava freshly harvested.

Test 1

In test 1, the top shelf of one of the three drying racks was loaded with 49.1 kg of cassava with an initial moisture of 62% (w.b) and spread over an area of 4.68 m^2. A control experiment was carried out by spreading the same quantity of cassava over an area of 4.7 m^2 in the sun. In the control experiment, cassava was dried on a raised platform at height of 1m above the ground in the sun. This test was conducted from 7:15 am (local time) on 2 October to 5 October 1997. During this test, the weight of the entire crop mass was taken at the beginning and close of each day of drying.

Test 2

In test 2, the bottom shelves of two of the drying racks were loaded with 65.88 kg of cassava, at an initial moisture content of 64% (w.b), over an area of 6.24 m^2. Test B was started on 8 October at 1:00 p.m. and terminated at 5:10 p.m on 12 October. Unlike test 1, the weight of the material was taken at the end of each day of the experiment.

Test 3

In test 3, part of the top and the bottom shelves of the middle drying rack were used for drying. About 81 kg of wet cassava at an moisture content of 62.5 % (w.b) was spread on the top shelf over an area of 5.4 m^2. About 80 kg of wet cassava with an moisture content of 62.5% (w.b) was spread on the bottom shelf covering an area of 5.4 m^2 directly below the crop on the top shelf. A control experiment was carried out by drying 10.91 kg of the same species of wet cassava in the sun on a raised platform over an area of 1 m^2. In this test, the weight of the crop being dried was taken after every 3 hours. This experiment was started at 9:30 am on 10 October and terminated on 13 October 1997. The aim of this experiment was to examine the effects of direct absorption of solar radiation and shading on the drying rate of cassava placed on the upper and lower shelves respectively.

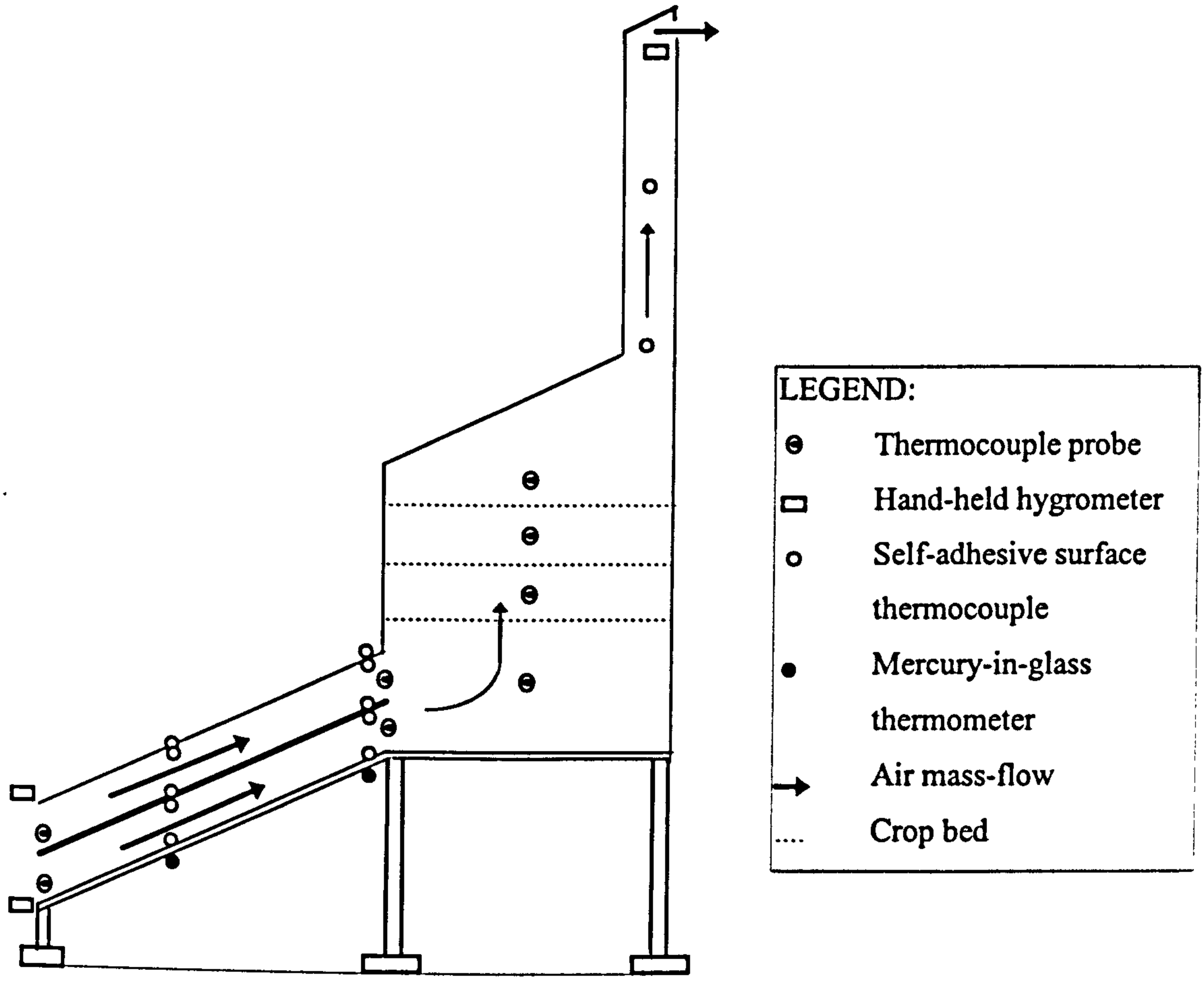

Figure 3.3: Schematic illustration of the laboratory dryer showing the locations of the temperature measuring sensors.

CHAPTER FOUR

FORMULATION OF MATHEMATICAL MODELS

4.0 Introduction

In this chapter, the mathematical models developed for predicting and evaluating the performance of the MNCSCD are presented. Three models are presented namely; the air-heating model, the drying model, and the technical performance model. The air-heating model, as presented in section 4.1, incorporates a model for predicting the intensity of solar radiation on the plane of the collectors (the primary and secondary collectors) and utilises the psychrometric model based on equations (2.70) through (2.85). The drying model, as presented in section 4.2, incorporates a design model which is based on equations (A1) through to (A23). The technical performance model is presented in section 4.3.

4.1 Formulation of the solar air-heating model

In this section a mathematical model of a single-pass, double-duct solar air-heater (SPDDSAH) is described. The model provides a design tool capable of predicting: the solar energy incident on the collector surface per unit area over a specified time (insolation), heat transfer coefficients, the mean air-flow rate, the average air temperature and its relative humidity at the collector exit.

The equations governing the performance of the system are formulated by coupling energy balance equations on the components of the air-heater with those for the useful heat extracted in the two channels, and making the following assumptions:

1. The air-heater operates under steady-state conditions.
2. The capacitance of the absorber plate is negligible.
3. The air-heater is subjected to constant insolation and hence, the operating temperatures of its components; the absorber, the bottom, and the cover plates are constant.

4. The area of the absorber plate is equal to the aperture area of the primary collector.
5. The temperature of the air varies only in the direction of the flow (x-direction).
6. The sky is considered a black-body for long wavelength radiation.
7. The heat flow through the glazing and the bottom plate is one-dimensional and in the y-direction.
8. The air-heater is treated as an inclined chimney.
9. The air-heater is considered to be made up of sections of equal length in the direction of air flow with each section receiving heated air from the previous section and delivering heated air to the following one.
10. The physical properties of air are assumed to vary linearly with temperature in the range 293 K < T < 333 K.
11. The ambient temperature and wind speed are constant and equal to the long-term, monthly-average day-time values.

4.1.1 Energy balance equations

The energy-balance equations on the three components of the SPDDSAH, as illustrated in fig. 4.1, and two expressions relating the useful energy absorbed by the heated air in the two channels to the incident energy (solar radiation) on the system are given below:-

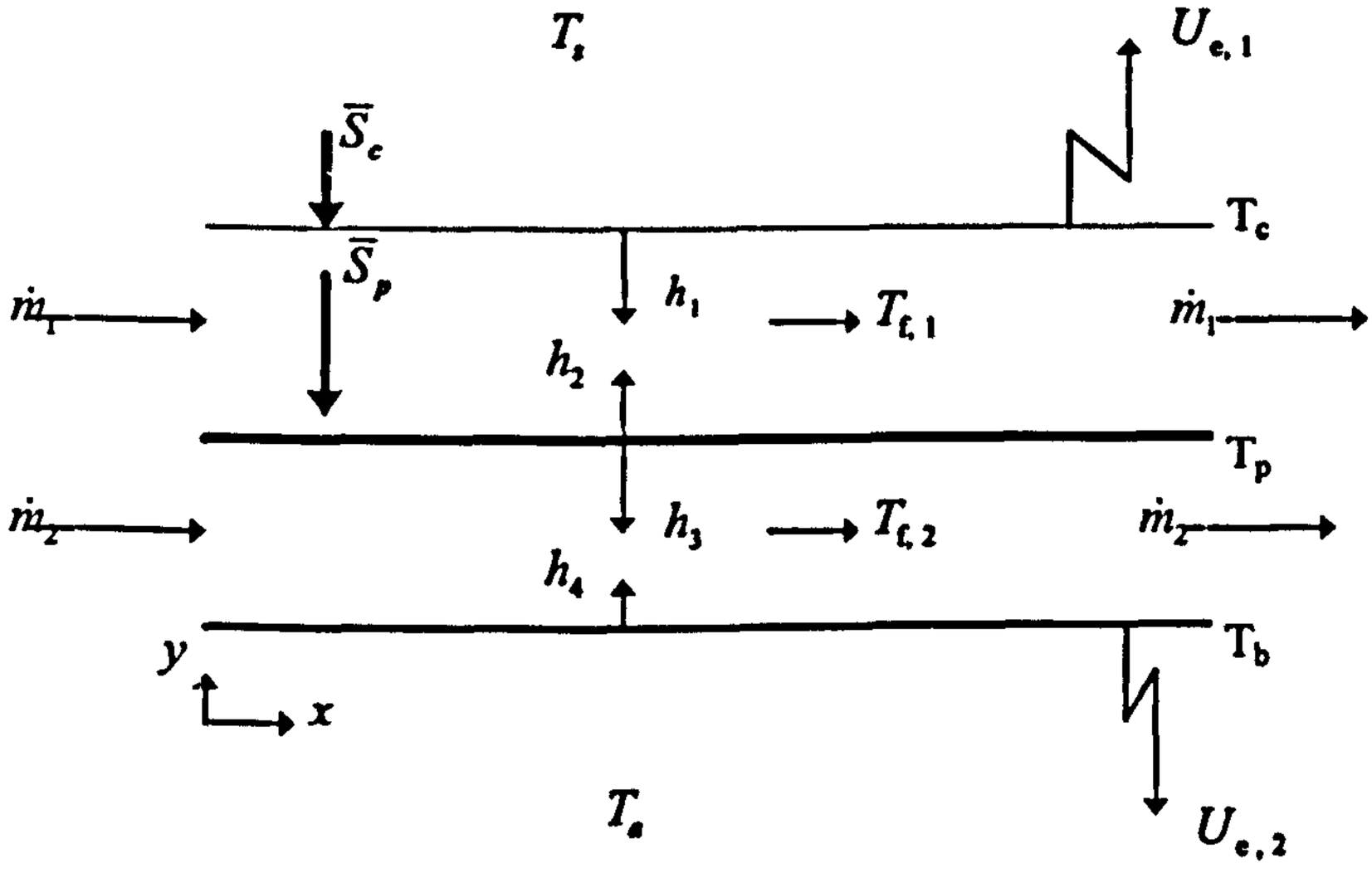

Figure 4.1: Energy balance on the components of the air-heater and its surroundings

cover plate:

$$\overline{S_c} + h_{r,pc}(T_p - T_c) + h_1(T_{f,1} - T_c) = h_w(T_c - T_a) + h_{r,cs}(T_c - T_s) \tag{4.1}$$

air stream 1 (Air in top channel):

$$h_2 W(T_p - T_{f,1}) = h_1 W(T_{f,1} - T_c) + \dot{m}_1 C_a \frac{dT_{f,1}}{dx} + U_{e,1} s_1 (T_{f,1} - T_a) \tag{4.2}$$

a***bsorber plate:***

$$\overline{S_p} = h_3(T_p - T_{f,2}) + h_2(T_p - T_{f,1}) + h_{r,pb}(T_p - T_b) + h_{r,pc}(T_p - T_c) \tag{4.3}$$

air stream 2 (Air in bottom channel):

$$h_3 W(T_p - T_{f,2}) = h_4 W(T_{f,2} - T_b) + \dot{m}_2 C_a \frac{dT_{f,2}}{dx} + U_{e,2} s_2 (T_{f,2} - T_a) \tag{4.4}$$

bottom plate:

$$h_4(T_{f,2} - T_b) + h_{r,pb}(T_p - T_b) = U_b(T_b - T_a) \tag{4.5}$$

Performance of the air-heater under a given set of conditions.

The overall effectiveness of the solar air-heater is indicated by its energy collection efficiency, η_c, which is a measure of how effectively the energy available in the solar energy incident upon the solar collector is transferred to the air flowing through it. It is defined as the ratio of the heat received by the drying air to the solar energy incident upon the absorber surface, in a given time interval, and is calculated from the equation:

$$\eta_c = \frac{\dot{m}_1 C_{p,1}(T_{f,1o} - T_{f,1IN}) + \dot{m}_2 C_{p,2}(T_{f,2o} - T_{f,2IN})}{I_c \times A_c} \tag{4.6}$$

4.1.2 Modelling of air flow rate

Air flow rate through a chimney is caused by natural draft resulting from temperature difference between the hot air at inlet to the chimney and the cold air outside it and is expressed as (Achenbach and Cole, 1949):

$$D_t = 47.9\,\rho_a'\,h'\left(\frac{T_{f,m}' - T_a'}{T_{f,m}'}\right) \tag{4.7}$$

where, D_t is the pressure drop (N/m^2), $T_{f,m}'$ is the mean temperature of the heated air inside the chimney ($^\circ$ F), T_a' is the temperature of ambient air ($^\circ$ F), h' is the vertical height of the stack (ft) and ρ_a' = mean density of ambient air (lb/ft^3). To account for heat losses in a chimney, the mean temperature, $T_{f,m}'$, valid for chimneys less than 9m high, is given by (Colborne and Moffat, 1959):

$$T_{f,m}' = T_a' - 0.65(T_a' - T_{f,o}') \tag{4.8}$$

where T_a' and $T_{f,o}'$ are temperatures at the inlet and outlet of the chimney respectively.

Neglecting inertia forces, the thermal pressure difference inside the collector is balanced by pressure drop due to friction across the collector and hence the mass flow rate of air in the *i*th channel is given by

$$\dot{m}_i = \rho_i W s_i C_{v,i} F_{v,i} \sqrt{2\left\{47.9\,\rho_a{}'\,h'\left(\frac{T_{f,o}' - T_a'}{T_{f,o}' + \frac{7}{13}T_a'}\right)\right\}} \tag{4.9}$$

where, $h' = L'\sin\beta$, $F_{v,i} = \sqrt{\dfrac{d_{h,i}}{f\,L\,\rho_i}}$, $d_{h,i}$ = hydraulic mean depth of the duct, L' = the length of the collector in feet and $C_{v,i}$ is the coefficient of velocity the values of which were found to range between 0.2 and 0.6 for both the top and bottom channels of the air-heater.

4.1.3 Estimation of heat transfer coefficients

The radiative heat transfer coefficients from the absorber plate to the cover plate (glazing), $h_{r,pc}$, and from the absorber plate to the bottom plate, $h_{r,pb}$ are given by an expression of the general form:

$$h_{r,pi} = \frac{\sigma\left(T_p^2 + T_i^2\right)\left(T_p + T_i\right)}{\frac{1}{\varepsilon_p} + \frac{1}{\varepsilon_i} - 1} \tag{4.10}$$

where, i represents c, b.

The heat transfer by radiation from the glazing of a solar collector to the sky (i.e. from a collector to the surroundings) is given by

$$h_{r,cs} = \sigma\varepsilon_c(T_c^2 + T_s^2)(T_c + T_s) \tag{4.11}$$

where T_s, the sky-temperature, is evaluated from an equation given by Swinbank (1963) as

$$T_s = 0.0552(T_a)^{1.5} \tag{4.12}$$

For a rough assessment of sky temperature, Whillier (1967) provides even a simpler expression

$$T_s = T_a - 6 \tag{4.13}$$

The effective sky temperature is related to the dew point temperature, dry bulb temperature, and the hour from midnight, t_h, by the following equation (Duffie and Beckman, 1991):

$$T_s = T_a(0.711 + 0.0056\theta_{dp} + 0.000073\theta_{dp}^2 + 0.013\cos(15t_h) \tag{4.14}$$

where T_s and T_a are in Kelvin and θ_{dp} is the dew point temperature in degree Celsius. The experimental data on which equation (4.14) is based is valid for dew points ranging from -20° C to 30° C. It is reported that in general the difference between the sky temperature and the ambient air temperatures range from 5° C in hot, moist climate to 30° C in a cold, dry climate. In this study equation (4.12) was used since it is relatively simple and also gives fairly accurate results. It has been noted that a cloud cover will tend to increase the sky temperature over that for a clear sky.

Hollands *et al* (1976) give the relationship between Nusselt number and Rayleigh number for free convective heat exchange through a tilted cavity with tilt angle, β, $0 \leq \beta \leq 60°$ and large aspect ratios, (L/s) ≥ 12 as:

$$Nu_x = 1 + 1.44\left(1 - \frac{1708(\sin 1.8\beta)^{1.6}}{Ra(\cos\beta)}\right)\left[1 - \frac{1708}{Ra(\cos\beta)}\right]^{*} + \left[\left(\frac{Ra(\cos\beta)}{5830}\right)^{1/3} - 1\right]^{*} \qquad (4.15)$$

where $[X]^{*}$ is defined by: $[X]^{*} = (|X| + X)/2$

The average value of the Nusselt number is related to the local value by the relation

$$\overline{Nu} = \tfrac{4}{3} Nu_x \qquad (4.16)$$

Equations 4.15 and 4.16 are used to evaluate the heat transfer coefficients, h_2 and h_4, between the hot air and the heated absorber plate for large aspect ratios ($L/s > 12$) and critical angles less than 60°. For small aspect ratios, (L/s) ≤ 12 and tilt angles less than the critical values β^c given in Table 4.1, it is suggested (Incropera and DeWitt, 1996) that reasonable results may be obtained for rectangular cavities as follows:

$$\overline{Nu}_L = \overline{Nu}_H \left[\frac{\overline{Nu}_v}{\overline{Nu}_H}\right]^{\beta/\beta^c} (\sin\beta^c)^{(\beta/4\beta^c)} \qquad (4.17)$$

Table 4.1 Critical angle for inclined rectangular cavities.

L/s	1	2	6	12	> 12
β^c	25°	53°	60°	67°	70°

Source: Incropera and DeWitt, 1996.

The convection heat transfer coefficient for a horizontal cavity, $\overline{Nu}_H$ with the heated plate below is obtained from equation (4.15) by making $\beta = 0$. For a vertical rectangular cavity, with aspect ratio from 2 to 10, $Pr < 10^5$ and $10^3 < Ra < 10^{10}$ the following correlation has been suggested (Incropera and Dewitt, 1996):

$$\overline{Nu}_v = 0.22\left(\frac{Pr}{0.2+Pr}Ra\right)^{0.28}\left(\frac{L}{s}\right)^{-1/4} \tag{4.18}$$

The characteristic length in the expression for Nusselt number for equations (4.15) to (4.18) is the depth of the corresponding air channel. In using these equations the properties of air are evaluated at the mean temperature of the plates enclosing the cavity.

The heat transfer coefficient, h_1 between hot air and the inner surface of the relatively cold tilted glass cover is estimated using the following correlation (Elsayed, 1990):

$$Nu = \frac{h_1 L^*}{k} = 0.27\left[(Gr\,Pr\cos\beta)^{1/3}\right] \tag{4.19}$$

where, L^* is the characteristic length and defined as the surface area of the enclosure divided by the perimeter that encompasses the area.

The heat transfer coefficient, h_3 is calculated using the correlation for calculating heat transfer coefficients between two horizontal plates (with the hot plate uppermost) and accounting for the tilt through multiplying by the appropriate factor as follows (Wong, 1977):

$$\overline{Nu} = 0.135(Gr\,Pr\cos\beta)^{1/3} \tag{4.20}$$

The wind heat transfer coefficient, h_w, is evaluated using correlation proposed by Othieno (1987) for angles of tilt in the range 0 to 20° as:

$$h_w = k(75 + 0.42\,\mathrm{Re}^{0.6}) / X \tag{4.21}$$

where the characteristic length, X, is four times the plate area divided by the plate perimeter.

The back loss coefficient U_b is given by Klein (1979) as:

$$U_b = 1/(x/k + 1/h_b) \tag{4.22}$$

where k and x are the thermal conductivity and thickness of the back insulation, respectively, and h_b is the convection heat transfer coefficient between the bottom of the insulation and the environment. The values of h_b are generally in the range of 12.5 to 25 $W/m^2 K$ (Tabor, 1958).

The edge heat losses are estimated by assuming one-dimensional sideways heat flow around the perimeter of the collector system. The edge loss heat transfer coefficient is referred to the collector area, A_c, and given by:

$$U_{e_1} = (UA)_{edge} / A_c = \{(k/x)\, s_i\} / W \tag{4.23}$$

4.1.4 Radiation incident on the collector surface

The monthly average daily extraterrestrial radiation on a horizontal surface, $\overline{H}_o$ is given as (Duffie and Beckman, 1991):

$$\overline{H}_o = \frac{24\times 3600}{\pi} G_{sc}\left(1+0.033\cos\frac{360\overline{n}}{365}\right)\left[\cos\phi\cos\delta\sin\omega_s + \frac{\pi\omega_s}{180}\sin\phi\sin\delta\right] \tag{4.24}$$

where G_{sc} = 1367 W/m^2, $\overline{n}$ = mean day (based on solar radiation) of the month, ϕ = latitude of the site, δ = declination and ω_s = sunset hour angle. Equation 4.24 is valid for evaluating $\overline{H}_o$, for latitudes in the range -60° to +60° (Duffie and Beckman, 1991).

The declination, δ, can be found from the equation of Cooper (1969):

$$\delta = 23.45 \sin(360 \frac{284 + \overline{n}}{365}) \tag{4.25}$$

The Angstrom-Page regression equation which relates monthly average daily radiation to the extraterrestrial radiation on a horizontal surface is:

$$\frac{\overline{H}}{\overline{H}_o} = a'' + b'' \frac{n}{\overline{N}} \tag{4.26}$$

where, $\overline{H}$ = monthly average daily radiation on a horizontal surface, n = monthly average daily hours of bright sunshine, a'', b'' are location-dependent empirical constants and $\overline{N}$ = monthly average of the maximum possible hours of bright sunshine and is given as:

$$\overline{N} = \frac{2}{15} \cos^{-1}(-\tan\phi \tan\delta) \tag{4.27}$$

The values of a'', and b'' for various climate types and locations are provided in Duffie and Beckman (1991). In the case study, the annual values of a'' and b'' determined for for Kumasi (Jackson and Akuffo, 1992) were used for lack of available values for the test site.

The mean monthly daily total radiation on a tilted surface, $\overline{H}_T$, is related to $\overline{H}$ and $\overline{R}$ as:

$$\overline{H_T} = \overline{R}\,\overline{H} \tag{4.28}$$

where, $\overline{R}$ is an estimate of the sum of three terms corresponding to the beam, diffuse, and ground-reflection on the inclined surface.

Klein and Theilacker (1981) formulated an algorithm for estimating $\overline{R}$ valid for any surface orientation, and for all latitudes and for any surface azimuth angle γ. For south facing collectors in the northern hemisphere ($\gamma = 0$), $\overline{R}$ is given by Klein and Theilacker (1981) as:

$$\overline{R}=\frac{\cos(\phi-\beta)}{d\cos\phi}\left\{\begin{array}{l}\left(a-\frac{\overline{H}_d}{\overline{H}}\right)\left(\sin\omega_s'-\frac{\pi}{180}\omega_s'\cos\omega_s''\right)\\ +\frac{b}{2}\left(\omega_s'\frac{\pi}{180}+\sin\omega_s'(\cos\omega_s'-2\cos\omega_s'')\right)\end{array}\right\}+\frac{\overline{H}_d}{\overline{H}}\left(\frac{1+\cos\beta}{2}\right)+\rho_g\left(\frac{1-\cos\beta}{2}\right) \quad (4.29)$$

where $\omega_s = \arccos(-\tan\phi\tan\delta)$ (4.30)

$$\omega_s''=\arccos(-\tan(\phi-\beta)\tan\delta \quad (4.31)$$

$$\omega_s' = \min(\omega_s, \omega_s'') \quad (4.32)$$

The values of a, b and d in equation (4.29) are given by Liu and Jordan (1977) and Collares-Pereira and Rabl (1979) as

$$a = 0.409 + 0.5016\sin(\omega_s - 60^\circ) \quad (4.33)$$

$$b = 0.6609 - 0.4767\sin(\omega_s - 60^\circ) \quad (4.34)$$

$$d = \sin\omega_s - \frac{\pi}{180}\omega_s\cos\omega_s \quad (4.35)$$

The above algorithm requires an estimate of $\overline{H}_d/\overline{H}$, the monthly average daily diffuse radiation fraction. Experiments have shown (Duffie and Beckman, 1991) that $\overline{H}_d/\overline{H}$ is related to the monthly average daily clearance index, $\overline{K}_T$ ($=\overline{H}/\overline{H}_o$) - the ratio of average daily total to extraterrestrial radiation. Duffie and Beckman (1991) recommend the use of the Erbs *et al*, (1982) correlation's for estimating $\overline{H}_d/\overline{H}$. Equations for the Erbs *et al*'s correlation of $\frac{\overline{H}_d}{\overline{H}}$ to $\overline{K}_T$ and ω_s are as follows:

For $\omega_s \leq 81.4^\circ$ *and* $0.3 \leq \overline{K}_T \leq 0.8$

$$\frac{\overline{H}_d}{\overline{H}} = 1.391 - 3.560\,\overline{K}_T + 4.189\,\overline{K}_T^{\,2} - 2.137\,\overline{K}_T^{\,3} \tag{4.36}$$

For $\omega_s > 81.4^\circ$ and $0.3 \leq \overline{K}_T \leq 0.8$

$$\frac{\overline{H}_d}{\overline{H}} = 1.311 - 3.022\,\overline{K}_T + 3.427\,\overline{K}_T^{\,2} - 1.821\,\overline{K}_T^{\,3} \tag{4.37}$$

According to Liu and Jordan (1977), the ground albedo, ρ_g, varies from 0.2 to 0.7 depending on the extent of the snow cover on the surface and for a surface not covered with snow they recommend the minimum value of 0.2.

The monthly average transmittance-absorptance product, $(\overline{\tau\alpha})_{av}$, is related to the monthly average radiation incident on the collector and the monthly average solar radiation absorbed per unit absorber plate area, $\overline{S}_{p,}$ as (Klein, 1979):

$$\overline{S}_{p,} = \overline{H}_T(\,\overline{\tau\alpha}\,)_{av} = \overline{R'}\,\overline{H} \tag{4.38}$$

The radiation absorbed by the absorber per unit area ($\overline{S}_{p,}$), is evaluated by combining equations (4.38) and (4.39) and also introducing a factor to account for the effects of dust and shading on the collector performance. Hence the effective monthly average daily absorbed radiation (by the absorber) is given by:

$$\overline{S}_{p,} = \zeta\,\overline{R}'(a'' + b''\frac{n}{\overline{N}})\,\overline{H}_o \tag{4.39}$$

In this model, it is assumed that solar radiation is collected over a time interval of N_{ds}, corresponding to day length for drying, (in hours) on each day of the month. Hence the steady-state value of the intensity of the monthly-mean absorbed solar radiation (by the absorber) is given as:

$$\overline{S}_p = \zeta\,\overline{R}'(a'' + b''\frac{n}{\overline{N}})\frac{\overline{H}_o}{N_{ds}\times 3600} \tag{4.40}$$

where, ζ (= 0.96) is a factor to account for the combined effects of shading and dust and n is the number of bright sunshine hours on the mean day of the month.

The intensity of solar radiation absorbed by the collector cover per unit area is given by

$$\overline{S}_c = \alpha_c \overline{R}\,\overline{K}_T \frac{\overline{H}_o}{N_{ds} \times 3600} \tag{4.41}$$

The effective transmittance-absorptance product of the diffuse and ground reflection components of the incident radiation on the tilted surface can be approximated by a relation of the form:

$$(\overline{\tau\alpha})_j \cong 1.01\,\tau_j\,\alpha_j \tag{4.42}$$

where,

$$\frac{\alpha_j}{\alpha_n} = 1 + 2.0345\times10^{-3}\,\theta_j - 1.990\times10^{-4}\,\theta_j^{\,2} + 5.324\times10^{-6}\,\theta_j^{\,3} - 4.799\times10^{-8}\,\theta_j^{\,4}, \tag{4.43}$$

$$\theta_j = \begin{cases} 60^\circ & \text{beam component} \\ 59.68 - 0.0138\beta + 0.001497\beta^2 & \text{diffuse component} \\ 90 - 0.5788\beta + 0.002693\beta^2 & \text{reflected component} \end{cases} \tag{4.44}$$

and β is the collector tilt. The effective transmittance-absorptance product of the beam component of the incident radiation, $(\overline{\tau\alpha})_b$, is calculated using the following expression of the incidence angle modifier (Duffie and Beckmann, 1991) :

$$\overline{\tau\alpha}_b = \left(1 + b_o\left\{\frac{1}{\cos\theta} - 1\right\}\right)(\overline{\tau\alpha})_j \tag{4.45}$$

where θ is the solar incidence angle on the glass cover and $b_o = -0.1$ for a collector with a single glass cover (ASHRAE, 1977). Equation 4.45 is used to calculate $(\overline{\tau\alpha})_b$ after putting $\theta = 60^\circ$ as suggested by Brandemuehl and Beckman (1980).

4.1.5 Thermo-physical properties of air in the plenum

The air inside the plenum is a combination of the air streams exiting the two channels. In estimating the temperature of the air in the plenum, adiabatic mixing of the two air streams from the channels is assumed to achieve a conservative estimate of the air temperature inside the plenum. This assumption is made on the premise that, once the air is inside the plenum there is no radiative or conductive heat transfer to the air. In real terms, the effect of heat losses is accounted for by the factors (ξ and γ) based on experimentation. The expression for the average temperature of the air in the plenum is given by:

$$T_f = \xi \frac{\dot{m}_1 c_{p,1} T_{f,1} + \dot{m}_2 c_{p,2} T_{f,2}}{(\dot{m}_1 + \dot{m}_2)} + \gamma \qquad (4.47)$$

where ξ and γ are constants determined experimentally. A linear regression using data (208 observations) from experiments on both the full-scale and the small-scale models and based on equation (4.47) produced $\xi = 0.94$ and $\gamma = -0.56$ with $R^2 = 0.96$.

The thermo-physical properties of air (density, thermal conductivity, specific heat and kinematic viscosity) are assumed to vary linearly with temperature T (K). The following relations valid for 293 K < T < 333 K are assumed for various thermo-physical properties of air:

$$\rho = -0.0038T + 2.3180 \qquad (4.48)$$

$$k = [0.0732\,T + 4.1672] \times 10^{-3} \qquad (4.49)$$

$$C_p = 0.0000098\,T + 1.0038 \qquad (4.50)$$

$$\nu = [0.0942\,T + 2.3180] \times 10^{-6} \qquad (4.51)$$

The recommended (Kern and Harris, 1975; Duffie and Beckman, 1991) value of the collector tilt, β, for maximum annual collection of solar radiation is the latitude of the site. However, from experiments the minimum slope for rain-water to drop off a sloped surface is 6^{o}. Hence, the minimum value of the collector tilt is 6^{o}.

4.1.6 Solution procedure

By manipulating equations (4.1) and (4.5), we obtain

$$T_b = \frac{1}{U_b + h_{r_{pb}} + h_4}\left[U_b T_a + h_{r_{pb}} T_p + h_4 T_{f_2}\right] \tag{4.52}$$

$$T_c = \frac{1}{h_{r_{ca}} + h_w + h_1 + h_{r_{pc}}}\left[\overline{S}_c + h_{r_{pc}} T_p + h_1 T_{f_1} + h_w T_a + h_{r_{ca}} T_s\right] \tag{4.53}$$

Eliminating T_b and T_c from equations (4.2), (4.3) and (4.4), yield the following three equations:

$$A_1 T_p = B_1 T_{f_1} + C_1 T_{f_2} + \gamma_3 \tag{4.54}$$

$$\frac{dT_{f_1}}{dx} = \lambda_1 T_{f_1} + \mu_1 T_{f_2} + \gamma_1 \tag{4.55}$$

$$\frac{dT_{f_2}}{dx} = \lambda_2 T_{f_1} + \mu_2 T_{f_2} + \gamma_2 \tag{4.56}$$

where: $\gamma_3 = D_1 T_a + E_1 T_s + F_1 \overline{S}_c + \overline{S}_p$;

$$\gamma_2 = \frac{1}{\dot{m}_2 C_a}\left[\left(\frac{A_3 D_1}{A_1} + D_3\right) T_a + \frac{A_3 E_1}{A_1} T_s + \frac{A_3 F_1}{A_1}\overline{S}_c + \frac{A_3}{A_1}\overline{S}_p\right]; \quad F_2 = W\left(\frac{h_1}{E}\right);$$

$$\gamma_1 = \frac{1}{\dot{m}_1 C_a}\left[\left(\frac{A_2 D_1}{A_1} + D_2\right) T_a + \left(\frac{A_2 E_1}{A_1} + E_2\right) T_s + \left(\frac{A_2 F_1}{A_1} + F_2\right)\overline{S}_c + \frac{A_2}{A_1}\overline{S}_p\right] \;;$$

$$\lambda_1 = \frac{1}{\dot{m}_1 C_a}\left(\frac{A_2 B_1}{A_1} - B_2\right); \qquad \lambda_2 = \frac{1}{\dot{m}_2 C_a}\left[\frac{A_3 B_1}{A_1}\right]; \qquad \mu_1 = \frac{1}{\dot{m}_1 C_a}\left[\frac{A_2 C_1}{A_1}\right];$$

$$\mu_2 = \frac{1}{\dot{m}_2 C_a}\left[\frac{A_3 C_1}{A_1} - B_3\right]; \; F_1 = \frac{h_{r_{pc}}}{E}, \; F = U_b + h_{r_{pb}} + h_4; \; A_2 = W\left(h_2 + \frac{h_1 h_{r_{pc}}}{E}\right);$$

$$E = h_{r_{ca}} + h_w + h_1 + h_{r_{pc}}; \; A_1 = h_3 + h_2 + h_{r_{pb}} - \frac{h_{r_{pb}}^2}{F} + h_{r_{pc}} - \frac{h_{r_{pc}}^2}{E};$$

$$B_1 = h_2 + \frac{h_{r_{pc}} h_1}{E}; \qquad C_1 = h_3 + \frac{h_{r_{pb}} h_4}{F}; \qquad D_1 = \left(h_{r_{pb}} U_b / F\right) + \left(h_{r_{pc}} h_w / E\right);$$

$$E_1 = \frac{h_{r_{pc}} h_{r_{ca}}}{E}; \qquad E_2 = W\left(\frac{h_1 h_{r_{ca}}}{E}\right); \qquad B_2 = W\left(h_2 + h_1 - \frac{h_1^2}{E} + \frac{U_{e_1} s_1}{W}\right);$$

$$A_3 = W\left(h_3 + \frac{h_4 h_{r_{pb}}}{F}\right); \qquad D_2 = W\left(\frac{h_1 h_w}{E} + \frac{U_{e_1} s_1}{W}\right);$$

$$B_3 = W\left(h_3 + h_4 - \frac{h_4^2}{F} + \frac{U_{e_2} s_2}{W}\right); \; D_3 = W\left(\frac{h_4 U_b}{F} + \frac{U_{e_2} s_2}{W}\right);$$

Equations 4.55 and 4.56 form a linear non-homogenous coupled differential equation system with coefficients that are dependent on the plate temperature T_p , the cover temperature T_c, the bottom plate temperature T_b, the solar intensity S and the ambient temperature T_a (Pawar *et al*, 1994). The two input variables of the model, namely the solar intensity and the ambient temperature are periodic in nature, and hence the values of the plate temperature T_p, fluid temperatures $T_{f,1}$, $T_{f,2}$ which are dependent on S and T_a will also be periodic. Putting T_p as a constant and eliminating $T_{f,1}$ and $T_{f,2}$ from equations (4.55) and (4.56) respectively by making use of equation (4.54) yield,

$$\frac{dT_{f_1}}{dx} = \phi_1 T_{f_1} + \phi_2 \tag{4.57}$$

$$\frac{dT_{f_2}}{dx} = \phi_3 T_{f_2} + \phi_4 \tag{4.58}$$

where: $\phi_1 = \lambda_1 - \frac{\mu_1 B_1}{C_1}$; $\phi_2 = \frac{\mu_1 A_1}{C_1} T_p - \frac{\mu_1 \gamma_3}{C_1} + \gamma_1$; $\phi_3 = \mu_2 - \frac{\lambda_2 C_1}{B_1}$ and

$\phi_4 = \frac{\lambda_2 A_1}{B_1} T_p - \frac{\lambda_2 \gamma_3}{B_1} + \gamma_2$

The finite difference technique is employed to solve equations (4.57) and (4.58) together with their boundary conditions. An explicit forward differencing method is used with an iterative technique by expressing these equations (4.57) and (4.58) in the form:

$$T_{f1_o} = \frac{1}{(2-\phi_1 \Delta x)} \left\{ (\phi_1 \Delta x + 2) T_{f1_{IN}} + 2\phi_2 \Delta x \right\} \quad (4.59)$$

$$T_{f2_o} = \frac{1}{(2-\phi_3 \Delta x)} \left\{ (\phi_3 \Delta x + 2) T_{f2_{IN}} + 2\phi_4 \Delta x \right\} \quad (4.60)$$

where $T_{fi} = \frac{1}{2}(T_{fi_{IN}} + T_{fi_o})$

The model assumes that at steady-state, the temperatures of the cover, absorber and the bottom plate (the walls) are each characterised by a constant value. The collector is imagined to be divided into a finite number of short sections each with a mean air temperature equal to the average of the inlet and outlet air temperatures. An iteration process is then started. The temperatures of the walls are initially guessed. The heat transfer coefficients are estimated using these guessed values. The initial values of the parameters defined, in equations (4.54) to (4.58) are then determined. Equations 4.59 and 4.60 are then used to determine the first approximations of exit temperature of the air in the first section. Equations 4.52 through to 4.54 are then used to calculate new values of cover temperature, T_c, the absorber temperature, T_p, and the bottom plate temperature, T_b. The newly calculated values of T_c, T_p and T_b are compared with the initially guessed values. The absolute criterion of convergence in the form $\left|T_i^{(n+1)} - T_i^{(n)}\right| \leq 0.01$ is employed to test for convergence of the values T_c, T_p and T_b. When convergence is established, the accepted values of T_c, T_p, T_b, $T_{f,1}$ and $T_{f,2}$ are used in determining the mass flow rates in the two channels. Subsequently, the criterion of convergence of the form $\left|\dot{m}_i^{(n+1)} - \dot{m}_i^{(n)}\right| \leq 0.001$ is used to establish convergence of the mass flow rate values. If the mass flow rate does not

converge, the iteration process is repeated with last calculated values of T_c, T_p, T_b, $T_{f,1}$ and $T_{f,2}$ as the initial values for the entire iteration process. On the other hand, if the convergence of the mass flow rate is also established then established values of the parameters (ϕ_1, ϕ_2, ϕ_3 and ϕ_4) in equations (4.59) and (4.60) are assumed constant and carried along with the flow. The accepted temperatures of the air at the exit of the first section are used as the inlet temperature of the air to the second section, if any. Equations 4.59 and 4.60 are used to calculate the outlet temperature of the air in the second section. The last process is repeated until the entire length of the collector is covered.

4.2 Formulation of the drying model

The deep-bed drying process is approached by writing energy and mass balance equations on an arbitrary elemental layer of the fixed crop bed. The drying of this element can be simulated by considering changes that occur in the crop and the drying air as represented in fig. 4.2. The drying air is passed through this elemental layer of crop for a time interval (Δt). During this period, moisture is evaporated from the crop bed into the drying air causing the moisture content of the crop to decrease and the absolute humidity of the air to increase. For a specified air flow rate, the values of the following variables are determined after each incremental drying period (Δt): T, the drying air temperature; T_{pt}, the crop temperature; H, the absolute humidity of the drying air; and M, the average moisture content.

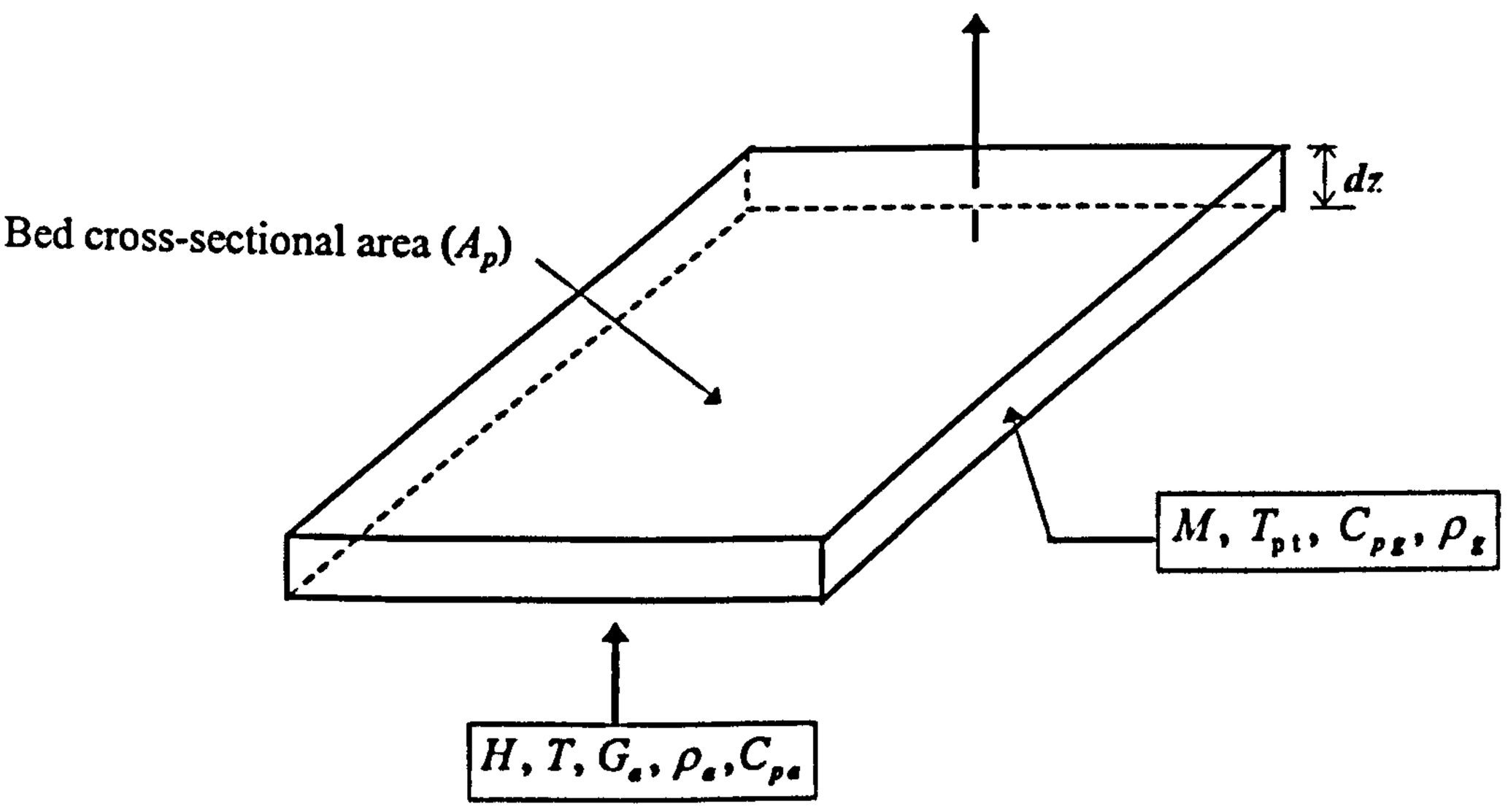

Figure 4.2: Elemental volume of crop bed

In deriving the mathematical model for analysing the drying process, the following assumptions are made:

1. no temperature gradients exist within each material particle;
2. particle to particle conduction is negligible;
3. air flow through the crop bed is uniformly distributed;
4. heat capacities of the air and of the wet crop are constant during the short time interval of the passage of the drying air;
5. the changes in temperature and humidity of air over an elemental layer of the crop bed are more significant than the changes that occur in a short time interval;
6. at the commencement of the drying process, the drying air displaces all air within the dryer without heat or mass transfer taking place. This assumption although not exact, it allows for the initial boundary conditions of the process to be specified;
7. moisture evaporated from the crop is at a temperature equal to that of the drying material;
8. the crop-bed is a rectangular slab with void spaces;
9. the change in enthalpy of the air trapped in the crop-bed void spaces is negligible compared to the change in the enthalpy of the flowing air.
10. there is no condensation on the walls of the drying chamber;
11. thermal capacitance of the drying chamber is significant; and
12. the convective film resistance on the outer surface of the drying chamber is negligible.

4.2.1 Heat and mass transfer in layer drying

When a thin layer of material is dried by passing air through the bulk of the crop bed (i.e. by through-flow of air), the conditions of the material and of the air are altered. The changes that occur are specified by the changes in the humidity and temperature of the air and the moisture content and temperature of the material. Four independent equations are needed to determine the changes in these four conditions: the drying rate equation, the mass balance equation on the drying air, the heat balance equation on the drying air and the heat balance on the crop (O'Callaghan, 1971). In this model, the drying chamber walls are not considered to be adiabatic therefore a fifth equation, an energy balance on the chamber

walls is added to evaluate its steady-state temperature. These five equations are derived as explained in the subsequent sections.

4.2.2 The drying rate equation

The rate of moisture removal from the crop can be expressed by the diffusion equation, (equation 2.5) which describes the removal of water vapour from the wet product. The solution of this equation for a slab-shaped crop bed is given as (Crank, 1975):

$$\frac{\overline{M} - M_e}{M_o - M_e} = \frac{8}{\pi^2} \sum_{n=0}^{\infty} \frac{1}{(2n+1)^2} \exp\left[-(2n+1)^2 D\pi^2 t / z^2\right] \tag{4.63}$$

where, D is the diffusion coefficient of the wet material, z is the thickness of the crop bed and t is the drying time. A simplified solution is sought by using the first few terms of the series solution of equation (4.63). The diffusion coefficient is a function of the material moisture content, the drying air temperature and the drying air relative humidity and for cassava the expression for the diffusion coefficient by Igbeka (1982) is modified as:

$$D = \Psi\left(-0.0274 - 5.74\times10^{-6} M + 5.98\times10^{-6} e^{M} + 0.0275 e^{-1/T} + 2.23\times10^{-6}\{-2RH + 1.2\}\right) \tag{4.64}$$

where, Ψ is a multiplying factor the value of which is dependent on the range of the moisture content of the product. Results from a series of experimental drying curves for cassava, of moisture contents in the range 202% down to 15%, showed that drying proceeds only in the falling-rate period. Four stages of falling-rate periods were identified; the values of the multiplying factors for all the stages are as follows:

$M \geq 1.2$	$\Psi = 0.07$;	$0.7 \leq M < 1.2$	$\Psi = 0.01$;
$0.4 \leq M < 0.7$	$\Psi = 0.0063$;	$M < 0.4$	$\Psi = 0.003$.

A generalised empirical relation is used to describe the equilibrium moisture content isotherms for hygroscopic materials. This relation is of the form (Teter and Citelly, 1970; Roa, 1974):

$$\ln\left(\frac{M_e}{p_o + p_1 RH + p_2 RH^2 + p_3 RH^3}\right) = q_o + \left(q_1 + q_2 RH + q_3 RH^2 + q_4 RH^3 + q_5 RH^4\right)T \tag{4.65}$$

In equation (4.65), p_i and q_i are product-dependent constants.

4.2.3 Mass balance equation on the drying air

This simply relates the exchange of moisture between material being dried and the drying air. Consider an element of material in a deep-bed dryer and the associated quantities (see fig. 4.2). Under steady-state, the difference between the amount of moisture flowing into and out of the control volume during the time interval *dt* is equal to the moisture leaving the material in the control volume. The change in humidity of the air in the void spaces can be neglected (Brooker *et al*, 1974).

The amount of water vapour flowing into the control volume at time *dt* past the plane at locations *z* and $(z + dz)$, respectively are equal to

$$G_a A_p H dt \text{ and } G_a A_p (H + \frac{\partial H}{\partial z} dz) dt$$

The amount of water removed from the material in the control volume in the time *dt* within which the drying air passes from locations *z* to $(z + dz)$ is given as

$$\rho_p A_p dz \frac{\partial M}{\partial t} dt$$

Under steady-state, assuming no condensation on the walls of the drying chamber, the mass balance on the control volume results in

$$G_a A_p H dt - G_a A_p (H + \frac{\partial H}{\partial z} dz) dt = \rho_p A_p dz \frac{\partial M}{\partial t} dt \tag{4.66}$$

which simplifies to:

$$G_a \frac{\partial H}{\partial z} = -\rho_p \frac{\partial M}{\partial t} \tag{4.67}$$

where, G_a (kg/s-m^2) is the mass-flux of air through the drying chamber and is related to the mass-flow rate and the effective cross-sectional area of the drying chamber by the relation:

$$G_a = \frac{\dot{m}}{A_{dc}} \tag{4.68}$$

The derivation of the expression for the mass flow rate ($\dot{m}$) is considered in section (4.2.7).

4.2.4 Heat balance on the drying air

The statement of energy balance on the air is:

heat transferred to the drying material and the tray (including the latent heat for vaporising the moisture) plus heat transferred to the drying chamber walls must equal the heat loss from the air less the enthalpy of the vapour gained during its passage through the drying bed.

Thus,

the change in enthalpy of the air = heat lost to the product and the drying chamber + heat carried by vapour to the air.

The enthalpy of the air flowing into the control volume in time dt at location z is

$$G_a A_p \left[\left(C_{pa} + C_{pw} H(z)\right) T(z) + L_a H(z)\right] dt$$

Similarly, the enthalpy of the air flowing out of the control volume in the same time dt from location $(z + dz)$ is

$$G_a A_p \left[\left(C_{pa} + C_{pw} H(z+dz)\right) T(z+dz) + L_a H(z+dz)\right] dt$$

But the heat lost from the drying air to the product and the walls of the drying chamber is

$$= \left[h_v A_p \left(T - T_{pt}\right) + h_v A_w (T - T_w)\right] dz\, dt$$

Assuming that moisture is evaporated from the wet material at the same temperature of the crop, the enthalpy of vapour gained during the passage of air through a crop bed in time (dt) is given by

$$\left(C_{pw} T_{pt} + L_a\right) \rho_p A_p \frac{\partial M}{\partial t} dz\, dt$$

The change in enthalpy of the drying air is given by the difference between the enthalpies of the air flowing into and out of the control volume as:

$$G_a A_p \left[\left(C_{pa} + C_{pw} H(z)\right) T(z) + L_a H(z)\right] dt -$$
$$G_a A_p \left[\left(C_{pa} + C_{pw} H(z+dz)\right) T(z+dz) + L_a H(z+dz)\right] dt$$

Simplifying and re-arranging the terms of the mathematical statement of the energy balance for the drying air results in the relation:

$$G_a A_p \left[\left(C_{pa} + C_{pw} H\right) \frac{\partial T}{\partial z} + C_{pw} T \frac{\partial H}{\partial z} + L_a \frac{\partial H}{\partial z}\right] dt dz$$
$$= -h_v A_p (T - T_{pt})\, dt dz - \left(\rho_p C_{pw} T_{pt} + \rho_p L_a\right) A_p \frac{\partial M}{\partial t} dt dz - h_v A_w \left(T - T_w\right) dt dz \qquad (4.69)$$

Substituting equation (4.66) into equation (4.69), the following expression relating the average temperature, T, at which air transfers heat in the control volume, to the drying conditions is obtained as:

$$\frac{\partial T}{\partial z} = \frac{1}{G_a (C_{pa} + C_{pw} H)} \left[h_v \left(T_{pt} - T\right) + \rho_p C_{pw} \left(T - T_{pt}\right) \frac{\partial M}{\partial t} - \frac{h_v A_w}{A_p} (T - T_w)\right] \qquad (4.70)$$

4.2.5 Heat balance on the wet material

In writing the energy balance on the wet material, it is assumed that the external energy supplied to the drying chamber is used by the wet material and the drying chamber walls during the drying period in the following ways:

- heat to evaporate moisture from the wet material and heat to raise the evaporated moisture temperature to that of the drying air
- heat to raise the temperature of the dry solid and its residual moisture
- heat lost from the crop through the chamber walls to the surrounding
- heat to raise the temperature of the drying trays and the chamber walls.

It is further assumed that the moisture evaporated from the wet material in time (*dt*) is carried away by the drying air.

Thus,

the change in enthalpy of the crop = convective and radiant energy transferred to the crop − Heat supplied to evaporate the moisture from the wet material to the drying air − Heat lost from the crop to the chamber walls by radiation − radiation heat exchange from a layer of the crop bed to the adjacent layer(s).

In addition to convective heat from the solar heated air passing through the elemental layer, solar energy is transferred directly to the top layer by radiation from the top and through the sides of the drying chamber to all other layers. As a result, the effective surface temperature of the wet material will rise above the wet-bulb temperature of the air and this will subsequently reduce the rate at which heat is drawn from the heated air, but will increase the rate of evaporation. The incident solar energy absorbed by an elemental layer at the top layer is progressively reduced by the absorptance-transmittance factor of the subsequent layers. Following from this assumption, the intensity of solar radiation on each layer, $\overline{H}_s$ is approximately modelled as an exponential decaying function with its maximum value, $\overline{H}_T$ at the top layer and one-half its maximum halfway through the entire bed and is represented by

$$\overline{H}_s = \overline{H}_T \exp(2\ln 2\,\{JM(dz)/z_o - 1\}) \tag{4.71}$$

At the beginning of the time step t, the enthalpy of the material is

$$A_p \rho_p dz \{C_{pg} + C_{pl} M(t)\} T_{pt}(t)$$

and at time $t+dt$, is

$$A_p \rho_p dz \left(C_{pg} + C_{pl} M(t)\right) T_{pt}(t+dt)$$

The difference in the enthalpy of the material is given by

$$\rho_p \left(C_{pg} + C_{pl} M\right) A_p dz \frac{\partial T_{pt}}{\partial t} dt$$

The amount of moisture evaporated in the time dt is equal to the change in the humidity ratio of the air as it passes through the elemental volume, $A_p dz$, of the crop bed and is given as

$$G_a A_p dz \frac{\partial H}{\partial z} dt$$

The energy required for the evaporation of moisture from the wet material in the time dt is

$$L_a G_a A_p \frac{\partial H}{\partial z} dz\, dt$$

The energy required for heating the moisture evaporated from the wet material at temperature T_{pt} to air temperature in time dt is

$$C_{pl}(T - T_{pt}) G_a A_p dz \frac{\partial H}{\partial z} dt$$

The energy required to raise the temperature of the mass of the drying chamber is given by

$$C'' m'' \frac{\partial T_{pt}}{\partial t} dz\, dt$$

The enthalpy balance on the wet material is

$$(\rho_p A_p (C_{pg} + C_{pl} M) + C'' m'') \frac{\partial T_{pt}}{\partial t} dt\, dz = \alpha_p \tau_p \overline{H}_s A_{sc} dt\, dz + h_v A_{dc} (T - T_{pt}) dt\, dz$$
$$- \rho_p A_p \frac{\partial M}{\partial t} \left[C_{pl} (T - T_{pt}) + L_g \right] dt dz - h_{rpw} A_w (T_{pt} - T_w) dt\, dz \qquad (4.72)$$

$$\frac{\partial T_{pt}}{\partial t} = \frac{1}{\rho_p (C_{pg} + C_{pl} M) + C'' m''} \left[\alpha_p{}' \tau_p \frac{\overline{H}_s}{\cos\beta} + \frac{h_v A_w}{A_p} (T - T_{pt}) \right.$$
$$\left. G_a \frac{\partial H}{\partial Z} \left[C_{pl} (T - T_{pt}) + L_g \right] - \frac{h_{rpw} A_w}{A_p} (T_{pt} - T_w) \right] \qquad (4.73)$$

4.2.6 Energy balance on the walls of the drying chamber

The energy balance on the walls of the drying chamber gives

$$\alpha \overline{S}_c A_{w_T} + h_v A_{w_p} (T - T_w) + h_{r_{pw}} A_{w_p} (T_{pt} - T_w) = h_{r_{ws}} A_{w_p} (T_w - T_s) + h_w A_{w_p} (T_w - T_a) \qquad (4.74)$$

It is assumed that there is no condensation in the inside of the cover of the drying chamber. The above equation is used to establish the temperature of the walls of the drying chamber as:

$$T_w = \frac{\alpha_c \overline{S}_c + h_{r_{pw}} T_{pt} + h_{r_{ws}} T_s + h_w T_a + h_v T}{h_w + h_{r_{ws}} + h_v + h_{r_{pw}}} \qquad (4.75)$$

4.2.7 Mass flow rate

The pressure difference, ΔP, generated by the buoyancy forces in a duct of vertical height, H_v, at a temperature, ΔT, above ambient is given by

$$\Delta P = g \beta' \rho_a \Delta T H_v \qquad (4.76)$$

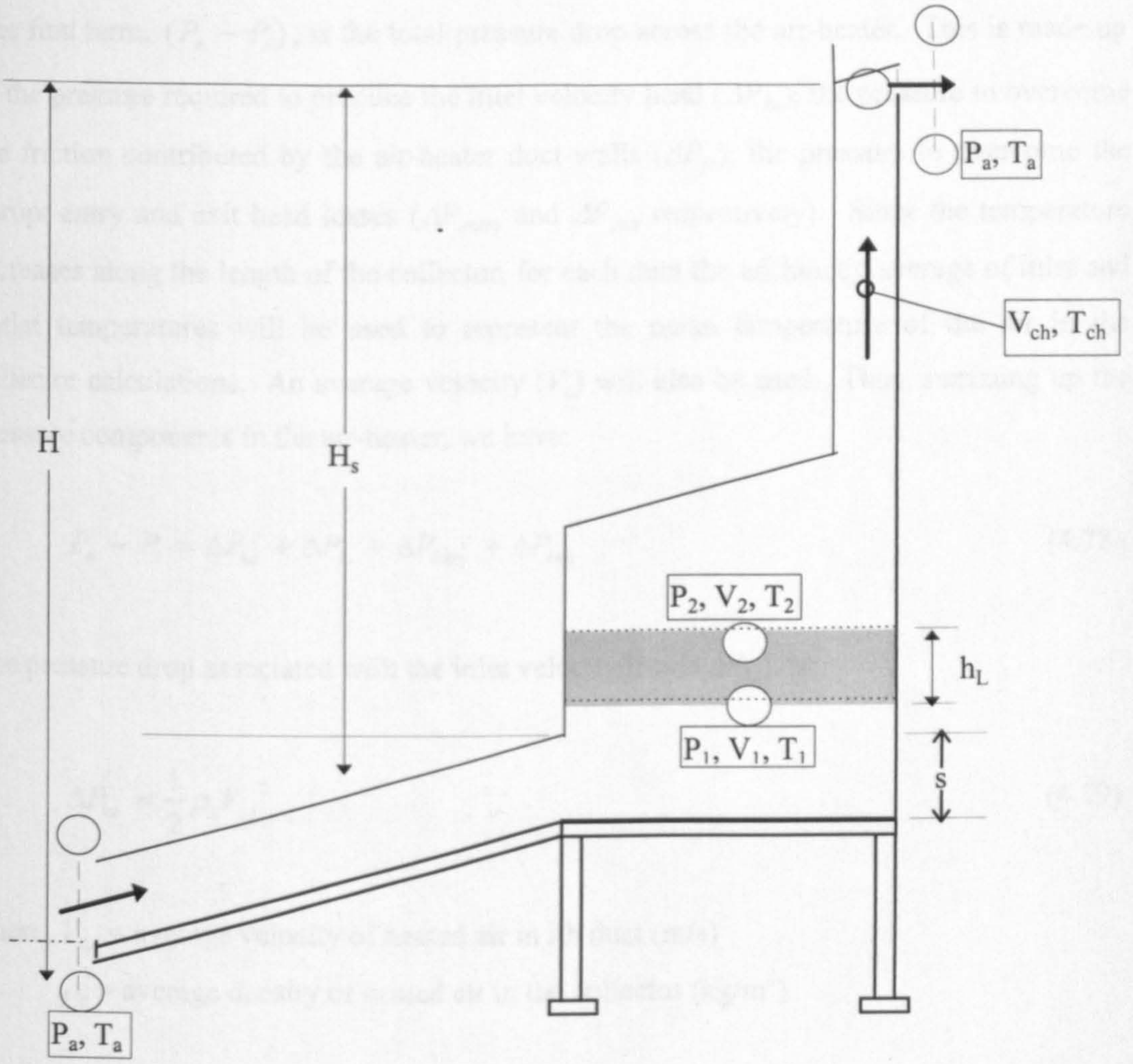

Figure 4.3: Schematic illustration of the MNCSCD for air flow rate analysis

Each component of the dryer, as shown in fig. 4.3, contributes to the total pressure drop. The flow rate is determined by considering and summing the pressure differences between pairs of points around the system. For an incompressible, steady-state flow condition, a closed-loop equation of the pressure differences along the points (a), (1), (2), (3), (4) and (a) can be written as:

$$(P_a - P_1) + (P_1 - P_2) + (P_2 - P_3) + (P_3 - P_a) = 0 \qquad (4.77)$$

The total pressure drop across the dryer is obtained by considering the pressure drop components of each of the terms in equation (4.77).

The first term, $(P_a - P_1)$, is the total pressure drop across the air-heater. This is made up of the pressure required to produce the inlet velocity head (ΔP_{ke}), the pressure to overcome the friction contributed by the air-heater duct walls (ΔP_{fc}), the pressure to overcome the abrupt entry and exit head losses (ΔP_{entry} and ΔP_{exit} respectively). Since the temperature increases along the length of the collector, for each duct the arithmetic average of inlet and outlet temperatures will be used to represent the mean temperature of the air in the collector calculations. An average velocity (V_c) will also be used. Thus, summing up the pressure components in the air-heater, we have:

$$P_a - P_1 = \Delta P_{ke} + \Delta P_{fc} + \Delta P_{entry} + \Delta P_{exit} \tag{4.78}$$

The pressure drop associated with the inlet velocity head (ΔP_{ke}), is:

$$\Delta P_{ke} = \frac{1}{2}\rho_c V_{c,i}^{\ 2} \tag{4.79}$$

where, $V_{c,i}$ = average velocity of heated air in ith duct (m/s)

ρ_c = average density of heated air in the collector (kg/m^3)

From continuity equation, the average velocity (V_c) can be expressed in terms of the velocity in the plenum (V_1) as:

$$V_c = (A_1 / A_c)(\rho_1 / \rho_c)V_1 \tag{4.80}$$

Equation (4.79) then becomes:

$$\Delta P_{ke} = C_{ke}\frac{\rho_1 V_1^{\ 2}}{2} \tag{4.81}$$

where A_c = the cross sectional area of the air duct (m/s)

A_1 = cross sectional area of the plenum (which equals the crop bed area) (m^2)

$C_{ke} = (A_1/A_c)^2(\rho_1/\rho_c)$.

The pressure drop due to the friction of the air-heater duct walls is given by:

$$\Delta P_{fc} = \frac{4fLG_a^{\,2}}{2\rho_c d_h} \tag{4.82}$$

where $G_a = \dfrac{\dot{m}}{A_c} = \dfrac{\rho_1 A_1 V_1}{A_c}$

L = collector length /(m)

$\dot{m}$ = mass flow rate of air in the drying system / (kg/s)

d_h = hydraulic diameter of the duct / (m) = $4A_c/P$

$V_c = V_{c,1} + V_{c,2}$

f = friction factor

P = perimeter of the air duct / (m).

Upon substitution and simplification we obtain:

$$\Delta P_{fc} = C_{fc}\frac{\rho_1 V_1^{\,2}}{2} \tag{4.83}$$

where $C_{fc} = \dfrac{4fL}{d_h}(\rho_1/\rho_2)(A_1/A_c)^2$

$f = 0.079\,\mathrm{R_e}^{-0.25}$ and

$$\mathrm{Re} = \frac{\mathrm{V_c} d_h}{\upsilon_c} = \frac{\dot{m} d_h}{A_c \rho_c \upsilon_c} = \frac{2\dot{m}}{(L+s)\rho_c \upsilon_c} \tag{4.84}$$

The pressure drop due to the abrupt collector entry is:

$$\Delta P_{entry} = 0.5\frac{\rho_c V_c^{\,2}}{2} = C_{entry}\frac{\rho_1 V_1^{\,2}}{2} \tag{4.85}$$

$$C_{entry} = 0.5(\rho_1/\rho_c)(A_1/A_c)^2$$

The pressure drop due to the abrupt air-heater exit is:

$$\Delta P_{exit} = \frac{(1 - A_c / A_1)^2 \rho_c V_c^2}{2} = C_{exit} \frac{\rho_1 V_1^2}{2} \tag{4.86}$$

$$C_{exit} = (1 - A_c / A_1)^2 (\rho_1 / \rho_c)(A_1 / A_2)^2$$

The second term (P_1 - P_2), is the pressure drop due to the resistance offered by the crop bed. The velocity of drying air through the crop mass is related to the pressure drop through it by the expression (Exell, 1980):

$$V_1 = c_1 \left(\frac{\Delta P_{bed}}{h_L} \right) \tag{4.87}$$

V_1 = the velocity of air entering and leaving the crop bed (m/s)

c_1 = empirical product-dependent constant.

The third term , (P_2 - P_3), is the total pressure drop within the stack above the drying bed. This pressure drop is made up of the change in kinetic energy between the two points (ΔP_{ke}), the pressure difference associated with the weight under gravity of the air between the two points (ΔP_{sw}), the pressure drop associated with the frictional losses (ΔP_{fch}), the pressure difference associated with the changes in the stack cross sectional area (ΔP_{xcs}) and the exit pressure loss term ($\Delta P_{exitchm}$). Therefore:

$$\Delta P_{ch} = \Delta P_{ke} + \Delta P_{sw} + \Delta P_{fch} + \Delta P_{cxs} + \Delta P_{cv} \tag{4.88}$$

where $\Delta P_{ke} = \frac{\rho_3 V_3^2}{2} - \frac{\rho_2 V_2^2}{2}$

The mass flow rate of air in the stack above the crop bed is assumed constant and can be expressed as follows:

$$\dot{m} = \rho_s A_s V_s = \rho_2 A_2 V_2 = \rho_3 A_3 V_3 \tag{4.89}$$

Upon substitution and simplification we obtain:

$$\Delta P_{ke} = \left(\frac{\rho_s}{\rho_3} (A_s / A_3)^2 - \frac{\rho_s}{\rho_2} (A_s / A_2)^2 \right) \frac{\rho_s V_s^2}{2} = K_{ke} \frac{\rho_s V_s^2}{2} \tag{4.90}$$

The static pressure difference is given by:

$$\Delta P_{sw} = \rho_s g H \tag{4.91}$$

where, H = overall height of the system (m)

ρ_s= average density of air in the chimney (kg/m^3)

The pressure difference associated with the chimney wall friction (ΔP_{fch}) is given as:

$$\Delta P_{fch} = \frac{4 f H_s \rho_s V_s^2}{2 d_{hch}} = K_{fch} \frac{\rho_s V_s^2}{2} \tag{4.92}$$

where, $K_{fch} = \dfrac{4 f H_s}{d_{hch}}$

H_s = height of stack portion above the crop bed / (m)

d_{hch} = hydraulic diameter of the chimney / (m)

f = friction factor = $0.079 \left(\dfrac{2\dot{m}}{(W + B)\rho_s \upsilon_s} \right)^{-0.25}$

The pressure loss due to the contraction of the outlet vent is given by:

$$\Delta P_{cv} = 0.5 \frac{\rho_3 V_3^2}{2} = K_{cv} \frac{\rho_s V_s^2}{2} \tag{4.93}$$

where C_c is the coefficient of contraction based on the vent area.

The pressure loss due to the contraction of the stack above the crop bed is given by:

$$\Delta P_{cxs} = \left(\frac{1}{C_c} - 1\right)^2 \frac{\rho_s V_s^2}{2} = K_{cxs} \frac{\rho_s V_s^2}{2} \tag{4.94}$$

The pressure difference between the outlet and the inlet levels (P_3 - P_a), is the static head pressure difference of the ambient air between the two points:

$$P_3 - P_a = \rho_o Hg \tag{4.95}$$

By substituting the relevant expressions into equation (4.77) we obtain the total pressure drop around the system as:

$$C_T \frac{\rho_1 V_1^2}{2} + h_L \left(\frac{V_1}{c_1}\right) + K_T \frac{\rho_s V_s^2}{2} = (\rho_0 - \rho_s) Hg \tag{4.96}$$

$$C_T \frac{\rho_1 V_1^2}{2} + h_L \left(\frac{V_1}{c_1}\right) = (\rho_0 - \rho_s) Hg - K_T \frac{\rho_s V_s^2}{2} \tag{4.97}$$

Equation (4.97) contains two different velocity terms (.i.e. V_1 and V_s) but it has been shown (Colborne and Moffat, 1959) that for a chimney operating under non-isothermal conditions the available draft, D_a, is related to the inlet conditions of the chimney by the relation:

$$D_a = Hg\Delta\rho_s - \frac{\Delta\rho_s}{\Delta\rho} \frac{\rho_1 V_1^2}{2} \tag{4.98}$$

By substituting the above expression for the available draft into equation (4.97) we obtain:

$$C_T \frac{\rho_1 V_1^2}{2} + h_L \left(\frac{V_1}{c_1}\right) + K_T \frac{\Delta\rho_s}{\Delta\rho} = Hg\Delta\rho_s \tag{4.99}$$

Equation (4.99) is rewritten in terms of the air mass flow through the system as

$$\frac{C_T}{2\rho_1 A_1^2}\dot{m}^2 + \frac{h_L}{c_1\rho_1 A_1}\dot{m} + \left(K_T\frac{\Delta\rho_s}{\Delta\rho} - Hg\Delta\rho_s\right) = 0 \qquad (4.100)$$

where $\Delta\rho_s = (\rho_o - \rho_s)$ (kg/m^3) and $\Delta\rho = (\rho_o - \rho_1)$ (kg/m^3).

4.2.8 Mean air temperature inside the chimney

The heated air rises in the chimney and escapes from the vent. The walls of the chimney absorb solar radiation. There is also loss of energy from the heated air in the chimney through its walls to the surrounding. A steady-state heat balance on a section of the chimney, as illustrated in fig. 4.4, gives:

$$\dot{m}C_a\left(T_{ch} - (T_{ch} + \frac{\partial T_{ch}}{\partial y}\delta y)\right) - PU_L(T_{ch} - T_a)\delta y + \alpha P\overline{H}_T\delta y = 0 \qquad (4.101)$$

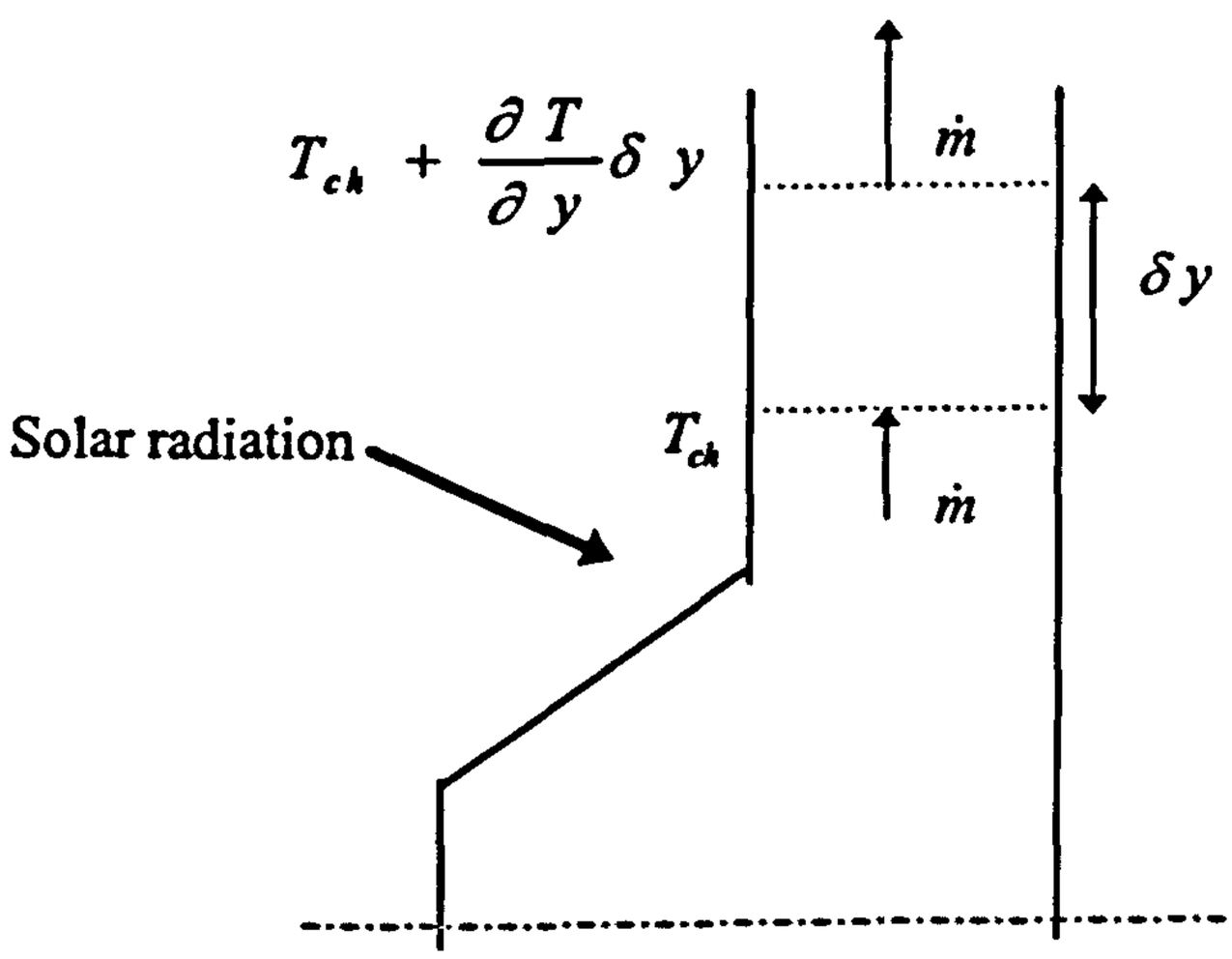

Figure 4.4: Temperatures and air mass flow in a chimney section of the MNCSCD

Rearranging, equation (4.101) gives a first-order differential equation in the form:

$$\frac{\partial T_{ch}}{\partial y} + RT_{ch} - (RT_a + R_1\overline{H}_T) = 0 \qquad (4.102)$$

Solving equation (4.102) the mean temperature distribution within the chimney is obtained as:

$$T_{ch} = T_a + \frac{R_1}{R}\overline{H}_T + \left(T_i - T_a - \frac{R_1}{R}\overline{H}_T\right)e^{-Ry} \qquad (4.103)$$

The mean air temperature within a chimney of height H_s is given by:

$$\overline{T}_{ch} = \frac{\int_0^{H_s} T_{ch}}{\int_0^{H_s} \partial y} \qquad (4.104)$$

Substituting for T_{ch} from equation (4.103) and integrating gives a mean temperature of

$$\overline{T}_{ch} = T_a + \frac{R_1}{R}\overline{H}_T + \frac{T_i - T_a - \frac{R_1}{R}\overline{H}_T}{RH_s}\left(1 - e^{-RH_s}\right) \qquad (4.105)$$

where, H_s = height of the stack portion above the crop bed / (m)

P = the perimeter of the chimney cross section/ (m)

U_L = is the overall heat transfer coefficient/ (W/m^2 K)

$R = \frac{PU_L}{\dot{m}C_a}$ and $R_1 = \frac{\alpha P}{\dot{m}C_a}$.

For steady-state heat transfer, the heat flowing from fluid A to the wall is equal to the heat flowing through the wall, which is also equal to the heat flowing from the wall to the fluid B. We therefore have:

$$\dot{q} = h_i(\overline{T}_{ch} - T_{wi}) = \frac{k}{x}(T_{wi} - T_a) \tag{4.106}$$

Rewriting these equations in terms of temperatures and adding corresponding sides of the three resulting equations, gives:

$$(\overline{T}_{ch} - T_{wi}) + (T_{wi} - T_a) = \dot{q}\left(\frac{1}{h_i} + \frac{x}{k}\right) \tag{4.107}$$

Equation (4.107) can be re-written as:

$$\dot{q} = U_L(\overline{T}_{ch} - T_a) \tag{4.108}$$

where,

$$U_L = \left(\frac{1}{h_i} + \frac{x}{k}\right)^{-1} \tag{4.109}$$

The heat transfer coefficient between a hot vertical wall at a temperature T_w and the surrounding fluid at temperature T_∞ can be evaluated from the expression (Cengel, 1998):

$$\mathrm{Nu} = \left\{0.825 + \frac{0.387\mathrm{Ra}^{1/6}}{(1 + [0.492/\mathrm{Pr}]^{9/16})^{8/27}}\right\}^2 \tag{4.110}$$

where, $\mathrm{Ra} = \dfrac{g\beta(T_w - T_\infty)\delta^3}{\upsilon^2}\mathrm{Pr}$

δ is characteristic length and is equal to the height of the vertical wall (m)

$\beta = \dfrac{1}{T_f}$

Equation (4.110) is valid for all Raleigh numbers. All properties of air are determined at the film temperature $T_f = (T_w + T_\infty)/2$. For air $\mathrm{Pr} \approx 0.709$, and therefore equation (4.110) simplifies to:

$$\mathrm{Nu} = \frac{h\delta}{k} = \left\{0.825 + 0.3244\mathrm{Ra}^{1/6}\right\}^2 \qquad (4.111)$$

4.2.9 Finite difference formulation of the drying simulation model.

The finite difference numerical technique is used to discretise the governing equations of the deep-bed drying mathematical model. A first-order implicit finite difference scheme (in both time and space), is employed to solve the governing equations described. The dependent variables (H and T) are to be evaluated at the time ($t + dt$). The independent variables (M and T_{pt}) are evaluated as the mean value of each layer representative of a given time interval. The following definitions are also applied in arriving at the finite difference model:

$$T_{z+\frac{1}{2}\Delta z,t+\Delta t} = \frac{T_{z+\Delta z,t+\Delta t} + T_{z,t+\Delta t}}{2} \qquad (4.112)$$

$$H_{z+\frac{1}{2}\Delta z,t+\Delta t} = \frac{H_{z+\Delta z,t+\Delta t} + H_{z,t+\Delta t}}{2} \qquad (4.113)$$

$$\frac{\partial M}{\partial t} = \frac{M_{z+1/2\Delta z,t+\Delta t} - M_{z+1/2\Delta z,t}}{\Delta t} \qquad (4.114)$$

$$\frac{\partial H}{\partial z} = \frac{H_{z+\Delta z,t+\Delta t} - H_{z,t+\Delta t}}{\Delta z} \qquad (4.115)$$

$$\overline{M} = M_{z+1/2\Delta z,t+\Delta t} \qquad (4.116)$$

$$\overline{T} = T_{z,t+\Delta t} + T_{z+\Delta z,\,t+\Delta t} \qquad (4.117)$$

Equations (4.63), (4.67), (4.70), and (4.73) can be written as

$$M_{z+1/2\Delta z,t+\Delta t} = M_e + (M_o - M_e)\frac{8}{\pi^2}\sum_{n=0}^{\infty}\frac{1}{(2n+1)^2}\exp\left[-(2n+1)^2 D\pi^2 t / z^2\right] \qquad (4.118)$$

$$H_{z+\Delta z,t+\Delta t} = H_{z,t+\Delta t} - \frac{\rho_p}{G_a}\frac{dz}{dt}\left(M_{z+\frac{1}{2}\Delta z,t+\Delta t} - M_{z+\frac{1}{2}\Delta z,t}\right) \qquad (4.119)$$

$$\frac{T_{z+\Delta z,t+\Delta t}-T_{z,t+\Delta t}}{dz}=\frac{1}{G_a\left(C_{pa}+C_{pw}H_{z+\frac{1}{2}\Delta z,t+\Delta t}\right)}\left[\begin{array}{l} h_v\left(T_{pt_{z+\frac{1}{2}\Delta z,t+\Delta t}}-T_{z+\frac{1}{2}\Delta z,t+\Delta t}\right)+ \\ \rho_p C_{pw}\left(T_{z+\frac{1}{2}\Delta z,t+\Delta t}-T_{pt_{z+\frac{1}{2}\Delta z,t+\Delta t}}\right)\left(\frac{\partial M}{\partial t}\right) \\ -\frac{h_v A_w}{A_p}\left(T_{z+\frac{1}{2}\Delta z,t+\Delta t}-T_w\right) \end{array}\right] \tag{4.120}$$

$$\begin{aligned} T_{pt_{z+\frac{1}{2}\Delta z,t+\Delta t}} &= T_{pt_{z+\frac{1}{2}\Delta z,t}}+[\{\alpha_p{}^{t}\tau_g\overline{H}/\cos\beta\}dt \\ &+G_a\Delta t/dz(H_{z+\Delta z,t}-H_{z,t})(L_g+C_{pl}(T_{pt_{z+\frac{1}{2}\Delta z,t}}-\frac{T_{z+\Delta z,t}+T_{z,t}}{2}))-\frac{h_{rws}A_w dt}{A_p}(T_w{}^4-T_s{}^4) \\ &-\frac{h_{rpw}A_w}{A_p}(T_{pt_{z+\frac{1}{2}\Delta z,t}}-T_w)+h_v dt(\frac{T_{z+\Delta z,t}+T_{z,t}}{2}-T_{pt_{z+\frac{1}{2}\Delta z,t}})-\frac{h_v A_w dt}{A_p}(\frac{T_{z+\Delta z,t}+T_{z,t}}{2}-T_w)] \\ &/(\rho_p C_{pg}+\rho_p C_{pl}M_{z+\frac{1}{2}\Delta z,t}+C''m'') \end{aligned} \tag{4.121}$$

Additionally, the relative humidity of the drying air is evaluated from the following expressions:

$$P_w=\frac{p(H_{z+\Delta z,t+\Delta t}+H_{z,t+\Delta t})/2}{(0.62198+\{H_{z+\Delta z,t+\Delta t}+H_{z,t+\Delta t}\}/2)} \tag{4.122}$$

$$P_{ws}=C_8/DTMT+C_9+C_{10}(DTMT)+C_{11}(DTMT)^2+C_{12}(DTMT)^3+C_{13}\ln(DTMT) \tag{4.123}$$

where, $DTMT=(T_{z+\Delta z,t+\Delta t}+T_{z,t+\Delta t})/2$

and, $RH=\frac{P_w}{P_{ws}}$.

The finite difference formulation of equations (4.64), (4.65) and (4.75) are obtained by replacing (M and T) by ($\overline{M}$ and $\overline{T}$) respectively.

4.2.10 Solution procedure

To solve equations (4.118), (4.119), (4.120) and (4.121), the finite difference model, the values of M, H, T and T_{pt} must be initialised at each position within the bed. First the following initial conditions are applied:

$$M_{z,0} = M_o \;;\; H_{z,0} = H_{\text{inlet}} \;;\; T_{z,0} = T_{\text{inlet}} \;;\quad T_{\text{pt,(z,0)}} = T_{\text{pt, initial}} \;;\quad \text{and} \quad T_{pt,(0,0)} = T_a.$$

Second, equations (4.118), (4.119), (4.120) and (4.121) are solved from the bottom elemental layer to the top layer of the crop bed. This then completes the initialisation process. The temperature of the material at the first time step is estimated as the average of the initial air and product temperature.

The discretised equations are solved as an uncoupled set. After the calculation of the first time step is completed, the following calculations are pursued until the required solution is achieved:

i) Guess the air mass flow rate, $\dot{m}_g$ through the system and the chimney wall temperature, T_{ch}.

ii) Using equations (4.100) and (4.105), the air mass flow rate, $\dot{m}$, through the system and the chimney wall temperature are estimated. The criterion of convergence of the form $|\dot{m} - \dot{m}_g| \leq 0.001$, is used to establish convergence of the air mass flow rate. Subsequently, this accepted air mass flow rate is used in estimating the chimney wall temperature. If the absolute value of the difference between the calculated value of the chimney wall temperature and the guessed value is less than 1 K, then convergence is established. Otherwise step (i) is revisited with last calculated values of $\dot{m}$ and T_{ch} as the guessed values.

iii) Progress the drying time from t to $t + dt$. The value of increment in time, dt , is calculated using equation (4.124).

iv) Solve equation (4.121) for temperature of the material at the current time.

v) Solve equation (4.118) for moisture content of the material.

vi) Solve equation (4.119) for relative humidity of the drying air.

vii) Solve equation (4.120) for the temperature of the air.

viii) Increase z by dz and repeat steps (iii) through to (vii) until the top layer is reached. Calculate the average moisture content, $\overline{M}$, of the entire crop bed after the time $(t + dt)$. Compare the average moisture content after time $(t + dt)$ with the desired moisture content, $\overline{M}_f$. The program is then terminated subject to the conditions for the termination of the program (see section 4.2.11). Otherwise you go back to step (ii) and then follow the subsequent steps through to step (vii).

The size of the increments dz and dt are critical since their choice will affect the stability of the solution procedure. Bakker-Arkema *et al* (1974) pointed out that if their values are too large, the equations will diverge from the true solution and if too small, the solution will require excessive computation time. To determine the expression for evaluating the time step the mass transfer terms in equations (4.71) and (4.72) are neglected. Furthermore, it is assumed that the change in temperature of the drying air is approximately equal to the change in the temperature of the product; then dividing equation (4.71) by (4.72) an approximate expression for evaluating the time step is obtained as:

$$dt \cong dx \frac{(\rho_p C_{pg} + \rho_p C_{pl} M + C'' m'')\cos\beta}{(G_a C_{pa} + G_a C_{pw} H)\alpha_g \tau_g \bar{H}_s} \qquad (4.124)$$

Equation 4.124 is used to evaluate the time step during the simulation run.

4.2.11 Program termination

The drying model terminates in one of the following ways:

(i) when a desired or specified drying time has been attained (in this programme the time should be less than 30 hours); and /or

(ii) when the average moisture content in the drying bed falls below a specified value.

4.3 Technical performance criteria model

In this model, the equations that allow for the thermodynamic assessment of the performance of the dryer are considered. For solar drying, three criteria have been defined (Brenndorfer *et al*, 1987): the system drying efficiency, the collector efficiency and the pick-up efficiency. However, to asses the effect of the inertia mass of the drying chamber on the performance of the system, another parameter the nocturnal moisture absorption or desorption index is introduced. These main performance characteristics evaluated are defined below.

4.3.1 The system drying efficiency, η_d

This parameter is defined as the ratio of the energy required to evaporate the moisture to the energy supplied to the dryer. The energy supplied to the dryer is the quantified as the solar energy incident on energy collection surfaces of the dryer over a given time interval. The system drying efficiency is a measure of the overall effectiveness of the system and is calculated from the following mathematical formula:

$$\eta_d = \frac{W_m L_t}{\overline{H}_T A_c t} \tag{4.125}$$

where, W_m (kg) is the mass of moisture evaporated in time t, L_t (J/kg) is the latent heat of evaporation of water from the product, $\overline{H}_T$ (W/m^2) is the insolation on the energy collection surfaces in a given time interval, A_c (m^2) is the effective energy collection area, and t (s) total drying time. Equation (4.125) is redefined in terms of the moisture content of the product as:

$$\eta_d = \frac{W_d (M_{i,db} - M_{f,db}) L_t}{\overline{H}_T A_c t} \tag{4.126}$$

It evident from equation (4.126) that for a given dryer, the load will have a significant effect on the drying efficiency. To isolate the effect of the initial crop mass on the drying efficiency, its value is normalised to obtain the normalised drying efficiency defined as:

$$\eta_{dN} = \frac{\eta_d}{W_d} \tag{4.127}$$

where W_d is the mass of dry matter (i.e. bone dry matter) in the initial crop mass. Equation (4.127) gives an indication of the efficiency of the drying system reckoned per mass of the crop.

4.3.2 The collector or air-heating efficiency η_c

This is a measure of how well the energy supplied to the air-heater is transferred to the air flowing through it. It is defined as the ratio of the heat received by the drying air to the solar energy incident on the air-heater in a given time interval and is calculated from the equation:

$$\eta_c = \frac{\dot{m}_1 C_{p,1}(T_{f,1o} - T_{f,1IN}) + \dot{m}_2 C_{p,2}(T_{f,2o} - T_{f,2IN})}{\overline{H}_T \times A_c} \tag{4.128}$$

Equation 4.128 is a definition and does not necessarily predict the performance of the air-heater. It must be noted that the conditions under which an air-heater operates affects the value of the collection efficiency significantly. The collector efficiency enables an assessment of the performance of the collector to be made.

4.3.3 The pick-up efficiency η_p

This parameter is used for evaluating the actual evaporation of moisture from the commodity inside the dryer. It is a direct measure of how efficiently the capacity of the (solar) heated air is utilised to dry a commodity, i.e. drying performance. The pick-up

efficiency is defined as the ratio of the moisture picked up by the air in the drying chamber to the theoretical capacity of the air to absorb moisture. Pick-up efficiency of 30 %, as an average over the whole drying period, is considered to be relatively good (Brenndorfer *et al*, 1987). The pick-up efficiency can be calculated from the formula:

$$\eta_p = \frac{W_o - W_t}{\dot{m}t(H_s^* - H_i)} \tag{4.129}$$

where, W_o (kg) is the initial mass of the commodity, W_t (kg) is the mass of the commodity at the time t, H_s^* (kg dry water/kg air) adiabatic saturation humidity of the air entering the drying chamber, H_i (kg dry water/kg air) is the absolute humidity of the ambient air (which is theoretically the same as the absolute humidity at the exit of the air-heater). The calculation of the pick-up efficiency necessitates the use of the psychrometric chart and or empirical relations to determine the adiabatic saturation humidity and the absolute humidity of the heated air at the inlet of drying chamber. On the psychrometric chart, the intercept of the ambient air vertical dry bulb temperature line and relative humidity defines the condition of the ambient air. Taking a horizontal line from this point to the absolute humidity axis enables the absolute humidity of the ambient air to be estimated. The saturation humidity of the heated at entry to the drying chamber is determined by following an adiabatic cooling line (line of constant enthalpy) to its intercept with the 100% saturation curve (wet-bulb temperature line).

Alternatively, the adiabatic saturation humidity is evaluated from the following expression:

$$H_s^* = \frac{H_i(2501 + 1.805\theta_i - 4.186\theta^*) + (\theta_i - \theta^*)}{2501 - 2.381\theta^*} \tag{4.130}$$

where, θ_i ($^\circ$C) is the dry-bulb temperature of air entering the drying chamber, and θ^* ($^\circ$C) is the wet-bulb temperature of the air entering the drying chamber. Combining equations (4.130) and (2.11), equation (4.129) is redefined as:

$$\eta_p = \frac{W_d(M_{i,db} - M_{t,db})(2501 - 2.381\theta_i^*)}{\dot{m}t(\theta_i - \theta_i^*)(1.805H_i + 1)} \tag{4.131}$$

The determination of the wet bulb-temperature of the heated air involves a try and error method. While equation (4.131) is to be used in mathematical models, equation (4.129) is easy to use in situations in which a physical experiment has been conducted.

4.3.4 The nocturnal moisture absorption or desorption index N_{arf}

The inertia mass of the drying chamber can be considered as a day-time heat sink and a night time heat source. By considering the weight loss or weight gain in the commodity being dried between sunset and sunrise, the preceding statement can be justified or refuted. The nocturnal moisture absorption or desorption index is defined as the ratio of the gain or loss of moisture between sunset and sunrise to the moisture content value at sunset of the preceding day. It is calculated from the relation:

$$N_{arf} = \frac{\Delta M}{M_{c,ss}} \tag{4.132}$$

where, ΔM is the nocturnal moisture loss and is given by

$$\Delta M = W_d(M_{d,ss} - M_{d,sr}) \tag{4.133}$$

$M_{d,ss}$ and $M_{s,sr}$ are the moisture contents (dry basis) of the product at sunset and sunrise, respectively. Positive values of N_{arf} indicate absorption of moisture while negative values indicate further moisture loss.

CHAPTER FIVE

EXPERIMENTAL RESULTS AND DISCUSSION

5.0 Introduction

In this chapter, the results from the experiments using the two physical dryers (i.e. the laboratory and the commercial-scale dryers) are presented and discussed under two sections. In section 5.1, the results of the experimental investigation of the small-scale laboratory dryer are presented and discussed while the results from field experiments using the commercial-scale dryer are presented and discussed in section 5.2.

5.1 Laboratory experiments: results and discussion

Laboratory experimental investigations of the small-scale dryer were conducted under no load (air-heater effect) and load conditions. The results and discussion are, therefore, presented under two subsections: subsection 5.1.1 is devoted for tests under no load; and subsection 5.1.2, for tests under load conditions. Though experimental results of a loaded dryer cannot be strictly compared with those of an unloaded dryer, nevertheless, the no-load tests conducted on the dryer enabled a choice to be made regarding the best positioning of the absorber plate of the SPDDSAH for optimal performance of the dryer.

5.1.1 Tests under no load conditions

Three tests (Tests 1, 2 and 3) were conducted under no load conditions. In test 1, the movable absorber plate of the SPDDSAH was suspended at a height of 55 mm from the base plate and 20 mm from the cover plate making the upper (top) channel flow duct of a cross-sectional area approximately 0.36 times that of the lower (bottom) channel. In tests 2 and 3, the absorber plate was suspended at heights of 36 and 17 mm respectively from the base plate, resulting in the upper channel duct having an area approximately 1.08 and 3.4 times that of the bottom channel.

An overview of the results of the tests are presented in Tables 5.1 to 5.3. The measured, and the calculated parameters presented in the tables are based on a constant or steady-state incident irradiation of 464 W/m^2 over the entire duration of the tests considered. For each test, the daily minimum, mean, maximum, and the standard deviation of the measured and calculated parameters listed below are presented: ambient air speed, temperature and relative humidity; the temperatures of the air-heater components (cover, absorber and base plates); the heated air temperature and velocity inside the heater; the air drying temperature inside the plenum; the air temperature in the drying chamber and the chimney; the relative air heating index; and the air-heater energy collection efficiency. A comparison of the overall performance of the dryer under no load conditions for the three tests is also provided in Table 5.4. Typical performance characteristics of the dryer under no load conditions, for three selected days, are illustrated in figs. 5.1 to 5.8. These graphs have been drawn for three representative experimental runs, one for each test, for the days during which each of the three experimental runs was conducted over the same length of time. The results for the other days follow the same trend.

As can be seen from Tables 5.1-5.3, the wind speeds recorded in the laboratory were extremely low; their values did not change appreciably with time. An average value of 0.01 m/s was consistently recorded, over the period of the tests, with a peak value of 0.02 m/s noted in all the tests (Table 5.4). A desirable implication of the lower prevailing wind speeds is the expected lower convective heat losses from the cover materials of the air-heater.

The diurnal variation in the ambient air temperature with time is shown in fig. 5.1. In test 1, an average ambient air temperature of 23.1° C was recorded under the laboratory conditions with the values ranging from 22 to 24.4° C. In test 2, average ambient air temperatures ranging from 24.4 to 28.7° C were recorded with a mean value of 27.3° C. A mean ambient air temperature of 26.9° C was observed in Test 3, against the minimum and maximum values of 23.1 and 29.2° C, respectively. Figure 5.2 demonstrates the variation of the ambient air relative humidity over the test period for the selected days. As depicted in fig. 5.2, comparatively higher ambient air relative humidity values were recorded during test 3. More precisely, their values ranged between 31.4 and 39.5% for test 1; 35.8 and 47.9% for test 2; and 35.1 and 56.6% for test 3, over the entire duration of the tests. The

mean ambient air relative humidity values recorded during tests 1, 2, and 3 were 36.7, 42.5 and 44.5%, respectively. The daily variations in the ambient air temperature and relative humidity over the test periods were generally small (Tables 5.1 to 5.3). Roughly, the prevailing laboratory ambient conditions in all the tests did not differ from their respective mean values by more than 1.96 of the corresponding standard deviation, with exception of test 3 in which the maximum relative humidity value differed from the mean by about 2.33 standard deviations (see Table 5.4). Following from these results, it can be concluded that the above laboratory experiments were conducted under a more controlled conditions compared to the fluctuations of the weather conditions outside. These observations coupled with the fact that the thermal capacitance of air is small confirm that transient analysis in the theoretical model formulated would not be essential.

The performance of a solar air-heater depends on the magnitude of the heat losses from the heater surfaces which is in turn dependent on the temperatures of the surface components. For instance, the principal heat loss, the cover heat loss, q_{lc}, may be quantified as:

$$q_{lc} = \sigma E_g (T_c^4 - T_s^4) + h_c (T_c - T_s) \qquad (5.1)$$

From equation (5.1) it is clear that if there is a reduction in the cover temperature there will be a corresponding reduction in the cover heat loss. Changes in the component temperatures of the air-heater can produce significant effects on its performance. Figure 5.3 illustrates the variation in the temperatures of the components of the air-heater for the selected typical runs. It can be seen from fig. 5.3, that the peak temperature difference for each of the components was less than 8° C. A similar trend of results was obtained on the other days (see Tables 5.1-5.3). For example in test 1, the average hourly values of the measured temperatures of the air-heater components over the test period, as can be seen in Table 5.4, were: mean absorber plate temperature, 55.8° C; mean cover plate temperature, 46.5° C; and mean base plate temperature, 27.2° C. Mean absorber plate temperature of 54° C was recorded in test 2, and the corresponding cover and base plate temperatures were 45.3° C and 29° C, respectively. In test 3, the average hourly values measured were: mean absorber plate temperature, 52.7° C; mean cover plate temperature, 44.3° C; and mean base plate temperature 33.0° C (Table 5.4). A comparison of the results show that, for a double duct air-heater of fixed overall width and depth, a decrease in the bottom channel depth in

relation to the top channel depth leads to a reduction in the cover plate temperature and a significant increase in bottom plate temperature with a corresponding drop in the absorber plate temperature. There is, in effect, a re-distribution of the available energy incident on the air-heater. A daily mean rise in the bottom plate temperature of 6.1° C over the ambient was noted in test 3 (Table 5.4 and Fig. 5.3), compared to the increments of 4.1 and 1.7° C realised in tests 1 and 2, respectively. The relative magnitude of the cover plate temperatures suggest that, the air-heater cover heat losses in test 3 would be lower than the losses experienced in test 2 which will in turn be lower than the heat losses in test 1. It is implicative from the results that increasing the temperature of the base plate with a corresponding reduction in the cover plate temperature might result in an improvement of the performance of the air-heater. It can be theorised from the above in support of previous experimental investigation on porous absorbers that a way of possibly further increasing the energy absorption capacity of the base plate with an attendant reduction in the absorber plate temperature of an SPDDSAH, is to consider replacing the conventional non-porous absorber plate with a blackened wire-screen of about 50% hole area; this way about half of the radiation would pass through the wire-screen and be absorbed at the lower surface of the bottom channel.

The variation in the drying air temperatures with time at the outlets from both the upper and lower channels of the air-heater, $T_{f,1}$ and $T_{f,2}$, respectively, are shown in fig. 5.4. Figure 5.4 shows that in test 1, there is significant rise in the drying air temperature at the outlet of the upper channel of between 25.2 and 26.1° C above that of the ambient, while the temperature elevations for the drying air in the bottom channel were remarkably minimal and in the range of 1.4 to 1.7° C. In test 2, the temperature elevation of the air in the upper channel ranged from 8.5 to 12.3° C, with a significant bottom channel temperature rise ranging between 5 and 6° C. The temperature elevations of the heated air in the upper channel recorded in test 3, was between 7 and 7.5° C and in the lower channel between 11.5 and 11.9° C. These results suggest that, for a given overall flow duct depth, as the channel flow area of any channel decreases relative to the other channel there is an increase in the temperature of air flowing through that channel. However, as can be seen from fig. 5.4, when the upper channel is made narrower relative to the lower channel, as in test 1, there is a significant increase in the temperature of drying air exiting that channel

compared with a similar situation in which the lower channel was made more narrower, as in test 3. The above general observation can be explained as follows: a decrease in the depth of a particular channel causes an increase in the resistance to the flow of air resulting in higher temperature of the air flowing through that channel. When the upper channel is made narrower compared to the situation in which the bottom channel is made narrower, the air stream in the top channel flows between two plates at relatively higher temperatures thus the convective heat transfer in the top channel is better than the other situation in which the air stream passing through the bottom channel contact plates at relatively lower temperatures.

A qualitative evaluation of the performance of an air-heater can be made by examining the mean temperature of the heated air at its outlet. For such purpose, the mean temperature of the heated-air in the base of the drying chamber (i.e. in the plenum) was measured. The mean plenum air temperature elevations (above the ambient air) recorded during the tests were 4.1, 5.4 and 10.8° C in tests 1, 2 and 3, respectively. The mean plenum air temperatures recorded in tests 1, 2, and 3 were, respectively, 27.1° C, 32.3° C and 37.4° C. These results of the drying air temperatures inside the plenum (fig. 5.4 and Table 5.4) showed that the performance of the air-heater was best when the suspended absorber plate was placed as near as possible to the bottom plate of the collector, i.e. to obtain an upper channel of larger airflow area compared to bottom flow duct. The effect of the reduced overall cover heat loss from the air-heater coupled with better convective and radiative heat exchanges between the air mass and the air-heater components could account for this observation.

The relative humidity of the drying air at the outlet of the air-heater was not measured because of limited access, instead its values were taken at the outlet of the chimney.
Figure 5.2 shows a diurnal variation in the heated air relative humidity at the outlet of the chimney. As can be seen from fig. 5.2, the relative magnitude of the reduction in the ambient relative humidity was more significant in test 3 compared to tests 1 and 2. A decrease in the mean air relative humidity of the order of 6.3% (below the mean ambient value) was obtained in test 3 compared to the values 3.2 and 4.7% recorded in tests 1 and 2, respectively (see Tables 5.1-5.3). A similar trend of results were recorded on the other days (Table 5.1-5.3).

The diurnal variations in the drying air flow rates at the outlets (upper and lower channels) of the air-heater are illustrated in fig. 5.5. Figure 5.5 shows that, when the top channel depth is made greater than the bottom channel, the air flow rate from the upper channel is higher than that from lower channel; the reverse phenomenon occurs when the bottom channel depth is made greater than the top channel depth. The mean hourly air flow rates recorded over the entire test period at the outlet of the upper channel in tests 1, 2, and 3 were: 0.18, 0.29 and 0.46 m/s, respectively; whereas values of 0.48, 0.29, and 0.13 m/s were obtained in the bottom channel for tests 1, 2, and 3, respectively (Table 5.4). As expected, the air mass flow rates and temperatures of the heated air at the heater outlet vary in inverse proportion (see Tabless 5.1 to 5.4).

The temperature profile along the axis of the drying chamber was obtained by measuring heated air temperature inside it at the middle and the top sections. Figure 5.6 shows the diurnal variation in the temperature profile measured at locations 180 mm and 220 mm inside the drying chamber from the base of the chamber. It is clear from fig. 5.6 that, the drying air temperature inside the drying chamber increases with increasing distance from the base of the drying chamber. In test 1, the mean temperature of the air inside the drying chamber was 36.4° C, with the values ranging between 34.8° C and 37.5° C, respectively. In test 2, the mean air temperature experienced inside the drying chamber was 37.1° C but a higher value of 40.2° C was recorded in test 3. The minimum and maximum drying air temperatures obtained inside the drying chamber were: 34.8 and 38.5° C, in test 2; and 38.6 and 41.5° C, in test 3. As can be observed in figs. 5.4 and 5.6, the chamber temperatures were generally higher than the plenum air temperatures. For instance, in test 1 the mean air temperature observed inside the drying chamber over the duration of the test was 8.9° C above the average temperature of air inside the plenum. In tests 2 and 3, drying air temperatures recorded inside the drying chamber were above the plenum air temperatures by 5.3 and 2.9° C, respectively. This behaviour, generally, arises because as the air progresses through the chamber it absorbs further energy from radiant energy incident on the transparent chamber thus increasing its temperature over that in the plenum.

Typical diurnal variations in the air temperatures measured at the lower and the middle section inside the chimney under no-load conditions are illustrated in fig. 5.7. It is seen that higher chimney air temperatures were recorded in test 3 compared to tests 1 and 2. For

instance in test 3, typical values of peak chimney air temperatures were between 31.3 and 36.6° C compared with ambient temperatures ranging from 23.1 to 29.2° C (Table 5.3). Corresponding peak temperature elevations above the ambient air temperatures were between 9.6 and 10.7° C, approximately. However, no significant temperature rise was recorded across the chimney in each of the tests; the curves for the temperatures recorded in the middle and lower portions of the chimney nearly coincided for all the tests. Temperature differences of less than 1° C were recorded in all the tests (Tables 5.1 to 5.3).

A comparison between the air temperatures recorded inside the drying chamber and the chimney (figs. 5.6 and 5.7) shows that the chimney temperatures were consistently lower than the chamber temperatures because of higher heat losses from the chimney. For drying purposes, this is desirable since the moisture absorbed by the air during the drying will lower the chamber air temperature. Mean temperature differences between the chamber and chimney of the order 0.2, 0.2 and 5.7° C were recorded in tests 1, 2 and 3, respectively. The results possibly suggest that the solar chimney does not possibly collect substantial radiant energy compared to the drying chamber and therefore no appreciable heating of the air column takes place within the chimney. Hence, as the air progresses through the chimney its temperature is not further increased, rather the air loses energy to its surroundings through friction. Since radiant energy is transmitted through the walls of the chimney; the inclusion of additional absorbing surfaces within the transparent chimney may further improve the performance of the solar chimney. This way the convective and the radiative heat exchange between the air and the absorbing surfaces inside the chimney will be further enhanced and thereby increasing the chimney air temperatures. The chimney air temperature elevation above ambient air temperature can be used as an index for evaluating the performance of the solar chimney in enhancing the air mass flow rate through the system. The mean chimney temperature elevation above the ambient recorded during the tests were 12.8, 10.5 and 8.0° C in tests 1, 2 and 3, respectively. This observation, explains the relatively higher air mass flow rates of 0.0174 kg/s recorded at the outlet of the air-heater in test 1, compared to the values of 0.0126 and 0.0155 kg/s obtained during tests 2 and 3.

The overall performance of three configurations of the air-heater was assessed from the energy collection efficiency values calculated using equation (4.128) on the basis of the

ratio of energy absorbed by the drying as it flows through the air-heater to amount of radiation incident on the absorber surface over a period of time. Figure 5.8 shows the typical diurnal variations in the cumulative energy collection efficiencies of the air as it progresses through the air-heater. The calculated efficiency values were in the range of 40.5-54% with an average value 48.3% for test 1 compared with values in the range of 51.1-67.9% with an average of 63.5% for test 2 (Tables 5.1 and 5.2). In test 3, the efficiency values ranged between 69.2 and 73.1% with an average value of 71%. The values of the collector efficiency obtained in test 3 compare very well with the instantaneous optimum efficiency, $\eta_{c,\max}$, of an air-heater which is given by the product of the effective transmissivity of the cover plate(s) and the absorptance of the absorber plate. The value of the mean energy collection efficiency obtained in test 3 compares very well with the optimum value of 82% for the air-heater obtained from theoretical considerations using equation (2.127). This supports an earlier inference from the low wind speeds recorded that, convective heat loss from the cover materials of the air-heater was expected to be minimal. In comparison with the optimum expected efficiency of the air-heater for the material used, the relatively higher values of the air-heater energy collection efficiency values of 40.5-73.1% recorded for the three configuration of the SPDDSAH illustrates the effectiveness of the air-heater employed in this study and the choice for a SPDDSAH in preference to SPRDAH or SPFDAH.

Generally, the results indicate that as a result of the incident energy gains through the walls and the structural members inside the drying chamber, the drying air gets heated up as it flows through it. The mean temperature of the air inside the chimney, under no load conditions, remained almost the same throughout the system. The most important conclusion that can be drawn from Tables 5.1-5.4 and figs. 5.1 through 5.8 is that, it would be desirable to design a SPDDSAH making the airflow passages of the bottom channel with smaller cross-sectional area than that of the upper channel. This geometry increases the heat collection capacity of the air stream as it flows through the heater; it also results in a significant drop in the relative humidity of the heated air compared to the other options. The above experimental results pinpoints the superiority of using a SPDDSAH type with air flow ducts of narrower lower channel and wider top channel.

Table 5.1: Overview of daily results for laboratory test 1 (No load test with absorber plate of air-heater located at 55 mm from the base plate)

	TEST 1		
Measured and calculated performance parameters	DAY 1	DAY 2	DAY 3
Duration of test (h)	6	5	7
Minimum ambient air velocity (m/s)	0.01	0.01	0.01
Mean ambient air velocity (m/s)	0.01	0.01	0.01
Maximum ambient air velocity (m/s)	0.02	0.02	0.02
Min. ambient air relative humidity (%)	37.10	31.40	37.2
Mean ambient air relative humidity (%)	38.30	33.0	38.20
Max. ambient air relative humidity (%)	39.20	34.00	39.5
Ambient air relative humidity (Std.) (%)	0.704	1.06	0.665
Minimum ambient air temperature (° C)	21.9	22	22
Mean ambient air temperature (° C)	23.1	22.4	23.4
Maximum ambient air temperature (° C)	24.3	22.8	24.4
Ambient air temperature (Std.) (° C)	0.75	0.31	0.79
Minimum glazing temperature (° C)	44.95	44.28	44.95
Mean glazing temperature (° C)	46.75	45.46	46.92
Maximum glazing temperature (° C)	47.87	45.95	47.91
Glazing temperature (Std.) (° C)	0.95	0.66	0.97
Minimum absorber plate temperature (° C)	54.43	53.38	54.45
Mean absorber plate temperature (° C)	56.08	54.93	56.24
Maximum absorber plate temperature (° C)	57	55.58	57.1
Absorber plate temperature (Std.) (° C)	0.87	0.84	0.87
Minimum bottom plate temperature (° C)	26.20	25.18	25.79
Mean bottom plate temperature (° C)	27.45	26.15	27.65
Maximum bottom plate temperature (° C)	28.61	26.72	28.7
Bottom plate temperature (Std.) (° C) (° C)	0.76	0.58	0.96
Minimum heated air temperature (Upper) (° C)	45.2	47.7	47.35
Mean heated air temperature, Upper (° C)	46.10	48.11	49.31
Maximum heated air temperature, Upper (° C)	47.1	48.63	50.5
Heated air temperature (Std.) (° C)	0.90	0.43	0.98
Minimum heated air flow velocity (Upper) (° C)	0.16	0.18	0.16
Mean heated air flow velocity (Upper) (° C)	0.18	0.18	0.17
Maximum heated air flow velocity (Upper) (° C)	0.2	0.2	0.18
Heated air flow velocity (Std. Upper) (° C)	0.016	0.015	0.009
Minimum heated air temperature (Lower) (° C)	23.66	23	23.66
Mean heated air temperature (Lower) (° C)	24.9	23.39	25.08
Maximum heated air temp. (Lower) (° C)	26.04	23.87	26.14
Heated air temp. (Std) (Lower) (° C)	0.81	0.40	0.87
Minimum heated air flow velocity (Lower) (m/s)	0.48	0.50	0.48
Mean heated air flow velocity (Lower) (m/s)	0.56	0.54	0.56
Maximum heated air flow velocity (Lower) (m/s)	0.65	0.55	0.65
Heated air flow velocity (Std. Lower) (m/s)	0.06	0.02	0.06
Min. average heated air temp. (Overall) (° C)	25.8	24.6	25.8
Mean-Ave. heated air temp. (Overall) (° C)	27.48	25.92	27.7
Max.-average heated air temperature (O) (° C)	28.9	26.5	29
Average heated air temperature (Std.) (° C)	0.93	0.72	1.01
Minimum chimney air temperature (° C)	34.75	33.25	34.75
Mean chimney air temperature (° C)	36.17	34.55	36.36
Maximum chimney air temperature (° C)	37.5	35	37.5
Chimney air temperature (Std) (° C)	0.75	0.68	1.00

Table 5.1: continued.

Measured and calculated performance parameters	DAY 1	DAY 2	DAY 3
Min. air relative humidity at chimney outlet (%)	34.6	30.1	34.6
Mean air relative humidity at chimney outlet (%)	34.95	30.42	34.99
Max. air relative humidity at chimney outlet (%)	38.40	33	39.4
Minimum relative heating index (Upper)	0.396	0.40	0.395
Mean relative heating index(Upper)	0.406	0.403	0.407
Maximum relative heating index(Upper)	0.41	0.407	0.412
Relative heating air index (Std)	0.005	0.004	0.005
Min. relative heating index (Lower)	0.023	0.009	0.021
Mean relative heating index(Lower)	0.025	0.014	0.026
Max. relative heating index (Lower)	0.027	0.017	0.027
Relative heating air index (Std)	0.002	0.003	0.002
Minimum-average relative heating index	0.210	0.204	0.208
Mean-average relative heating index	0.216	0.209	0.216
Maximum-average relative heating index	0.218	0.212	0.219
Relative heating index (Std.)	0.003	0.003	0.003
Minimum air temp. inside drying chamber (° C)	34.8	33.6	34.8
Mean air temp. inside drying chamber (° C)	36.38	34.78	36.56
Maximum air temp. inside drying chamber (° C)	37.5	35.3	37.6
Average air temp. in drying chamber (Std.) (° C)	0.90	0.66	0.94
Minimum exit air temperature (° C)	25.90	25.3	25.90
Mean exit air temperature (° C)	26.98	26.68	27.4
Maximum exit air temperature (° C)	27.80	29.70	27.80
Exit air temperature (Std.) (° C)	0.65	1.61	0.62
Minimum air mass flow rate (kg/s)	0.0159	0.0165	0.0160
Mean air mass flow rate (kg/s)	0.0164	0.0179	0.0184
Maximum air mass flow rate (kg/s)	0.021	0.0184	0.0207
Air mass flow rate (kg/s)	0.0018	0.0072	0.0016
Minimum drying air temp. rise (Upper) (° C)	25.15	25.29	25.05
Mean drying air temperature rise (Upper) (° C)	25.80	25.61	25.85
Maximum drying air temp. rise (Upper) (° C)	26.05	25.83	26.15
Drying air temperature rise (Std. Upper) (° C)	0.32	0.23	0.35
Min. drying air temperature rise (Lower) (° C)	1.4	0.6	1.36
Mean drying air temperature rise (Lower) (° C)	1.6	0.89	1.62
Maximum drying air temp. rise (Lower) (° C)	1.74	1.07	1.74
Drying air temp. rise (Std. Lower) (° C)	0.12	0.199	0.122
Minimum collector efficiency.(Overall) (%)	40.51	37.12	41.11
Mean collector efficiency(Overall) (%)	48.31	40.63	47.34
Maximum collector efficiency (Overall) (%)	53.95	45.71	50.52
Collector efficiency (Std.) (%)	5.35	3.13	3.53

Table 5.2: Overview of daily results for laboratory test 2 (No load test with absorber plate of air-heater located at 36 mm from the base plate)

	TEST 2		
Measured and calculated performance parameters	DAY 1	DAY 2	DAY 3
Duration of test (hours)	6	7	7
Minimum ambient air speed (m/s)	0.01	0.01	0.01
Mean ambient air speed (m/s)	0.01	0.01	0.011
Maximum ambient air speed (m/s)	0.02	0.02	0.02
Min. ambient air relative. humidity (%)	35.8	45	37.5
Mean ambient air relative. humidity (%)	40.5	45.78	41.08
Max. ambient air relative. humidity (%)	47.9	45.8	45
Ambient air relative. humidity(Std.)	3.83	0.506	2.68
Min. ambient air temperature (° C)	24.4	24.5	24.1
Mean ambient air temperature (° C)	27.09	27.14	26.98
Max. ambient air temperature (° C)	28.3	28.2	27.7
Ambient air temperature (Std.) (° C)	1.03	0.63	0.50
Min. glazing temperature (° C)	39.15	44.45	44.23
Mean glazing temperature (° C)	44.82	45.87	44.99
Max. glazing temperature (° C)	46.98	46.67	45.99
Glazing temperature (Std.) (° C)	2.59	0.69	0.66
Min. absorber plate temp. (° C)	52	53.00	51.58
Mean absorber plate temp. (° C)	54.5	54.54	52.97
Max. absorber plate temp. (° C)	55.46	55.21	54.40
Absorber plate temp. (Std.) (° C)	1.21	0.70	1.07
Min. bottom plate temp. (° C)	27.1	28.32	27.89
Mean bottom plate temp. (° C)	28.96	29.67	28.44
Max. bottom plate temp. (° C)	30.0	30.44	29.43
Bottom plate temp.(Std.) (° C)	0.95	0.66	0.56
Min. heated air temp. (Upper) (° C)	34	37.67	36.65
Mean heated air temp. (Upper) (° C)	38.87	38.43	37.44
Max. heated air temp.(Upper) (° C)	40.35	38.87	38.16
Heated air temperature (Std.) (° C)	2.19	0.45	0.53
Min. heated air flow velocity(Upper) (° C)	0.27	0.28	0.3
Mean heated airflow velocity (Upper) (° C)	0.28	0.29	0.31
Max. heated air flow velocity (Upper) (° C)	0.29	0.31	0.32
Heated air flow velocity (Std. Upper) (° C)	0.006	0.01	0.006
Min. heated air temp. (Lower) (° C)	30.5	32.71	32.6
Mean heated air temp. (Lower) (° C)	33.17	33.65	33.03
Max. heated air temp. (Lower) (° C)	34.29	34.4	33.51
Heated air temp. (Std. (Lower) (° C)	1.26	0.48	0.31
Min. heated air flow velocity (Lower) (° C)	0.29	0.30	0.33
Mean heated airflow velocity(Lower) (° C)	0.30	0.31	0.33
Max. heated airflow velocity (Lower) (° C)	0.31	0.32	0.34
Heated air flow velocity (Std. Lower) (° C)	0.007	0.008	0.005
Min. Ave. heated air temp.(Overall) (° C)	30	31.5	31.2
Mean-Ave. heated air temp.(Overall) (° C)	31.87	32.94	31.99
Max.-average heated air temperature, (O)	33	33.5	33
Average heated air temp.(Std.) (° C)	1.07	0.61	0.56
Min. chimney air temp. (° C)	35.75	35.5	35.75
Mean chimney air temp. (° C)	37.43	37.54	37.39
Max. chimney air temp. (° C)	38.75	38.75	38.7
Chimney air temp. (Std) (° C)	0.99	1.00	0.92

Table 5.2: continued.

Measured and calculated performance parameters	TEST 2		
	DAY 1	DAY 2	DAY 3
Min. air relative humidity at chimney outlet (%)	32.8	36	32.8
Mean air relative humidity at chimney outlet (%)	35.83	38.86	36.37
Max. air relative humidity at chimney outlet (%)	47.9	47.7	42
Min. relative heating index (Upper)	0.134	0.165	0.163
Mean relative heating index(Upper)	0.179	0.172	0.165
Max. relative heating index(Upper)	0.193	0.177	0.168
Relative heating air index (Std)	0.020	0.004	0.001
Min. relative heating index (Lower)	0.070	0.085	0.092
Mean relative heating index(Lower)	0.089	0.097	0.096
Max. relative heating index (Lower)	0.095	0.101	0.102
Relative heating air index (Std)	0.011	0.006	0.003
Min.-average relative heating index	0.106	0.125	0.128
Mean-average relative heating index	0.135	0.134	0.131
Max.-average relative heating index	0.149	0.140	0.134
Relative heating index (Std.)	0.013	0.005	0.002
Minimum air mass flow rate (kg/s)	0.0111	0.0112	0.0123
Mean air mass flow rate (kg/s)	0.0123	0.0126	0.0126
Maximum air mass flow rate (kg/s)	0.0136	0.0128	0.0129
Air mass flow rate (std)	0.0002	0.0003	0.0002
Min. air temp. inside drying chamber (° C)	34.8	36	36
Mean air temp. inside drying chamber	37.08	39.28	38.76
Max. air temp. inside drying chamber (° C)	38.5	41	41
Average air temp. in drying chamber (Std.)	1.22	1.63	1.77
Min. exit air temperature (° C)	31.5	30.9	30.7
Mean exit air temperature (° C)	33.1	31.68	31.47
Max. exit air temperature (° C)	35.4	32.9	32.8
Exit air temperature (Std.) (° C)	1.41	0.85	0.77
Min. drying air temperature rise (Upper) (° C)	8.5	10.5	10.38
Mean drying air temperature rise (Upper) (° C)	11.34	10.92	10.51
Max. drying air temperature rise (Upper) (° C)	12.25	11.27	10.66
Drying air temperature rise (Std. Upper) (° C)	1.28	0.23	0.09
Min. drying air temperature (Lower) (° C)	5.0	5.4	5.81
Mean drying air temperature rise (Lower) (° C)	5.63	6.13	6.10
Max. drying air temperature rise (Lower) (° C)	6.01	6.61	6.5
Drying air temp. rise (Std. Lower) (° C)	0.38	0.40	0.21
Min. collector efficiency (Overall) (%)	51.13	63.76	67.02
Mean collector efficiency (Overall) (%)	63.50	66.06	68.88
Max. collector efficiency (Overall) (%)	67.91	70.48	70.99
Collector efficiency (Std.) (%)	5.73	2.19	1.17

Table 5.3: Overview of daily results for laboratory test 3 (No load test with absorber plate of air-heater located at 17 mm from the base plate)

	TEST 3			
Measured and calculated performance parameters	DAY 1	DAY 2	DAY 3	DAY 4
Duration of test (h)	6	7	7	5
Minimum air flow velocity (m/s)	0.01	0.01	0.01	0.01
Mean air flow velocity (m/s)	0.01	0.01	0.01	0.01
Maximum air flow velocity (m/s)	0.02	0.01	0.02	0.02
Min. ambient air relative humidity (%)	43.2	38.1	35.1	45.5
Mean ambient air relative humidity (%)	45.3	45.1	37.6	50.1
Max. ambient air relative humidity (%)	51.2	54	41.9	56.6
Ambient air relative humidity(Std.) (%)	2.61	4.87	2.13	4.20
Min. ambient air temperature (° C)	25	25	25.6	23.1
Mean ambient air temperature (° C)	26.86	27.24	27.2	24.5
Max. ambient air temperature (° C)	28.3	29.2	28	25.8
Ambient air temperature (Std.) (° C)	0.90	1.23	0.68	0.83
Min. glazing temperature (° C)	43.4	43.5	42.6	40.6
Mean glazing temperature (° C)	45.3	45.13	44.43	41.94
Max. glazing temperature (° C)	46.8	46.7	45.3	42.8
Glazing temperature (Std.) (° C)	1.11	0.95	0.91	0.80
Min. absorber plate temperature (° C)	50.8	52.2	51.5	49.6
Mean absorber plate temperature (° C)	52.55	53.77	53.31	50.7
Max. absorber plate temperature (° C)	54.0	55.3	54.2	51.4
Absorber plate temperature (Std.) (° C)	1.02	0.87	0.87	0.63
Min. bottom plate temperature (° C)	31.5	32.7	30.8	30
Mean bottom plate temperature (° C)	33.08	33.88	33.51	30.74
Max. bottom plate temperature (° C)	34.2	34.8	34.4	31.3
Bottom plate temperature (Std.) (° C)	0.88	0.62	1.20	0.48
Min. heated air temperature (Upper) (° C)	33.2	32.8	33.3	30
Mean heated air temperature (Upper) (° C)	34.47	34.27	33.64	31.1
Max. heated air temp.(Upper) (° C)	35.8	35.6	34.3	32
Heated air temperature (Std.) (° C)	0.84	0.85	0.43	0.73
Min. heated air flow velocity (Upper) (m/s)	0.4	0.38	0.45	0.45
Mean heated air flow velocity (Upper) (m/s)	0.42	0.47	0.48	0.47
Max. heated air flow velocity (Upper) (m/s)	0.44	0.5	0.50	0.5
Heated air flow velocity (Std., Upper) (m/s)	0.014	0.04	0.02	0.02
Min. heated air temperature (Lower) (° C)	37.2	37.1	34.3	34.2
Mean heated air temperature (Lower) (° C)	38.87	38.37	37.86	35.16
Max. heated air temperature (Lower) (° C)	40	39.4	39	35.8
Heated air temperature (Std., Lower) (° C)	0.90	0.68	1.52	0.57
Min. heated air flow velocity (Lower) (m/s)	0.14	0.13	0.15	0.15
Mean heated air flow velocity (Lower) (m/s)	0.15	0.17	0.18	0.17
Max. heated air flow velocity (Lower) (m/s)	0.16	0.20	0.20	0.18
Heated air flow velocity (Std., (Lower) (m/s)	0.01	0.02	0.02	0.02
Min. average heated air temp.(Overall) (° C)	35.4	37.5	37.2	34
Mean-Ave. heated air temp. (Overall) (° C)	37.1	38.5	37.99	35.18
Max.-average heated air temp. (Overall) (° C)	38.5	39.6	38.6	35.8
Average heated air temperature (Std.) (° C)	1.00	0.64	0.54	0.69
Min. chimney air temperature(° C)	33.3	34.9	33.8	31.3
Mean chimney air temperature(° C)	34.55	35.73	34.83	32.48
Max. chimney air temperature(° C)	35.6	36.6	35.2	33.3
Chimney air temperature (Std) (° C)	0.71	0.53	0.44	0.74

Table 5.3: continued

Measured and calculated performance parameters	TEST 3			
	DAY 1	DAY 2	DAY 3	DAY 4
Min. air relative humidity at chimney outlet (%)	37.80	33.40	29.8	40.0
Mean air relative humidity at chimney outlet (%)	39.81	35.47	32.23	42.24
Max. air relative humidity at chimney outlet (%)	51.20	50.6	42	56.70
Min. relative heating index (Upper)	0.11	0.10	0.085	0.097
Mean relative heating index (Upper)	0.11	0.11	0.098	0.098
Max. relative heating index (Upper)	0.12	0.12	0.11	0.102
Relative heating air index (Std)	0.004	0.006	0.01	0.004
Min. relative heating index (Lower)	0.181	0.161	0.126	0.154
Mean relative heating index (Lower)	0.184	0.170	0.164	0.163
Max. relative heating index (Lower)	0.187	0.187	0.176	0.170
Relative heating air index (Std)	0.002	0.008	0.016	0.005
Min.-average relative heating index	0.146	0.131	0.118	0.124
Mean-average relative heating index	0.149	0.138	0.131	0.131
Max.-average relative heating index	0.153	0.154	0.137	0.136
Relative heating index (Std.)	0.002	0.007	0.006	0.004
Minimum air mass flow rate (kg/s)	0.0135	0.0127	0.0127	0.0150
Mean air mass flow rate (kg/s)	0.0139	0.0157	0.0157	0.0162
Maximum air mass flow rate (kg/s)	0.0141	0.0168	0.0166	0.0169
Air mass flow rate (std) (kg/s)	0.0004	0.0013	0.0013	0.0006
Min. air temp. inside drying chamber(° C)	38.6	40	40	37
Mean air temp. inside drying chamber(° C)	40.18	41.33	40.84	38.14
Max. air temp. inside drying chamber(° C)	41.5	42.7	41.5	38.8
Average air temp. in drying chamber (Std.) (° C)	0.95	0.80	0.54	0.67
Min. exit air temperature(° C)	29.5	30.8	29.5	27.1
Mean exit air temperature(° C)	30.37	31.68	30.47	28.90
Max. exit air temperature(° C)	31.1	32.7	31.8	29.8
Exit air temperature (Std.) (° C)	0.52	0.60	0.64	1.12
Min. drying air temperature rise (Upper) (° C)	7	6.4	5.4	5.9
Mean drying air temperature rise (Upper) (° C)	7.3	6.71	6.21	6.26
Max. drying air temperature rise (Upper) (° C)	7.5	7.6	7	6.5
Drying air temperature rise (Std., Upper) (° C)	0.24	0.38	0.44	0.22
Min. drying air temperature (Lower) (° C)	11.5	10.2	8.0	9.8
Mean drying air temperature rise (Lower) (° C)	11.67	10.8	10.42	10.32
Max. drying air temperature rise (Lower) (° C)	11.9	11.9	11.2	10.8
Drying air temperature rise (Std., Lower) (° C)	0.13	0.53	1.02	0.32
Min. collector efficiency (Overall) (%)	69.22	67.4	66.1	69.2
Mean collector efficiency (Overall) (%)	71.02	73.58	71.30	70.31
Max. collector efficiency (Overall) (%)	73.1	77.47	77.17	76.67
Collector efficiency (Std.) (%)	1.15	3.21	3.34	3.37

Table 5.4: Comparison of the mean daily results for laboratory tests 1, 2, and 3

Measured and calculated performance parameters	TEST 1	TEST 2	TEST 3
Minimum air flow velocity (m/s)	0.01	0.01	0.01
Mean air flow velocity (m/s)	0.01	0.01	0.01
Maximum air flow velocity (m/s)	0.02	0.02	0.02
Min. ambient air relative. humidity (%)	31.40	35.8	35.1
Mean ambient air relative. humidity (%)	36.68	42.54	44.5
Max. ambient air relative. humidity (%)	39.5	47.9	56.6
Ambient air relative. humidity(Std.) (%)	2.59	3.71	5.66
Min. ambient air temperature (° C)	21.9	25.5	23.1
Mean ambient air temperature (° C)	23.0	26.93	26.58
Max. ambient air temperature (° C)	24.4	28.2	29.2
Ambient air temperature (Std.) (° C)	0.79	0.85	1.40
Min. glazing temperature (° C)	44.28	39.15	40.6
Mean glazing temperature (° C)	46.45	45.25	44.34
Max. glazing temperature (° C)	47.91	46.98	46.8
Glazing temperature (Std.) (° C)	1.08	1.60	1.57
Min. absorber plate temperature (° C)	53.38	51.58	50.8
Mean absorber plate temperature (° C)	55.82	53.97	52.74
Max. absorber plate temperature (° C)	57.1	55.46	55.3
Absorber plate temperature (Std.) (° C)	1.02	1.25	1.41
Min. bottom plate temperature (° C)	25.18	27.1	30
Mean bottom plate temperature (° C)	27.17	29.03	32.96
Max. bottom plate temperature (° C)	28.7	30.44	34.8
Bottom plate temperature (Std.) (° C)	1.02	0.90	1.43
Min. heated air temperature (Upper) (° C)	45.20	34	30
Mean heated air temperature (Upper) (° C)	47.90	38.21	33.51
Max. heated air temperature (Upper) (° C)	50.5	40.35	35.8
Heated air temperature (Std.) (° C)	0.98	1.40	1.44
Min. heated air flow velocity (Upper) (° C)	0.16	0.27	0.38
Mean heated air flow velocity (Upper) (° C)	0.178	0.294	0.46
Max. heated air flow velocity (Upper) (° C)	0.2	0.32	0.50
Heated air flow velocity (Std. Upper) (° C)	0.014	0.014	0.04
Min. heated air temperature (Lower) (° C)	23	30.5	34.2
Mean heated air temperature (Lower) (° C)	23.39	33.29	37.7
Max. heated air temperature (Lower) (° C)	24.55	34.4	40
Heated air temperature (Std., Lower) (° C)	1.04	0.82	1.67
Min. heated air flow velocity (Lower) (m/s)	0.48	0.29	0.13
Mean heated air flow velocity (Lower) (m/s)	0.56	0.317	0.17
Max. heated air flow velocity (Lower) (m/s)	0.65	0.34	0.20
Heated air flow velocity (Std., Lower) (m/s)	0.051	0.015	0.018
Min. average heated air temp. (Overall) (° C)	24.6	30	34
Mean-average heated air temp. (Overall) (° C)	27.13	32.29	37.36
Max.-average heated air temp. (Overall) (° C)	29	33.5	39.6
Average heated air temperature (Std.) (° C)	1.18	0.91	1.40
Min. chimney air temperature (° C)	33.25	35.75	31.3
Mean chimney air temperature (° C)	35.79	37.45	34.54
Max. chimney air temperature (° C)	37.5	38.75	36.6
Chimney air temperature (Std) (° C)	1.19	0.98	1.27

Table 5.4: Continued.

Measured and calculated performance parameters	TEST 1	TEST 2	TEST 3
Min. air relative humidity at chimney outlet (%)	30.10	32.8	29.80
Mean air relative humidity at chimney outlet (%)	36.68	35.83	36.96
Max. air relative humidity at chimney outlet (%)	39.40	47.9	56.70
Min. relative heating index (Upper)	0.395	0.134	0.085
Mean relative heating index (Upper)	0.406	0.172	0.104
Max. relative heating index (Upper)	0.412	0.172	0.12
Relative heating air index (Std.)	0.005	0.014	0.008
Min. relative heating index (Lower)	0.009	0.070	0.126
Mean relative heating index (Lower)	0.022	0.094	0.137
Max. relative heating index (Lower)	0.027	0.102	0.154
Relative heating air index (Std)	0.006	0.008	0.009
Min.-average relative heating index	0.08	0.10	0.31
Mean-average relative heating index	0.125	0.156	0.33
Max.-average relative heating index	0.15	0.19	0.39
Relative heating index (Std.)	0.005	0.009	0.009
Minimum air mass flow rate (kg/s)	0.0159	0.0111	0.0127
Mean air mass flow rate (kg/s)	0.0174	0.0126	0.0155
Maximum air mass flow rate (kg/s)	0.021	0.0129	0.0169
Air mass flow rate (std) (kg/s)	0.0015	0.0003	0.0017
Min. air temp. inside drying chamber (° C)	33.6	32.5	37
Mean air temp. inside drying chamber (° C)	36.00	37.62	40.28
Max. air temp. inside drying chamber (° C)	37.6	41	42.7
Average air temp. in drying chamber (Std.) (° C)	1.15	2.69	1.37
Min. exit air temperature (° C)	25.3	30.7	27.1
Mean exit air temperature (° C)	26.92	32.03	30.47
Max. exit air temperature (° C)	29.70	35.4	32.7
Exit air temperature (Std.) (° C)	1.02	1.25	1.20
Min. drying air temperature rise (Upper) (° C)	25.05	8.5	5.4
Mean drying air temperature rise (Upper) (° C)	25.77	10.92	6.62
Max. drying air temperature rise (Upper) (° C)	26.15	12.55	7.6
Drying air temperature rise (Std., Upper) (° C)	0.32	0.87	0.54
Min. drying air temperature rise (Lower) (° C)	0.6	4.43	8.0
Mean drying air temperature rise (Lower) (° C)	1.41	6.00	10.8
Max. drying air temperature rise (Lower) (° C)	1.74	6.61	11.9
Drying air temperature rise (Std., Lower) (° C)	0.36	0.51	0.81
Min. collector efficiency (Overall) (%)	37.12	51.13	66.1
Mean collector efficiency (Overall) (%)	45.75	66.46	71.67
Max. collector efficiency (Overall) (%)	53.95	72.43	77.47
Collector efficiency (Std.) (%)	5.29	4.84	3.18

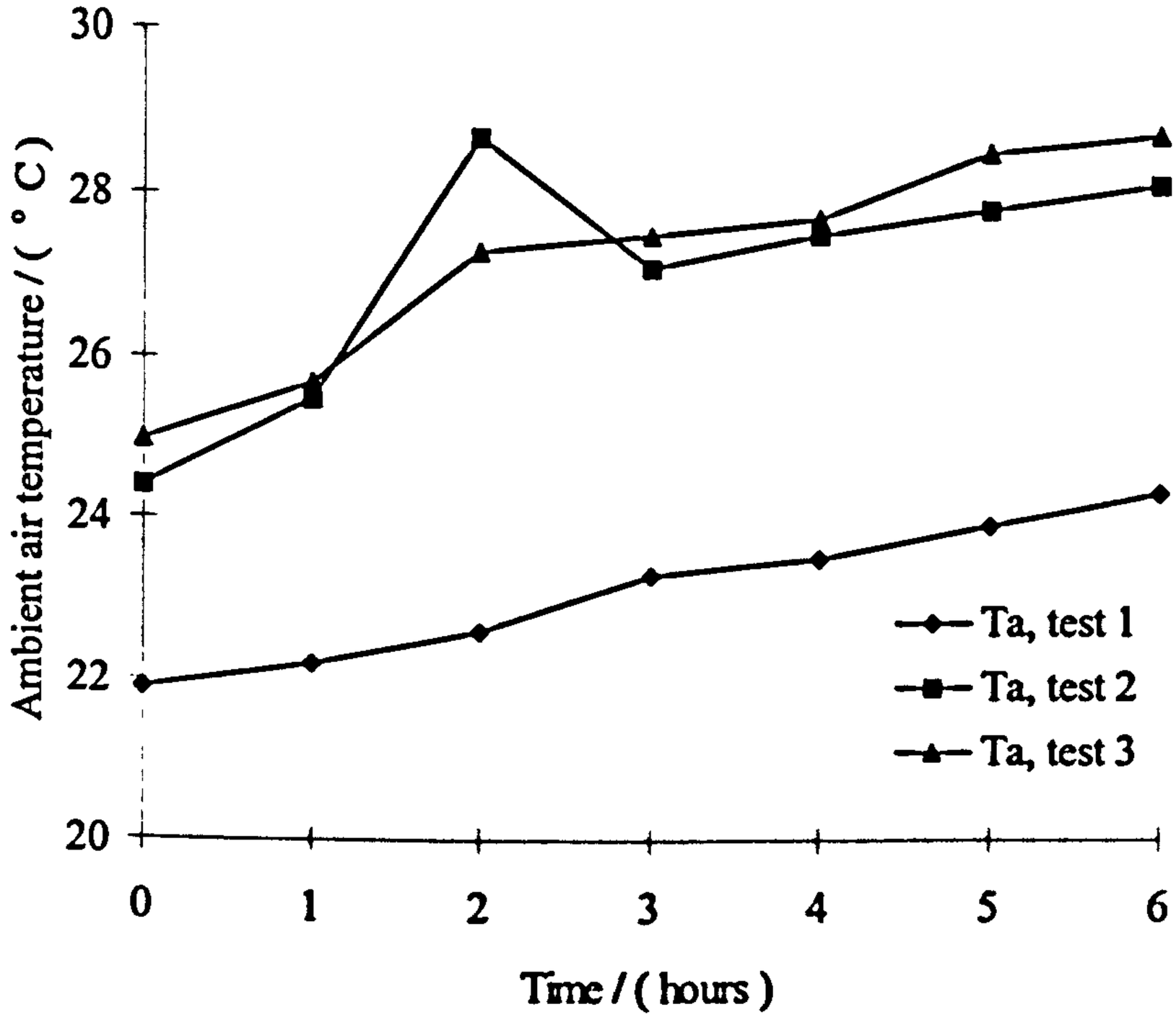

Figure 5.1: Diurnal variation in the ambient air temperature with time during tests 1-3 for three selected days.

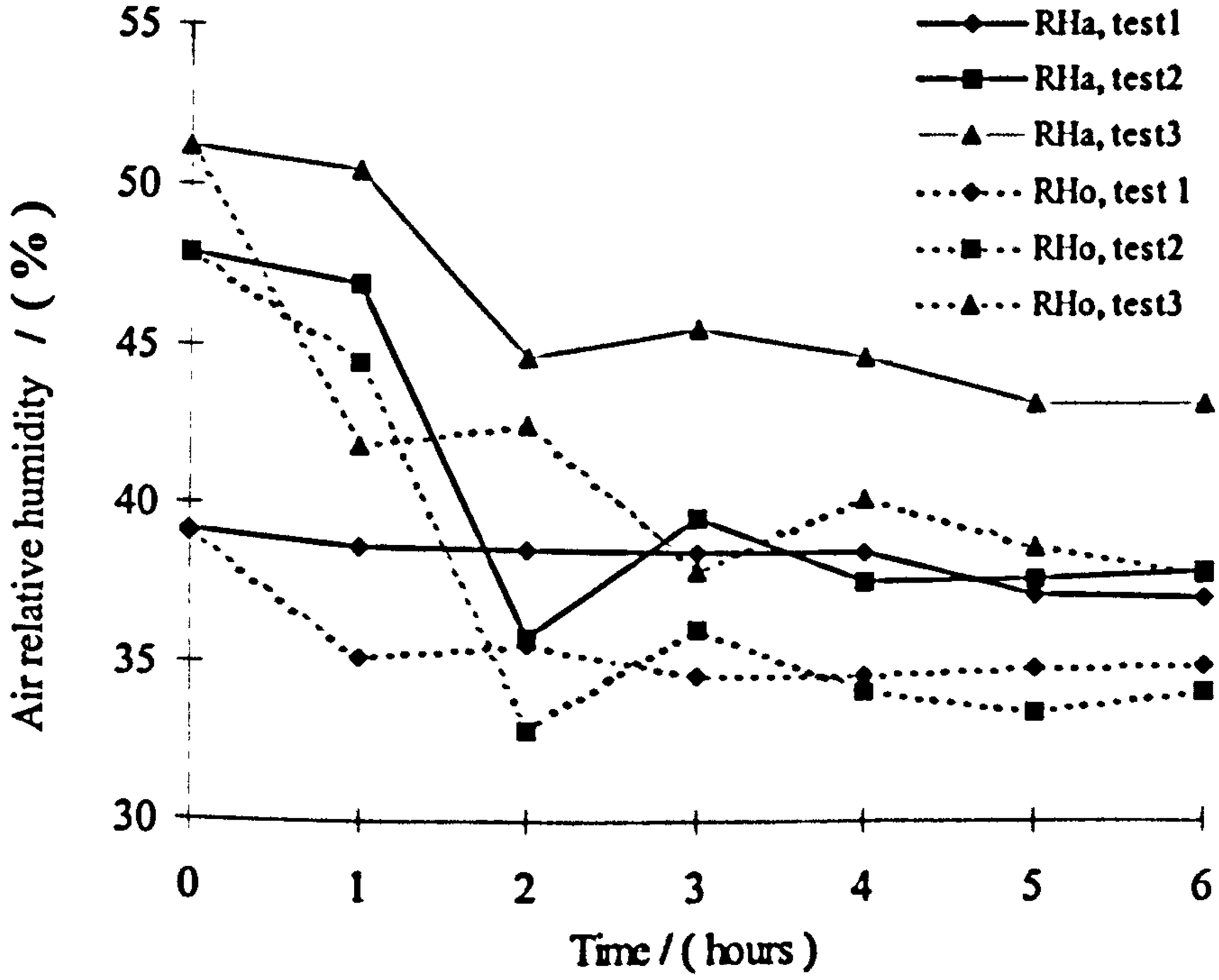

Figure 5.2: Variation of ambient and exhaust air relative humidity with time during tests 1 - 3 for three selected days .

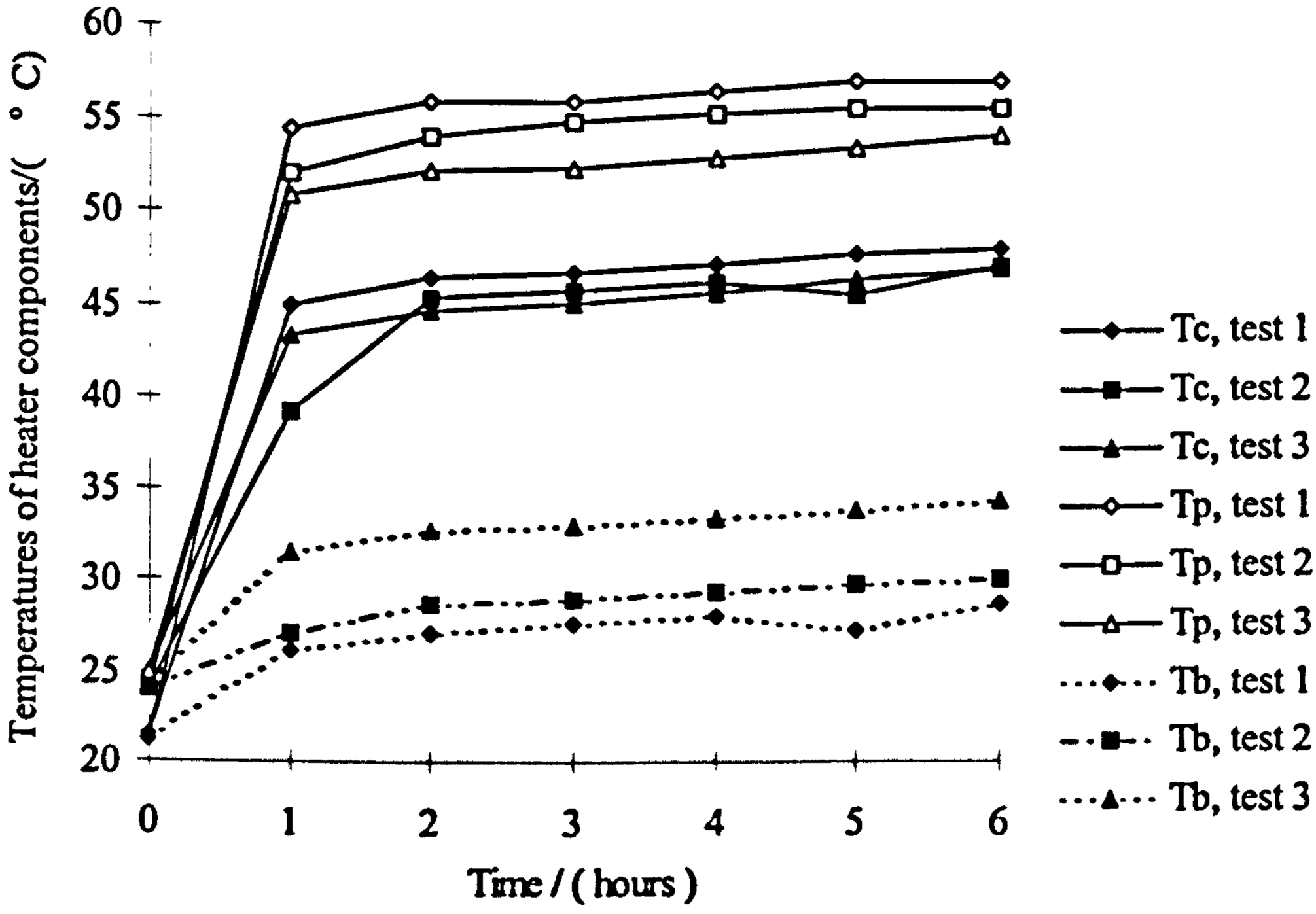

Figure 5.3: Variation in the temperatures of the air-heater components with time during tests 1-3 for three selected days.

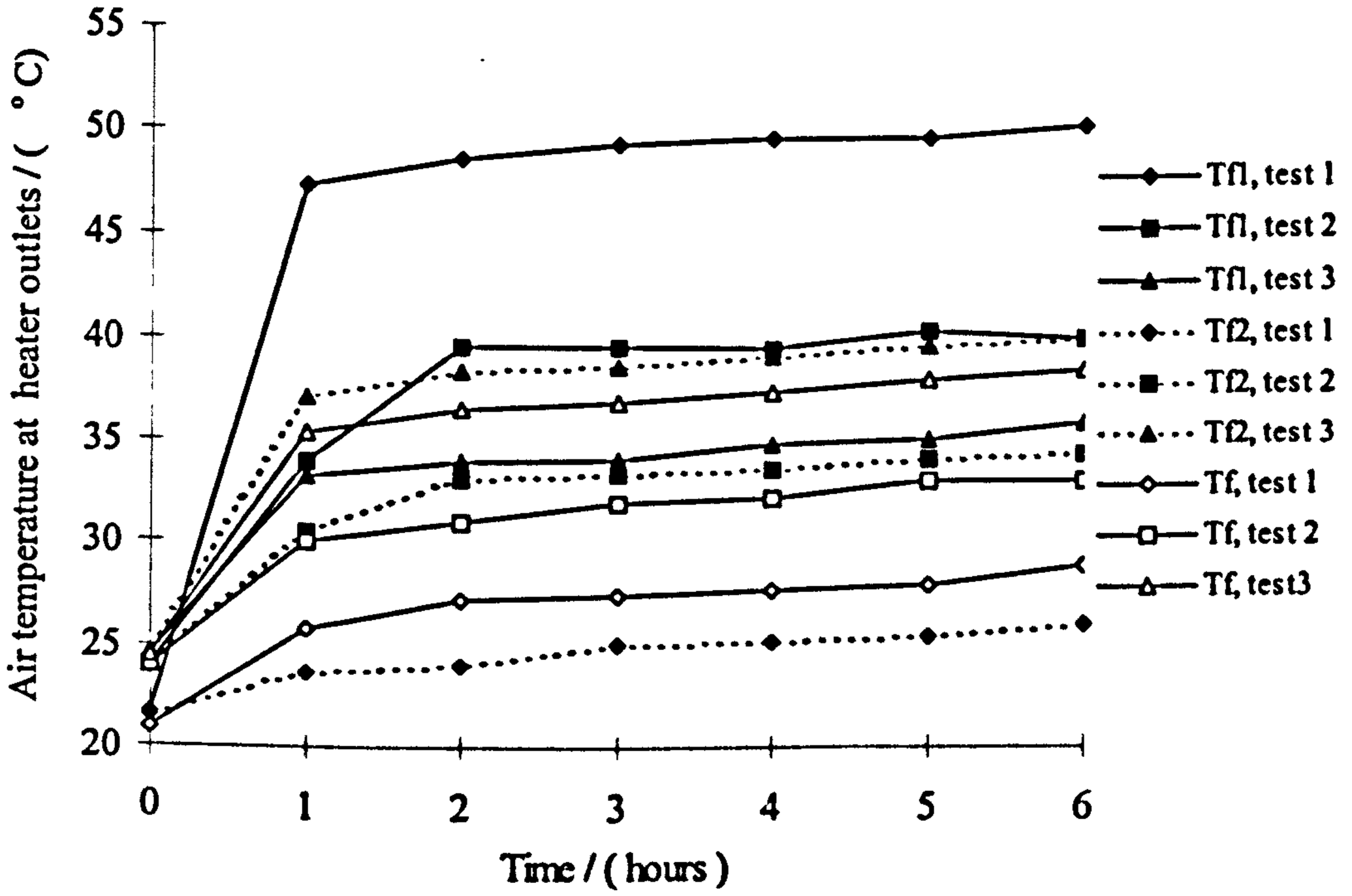

Figure 5.4: Variations in the drying air temperatures at outlets of the air-heater channels with time during tests 1-3 for three selected days.

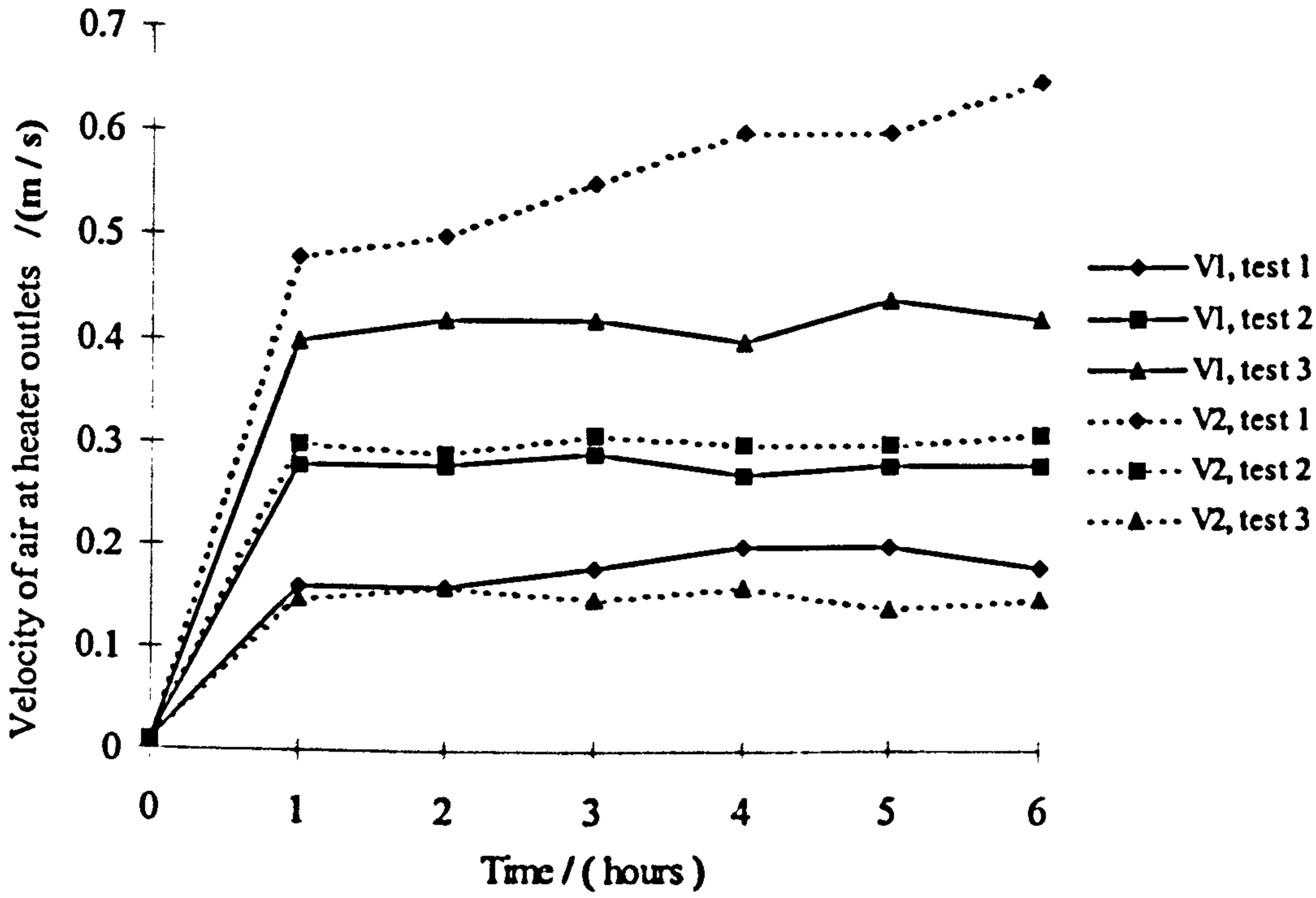

Figure 5.5: Diurnal variations in the drying air velocity at the oulets of the air-heater during tests 1-3 for three selected days

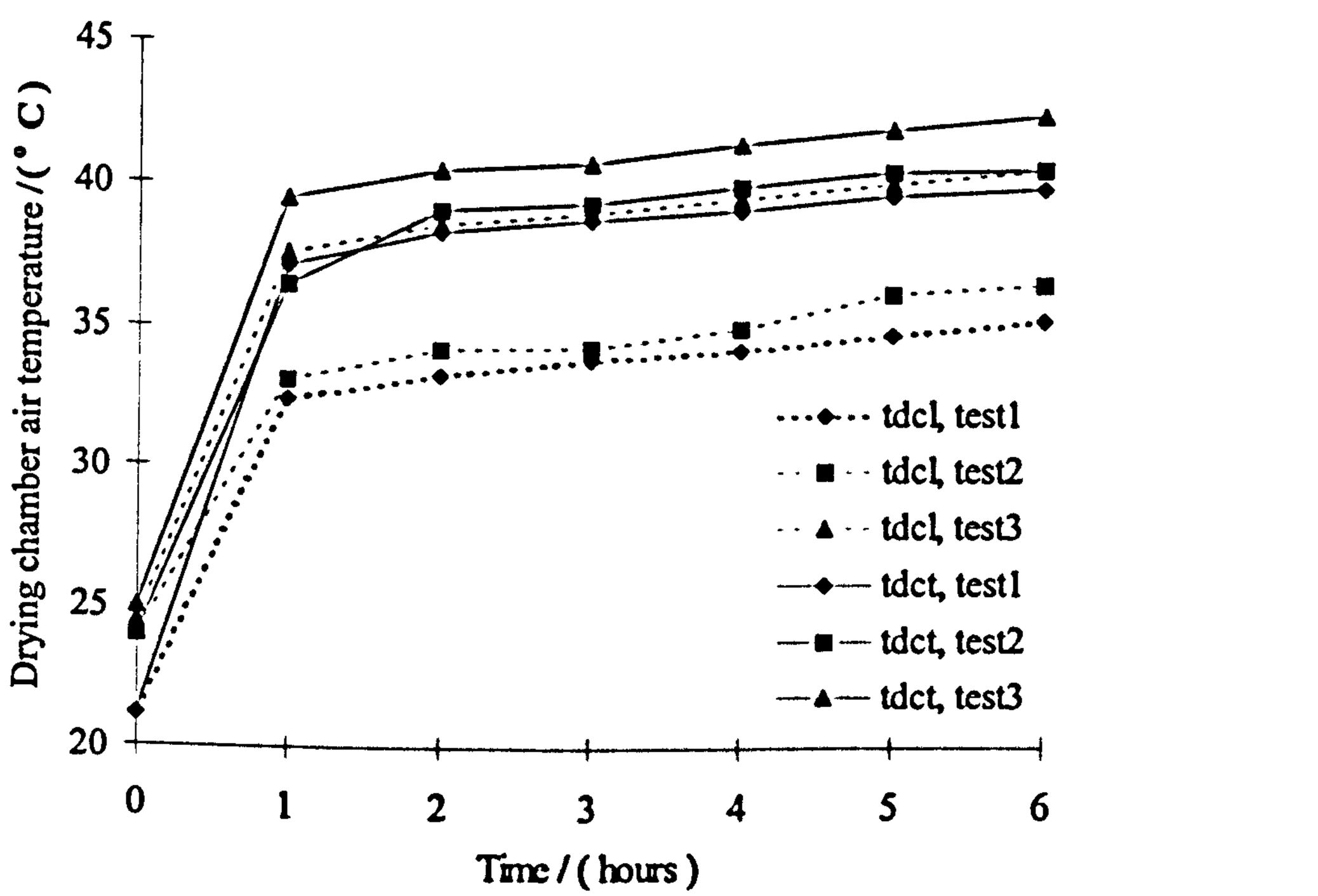

Figure 5.6: Diurnal variation in the drying air temperature profile at two locations in the drying chamber during tests 1-3 for three selected days.

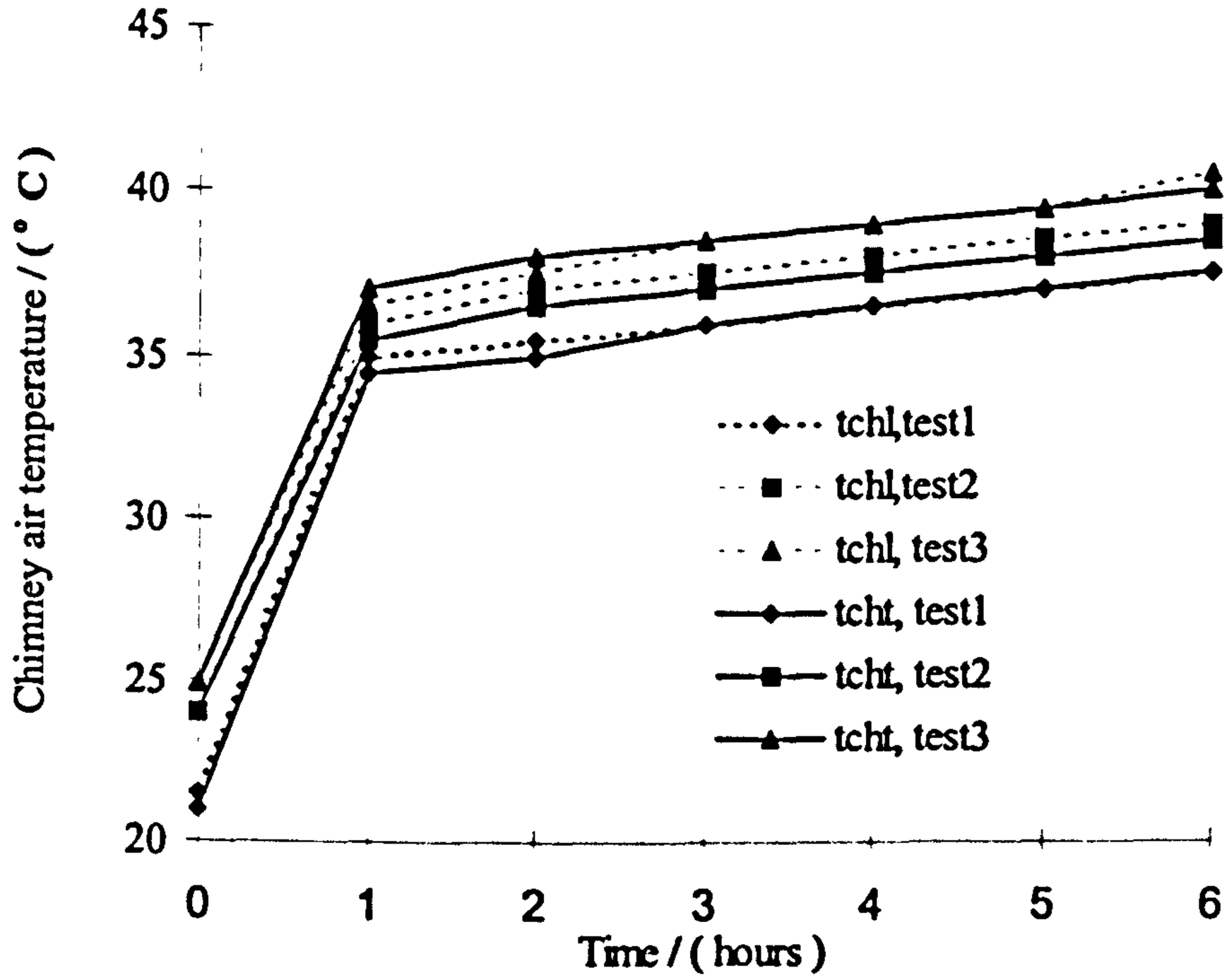

Figure 5.7: Diurnal variations in the air temperature measured at the bottom and middle sections of the chimney with time during tests 1-3 for three selected days.

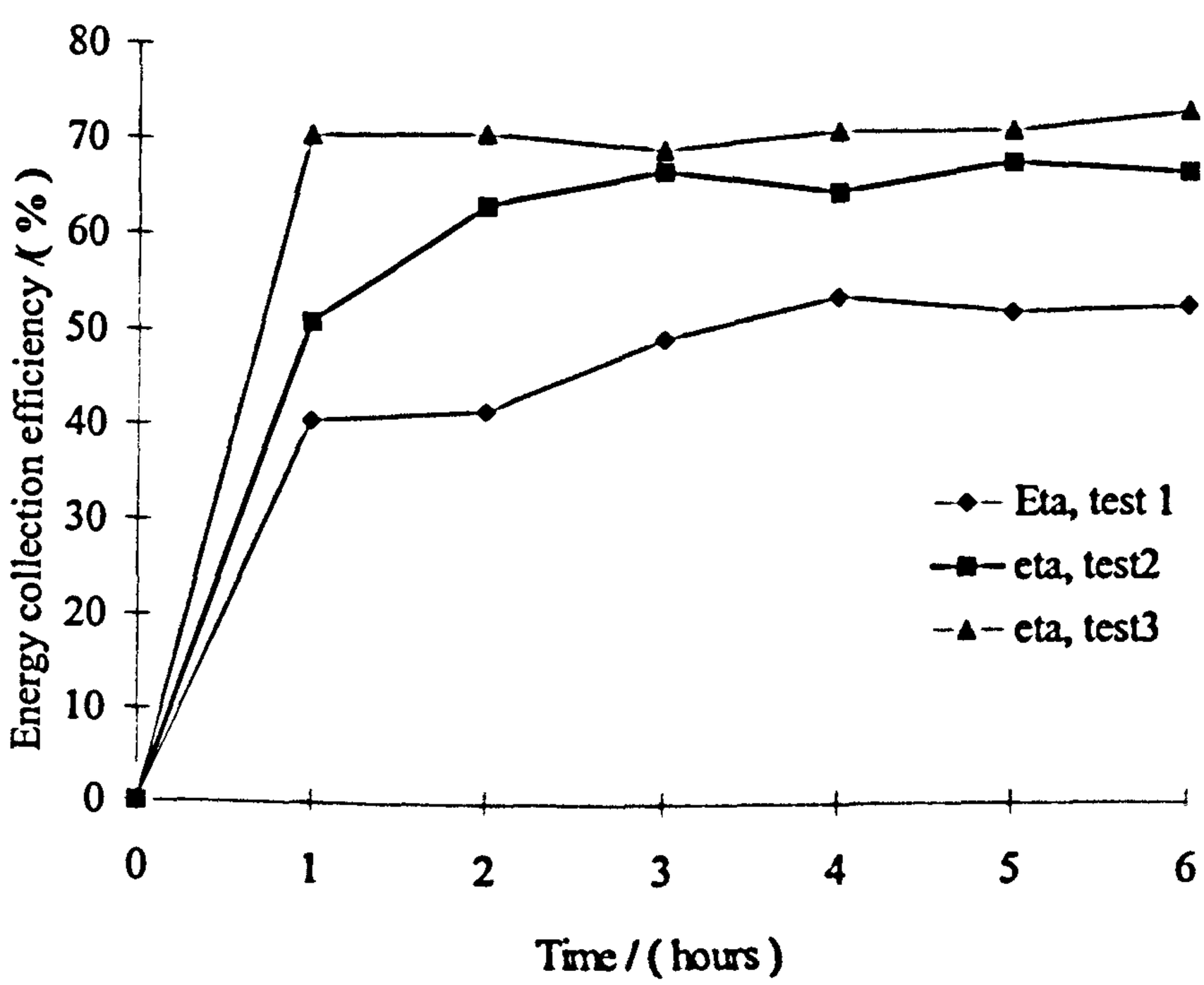

Figure 5.8: Diurnal variation in the cumulative energy collection efficiency of the air-heater during tests 1-3 for three selected days.

5.1.2 Tests under load conditions

Two sets of drying tests were performed under load conditions: (a) tests in which the drying was carried out continuously until a set time was reached (as in Tests 4, 5 and 6), and (b) tests in which the drying was carried out on day to day basis until the desired moisture content was achieved or a set time was reached (as in Tests 7 through 13).

In Tests 7 through 13, because drying was performed on daily basis, the experimental plots of the results of these tests have humps that flatten out over a length of time or are bounded between two vertical lines. In such plots (Figs. 5.19 through 5.38), the number of humps represents the number of days of operation of the dryer with the hump interval corresponding to the duration of the test on that day. In tests 9 through 13, the absorber plate of the air-heater was located at 17 mm from the base plate (as in tests 3 and 6).

Tests 4, 5, and 6 (continuous drying tests using air-heater options A, B and C, respectively)

Tests 4, 5 and 6 were carried out to evaluate the drying performance of the MNCSCD using the three configurations of the SPDDSAH described earlier (see section 5.1.1). To compare the dryers' performance with open-air drying, a control experiment was carried out by drying 122g of cassava chips in open-air under the same laboratory conditions during test 4. A lower loading density of 2.8 kg/m^2 was employed in the open-air drying. The average initial moisture contents of the cassava for all tests were about 202%, dry basis (i.e. about 67% wet basis) and the drying was performed continuously, in each test, for a period of 22 hours. No mould growth on the surface of the dried cassava was observed in any of the tests. In each of the three drying tests, between 1458 and 1461 g of cassava was spread on a drying tray of surface area 0.16 m^2 suspended on a cantilever beam at a height of 190 mm from the base of the drying chamber by means of four light inextensible strings of equal lengths. The desired moisture content level (20.4%, dry basis) for safe storage could not be attained within the cumulative drying time of twenty-two hours in any of the tests (see fig. 5.11).

An overview of the results of these experimental tests is presented in Table 5.5. As in 5.1.1, the data presented in Table 5.5 were computed over the drying period using a steady-

state incident radiation intensity of 464 W/m^2. In calculating the overall drying efficiencies, the energy collection area was taken as the sum of the primary and secondary collector areas to capture the effect of the contribution of the direct radiant energy incident on the drying chamber on the overall drying performance. The overall efficiency values computed for each test were then 'normalised' against the total initial crop weight to isolate, if any, the differences in drying load densities and its effect on the drying efficiency. The values of the mean pick up efficiency presented in Table 5.5 were obtained with the aid of psychrometric chart and equation (4.129).

The variation of the ambient air temperatures recorded over the drying periods in all the three tests was small (Fig. 5.9); differences of only up to 4° C were observed between the maximum and minimum ambient air temperatures (Table 5.5). Comparatively low levels of ambient air relative humidity were observed (see fig. 5.10). In test 4, the values ranged between 35.4 and 43.1% with a mean value of 40.1%, whereas in test 6 the values varied from 32.7 to 42% with a mean of 34.9%. The relative humidity values were not recorded in test 5 because of the non availability of the hand held relative humidity/temperature measuring instrument on that day. Diurnal variations in the relative humidity of the air at the outlet of the chimney (exhaust air) are shown in Fig. 5.10. In test 6, the exhaust air relative humidity increased by about 21% over the ambient value in the first hour, compared to the increment of 16% obtained in tests 4. The maximum values of the exhaust air relative humidity observed during the tests were 60.5 and 59.4% in tests 6 and 4, respectively. The increase in the exhaust air relative humidity over the ambient values can be explained as follows: as the air flows up the drying chamber it absorbs the evaporated moisture from the crop with a simultaneous loss of heat to the crop resulting in an increase in its relative humidity. But as can be seen from Fig. 5.10, as the drying progresses, the relative humidity of the exhaust air decreases because the moisture content of the product decreases and therefore less moisture gets entrained in the drying air leaving the chimney. In general, the mean ambient air and exhaust air relative humidity values recorded over the test period were lower than the maximum value of 60% recommended by Cheema (1978) for rapid drying of cassava. These conditions, naturally, favoured the drying of the cassava chips.

Three plots illustrating the drying behaviours accomplished in the experimentation are shown in Figs. 5.11 to 5.13. The plots of the comparative changes in the moisture contents (drying curves) with time throughout the drying progress of the tests are shown in Fig. 5.11. The curves show that, as expected, the rate of drying of the cassava chips was much higher in the dryer than in the open-air drying (shown in Figs. 5.11 to 5.13 as control) under the same heat source and laboratory conditions. It can be seen from fig. 5.11 that, for example, the drying times required to dry cassava chips from 201.6% to 76.1% dry basis were: 10.5 hours in test 6; 12 hours in test 5; 14.5 hours in test 4; and 22 hours in the open-air drying. The better performance of drying in the dryer compared to the open-air drying could be attributed partly to the better mass flow rate of heated air entering the drying chamber due to the chimney effect. Furthermore, the product dried in the dryer received energy from both the heated air from the air-heater and the direct incident radiation, while the open-air dried sample received only the direct incident radiation and lost significant energy to the surroundings. The hourly changes in the drying rates are also illustrated as functions of time and of moisture content in Figs. 5.12 and 5.13, respectively. Figure 5.12 indicates that, for a loading density of approximately 9.13 kg/m^2 employed in all the tests using the dryer, the drying rates were higher in test 6 (when the movable absorber plate of the SPDDSAH was positioned closer to the base plate than the transparent cover) than in tests 4 and 5 at all moisture contents. The higher mass flow rates achieved in test 6 compared to tests 4 and 5 (see fig. 5.14) partly accounts for the higher drying rates observed in test 6. It can be observed from Fig. 5.13 that, for the product dried in the dryer, the improvement in the rate of drying is noticeable for test 6 in the later stages of drying. For example, at a moisture content level of 50% the drying rate of the cassava chips in test 6 was 0.0048 $kg_w/kg_s.h$; whereas the drying rates at the same moisture content level in tests 5 and 4 were 0.0026 and 0.004 $kg_w/kg_s.h$, respectively. A possible explanation for this observation is that in the final stages of drying (i.e. at low moisture contents), the rate of drying tends to be controlled by the rate of moisture movement from the interior of the drying body to the surface. This, in turn, is controlled by the temperature of the body which is governed by the temperature of the surrounding air. It can be postulated, therefore, that the higher rate of drying at low moisture contents is attributable to the higher air temperatures and relatively higher mass flow rates attained in the drying chamber, as in test 6, compared to the values obtained in tests 4 and 5 (Fig. 5.15). It can be seen from figs. 5.12 and 5.13 that, no constant rate period was observed in the drying

cassava from a moisture of 201.6% to 24% dry basis in any of the tests. In previous research Chirife *et al*, (1969) observed a similar trend in the drying of cassava from a moisture content of 66 to 14% on wet basis (i.e., about 200 to 16% dry basis).

The variations in the plenum air temperature for the three tests over the drying time, is illustrated in fig. 5.15. The curves of the variations in the ambient air temperature have been superimposed for purposes of comparison. Figure 5.15 shows moderate rises in the drying air temperature inside the plenum above ambient values. Peak temperature elevations of 4, 6.6 and 8° C were experienced in tests 4, 5 and 6, respectively. In test 6, the maximum drying air temperature recorded was 33.3° C compared to the values of 27.3° C and 31.8° C realised in tests 4 and 5, respectively. However, the average temperatures experienced in the plenum with the dryer loaded were far less compared to the cases in which the dryer was not loaded. For example, with the dryer unloaded and employing the same SPDDSAH configuration used in test 6, a daily mean rise in the plenum air temperature of 10.5° C over ambient was obtained (see Fig. 5.4 and Table 5.4).

Figure 5.14 shows the variation in the mean mass flow rates at the outlet of the air-heater during tests 4, 5 and 6. It can be observed that higher air mass flow rates were obtained during test 6 compared with the corresponding values in tests 4 and 5. The higher mass flow rates and drying air temperatures coupled with the lower drying air relative humidity recorded in test 6 compared with the corresponding values achieved in tests 4 and 5, is indicative that the drying potential of the plenum air in test 6, would be greater than that of test 4 or 5.

Mean drying air temperatures recorded in the drying chamber over the test series were between 33.9-37.2° C in test 6; 31-34.8° C in test 4 and 33.1-37.4° C in test 5. However, in the corresponding tests under no load conditions higher drying chamber temperatures were recorded (see Table 5.1-5.3). The variation in the mean drying air temperatures (inside the drying chamber) with distance from the base of the chamber is illustrated in Fig. 5.16. Figure 5.16 shows that, in general, the air temperature inside the chamber increases with distance from the base of the drying chamber. This observation can be explained along the following lines: as the air flows up the drying chamber it absorbs the evaporated moisture from the crop with a simultaneous loss of heat to the crop resulting in an increase in its

relative humidity; however, it is heated in turn by the direct radiant energy reaching the chamber.

Figure 5.17 shows the variation in the exhaust temperature along the length of the chimney. Comparing figs. 5.16 and 5.17, it can be seen that in the initial stages of drying, the chimney temperatures are higher than the drying chamber air temperatures but as the drying progresses the chamber air temperature increases and eventually becomes higher than the chimney air temperature. The chamber temperatures becoming higher than the chimney temperature at some point during drying is suggestive that the drying potential of the heated air was possibly under utilised in all the three tests. The air temperatures recorded in the drying chamber and the chimney under load conditions were lower than the corresponding air temperatures recorded under no load conditions (see figs. 5.6, 5.7, 5.16 and 5.17). For example, under nearly the same laboratory conditions, a peak temperature of 39° C was recorded inside the drying chamber in test 5 compared to the value of 42.7° C observed in test 3 (fig. 5.12). This observation denotes that the positional changes in the air temperature within the dryer depended not only on incident energy, but also on the moisture content of the cassava being dried. The range of drying air temperatures recorded for the dryer studied were less than optimum value of 84° C for the cassava to get scorched under the drying conditions experienced.

The calculated relative heating index values, as can be seen from Tables 5.4 and 5.5, ranged between 0.09 and 0.26 for tests 4, 5 and 6 compared with values of 0.08-0.39 obtained in tests 1, 2 and 3. It must be noted from these results that the air-heater outlet temperatures are affected by the loading capacity of the dryer and therefore should be taken into account in the design of a dryer.

The variations in the normalised overall drying efficiencies with time are shown in fig. 5.18. It can be seen that the value of the cumulative efficiency for each test decreases as the drying progresses. However, as mentioned earlier, the drying air temperatures and mass flow rates inside the chamber increased as the drying progressed in all the tests (see figs. 5.14 and 5.15). These observations point to the fact that the drying efficiency is strongly linked up with the reduced moisture content of the product being dried. It can be seen from fig. 5.18 that cumulative drying efficiency at the end of the 22 hours of drying

was higher in test 6 (8.75%) compared to the values of 7.6% and 7.95% in tests 4 and 5, respectively, however, the pick-up efficiency of the dryer for test 4 was 17.5% compared to a lower value of 11.5% obtained in test 6. Though the drying air conditions in test 6 were far better than those of test 4, yet the higher value of the pick-up efficiency obtained during test 4 compared to a value of 11.5% obtained in test 6 indicates that the potential of the heated air from the air-heater in test 6 was highly under-utilised.

Table 5.5: Overview of results for laboratory tests 4, 5 and 6

(Test 4 - test under load with air-heater option A, absorber plate of 55 mm from base plate;
Test 5 -test under load with air-heater option B, absorber plate of 36 mm from base plate;
Test 6 - test under load with air-heater option C, absorber plate of 17 mm from base plate)

Measured and calculated performance parameters	TEST 4	TEST 5	TEST 6
Starting time	11.40 am	11.20 am	11.20 am
Duration of drying (h)	22	22	22
Initial weight of crop mass (grams)	1458.3	1460	1460.1
Initial product moisture content ($kg_{water}/kg_{drv\ solid\ matter}$)	201.6	201.6	201.7
Final product moisture content ($kg_{water}/kg_{drv\ solid\ matter}$)	49.7	28.1	24.0
Minimum ambient air relative humidity (%)	35.40	-[a]	32.7
Mean ambient air relative. humidity (%)	40.10	-[a]	34.9
Maximum ambient air relative. humidity (%)	43.10	-[a]	42
Minimum ambient air temperature (°C)	22.1	21	21.2
Mean ambient air temperature (°C)	23.2	24.8	24.9
Maximum ambient air temperature (°C)	23.9	25.4	25.3
Min. glazing temperature (°C)	45.2	44	42.3
Mean glazing temperature (°C)	46.2	45.1	44.0
Maximum glazing temperature (°C)	47.7	46.2	44.6
Minimum absorber plate temperature (°C)	54.0	52.0	49.9
Mean absorber plate temperature (°C)	55.3	53.6	51.3
Maximum absorber plate temperature (°C)	56.6	55.0	52.1
Minimum bottom plate temperature (°C)	25.20	27.1	28.3
Mean bottom plate temperature (°C)	26.9	29.1	31.1
Maximum bottom plate temperature (°C)	27.7	30.4	31.6
Minimum heated air temperature in upper channel (°C)	47.9	40.0	31.8
Mean heated air temperature in upper channel (°C)	49.3	45.1	32.9
Maximum heated air temperature in upper channel (°C)	50.7	47.5	33.2
Min. heated air flow velocity in upper channel (°C)	0.10	0.27	0.42
Mean heated air flow velocity in upper channel (°C)	0.13	0.29	0.45
Max. heated air flow velocity in upper channel (°C)	0.18	0.31	0.49
Minimum heated air temperature in lower channel (°C)	23.3	33	38.6
Mean heated air temp. in lower channel (°C)	24.2	35.2	40.5
Maximum heated air temp. in lower channel (°C)	25.3	38	41
Min. heated air flow velocity in lower channel (°C)	0.30	0.26	0.14
Mean heated air flow velocity in lower channel (°C)	0.46	0.30	0.16
Max. heated air flow velocity in lower channel (°C)	0.50	0.33	0.20

Table 5.5: continued.

Measured and calculated performance parameters	TEST 4	TEST 5	TEST 6
Minimum heated air temperature in plenum (°C)	25.0	27	29.9
Mean heated air temperature in plenum (°C)	26.6	30.7	32.7
Maximum heated air temperature in plenum (°C)	27.3	31.8	33.3
Minimum chimney air temperature (°C)	31.3	32	33
Mean chimney air temperature (°C)	34.2	34.5	34.9
Maximum chimney air temperature (°C)	35	35.5	36
Minimum relative heating index	0.09	0.16	0.21
Mean relative heating index	0.10	0.17	0.24
Maximum relative heating index	0.12	0.18	0.26
Minimum air temperature inside drying chamber (°C)	31.3	32.6	30.3
Mean air temperature inside drying chamber (°C)	33.9	35.7	34.6
Maximum air temperature inside drying chamber (°C)	34.8	37.5	37.1
Minimum exit air temperature (°C)	24.8	25	26.2
Mean exit air temperature (°C)	26.0	26.5	27.7
Maximum exit air temperature (°C)	27.1	27.6	28.9
Min. drying air temperature rise in upper channel (°C)	25.0	19	6.8
Mean drying air temperature rise in upper channel (°C)	26.0	20.3	7.8
Max. drying air temperature rise in upper channel (°C)	27.0	22.5	8.3
Min. drying air temperature rise in lower channel (°C)	0.47	12	15.1
Mean drying air temperature rise in lower channel (°C)	1.0	10.4	8.0
Max. drying air temperature rise in lower channel (°C)	1.9	13.3	16.0
Minimum air mass flow rate (kg/s)	0.0078	0.011	0.0142
Mean air mass flow rate (kg/s)	0.0115	0.0131	0.0152
Maximum air mass flow rate (kg/s)	0.0132	0.0143	0.0163
Minimum exhaust air relative humidity (%)	33	-[a]	28.9
Mean exhaust air relative humidity (%)	45.1	-[a]	36.4
Maximum exhaust relative humidity (%)	59.4	-[a]	46.5
Mean pick-up efficiency (%)	17.5	-[a]	11.5
Overall drying efficiency (%)	11.0	11.6	12.3
Normalised drying efficiency (% / kg mass)	7.6	7.95	8.43

[a] Value not recorded or estimated.

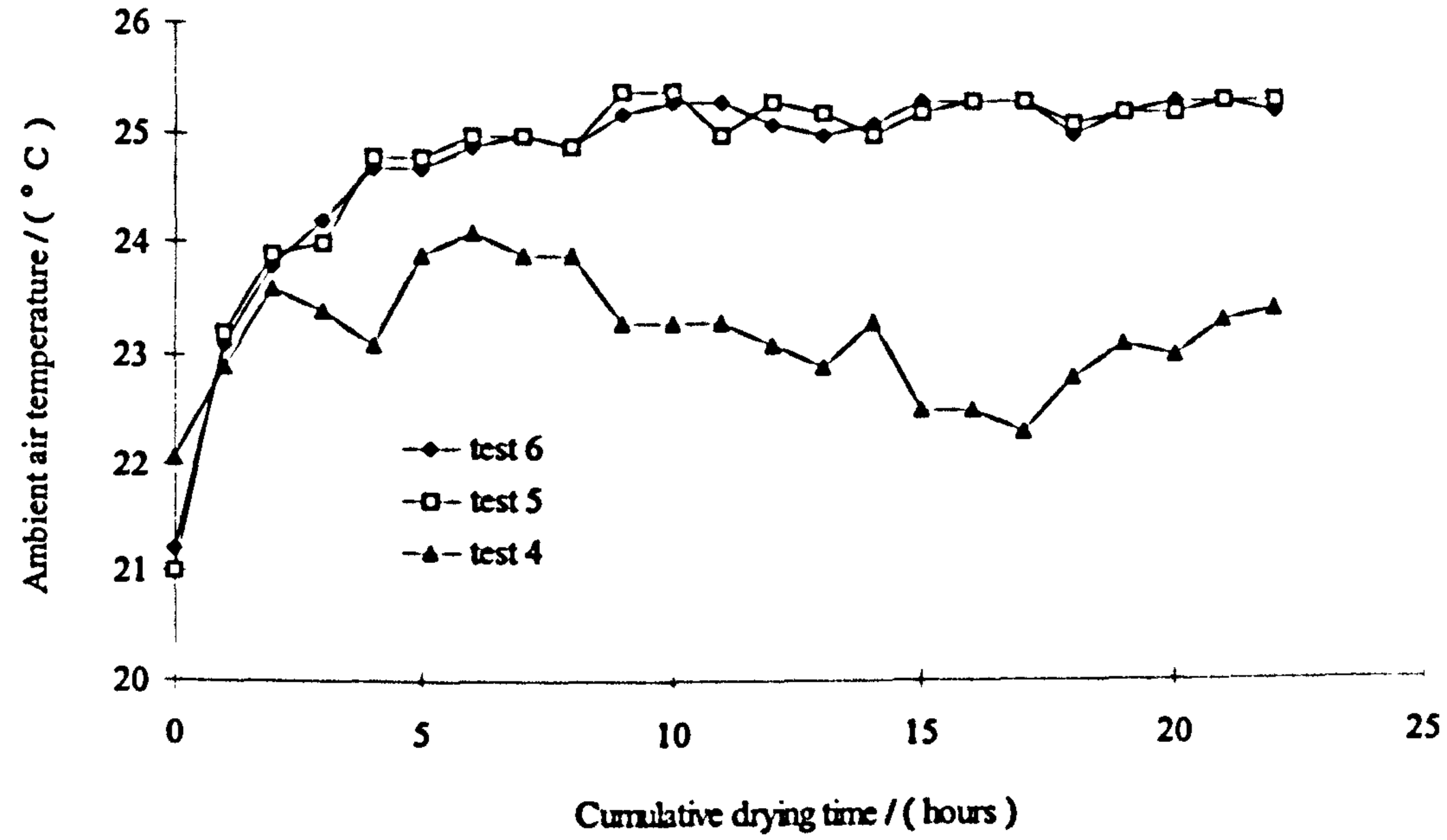

Figure 5.9: Variation in the ambient air temperature with time during tests 4, 5 and 6.

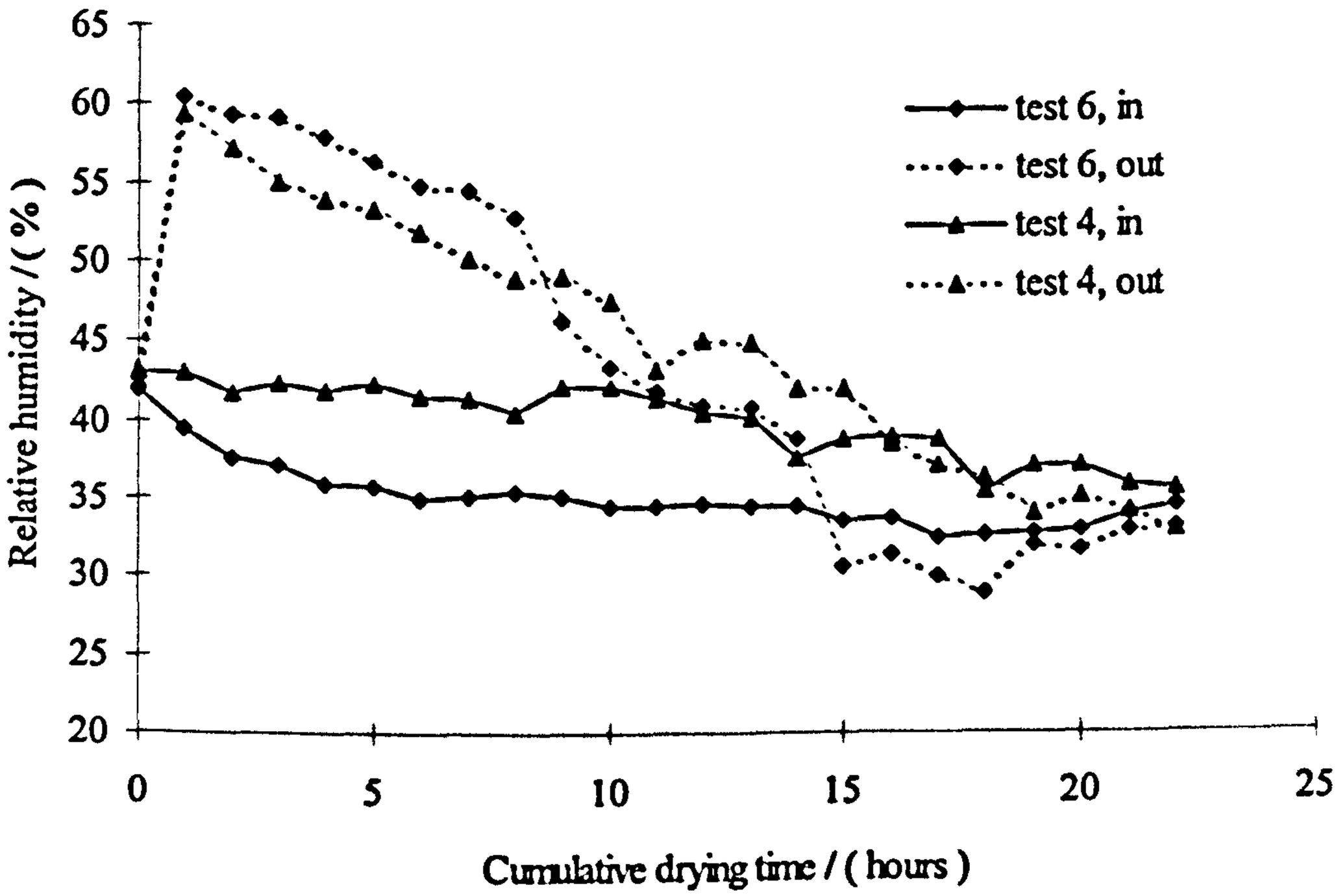

Figure 5.10: Variation in the ambient air and exhaust air relative humidity with time during tests 4, 5 and 6.

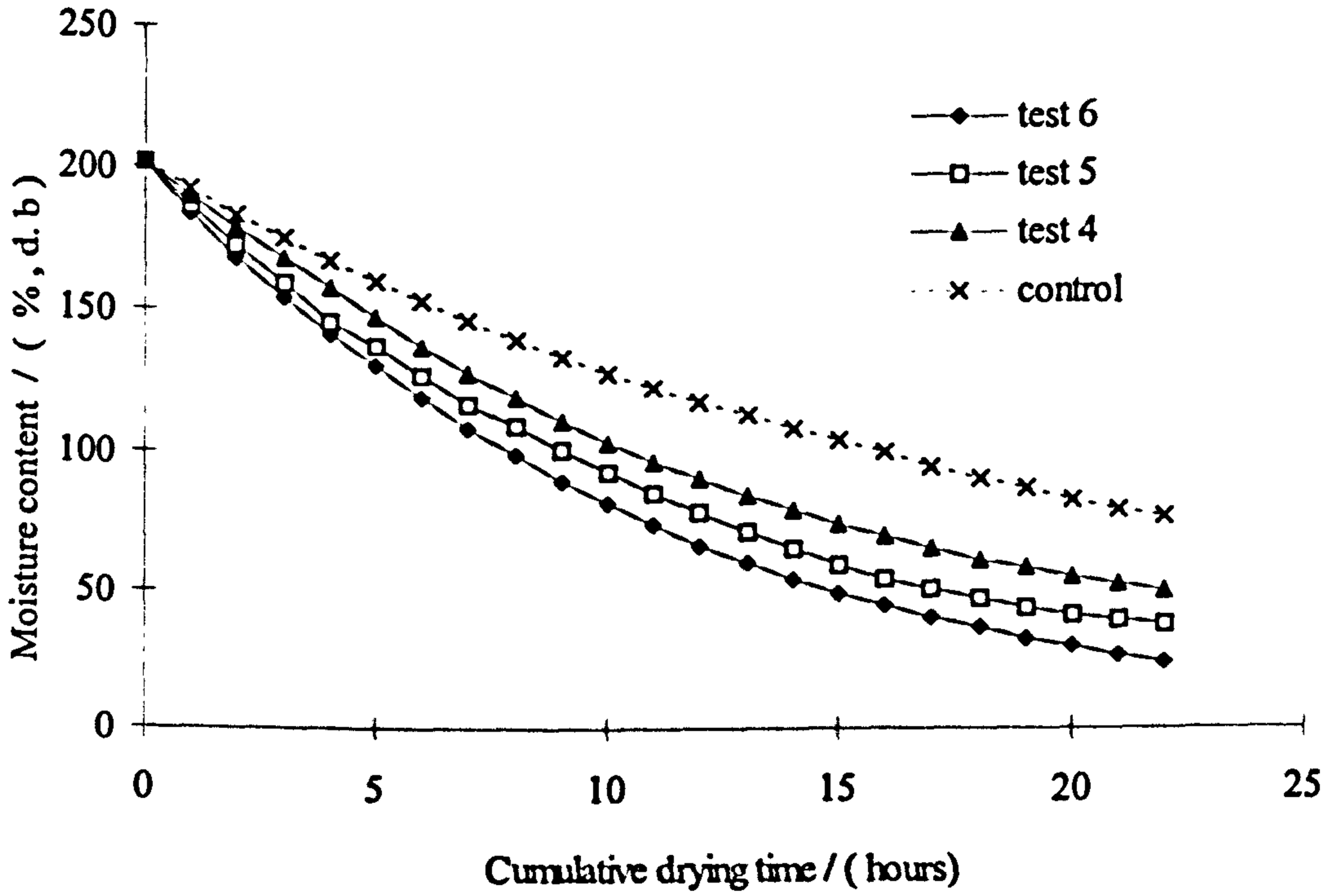

Figure 5.11: Comparative changes in moisture content with time during tests 4, 5 and 6

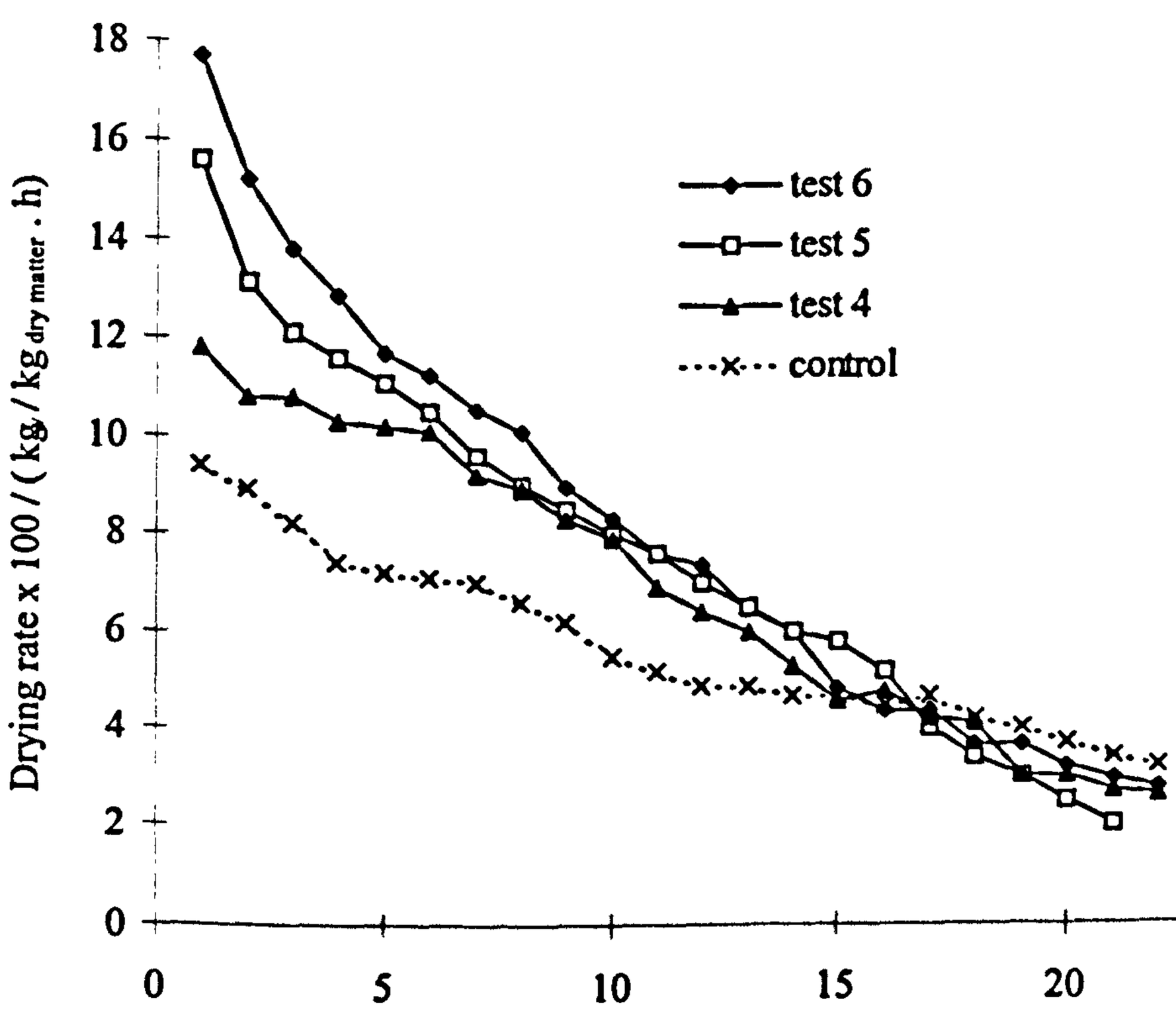

Figure 5.12: Variation in the drying rate of cassava chips with time during tests 4, 5 and 6.

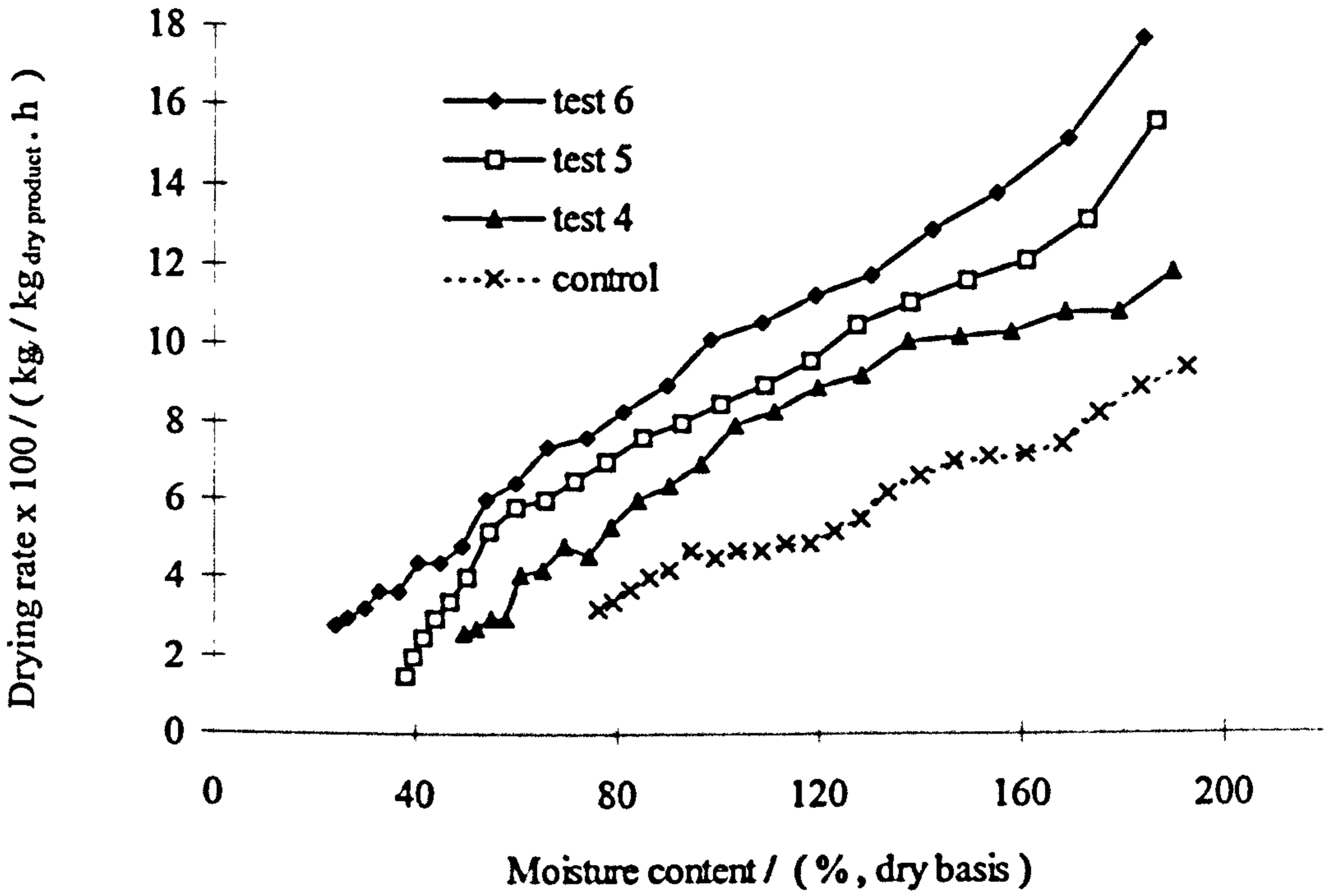

Figure 5.13: Variation in the drying rate of cassava chips with moisture content during tests 4, 5 and 6.

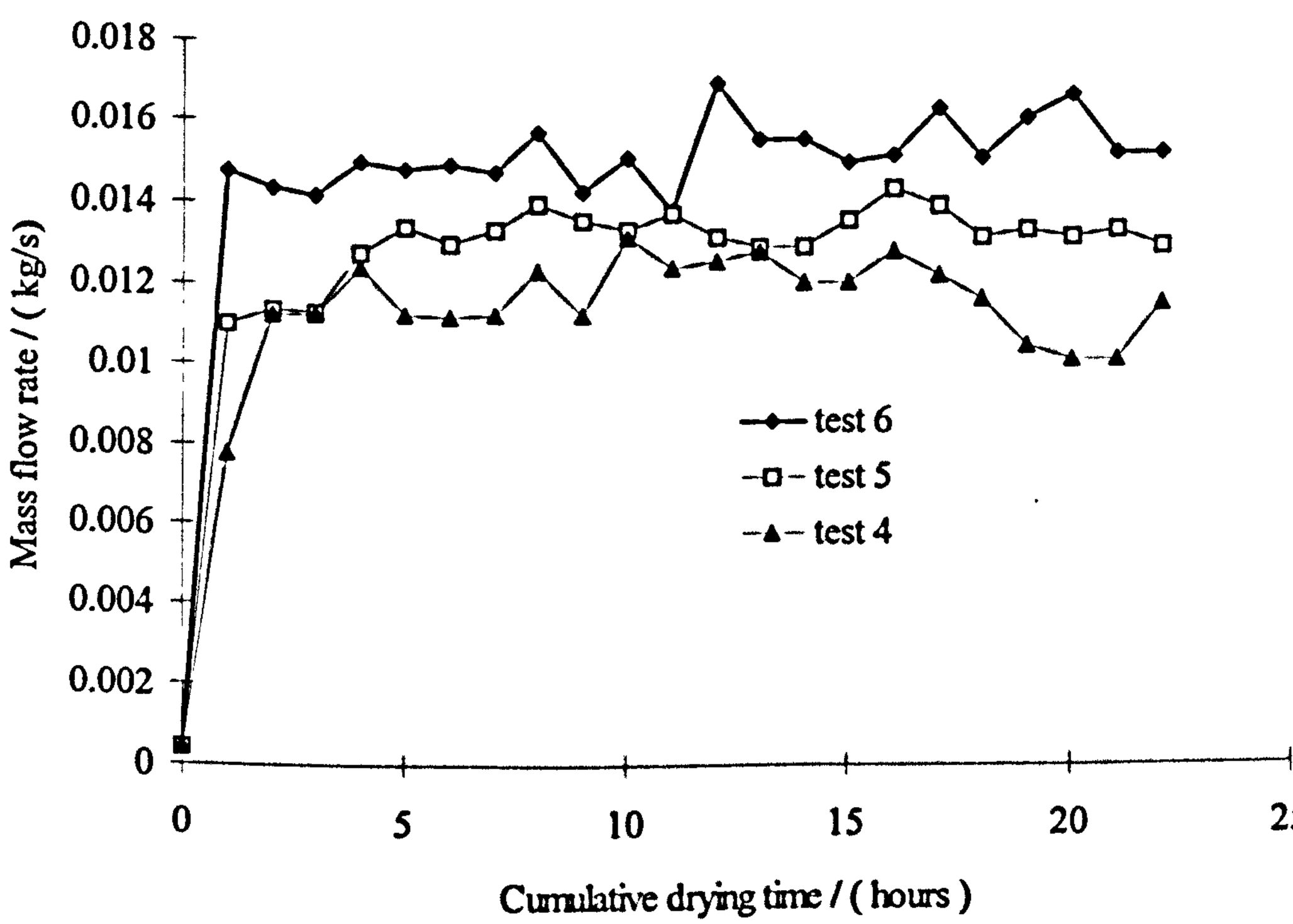

Figure 5.14: Variation in the air mass flow rate with time during tests 4, 5 and 6.

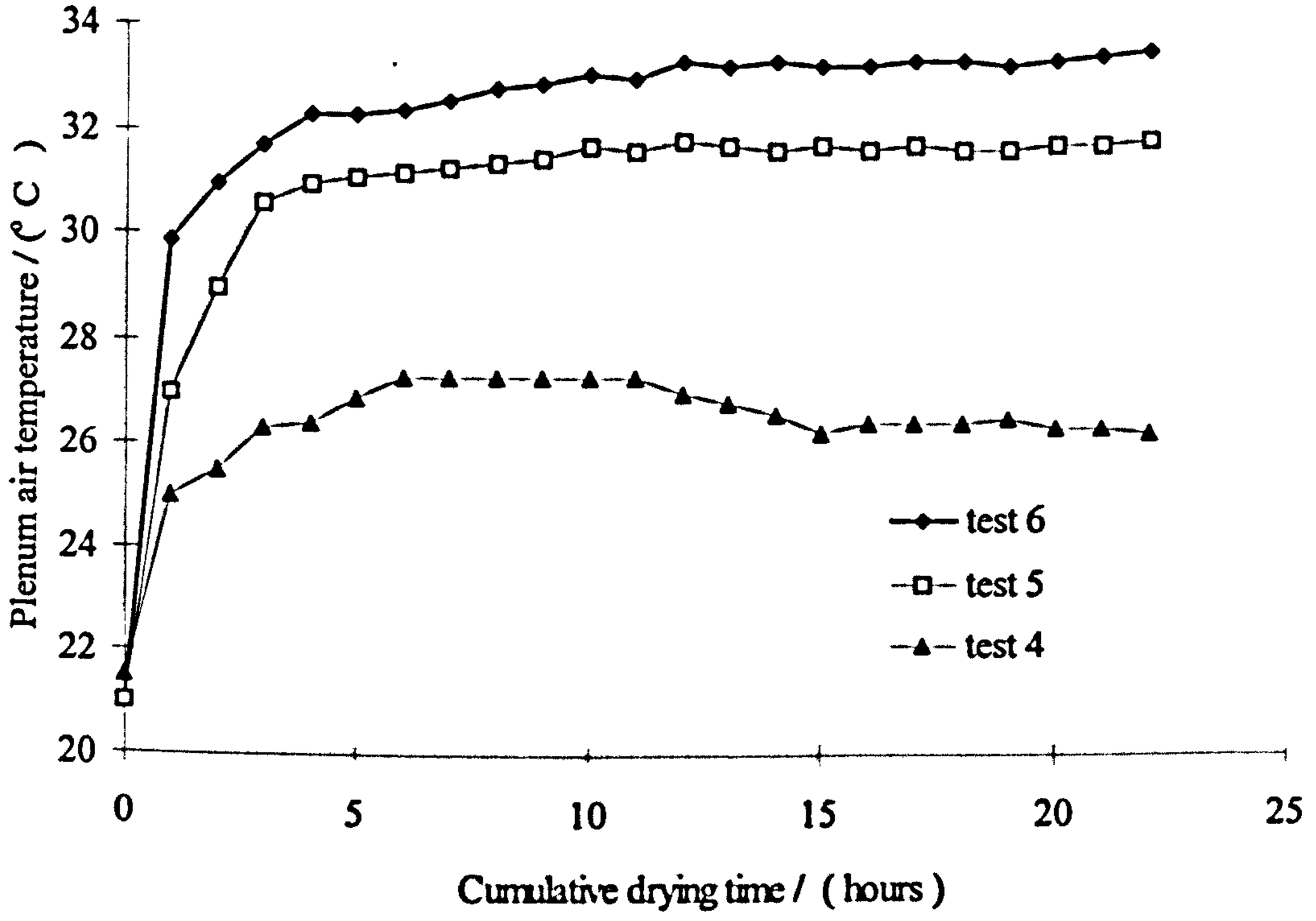

Figure 5.15: Variation in the plenum air temperature with time during tests 4, 5 and 6.

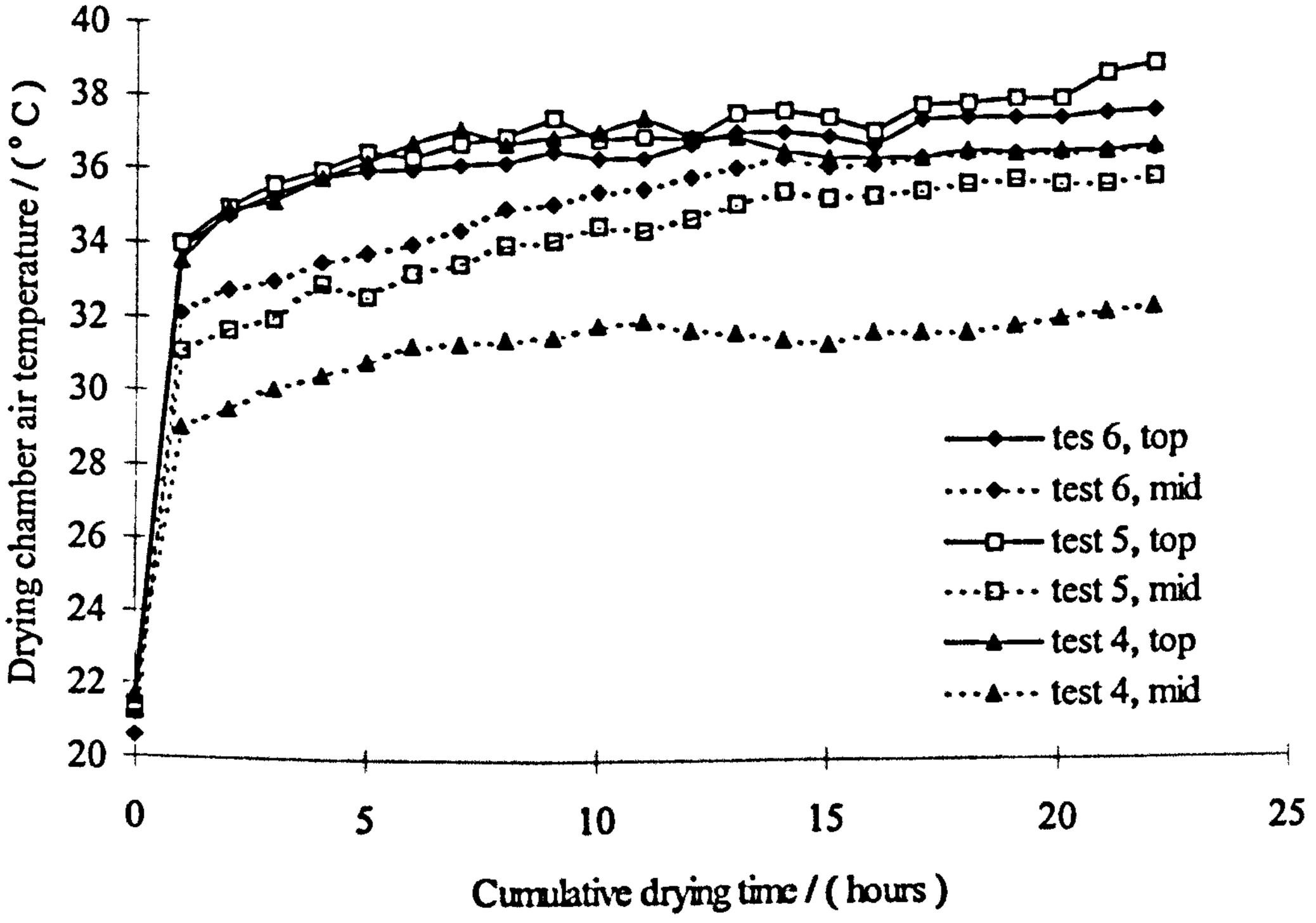

Figure 5.16: Variation in the drying chamber air temperature with time during tests 4, 5 and 6.

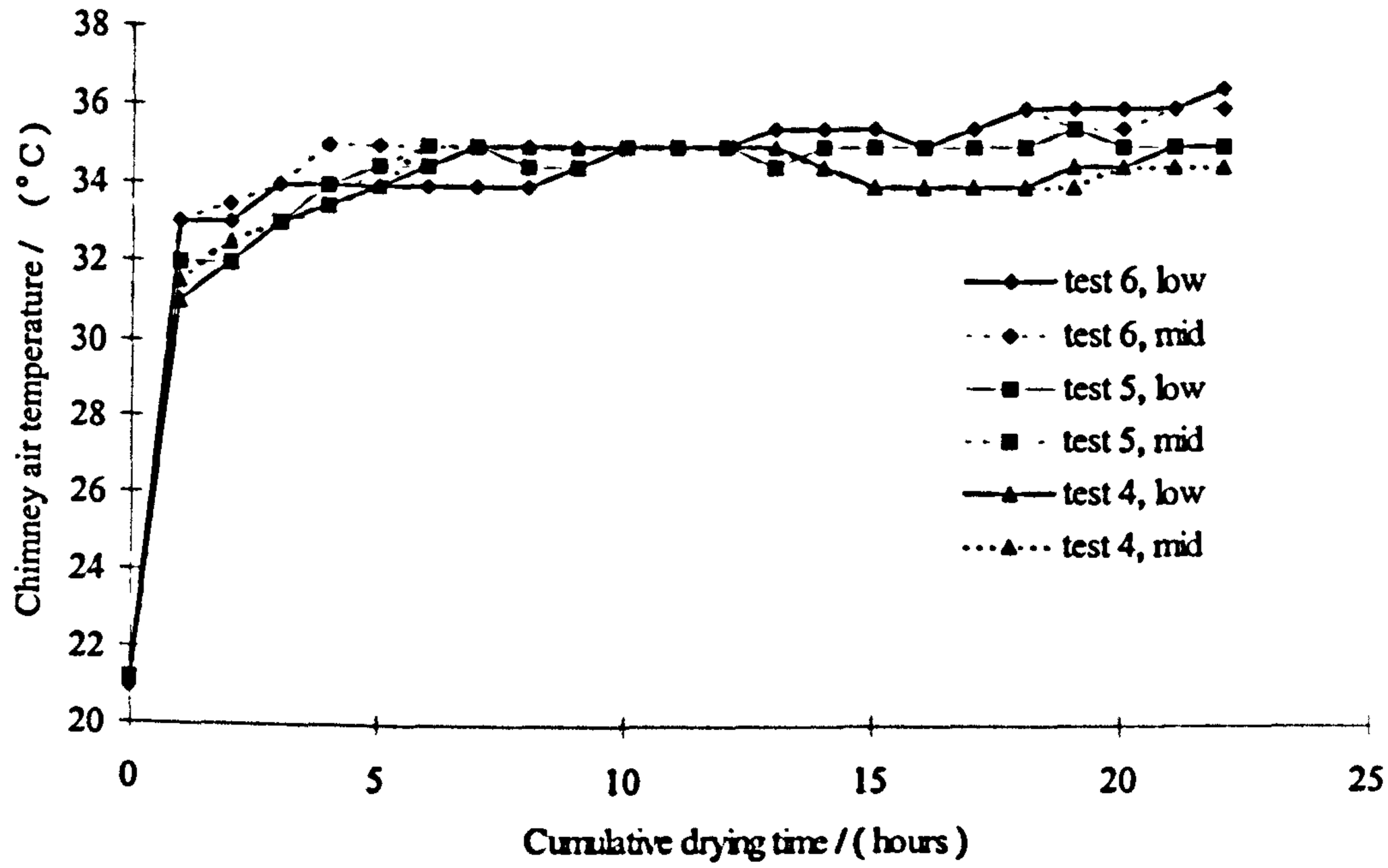

Figure 5.17: Variation in the chimney air temperature with time during tests 4, 5 and 6.

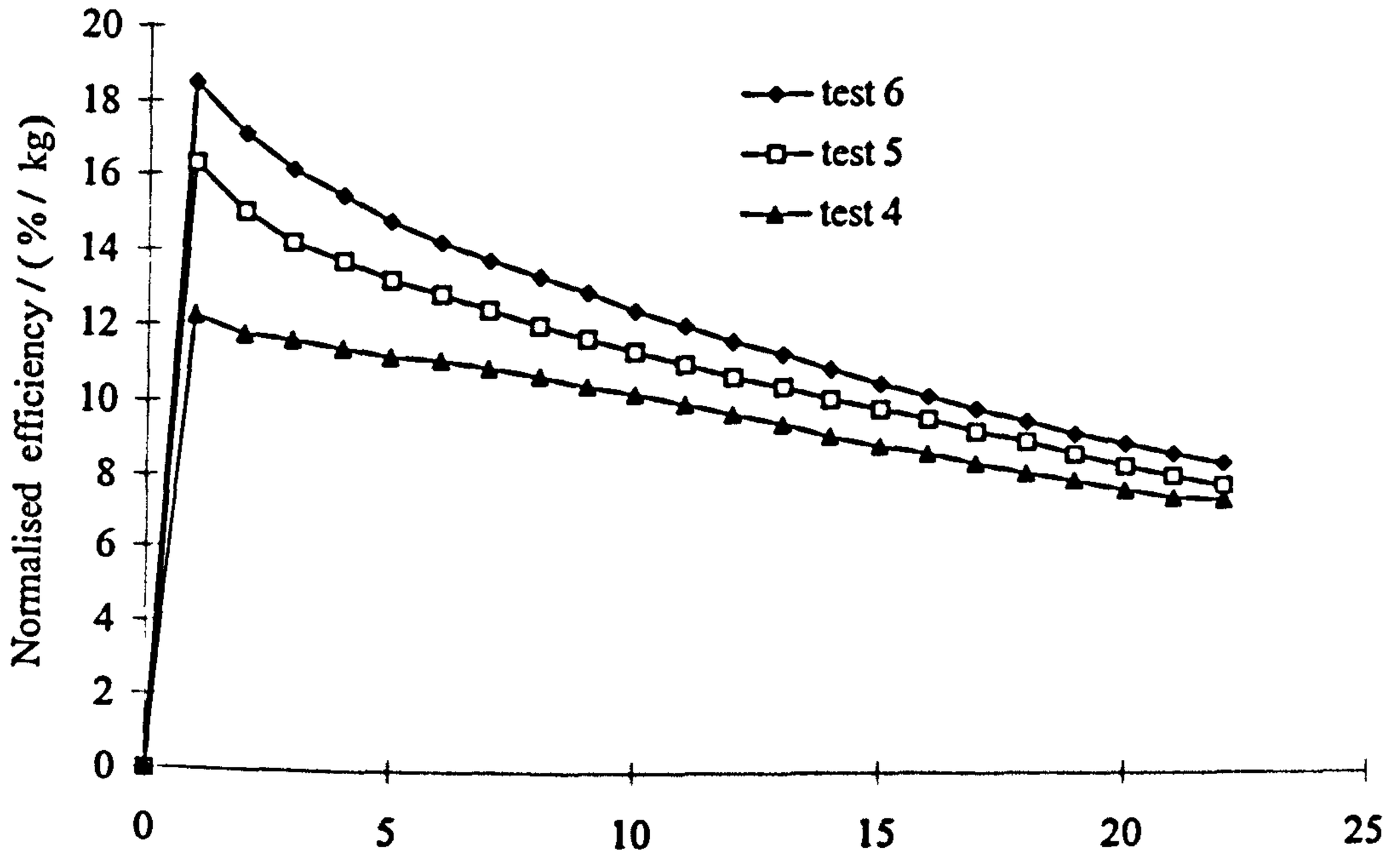

Figure 5.18: Variation in the cumulative normalised drying efficiency with time during tests 4, 5 and 6.

Test 7, 8 and 9 (day to day drying tests with air-heater options A, B and C, respectively)

The same configurations of the air-heater employed in tests 4, 5 and 6 were used in tests 7, 8 and 9, respectively. These tests were, as stated in section 3.3.1, conducted to evaluate the effect of the thermal mass of the dryer on its performance. During the tests, the crop mass was left in the dryer at the close of a day's experimental run while the solar simulator was switched off, thus providing no externally supplied energy until the beginning of the next day's run. In the calculation of the overall drying efficiency values presented in Table 5.6, the time was based on the length of time over which the solar simulator was effectively in operation during the days. The average initial moisture content of the cassava dried in each of these tests was 201.7%.

The results of tests 7, 8 and 9 are hereafter presented and discussed by comparing them with some pertinent results from tests 4, 5 and 6. A summary of the mean values of the laboratory test conditions in tests 4, 5, and 6 are provided alongside those obtained in tests 7, 8 and 9 in Table 5.6. An overview of the results of tests 7-9 is provided in Table 5.8.

Table 5.6: Mean values of the prevailing laboratory test conditions during tests 4 to 9

Test condition	Test 4	Test 5	Test 6	Test 7	Test 8	Test 9
Ambient relative humidity (%)	40.1	-[a]	34.9	49	30.7	39.2
Ambient air temperature (°C)	23.2	24	24.9	24.1	23.7	24.7
Ambient wind speed (m/s)	0.01	0.01	0.01	0.01	0.01	0.01

[a] Value not recorded during the test

It can be seen from Table 5.6 that, the ambient air relative humidity values were slightly higher in tests 7 and 9 than the values recorded during tests 4 and 6. No significant differences in the ambient air temperatures were observed in these comparative tests, except for tests 4 and 7 in which a mean difference of nearly 1° C was recorded.

Figure 5.19 shows the mean drying curves for tests 7, 8 and 9. The vertical portions of the 'curves' represent the night time drying with their end points denoting the moisture contents at the end of a particular day's run and the beginning of the following day's run. The broken horizontal line indicates the safe storage moisture content of 20.4%, dry basis. The drop in the moisture contents over the nights in each of the tests (see fig. 5.19) indicates that drying took place during the nights in all the tests. Comparing the drying curves in

figs. 5.11 and 5.19, it can be seen that the rate of drying was generally faster in tests 7, 8 and 9 than in tests 4 to 6. For example, for the same 22 hours of external energy supplied to the dryer, the product dried on daily basis in test 9 reached a content of 16.7% (dry basis) whereas the product dried on a continuous basis in test 6 reached a moisture content of 24% even though lower relative humidity values were observed in test 6 compared to test 9. As can be seen from fig. 5.19, when the cassava chips were dried in the dryer on daily basis, the worst rate of drying was realised in test 7; nonetheless, within 22 hours of external energy input the final moisture content of the cassava chips dried during test 7 was 23.9% compared to a value of 49.7% obtained with the same air-heater configuration in test 4. Since the laboratory test conditions during tests 7, 8 and 9 were no better than those recorded during tests 4 to 6, the faster rates of drying achieved in tests 7, 8 and 9 compared to the drying rates observed in tests 4, 5 and 6 (see Table 5.6), in which drying was carried out continuously on under almost exactly similar test conditions, can be attributed primarily to the contribution of nocturnal drying in tests 7, 8 and 9. The total nocturnal moisture loss in tests 7 , 8 and 9 were computed using equation 4.133 and found to be 136.5g, 181.4g and 48.8g respectively, compared to the total moisture loss over the drying period their values of which were found to be 840, 607.3 and 684.2 g, respectively. Thus, the nocturnal moisture accounted for 16.3, 29.9 and 7.1% of the total moisture lost in tests 7, 8 and 9, respectively to bring the products to the final moisture levels attained. The nocturnal moisture loss can be explained as follows: during the day, part of the energy transmitted through the transparent chamber is absorbed by the structural members. This energy which would have otherwise been lost to the surroundings is released at night to the system, thus maintaining the temperature inside the chamber slightly above the product temperature and extending the drying time well into the night. The magnitude of the nocturnal moisture loss is influenced by two factors, namely: the vapour pressure of water in the surrounding air (which is a function of the air's temperature and relative humidity) and the vapour pressure of moisture in the crop (which is a function of the moisture content). The higher nocturnal moisture loss observed during the first night in test 8 compared to the values observed during the first nights in tests 7 and 9 could be attributed to the low ambient relative humidity values and higher product moisture content. It can be seen from fig. 5.19, that the nocturnal moisture loss decreases as the drying progresses. This observation is due to the fact that as the drying progresses, the vapour pressure of the moisture in the product decreases thus resulting in a further reduction of the nocturnal

moisture loss. Since the rate of moisture loss from a material is strongly tied up with lower relative humidity of the surrounding air, a possible way of increasing the nocturnal moisture loss is to consider introducing desiccants in the drying chamber to absorb moisture within the chamber at night particularly during wet season drying.

The variations in the drying rates as functions of time and moisture content are illustrated in figs. 5.20 and 5.21, respectively. Figure 5.20 shows clearly that the drying rates were higher in test 9; in 19.6 hours the product moisture content was reduced from an initial value of 201.7% to the desired level of 16.8%. In the case of tests 7 and 8, at the end of 19.6 hours of external energy supply, the product moisture contents were 40 and 20%, respectively. Figure 5.21 shows that the drying rates recorded during test 9 were higher than the values noted in tests 7 and 8, at all moisture content levels.

Since nocturnal moisture loss contributed significantly to the total moisture loss in tests 7, 8 and 9, it can be concluded from the above experimental observations that connecting or incorporating a physical heat storage equipment to dryers to store up energy which would otherwise be lost during the day for drying during the night can be justified, particularly in solar drying.

The normalised overall drying efficiencies plots in fig. 5.22 show that at the end of 19.6 hours of external energy input their values were: 8.64 %/kg for test 7; 9.60 %/kg for test 8; and 9.80 %/kg for test 9. These values are greater than the corresponding values of 7.8, 8.4 and 9.0 %/kg obtained in tests 4, 5 and 6 (see fig. 5.18), emphasising the added advantage in utilising the energy stored up in the structural members of the dryer for drying at night.

Test 10 (day to day drying test with air-heater option C and drying bed at a height of 240 mm from the base of the drying chamber)

In test 10, about 1117g of cassava chips were dried on a single tray suspended at a height of 240 mm from the base of the drying chamber. The same configuration of the air-heater was used in tests 9 and 10. However, in test 9, 1116.3g of cassava chips were dried on a single tray suspended at a height of 190 mm from the base of the drying chamber. For purposes of comparison, the results of test 10 are presented alongside those obtained in test 9.

The diurnal variations in the ambient air relative humidity and temperature, and in the heated air temperature inside the plenum and drying chamber, for tests 9 and 10, are illustrated in figs. 5.23(a) and 5.23(b). The results indicate a slight predominance of higher drying air temperatures inside the plenum and the chamber during test 10 over test 9. The hourly average heated air temperatures recorded over the drying periods in the plenum and the chamber respectively were between: 30.6-34.7° C and 31.6-38.9° C for test 9; and 31 - 33.5° C and 32.9 -39° C for test 10. The corresponding mean values of the drying air temperatures recorded inside the plenum, drying chamber and chimney over the test periods were: 33, 36.5 and 35° C and 33.3, 36 and 31.2° C in tests 10 and 9, respectively. However, ambient air relative humidity values recorded over the drying periods were higher in test 10 than in test 9. The ambient air relative humidity values recorded in test 9 were between 35.7 and 45.2% compared to values of 35.8 to 53.2 % obtained in test 10. The mean ambient air temperature and relative humidity values recorded over the two test periods were: 24.9° C and 35.5% for test 9; and 24.4° C and 41.7% for test 10.

The mean air mass flow rates over the drying periods ranged between 0.0132 - 0.0159 kg/s for test 9, and 0.0127 - 0.0169 kg/s for test 10 (see fig. 5.24). Comparatively, higher air flow rates were observed in test 10 than during test 9.

The mean drying curves for tests 9 and 10 are shown in figs. 5.25 to 5.27. Figure 5.25 shows the variations in moisture content with time; while figs. 5.26 and 5.27 illustrate the variations in the drying rates with time and moisture content, respectively. Figure 5.25 shows that the rate of drying in test 10 was marginally faster than in test 9. For 19 hours of external energy supply, 1117.2g of cassava chips were dried from a moisture content of 210.6% to a final value of 20.7% in test 9; whereas the final moisture content attained in test 10 after the same length of time was 18.3%, dry basis. As can be seen from figs. 5.26 and 5.27, during the first day (at higher moisture contents) the hourly rates of drying were generally faster in test 9 compared to the rates achieved in test 10. During the second and third days, (at low moisture content level) the drying rates were consistently higher in test 10 than in test 9, at all moisture contents over the test periods. It is clear from the experimental data that the radiative and convective heat fluxes as well as the air mass flow rate reaching the drying bed were greater in test 10 than in test 9. Since the relative humidity of the air stream is the only other external parameter that can possibly affect the

rate of drying, it could be hypothesised that the lower relative humidity values observed in test 9 was the dominant factor responsible for the faster drying rates experienced in test 9 on the first day compared to the slower drying rates observed in test 10. Against the backdrop of the lower air relative humidity values recorded in test 9, the faster drying rates observed in test 10 (compared to the drying rates in test 9) during the second and third days of drying could probably be due to the dominance of the combined effects of better radiative and convective heat fluxes as well as the mass flow rates over the influence of lower air relative humidity values. Two important factors that emerge from the results of the comparative tests 9 and 10 are to be noted:

- In the early (initial) stages of drying, moderate air mass flux of lower relative humidity is desired to optimise the use of energy for drying. During this stage the moisture migration from the interior of the crop to the surface is at a faster rate and therefore higher air velocities and lower relative humidity is required to remove the moisture from the surface of the crop.

- In the final (later) stage of drying (at low moisture contents), moderate mass flow rates combined with high product temperatures will provide a more rapid drying. In this stage, the moisture content level of the crop is low, hence the moisture gradient across the crop from its interior to the surface is small and therefore high product temperatures are required for higher vapour pressure gradients to enhance drying.

From fig. 5.25, it can be seen that after 7 hours of drying during the first day, in both cases, the moisture content (dry basis) at the close of the day were 98.5 and 110.3% in tests 9 and 10, respectively. Subsequently, the nocturnal moisture loss on the first night (represented by the vertical portions of the curves in fig. 5.19) was higher in test 10 than in test 9. The tests were ended on the second day of drying at moisture contents of 41.7% and 44% in tests 9 and 10, respectively. It is clear from fig. 5.25 that, the nocturnal moisture loss on the second night was greater in test 10. From these observations, it can be concluded that the nocturnal moisture loss is a function of the prevailing moisture content of the material being dried.

The drying curves (see the intersection of the horizontal broken line with the curves in fig. 5.25) show that the cumulative time required for drying approximately 1116 g of cassava chips from a moisture content of 201.7% to a desired level of 20.4% dry basis was reduced by 2 hours by simply raising the drying bed nearer the radiant heat source. Comparing the prevailing conditions under which tests 9 and 10 were performed, it can be alluded that, for the same convective heat flux into the system, higher drying rates can be achieved by increasing the radiant energy reaching the drying chamber. In solar drying, the use of a transparent chamber as opposed to an opaque one for the same drying system can therefore be strongly justified. It can also be postulated from the results that in the initial stages of drying, the single most important parameter that controls the rate of dying is lower air relative humidity.

Tests 11 and 12 (day to day drying tests with air-heater option C and employing same load but using three and two tiers of drying shelves, respectively)

One way of increasing the drying capacity of a solar dryer is by enlarging the drying surface area through an increase in the chamber cross sectional area. The alternative way of increasing the drying capacity, without necessarily enlarging the chamber surface area, is to employ tiers of trays or shelves arranged vertically and spaced apart for a given drying chamber volume. For a given load and chamber volume, the layer density per bed is reduced by either using multiple trays/shelves or by increasing drying chamber surface area. The purpose of tests 11 and 12 in this study, was to investigate the effect of reducing crop bed layer density by employing tiers of trays during drying.

The same quantity of cassava chips (about 1329 g) were dried in each of these tests. However, the product was spread on three and on two drying shelves in tests 11 and 12, respectively. With the drying trays loaded and arranged one vertically above the other and spaced out, the lower shelves receive some amount of direct incident radiation but most of the product is shaded by the upper shelves. The uppermost shelf is not shaded and therefore receives the maximum direct radiation coming through the roof (secondary collector) of the chamber. With the fixed solar simulator employed in this study, the heat source radiated energy directly onto the roof of the chamber with very little or no radiation incident on the crop surface from the sides of the chamber.

The changes in the drying air temperature across the drying beds together with the changes in the ambient air temperature and relative humidity observed during test 11 are illustrated in figs. 5.28. Figure 5.28 shows the temperature variation across the three drying beds during the four days of drying. The figure clearly illustrates that during the first day of drying, the temperature of the air stream leaving the middle layer was consistently lower than the temperature of the air stream entering it, but higher than the temperature of the air stream encountering the bottom layer (i.e. plenum temperature). On the other hand, the temperature of the air current leaving the top shelf was greater than all the temperatures recorded inside the drying chamber. From the second day onwards, it can be seen that higher temperatures of the air stream were recorded at the same locations inside the chamber. These observations can be explained along the following lines: In the operation of the dryer, ambient air is heated on its way to the chamber. The air transfers its sensible heat to the drying shelves, and to the product on its passage through the chamber, and leaves through the vent provided along the chimney. Upon encountering the bottom crop layer, the temperature of the heated air decreases as it gains moisture through drying of the product. The lower shelves receive incident radiation, but mostly they are shaded by the top shelf. During the drying run, the temperature of the air stream as it passes through the bottom layer drops but it is raised subsequently by the radiant energy reaching the chamber before it encounters the middle layer. An explanation along the same lines can be put up to justify the temperature of the air stream exiting the top bed. However, since the top bed is subjected to higher incident radiation than the lower beds, the air stream temperature coming out of the top bed is higher than the values recorded at the lower locations.

The hourly variations of the moisture content with time over the period of drying are presented in fig. 5.29. The figure shows that the bottom layer dried faster than the top and the middle layers. At the end of nearly 25 hours of external energy supply, the mean moisture content of the three layers were: 25.9% for the top layer; 28.5% for the middle layer; and 21.4% for the bottom layer. The overall mean product moisture content was 23.4% (dry basis). Figure 5.30 shows that during the first day of drying, the drying rate was higher for the bottom layer than the top and middle layers. Since the product moisture content was sufficiently high during the first day, it can be hypothesised from earlier results that the better air circulation and the relatively lower air stream relative humidity encountered by the bottom layer accounted for the higher hourly drying rates of the bottom

layer compared to the top and middle layers. It can be seen from fig. 5.30 that during the second day higher drying rates were recorded for the top layer. Following the first day of drying, the resistance of the product mass to the flow of air decreases hence the air circulation around the top bed improves. The improvement in the air circulation coupled with better radiant heat flux reaching the top bed possibly accounts for the higher drying rates recorded for the top bed compared to the middle and bottom layers. On the third and fourth days the air circulation to all the beds gets better and in addition the radiant heat flux reaching the lower beds is further improved. The rate of drying of the crop then becomes a function of the product moisture content. The relatively higher rates of drying recorded for the middle layer during the third and fourth nights than the top and bottom layers, is therefore explainable.

Figure 5.31 shows, in absolute terms, that the drying rate at all moisture contents was generally higher for the bottom layer, followed by the top then the middle layers. Following from this observation, it can be postulated that a better convective heat flux is perhaps more favourable than direct radiated heat flux for a drying process.

The mean drying curves, showing the variations in the product moisture content with time, for the two beds are shown in figs 5.32. The mean moisture content is lower for the top layer compared to the bottom layer at all times. After twenty-one hours of external supply of energy, the top and bottom layers dried from a moisture content of about 202% to 17.7 % and 28.1%, respectively while the mean product moisture content was 23.7% (dry basis). Figure 5.33 clearly indicates that the drying rates were higher for the top layer than the bottom layer at all moisture contents over the whole drying period. This observation can be explained as follows: The top layer was not shaded and therefore received maximum amount of direct incident radiation coming through the roof of the chamber compared to the bottom layer which is shaded by the top layer. The temperature of the top bed is expected to be higher than the bottom layer, hence crop moisture vapour pressure difference would therefore be higher for the top layer than the bottom layer. In addition, the air circulation through the top layer is better in test 12, thus the coupled effect of better air circulation and higher radiant energy reaching the top bed accounts for the faster drying rate of the top bed compared with the bottom layer. It is to be noted from the results of

tests 11 and 12 that, drying rates can be improved under the combined influence of radiant and convective heat fluxes.

Figure 5.34 shows the variation in the prevailing laboratory air conditions (temperature and relative humidity) and the heated air temperature profile of the beds. It can be observed that there was no notable difference in temperature between the air stream arriving at the bottom layer (plenum air temperature) and the ambient air temperature. Instead, the temperature of the air current entering the top layer is seen to be significantly higher than the temperature of air leaving the bottom layer. Thus the top layer was subjected to better convective heat flux and radiant energy than the bottom layer on all the days of the experiment, hence the faster drying rate of the top bed as observed during the test.

Test 13 (day to day drying test with air-heater option C and dryer loaded to design capacity of 3 kg, and dying bed at a height of 340 mm from the base of drying chamber)

In this test, the design capacity of the dryer was evaluated by loading it with 3 kg of cassava chips on a crop bed located at 340 mm from the chamber base. It can be inferred from the positioning of the crop bed relative to the heat source that during this test the crop bed received the maximum amount of direct radiant energy from the heat source than in any of the tests. Mould growth on the surface of the product being dried was detected on the second day of drying. The extent of the mould growth in test 13 was quite substantial compared with that during test 11.

The variations in the drying air conditions are illustrated in fig. 5.35. The figure clearly shows that during the first day of drying, no significant differences between the plenum, the chamber and the chimney air temperatures were observed. However, on the subsequent days the mean drying chamber and plenum air temperatures recorded were consistently lower than the chimney air temperatures. The hourly exhaust air relative humidity values recorded were consistently higher than the corresponding ambient air values. The magnitude of the exhaust air relative humidity is an indication of the amount of moisture evaporated from the product. The fact that its values remained well above those of the ambient over the entire duration of the test is suggestive that the drying chamber was saturated with vapour over the length of the test. The mean value of the exhaust air relative

humidity recorded over the duration of the test was 48.6% compared to the ambient mean value of 39.4%.

The variation in the mean moisture content with time is illustrated in fig. 5.36. It can be seen that, over the period of the test, the mean moisture content of the product was reduced from 201.7% to 21.1% (dry basis) in twenty-one hours. The nocturnal moisture loss over the period accounted for about 23.9% of the total amount of moisture removed from the product to bring it to a final moisture content of 21.1%. Figures 5.37 and 5.38 illustrate the variation in the hourly drying rates with time and moisture content, respectively. The drying rates were lower than the corresponding values achieved during test 11 and 12 (see figs. 5.30 and 5.33). The cumulative normalised drying efficiency was evaluated and found to be 7.5% lower than the value obtained in test 6, for instance. However, the pick - up efficiency was evaluated and found to be 28.2%. Though the drying air conditions in test 13 was no better than the conditions of the drying air in test 6, the higher pick-up efficiency realised in test 13 suggests that, the drying potential of the heated air was better utilised than in test 6. It is noted from the above that, the pick-up efficiency is perhaps most useful for evaluating the performance of a dryer used to dry different quantities of the same commodity. It would not be misleading to postulate that, it would be most important performance parameter in judging the performance of two or more dryers employed in drying the same product. The pick-up efficiency of 28.2% achieved in test 13 compares very well with the suggested optimal value of 30% for a dryer. Perhaps, the optimal load capacity for the dryer studied was in effect around 3 kg.

Quality of the dried products

Results from this study show that the peak air temperature observed in any of the tests was less than the recommended temperature ranges of 75° C and above (Cheema, 1978) at which the enzyme linamarase which produces the highly poisonous hydrocyanic acid in cassava is completely destroyed. No detailed pathological evaluation of the dried product was undertaken. However, visual examination of the products dried during the tests showed mould growth on the surface of the product in tests 11 and 13. The mould growth observed in test 13 was more severe than that realised in test 11. For test 11, the mould growth was higher on the middle layer than the bottom layer. The product dried on the top bed in test 11 showed no significant traces of mould growth.

The growth of the mould on the product surfaces during tests 11 and 13 may be attributed to the poor conditions of the drying air in contact with the product and/or excess drying load. Excess drying load is definitely not the cause for the mould growth observed in test 11. For example, in tests 4 and 8 greater loads (1430g and 1023.3g of cassava chips) were dried but no mould growth was detected. From Table 5.7, it can be seen the drying air conditions in test 11 were in some respects less favourable compared to the conditions in test 12, where no mould growth was observed. It can consequently be postulated that the poor air circulation and higher air relative humidity were responsible for the mould growth observed in test 11.

In test 13, the ambient air temperature and relative humidity values recorded were between 21.6-25.5° C and 32.3-47.3% with corresponding average values of 24.6° C and 39.4%, respectively. The mean air temperatures in the plenum, chamber and chimney were 31.7, 32.8 and 33.8° C, respectively. The mean exhaust air relative humidity and mass flow rate were 48.6% and 0.0145 kg/s, respectively. A cursory look at the test conditions that prevailed during tests 7, 12 and 13 shows that, the mean air conditions in test 13 were somehow better compared to the conditions observed in tests 7 and 12 (Table 5.6 and 5.8). However, no mould growth was observed in either test 7 or 12. The mould growth observed in test 13 is therefore attributable to the higher product load in relation to the drying air conditions experienced. It can be presumed that the 3 kg of wet cassava placed in the dryer was perhaps slightly on the higher side than would be allowed for a drying surface area of 0.16 m^2. Really, the loading density of 18.75 kg/m^2 employed during test 13 was far more than the recommended maximum layer density of 15 kg/m^2 (Keey, 1972) for rapid drying of cassava chips and hence the likely cause for the mould growth.

Table 5.7: Mean drying air conditions observed during tests 11 and 12

Drying air condition	Test 11	Test 12
Mean ambient air temperature (° C)	23.6	24.1
Mean ambient air relative humidity (%)	52.7	48.6
Mean exhaust air relative humidity (%)	43.9	43.1
Mean plenum air temperature (° C)	31.8	32.6
Mean chimney air temperature (° C)	35.6	35.6
Mean drying chamber air temperature (° C)	34.3	31.9
Mean mass flow rate (kg/s)	0.0132	0.0145

Table 5.8: An overview of results for tests 7, 8 and 9

Measured and calculated performance parameters	TEST 7				TEST 8			TEST 9		
	DAY 1	DAY 2	DAY 3	DAY 4	DAY 1	DAY 2	DAY 3	DAY 1	DAY 2	DAY 3
Starting time	10:55	10:25	10:00	10:25	10:07	08:50	09:55	10:15	10:00	09:05
Duration of drying (h)	7	7	7	6	3.6	9	7	7	7	8
Initial weight of the crop mass (grams)	1425	1029	748	594.5	1023.3	715.1	459.3	1116.7	735	502.2
Initial crop moisture content (kg_{water}/ $kg_{drv\ solid\ matter}$)	201.7	117.7	58.3	25.8	201.6	110.7	35.3	201.6	91.3	35.7
Final crop moisture content (kg_{water}/ $kg_{drv\ solid\ matter}$)	132.2	72.7	35.0	19.7	151.4	48.1	22.6	98.5	41.7	16.8
Minimum ambient air relative humidity (%)	45.2	46.3	49	50.1	30.7	29.4	25.2	37.4	35.7	35.9
Mean ambient air relative humidity (%)	47.3	47.2	49.7	51.9	31.7	32.3	28	39.1	38.3	38.5
Maximum ambient air relative humidity (%)	51.4	53.1	52.2	60.5	36.7	35.4	32.5	45.2	42.1	45.1
Minimum ambient air temperature (°C)	21.4	21.5	22	21	21	21.2	22.3	22.4	22.5	23
Mean ambient air temperature (°C)	24.3	24.4	23.7	23.9	24.5	23.4	23.8	24.3	25.1	25.5
Maximum ambient air temperature (°C)	25.3	25.3	24	24.2	25.8	25.1	25.1	25.4	26.7	26
Minimum glazing temperature (°C)	46.4	45.6	46.6	47.0	42.3	41.8	41.8	40.7	40.1	49.7
Mean glazing temperature (°C)	47.8	48.0	47.7	47.9	43.1	49.2	42	42.4	41.7	42.5
Maximum glazing temperature (°C)	49.1	49.1	48.0	48.3	43.6	42.9	42.1	43.9	43.2	44.1
Minimum absorber plate temperature (°C)	54.9	54.4	55.0	55.6	48.7	48.4	48.2	48.1	49.1	49.7
Mean absorber plate temperature (°C)	56.4	56.5	56.2	56.2	49.6	49.2	48.4	50.0	50.5	50.7
Maximum absorber plate temperature (°C)	57.6	57.6	56.5	56.6	50.1	49.8	48.6	51.4	51.7	51.2
Minimum bottom plate temperature (°C)	24.9	26.5	25.3	25.7	25.4	25.0	25.7	27.8	28.7	29.8
Mean bottom plate temperature (°C)	26.2	27.0	26.5	26.7	26.4	26.5	26.2	29.6	30.3	31.7
Maximum bottom plate temperature (°C)	27.2	27.4	26.8	27.1	27.0	26.9	26.4	30.6	31.6	32.9
Minimum heated air temp. in upper channel (°C)	49.7	49.4	49.9	50.7	35.3	33.9	33.7	29.3	28.8	31.7
Mean heated air temp. in upper channel (°C)	51.3	51.5	51.0	51.5	35.7	34.8	34.0	30.5	30.6	32.8
Maximum heated air temp. in upper channel (°C)	52.6	52.3	51.2	51.9	36	35.2	34.3	31.7	32.2	33.6
Minimum heated air temp. in lower channel (°C)	24	25.4	24.2	24.7	30.6	29.8	29.9	32.9	33.1	35.8
Mean heated air temperature in lower channel (°C)	25.0	25.9	24.8	25.4	31.2	30.6	30.1	34.6	34.8	37.1
Maximum heated air temp. in lower channel (°C)	25.8	27.2	25	25.6	31.6	30.8	30.4	35.7	36.1	37.7
Min. heated air velocity in lower channel(m/s)	0.36	0.38	0.4	0.4	0.36	0.4	0.38	0.4	0.4	0.38
Mean heated air velocity in lower channel(m/s)	0.40	0.42	0.43	0.45	0.39	0.42	0.42	0.42	0.44	0.45

Table 5.8: continued.

Measured and calculated performance parameters	DAY 1	DAY 2	DAY 3	DAY 4	DAY 1	DAY 2	DAY 3	DAY 1	DAY 2	DAY 3
Max. heated air velocity in lower channel(m/s)	0.43	0.44	0.48	0.48	0.4	0.48	0.48	0.45	0.48	0.48
Min. heated air velocity in upper channel(m/s)	0.12	0.14	0.14	0.13	0.3	0.32	0.3	0.14	0.11	0.11
Mean heated air velocity in upper channel(m/s)	0.14	0.15	0.14	0.15	0.32	0.33	0.35	0.15	0.13	0.15
Max. heated air velocity in upper channel(m/s)	0.16	0.18	0.15	0.16	0.32	0.38	0.38	0.18	0.16	0.18
Minimum heated air temperature in plenum (°C)	24.8	26.9	25.8	26.9	27.3	27	27.5	30.6	31.9	33
Mean heated air temperature in plenum (°C)	26.3	27.3	26.7	27.0	28.2	27.8	28	32.4	33.4	34
Maximum heated air temperature in plenum (°C)	27.3	28.1	27.3	27.3	28.6	28.2	28.2	34	34.8	34.5
Minimum chimney air temperature (°C)	32.8	35	35	36.5	31.8	33	34	28.6	29.7	30.8
Mean chimney air temperature (°C)	34.0	36.1	35.8	36.9	33	34.3	34.3	30.1	31.2	32.1
Maximum chimney air temperature (°C)	35.3	37.5	36.3	33.6	32.5	34.8	34.3	31.7	32.8	33.9
Minimum relative heating index	0.05	0.08	0.11	0.11	0.09	0.10	0.09	0.22	0.18	0.24
Mean relative heating index	0.08	0.11	0.12	0.12	0.11	0.14	0.13	0.25	0.24	0.25
Maximum relative heating index	0.09	0.14	0.13	0.15	0.13	0.20	0.16	0.28	0.26	0.28
Minimum air temp. inside drying chamber (°C)	28.5	31.1	30.5	32.7	30.3	31.7	35.7	31.6	33.7	34.6
Mean air temperature inside drying chamber (°C)	29.8	32.2	31.9	33.4	31.5	34.3	35.9	33.8	36.2	37.7
Max. air temperature inside drying chamber (°C)	30.7	34.6	32.6	33.6	32.5	35.8	36.2	35.8	38.1	38.9
Minimum exit air temperature (°C)	25.9	26	26.3	26.6	26	24.5	26.9	25.7	26.3	27
Mean exit air temperature (°C)	27.0	27.1	26.9	27.2	26.2	26.7	28.1	26.8	27.9	28.5
Maximum exit air temperature (°C)	28.4	27.9	27.5	27.5	26.3	28.3	28.8	28.3	29.4	31.3
Minimum exit air relative humidity (%)	46.3	43.2	41.3	40.2	40.9	29.8	26.4	42.4	33	28.5
Mean exit air relative humidity (%)	51.5	46.7	42.9	41.7	42.5	31.5	31.6	44.8	36.7	38.6
Maximum exit air relative humidity (%)	56.5	53.2	44.5	45.6	44.3	35.1	35	50	41.7	37.6
Min. drying air temp. rise in upper channel (°C)	26.2	25.9	26.9	27.5	10.1	9.7	9.2	6.0	4.1	6.6
Mean drying air temp. rise in upper channel (°C)	27	27.0	27.2	27.6	11.2	11.4	10.2	6.2	6.5	6.4
Max. drying air temp. rise in upper channel (°C)	27.3	26.9	27.6	28.1	12.1	13.3	11.1	6.5	6.0	7.9
Min. drying air temp. rise in lower channel (°C)	0.5	0.56	0.97	1.4	5.69	5.54	5.0	9.6	8.1	10.8
Mean drying air temp. rise in lower channel (°C)	0.7	1.5	1.1	1.5	6.7	7.2	6.3	10.3	9.7	11.6
Max. drying air temp. rise in lower channel (°C)	1.2	1.3	1.3	1.8	7.4	9.4	7.1	10.8	10.5	12.3
Overall drying efficiency (%)	14.8	14.5	11.9	10.1	13.5	12.7	9.9	17.2	13.4	10.3
Normalised drying efficiency (% / kg)	10.4	9.7	8.3	7.1	13.2	12.4	9.4	15.5	12.0	8.8

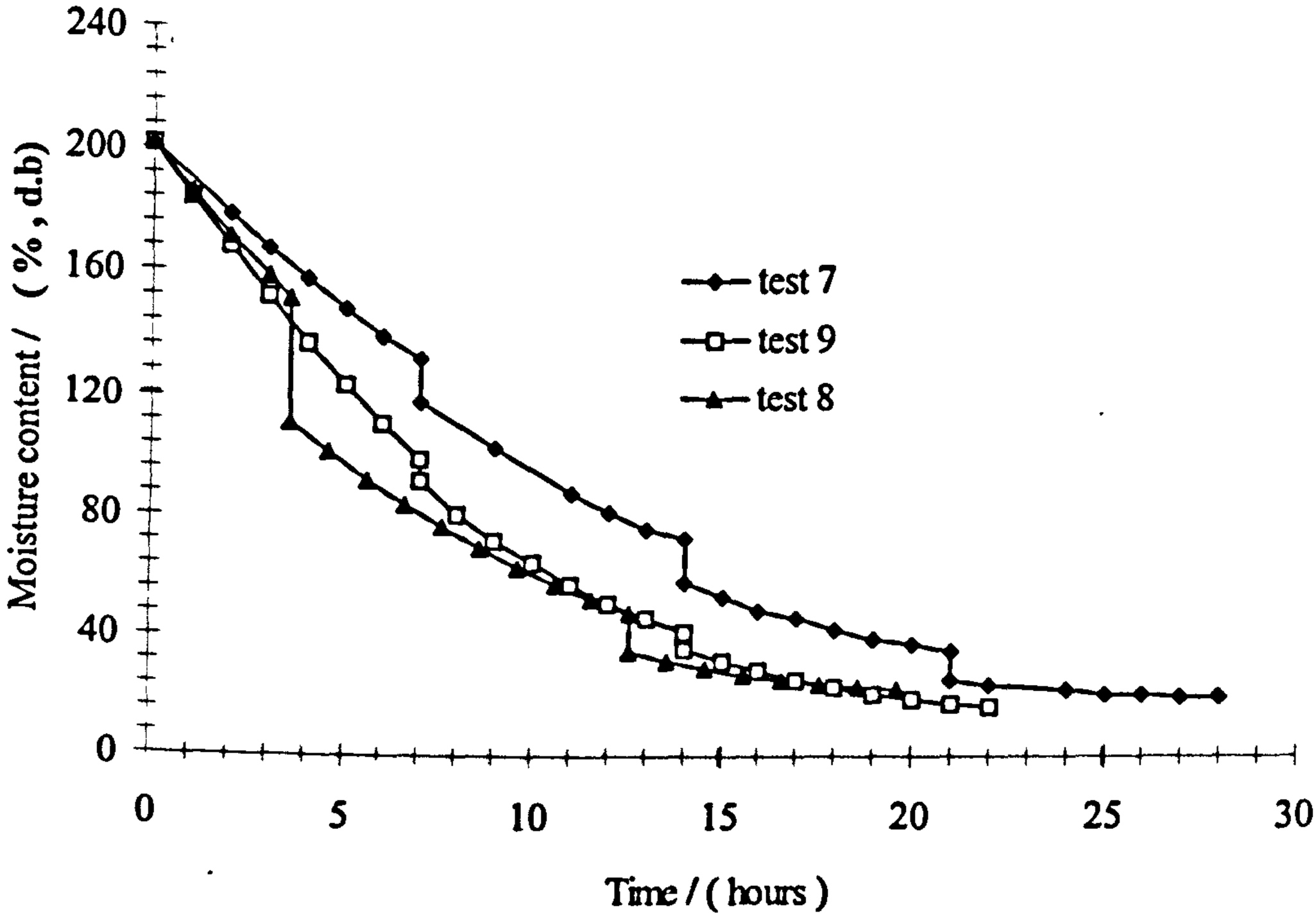

Figure 5.19: Mean drying curves for tests 7, 8 and 9

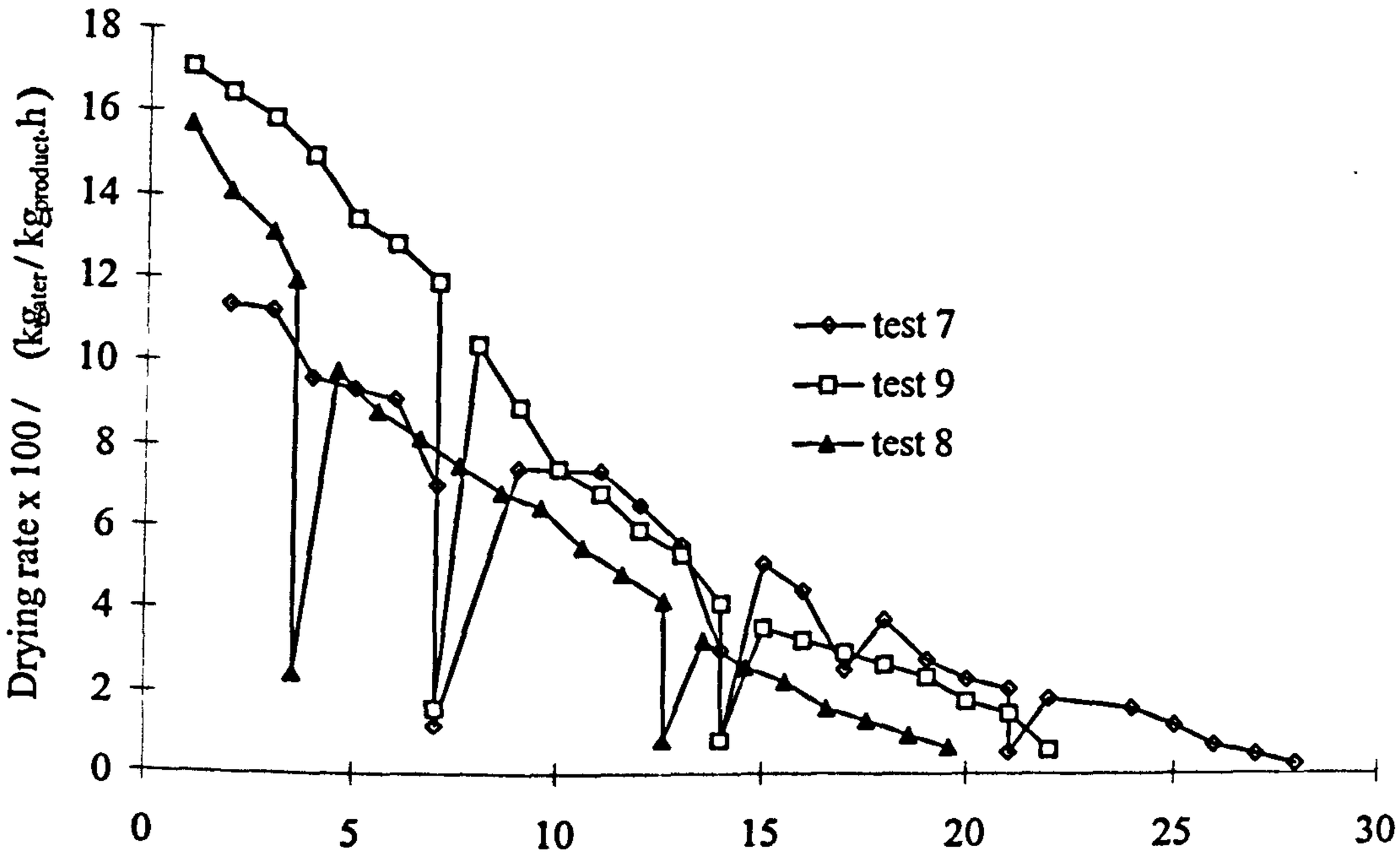

Figure 5.20: Variation in the drying rate of cassava chips with time during tests 7, 8 and 9.

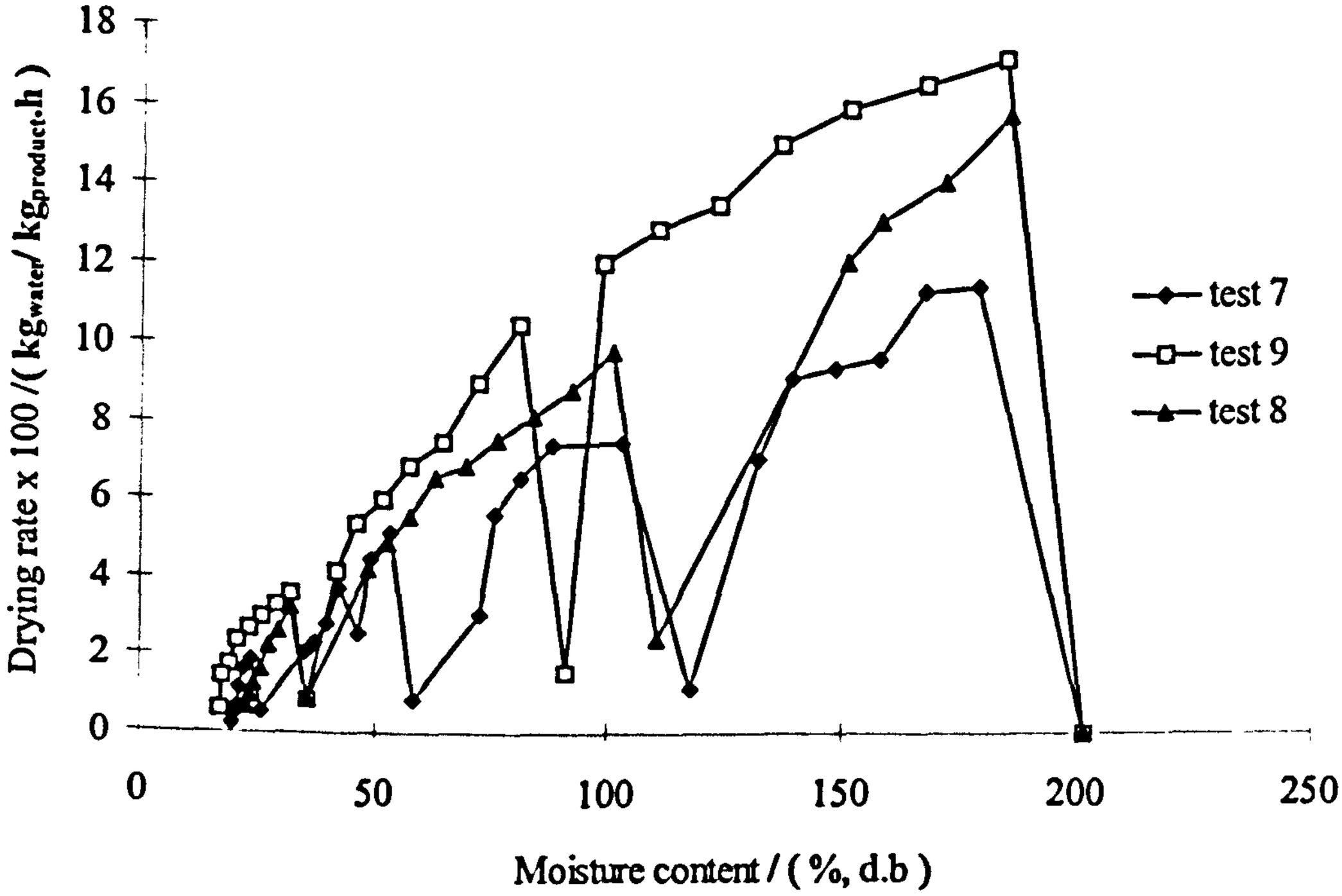

Figure 5.21: Variation in the drying rate of cassava chips with moisture content during tests 7, 8 and 9.

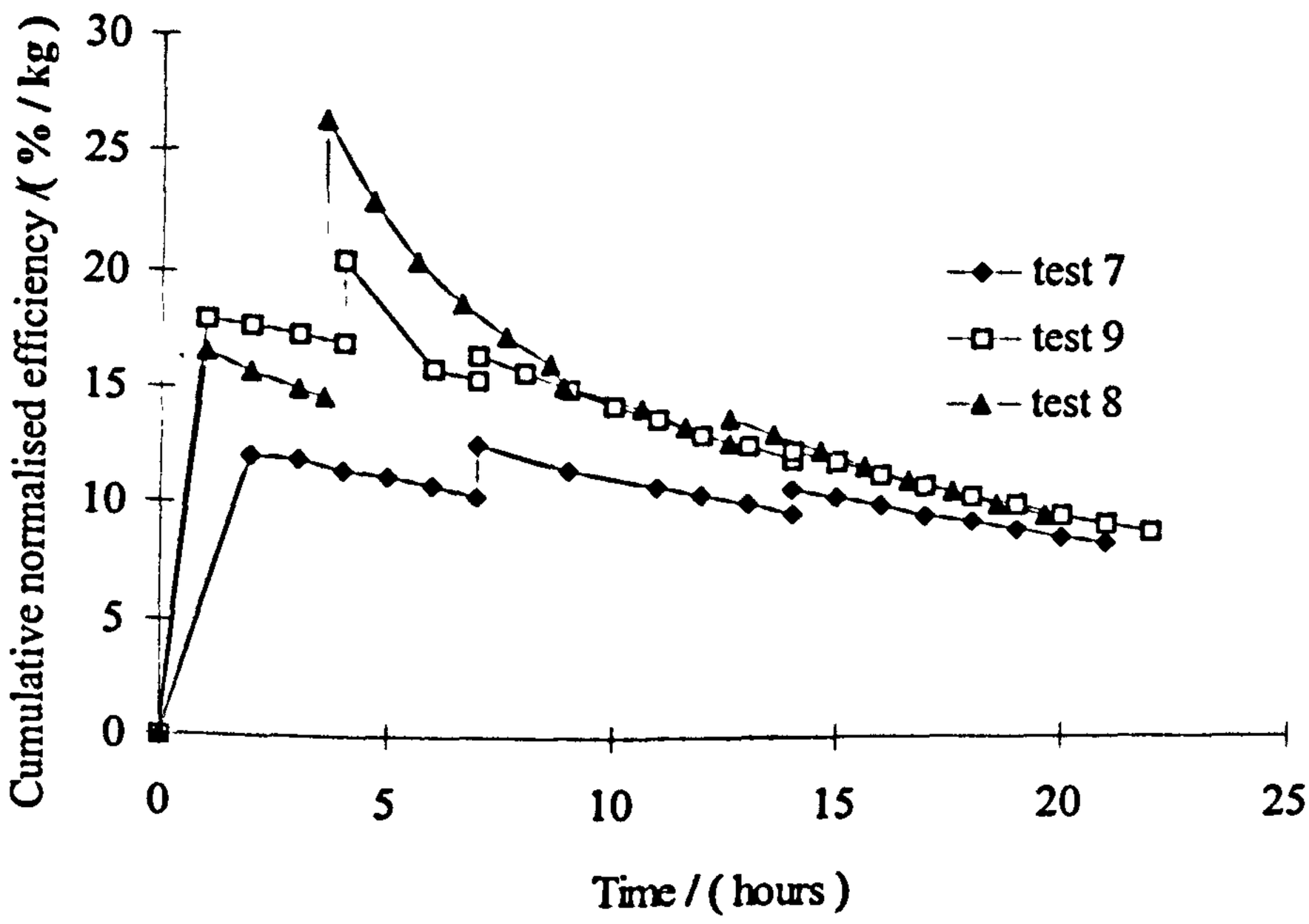

Figure 5.22: Variation in the cumulative normalised drying efficiency with time during tests 7, 8 and 9

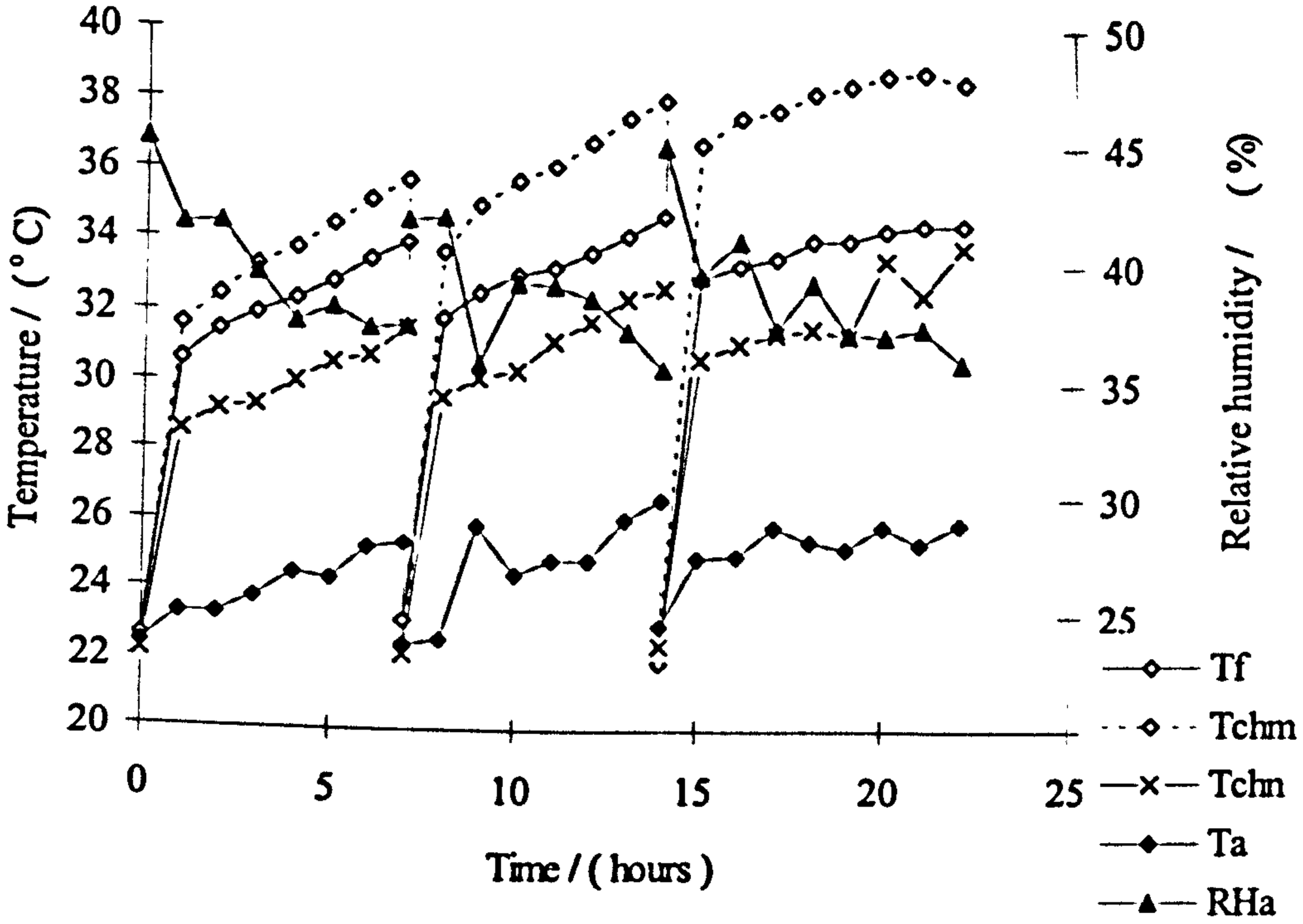

Figure 5.23a: Variation in the drying air conditions with time during test 9

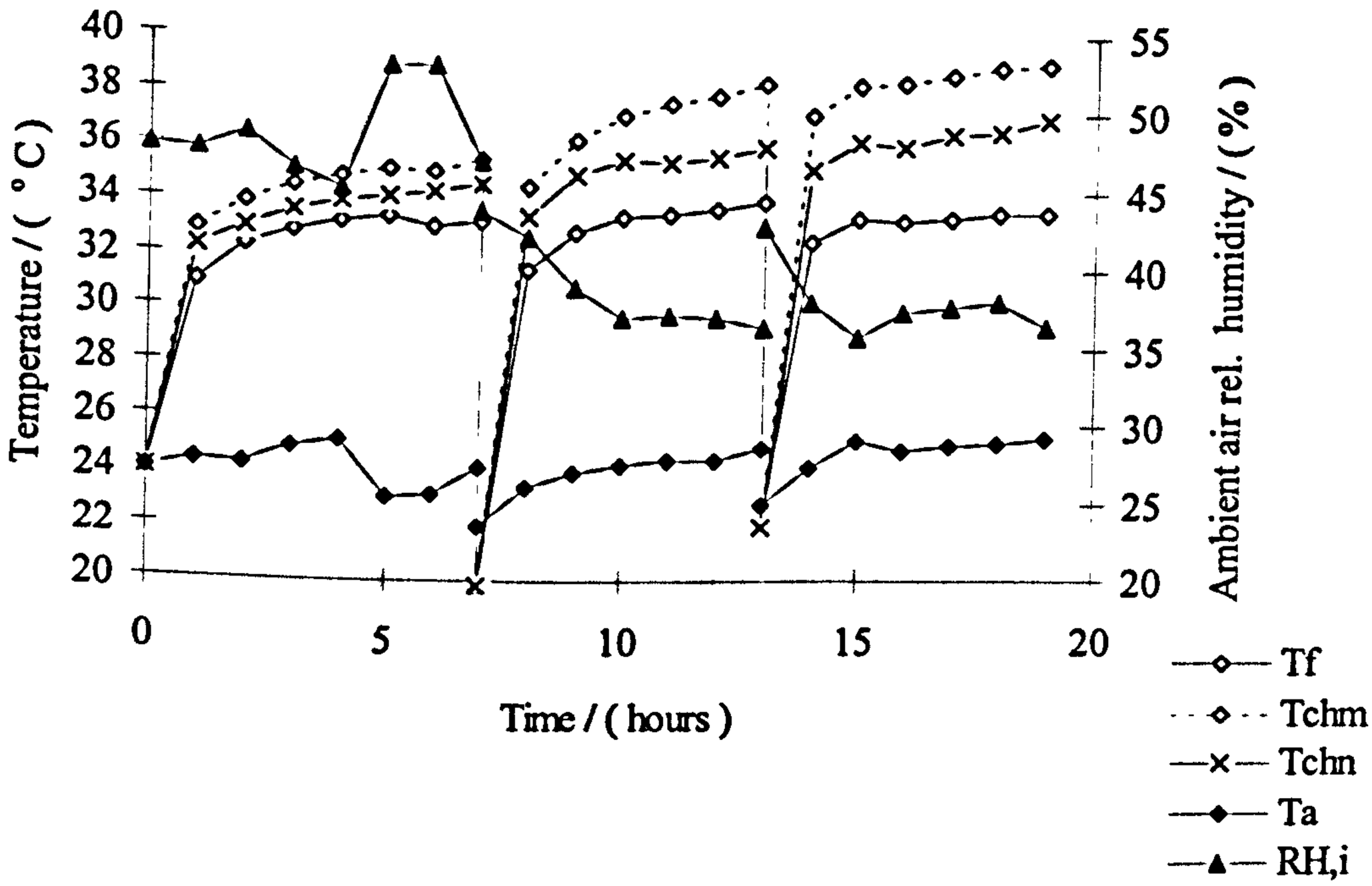

Figure 5.23b: Variation in the drying air conditions with time during test 10.

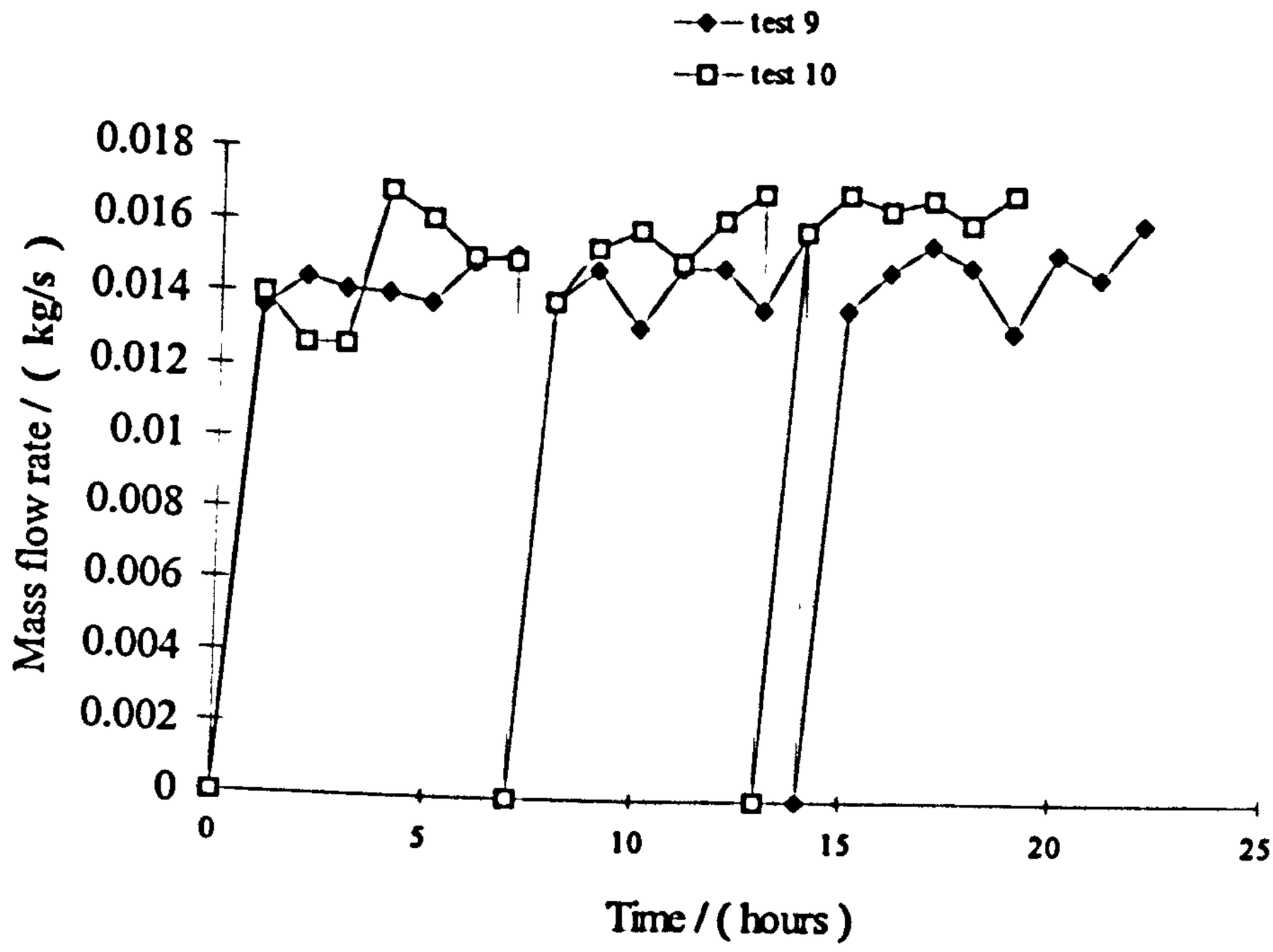

Figure 5.24: Variation in the air mass flow rate with time during tests 9 and 10.

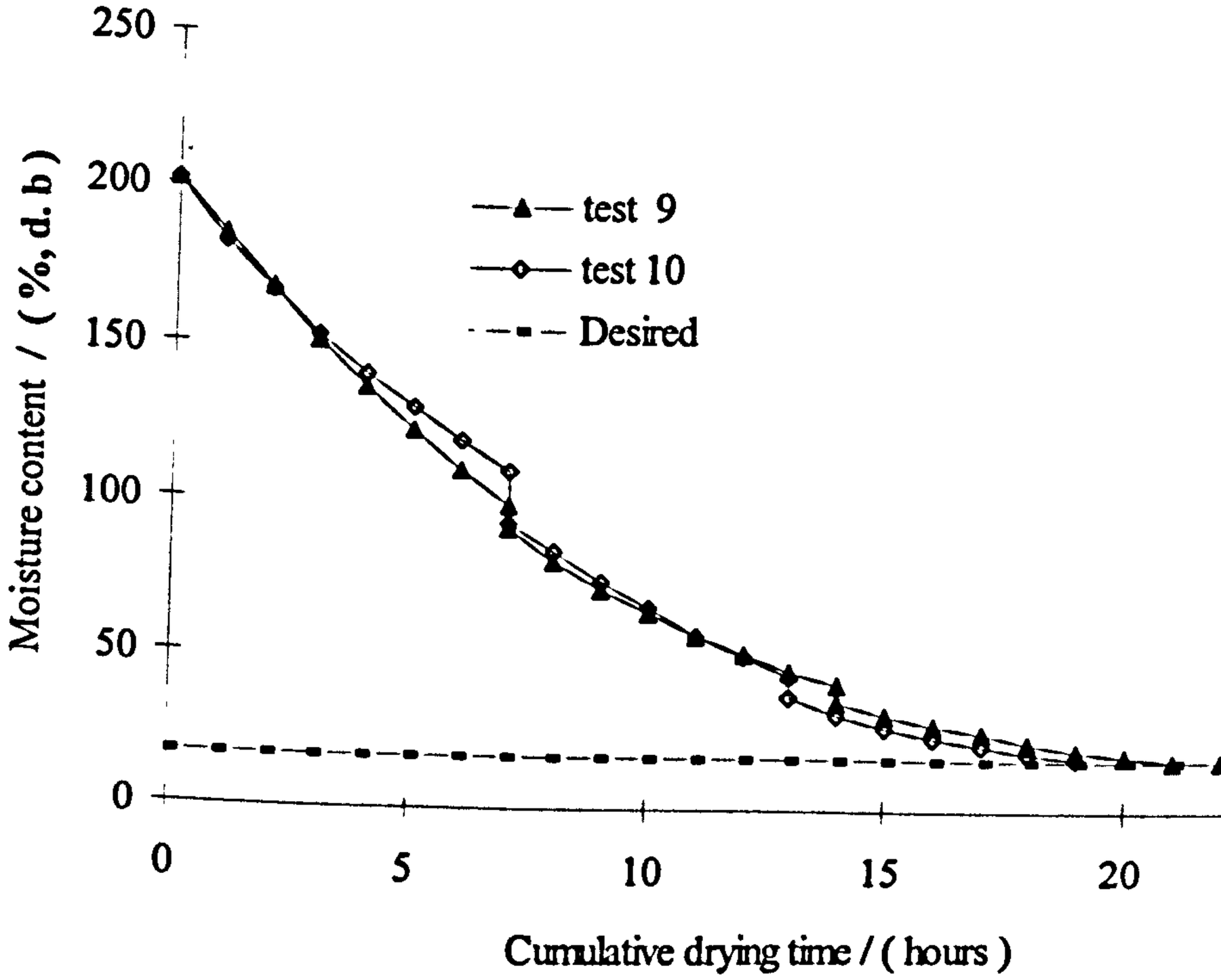

Figure 5.25: Changes in the product moisture content with time during tests 9 and 10.

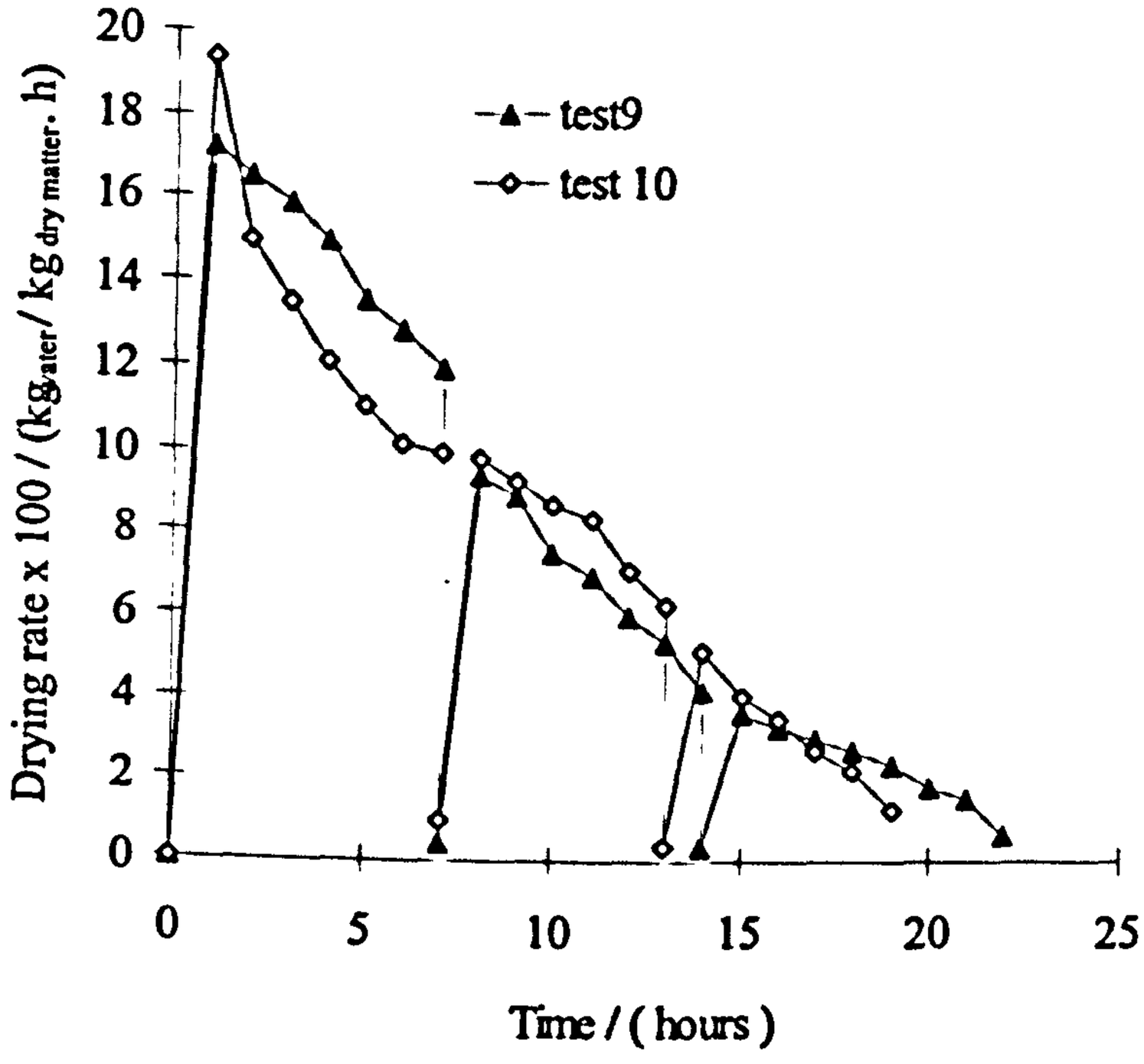

Figure 5.26: Variation in the drying rate of cassava chips with time during tests 9 and 10.

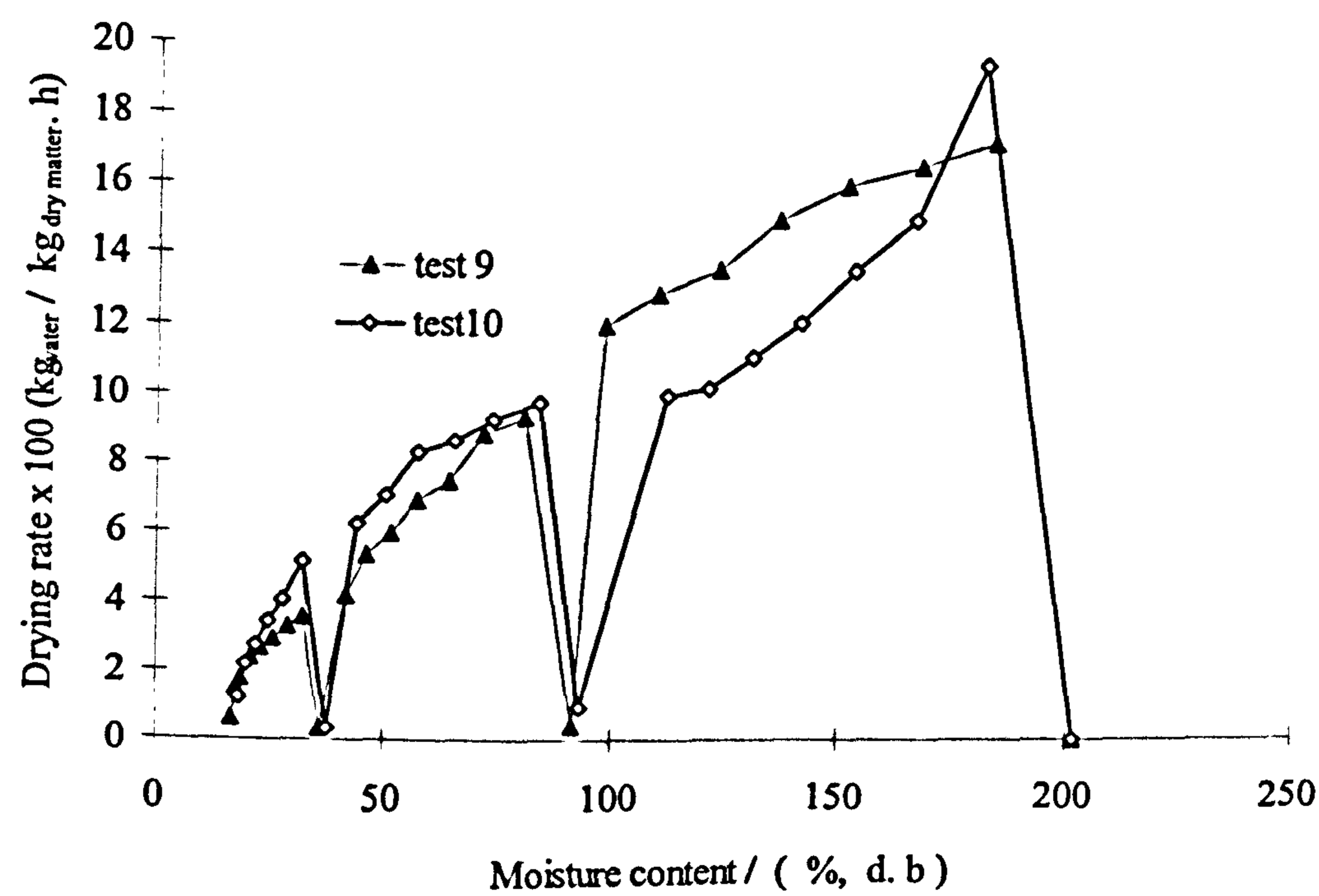

Figure 5.27: Variation in the drying rate of cassava chips with moisture content during tests 9 and 10

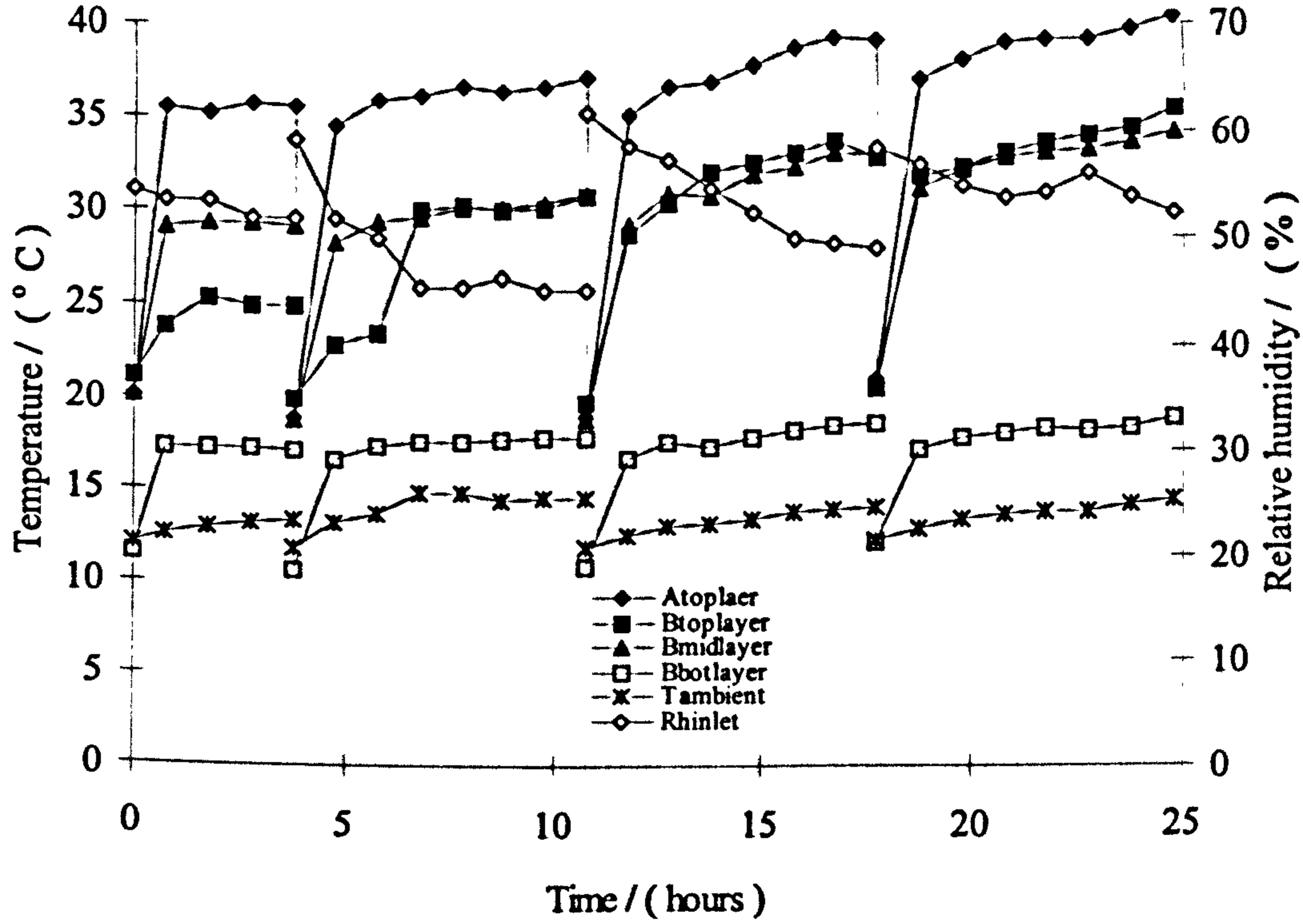

Figure 5.28: Variation in the drying air conditions with time during test 11.

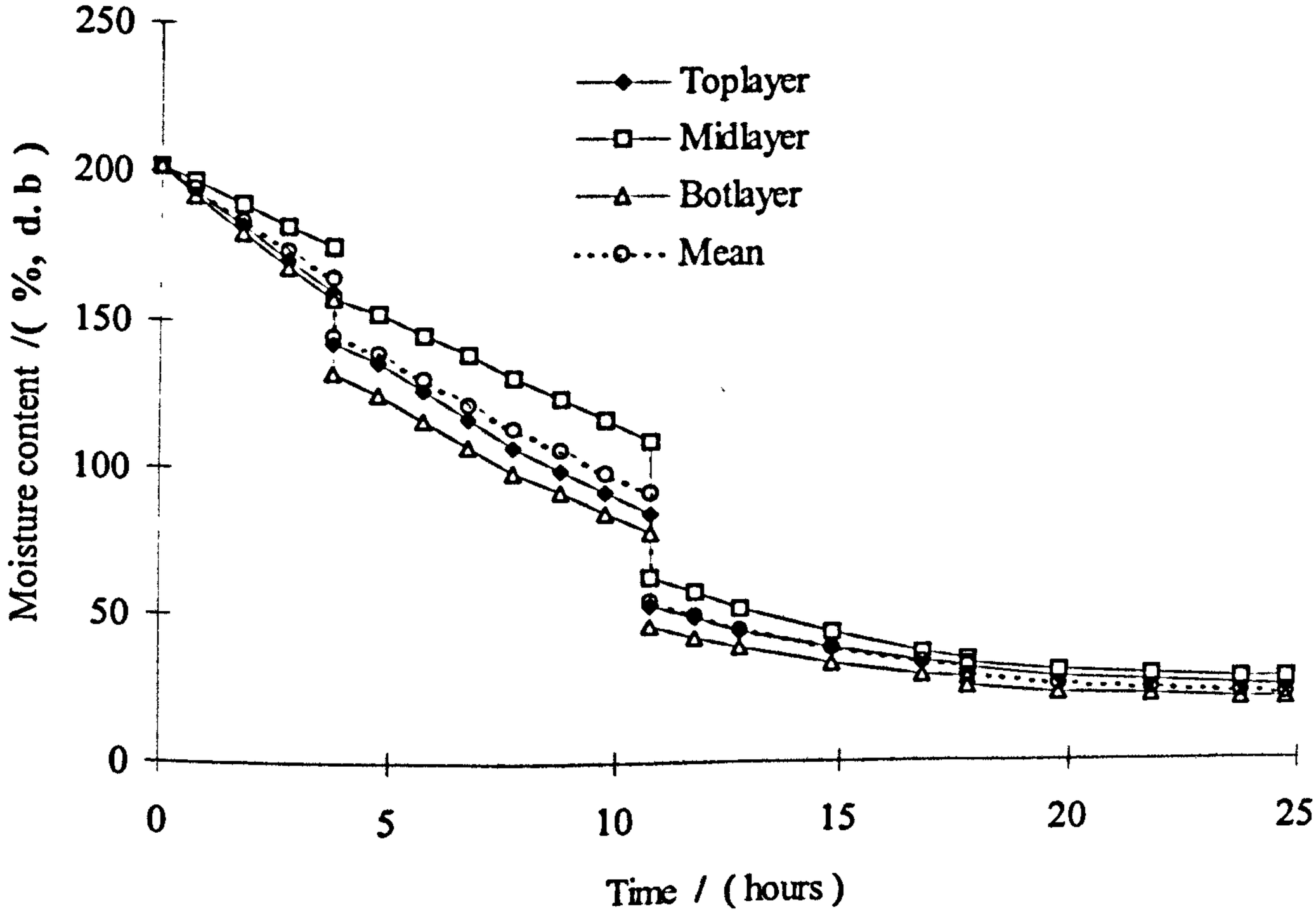

Figure 5.29: Variation in the product moisture content with time during test 11

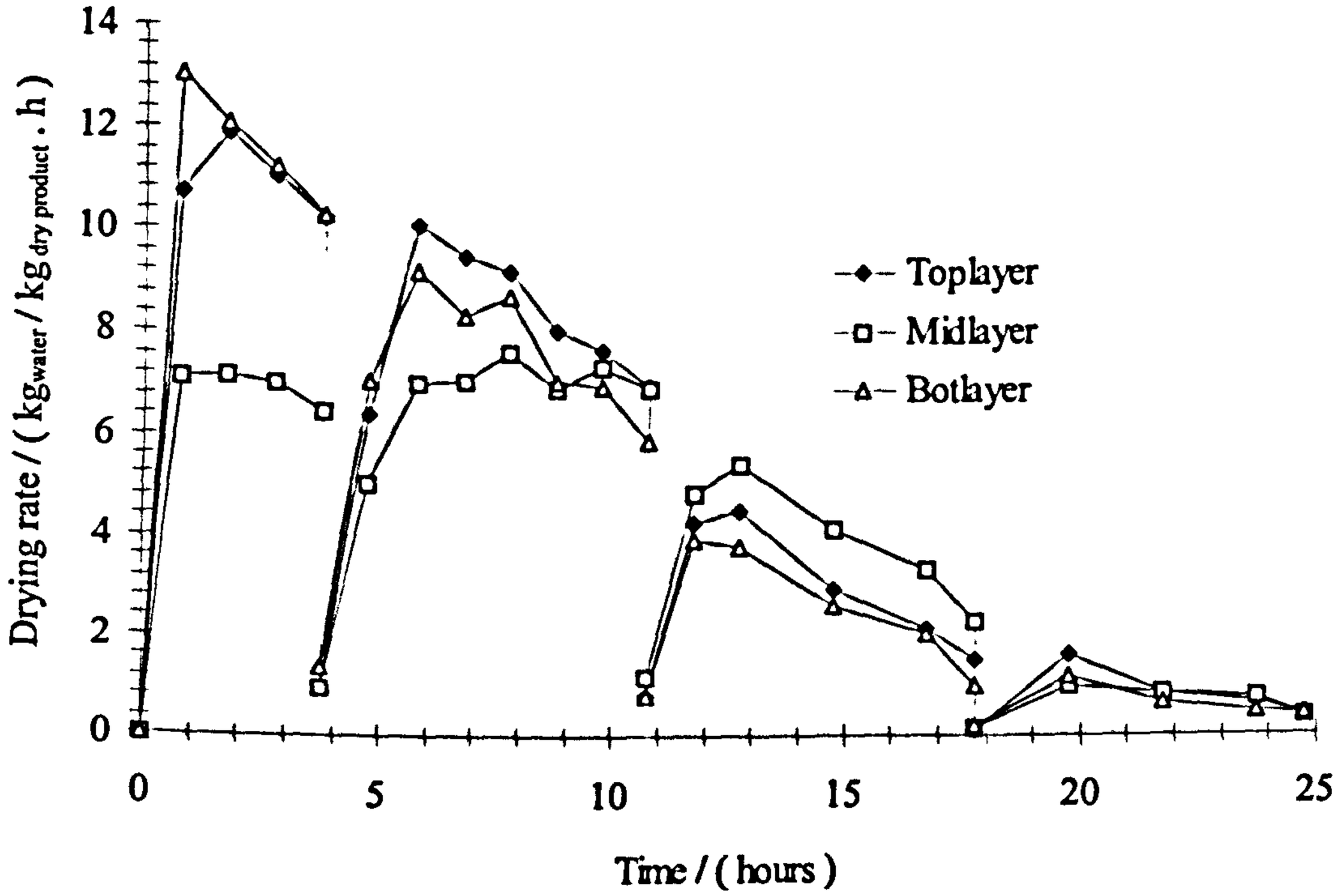

Figure 5.30: Variation in the drying rate of cassava chips with time during test 11.

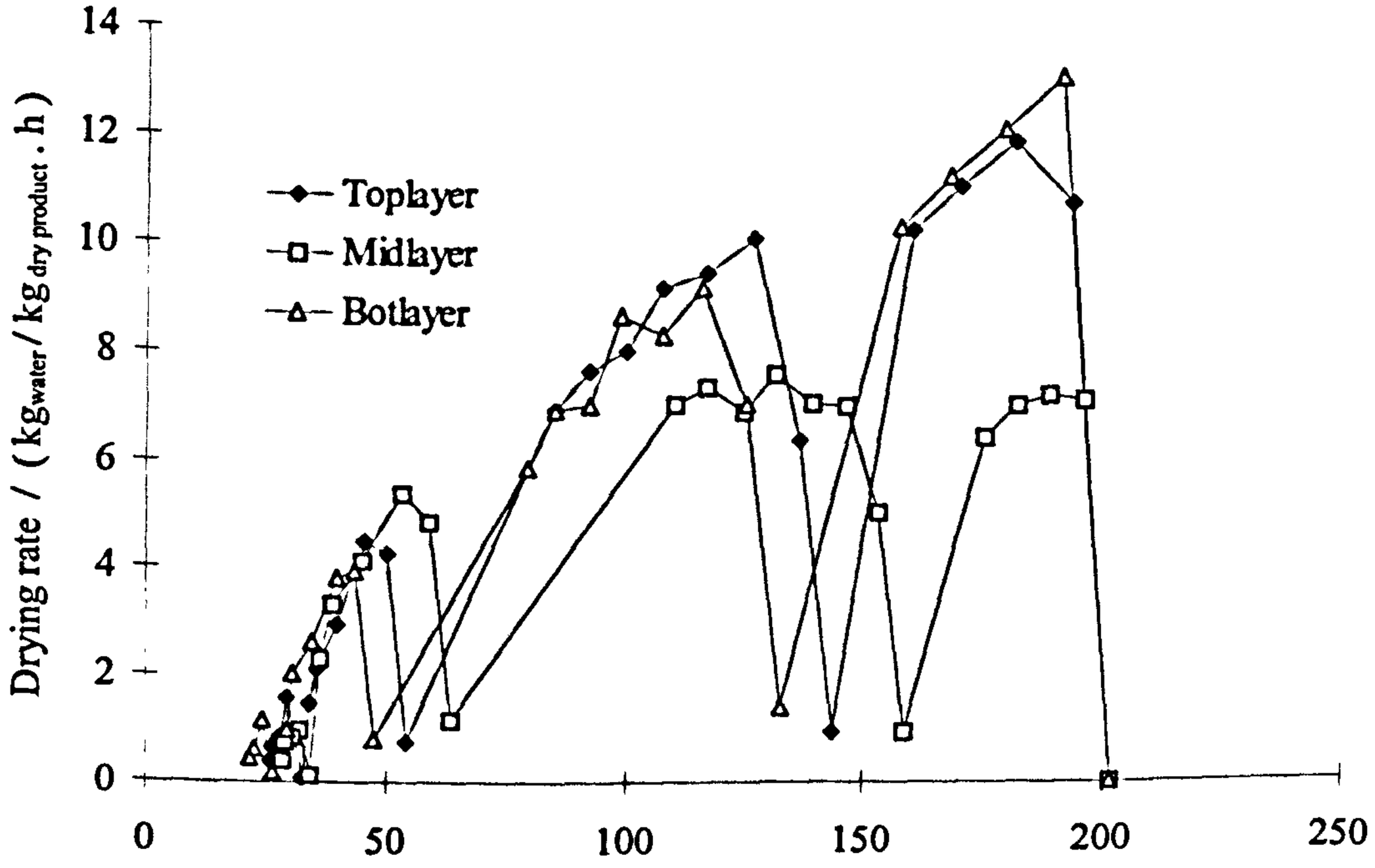

Figure 5.31: Variation in the drying rate of cassava chips with moisture content during test 11.

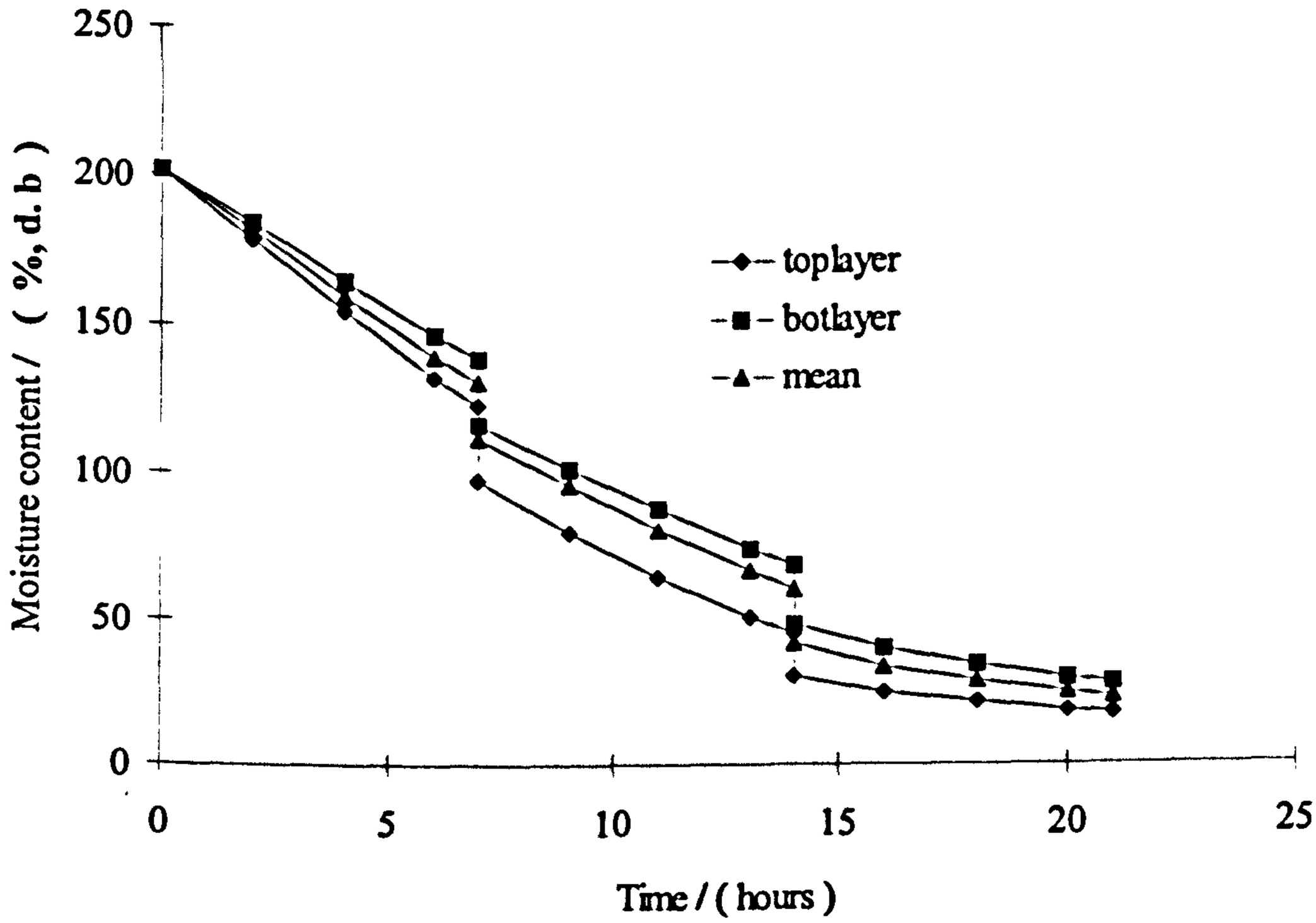

Figure 5.32: Variation in the moisture content of cassava chips dried in two layers with time during test 12

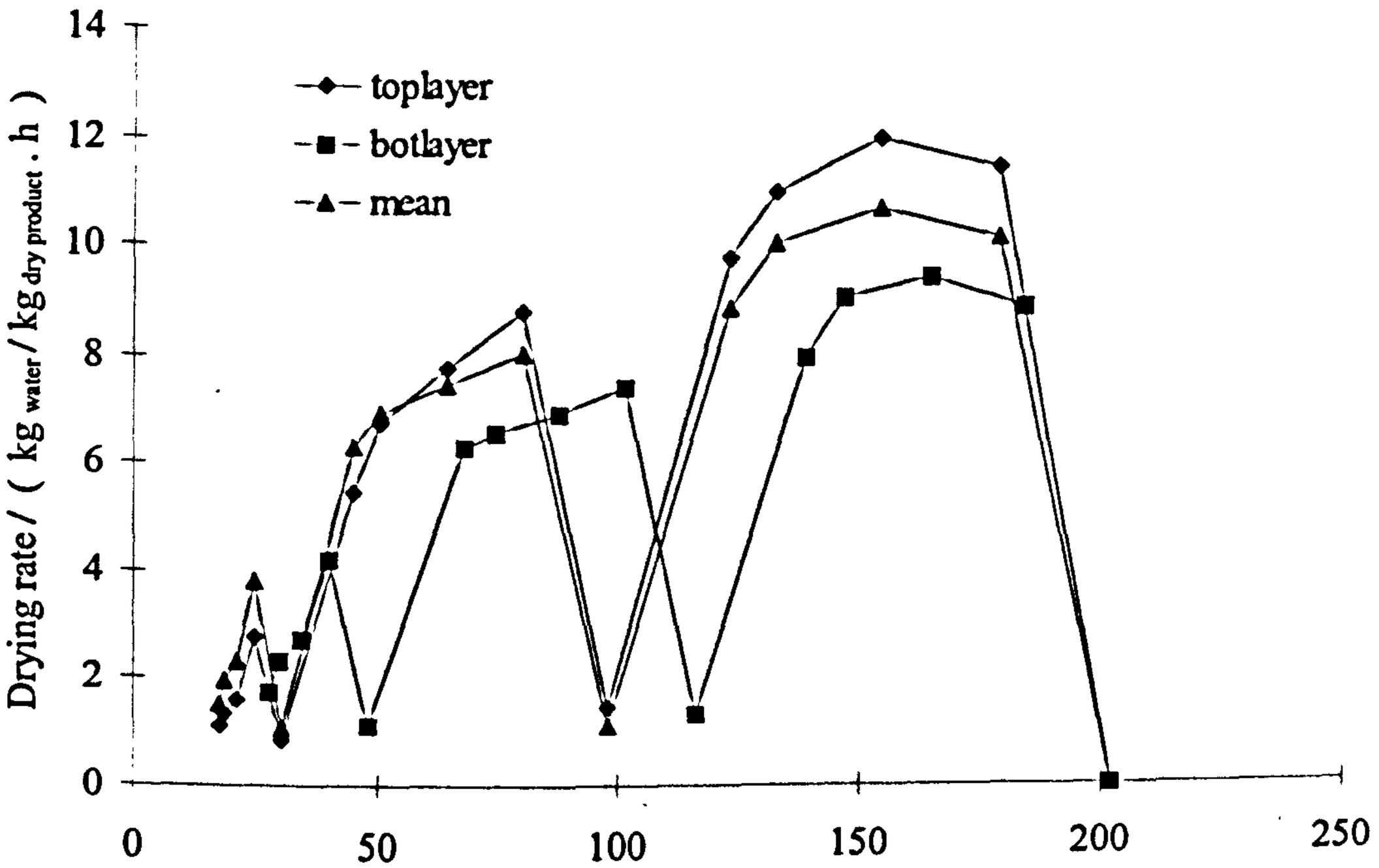

Figure 5.33: Variation in the drying rates of cassava chips dried in two layers with moisture content during test 12.

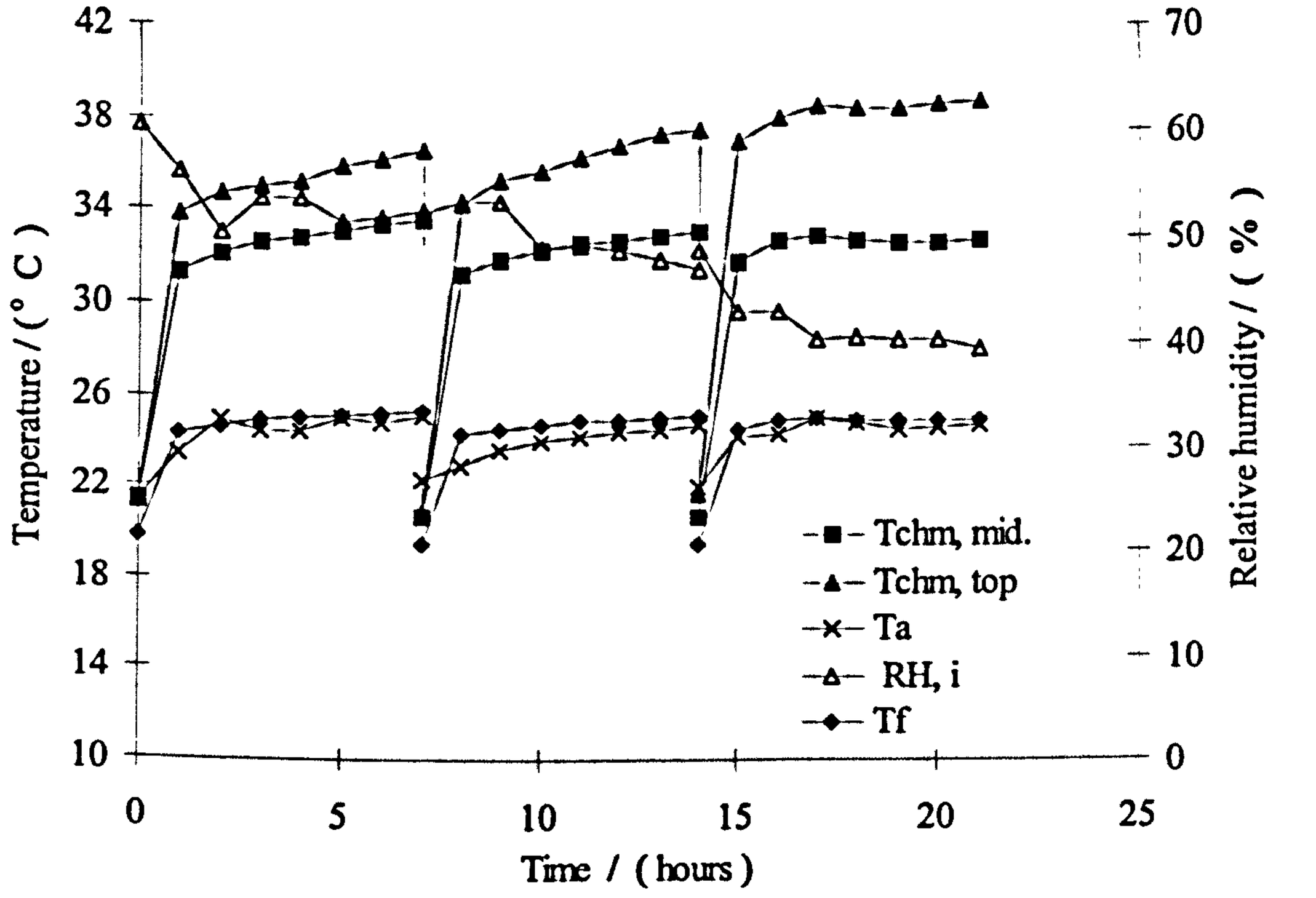

Figure 5.34: Variation in the ambient air relative humidity and the temperature profile of the drying air inside the drying chamber with time during test 12.

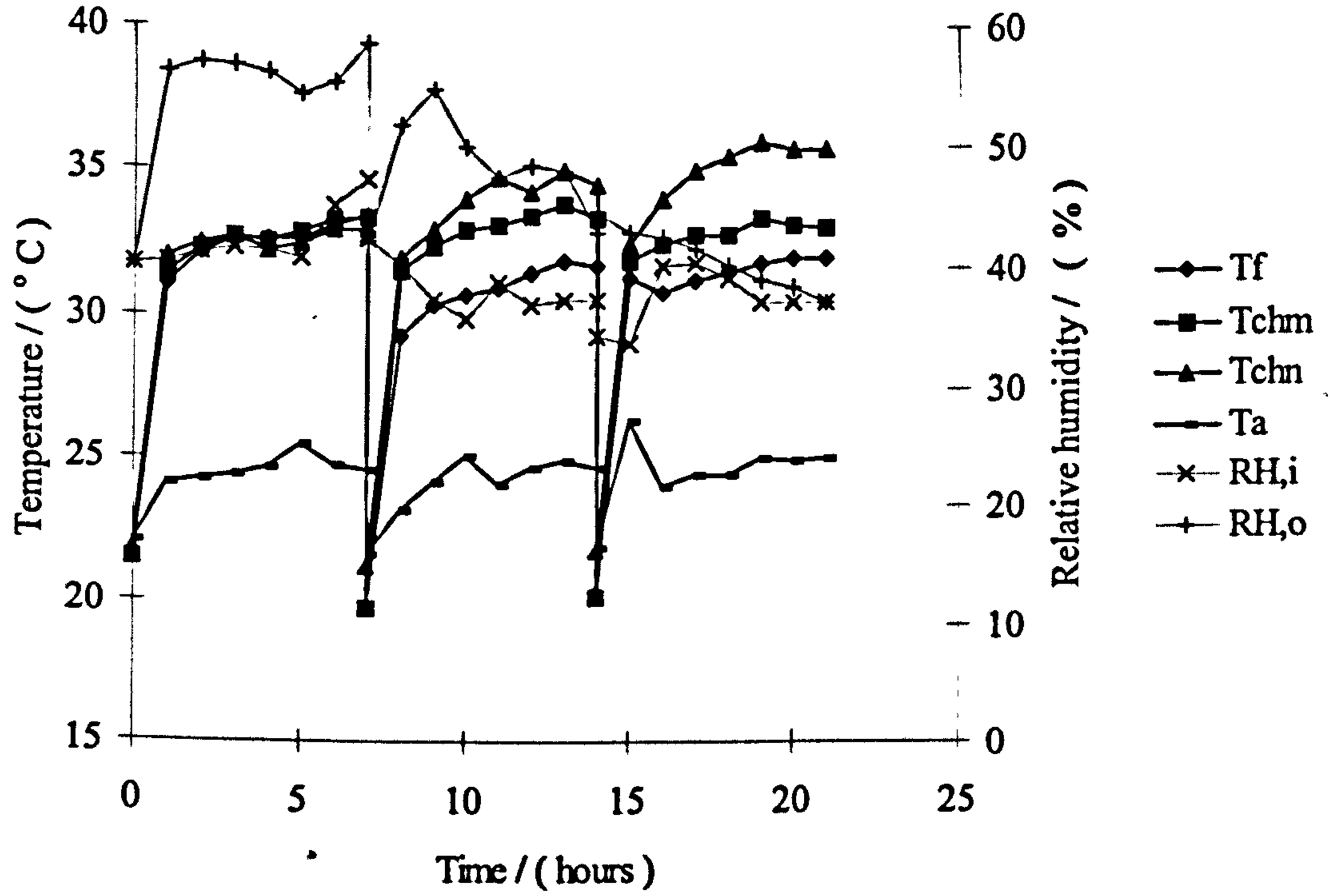

Figure 5.35: Variation in the ambient and exhaust air relative humidity and drying air temperature profile inside the dryer with time for test 13.

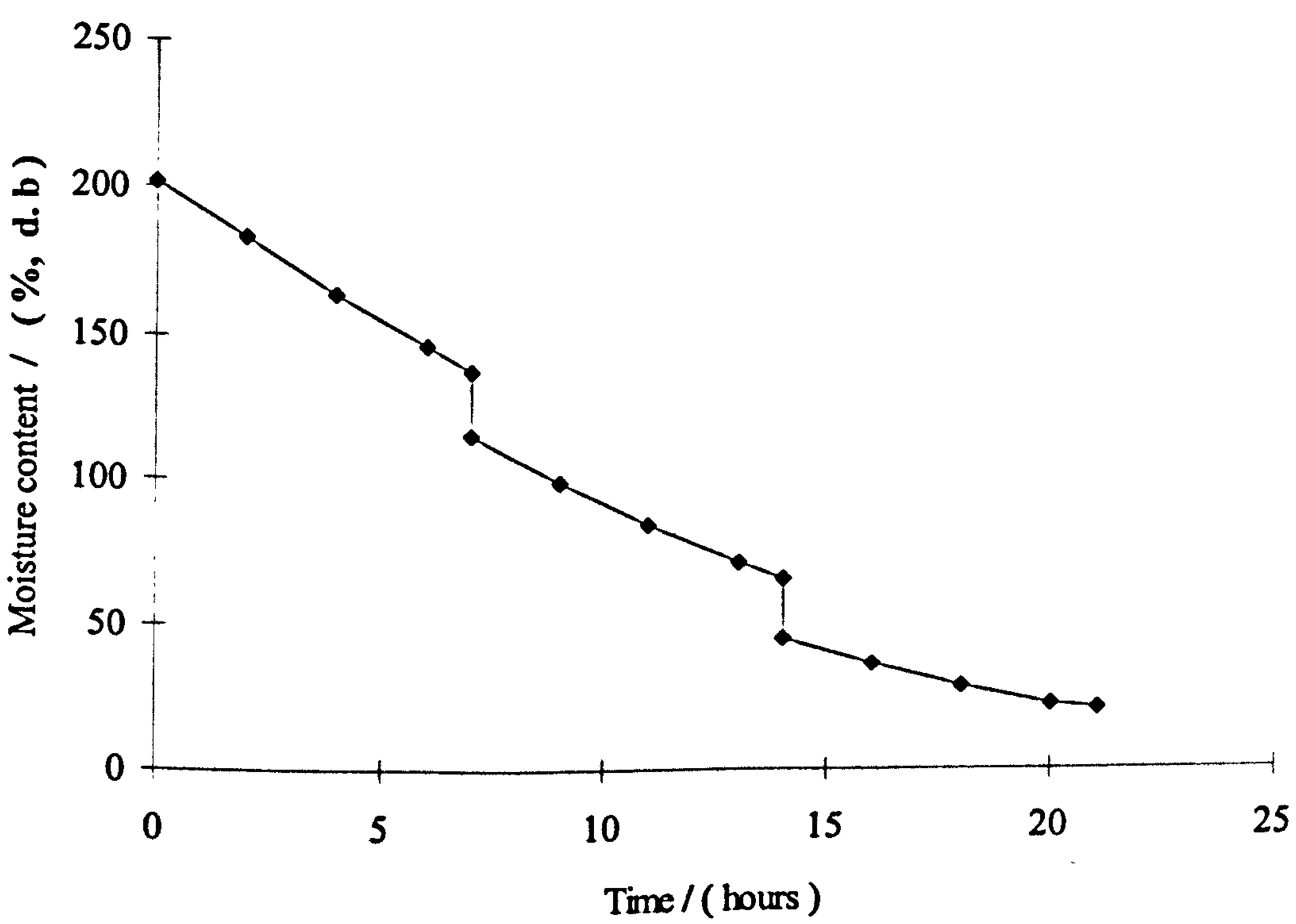

Figure 5.36: Variation in moisture content of cassava chips with time during test 13.

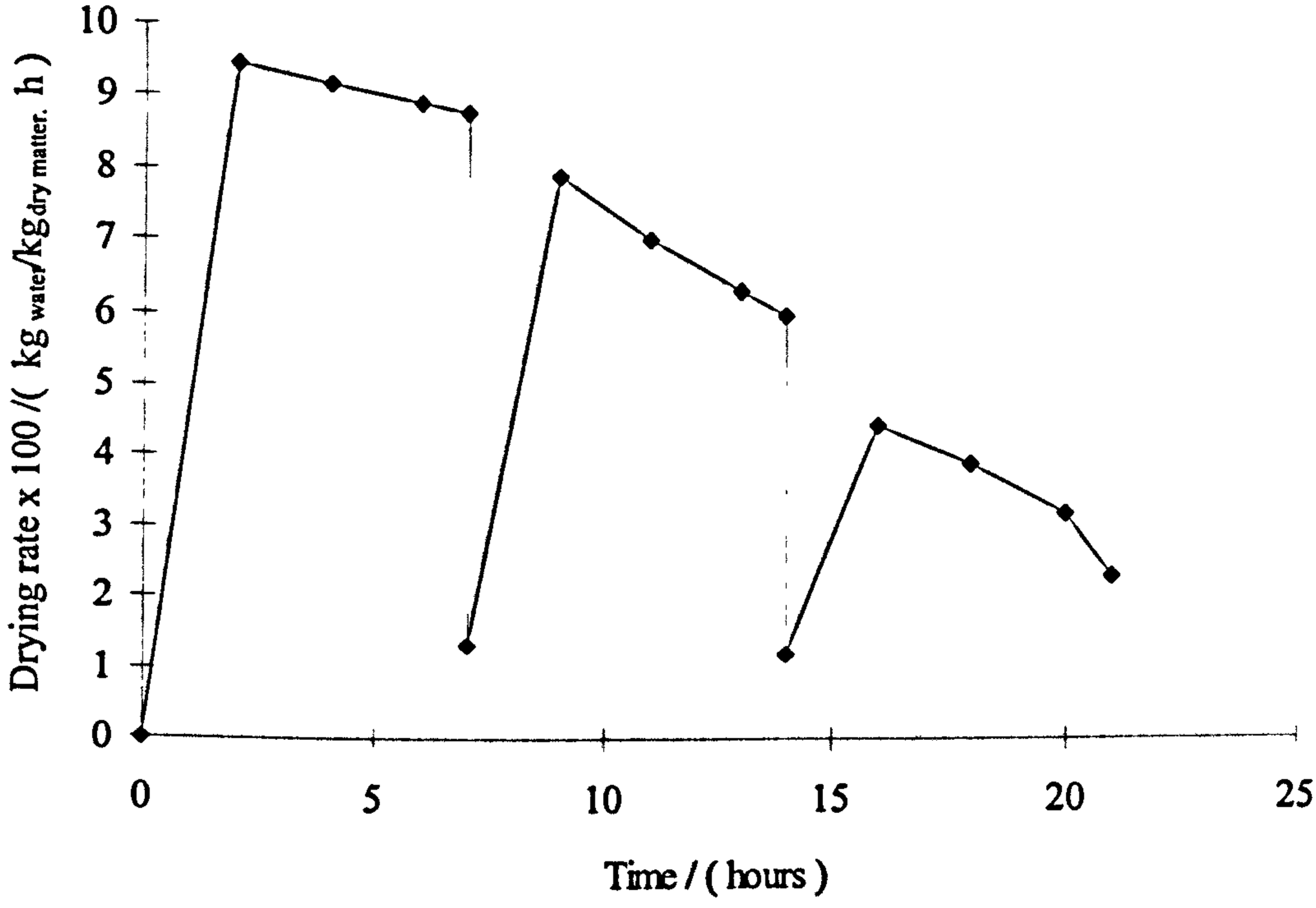

Figure 5.37: Variation in the drying rate of cassava chips with time during test 13.

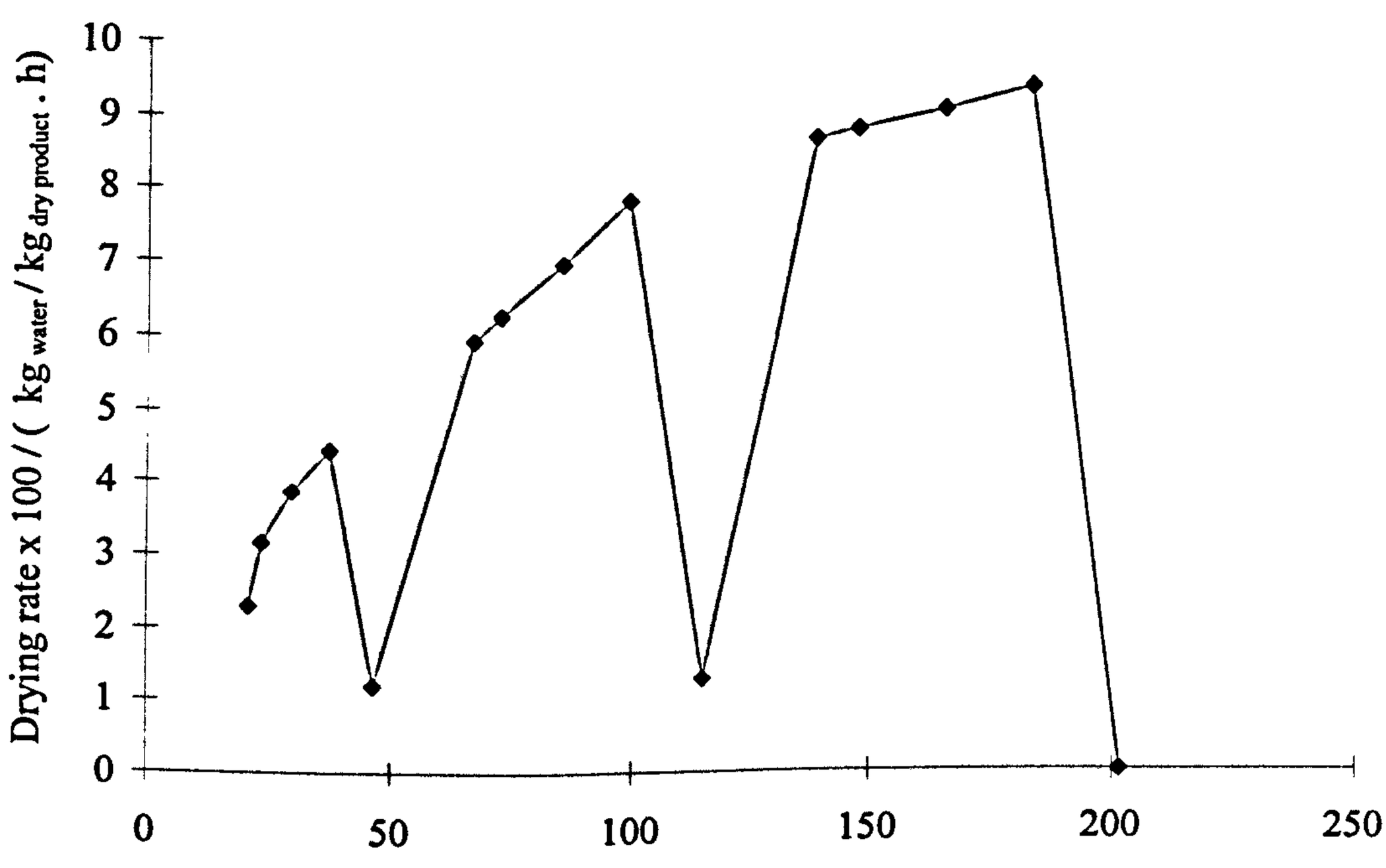

Figure 5.38: Variation in the drying rate of cassava chips with moisture content during test 13.

5.2 Field experimental study: results and discussion

The field experimental study was carried out, in Ghana, on a commercial-scale MNCSCD from 1700 (local time) on 1 October 1997 to 1715 on 14 October 1997. Unlike the laboratory experiments, tests were carried out on the dryer under load conditions only because of the limited time. Three drying tests, hereinafter referred to as Tests 1, 2 and 3, were conducted over the relatively short experimental period. During each test, the dryer was loaded with cassava freshly harvested. The total initial crop weights of the cassava chips dried (in the dryer) during tests 1, 2 and 3 were 49.1, 65.9 and 161.5 kg, respectively. To compare the dryers' performance with an open-air sun drying, a control experiment was undertaken during test 1 by drying 49.1 kg of cassava chips spread on a mat of area 4.6 m^2 placed on a raised platform. The initial moisture content of each batch of cassava dried was determined by the oven method. A representative sample of the cassava for each test was taken to a local secondary school science laboratory, about one kilometre away from the test site, for the moisture content determination. The initial crop moisture contents during tests 1, 2 and 3 were found to be 163.2%, 177.8% and 166.7% (dry basis), respectively.

The daily average values of the wind speed recorded over the period is provided in table 5.9. The daytime and nocturnal average values of the parameters measured over the test period is provided in Table 5.10. The daily daytime and nocturnal average values of the systems' parameters measured are provided in tables 5.11 and 5.12, respectively. An overview of the mean hourly values of the prevailing weather conditions and the day to day performance of the dryer during each test is provided for tests 1, 2, and 3 in Tables 5.13, 5.14 and 5.15, respectively.

Wind speeds recorded over the period were generally low, though varying widely with time; its values ranged between 0.2 and 1.4 m/s (Tables 5.13-5.15), with an average value of 0.72 m/s (Table 5.9). An implication of the low wind speed is perhaps the lower convective heat losses from the cover material (glazing) of the air-heater.

Figures 5.39 to 5.52 show the variations in the measured average hourly weather conditions and systems' parameters with time of the day, over the entire duration of the tests. Summaries of the drying data for tests 1, 2 and 3 are provided in Tables 5.13, 5.14 and 5.15, respectively.

The variation in the measured average hourly values of the total insolation is shown in fig. 5.39. The hourly values of the insolation recorded between 0700 and 1800 hours (day-time) over the entire experimental period ranged between 1.625 and 994 W/m^2, with an average value of 341 W/m^2. The fluctuations in the levels of insolation recorded over the test period was due to the variable cloud cover. The day-time daily mean global insolation over the period varied between 121-500.3 W/m^2 (Table 5.11). The lowest global day-time insolations were recorded during tests 2 and 3 on 10 October 1997. The measured values ranged between 18.5 and 266.4 W/m^2 with an average of 121.4 W/m^2, while the maximum day-time hourly average value of 500.3 W/m^2 was recorded on 12 October 1997 with the hourly values varying between 35.6 and 936 W/m^2 (see fig. 5.39).

The average hourly variation in the ambient air temperature over the period of the tests is shown in fig. 5.40. The effect of the fluctuations in the global insolation on the ambient air temperature is evident from figs. 5.39 and 5.40. It can be observed that, the ambient air temperatures peak and fall in agreement with global insolation variation over the day. The daily mean ambient air temperature over the test period varied from 26.1° C to 31.7° C during the day and 22° C to 24.8° C during the nights (Tables 5.11 and 5.12). Mean daytime and nocturnal ambient air temperatures over the entire period were respectively 30.1° C and 24.1° C with corresponding peak values of 35.4° C and 26° C.

The hourly variations in the ambient air and drying air relative humidity values over the duration of the test are illustrated in figs. 5.41 and 5.42. The daily mean of the ambient air relative humidity over the test period varied from 52.1% to 75.7%. Mean ambient air relative humidity recorded over the entire period was 60.9% with a peak value of 85% recorded on 7 October 1997. The effect of the fluctuations in the global insolation on the ambient air and drying air relative humidity is evident from figs. 5.39, 5.41 and 5.42. The variation of ambient air and drying air relative humidity with insolation shows a strong linear correlation (see fig. 5.43) with correlation coefficients (R) of 0.97 and 0.85 for the ambient and drying air, respectively. The mean ambient air relative humidity value of 60.9% recorded over the test period was generally higher than the recommended value of 60% for fast drying of cassava chips (Cheema, 1978), however, the mean drying air relative humidity recorded at the outlet of the air-heater was 43.1% (Table 5.10). For the purpose of drying cassava under such

humid conditions, the need for an air-heater to supply pre-heated air at reduced relative humidity into the drying chamber is evident.

The daily mean drying air temperatures recorded inside the plenum were between 30.1° C and 41.5° C compared with the daily mean ambient air temperatures of between 26.1 and 31.6° C (Table 5.11). The mean day-time plenum air temperature elevation above the ambient, over the experimental period, ranged from 4.0 to 9.5° C compared with the corresponding nocturnal values of between 1.8 and 3.1° C (see Tables 5.11 and 5.12). The diurnal variations in the plenum air temperature is shown in fig. 5.44. The results indicate that the range of drying air temperatures recorded for the dryer studied were within the desired limit 70° C for the drying of cassava (Imre, 1997). The results further indicate that the daily mean nocturnal plenum air temperatures were between 24.5 and 27.5° C compared with the ambient nocturnal air temperatures of between 22 and 25.2° C. Though there were heat losses from the system to the surrounding at night, over the test period the mean nocturnal plenum air temperature's were consistently higher than ambient air temperatures by about 1.5-4.8° C, approximately. The higher nocturnal plenum air temperatures attained compared to the ambient air temperatures are desirable for drying purposes. Comparing the nocturnal temperature elevations inside the dryer (between 1.8 and 3.1° C) and the corresponding day-time temperature elevations of 4.0-9.5° C, it could be said that the thermal mass of the system acts effectively as a heat storage equipment. The heat stored in the thermal mass during the day is subsequently released at night thus maintaining the temperature inside the chamber well above the ambient temperature.

The variations in the average hourly drying air temperatures exiting the upper and lower channels of the SPDDSAH are illustrated in figs. 5.45 and 5.46, respectively. Comparing figs. 5.45 and 5.46 it can be seen clearly that, during the daytime the temperature of the heated air exiting the upper channel is consistently higher than the temperature of the drying air exiting lower channel. The reverse phenomenon is observed at night. The daytime values of the mean temperature of heated drying air exiting the upper and lower channels of the air-heater were 40.2 and 35.4° C, respectively, compared with nocturnal values of 24.9° C and 26.5° C. Though the top and the bottom channels were of equal depth, the temperatures of the air recorded at the outlet of the upper channel were consistently higher than the air temperatures measured at the outlet of the lower channel. Differences of up to 12.1° C were

observed. This experimental observation is at variance with the theoretical predictions by Ong (1995a) and Pawar *et al* (1994). However, a similar trend of experimental results have been reported from studies on a SPDDSAH (Ong, 1995b). The theoretical models of Ong (1995a) and Pawar *et al* (1994) need some modification, if they are to be employed for predicting the performance of SPDDSAH's.

The variations in the mean hourly air velocity at the outlets of the channels (i.e. the top and bottom channels) are shown in figs. 5.47 and 5.48. From figs. 5.47 and 5.48, it is observed that the hourly values mean air speed recorded at the outlet of the top channel were consistently lower than the airspeed at the outlet of the bottom channel. The mean air velocities measured at outlets of the top and bottom channels during the day were between 0.09-0.19 m/s and 0.12-0.24 m/s, respectively. These observed velocities are in the lower end of the range of typical values of 0.2-0.4 m/s reported by Macedo and Altemani (1978) following their extensive experimental investigation on differing constructions of natural convection solar air-heaters not connected to any drying chamber. Whereas the values obtained in this study are lower than those reported by Macedo and Altemani (1978), it can be argued that the results are reasonable considering the combined effect of the pressure drop offered by the drying chamber and the heat losses through the numerous openings observed in the air-heater. These losses contributed to the lower air velocities recorded.

The variations in the mean temperatures of the components of the air-heater are shown in figs. 5.49 to 5.51. It can be seen clearly that, during the day the absorber plate temperature is consistently higher than cover plate temperature which is in turn greater than the base plate temperature. The nocturnal values of the base plate temperatures recorded were consistently greater than the absorber plate temperature; while the absorber plate temperatures were also consistently higher than the cover plate temperatures. The reversal in values of the nocturnal plate temperatures is due to the fact during the day the base plate (plywood) stores up energy and releases it at night thus acting as heat sink during the day and a heat source during the night. The air-heater component temperatures peak and fall in agreement with the fluctuation in the insolation.

The drying results of test 1 are presented in Tables 5.13 and 5.16. It is clear that the product placed in the dryer dried at a faster rate than the open-air sun drying. Within four days of

drying, the cassava chips placed in the solar dryer reached a moisture content of 20.9% (dry basis) compared to a value 39.6% attained in the open air sun drying. At the end of the fifth day, the moisture content of the sun dried product was 33.6% when the experiment was terminated. Notwithstanding the overall slow rate of drying by the traditional sun drying method, no appreciable difference was observed in the drying rates of the product dried in the solar dryer and in open-air during the first day of drying (Table 5.13). The final product moisture content at the end of the first day of drying were 95.3 and 97% in the solar dryer and in the open air sun drying, respectively. From the second day onwards, it is observed that the drying rate of the product in the dryer was significantly higher compared to the drying rate of the product dried in open air. These observations can be explained as follows: During the early stages of drying, free water is extracted from the product and therefore air flow rate exerts an important influence on drying. Hence, the ambient wind speed of 0.8 m/s was sufficient to sustain the higher drying rates within the first day during the open-air sun drying. The comparable higher drying rates observed in the open-air sun-drying during the first day could also be attributed to the higher insolation values (Table 5.11). However, in the latter stages of drying bound water inside the product is evaporated. The higher rate of drying of the solar dried product is attributable mainly to the relatively higher drying air temperature and lower air relative humidity inside the drying chamber. The mean wind speeds were comparatively higher during the second and fourth days of drying, nonetheless slower rates of drying were observed for the product dried in the sun. It is suggested from this observation that in the latter stages of drying of cassava, at moisture contents less than 100% dry basis, air speed has practically no influence on the drying kinetics. As the drying proceeds the transfer boundary moves further inside the product. Temperature therefore exhibits a very great influence on the drying rates in the later stages of drying. Increasing the temperature of the air reduces the partial pressure of the water in the air, and increases the saturation pressure at the product-air interface. For this reason, from the second day onwards the air inlets can be partially closed. This will cause a reduction in the air flow rate and subsequently an increase in the temperature of the heated air at the exit of the air-heater.

In test 2, 65870 grams of cassava chips were placed on two top beds covering a total area of 6.24 m^2 thus maintaining loading density 10.6 kg/m^2 . From Table 5.17, it is observed that the crop moisture content was reduced from an initial value of 177.8% to a final value of 20.5% at the end of the fifth day of drying. The slow rate of drying recorded for this test

compared to the preceding test can be attributed mainly to the higher relative humidity of the drying air recorded during this test (especially on the third day of drying) though, in addition, the crop used in this test had a higher initial moisture content than in the preceding test.

Table 5.18 shows the results of the drying experiment for test 3. As stated earlier, 81 kg and 80.5 kg of cassava chips were placed on the top and bottom layers, respectively, with each batch covering an area of 5.4 m^2. The product on the bottom shelf was placed vertically below what was on the top bed. Comparing the moisture contents values presented in table 5.18, it is clear that during the first day, the cassava on the bottom bed dried faster than the product on the top bed. The cassava placed on the bottom shelf dried to a moisture content of 141.9% compared to a value of 144.2% attained by the product on the top bed. Whereas the product on the top bed receives higher direct solar radiation compared with that placed on the bottom shelf; the cassava chips placed on the bottom bed were subjected to a better circulation of drying air through the crop bed than the product on the top bed. The faster rate of drying observed on the first day for the product on the bottom bed suggests that during the first day (early stages of drying), as stated earlier, the convective heat flux controlled the drying kinetics. From the second day onwards, the top bed dried at a faster rate than the bottom bed. Since the product on the top bed absorbs much more direct solar radiation than the bottom layer, and since the air above it is also warmer, these combined effects account for the higher drying rates of the top bed from the second day onwards, as is shown by the result. In four days, 161.5 kg of cassava chips were reduced from a moisture content of 166.7% (dry basis) to a mean moisture content of 20.7% suggesting that the drying was higher compared with the rate of drying in test 2. From the view point of increased throughput per drying batch and faster drying rates, two layer drying is recommended as a follow up of the experimental results attained.

In general, the drying results obtained from this study compare favourably with other solar drying tests using cassava. Drying periods of between 1-6 days for cassava have been reported (Ezekwe, 1981; Ayensu and Bondzie, 1986; Roa, 1974; Fleming *et al*, 1986) in the literature using differing constructions of solar dryers. Based on the average daily insolation of 341.3 W/m^2 over the period of the experiment, the air-heater efficiency was assessed using equation (4.6) and found to be 9.5%. This value is lower than values reported in the literature.

The significant amount of heat losses through the many small openings in the air-heater accounts for the discrepancy.

The expected drying air temperature rise over the ambient value is an important factor needed for the design of a solar air-heater. In this study, the variation of the instantaneous values of the mean plenum air temperature rise over the ambient air temperature ($T_f - T_a$), recorded were correlated to the instantaneous mean hourly values of the solar radiation intensity (H_T) measured over the entire period of the test. A strong linear correlation (see fig. 5.52) of the form:

$$(T_f - T_a) = 0.0113 H_T + 3.636 \qquad (5.2)$$

with a correlation coefficient, R of 0.88 was obtained for the day-time temperature rise of the plenum air temperature over the ambient air temperature, for the air-heater studied.

Table 5.9: Daily mean values of the prevailing wind speed recorded during the field test

Day in Oct. '97	2	3	4	5	6	8	9	10	11	12	13
Speed (m/s)	0.8	1.0	0.7	1.0	0.5	0.4	0.8	0.5	0.8	0.6	0.6

Table 5.10: Average values of the measured parameters over the duration of the test

	Tp (°C)	Tb (°C)	Tc (°C)	TF1 (°C)	TF2 (°C)	TF (°C)	Ta (°C)	V1 m/s	V2 m/s	RH,i (%)	RH,o (%)	RAD W/m^2
Day	42.4	36.5	41.4	40.2	35.4	37.6	30.1	0.15	0.19	60.9	43.1	341.3
Night	25.6	27.9	23.7	24.9	26.5	26.5	24.1	-[a]	0.01	-[a]	-[a]	0.054

[a] Values manually recorded during the day, hence nocturnal values were not recorded.

Table 5.11: Daytime[c] daily mean values of measured parameters.

Day	T_p (°C)	T_b (°C)	T_c (°C)	$T_{f,1}$ (°C)	$T_{f,2}$ (°C)	T_f (°C)	T_a (°C)	V_1 m/s	V_2 m/s	RH,i (%)	RH,o (%)	H_T W/m^2
2 Oct	46.9	39.4	46.1	44.3	38.3	41.2	31.7	0.145	0.181	52.1	34.9	488.1
3 Oct	45.1	38.5	44.0	42.1	37.2	39.3	31.6	0.160	0.200	58.6	38.3	398.6
4 Oct	41.1	36.0	39.9	38.7	34.8	36.2	30.2	0.133	0.166	58.2	43	294.3
5 Oct	40.4	35.3	39.6	39.1	34.6	36.3	29.7	0.120	0.142	56	42.8	289.6
6 Oct	40.5	35.6	39.9	38.6	34.4	36.2	29.0	0.163	0.203	59.7	40.3	326.8
7 Oct	40.8	34.9	39.6	38.4	33.8	36.4	29.1	0.177	0.230	70	60	122.8
8 Oct	45.4	38.3	43.9	42.1	37.1	39.8	31.1	0.187	0.239	60.1	36.3	424.0
9 Oct	44.5	38.0	43.8	42.7	36.9	38.9	30.9	0.127	0.156	62.5	39.5	389.9
10 Oct	31.9	30.3	30.9	30.8	29.3	30.1	26.1	0.092	0.115	75.7	66.7	121.4
11 Oct	40	34.4	38.8	37.9	33.3	35.6	28.5	0.189	0.231	63.0	47.6	343.5
12 Oct	47.7	39.6	46.9	45.4	38.7	41.5	31.6	0.140	0.171	53.1	28.6	500.3
13 Oct	44.4	37.8	43.2	42.1	36.7	39.7	31.3	0.187	0.225	59.3	35.0	396.3

[c] The day-time as used in this study represents the period between 0700 and 1800 hours.

Table 5.12: Nocturnal[d] daily hourly mean values of measured parameters

Day	T_p (°C)	T_b (°C)	T_c (°C)	$T_{f,1}$ (°C)	$T_{f,2}$ (°C)	T_f (°C)	T_a (°C)	V_2 (m/s)	H_T (W/m^2)
1 Oct	25.9	28.3	24.0	25..1	26.7	27.0	24.1	0.007	0.281
2 Oct	25.6	28.3	23.2	24.6	26.5	26.8	23.7	0.022	0.045
3 Oct	26..0	28.5	23.8	25.2	26.9	26.8	24.3	0.015	0.033
4 Oct	25.5	27.8	23.6	24.7	26.3	26.4	24.1	0.010	0.015
5 Oct	26.2	28.3	24.5	25.5	26.9	27.1	24.6	0.013	0.020
6 Oct	23.4	26.0	21.6	22.6	24.3	24.5	22.0	0.018	0.031
7 Oct	26.2	28.1	24.5	25.7	27.0	27.0	24.7	0.006	0.029
8 Oct	26.8	28.9	24.9	26.2	27.6	27.5	25.2	0.008	0.079
9 Oct	26.3	28.6	24.3	25.7	27.2	27.1	24.7	0.015	0.012
10 Oct	23.9	25.9	22.1	23.2	24.6	24.6	22.8	0.016	0.016
11 Oct	25.4	27.4	23.7	24.7	26.1	26.2	24.1	0.002	0.079
12 Oct	25.3	28.2	23.2	24.6	26.5	26.7	23.8	0.016	0.057
13 Oct	26.4	28.7	24.4	25.6	27.2	27.4	24.8	0.017	0.001

[d] The nocturnal period as used in this study represents the period between 1800 hours and 0700 hours.
- Nocturnal values of V1, RH,i and RH,o were not recorded and therefore their columns in table 5.12 have been omitted.

Table 5.13: An overview of drying results using the commercial-scale field dryer for Test 1.

Measured and calculated performance parameters	DAY 1 (2/10/97)	DAY 2 (3/10/97)	DAY 3 (4/10/97)	DAY 4 (5/10/97)	DAY 5 (6/10/97)
Duration drying the day (hours)	6	9	10	11	7
Minimum wind speed (m/s)	0.6	0.4	0.5	0.6	0.3
Mean wind speed (m/s)	0.8	1.0	0.7	1.0	0.5
Maximum wind speed (m/s)	1.4	1.4	0.9	1.3	1.0
Initial weight of the crop mass (grams)	2693 (2693)	1805 (2047)	1453 (1582)	1328 (1426)	- (1343)
Final weight of the crop mass	1999 (2057)	1491 (1620)	1347 (1438)	1238 (1352)	- (1302)
Initial crop moisture content (kg_{water}/ $kg_{drv\ solid\ matter}$)	163.2 (163.2)	76.4 (100)	42 (54.6)	29.7 (39.3)	- (31.2)
Final crop moisture content (kg_{water}/ $kg_{drv\ solid\ matter}$)	95.3 (109.2)	45.8 (58.2)	31.6 (40.4)	20.9 (32.1)	- (27.2)
Minimum total insolation (W/m^2)	45	10.81	11.7	10.03	1.625
Mean total insolation (W/m^2)	488.1	398.6	294.3	289.6	326.8
Maximum total insolation (W/m^2)	994	796	543.9	605.7	735
Minimum ambient air relative humidity (%)	45.1	42.3	46.4	40.9	50.8
Mean ambient air relative humidity (%)	52.1	58.6	58.2	56	59.7
Maximum ambient air relative humidity (%)	59.3	74.9	71.1	68.2	69.7
Min. air relative humidity at air-heater outlet(%)	23	24	31	31	26
Mean air relative humidity at air-heater outlet (%)	34.9	38.3	43	42.8	40.3
Max. air relative humidity at air-heater outlet(%)	56	62	59	58	69
Minimum ambient air temperature (°C)	25.9	24.5	23.9	24.1	24.2
Mean ambient air temperature (°C)	31.7	31.6	30.2	29.7	29
Maximum ambient air temperature (°C)	35.4	35.2	33.4	33.1	34.3
Minimum glazing temperature (°C)	28.6	26.3	24.3	24.9	24.7
Mean glazing temperature (°C)	46.1	44.0	39.9	39.6	39.9
Maximum glazing temperature (°C)	68.3	59.7	52.6	50.5	58.7
Minimum absorber plate temperature (°C)	29.5	27.5	26.1	25.8	26.4
Mean absorber plate temperature (°C)	46.9	45.1	41.1	40.4	40.5
Maximum absorber plate temperature (°C)	67.2	60.4	52.1	49.9	57.2

Table 5.13: continued.

Measured and calculated parameters	DAY 1	DAY 2	DAY 3	DAY 4	DAY 5
Minimum bottom plate temperature (°C)	28.1	27.5	27.1	27.1	27.2
Mean bottom plate temperature (°C)	39.4	38.5	36.0	35.3	35.6
Maximum bottom plate temperature (°C)	47.1	45.5	43.3	39.8	44.2
Minimum heated air temp. in upper channel (°C)	28.0	26.3	25.2	25.7	25.6
Mean heated air temperature in upper channel (°C)	44.3	42.1	38.7	39.1	38.6
Maximum heated air temp. in upper channel (°C)	57.5	53.0	48.4	47.4	53.5
Minimum heated air temp. in lower channel (°C)	27.2	26.5	26	26.4	26.3
Mean heated air temperature in lower channel (°C)	38.3	37.2	34.8	34.6	34.4
Maximum heated air temp. in lower channel (°C)	46.0	45.3	41.3	40.1	43.6
Minimum heated air velocity in lower channel(m/s)	0.01	0.03	0.012	0.003	0.027
Mean heated air velocity in lower channel(m/s)	0.181	0.200	0.166	0.142	0.203
Maximum heated air velocity in lower channel(m/s)	0.255	0.402	0.317	0.293	0.445
Minimum heated air velocity in upper channel(m/s)	0.01	0.02	0.01	0.00	0.02
Mean heated air velocity in upper channel(m/s)	0.145	0.160	0.133	0.120	0.163
Maximum heated air velocity in upper channel(m/s)	0.20	0.301	0.151	0.112	0.324
Minimum heated air temperature in plenum (°C)	28.8	27.5	26.2	26.1	26.4
Mean heated air temperature in plenum (°C)	41.2	39.3	36.2	36.3	36.2
Maximum heated air temperature in plenum (°C)	49.0	48.2	43.3	43.3	46.6

Table 5.14: An overview of drying results using commercial-scale dryer for test 2

Measured and calculated performance parameters	DAY 1 (8/10/97)	DAY 2 (9/10/97)	DAY 3 (10/10/97)	DAY 4 (11/10/97)	DAY 5 (12/10/97)
Duration of test (hours)	4.6	8	8.5	9	9
Minimum wind speed (m/s)	0.2	0.3	0.4	0.6	0.2
Mean wind speed (m/s)	0.4	0.8	0.5	0.8	0.6
Maximum wind speed (m/s)	0.8	1.0	1.0	1.4	1.0
Initial weight of the crop mass (grams)	65870	-	-	-	-
Final weight of the crop mass	51736	38014	34011	31176	28576
Initial crop moisture content (kg_{water}/ $kg_{drv\ solid\ matter}$)	178.8	-	-	-	-
Final crop moisture content (kg_{water}/ $kg_{drv\ solid\ matter}$)	118.2	60.3	43.4	31.5	20.5
Minimum total insolation (W/m^2)	16.21	4.39	8.45	10.2	35.6
Mean total insolation (W/m^2)	424	389.9	221.	343.5	500.3
Maximum total insolation (W/m^2)	959	825	266.4	685.1	936
Minimum ambient air relative humidity (%)	37.8	49.9	67.3	45.1	41.7
Mean ambient air relative humidity (%)	60.1	62.5	75.7	63.0	53.1
Maximum ambient air relative humidity (%)	79.2	75.2	82.4	79.5	70.7
Min. air relative humidity at air-heater outlet(%)	21	27	60	33	25
Mean air relative humidity at air-heater outlet (%)	36.3	39.5	66.7	47.6	28.6
Max. air relative humidity at air-heater outlet(%)	65	63	75	77	45
Minimum ambient air temperature (°C)	24.8	24.8	24.9	22.5	24.6
Mean ambient air temperature (°C)	31.1	30.9	26.1	28.5	31.6
Maximum ambient air temperature (°C)	35.1	34.7	27.3	32.0	35.2
Minimum glazing temperature (°C)	25.4	26.3	25.6	22.9	27.3
Mean glazing temperature (°C)	43.9	43.8	30.9	38.4	46.9
Maximum glazing temperature (°C)	59.1	56.6	36.1	50.8	65.8
Minimum absorber plate temperature (°C)	26.7	27.9	27	24.6	28.1
Mean absorber plate temperature (°C)	45.4	56.6	31.9	40	47.7
Maximum absorber plate temperature (°C)	58.5	44.5	36.9	51.3	63.4
Minimum bottom plate temperature (°C)	27.2	27.9	27.5	25.4	27.3
Mean bottom plate temperature (°C)	38.3	38	30.3	34.4	39.6
Maximum bottom plate temperature (°C)	45.4	45.9	32.9	40.1	65.8

Table 5.14: continued.

Measured and calculated performance parameters	DAY 1	DAY 2	DAY 3	DAY 3	DAY 4
Minimum heated air temp. in upper channel (°C)	26	26.8	26.2	23.7	27.1
Mean heated air temperature in upper channel (°C)	42.1	42.7	30.8	37.9	45.4
Maximum heated air temp. in upper channel (°C)	55.4	51.3	35.7	48.3	56.8
Minimum heated air temp. in lower channel (°C)	26.5	27.0	26.7	24.4	26.5
Mean heated air temperature in lower channel (°C)	37.1	42.7	29.3	33.3	38.7
Maximum heated air temp. in lower channel (°C)	44.2	45	32.1	38.8	45.5
Minimum heated air velocity in lower channel(m/s)	0.03	0.038	0.032	0.013	0
Mean heated air velocity in lower channel(m/s)	0.239	0.156	0.115	0.231	0.171
Maximum heated air velocity in lower channel(m/s)	0.513	0.263	0.222	0.421	0.307
Minimum heated air velocity in upper channel(m/s)	0.01	0.02	0.02	0	0
Mean heated air velocity in upper channel(m/s)	0.187	0.127	0.092	0.189	0.140
Maximum heated air velocity in upper channel(m/s)	0.41	0.21	0.164	0.34	0.251
Minimum heated air temperature in plenum (°C)	26.6	27.5	27.3	24.4	27.9
Mean heated air temperature in plenum (°C)	39.8	38.9	30.1	35.6	41.5
Maximum heated air temperature in plenum (°C)	51.1	49.2	33	42.8	49.7

Table 5.15: An overview of drying results using commercial-scale dryer for field test 3

Measured and calculated performance parameters	DAY 1 (10/10/97)	DAY 2 (11/10/97)	DAY 3 (12/10/97)	DAY 4 (13/10/97)
Duration of test (hours)	8.5	9	9	9
Minimum wind speed (m/s)	0.4	0.6	0.4	0.2
Mean wind speed (m/s)	0.5	0.8	0.6	0.6
Maximum wind speed (m/s)	1.0	1.4	1.1	1.0
Initial weight of the crop mass (grams)	161469 (10912)	136973 (9842)	99454 (7222)	79422 (5527)
Final weight of the crop mass	147171 (9914)	108362 (7625)	80759 (5679)	73186 (5200)
Initial crop moisture content (kg_{water}/ $kg_{dry\ solid\ matter}$)	166.7 (166.7)	126.2 (131.3)	64.2 (76.5)	31.2 (35.1)
Final crop moisture content (kg_{water}/ $kg_{dry\ solid\ matter}$)	143.1 (142.3)	79 (86.3)	33.4 (38.8)	20.9 (27.1)
Minimum total insolation (W/m^2)	8.45	10.2	35.6	20.7
Mean total insolation (W/m^2)	221.	343.5	500.3	396.3
Maximum total insolation (W/m^2)	266.4	685.1	936	694.1
Minimum ambient air relative humidity (%)	67.3	45.1	41.7	48.8
Mean ambient air relative humidity (%)	75.7	63.0	53.1	59.3
Maximum ambient air relative humidity (%)	82.4	79.5	70.7	73.6
Min. air relative humidity at air-heater outlet(%)	60	33	25	25
Mean air relative humidity at air-heater outlet (%)	66.7	47.6	28.6	35
Max. air relative humidity at air-heater outlet(%)	75	77	45	49
Minimum ambient air temperature (°C)	24.9	22.5	24.6	23.9
Mean ambient air temperature (°C)	26.1	28.5	31.6	31.3
Maximum ambient air temperature (°C)	27.3	32.0	35.2	34.2
Minimum glazing temperature (°C)	25.6	22.9	27.3	25.8
Mean glazing temperature (°C)	30.9	38.4	46.9	43.2
Maximum glazing temperature (°C)	36.1	50.8	65.8	56.9
Minimum absorber plate temperature (°C)	27	24.6	28.1	26.6
Mean absorber plate temperature (°C)	31.9	40	47.7	44.4
Maximum absorber plate temperature (°C)	36.9	51.3	63.4	57.2

Table 5.15: continued.

Measured and calculated performance parameters	DAY 1	DAY 2	DAY 3	DAY 4
Minimum bottom plate temperature (°C)	27.5	25.4	27.3	26.9
Mean bottom plate temperature (°C)	30.3	34.4	39.6	37.8
Maximum bottom plate temperature (°C)	32.9	40.1	65.8	43.4
Minimum heated air temp. in upper channel (°C)	26.2	23.7	27.1	25.6
Mean heated air temperature in upper channel (°C)	30.8	37.9	45.4	42.1
Maximum heated air temp. in upper channel (°C)	35.7	48.3	56.8	50.4
Minimum heated air temp. in lower channel (°C)	26.7	24.4	26.5	25.9
Mean heated air temperature in lower channel (°C)	29.3	33.3	38.7	36.7
Maximum heated air temp. in lower channel (°C)	32.1	38.8	45.5	41.8
Minimum heated air velocity in lower channel(m/s)	0.032	0.013	0	0.021
Mean heated air velocity in lower channel(m/s)	0.115	0.231	0.171	0.225
Maximum heated air velocity in lower channel(m/s)	0.222	0.421	0.307	0.388
Minimum heated air velocity in upper channel(m/s)	0.02	0	0	0.014
Mean heated air velocity in upper channel(m/s)	0.092	0.189	0.140	0.187
Maximum heated air velocity in upper channel(m/s)	0.164	0.34	0.251	0.30
Minimum heated air temperature in plenum (°C)	27.3	24.4	27.9	27.4
Mean heated air temperature in plenum (°C)	30.1	35.6	41.5	39.7
Maximum heated air temperature in plenum (°C)	33	42.8	49.7	41.8

Table 5.16: Summary of the field drying experiment:-TEST 1

Date/Time(hours)	Weight of product (grammes)		Moisture content (%, dry basis)	
	Solar dryer	Open air	Solar dryer	Open air
2 October 1997				
1115	49100	49100	163.2	163.2
1715	36440	36830	95.3	97.2
3 October 1997				
0815	32910	35500	76.4	90.1
1715	27180	31000	45.8	66.1
4 October 1997				
0715	26498	30300	42	62.3
1715	24556	28250	31.6	51.5
5 October 1997				
0831	24209	27750	29.7	48.8
1731	22569	26000	20.9	39.3
6 October 1997				
0805	-	25800	-	38.3
1505	-	24500	-	31.2

Table 5.17: Summary of the field drying experiment:-TEST 2

Day / Time (hours)	Weight of crop (grammes)	Moisture content (% dry basis)
8 October 1997		
1300	65870	177.8
1735	51736	118.2
9 October 1997		
0915	-	-
1715	38014	60.3
10 October 1997		
0930	-	-
1800	34011	43.4
11 October 1997		
0900	-	-
1800	31176	31.5
12 October 1997		
0810	-	-
1710	28576	20.5

Table 5.18: Summary of field drying experiment: - TEST 3

Date / time of day(hours)	Weight of product (grammes)		Moisture content (%, dry basis)	
	Dryer (Top bed)	Dryer (bottom bed)	Dryer (Top bed)	Dryer (bottom bed)
10 October 1997				
0930	81000	80469	166.7	166.7
1230	79608	78685	162.1	160.7
1530	77079	176018	153.8	151.9
1800	74185	72986	144.2	141.9
11 October 1997				
0900	69155	67818	127.7	124.7
1200	63319	62636	108.5	107.6
1500	56442	56318	85.8	86.6
1800	54099	54264	79.8	79.8
12 October 1997				
0810	49882	49572	64.3	64.3
1110	45609	45685	50.2	51.4
1410	42047	42281	38.4	40.1
1710	40366	40393	32.9	33.9
13 October 1997				
0815	39704	39718	30.7	31.6
1115	38333	38243	26.2	26.5
1415	37403	37375	23.1	23.5
1715	36576	36610	20.4	21.3

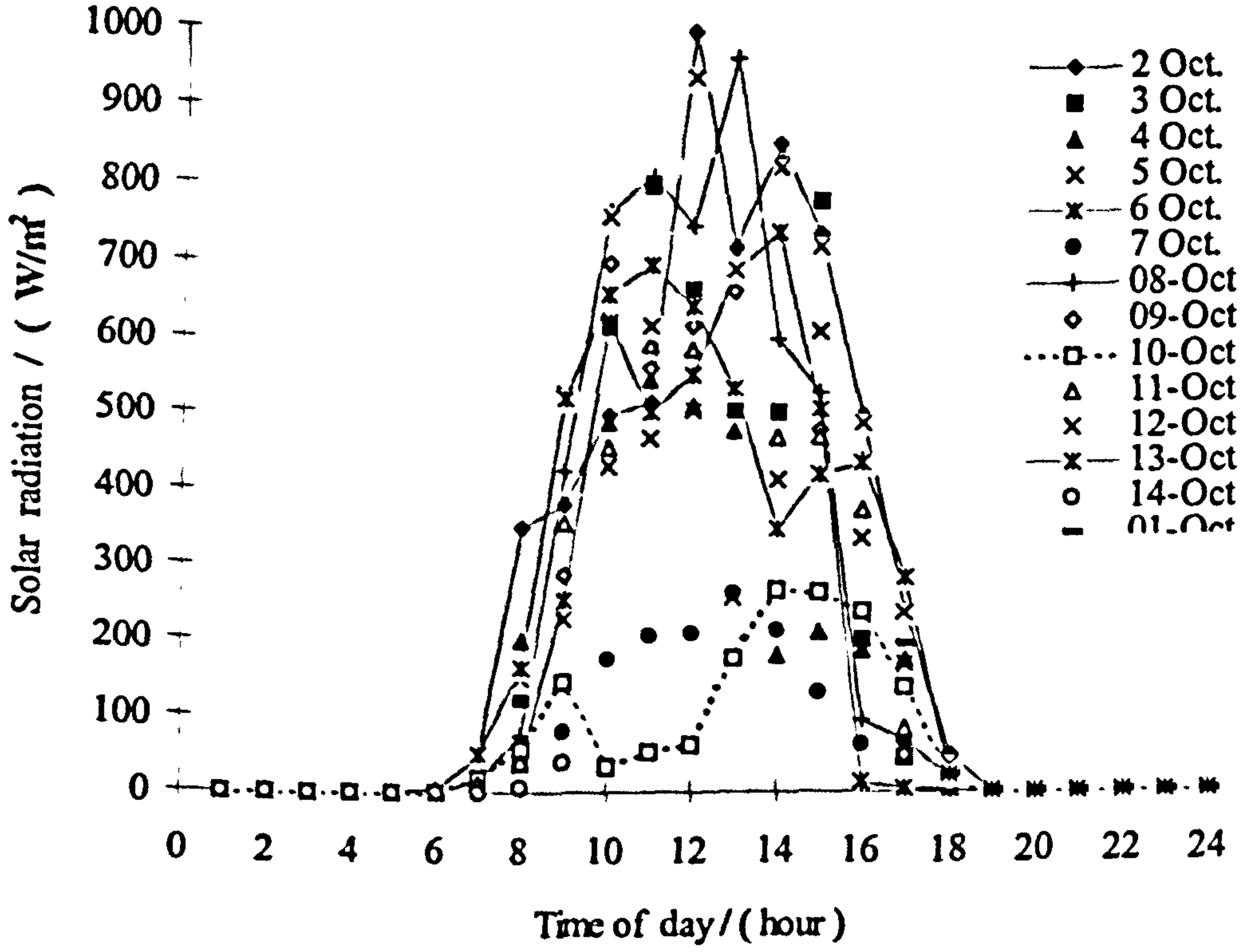

Figure 5.39: Variation in the hourly insolation with time of day recorded over the experimental period at Agona-Asafo, Ghana (2 - 14 October 1997)

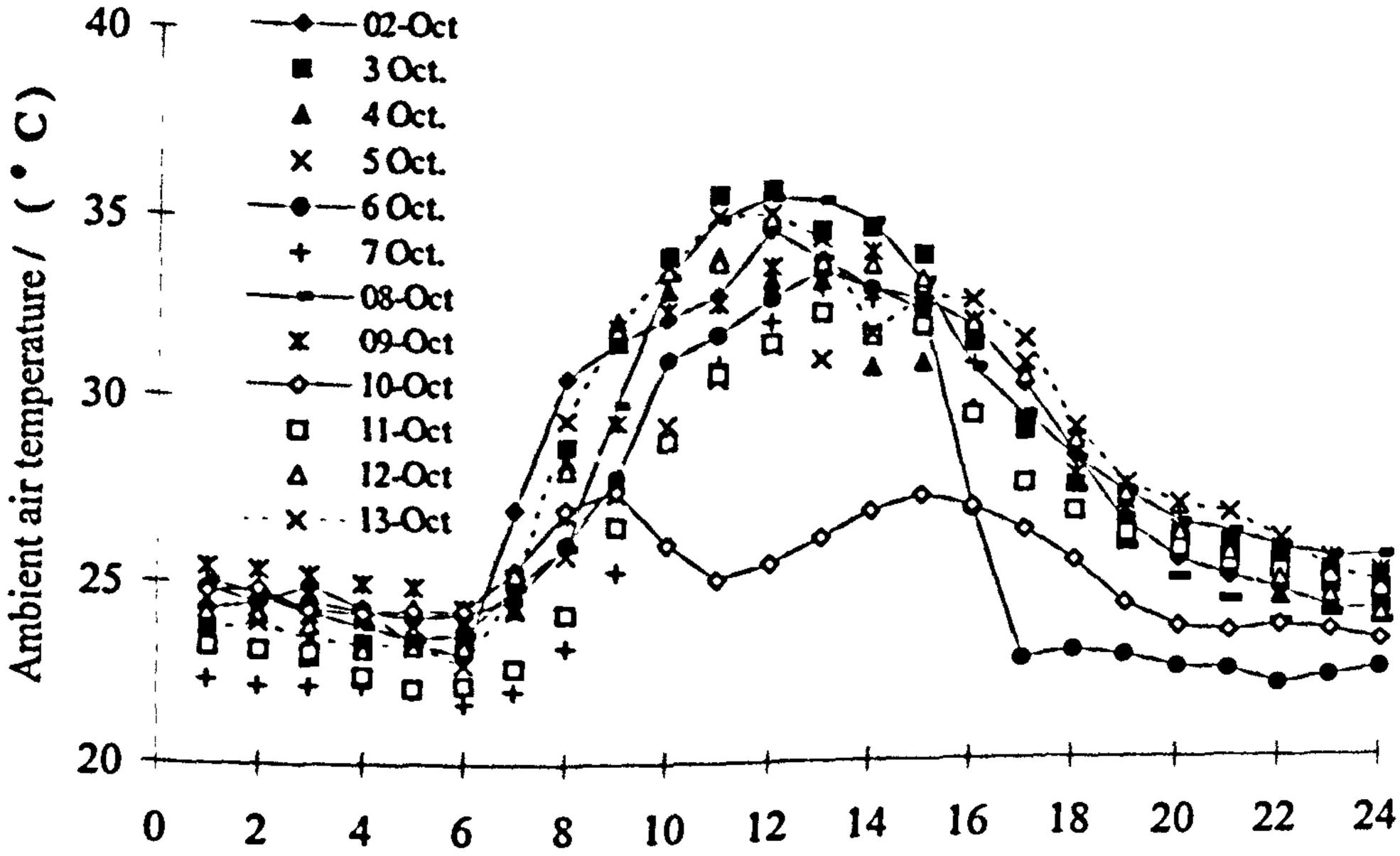

Figure 5.40: Variation in the ambient air temperature with time of day recorded over the experimental period at Agona-Asafo, Ghana (2-14 October, 1997).

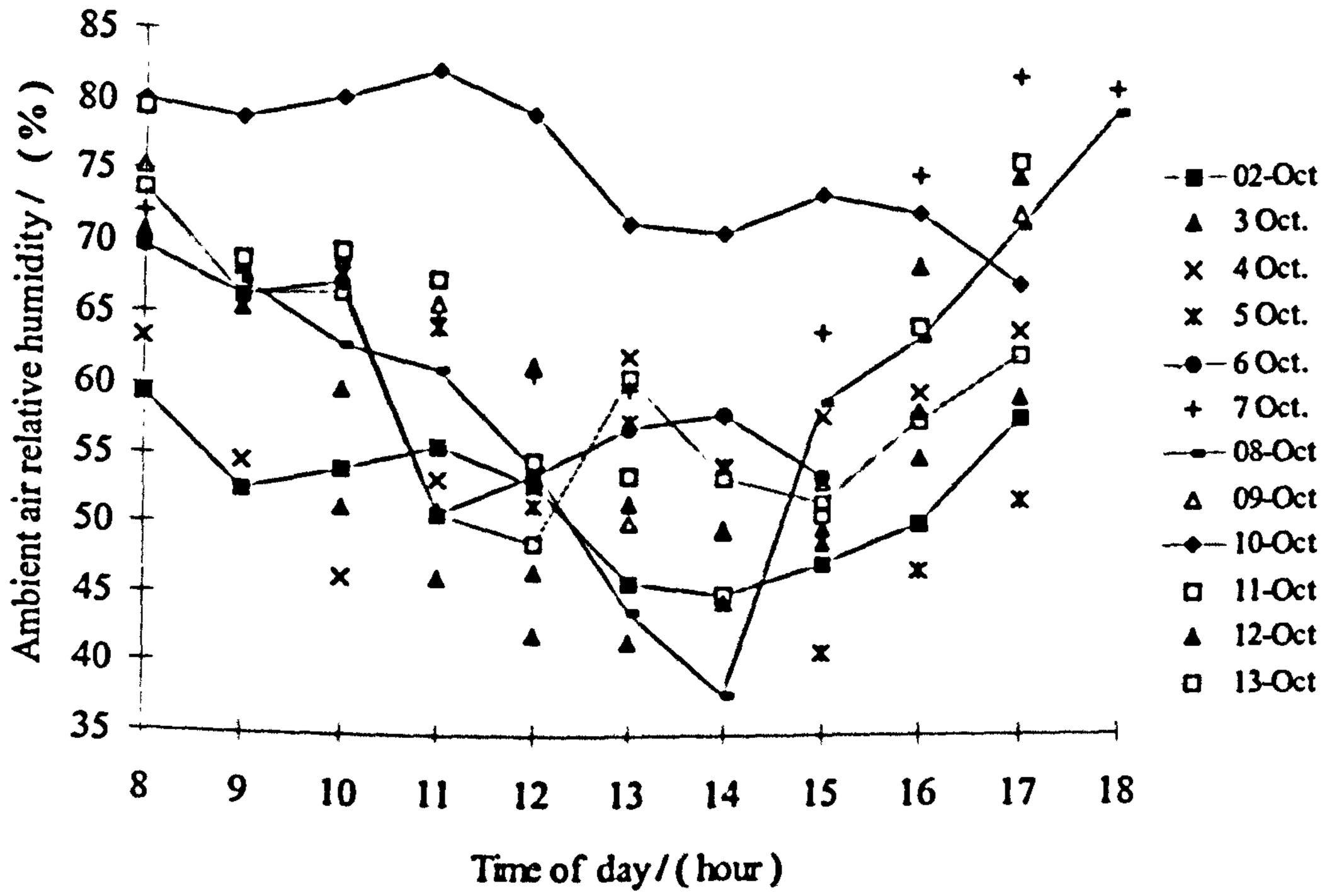

Figure 5.41: Variation in the hourly ambient air relative humidity with time of day recorded over the experimental period at Agona-Asafo, Ghana (2-14 October, 1997).

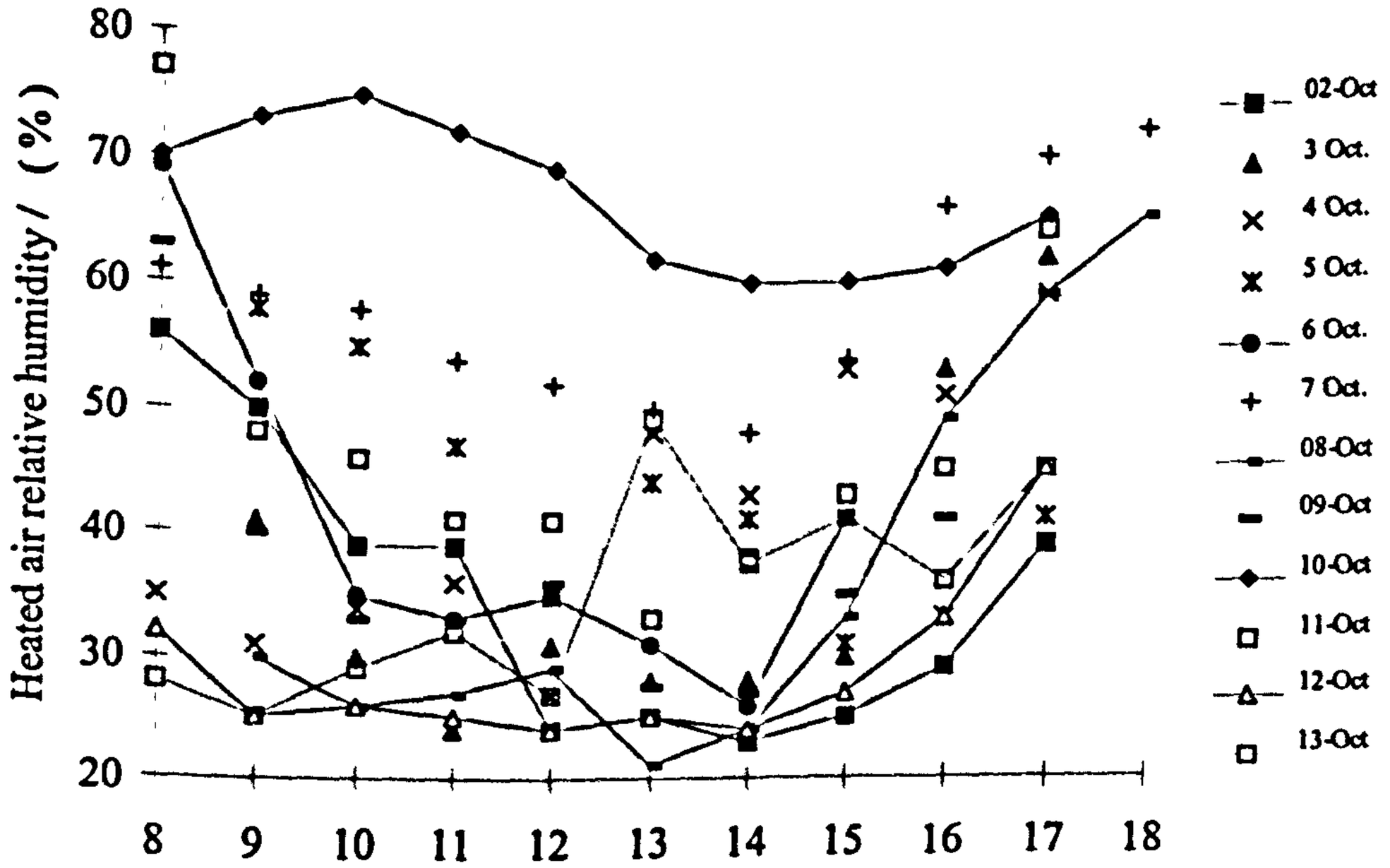

Figure 5.42: Variation in the hourly heated air relative humidity at outlet of the primary collector with time of day recorded over the experimental period at Agona-Asafo, Ghana (2-14 October, 1997).

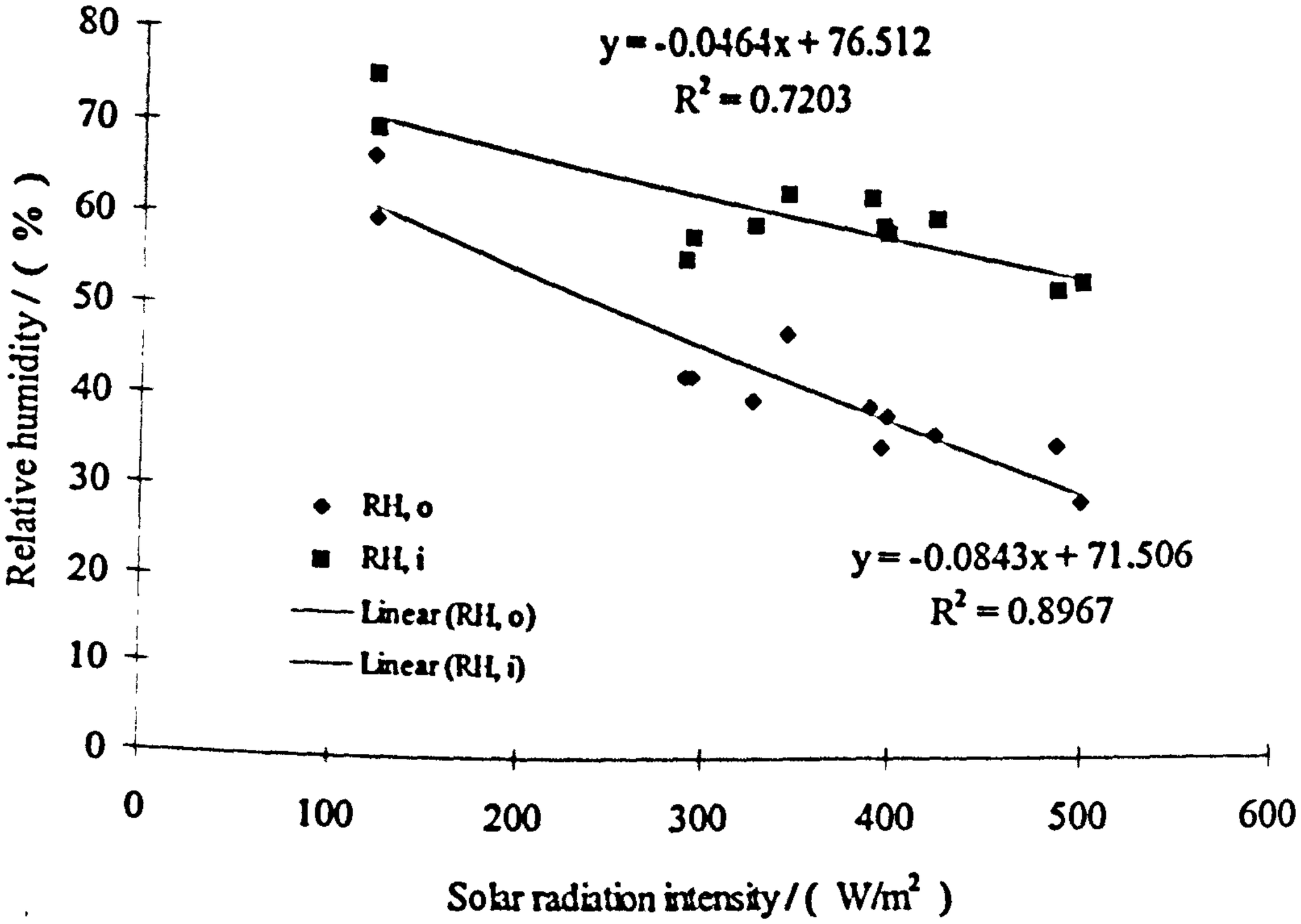

Figure 5.43: Variation in the daily mean values of the ambient and heated-air relative humidity with time of day recorded at Agona-Asafo, Ghana (2-14 October, 1997).

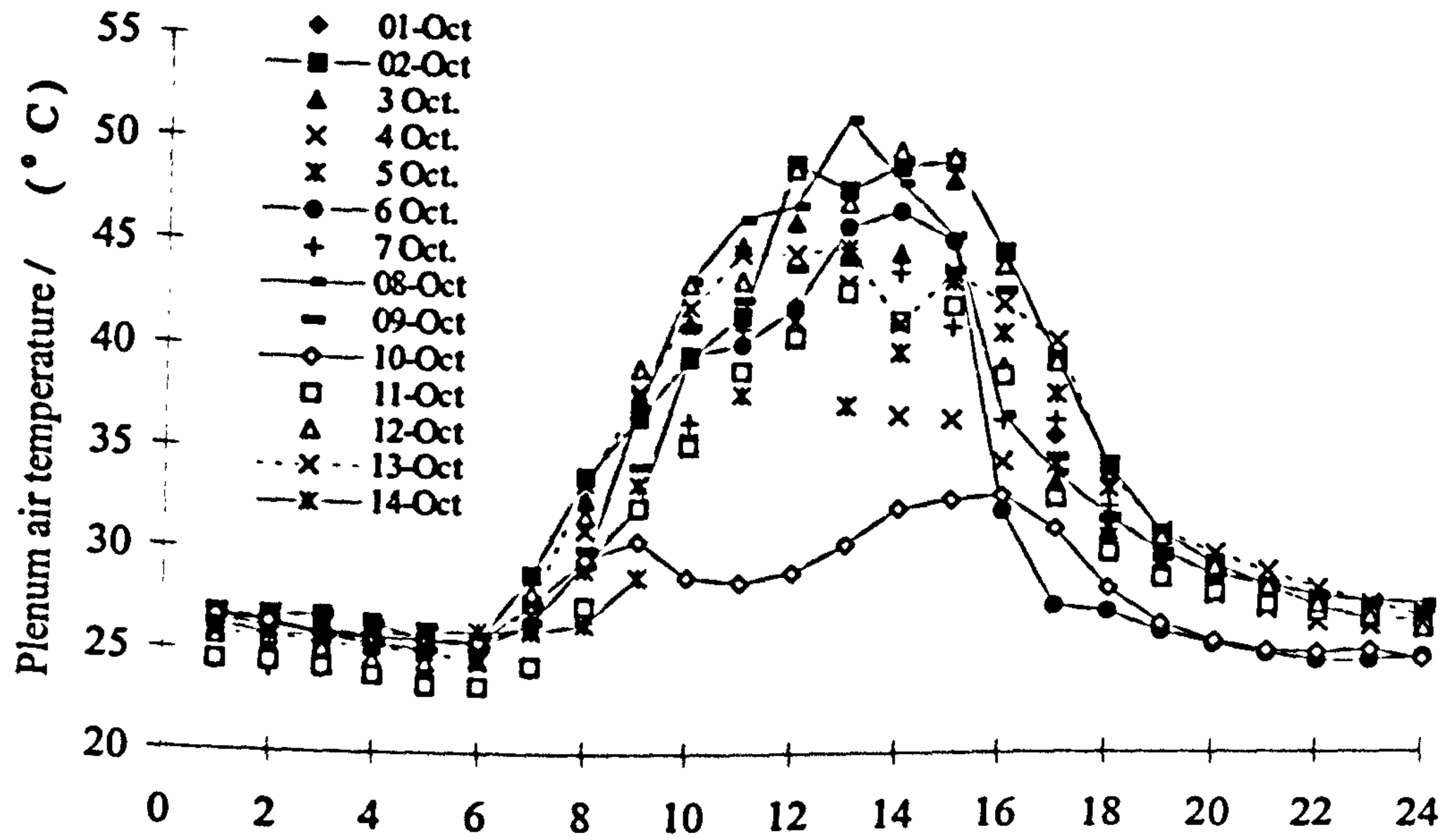

Figure 5.44: Variation in the hourly average values of the heated-air temperature with time of day recorded inside the plenum over the experimental period at Agona-Asafo, Ghana (2-14 October, 1997).

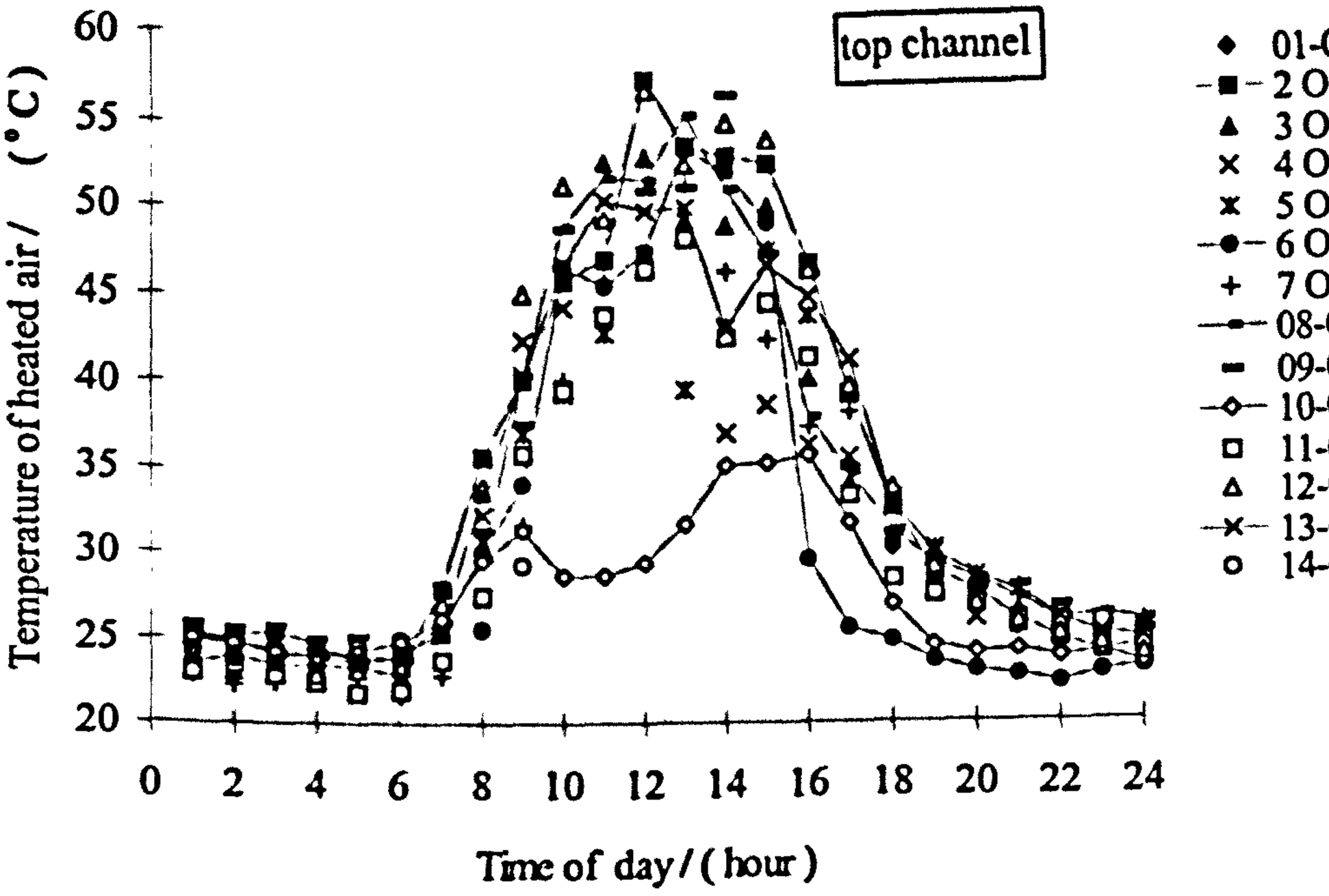

Figure 5.45: Variation in the top channel outlet air temperature with time of day recorded over the experimental period at Agona-Asafo, Ghana (2-14 October, 1997).

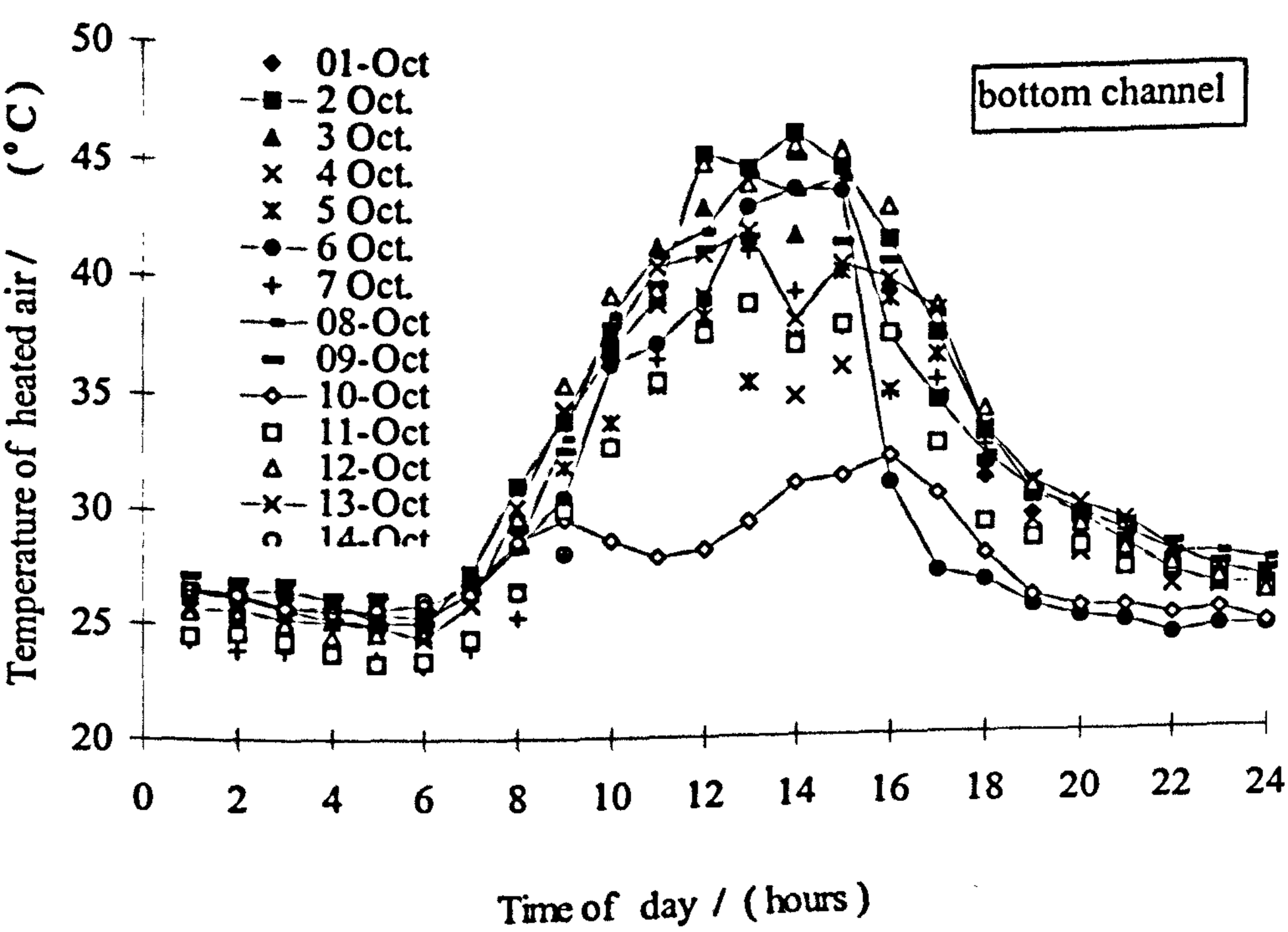

Figure 5.46: Variation in the bottom channel outlet air temperature with time of the recorded over the experimental period at Agona-Asafo, Ghana (2-14 October, 1997).

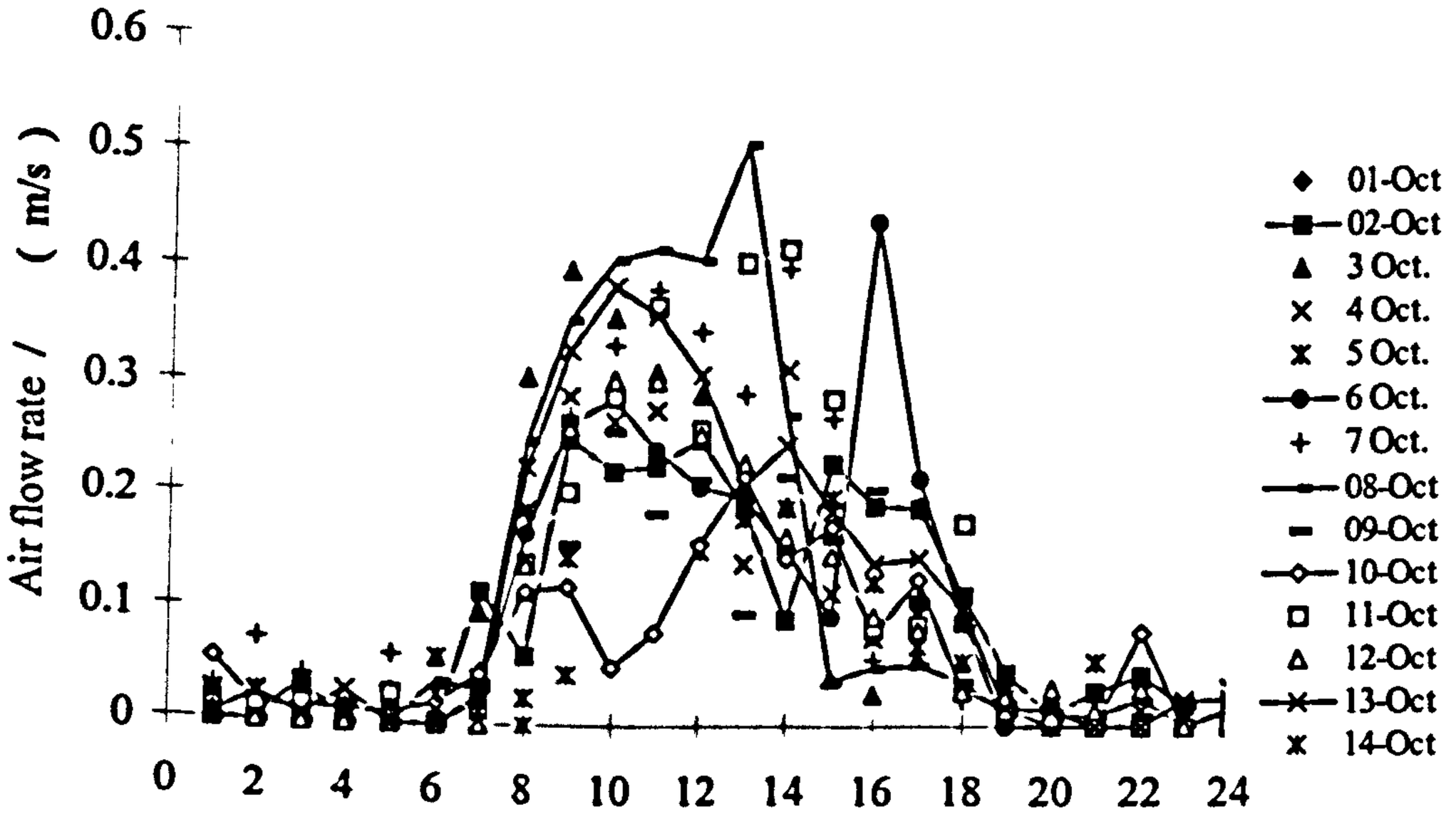

Figure 5.47: Variation in the heated air velocity at the outlet of the bottom channel with time of day recorded over the experimental period at Agona-Asafo, Ghana (2-14 October, 1997).

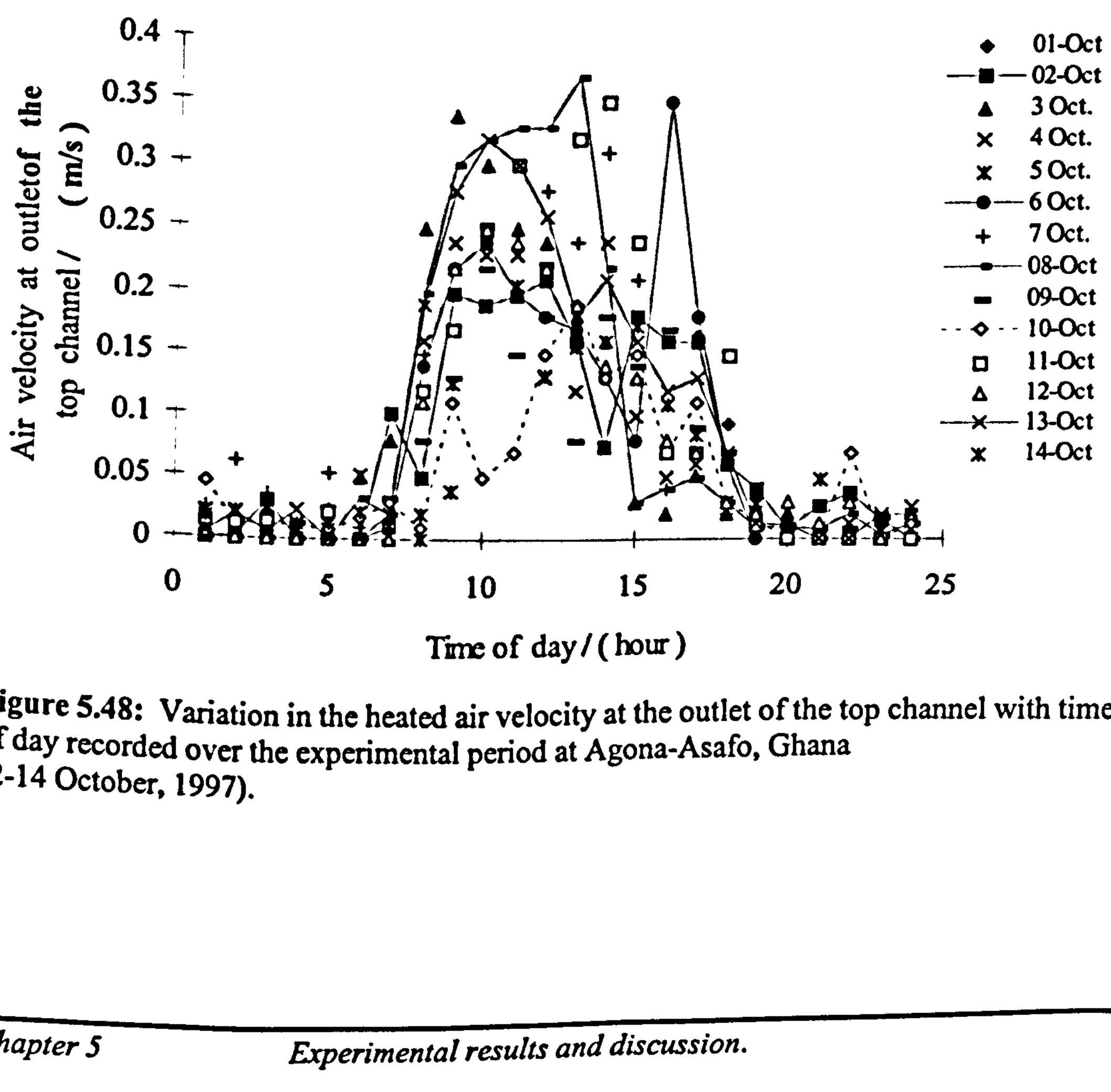

Figure 5.48: Variation in the heated air velocity at the outlet of the top channel with time of day recorded over the experimental period at Agona-Asafo, Ghana (2-14 October, 1997).

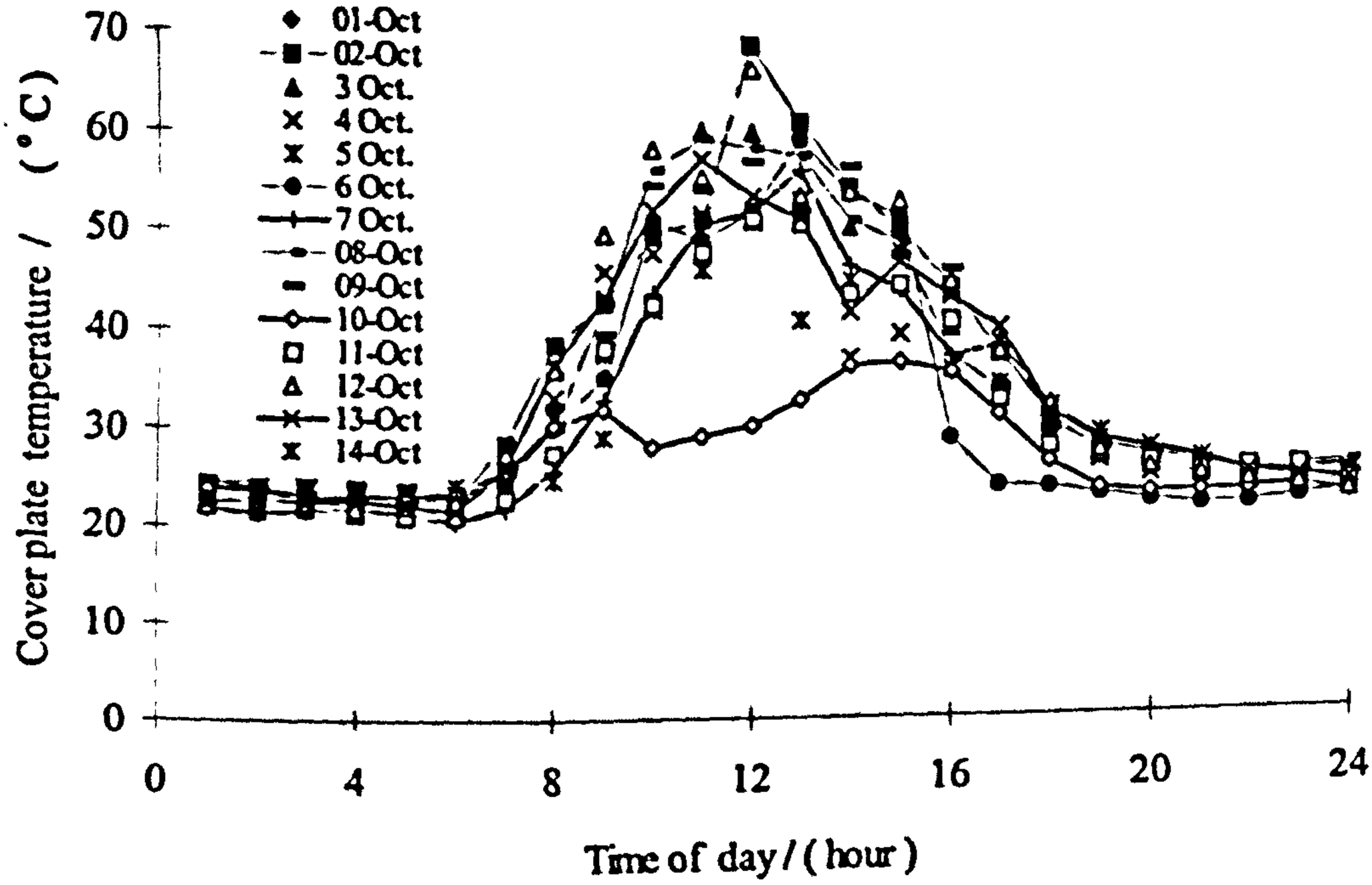

Figure 5.49: Variation in the cover plate temperature with time of day recorded over the experimental period at Agona-Asafo, Ghana (2-14 October, 1997).

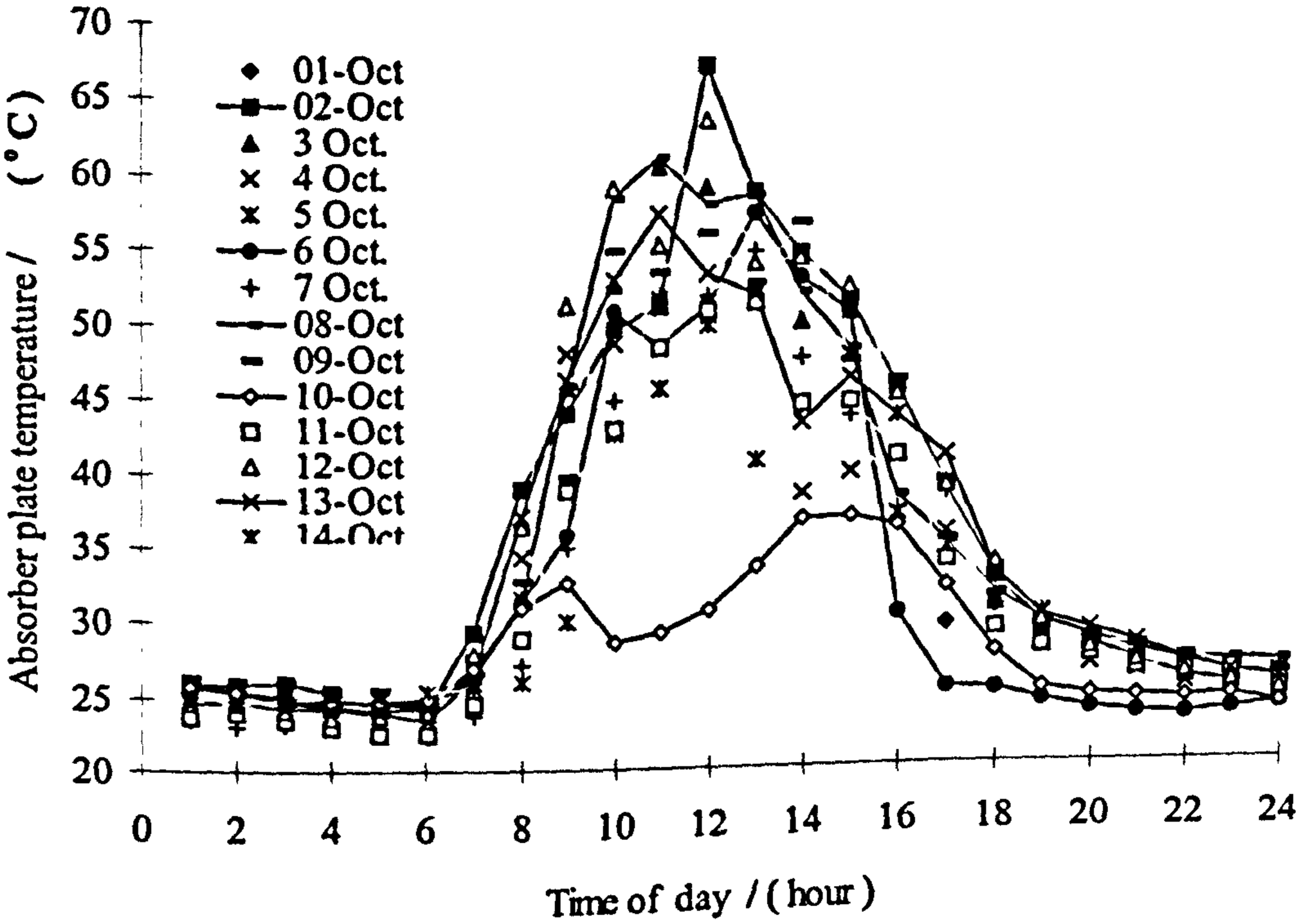

Figure 5.50: Variation in the absorber plate temperature with time of day recorded over the experimental period at Agona-Asafo, Ghana (2-14 October, 1997).

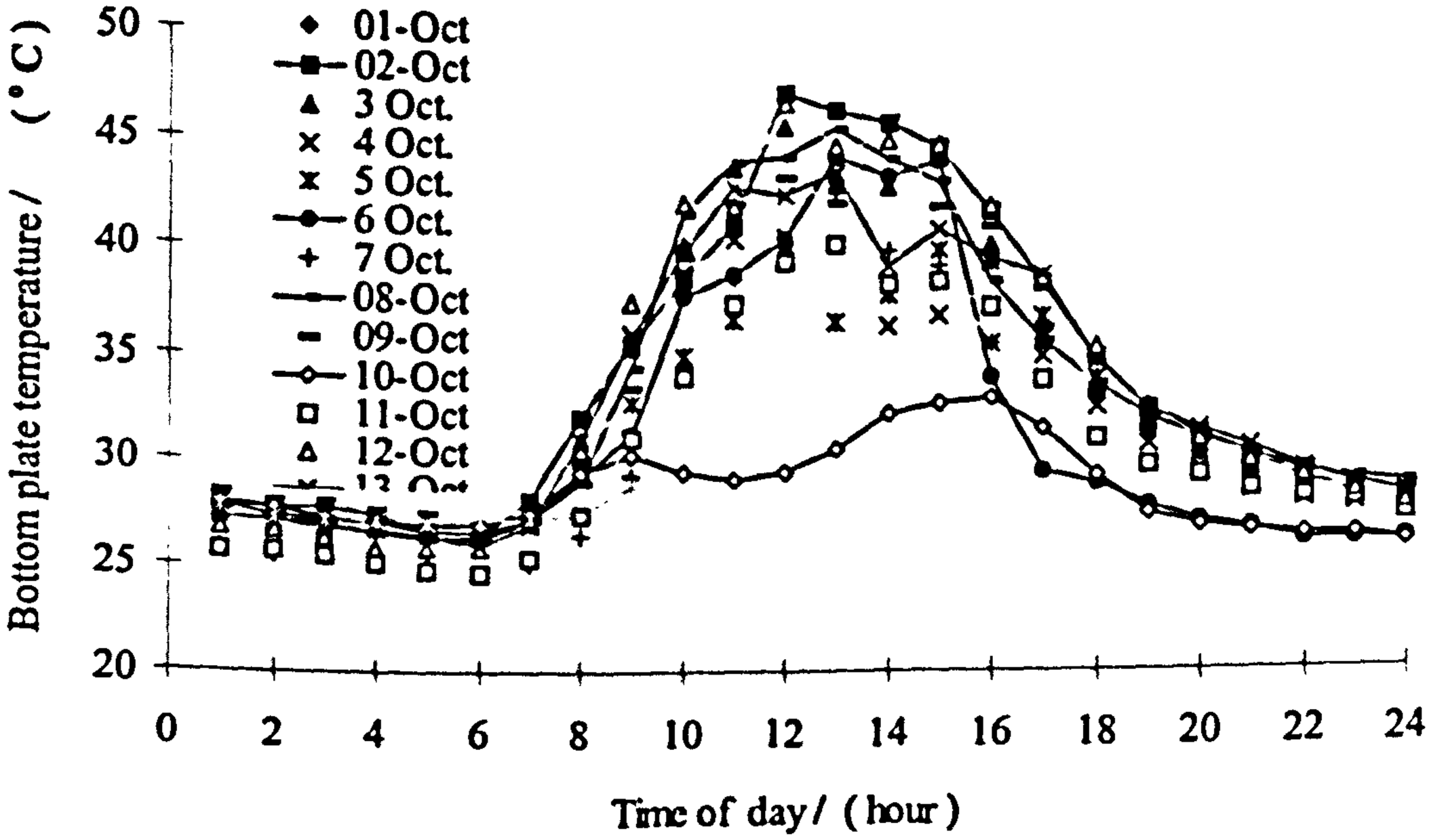

Figure 5.51: Variation in the bottom plate temperature with time of day recorded over the experimental period at Agona-Asafo, Ghana (2-14 October, 1997).

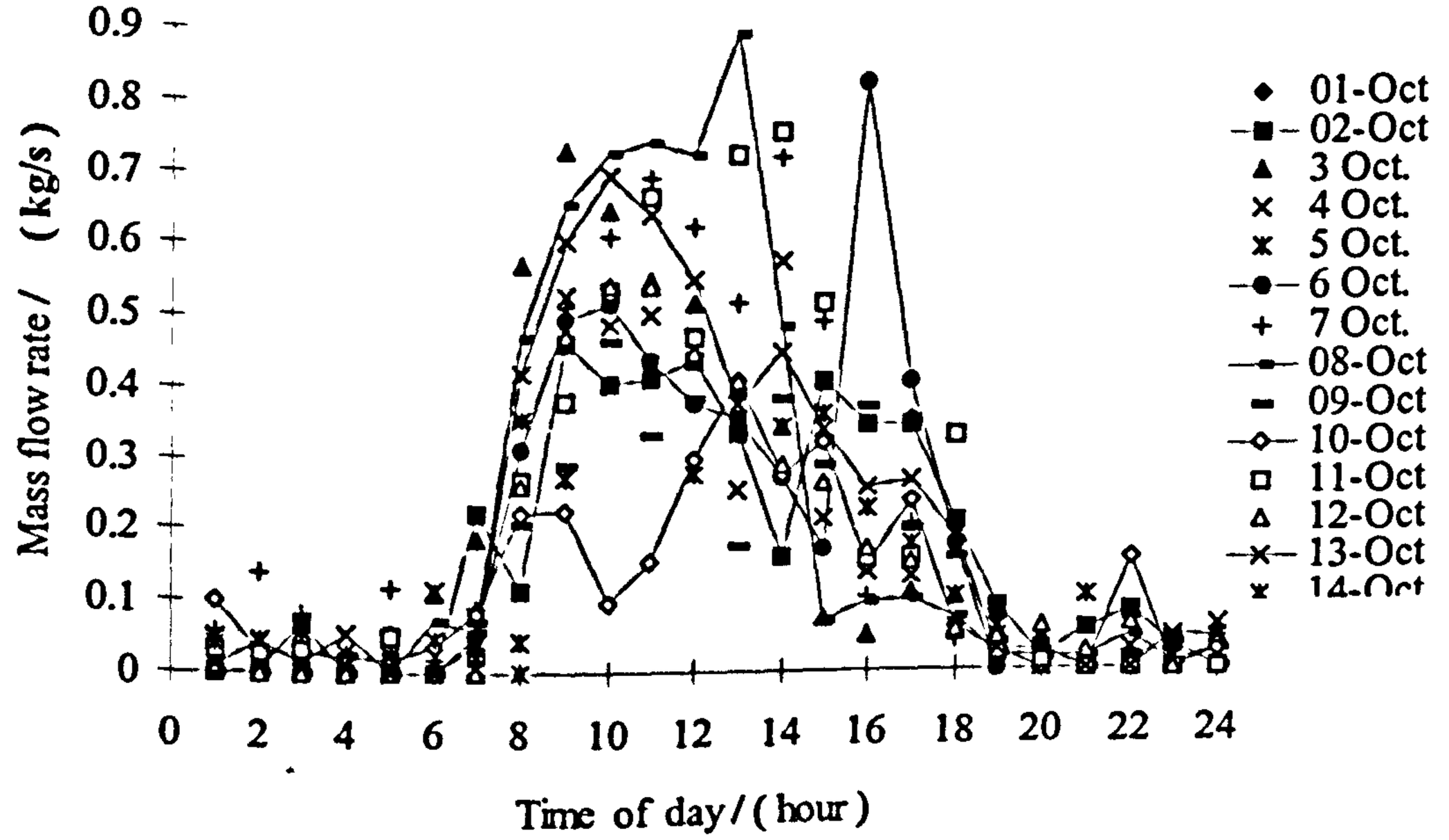

Figure 5.52: Variation in the total mass flow rate at inlet to the drying chamber with time of day recorded over the experimental period at Agona-Asafo, Ghana (2-14 October, 1997).

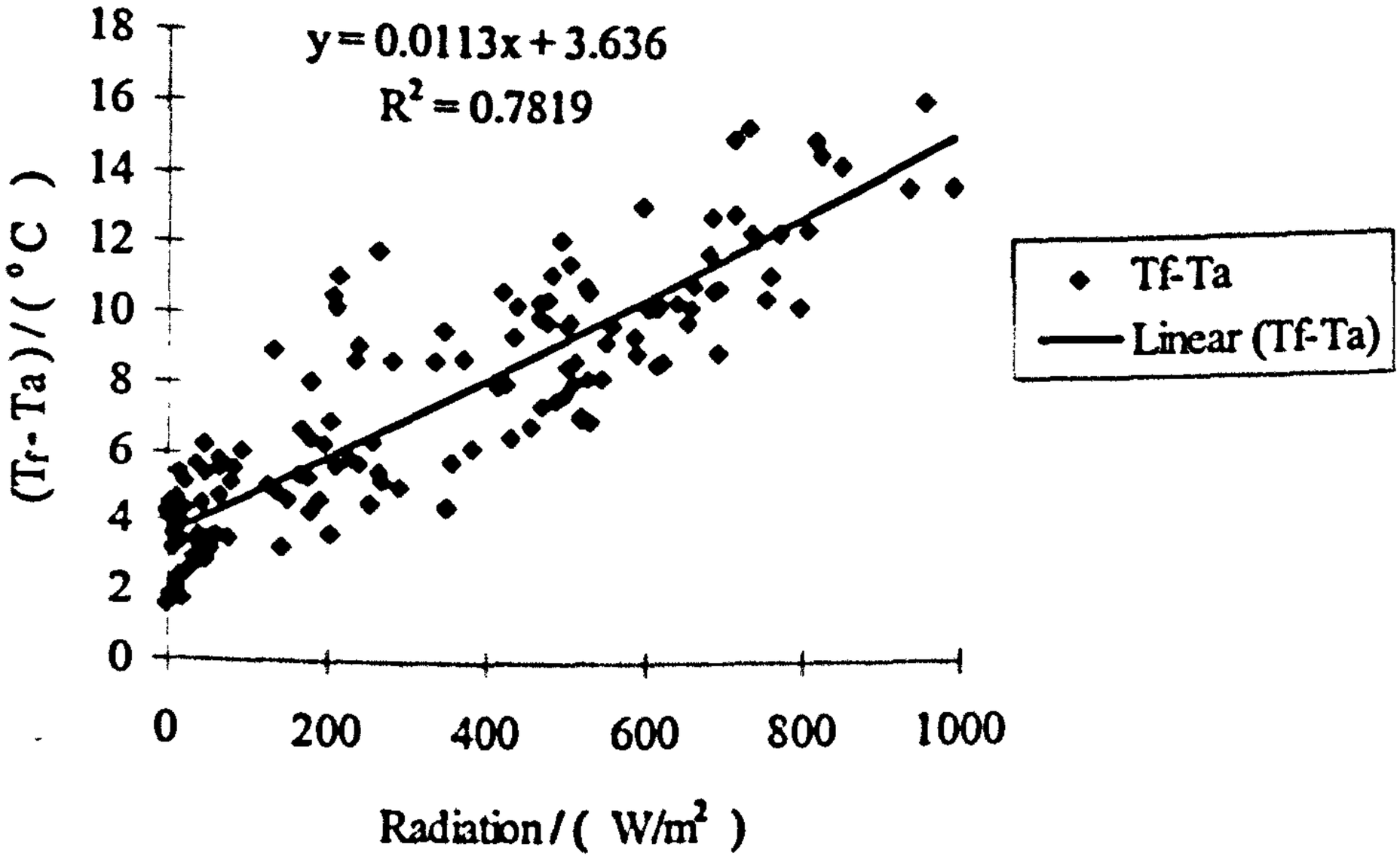

Figure 5.53: Variation of plenum air temperature rise above ambient with solar radiation intensity recorded over the experimental period at Agona-Asafo, Ghana (2 - 14 October, 1997).

CHAPTER SIX

COMPUTER SIMULATION: PROGRAMS, RESULTS AND DISCUSSION

6.0 Computer simulation programs

A complete testing of the air-heating and drying mathematical models developed in chapter 4 to predict the expected performance of the system was carried out by means of two computer simulation programs- SAH and LAYER- written using FORTRAN 77. The program SAH is for studying the performance of the air-heater and it includes four subroutines-RADTNA, GETSIX, GETFUR and SYCHART. The program LAYER, serves to determine the average temperature and moisture content variation of the material being dried and the variation in the properties of the drying air. The following data are required as user-supplied or internally-generated input in the execution of the program LAYER:

a) the temperature of heated air entering the drying chamber which is equal to the mean temperature of the air exiting the air-heater,
b) the average operating temperatures of the air heater components,
c) the relative humidity of air entering the drying chamber,
d) the velocity of heated air entering the drying chamber,
e) the intensity of solar radiation reaching the dryer,
f) the physical and transport properties of the material to be dried,
g) the ambient conditions (temperature and relative humidity of ambient air, and the wind speed)
h) the physical and thermal properties of the materials used for constructing the dryer, and
i) the dimensions of the system (length to width ratio, overall depth, and the top to bottom channel depth ratio of the air-heater; width to breadth ratio, the volume, and height to breadth ratio of the drying chamber; as well as the dimensions of the chimney).

In the main program LAYER, SAH is a subroutine, however each of the two computer simulation programs can be run independently. The main program co-ordinates all the subroutines as illustrated in fig. 6.1. To run LAYER independent of SAH, we need to enter manually values of items (a) to (e) above instead of calling their corresponding values from

subroutines SAH, GETSIX, SYCHART, GETFUR and RADTNA respectively. The listing of the main computer simulation program, LAYER, is provided in Appendix B.

All the variables in the main programs and subroutines are declared as double precision. This is to minimise the numerical errors associated with the calculations of very small quantities and minimise the overall programming errors.

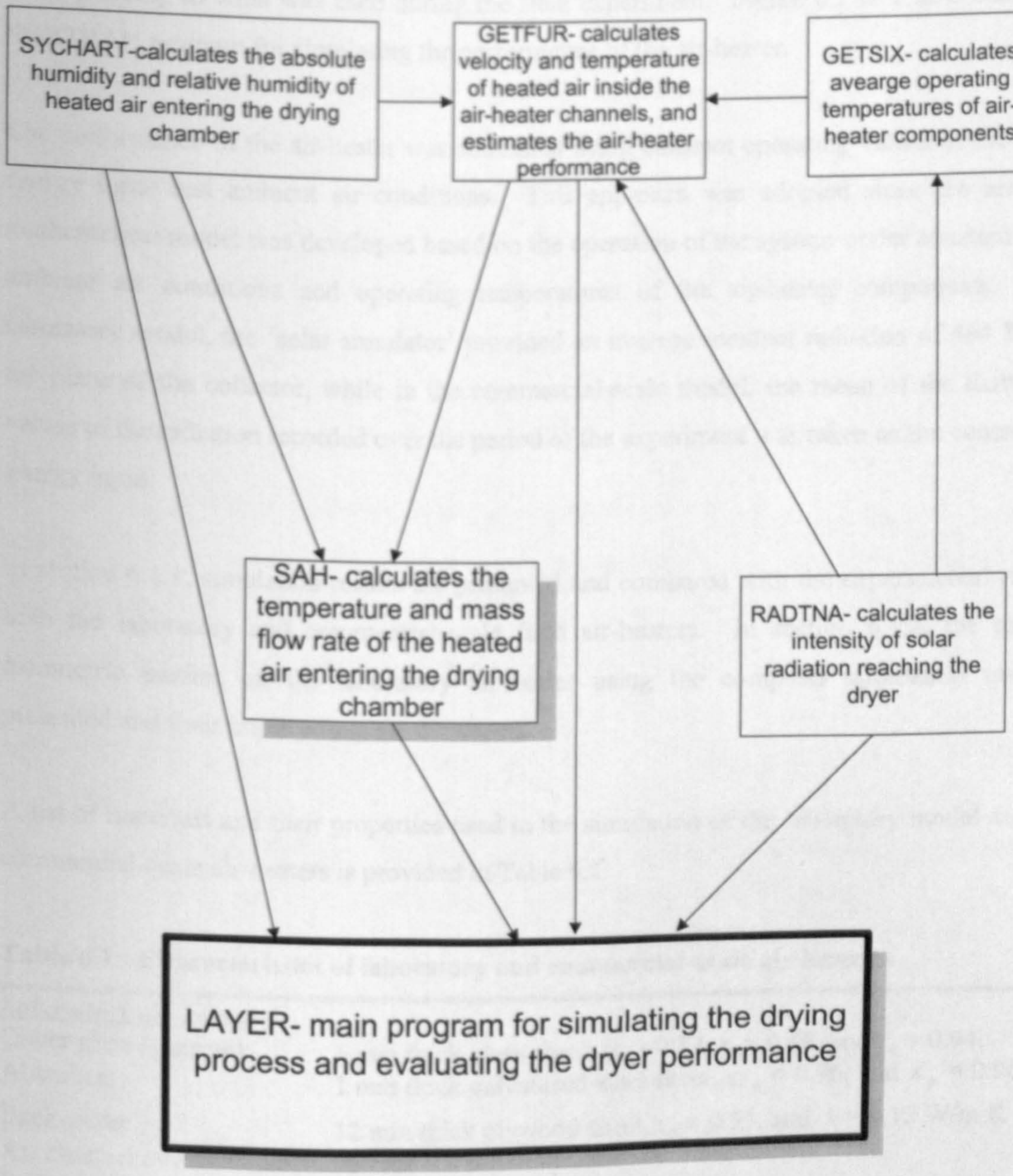

Figure 6.1: Schematic illustration of the co-ordination between the main program LAYER and the subroutines SAH, GETFUR, GETSIX, SYCHART and RADTNA

6.1 Air-heater performance simulation

The mathematical model developed for the air heating process was tested by comparing the predicted performance indicators with the experimentally determined values. In simulating the performance of the laboratory air-heater, the FORTRAN computer program SAH was run for the three configurations experimented on during the laboratory tests (see chapter 3). In the case of the commercial-scale dryer, only one computer simulation was executed for the configuration corresponding to what was used during the field experiment. Figure 6.2 is a flow-chart of the FORTRAN program for simulating the performance of the air-heater.

The performance of the air-heater was simulated using constant operating values of the incident energy input and ambient air conditions. This approach was adopted since the air-heating mathematical model was developed based on the operation of the system under constant average ambient air conditions and operating temperatures of the air-heater components. In the laboratory model, the 'solar simulator' provided an average incident radiation of 464 W/m^2 on the plane of the collector, while in the commercial-scale model, the mean of the daily hourly values of the radiation recorded over the period of the experiment was taken as the constant solar energy input.

In section 6.1.1, simulation results are presented and compared with the experimental results of both the laboratory and commercial-scale field air-heaters. In section 6.1.2, the results of parametric studies on the laboratory air-heater using the computer simulation model are presented and their implications are discussed.

A list of materials and their properties used in the simulation of the laboratory model and in the commercial-scale air-heaters is provided in Table 6.1.

Table 6.1: Characteristics of laboratory and commercial-scale air heaters.

Laboratory air-heater	
Cover plate (glazing):	6 mm thick glass sheet, $\alpha_c = 0.12$, $\tau_c = 0.88$, and $\varepsilon_c = 0.94$.
Absorber:	1 mm thick galvanised-steel sheet, $\alpha_p = 0.96$, and $\varepsilon_p = 0.96$
Back-plate:	12 mm thick plywood sheet, $\varepsilon_b = 0.93$, and $k = 0.12$ W/m K
Air channel overall depth:	75 mm
Inclination:	8° (β) with the horizontal
Side walls:	20 mm thick hardwood (oak), $\varepsilon_h = 0.92$, and $k = 0.17$ W/m K

Table 6.1: continued.

Commercial air-heater	
Cover plate:	3.2 mm poly-carbonate sheet, $\alpha_c = 0.16$, $\tau_c = 0.84$, and $\varepsilon_c = 0.94$
Absorber:	corrugated galvanised sheet painted matt black, $\alpha_p = 0.96$, $\varepsilon_p = 0.96$
Back-plate:	12 mm thick plywood, $\varepsilon_b = 0.93$, and $k = 0.12$ W/m K
Air heater overall depth:	280 mm
Inclination:	8° (β) with the horizontal facing directly south
Side walls:	12.5 cm concrete walls, $\alpha = 0.60$, $\varepsilon_b = 0.88$, and $k = 0.93$ W/m K

The following are required as additional input data for running the program SAH: the ambient conditions (wind speed, and ambient temperature); the site parameters (latitude, empirical constants in the Angstrom-Page regression, number of bright sunshine hours in the mean day of the month); miscellaneous parameters (the design day and the initial guess values of the mean operating temperatures of the glazing, absorber and back plates as well as the air mass flow rate).

6.1.1 Comparison of the simulation and experimental results

In this section, a comparison is made between experimental results and simulation data for the laboratory and field air-heaters to determine the accuracy of the predictions of the model. The following variables, were selected to assess the validity of the model.

i) the mean temperatures of the air-heater components- the glazing, the absorber, and the back-plate;
ii) the mean temperatures of the heated-air at the outlets of the top and bottom channels;
iii) the mean temperature of the air in the plenum of the drying chamber;
iv) the mean air mass flow rate at the outlet of the air-heater;
vi) the relative humidity of the heated-air inside the plenum; and
vii) the mean value of the solar irradiance.

The prevailing laboratory and field weather conditions together with the details of the air-heater configurations for all the simulation runs are provided in Tables 6.2 and 6.3. For the laboratory air-heater, the program SAH was run for three sets of conditions- corresponding to the conditions

of Day 1 for each of the Tests 1, 2, and 3 (see Tables 5.1 - 5.3)- and the three air-heater configurations, whereas for the field air-heater only one run was performed for the reason previously stated. The measured and the predicted values of the above identified variables for the assessment laboratory and field air-heaters are provided in Tables 6.4 and 6.5, respectively.

It is observed from Table 6.4 that very reasonable agreement is obtained between the predicted and the experimental values of the temperatures of the air-heater components, and of the drying air, but the comparison of the mass flow rates are not so good. The percentage difference between the measured and predicted values of the operating temperatures of the air-heater component were within 9.1% of the experimentally determined values; in the case of heated air temperatures, the difference between the measured and predicted values are within 9 % of the experimental values. For the three runs, the percentage difference between the experimental and predicted air mass flow rates were within 12.2% of the experimental values.

As can be seen from Table 6.5, the predicted values of the operating temperatures of the full-scale air-heater components and the fluid temperatures were consistently higher than the values measured experimentally by up to 12%. This is perhaps due to the fact that, the model over-predicted the solar irradiance by 40.5% of the experimentally determined value. A possible explanation for the discrepancy between the measured and the predicted values of the solar irradiance is that the exact values of the constants in the Angstrom-Page were unavailable and therefore conservative estimates for another site in the same country were used. Another possible cause for the discrepancy between the measured and the predicted solar irradiance is the influence of extremely low values of the incident solar radiation- of the order of 121 W/m^2 - recorded on two days during the twelve days over which the experiment was conducted. The results show that the simulated air mass flow at the exit of the air-heater approached quite closely the experimental results (Table 6.5) within 5.1% of the experimental value.

It is seen from Tables 6.4 and 6.5 that, in general, the air-heating model is capable of predicting the performance of the air-heater with reasonable accuracy. With, the exception of the solar irradiance values the difference between the other measured and predicted values are within 12.2% of the experimental results, and this may be regarded as satisfactory agreement considering the fact that a steady state solution is used to estimate an otherwise dynamic

phenomenon. A refinement of the air-heating model could possibly be achieved by incorporating a term in the model to account for heat capacity of the air-heater components.

Table 6.2: Values of the prevailing laboratory conditions and air-heater configurations

Parameter	RUN 1	RUN 2	RUN 3
Top to bottom channel depth ratio (P)	0.364	1.08	3.412
Length to width ratio (Q)	1.586	1.586	1.586
Ambient air temperature, °C	23.1	27.1	26.9
Ambient air relative humidity, %	38.3	40.5	45.3
Wind speed, m/s	0.01	0.01	0.01
Mean intensity of incident radiation, W/m^2	464	464	464
Area of the air-heater aperture, m^2	0.327	0.327	0.327
Overall depth of the air-heater, mm	75	75	75

Table 6.3: Values of prevailing field conditions and air-heater configurations

Parameter	Value
Top to bottom channel depth ratio (P)	1.0
Length to width ratio (Q)	2.08
Ambient air temperature, °C	23
Ambient air relative humidity, %	60.9
Wind speed, m/s	0.72
Mean intensity of incident radiation, W/m^2	341
Area of the air-heater aperture, m^2	76.23
Overall depth of the air-heater, mm	280

Table 6.4: Comparison of the average values of the measured and predicted values of the laboratory air-heater

		Parameter						
		T_c (°C)	T_o (°C)	T_b (°C)	$T_{f.1}$ (°C)	$T_{f.2}$ (°C)	T_f (°C)	$\dot{m}$ (kg/s)
Day 1, test 1	Measured	46.8	56.1	27.5	46.1	24.9	27.5	0.0164
RUN 1	Predicted	43.3	57.0	25.0	42.0	26.2	29.5	0.0144
Difference (± %)		-7.1	+1.6	-9.1	-8.9	+5.2	+7.3	-12.2
Day 1, test 2	Measured	44.8	54.5	29	38.9	33.2	31.9	0.0123
RUN 2	Predicted	44.8	56.5	29	36.8	31.8	34.3	0.0130
Difference[a] (± %)		0	+3.7	0	-5.4	-4.2	+7.5	+5.7
Day 3, test 3	Measured	45.3	52.6	33.1	34.5	38.9	37.1	0.0139
RUN 3	Predicted	43.4	55.4	31.6	34.1	36.1	34.4	0.0145
Difference (± %)		-4.4	+5.3	-4.5	-1.1	-7.2	-7.3	+4.3

Table 6.5: Comparison of the average values of the measured and predicted values of the full-scale air-heater.

	Parameter								
	T_c (°C)	T_p (°C)	T_b (°C)	$T_{f,1}$ (°C)	$T_{f,2}$ (°C)	T_f (°C)	$\dot{m}$ (kg/s)	RH_2 (%)	RAD (W/m^2)
Measured	41.4	42.4	36.5	40.2	35.4	37.6	0.369	43.1	341
Predicted	42.1	47.5	37.3	41.9	39.2	40.3	0.350	34.8	479
Difference (± %)	+1.7	+12	+2.2	+4.2	+10.7	+7.2	-5.1	-19.7	+40.5

[a] The negative percentage difference indicates that the predicted value was less than the observed value, and vice versa is true for the positive difference.

6.1.2 Parametric studies on the air-heaters

In order to optimise the design of the SPDDSAH, parametric studies were conducted on the laboratory air-heater using the simulation model. The study was designed to look at the factors that are within the control of a solar air-heater designer and which can be varied in order to improve its performance. The focus of the study, therefore, was concerned with determining the best air-heater design configuration without compromising on cost. The investigation assessed the effect of the following parameters on the performance of the air-heater:

i) the air flow channel top to bottom depth ratio, $P\ (=s_1/s_2)$,

ii) the length to width ratio, $Q\ (=L/W)$,

iii) the overall collector channel depth, $s\ (=s_1+s_2)$, and

iv) the area of the primary collector, A_c

Using the same baseline design parameters of the laboratory air-heater ($P = 0.364$, $Q = 1.586$, $s = 75$ mm and $A_c = 0.327\ m^2$), the value of any one of these parameters was varied keeping the others fixed and the effect of this change on the collector's predicted performance was obtained. A simulation process of this type was adopted because it is useful in predicting the effect of varying any one parameter on the air-heating process.

Figures 6.3(a) and 6.3(b) show that as the top to bottom channel depth ratio is increased ($P > 1$), for a given overall depth, there is an increase in the temperature and a reduction in the mass flow rate of the heated air flowing through the bottom channel; and the reverse phenomenon occurs in

the upper channel. As the top to bottom channel depth ratio decreases (P < 1), there is an increase in temperature of the air flowing through the upper channel and a reduction in the mass flow rate, as expected. However, in the bottom channel there is a decrease in the temperature of the flowing air and an increase in the mass flow rate, signifying that bottom losses are minimised resulting in an increase in the air flow rate. A decrease in the depth of a channel results in an increase in the flow resistance, thus leading to higher temperature of the heated air flowing through that channel. As is evident, there is a significant increase in the temperature when the upper channel depth is made narrower for a given overall depth, as compared to a similar situation in which the lower channel depth is made narrower. The latter behaviour suggests that the top losses are minimised as the top channel is made narrower compared to the situation where the bottom channel is made narrower. This trend of results is confirmed by the experimental results presented in Table 6.4.

Figure 6.3(c) shows a progressive increase in the efficiency of the air-heater as the top to bottom channel depth ratio is increased. Figure 6.3(d) shows that as the top to bottom channel depth ratio increases, the normalised relative humidity decreases. The study reveals that increasing the top to bottom channel depth ratio above the value of P = 1.1 will always result in an increase in the mean heated air temperature and mass flow-rate, and a reduction in the normalised relative humidity.

Figures 6.4(a) and 6.4(b) show that an increase in the value of s causes an increase in the mass flow rate and a decrease in the temperature of the heated air in both channels. The results can be interpreted as follows: an increase in the channel flow area over the baseline value results in lower flow resistance and hence a decrease in the temperature of the heated air as the channel depth is increased. Figure 6.4(c) shows that an increase in the overall channel depth results in an increase in the efficiency. Similar trends have been reported in the literature [10]. The useful heat transferred to the heated air flowing through any channel is given by $Q_u = \dot{m}C_p\Delta T$. Since ΔT decreases as the overall channel depth, s, is increased, the increase in the efficiency for a given set of values of P, Q, and A_c is suggestive that the increase in the mass flow rate outweighs the effect of the decrease in the corresponding temperature of the heated air. Thus, mass flow rate becomes the dominant determining factor governing the performance of the air-heater with an increase in the value of the overall collector depth. However, the extent to which s can be

increased to achieve an increase in collector efficiency is limited since for collectors with a tilt angle up to 60°, the aspect ratio (= *L/s*) should be between 20 and 200 (Bucherg *et al*, 1974). This restriction places a limit on the maximum value of *s* for an air-heater of a given area. It is also significant to note that, with this option, the increase in the useful energy is at the expense of reduced temperatures of the heated air and increase in the relative humidity as shown in figs. 6.4(a) and 6.4(c). Thus, increasing the air-heater overall channel depth will result in heated air conditions that are unfavourable for crop drying purposes. On the other hand, it can be inferred from the results that in order to achieve a higher air-stream temperature, a small flow channel depth is required. However, small flow channel depths will cause large frictional losses over the length of the air-heater resulting in a reduced mass flow rate.

Figures 6.5(a) and 6.5(b) show that as Q is increased the temperature of the air-stream in the channels increases while the mass flow rate decreases. As is evident, the temperature of the air in the top channel is always greater than that in the bottom channel, even for a situation in which both the upper and the lower channels are of equal depth (see fig. 6.4(a)). An increase in the value of Q implies a reduction in the value of the width of the collector and consequently an increase in the length. Thus, for a given configuration of the air-heater with s, P and A_c maintained constant, there is a reduction in the area of each of the flow channels. This leads to an increase in turbulence resulting in an increase in the mean heated air temperature and a decrease in the mass flow rate.

Figure 6.5(c) depicts a decrease in the efficiency of the air heater with increasing Q. But the temperature of the heated air increases as Q is increased and therefore the corresponding reduction in efficiency suggests that an increase in the mass flow rate becomes the more dominant factor governing the performance of the air-heater than the effect of an increase in temperature. Reducing the length to width ratio for a given collector is an alternate proposition for increasing its efficiency without compromising on cost but it is at the expense of decreasing temperatures and increasing relative humidity of the heated air. Figure 6.5(d) shows that increasing the length to width ratio, for a given area, results in lower values of the normalised relative humidity.

Figures 6.6(a) and 6.6(b) clearly illustrate that an increase in the collector area will lead to an increase in both the temperature and the mass flow rate, for a given air heater configuration. This

option does not necessarily alter the flow channel configuration, but the total solar radiation absorbed by the collector is increased and consequently the available energy increases. However, the efficiency of the collector decreases as the area is increased as shown in fig. 6.5(c). The possible explanation for this observation is that the increase in the useful energy does not match up to the energy supplied. Thus, increasing a collector area for a natural convection solar air heater might not necessarily lead to an increase in the collector efficiency. It is clear from fig. 6.5(d) that increasing the collector aperture area will result in a decrease in the relative humidity of heated air at entry to the drying chamber. For a given total energy collection area of a drying system, an increase in the air-heater surface area will imply reducing the cross-sectional area of the drying chamber. This option could possibly reduce the crop matter that can be dried in the drying chamber per batch.

It is revealing from the study, that for a SPDDSAH the single modification that can be made to achieve an improvement in the performance of the heater at minimum added cost is to consider re-positioning the absorber plate to obtain higher values of P.

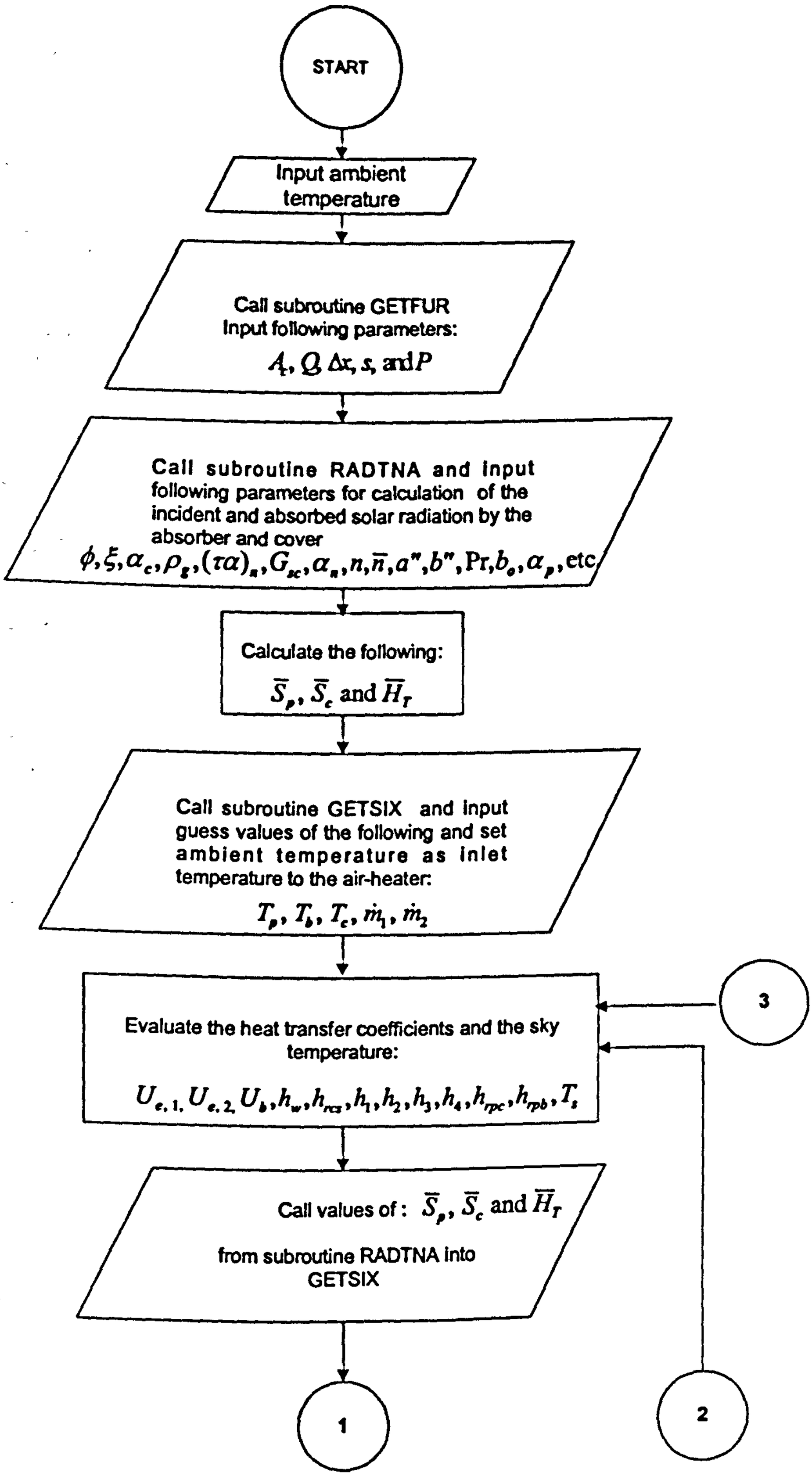
START
Input ambient temperature
Call subroutine GETFUR
Input following parameters:
$A, Q, \Delta x, s,$ and P
Call subroutine RADTNA and input following parameters for calculation of the incident and absorbed solar radiation by the absorber and cover
$\phi, \xi, \alpha_c, \rho_g, (\tau\alpha)_n, G_{sc}, \alpha_n, n, \bar{n}, a'', b'', \Pr, b_o, \alpha_p$, etc
Calculate the following:
$\bar{S}_p, \bar{S}_c$ and $\bar{H}_T$
Call subroutine GETSIX and input guess values of the following and set ambient temperature as inlet temperature to the air-heater:
$T_p, T_b, T_c, \dot{m}_1, \dot{m}_2$
Evaluate the heat transfer coefficients and the sky temperature:
$U_{e,1}, U_{e,2}, U_b, h_w, h_{rcs}, h_1, h_2, h_3, h_4, h_{rpc}, h_{rpb}, T_s$
Call values of : $\bar{S}_p, \bar{S}_c$ and $\bar{H}_T$
from subroutine RADTNA into GETSIX
3
1
2

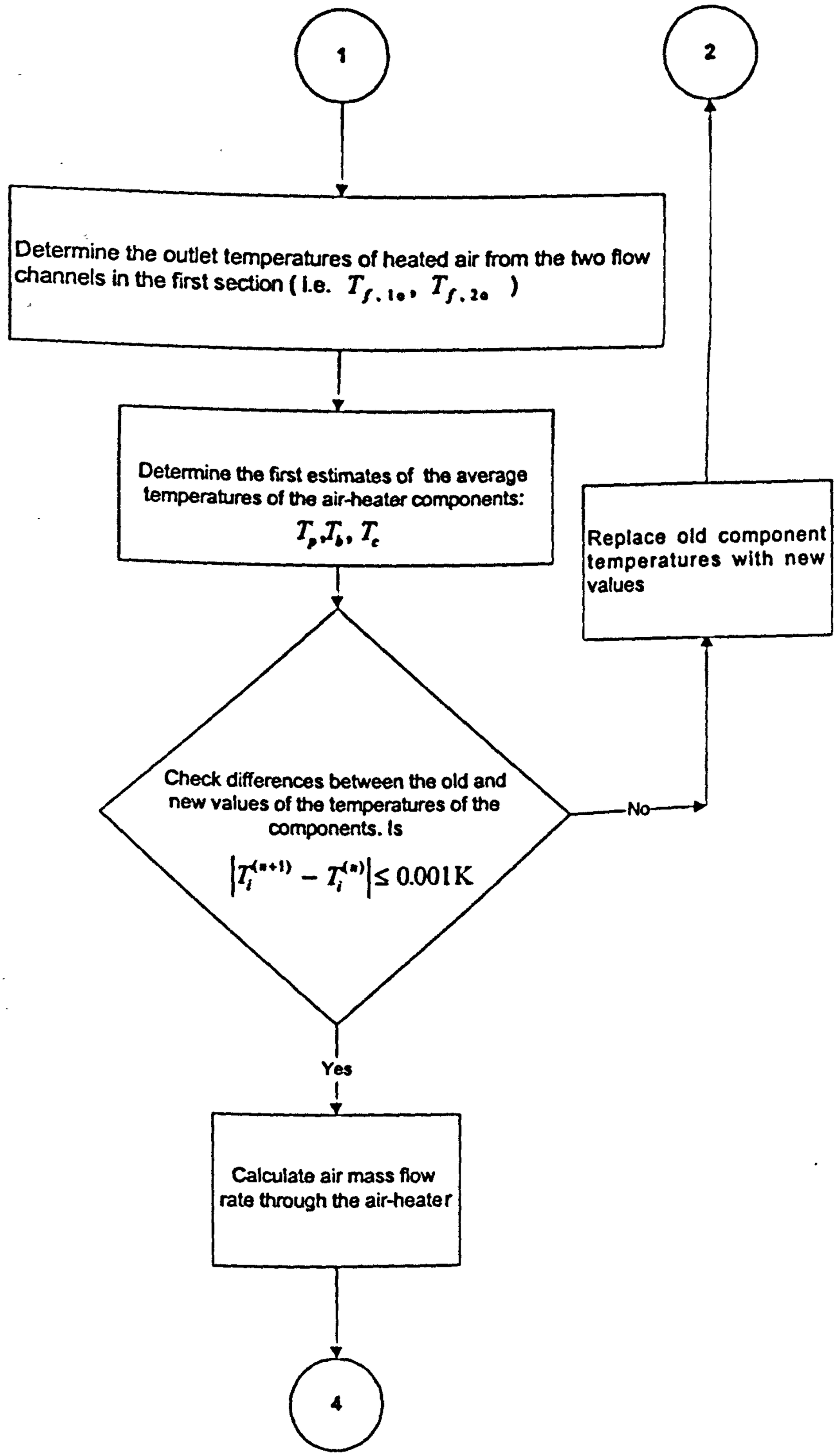
1
2
Determine the outlet temperatures of heated air from the two flow channels in the first section (i.e. $T_{f,1o}$, $T_{f,2o}$)
Determine the first estimates of the average temperatures of the air-heater components:
T_p, T_b, T_c
Replace old component temperatures with new values
Check differences between the old and new values of the temperatures of the components. Is
$|T_i^{(n+1)} - T_i^{(n)}| \leq 0.001\,\mathrm{K}$
No
Yes
Calculate air mass flow rate through the air-heater
4

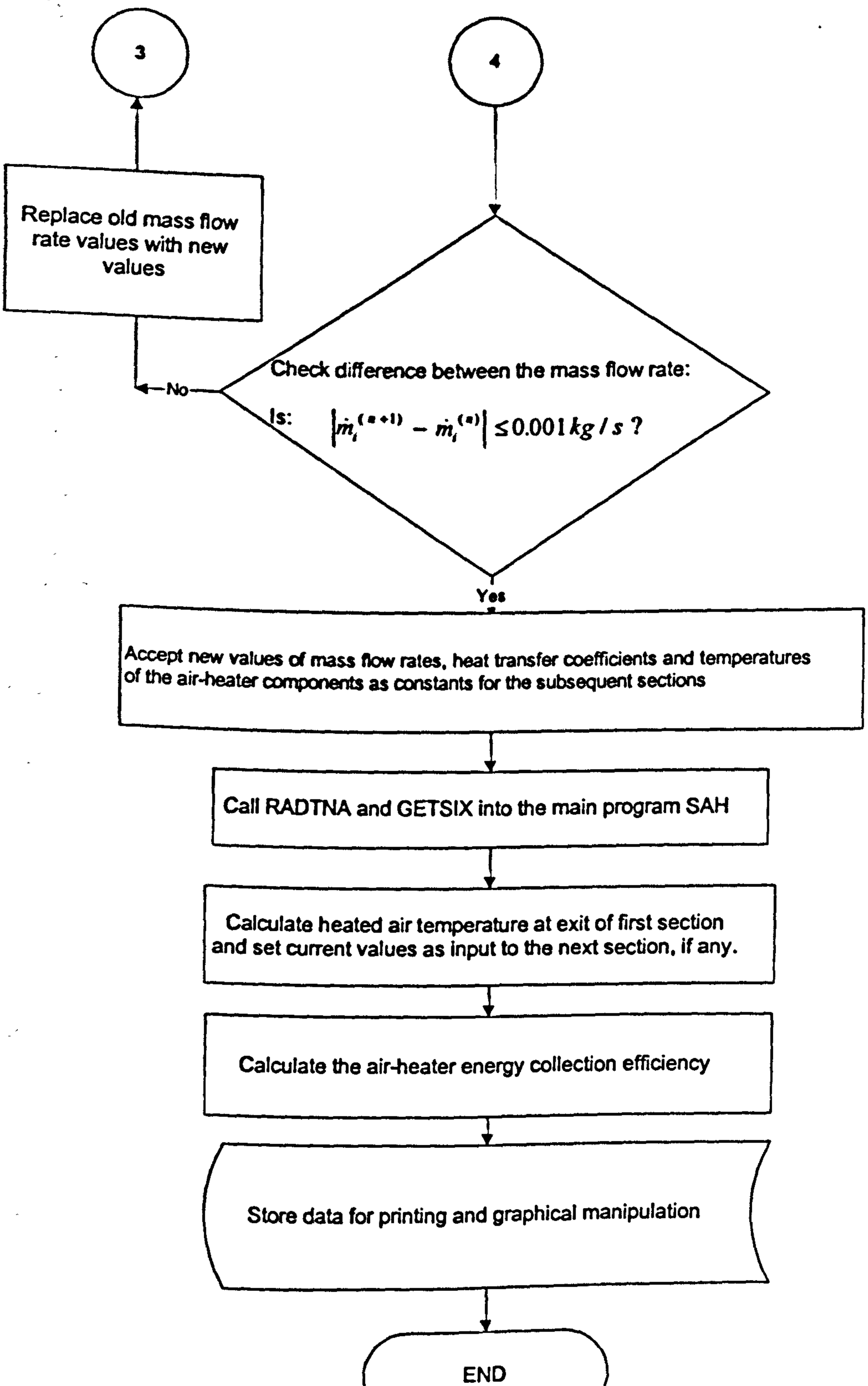

Figure 6.2: Flow chart of the FORTRAN program SAH

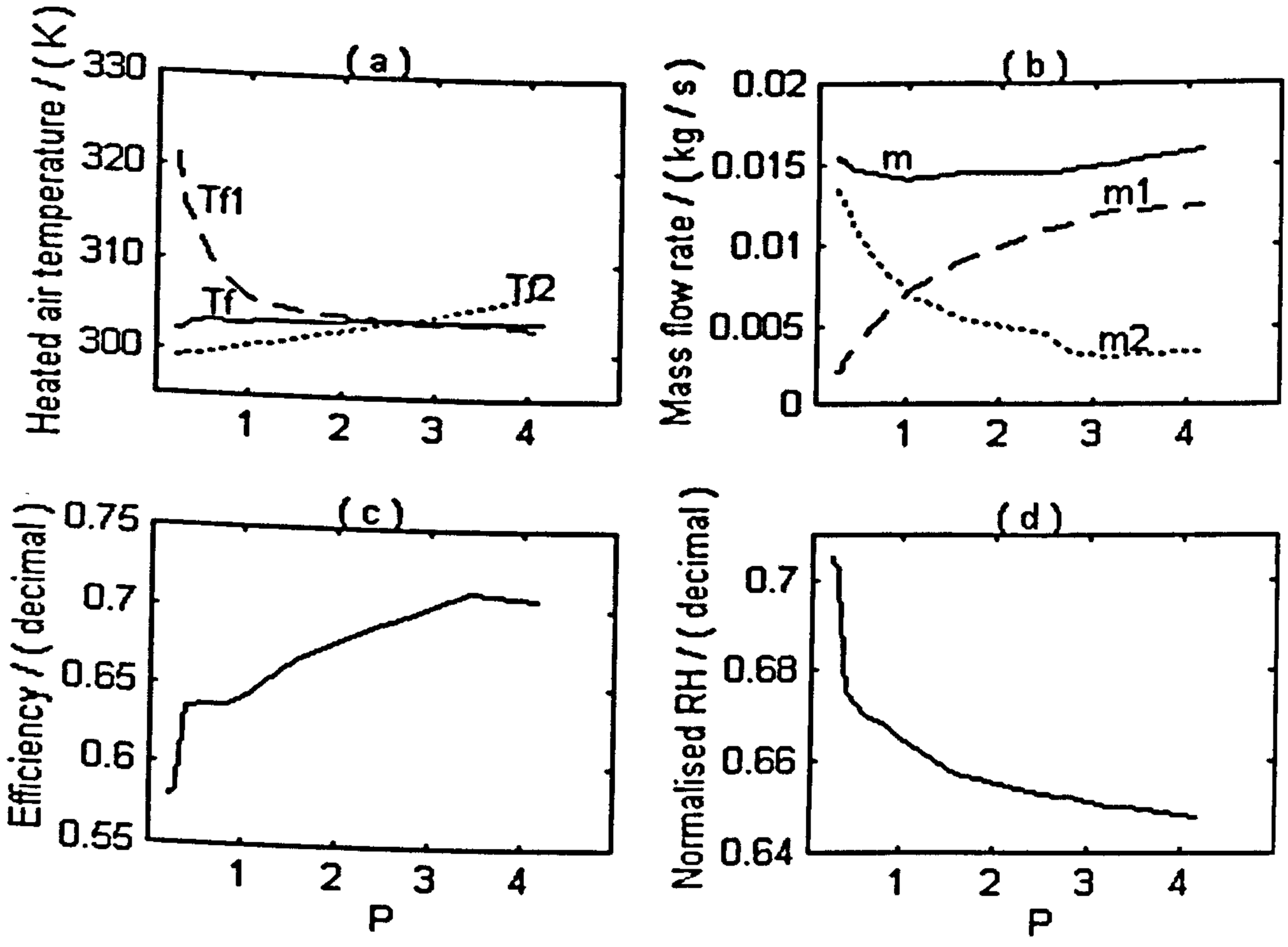

Figure 6.3: Simulation results of the effect of varying top to bottom channel depth ratio (P) on the performance of a SPDDSAH

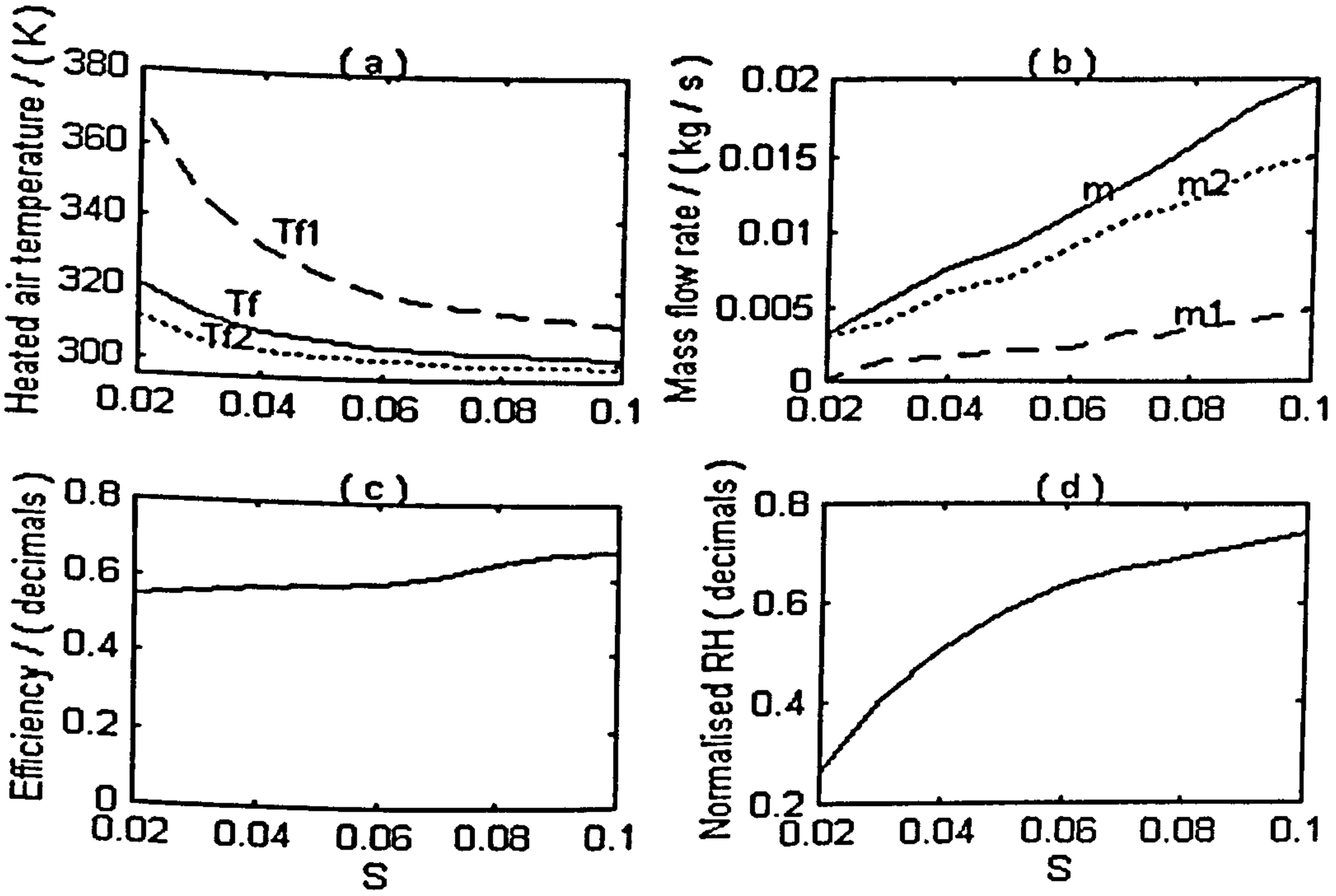

Figure 6.4: Simulation results of the effect of varying overall channel depth (s) on the performance of a SPDDSAH

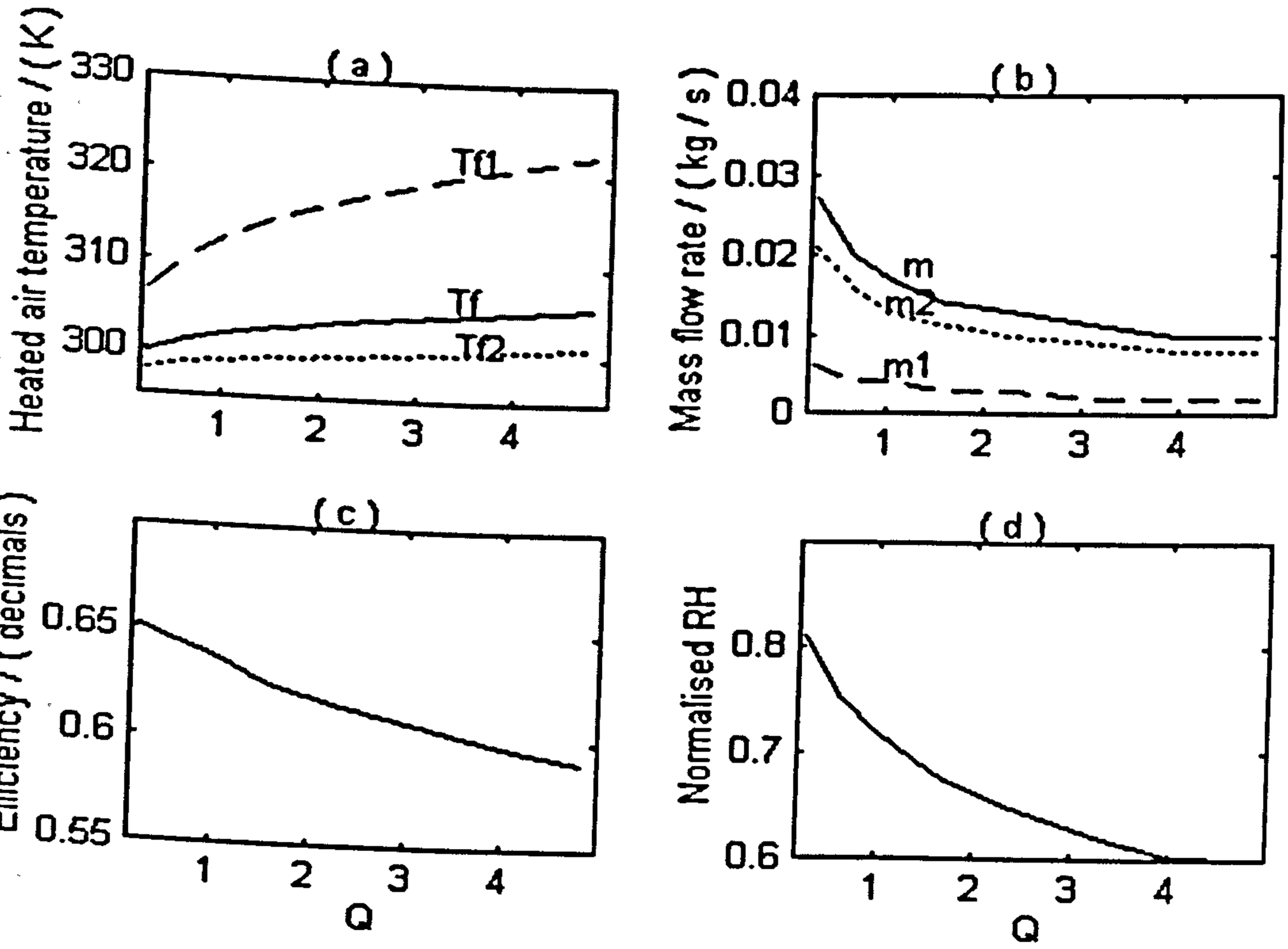

Figure 6.5: Simulation results of the effect of varying length to width ratio (Q) on the performance of a SPDDSAH

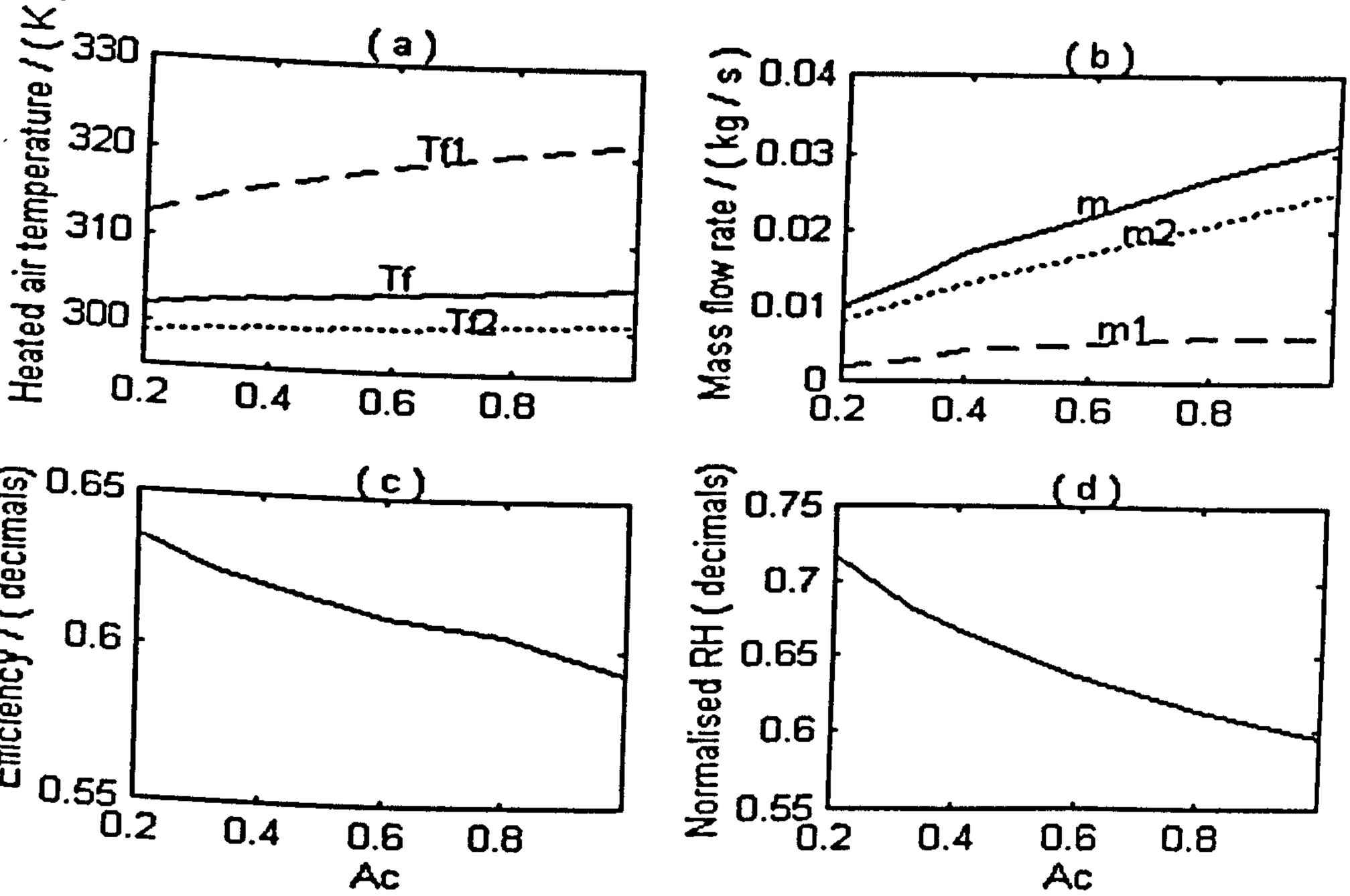

Figure 6.6: Simulation results of the effect of varying collector area (A_c) on the performance of a SPDDSAH

6.2 Simulation of the drying process

In simulating the performance of the drying process, the computer program LAYER, was used. The program was run using two of the three possible configurations of the laboratory dryer and under the prevailing conditions for runs 1 and 3- corresponding to Tests 4 and 6 of the laboratory experiments- as presented earlier in Table 6.2. No simulation was carried out for Test 5 for lack of the ambient air relative humidity. The other parameters required to specify the material properties, the site conditions, the program gimmicks, and the dryer configuration completely for the simulation of the drying process in addition to those presented in Table 6.2 were set at the following typical values for the two runs:

Bulk density, kg/m^3	552
Specific heat capacity of crop, J/kg K	840
Number of crop bed layers	1
Estimated time for termination of program, h	30
Number of incremental bed depths	1
Volume of the drying chamber, m^3	0.082
Height of the chimney, m	0.615
Drying chamber width to breadth ratio. ($X_2 = W/B$)	1.195
Atmospheric pressure, kN/m^2	101.325
Incremental time between output prints, h	1
Drying chamber height to width ratio, ($X_1 = h_1/W$)	0.982
Ratio of chimney to chamber cross sectional areas (B_{ch}/B)	0.224
Ratio of the chimney exhaust vent area to the chimney cross section, ($X/s \approx X/B_{ch}$)	0.4

The execution of the program LAYER also calls for user-supplied initial guess values of the mean air flow rate, mean temperature of the walls of the drying chamber and the mean temperature of the air exiting the crop bed. For the purpose of the two runs the values of the above were set for all the runs as, 0.1 kg/s, 28° C and 32° C.

6.2.1 Comparison of the simulation and the experimental results

The accuracy of the drying process was assessed in terms of the discrepancy between the following three parameters:

a) the experimental run time and the predicted time to reach the experimental final average moisture content,

b) the overall drying efficiency calculated using experimental and predicted values, and

c) the pick-up efficiency calculated using experimental and predicted values, as presented in Table 6.6.

The experimental crop bed moisture content profiles were also compared. Figure 6.6 shows the plots of the simulated (predicted) drying histories, which were done by using five terms of the diffusion equation (4.63), along with the drying histories observed during the continuous drying experiments in the laboratory. Figure 6.7 illustrates the simulated temperature variation of the product and of the air-stream temperatures. The figure shows that higher product temperatures were obtained in Test 6 compared to values obtained during Test 4. The drying air temperatures also increases with time during Test 6 whereas the opposite trend is observed in Test 4. Since the vapour pressure in the product increases as the temperature is increased, the product dries faster during Test 6 than in Test 4 (see fig. 6.7). Figure 6.6 shows that the simulated drying approached quite closely the experimental drying results.

As can be seen from Table 6.7 and fig. 6.8, the drying process mathematical model provides a good approximation of the physical process. For example in Test 4, it took 22 hours to dry 1458.3 grams of cassava from an initial moisture content of 201.7% (dry basis) to 49.7%, and the model predicts that this task can be accomplished within 20.4 hours of cumulative drying time with a percentage error of -7.3%. In the case of test 6, it took 22 hours to dry 1460 grams of cassava from an initial moisture content of 201.6% (dry basis) to 23.9% dry basis, and the model predicts a total drying time of 24.4 hours with a percentage error of +10.8%. The model predicts drying and pick-up efficiencies of 10.3% and 9.1% respectively for test 4, while values of 10.1% and 10.4% are predicted for test 6. The drying and pick-up efficiencies are within 6.3% and 11.4% of the experimentally determined values for test 4 and within 7.1% and 18.6% for test 6.

The simulated drying results presented here were obtained by using an incremental bed thickness equal to the entire crop bed thickness. Several other combinations of the incremental bed thickness were used in some trial simulation runs; however, they resulted in slightly more over-drying than the results presented here. It was also found that changes in the incremental bed thickness as well the air-heater incremental length produced significant effects on the temperature of the air entering the chamber and hence the drying time. For crop bed thickness of up to 66 mm investigated a single layer approach gave better results.

Table 6.6: Comparison between experimental and predicted values of the cumulative drying time, overall drying and pick-up efficiencies.

	TEST 4			TEST 6		
	Drying time	Drying Efficiency	Pick-up Efficiency	Drying time	Drying Efficiency	Pick-up Efficiency
Experimental	22 hrs.	11%	17.5%	22 hrs.	12.3%	11.2%
Predicted	20.4 hrs.	10.3%	15.5%	24.4	10.1%	10.4%
% Difference	-7.3	-6.3	-11.4	+10.8	-18.6	-7.1

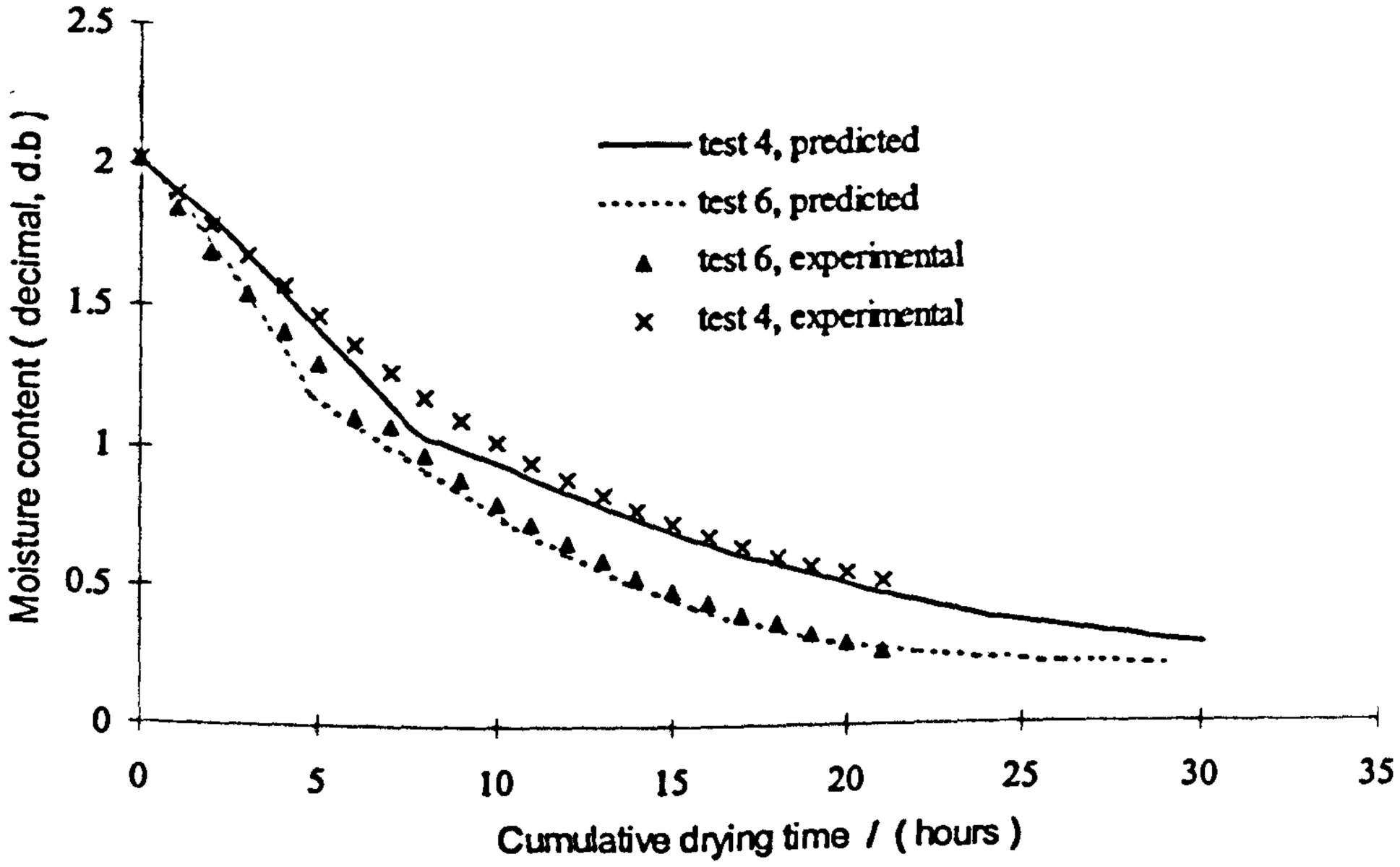

Figure 6.7: Comparison between experimental and predicted results of the variation in the product moisture content with drying time for Tests 4 and 6 of the laboratory drying experiment.

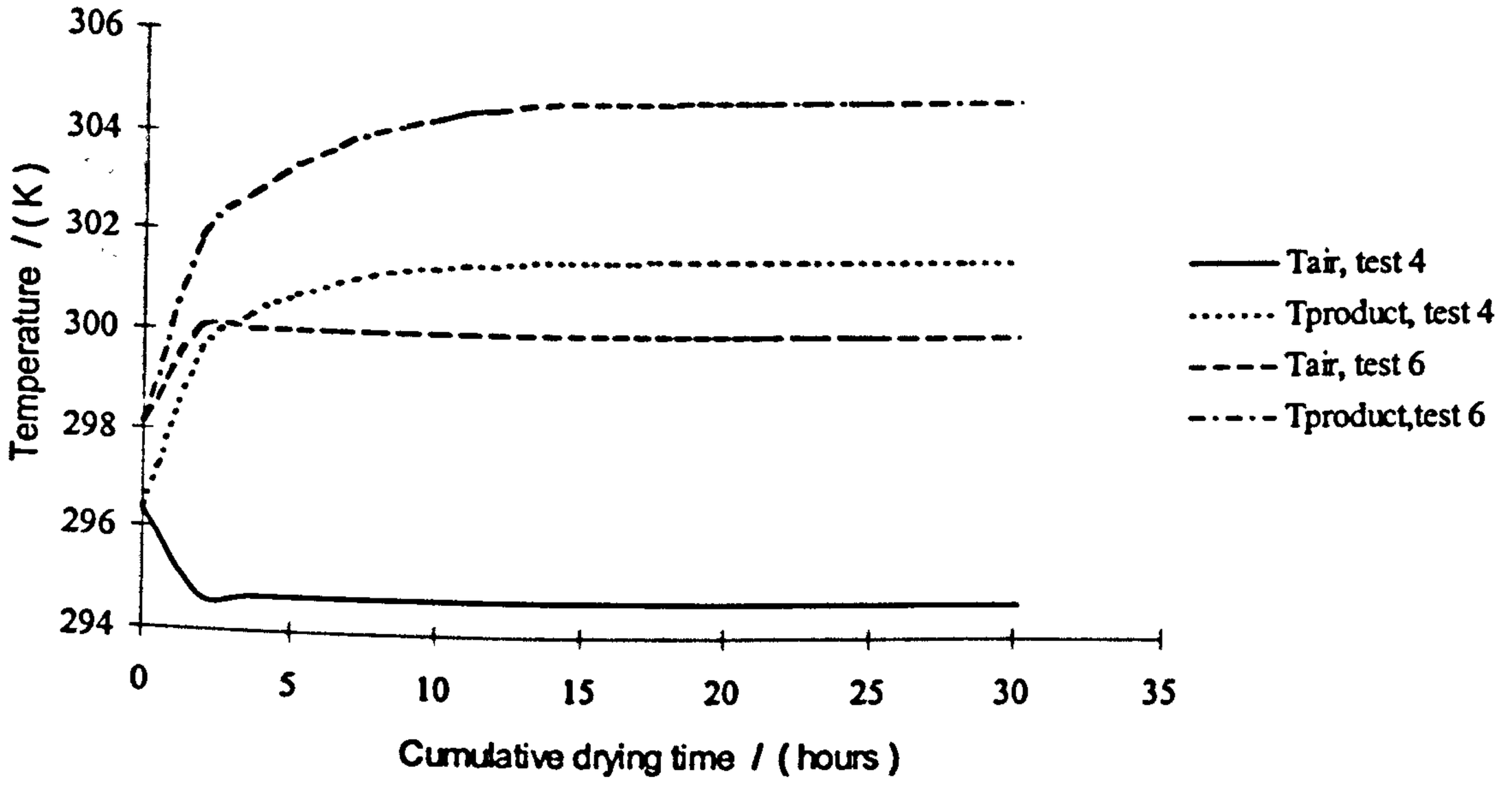

Figure 6.8: Comparison between predicted results of the product average temperature (Tproduct) and the average drying air temperature leaving the drying chamber (Tair) for Tests 4 and 6 of the laboratory experiment

6.2.2 Parametric studies of the drying system

The computer simulation model (LAYER) was used to perform parametric studies of the MNCSCD with a view to obtaining design options for optimising the performance of such dryers. The study was intended to explore and provide a range of conditions under which the MNCSCD can perform better than the baseline design conditions. The effects of varying the following parameters on the performance of the MNCSCD were considered:

a) the load capacity of the dryer,
b) the thermal capacity of the drying chamber,
c) the dimensions of the chimney and the exhaust air vent,
d) the volume of the dying chamber, and
e) the ratio of the primary to secondary collector areas for a given total energy collection area.

In (a) to (d) above, the effects of the various parameters were simulated under the assumption that there is no change in the ratio of the primary to the secondary collector areas. In (e), for purposes of comparison, the effect of varying the ratio of the primary to the secondary collector areas was examined. A summary of the effects of the above parameters on the air mass flux through the drying bed and the relative humidity of the air exiting the crop bed are provided in Table 6.8, whereas the hourly variations of the product moisture content, M_d; the temperature of the drying air exiting the crop bed, T_f; the average product temperature, T_p; the drying efficiency, η_d and the pick-up efficiency, η_p respectively resulting from the changes in the parameters considered are illustrated in figs. 6.9 to 6.17. In all, nineteen simulation runs, designated hereafter as R1 through R20, were executed. Table 6.7 summarises the cases that have been considered, and the values of the changed parameters in all the nineteen simulation runs are provided. The baseline values of all the parameters investigated are provided under R1. All the nineteen runs were executed using laboratory conditions that prevailed during Test 4. The parameters for the three different line weights used in figs. 6.9 through 6.17, for the simulation runs R1-R20 are defined in Table 6.9. For the efficiency curves in figs. 6.9-6.17, the red and the green line-styles are used for drying and pick-up efficiencies respectively.

Table 6.7: Values of the variable parameters for simulation runs R1 to R20.

		Value of the parameter changed in the simulation run								
Parameter	Unit	R1	R3	R4	R5	R6	R7	R8	R9	R10
W_T	kg	1.458	0.73	2.5	–	–	–	–	–	–
$m^w C^w$	J/K	9371	–	—	4686	18742	–	–	–	–
h_{ch}	m	0.615	–	–	–	–	0.308	1.23	–	–
A_{ch} / A_{dc}	-	0.224	–	–	–	–	–	–	0.112	0.448
A_{vent} / A_{vent}	-	0.40	–	–	–	–	–	–	–	–
V_{chm}	m^3	0.082	–	–	–	–	–	–	–	–
A_{dc} / A_c	-	0.53	–	–	–	–	–	–	–	–

		Value of the parameter changed in the simulation run								
Parameter	Unit	R11	R12	R13	R14	R15	R16	R17	R18	R19
W_T	kg	–	–	–	–	–	–	–	3.0	4.0
$m^w C^w$	J/K	–	–	–	–	–	–	–	–	–
h_{ch}	m	–	–	–	–	–	–	–	–	–
A_{ch} / A_{dc}	-	–	–	–	–	–	–	–	–	–
A_{vent} / A_{vent}	-	0.2	0.8	–	–	–	–	–	–	–
V_{chm}	m^3	–	–	0.163	0.041	–	–	–	–	–
A_{dc} / A_c	-	–	–	–	–	1.0	0.33	2.0	2.0	2.0

For R2 through R19 the value for each parameter changed in the particular simulation run is provided in table 6.7. The dashed line s (—) in the body of the table for a particular parameter for runs R3 to R17 shows that the value of that parameter is equal to the baseline value.

In fig. 6.9, the model is used to study the performance of the dryer at various load capacities, W_T. The results are shown in figs. 6.9(a)-6.9(d) for hourly variation of the M_d, T_f, T_p, η_d and η_p respectively. From fig. 6.9(a) it can be seen that as the load is increased, the drying rate decreases significantly. For example, when the load is increased from the baseline value of 1.458 kg to 2.50 kg, the final product moisture on dry basis attained after 30.1 hours is increased from 28.8% to 76.5% respectively. Figure 6.9(a) shows that the drying air temperature exiting the crop bed decreases with an increase in the loading capacity under the same ambient conditions. The effect of the crop loading capacity on the overall efficiency is also significant; it decreases with an increase in the crop capacity (fig. 6.9(d)). Figures 6.9(b) and 6.9(c) illustrate that the temperature of the

air exiting the crop bed and of the product temperature decrease with increasing crop loading density. As a result of the reduction in the product and the air temperatures, the vapour pressure of water in the product decreases and in addition the partial pressure of water vapour in the surrounding air increases; thus resulting in a reduction in the driving force for evaporation of moisture from the crop. Consequently, the drying efficiency decreases. The increase in the pick-up efficiency with increasing crop loading density suggests that the potential of the air is better utilised with an increase in the loading density. However, the pick up efficiency increases with increasing crop loading density up to 2.52 kg beyond which the relative humidity of air exiting the drying bed exceeds 100%. Therefore, for the present design under the same ambient conditions, the simulation results show that loads above 2.52 kg cannot be dried in the drying chamber in a single batch. The predicted results show that for loads above 2.52 kg, modifications in either the drying chamber and/or chimney configurations are/is required, if condensation is to be avoided. It is gratifying to note that by altering the ratio of the primary collector surface area to the crop bed surface area from 0.53 in R1 to 2.0 (in R18 and R19), for the same total energy collection area, condensation is avoided. The simulation runs R18 and R19 suggest that crop masses of 3.0 kg and 4.0 kg can be dried from a moisture content of 201.6% dry basis to final moisture contents of 30.2% and 56% respectively in 30.1 hours (see fig. 6.16(a)). Table 6.8 shows that the relative humidity of air exiting the crop bed for runs R18 and R19 are 53.8% and 77% respectively. But with the same ratio of drying bed cross-sectional area to the primary collector area (i.e. A_{dc}/A_c) of 2.0, a crop load of 5 kg resulted in RH $\approx$ 100%.

The effects of changing the thermal heat capacity, $m''C''$, of the drying chamber on the performance of the dryer were studied in runs R1, R5 and R6. Figures 6.10(a) to 6.10(d) show that increasing the thermal heat capacity of the drying chamber has no effect on the drying results. As can be seen from Table 6.8, an increase in the thermal heat capacity of the drying chamber does not have any change in the values of the air mass flux and the relative humidity of the air exiting the drying bed. It is seen from fig. 6.10(c) as the drying proceeds for all values of $m''C''$ product temperature increases with time. Since, the model assumes a variation in the temperature of the thermal mass of the drying chamber at the same rate as the as the product, it can be inferred that as $m''C''$ is increased more

energy would be stored in the thermal mass of the drying chamber with time during the day rather being utilised to further increase the product temperature. The benefit to be gained in increasing the thermal mass of the drying chamber of a solar drying system is that the energy stored up in the thermal mass during the day is released at night thus extending the drying to the non-sunny hours of the day.

Table 6.8: Values of the air mass flux ($\dot{G}_a$) and relative humidity of the drying air exiting the crop bed (RH_{exit}) for the various simulation runs

Values of $\dot{G}_a$ and RH_{exit} for each simulation run

Parameter	R1	R3	R4	R5	R6	R7	R8	R9	R10
$\dot{G}_a$ (kg/s-m^2)	0.045	0.046	0.044	0.045	0.045	0.038	0.055	0.045	0.045
RH_{exit} (%)	44.3	31.6	88.9	44.3	44.3	35.6	63	44.3	44.3

Values of $\dot{G}_a$ and RH_{exit} for each simulation run

Parameter	R11	R12	R13	R14	R15	R16	R17	R18	R19
$\dot{G}_a$ (kg/s-m^2)	0.024	0.072	0.053	0.040	0.038	0.048	0.030	0.030	0.030
RH_{exit} (%)	59.1	38.0	41.7	49	35.9	71.1	34.8	53.8	77

The value of the relative humidity of the air at inlet to the drying chamber for runs R1 through R14 is 27.4%,; for R15, R16 and R17 the values are 28.2%, 27.0% and 29.2% respectively.

The model was used to test the performance of the MNCSCD at various chimney heights, h_{ch}. The effect of changing h_{ch} was studied in computer runs R7 and R8. The results are compared with the basic run R1 in figures 6.11(a) to 6.11(d). From fig. 6.11 it can be concluded that, for a given load, increasing the chimney height above 0.30m leads to the following:

a) a decrease in the temperature of the drying air exiting the crop bed,
b) no significant change in the product temperature above its initial value for h_{ch} greater than the design value of 0.62 m,
c) a decrease in the time required to dry the crop to a desired final moisture content, and
d) an increase in the overall drying efficiency and a decrease in the pick-up efficiency.

The decrease in the pick-up suggests that the load capacity of the dryer can be increased above the baseline value of 1.458 kg. Figure 6.11(a) shows that increasing the chimney height from 0.615 m to 1.23 m does not affect the drying time significantly. The results

show that, it would take 30.1 hours to dry 1.458 kg of cassava from an initial moisture of 201.6% dry basis to a final moisture content of 24.6% when the chimney is 1.23m compared to the values of 34.1% and 28.8% achieved with a chimney heights of 0.31 m and 0.615 m respectively. As expected, an increase in the chimney height results in an increase in the air mass flux because of the increase in the buoyancy. However, because of the resulting increase in the relative humidity of the drying air (see Table 6.8), the drying efficiency is not significantly increased. It can be inferred from the above results that, though increasing the chimney height increases the air mass flux through the system, but drying efficiency is not significantly improved.

The effect of changing the ratio of the chimney cross sectional area to the drying bed area, $A_{ch} / A_{dc} = B_{ch} / B_{dc}$, was studied by considering only changes in the breadth of the chimney in order to maintain a constant drying bed cross section and the same air-heater configuration. The effect of varying B_{ch} / B_{dc} on the performance of the dryer was studied in simulation runs R1, R9 and R10. From Table 6.8 and Figs. 6.12(a) to 6.12(d) it is observed that altering the breadth of the chimney for a given drying bed area does not alter the performance of the dryer in all aspects.

The changes in the ratio of the exit air-vent (for escape of exhaust moist air) cross sectional area to the inlet air vent , *i.e.* $A_{exvent} / A_{invent} \approx x / s$, was studied by changing the height of the exit air-vent, x , for a fixed overall depth, s, of the air-heater. The effect of varying x for a fixed value of s was simulated in runs R1, R11 and R12. From Table 6.8, it is clear that increasing the height of the exit air event, for a fixed air-heater duct depth, results in an increase in the air mass flux through the crop bed and a reduction in the relative humidity of the air exiting the crop bed. These conditions have been established from the experimental data (see chapter 5) as favourable conditions for drying purposes.

From figs. 6.13(a) to 6.13(d) it can be summarised that increasing x generally leads to the following:

a) a slight increase in the product temperature, which tends to a constant value with time,

b) an increase in the temperature of drying air exiting the crop bed, but for $x > 0.03$ m an increase in x results in a rise in temperature of about 1.5^{o} C above the ambient value,

c) a significant reduction in the drying time, and

d) a significant increase in the overall drying efficiency and a corresponding reduction in the pick-up efficiency.

The model was used to test the effect of varying the volume of the drying chamber , V_{chm}, on the performance on the dryer. Simulation runs R1, R13 and R14 were used to explore the dependence of the dryer performance on the changes in the volume of the drying chamber. An increase in the volume of the drying chamber can be effected by either increasing the drying bed cross-sectional area and maintaining the height of the chamber or increasing the height of the chamber and maintaining the drying bed area. However, in order to preserve the drying bed surface area, the later option was adopted in this investigation.

From Table 6.8, it is clear that increasing the volume of the chamber for a given surface area of the drying bed results in an increase in the air mass flux and a reduction in the relative humidity of the air exiting the drying bed. Since the drying bed surface area is kept constant, an increase in V_{chm}, leads to an increase in the height of the air column thus enhancing buoyant flow of the drying air. Thus, the increase in the air mass flux resulting from the increase in V_{chm} is as expected. Figure 6.14(a) shows that the drying rate is increased for a given load and drying bed surface area, by increasing the volume of the drying chamber. No discernible differences were recorded in the values of T_f and T_p as the volume of the drying chamber was varied. The drying efficiency increases slightly as V_{chm} is increased, whereas the pick-up efficiency decreases (see fig. 6.14(d)).

The mathematical model was used to test the performance of the MNCSCD at various ratios of the secondary collector area to the primary collector area (A_{dc} / A_c) for a given total energy collection area. The effect of A_{dc} / A_c on the performance of the dryer was studied in simulation runs R1, R15, R16 and R17. From table 6.8 it can be seen that increasing the value of A_{dc} / A_c leads to a reduction in the air mass flux and a reduction in the air relative humidity exiting the crop bed. For a given crop load, since the loading density is reduced with an increase in the value of A_{dc} / A_c, it is expected that pressure drop across the crop bed should reduce and therefore result in an increase in the air mass flux. Increasing the ratio of A_{dc} to A_c, for a given total energy collection results in a drop

in the heated air temperature entering the drying chamber. The resultant is that there is a reduction in the air mass flux as the ratio of A_{dc} to A_c, is increased. The reduction in the relative humidity of air exiting the crop bed is attributable to the fact that since the layer density is reduced as A_{dc} / A_c is increased a greater percentage of the product is subject to intense radiation and hence the product temperature increases appreciably.

From figs. 6.15(a) through 6.15(d), it can be seen that as A_{dc} / A_c is increased, there is a significant increase in the product temperature and the temperature of the air exiting the drying bed. The resulting effect is that the drying rate increases and hence the overall drying efficiency increases. An increase in A_{dc} / A_c also results in an increase in the pick-up efficiency above the reference condition, signifying that an increase in the A_{dc} / A_c value for a given load results in a better utilisation of the energy of the heated air. Since the temperature of the heated air entering the drying chamber decreases with an increase in the value of A_{dc} / A_c, with the higher drying rates the pick-up efficiency increases as expected. The results further show that for $1 < A_{dc} / A_c < 2$, there is no observable difference in the performance of the dryer. This observation suggests that for optimum performance of the dryer A_{dc} / A_c can be set within the above limit. Following from the above, for higher inlet air temperatures to the drying chamber, it is recommended that in dimensioning a MNCSCD, the surface area of the primary collector (air-heater) should be set equal to the horizontal area of the drying chamber. This recommendation supports an earlier observation by Bassey (1986).

The simulation results in figs. 6.9-6.16 can be utilised to achieve efficient designs of the MNCSCD at no added cost. Consider, for example, a dryer in which the design parameters are set as listed below and working under the same environmental conditions as the baseline dryer:

$W_T = 1.458$ kg; $m''C'' = 9371$ J/K; $A_c / A_{dc} = 1.0$; $A_{chm} / A_{dc} = 0.224$; $h_{ch} = 0.615$ m; $V_{chm} = 0.163$ m^3; $A_{svent} / A_{ivent} = 0.448$; $P = 3.412$; $Q = 1.586$; $s = 0.075$ mm. A comparison between the simulated performance of this proposed dryer design and the baseline design is provided by means of fig. 6.17. It is clear from the results that in 22 hours, with the new design 1.458 kg of cassava can be dried from an initial moisture content of 201.6% dry basis to 21.9%, compared to final moisture content of 49.7%

achieved with the baseline design. A comparison of the air mass flux and the relative humidity of the drying air exiting the crop bed for the two possible dryer designs reveal that, whereas the baseline design results in an air mass flux and exit air relative humidity values of 0.045 kg/s and 44.3%, in the proposed design the mass flux will increase to 0.055 kg/s with a further reduction in the relative humidity to a value of 32.3%.

Figure 6.17 also shows that there is a significant increase in the product and the drying air temperatures with time, in contrast to the baseline design in which the drying air temperature decreases with time. It is apparent from the above results that the model can be used to size the dryer to achieve optimum performance.

Table 6.9: Distinction between the different line weights used in figures 6.9 to 6.17

	·····	——	------
Figure 6.9	W_T = 0.73 kg	W_T = 1.458 kg	W_T = 2.5 kg
Figure 6.10	$m''C''$ =4686 J/kg	$m''C''$ = 9373 J/kg	$m''C''$ = 18742 J/kg
Figure 6.11	h_{ch} = 0.31 m	h_{ch} = 0.615 m	h_{ch} = 1.23 m
Figure 6.12	A_{ch} / A_{dc} = 0.112	A_{ch} / A_{dc} = 0.224	A_{ch} / A_{dc} = 0.448
Figure 6.13	A_{xvent} / A_{ivent} = 0.20	A_{xvent} / A_{ivent} = 0.40	A_{xvent} / A_{ivent} = 0.80
Figure 6.14	V_{chm} = 0.041 m^3	V_{chm} = 0.082 m^3	V_{chm} = 0.163 m^3
Figure 6.15[a]	A_{dc} / A_c = 1.0	A_{dc} / A_c = 0.53	A_{dc} / A_c = 0.33
Figure 6.16	A_{dc} / A_c =2, W_T =4.0 kg	A_{dc} / A_c =0.53, W_T =1.46 kg	A_{dc} / A_c =2, W_T =3.0 kg
Figure 6.17		Baseline design	A proposed design

[a] In fig. 6.15, the line not defined in table 6.9 (·····) is for A_{dc} / A_c = 2.0.

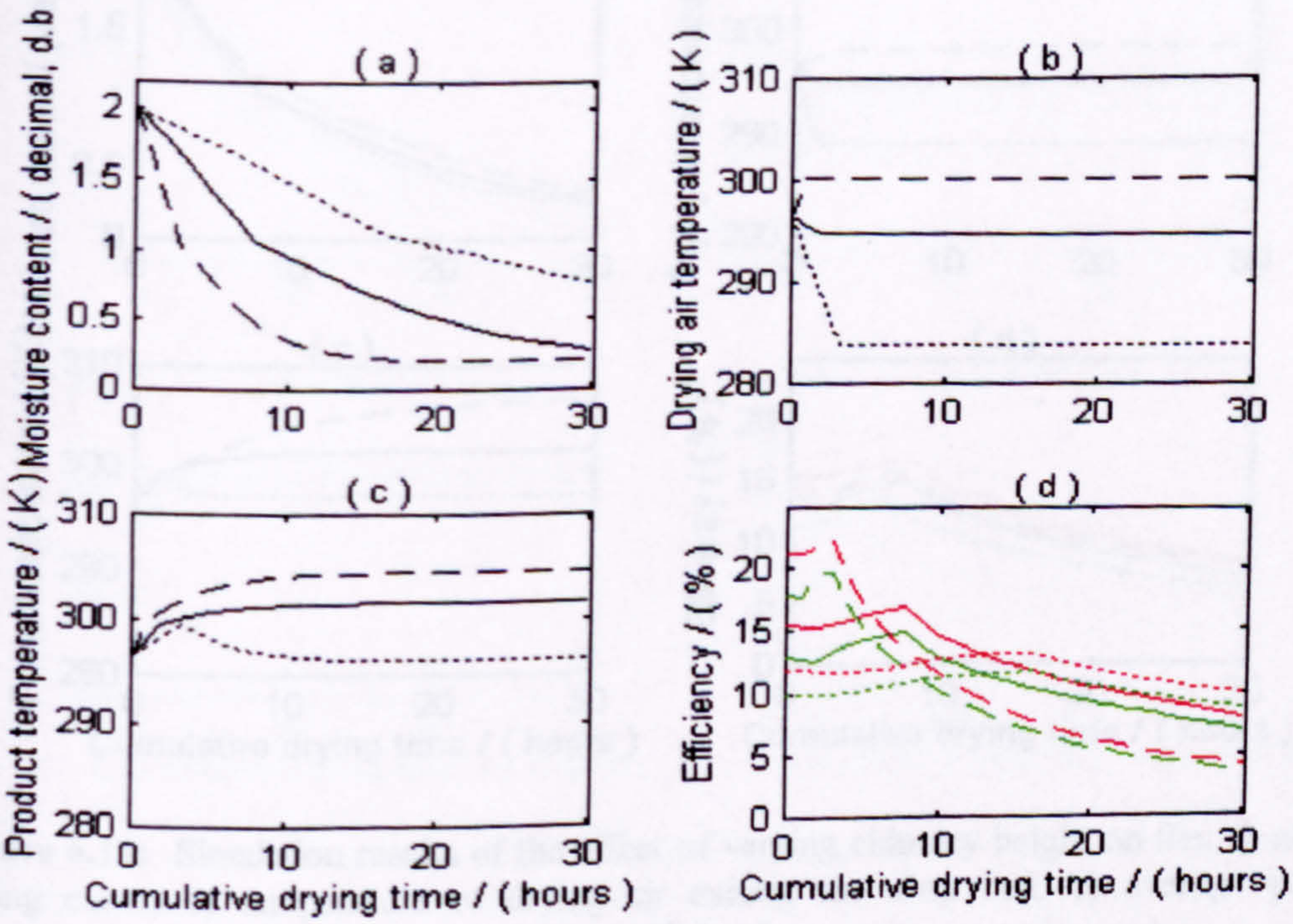

Figure 6.9: Simulation results of the effect of varying loading capacity on the: a) average drying curve, b) temperature of drying air exiting the crop bed, c) average product temperature, and d) the drying and pick-up efficiencies

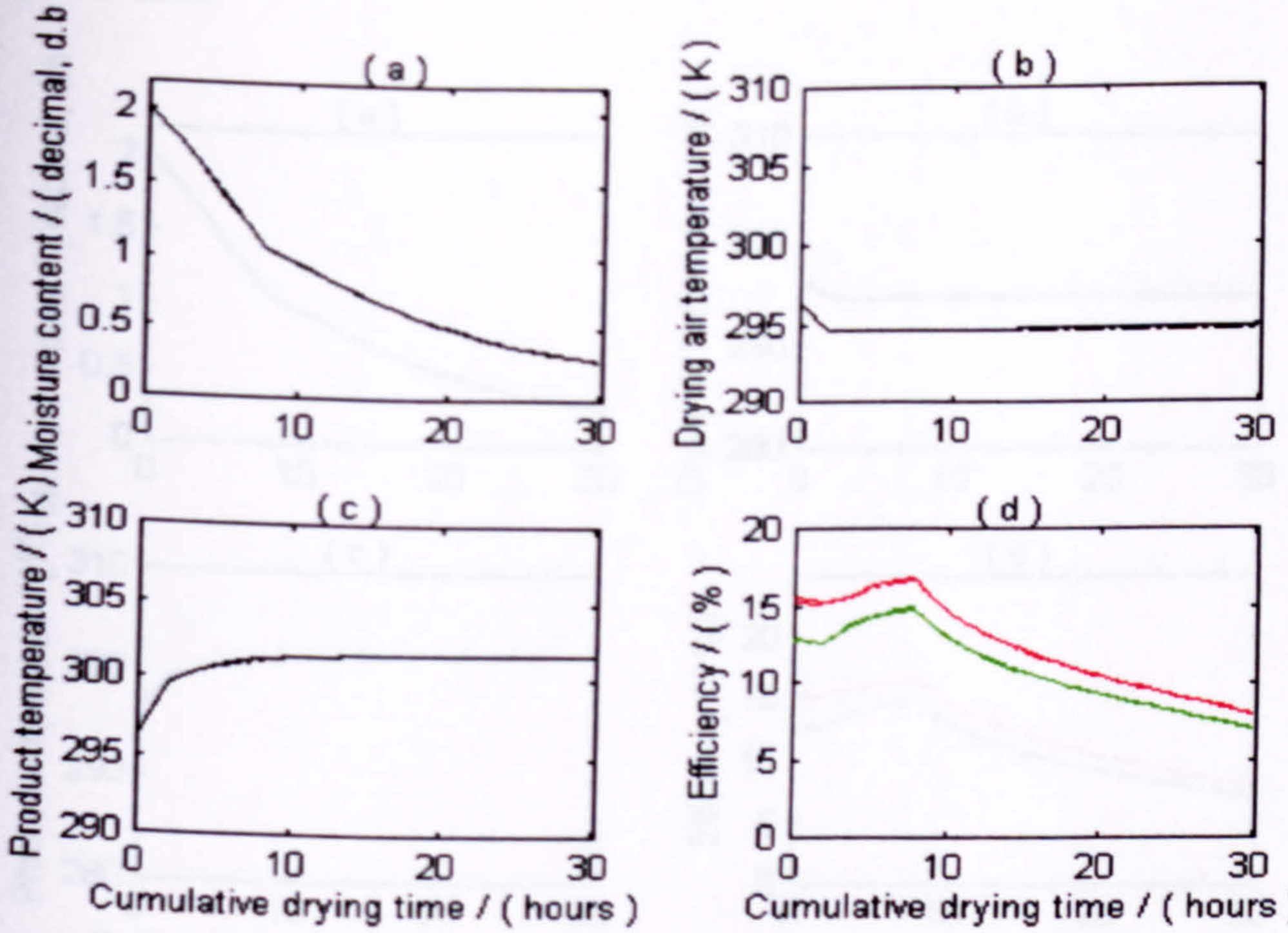

Figure 6.10: Simulation results of the effect of varying thermal capacity of the drying chamber on the: a) average drying curve, b) temperature of drying air exiting the crop bed, c) average product temperature, and d) the drying and pick-up efficiencies.

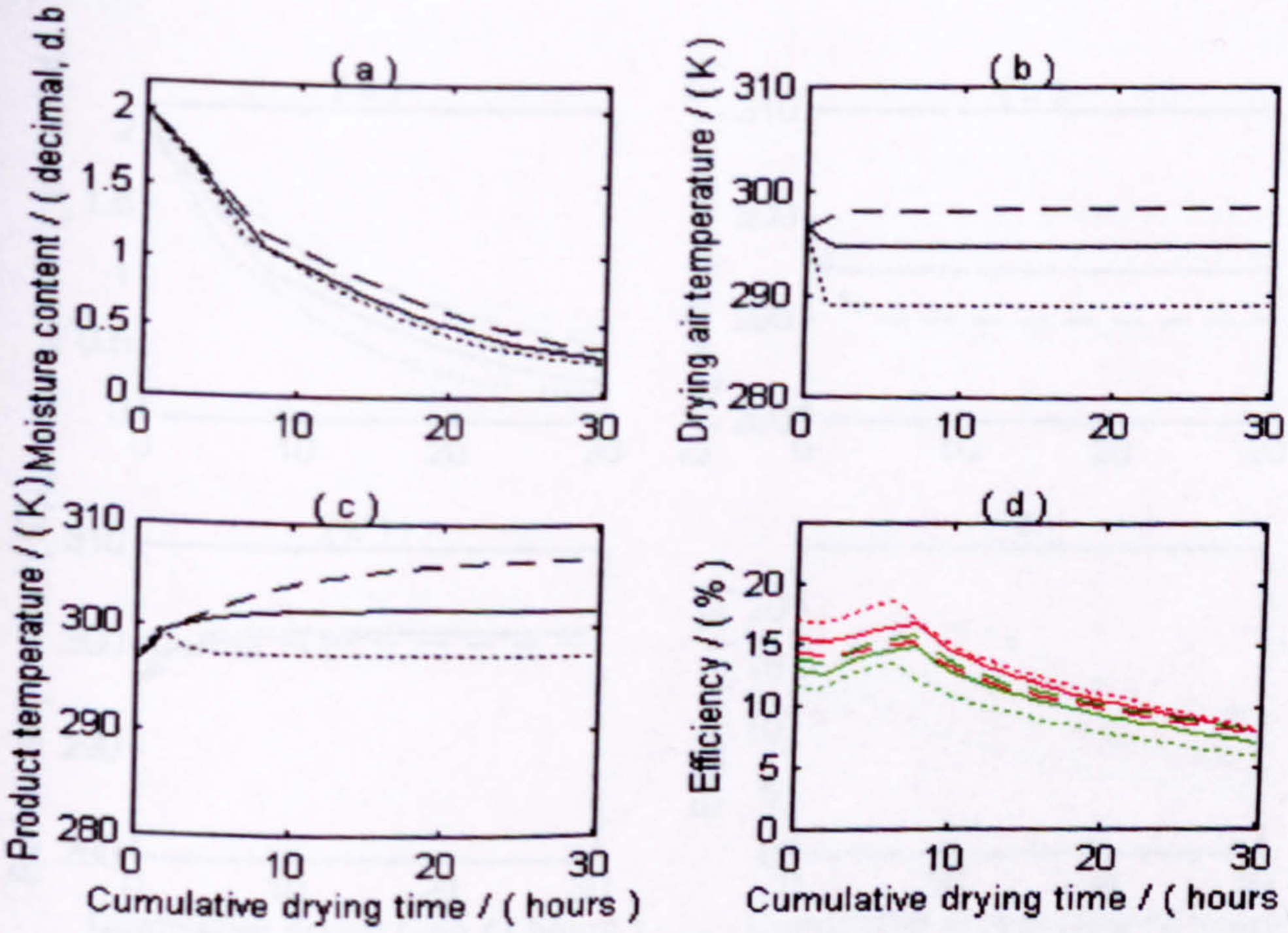

Figure 6.11: Simulation results of the effect of varying chimney height on the: a) average drying curve, b) temperature of drying air exiting the crop bed, c) average product temperature, and d) the drying and pick-up efficiencies

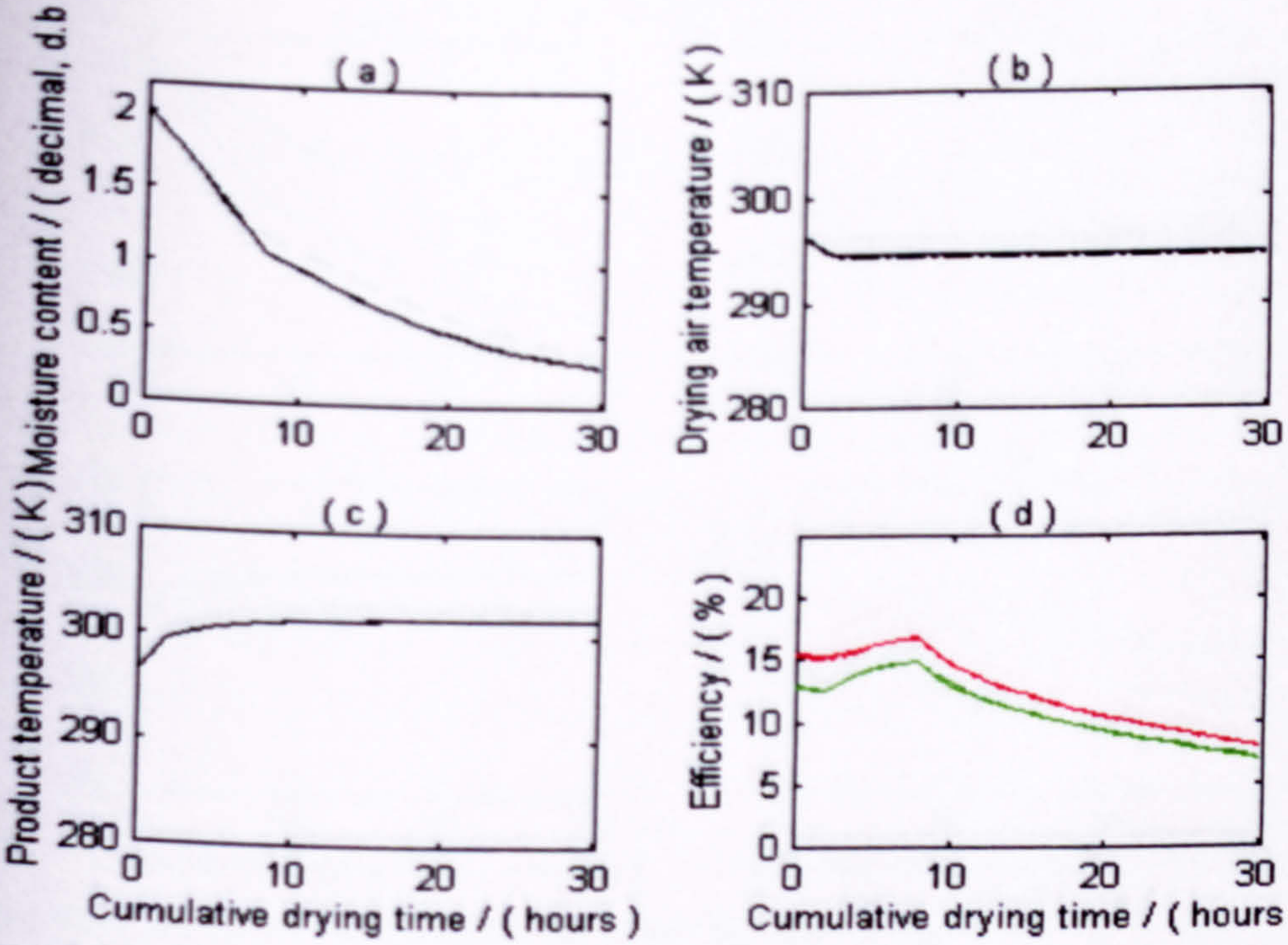

Figure 6.12: Simulation results of the effect of varying chimney cross-sectional area for a fixed chimney width on the: a) average drying curve, b) temperature of drying air exiting the crop bed, c) average product temperature, and d) the drying and pick-up efficiencies

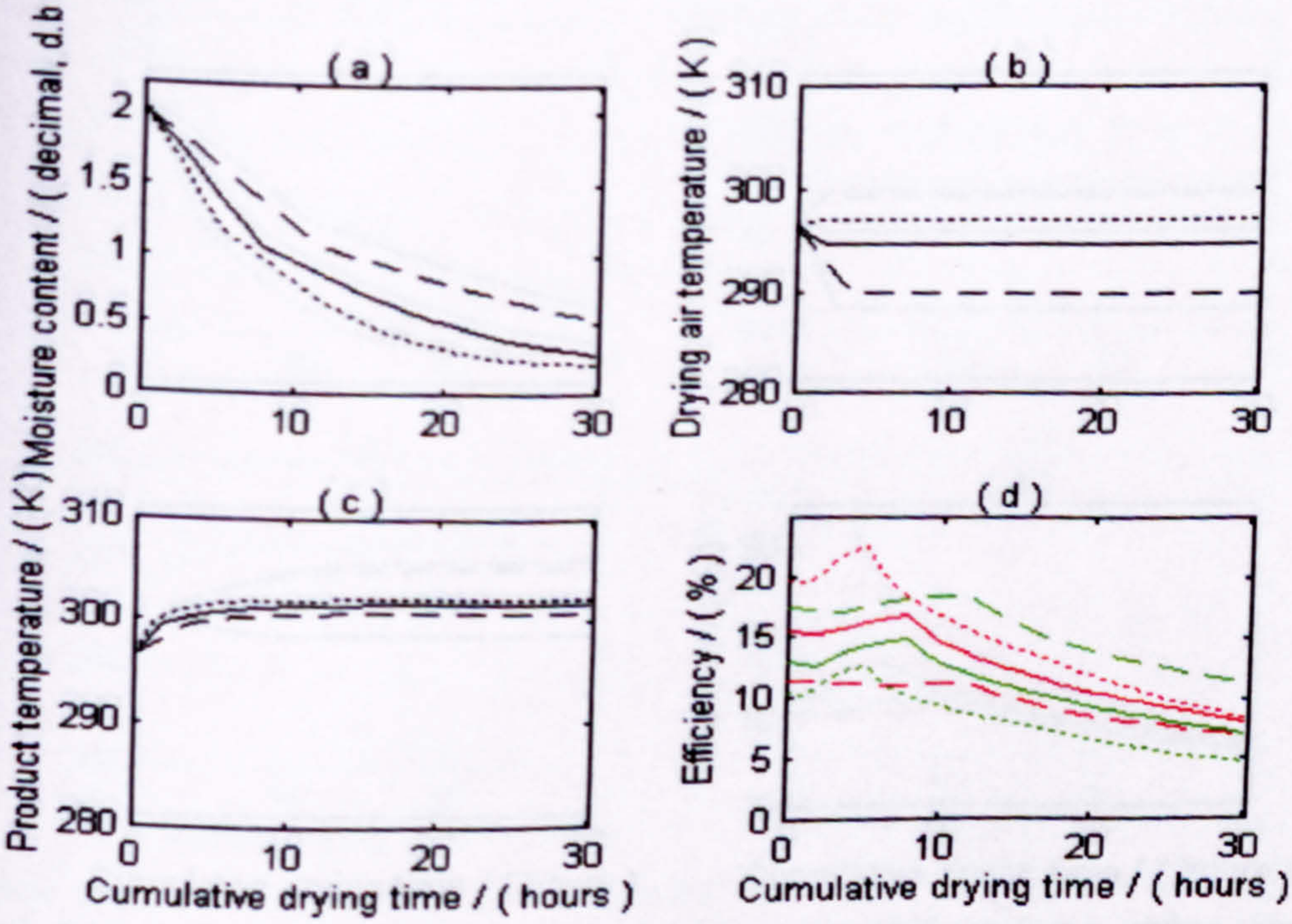

Figure 6.13: Simulation results of the effect of varying chimney exit vent height a fixed chimney width on the: a) average drying curve, b) temperature of drying air exiting the crop bed, c) average product temperature, and d) the drying and pick-up efficiencies

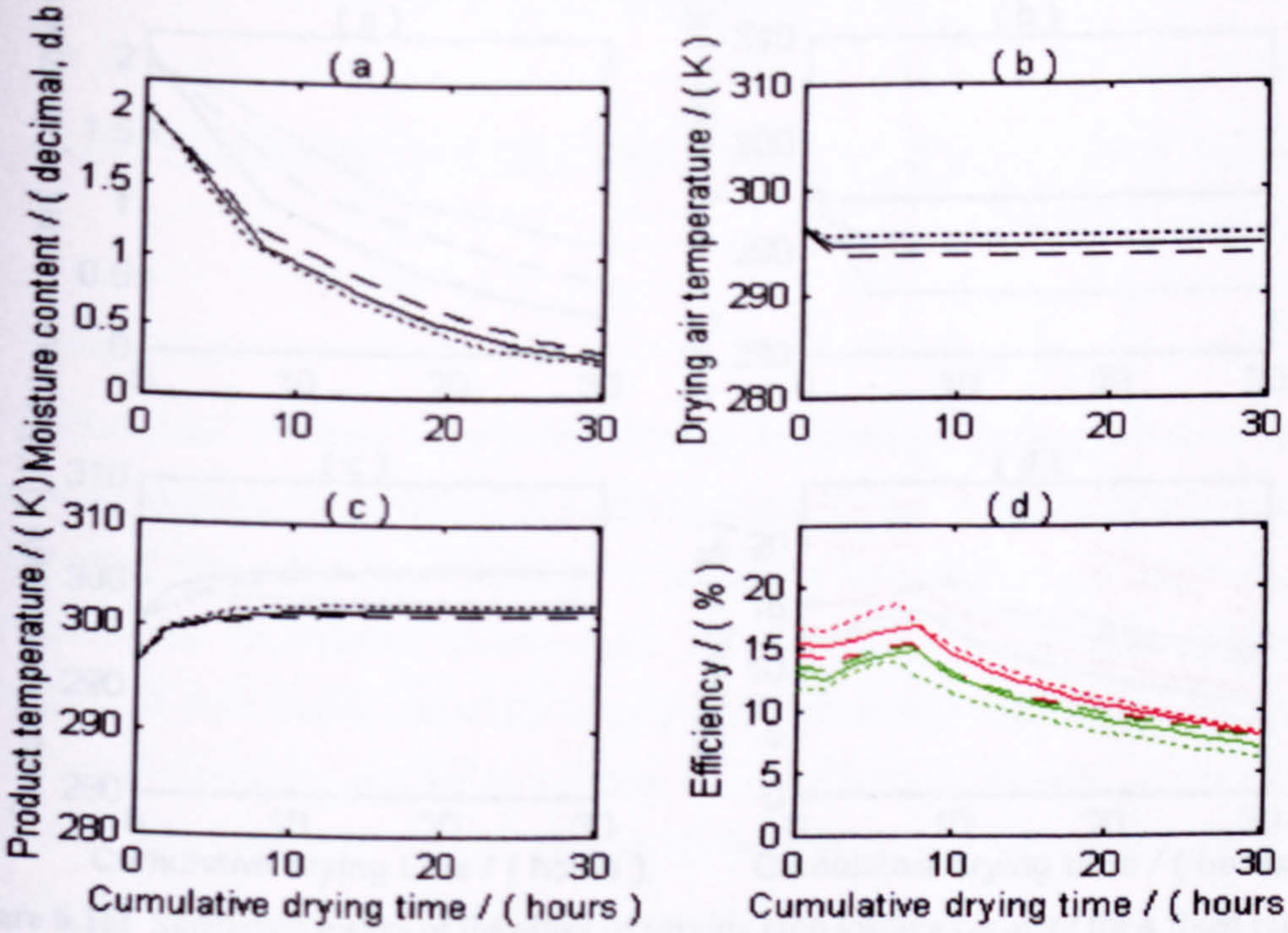

Figure 6.14: Simulation results of the effect of varying drying chamber volume for a fixed drying bed cross-sectional area on the: a) average drying curve, b) temperature of drying air exiting the crop bed, c) average product temperature, and d) the drying and pick-up efficiencies

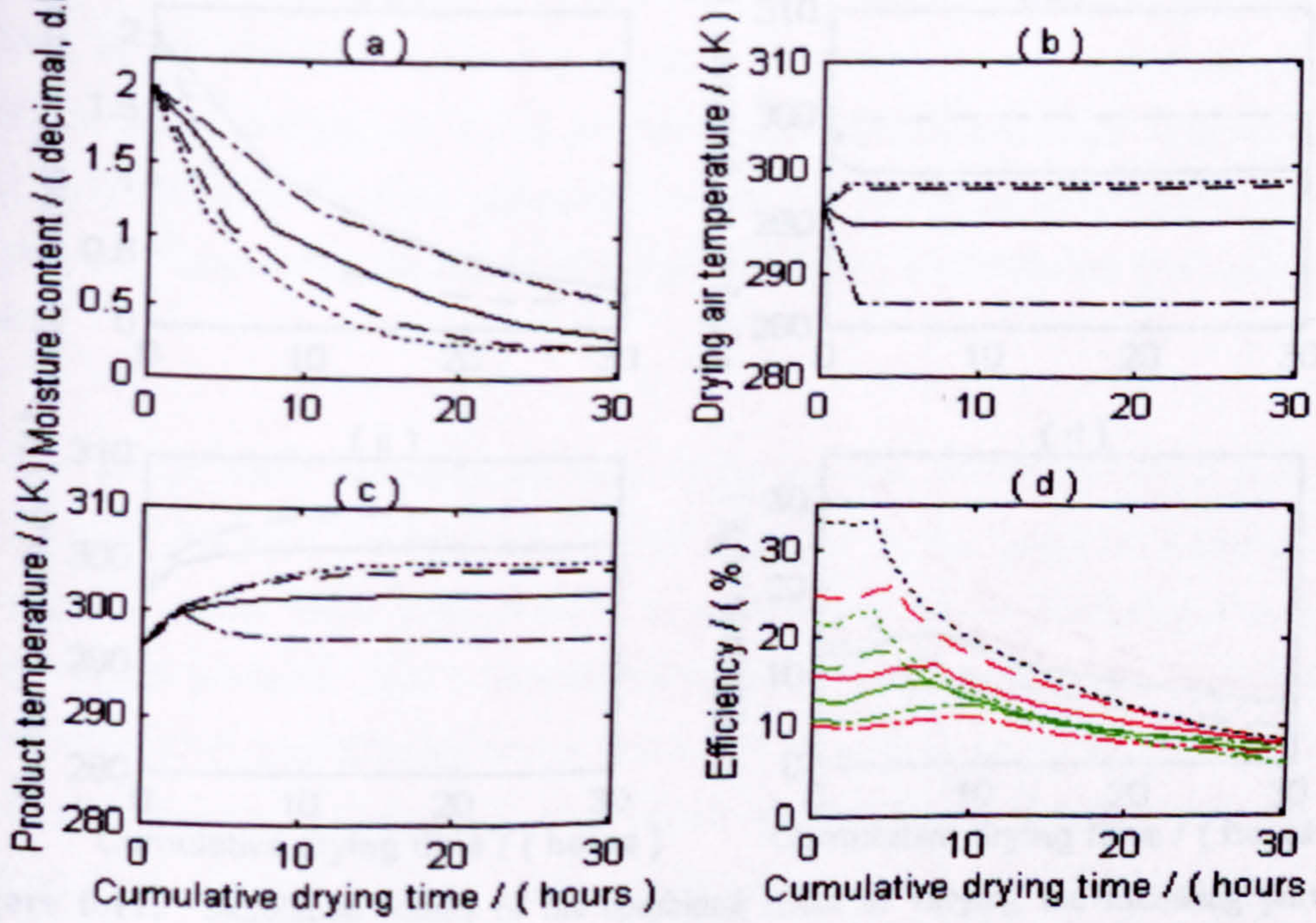

Figure 6.15: Simulation results of the effect of varying ratios of the air-heater surface area to the drying bed cross-sectional area for a fixed total energy collection area on the: a) average drying curve, b) temperature of drying air exiting the crop bed, c) average product temperature, and d) the drying and pick-up efficiencies

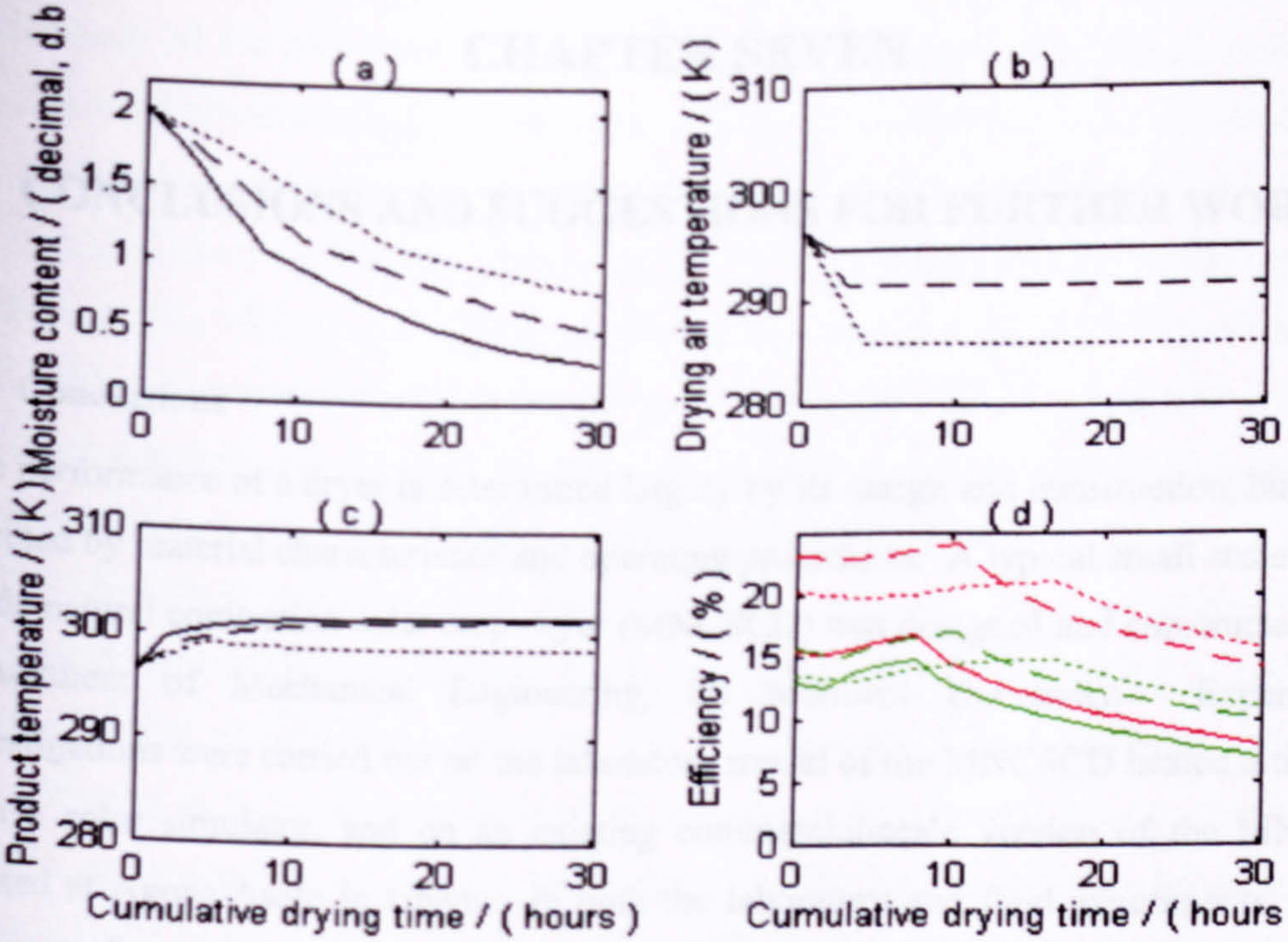

Figure 6.16: Simulation results of the effect of varying crop loading capacity for a fixed ratio of the air-heater surface area to the drying bed cross-sectional area on the: a) average drying curve, b) temperature of drying air exiting the crop bed, c) average product temperature, and d) the drying and pick-up efficiencies

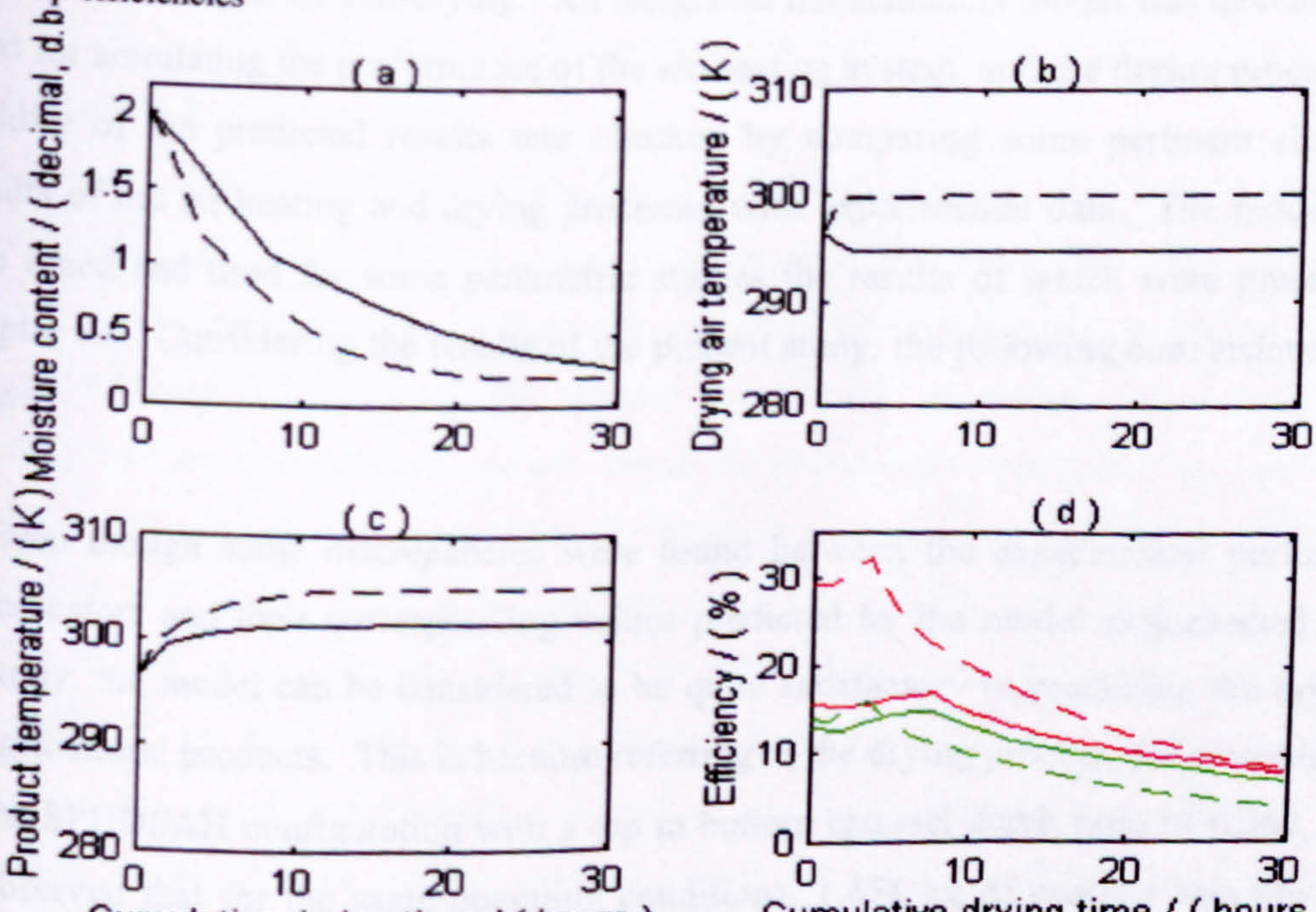

Figure 6.17: Simulation results of the combined effect of varying the following parameters, namely: height of the exit air vent; the volume of the drying chamber; air-heater top to bottom channel depth ratio; and ratio of the drying bed cross-sectional area to the air-heater surface area; for a fixed total collector area on the: a) average drying curve, b) temperature of drying air exiting the crop bed, c) average product temperature, and d) the drying and pick-up efficiencies

CHAPTER SEVEN

CONCLUSIONS AND SUGGESTIONS FOR FURTHER WORK.

7.0 Conclusions

The performance of a dryer is determined largely by its design and construction, but is also affected by material characteristics and operating procedures. A typical small-scale mixed-mode natural convection solar crop dryer (MNCSCD) was designed and constructed at the Department of Mechanical Engineering, De Montfort University. Experimental investigations were carried out on the laboratory model of the MNCSCD heated artificially with a solar simulator, and on an existing commercial-scale version of the MNCSCD located at Agona-Asafo in Ghana. In both the laboratory and field experiments, control drying tests were executed by drying cassava in open-air under the same ambient conditions as the dryers and their drying performance were compared with the data obtained from open air sun-drying. An integrated mathematical model was developed and used for simulating the performance of the air-heating system, and the drying process. The validity of the predicted results was checked by comparing some pertinent simulation results of the air-heating and drying processes with experimental data. The models were fine tuned and used for some parametric studies the results of which were presented in chapter six. Considering the results of the present study, the following conclusions can be drawn:

1) Even though some discrepancies were found between the experimental performance indicators and their corresponding values predicted by the model as presented in this study, the model can be considered to be quite satisfactory in predicting the drying of agricultural products. This is because referring to the drying process, for example using the SPDDSAH configuration with a top to bottom channel depth ratio of 0.364, it was observed that for the same operating conditions, 1.458 kg of cassava was physically dried from an initial moisture content of 201.6% to 49.7 % in 22 hours of continuous drying time. The model predicted a continuous drying time of 20.4 hours to reach the same final moisture content. In addition, each of the parameters selected to asses the

accuracy of the performance of the SPDDSAH was predicted within ± 20 % of the experimentally determined values, with exception of the incident radiation for which the experimental value was over-predicted by + 40.5 % (see Tables 6.4 and 6.5). The possible causes of the discrepancy in the incident solar radiation value have been discussed in chapter six. These discrepancies notwithstanding, the accuracy of the predicted drying results is such that the use of the models for other agricultural products seems justified; hence it will be useful as a design aid in future for development of typical designs of the MNCSCD to satisfy specific applications.

2) The simulation results coupled with the experimental data suggest that significant improvement in the SPDDSAH performance may be obtained through a careful choice of a number of collector parameters. For a given overall depth of a SPDDSAH, re-positioning of the absorber plate to obtain a design of larger top to bottom channel depth ratio, in particular $1.1 < P < 3.5$, will result in an increase in the temperature and mass flow rate, and a significant reduction in the relative humidity of the heated air entering the drying chamber. Higher length to width ratio of the air-heater is also desirable but since they result in lowering of the heated air mass flux a compromise value of $1.0 < Q < 2.0$ can be used in conjunction with higher values of P to achieve optimal performance of the air-heater.
3) The mass flow rate is the dominant factor that determines the effectiveness of a natural convection air-heater, hence for simulation purposes a careful estimation of the mass flow rate is essential. The air flow rate model as developed in this study expresses the inter-relationships between the various parameters governing the operation and performance of the proposed system, hence the model can be recognised as a very useful tool in the design and evaluation of future designs of the MNCSCD. The model predicted the air mass flux with a percentage error of -12.2 % to +5.7 per cent.
4) The results of the physical drying experiment show that, under the same ambient conditions, the traditional sun-drying method is improved significantly by carrying out the drying in an enclosed structure (see fig. 6.17). Sensitivity analysis carried out on the system showed that by making some structural changes in existing solar dryer designs they can be made even more efficient.

5) In the drying of cassava, simulation results showed that the loading density should be limited 14.6 kg/m^2 of drying surface area to avoid condensation, a situation that will lead to possible mould growth and thereby result in poor quality dried product.

6) For a MNCSCD under the same ambient conditions, the simulation results showed that when the ratio of the secondary to the primary collector surface area, that is A_{dc} / A_c, is increased the overall drying efficiency increases. However, for $A_{dc} / A_c > 1.0$ no significant difference in the performance of the dryer was observed. Thus, following from this study, it is recommended that the primary and the secondary collector areas should be made equal to achieve a better performance of the MNCSCD. This recommendation confirms the recommendation by Bassey *et al* (1986) but it is at variance with the recommended value of 0.33 by Exell (1982), for optimum performance of a MNCSCD.

7) Simulation results indicate that, the performance of the dryer can be improved by effecting the following changes to the drying chamber and the chimney:

   a) increasing the volume of the drying chamber,

   b) increasing the height of the chimney air vent such that $A_{xvent} / A_{ivent} \approx 0.8$

   c) and decreasing the chimney height.

8) Experimental results showed that the energy stored up in the thermal mass of the drying system during the day is released at night for drying. From three drying experiments conducted with the same dryer in the laboratory using three different configurations of a SPDDSAH of the same surface area, it was established that in a particular instance, the nocturnal drying accounted for up to 30 % of the total moisture removed from the product to bring it to a safe moisture content level. Simulation results also showed that increasing the thermal mass of the drying chamber has no significant effect on the drying process during the day. Since an increase in the thermal mass does not have an adverse effect on the dryer performance during the day but rather enhances drying at night, by marrying up the above complementing observations, it is recommended that the thermal mass of the drying chamber of a MNCSCD should be increased by incorporating possibly a rock bed storage system inside the chamber to store up energy during the day for extended drying operation during the non-sunny hours.

9) The experimental investigation also verified the effect of different loading arrangements on the drying rate of cassava. The same quantity of cassava was dried on one bed, two

beds or three beds and the rates of drying were monitored. The results showed that the cassava dried using two layers dried faster than the single layer or three bed layer arrangements. Hence, from the point of view of increased load per batch and faster drying rates, the two-layer drying is recommended in preference to either a single or three layer drying.

10)During the natural convection solar drying of cassava chips from a moisture content of 201% dry basis) to lower moisture contents of around 20% (wet basis), no constant-rate period was observed. The falling-rate period characterised the entire drying process from the start. Four stages of the falling-rate period were identified (see 4.2.2).

7.1 Suggestions for further work

A limited number of experiments were conducted on the laboratory and commercial-scale dryers as a result of time and financial constraints. Some of the simulation results were not validated with experimental data. It is apparent from the findings of this study that some further work is necessary in refining and verifying the theories considered. The following areas require further work to verify the simulation results adequately.

1. The simulation results suggest that an increase in the thermal mass of the drying chamber will not affect the dryer day time performance while experiments with product dried on a day to day basis suggested an improvement in the drying as a result of the thermal inertia of the system. It is recommended that drying experiments (both continuous and day to day drying experiments) should be conducted by incorporating different rock bed arrangements of known thermal inertia in the drying chamber. This way it would be possible to verify and confirm the simulation results and establish the validity of the deductions from the experimental results.
2. In the mathematical model developed to predict the performance of the MNCSCD, the effect of the thermal capacitance of the air-heater was neglected. However, as noted earlier, the drying experimental results of the laboratory tests 4, 5 and 6 suggest an improvement in the drying performance as a result of possible release of energy stored in the thermal mass of the system for drying at night. It will be useful if experiments are conducted on the different configurations of the SPDDSAH of varying thermal mass to

investigate the contribution of the thermal mass of the air-heater on the nocturnal drying performance.

3. As result of financial constraint, experiments could not be conducted on the commercial-scale loaded to full capacity. The full potential of the model will be realised only when they are applied to optimisation of commercial-scale solar drying systems. Adequate experimental data on the full capacity of the dryer must be established and used to validate the performance of the system in order to establish conclusively the findings of this study.

APPENDIX A

DETAIL DESCRIPTION OF THE DESIGN PRINCIPLES OF THE MIXED-MODE NATURAL CONVECTION SOLAR CROP DRYER (MNCSCD)

Introduction.

The design of a solar dryer is a complex task which can generally be considered under three phases as follows:

1. defining the drying process to be performed by the dryer in order to achieve the desired end-product quality and dryer performance
2. selecting the appropriate type of solar dryer to use, and
3. undertaking the detailed structural design of the solar dryer.

In this section the basic design principles underlying the structural design, of a typical small-scale mixed-mode natural convection solar crop dryer (MNCSCD) used in the laboratory experiment is outlined.

1 Conceptual design

Figure 1.1 shows a pictorial view of the laboratory model of the MNCSCD design achieved. The full description of the dryer is detailed in Chapter 3.

2 Design data

The drying requirements of agricultural products vary from product to product. The quantity of moisture to be removed from a particular product to make it safe for storage, which is determined by the initial moisture content of the product and the desired moisture content for safe storage of the dried product, varies from crop to crop. The maximum permissible temperature and relative humidity of the air used for removing the moisture from the crop during drying affect the drying rate significantly. Each crop, has its specific requirements for best quality. Another crucial consideration is whether the crop can be exposed to direct sunlight or not. Knowledge of these requirements and others is needed

for a good design of a crop-dryer. Information regarding the type of crop to be dried, loading density, its characteristics and the quantity per batch, is needed, together with data concerning the geographical location of the dryer and the climatic conditions during the harvest period. These were determined for the present design as explained below.

3 Crop Characteristics.

The dryer dimensions are based on the fact that the maximum quantity of the material to be dried per batch is 3 kg. The dryer is to be used for drying high moisture content crops for which the mass of water to be removed to bring it to a safe storage level could be as high as 50-70% of the initial weight of the product. If the desired final moisture content of the material is in the range 4 to 17% (w . b), then the initial moisture content of the crop would be in the range 52- 75% (w . b). Cassava, a typical tropical food crop that provides about 8-10% of the calorie requirements of human being (Roa, 1974), was used as the basis for the design calculations presented.

The following characteristics of cassava were either established experimentally or their values were taken from the literature:

Crop porosity:	0.44 (Roa, 1974)
Bulk density:	552 kg/m^3
Initial moisture content:	62-67% (wet basis)
Desired final moisture content:	17% w.b (Baker, 1997; Amouzou *et al*, 1986)
Loading bed void fraction:	0.40
Solid specific heat capacity:	840 J/kg K
Maximum permissible drying temperature:	70° C (Imre, 1997; Amouzou *et al*, 1986)
Maximum permissible drying air relative humidity:	60% (Cheema, 1978)
Percentage of dry matter content:	33-38% of the initial weight
Loading density:	5-15 kg/m^2 (Keey, 1972)
Drying ratio[a] for crop with initial moisture content of 62-67% wet basis:	between 11:5 and 5: 2

[a] Drying ratio is the ratio of the initial mass of crop before drying mass to the mass of the dried product.

4 Design constraints

i. The average velocity of the drying air, v_c , at the exit (or outlet) of the collector is expected to be between 0.20 and 0.40 m/s.

ii. The collector tilt (β_{opt}) for maximum collection of incident solar radiation for all year-round operation of a collector is to be taken as the latitude of the site where it is located in practice (Duffie and Beckman, 1991; Bucherg *et al*, 1974). The optimum azimuth angle, γ_{opt}, for maximum collection of solar energy is 0^{o} for south facing collectors or collectors sited in the northern hemisphere. Sinjeri and Kulistic, (1994) have shown that the change in the annual radiation collected is negligible if the azimuth angle is less than 30^{o}. For this design β_{opt} and γ_{opt} were taken as 6^{o} and 0^{o} respectively.

iii. The aggregate drying bed thickness, h_L, is not to exceed 200 mm, the maximum value expected for thin layer drying (Hall, 1975).

v. The maximum height of the hot air column was assumed to be 1.3m, from laboratory space considerations. That is, $H \leq 1.3$ m.

vi The air-heater aperture is to have an area (A_c) about two times that of the drying chamber area (A_{dc}).

vii. From previous research (Wayo, 1990), it was noted that with of incident solar energy in the range 400 to 600 W/m^2 and average air flow rate between 0.2 and 0.4 m/s, an effective drying time of 30 hours (2-5 days) can be assumed for a loading density in the range 10 to 20 kg/m^2.

viii. Light of intensity in the range of 400-600 W/m^2 is to be provided under laboratory conditions for drying experiments.

ix. Ambient air temperature in the laboratory was assumed to be 24 °C.

5 Sample design calculations

5.1 Air flow requirement.

The expected drying air temperature rise over the ambient value was calculated using a modified form of an empirical formulae suggested by Macedo and Altemani (1978):

$$\Delta T = 2\beta\,(T_b - T_c)(E / E_o) \qquad \text{(A1)}$$

Appendix A Detail description of the design principles of the mixed-mode natural convection solar crop dryer (MNCSCD).

where, $\Delta T = T_o - T_a$, is the temperature difference between the expected mean temperature of the heated air at the collector outlet and the ambient air temperature, β is a dimensionlesss parameters whose value is the range 0.14 to 0.25 (Macedo and Altemani, 1978), $(T_b - T_c)$ is the temperature difference between the boiling and freezing point of water at atmospheric pressure, E is the intensity of radiation incident on the plane of the collector and E_o is the maximum intensity of the source of radiation. The maximum intensity of the light source used (i.e. its intensity at a distance of 0 cm from the axis of the lamp), E_o, was determined to be 1454 W/m^2.

For this design, the mean value of β was taken as 0.20 to allow for moderate drying air temperature and moderate velocity for natural drying. Taking $T_b - T_c = 100^\circ$C, $E = 460$ W/m^2 and $\beta = 0.20$, the maximum expected temperature rise of the drying air at the exit of the primary collector is evaluated as 12.7° C.

The total quantity of moisture to be removed from the crop, was used to determine the total mass flow of air required for drying. The moisture to be removed (M_w) depends on the crop and can be found from the following relationship:

$$M_w = \frac{W_W\left[M_{i.wb} - M_{f.wb}\right]}{\left(1 - M_{f.wb}\right)} \qquad \text{(A2)}$$

where W_w = total crop mass, $M_{i.wb}$ = initial moisture fraction on wet basis, $M_{f.wb}$ = final moisture fraction on wet basis. The moisture fraction, on wet basis, defined as the ratio of the mass of water content to the total crop mass.

The total volume of air required (V_A) was then found from the equation:

$$V_A = \frac{M_w L_t R T_a}{C_{pa} P_a (T_o - T_f)} \qquad \text{(A3)}$$

where R_a = specific gas constant, P_a = partial pressure of dry air in the atmosphere,

---

Appendix A Detail description of the design principles of the mixed-mode natural convection solar crop dryer (MNCSCD).

C_{pa} = specific heat capacity of air at constant pressure, T_f = temperature of air leaving the drying bed, which value is assumed to be given by (T_a + 0.75{ΔT}) and the other parameters are as defined in Chapter 2. The value of the latent heat of evaporation in equation (A3) was estimated using the following expression (Liley and Gambill, 1973).

$$L_t = R_g T_c T_b \ln(P_c) \frac{(T_c - T_{pt})^{0.38}}{(T_c - T_b)^{1.38}} \qquad \text{(A4)}$$

where, R_g is the gas constant for water vapour, T_b is the boiling point of water, P_c is the critical pressure of water, T_{pt} is the temperature of the product and T_c is the critical temperature of water.

Since bound water is to be evaporated from the product the value of L_t estimated using equation (A4) is increased by a factor of 15%. The average temperature of the product during drying is estimated as the weighted mean of the temperatures of the air entering and leaving the crop bed ($T = 0.25\{3T_o + T_a\}$). The total volume of air required was found to be 1325 m^3.

The volume flow rate is calculated from the relation:

$$\dot{V} = \frac{V_A}{t} \qquad \text{(A5)}$$

where, t, is the total time required to dry a given sample of moist material to save storage level. Putting t = 108,000 seconds (30 hrs), the volume flow rate was obtained as 0.0123 m^3.

5.2 Area of drying chamber.

The cross-sectional area of the drying chamber Adc is obtained from first principles by relating the solid density of the wet material to its mass and the corresponding volume as:

$$A_{dc} = \frac{W_t}{\rho_s h_L (1 - \varepsilon_v)} = \frac{W_t}{\rho_{gr} h_L} \quad \text{(A6)}$$

where, W_t (= $W_m/3$, assuming three layers) is the mass of the crop on each layer, ρ_s is the solid density of the crop on wet basis, ρ_{gr} is the bulk density of the crop on wet basis and h_L is the layer drying bed thickness. The product of the solid density and the layer drying bed thickness is defined as the loading density. Assuming that a dryer is designed for a given loading density then a more dense material should be dried in thin layers and vice versa. Assuming an average loading density of 10 kg/m^2, the cross sectional area of the drying chamber is given as 0.167 m^2. Hence the area of the air-heater is found to be 0.34 m^2. Taking the ratio of the length of the air-heater to the width as 1.6, the collector length and width are detetermined as 0.73 m and 0.454 m respectively. The length of the drying chamber is made equal to the width (W) of the air-heater. Thus the breadth of the drying chamber is determined from the relation:

$$B = A_{dc} / W \quad \text{(A7)}$$

Putting the ratio of the drying chamber width to breadth to be 1.2, the breadth of the drying chamber was found to be 0.375 m satisfying the other constraints imposed on the design.

5.3 Total area of the system for collecting incident energy.

The total area surface of the dryer for collecting incident radiation is related to the overall system drying efficiency (η_d) which is given by:

$$\eta_d = \frac{M_w L_t}{H_t A_c t} \quad \text{(A8)}$$

where, A_c = total area of the dryer receiving incident radiation (the total surface area of the primary and secondary collectors of the dryer), t = total time , L_t = latent heat of vaporisation, and H_t is the intensity of radiation incident on a tilted surface.

In a physical system, H_t is the monthly average daily irradiation on a horizontal surface and is dependent on atmospheric transmittance and ground reflectivity. For the laboratory model, H_t was taken as the intensity of the incident radiation from the solar simulator. The overall drying efficiency of natural convection solar dryers reported in the literature have been shown to vary widely over the loading densities and weather conditions (Brenndorfer *et al*, 1987, Ekechukwu, 1987). Typical values reported for natural convection solar crop dryers range from 9 to 25%. To achieve a realistic design an overall efficiency value of 20% was assumed.

Putting M_p = 1.8 kg, L_t = 2.746 MJ/kg, t = 108,000 s, H_t = 460 W/m^2 into the efficiency equation (A8) above, and assuming a mean overall efficiency of 20% (i.e. η_d = 0.20), yields A_c = 0.496 m^2. The design concept is based on the fact that the following fundamental relation must be satisfied:

$$A_c \approx A_p + A_{dc} \tag{A9}$$

otherwise the ratio of the collector area to the drying chamber area should be altered.

5.4 Other dimensions of the dryer

The determination of the air duct depth is to some extent an iterative procedure. The depth of the collector air duct channel (s) is calculated and if this proves suitable for the desired volume flow rate and the average value of the velocity of air inside the air-heaters, then it is used. Otherwise, some or all the estimated or assumed values are altered and/ or the space configurations of the air-heaters are altered to achieve the desired value of s subject to all the constraints imposed on the design. Following from the continuity equation for one dimensional steady flow, the weighted average velocity at the exit of the air-heater is related to the channel overall cross section by the relation:

$$V_c = \frac{\dot{V}}{sW} \tag{A10}$$

Putting $V_c = 0.30\ m^3/s$, $\dot{V} = 0.0123\ m^3/s$, $W = 0.454$ m gives $s = 0.08$ m.

The surface area of the absorber of the absorbing is approximately equal to the area of the air heater cover, A_c ; this is related to the length and width of the cover as follows:

$$A_c = L \times W \tag{A11}$$

Following from the suggestion by Bruce (1978) regarding inlet and outlet vents areas for natural ventilation, the cross-sectional area of the chimney was related to the air-heater duct area by the relation,

$$A_d = 2A_v \tag{A12}$$

From the above relation the height of the chimeny vent was determined to be 35 mm. Relating chimney cross-section and the air vent in the chimney, the dimensions of the vent were obtained (0.375 m wide and 77 mm in height).

It is must be noted that because of constructional difficulties some of the dimensions were altered slightly to allow for easy assembly and disassembly of the members.

5.5 Pressure drop through the drying bed.

According to Jindal and Gunasekaran (1982), the resistance to the flow of air through a packed bed of agricultural produce is expressed in the form:

$$u = a\left(\frac{\Delta P_B}{h_L}\right)^b \tag{A13}$$

wher u = air velocity, h_L = drying bed thickness and a, b are constants whose values are determined experimentally. For natural circulation of air through a thin layer of cassava chips ($h_L \leq 0.20$ m) their conservative estimates were found to be 0.001 and 0.9, respectively. The air velocity (u) can be found from the continuity equation. The pressure

drop across the crop bed (ΔP_B) was calculated (for the present design it was found to be 0.676 Pa).

5.6 Pressure drop through the collector.

The pressure drop through each rectangular channel of the collector is given by the expression:

$$\Delta P_c = f\frac{L(d+B)}{2dB}\tfrac{1}{2}\rho^* V_C^2 \qquad \text{(A14)}$$

where f = the friction factor, d = depth of each collector air channel, ρ^* = average air density in the collector (which can be determined from the equation of state) and the other symbols are as previously defined. The flow of air in the airway is practically turbulent and therefore f varies with the roughness ratio of the channel walls. The equivalent roughness of cement or plaster faced airways and galvanized steel jointed ductwork are known. The design values of $V_C = 0.20$ m/s, $d = 0.077$ m, and $W = 437$ mm were obtained after several iterations in order to satisfy all the constraints of the design. f was estimated from the well-known Moody chart summarizing the researches and formulations of Prandtl, van Karman, Nikuradse and Colebrook, as 0.015. The pressure drop through each channel of the collector on each wing of the drying chamber was obtained as 0.0022 Pa.

5.7 Height of the hot air column.

It is the minimum height of the exit vents above the collector inlet for moist air escape to the ambient under air circulation by natural convection. In arriving at the height of the air column it is assumed that the dryer functions under steady state conditions. Hence the steady state values of the ambient air temperature and density are T_a and ρ_a, respectively. It is further assumed that:

- the depth of the drying bed, h_L, is small compared to height, H, of the hot air column

- the whole structure is air tight and ambient air enters through the inlet and the moist warm air escapes through the vent(s) in the chimney
- the steady state average values of the temperature and density of the hot air inside the chimney are T_o and ρ^*, respectively.

Applying Bernoulli's equation between the relevant sections of the dryer and simplifying the resulting expressions leads to the relation:

$$H = \frac{\Delta P_a + \Delta P_c}{g(\rho_a - \rho^*)} = \frac{\Delta P_T}{g(\rho_a - \rho^*)} = \frac{\Delta P_T}{g(1/T_a - 1/T_o)P/R} \qquad \text{(A15)}$$

where ΔP_T, is the total pressure drop through the dryer. The value was obtained as 0.678 Pa and thus the height of the hot air column above the air inlet H was found to be 1.3m. In the construction of the dryer an extra allowance should be made for the height of the chimney and the height of the solar air-heater inlet above the ground. The height of the air-heater inlet should be at least 0.40 m to allow air to flow naturally through it.

6 Design of the cantilever system

The standard procedure for the measurement of tensile or compressive direct strains utilises the *full-bridge* circuit for measurement of the small changes in the resistance of the strain gauges. This arrangement is preferred because the sensitivity of a full-bridge circuit is increased by a factor of 2.6 over that which would be achieved using a single linear gauge (Hearn, 1997). In the determining the thickness of the beam the following factors were taken into consideration:

i. the load capacity should be limited to 3 kg,
ii. the maximum deflection of the cantilever should correspond to the maximum allowable reading of the microstrain indicator (1999 με),
iii. the effective length of the cantilever should be about half the width of the drying chamber (i.e. $L = 200$ mm). This is to ensure symmetric loading.
iv. a standard cantilever beam of width, b = 25 mm was assumed,

For a simple cantilever of constant cross section as shown in fig. A1, the moment of the load F about the root of the strain guage is given by

$$M = \frac{I\sigma}{y} = \frac{6FL}{bh^2} \qquad \text{(A16)}$$

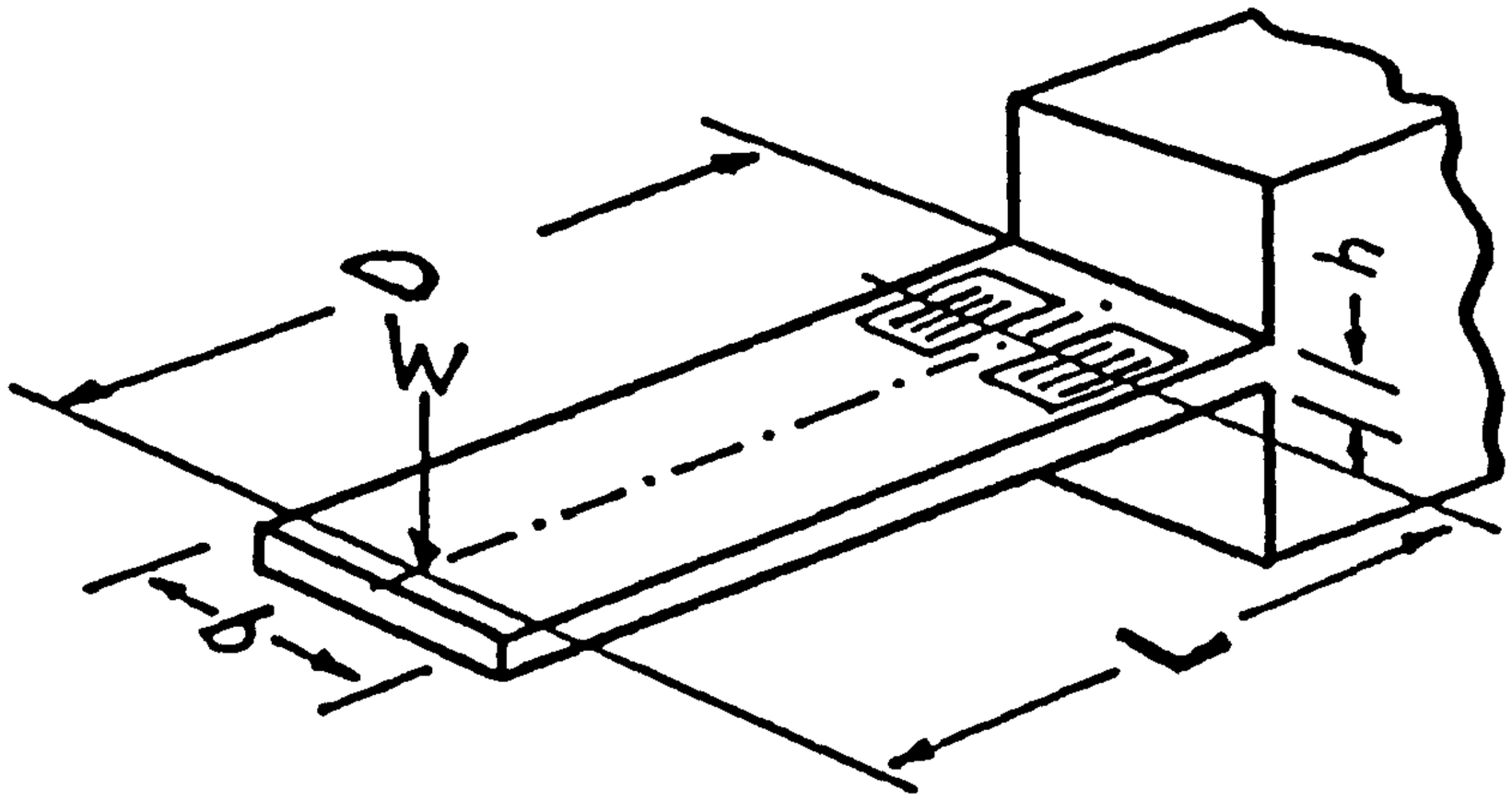

Figure A1: A simple cantilever beam of constant cross section (Pople, 1979)

where,

M = bending moment of the load F about the root of each strain guage.

y = distance of a fibre of the beam from its neutral axis of bending (y = 0.5 h)

I = second moment of area for the beam cross section ($I = bh^3 / 12$)

h = beam thickness

b = beam width (25 mm)

L = distance between the applied load F and the active length centre of the gauge (220 mm)

D = distance between the applied load and the root of the cantilever

δ = beam tip deflection

E = Young's Modulus of elasticity (for steel E = 21 x 10^{10} N/m^2).

The surface strain of the beam, indicated by a single linear gauge, is related to the stress experienced under the action of the applied load and the Young's modulus by the relation

$$\varepsilon = \sigma / E \tag{A17}$$

Thus combining Equations (A16) and (A17) we obtain

$$\varepsilon = \frac{6FL}{bh^2E} \tag{A18}$$

where ε is the strain recorded when a single active gauge is attached to the cantilever subjected to a load F, and is given as:

$$\varepsilon = \frac{\text{total permissible strain recorded by the microstrain indicator}}{\text{sensitivity of the bridge circuit}}$$

Noting that the sensitivity of the bridge circuit is 2.6, the maximum deflection of the beam was found to be 768.8 με. By considering the beam to experience this maximum strain, the desired plate thickness, *h*, of the cantilever beam was calculated from equation (A18). The plate thickness was found to be 2.95 mm, hence a steel plate bar of standard thickness approximately 3 mm was chosen.

Appendix A Detail description of the design principles of the mixed-mode natural convection solar crop dryer (MNCSCD).

APPENDIX B

PROGRAM TO SIMULATE THE PERFORMANCE OF THE MNCSCD

```
      PROGRAM LAYER
C—      PROGRAM TO SIMULATE LAYER DRYING OF AGRICULTURAL PRODUCTS
      COMMON WMT,TMT,RHT,DELT,WMCN,KAB
      INTEGER IEXIT,NL1,NDIBO,ITERCT,NL,KAB,NCOND,JK,JM ,ike,ndim
      DOUBLE PRECISION WMT,TMT,RHT,DELT,WMCN,CPA,CPL,CPW,CPG,CT,BTA,
     SRHOM,HFG,PATM,RHTP,TM,HR,DEEP,WMC,TA,MFDOT,TCH,HV,HA,TOP1,TXWB
      DOUBLE PRECISION Z,DELZ,TIME,PRT,WMEND,D,GA,PR,WATER,ETAD,A1AC
      DOUBLE PRECISION MFDOTG,KW,TW,TTP,TATM,QDOT,RA,BETAAIR,TF,AW
      DOUBLE PRECISION HRWS,CC,F1B,L,TACHG_AV,BHT,TCHG,TOP4,TOP3,TOF
      DOUBLE PRECISION RHOA,WT,TAUG,CMPRM,DEPTH,ALPHAM,R,F1T,TAIR,W
      DOUBLE PRECISION TAIPIG,ALPHAG,KTY,KVISTY,HI,UL,ENERGY,T1WBC,BHT
      DOUBLE PRECISION RHOINC1,RHOINC2,ADC,CFA,CKE,SUM,WMAVE,G1,T1WB
      DOUBLE PRECISION RHO1,RHOC,RE,KVISTYC,DHC,CFC,FC,CENTRY,RHOIPIG
      DOUBLE PRECISION CEXIT,ACH,AVENT,ACHVENT,ACHDC,RHOCHG,KKE,KVISCH
      DOUBLE PRECISION DHCH,FCH,KFCH,KCV,KCXS,KT,A,B,C,WME,TT,TABS,T1DB
      DOUBLE PRECISION A1,B1,C1,D1,D2,D3,D4,E1,F1,A3,B3,F2,C14,C15,C16
      DOUBLE PRECISION C17,C18,C25,C26,C27,C28,DR,SS,PP,C_1,HS,PWS1B,PV
      DOUBLE PRECISION C29,C30,C31,C32,C33,C34,C35,C36,C37,RO,PVS,T1DBC
      DOUBLE PRECISION T1DPC,DBTPR,TBTNPR,W1STAR,P1V,A1LF,TANC,TMMEAN
      DOUBLE PRECISION WMCNWB,WMAVEWB,PI,F,GM,PUM,XR,PUN,PAN,QP,TAMEAN
      DOUBLE PRECISION AC,DEPTH,Q,TF1OIN,TF2OIN,HR2,TA,P,SBARC,SBARP
      DOUBLE PRECISION TF1IN,TF2IN,X2,X1,MSCSF,SHCSF,MSCV,SHCV,AOCV,RHN
      DOUBLE PRECISION MSDTRAY,SHDTRAY,VOLDCHM,BDC,HDC,HCH,LOS,RH2,RH1
      DOUBLE PRECISION TP,TB,TC,M1,M2,M,V1SIN,V2SIN,S1,S2,DELTAY,ETACIN
      DOUBLE PRECISION V1S(2000),V2S(2000),TF1O(2000),TF2O(2000),TAIN
      DOUBLE PRECISION HRN,HRN1,BCH,XVENT,W_t,PICKUP_E,PCL,TBL,TCL,RCL
      DOUBLE PRECISION HSSTAR,HIN,FSILONV,T2WB
      DIMENSION WMC(100),TAIR(101,2),TM(100),HR(101,2),DEEP(20)
      DIMENSION F(400),RH(101)
      PARAMETER(RHTP=0.98,G=9.807,ndim=2000)
      PARAMETER(WT=1.4583,X=0.003,KW=1.0,PR=0.71,SHCV=1465,
     $ CC=0.61,BCH=0.085,BTA=0.1135,TAUG=0.83,FSILONV=0.50,
     $ ALPHAM=0.76,ALPHAG=0.086,C_1=0.465,MPULOS=1.092,SHCSF=502,
     $ XVENT=0.03,MPUAOCV=3.58,SHDTRAY=502,PI=3.142,MSDTRAY=0.599)
      OPEN (UNIT=1, STATUS='new', FILE='FORSONGx.DAT')
      OPEN (UNIT=2, STATUS='new', FILE='FRANCISGx.DAT')
      call SAH(TF,TA,W,AC,DEPTH,P,Q,TF1OIN,TF2OIN,RH2,BHT,HR2,
     $ m1,m2,m,v1sin,v2sin,etacin,rh1,T2WB)
      call GETFUR(ndim,V1S,V2S,TF1O,TF2O,S1,S2,W,TF1IN,TF2IN,TA,
     $  V1SIN,V2SIN,AC,DEPTH,P,Q,DELTAY,ETACIN,TP,TB,TC,BHT,TF,RH2,
     $  M1,M2,M1,RH1,RHN)
      call RADTNA(SBARC,SBARP,BHT)
      call sychart(TF,TA,RH2,RH1,RHN,HR2,T2WB)
C—      DATA ON ATMOSPHERIC CONDITIONS
      WRITE(*,*)'INPUT  PATM (kN/m^2):='
      READ (*,*) PATM
C—      DATA ON DRYING CHAMBER DESIRED SPECIFICATIONS
      WRITE (*,*)'INPUT X2 :='
      READ (*,*) X2
      WRITE (*,*)'VOLDCHM (M^3):='
      READ (*,*) VOLDCHM
      WRITE (*,*)'INPUT HCH (m):='
      READ (*,*) HCH
      WRITE(*,*) 'INPUT CPG (J/kg K) :='
      READ (*,*) CPG
      WRITE(*,*) 'INPUT RHOM (kg/m^3):='
      READ(*,*) RHOM
C—      OVERALL DEPTH, NUMBER OF LAYERS
      WRITE(*,*)'INPUT NL (integer):='
      READ (*,*) NL
C—      DRYING AIR TEMPERATURE AT INLET OF THE DRYING CHAMBER
      If (P.LT.1.0) THEN
        TAIN =  TF+0
      end if
      If ((P.GT.1.0).AND.(P.LT.2.0)) THEN
       TAIN = TF+0
      end if
      If (P.GT.2.0) THEN
       TAIN = TF+0
```

```
      end if

C---        OTHER INPUT CONDITIONS FOR THE DRYING SIMULATION
      WRITE(*,*) 'INPUT NDIBO (integer):='
      READ(*,*) NDIBO
      WRITE(*,*)'INPUT TBTNPR (hr):='
      READ (*,*) TBTNPR
C---        GUESS VALUES OF AIR MASS FLOW RATE, CHIMNEY TEMPERATURE, DRYING
C---        CHAMBER TEMPERATURE,MEAN AIR TEMPERATURE IN THE HEATER, DRYER WALL
C---        TEMPERATURE
      WRITE(*,*) 'INPUT TACHG (K):='
      READ (*,*) TACHG
      TAHG = (TF1IN + TF2IN)/2.
      WRITE(*,*)'INPUT MFDOTG (kg/s):='
      READ (*,*) MFDOTG
      WRITE(*,*) 'INPUT TWG (K):='
      READ (*,*) TWG
       TATM=TA
       HRNI = HR2
       WRITE(*,*) HRNI,tf1in,tf2in
       RHOA =3.52981E2/(TATM*(1+1.6078*HRNI))
       TS = 0.0552*TATM**1.5
       WRITE(*,*) TS,BHT,HR2
       write(*,*) w,ac,q
       TCHG = TACHG
       WRITE(*,*)TF
       TOF = TAHG - 2.5
       HRWS = 5.67E-8*0.92*(TWG**2 + TS**2)*(TWG + TS)
       RHO1 = 3.52981E2/(TOF*(1 + 1.6078*HRNI))
       RHOCHG = 352.981/(TCHG*(1 + 1.6078*HRNI))
       I=0
  131 IF(I.LT.100) THEN
C---        CALCULATE MASS FLOW RATE AND MASS FLOW PER UNIT BED AREA
       WDC=SQRT(AC/Q)
        L=SQRT(Q*AC)
        BDC = WDC/X2
      X1=((VOLDCHM/WDC)-0.5*((BDC**2)-0.5*DEPTH**2)*sin(BTA)/cos(BTA))
     $  /(BDC**2)
      HDC =BDC*X1
      H=HDC + DEPTH + BDC*sin(BTA)/cos(BTA) + HCH
      TADCG = TACHG - 3
      TFLUID = (TWG + TADCG)/2.
      TACHG_AV = TFLUID
      BETAAIR = 1/TACHG_AV
      KVISTY= (0.0942*TFLUID + 2.318)/1000000.
      RA = (G*BETAAIR*(TACHG_AV-TWG)*(HCH**3)*PR)/(KVISTY**3)
      KTY = (0.0732*TFLUID + 4.1672)/1000.
      HI = KTY*(0.825 + 0.3244*(RA**1./6))/X
      UL = 1/(1/HI + X/KW)
      QDOT = UL*(TACHG - TATM)
      RHOINC1 = 352.981/(TF1IN*(1 + 1.6078*HRNI))
      RHOINC2 = 352.981/(TF2IN*(1 + 1.6068*HRNI))
      RHOC = (RHOINC1 + RHOINC2)/2.
      WRITE(*,*) RHOC
      AW= 2*(WDC+BDC)*HCH
      ADC = WDC*BDC
      write(*,*)ADC
      CFA = WDC*DEPTH
      A1AC = ADC/CFA
      CKE =(A1AC**2)*RHO1/RHOC
      KVISTYC = (0.0942*TOF+2.318)/1000000.
      RE = (2*MFDOTG)/((WDC + DEPTH)*RHOC*KVISTYC)
      FC = 0.079*(RE**(-0.25))
      DHC =(2*DEPTH*WDC)/(DEPTH + WDC)
      CFC=4*FC*L*(RHO1/RHOC)*(A1AC**2)/DHC
      CENTRY= 0.5*(RHO1/RHOC)*(A1AC**2)
      CEXIT= ((A1AC - 1)**2)*(RHO1/RHOC)
      CT = CKE + CFC + CENTRY + CEXIT
      TAIPIG=TATM + QDOT*X/KW
      RHOIPIG=352.981/(TAIPIG*(1+1.6078*HRNI))
      ACH=WDC*BCH
      AVENT=BCH*XVENT
      ACHVENT=ACH/AVENT
      ACHDC = ACH/ADC
```

```
      KKE=ACHVENT**2 - (RHOCHG/RHOIPIG)*(ACHDC**2)
      KVISCH= (0.0942*TACHG + 2.318)/1000000.
      DHCH=(2*WDC*BCH)/(WDC+BCH)
      FCH=0.079*((2*MFDOTG)/((WDC+BCH)*RHOCHG*KVISCH))**(-0.25)
      KFCH=4*FCH*HCH/DHCH
      KCV=0.5
      KCXS=((1/CC) - 1)**2
      KT = KKE +KFCH + KCV + KCXS
      A = (1./(2*RHO1*ADC**2))*(CT + (KT*(RHOA-RHOCHG))/(RHOA-RHO1))
      Z = (WT*X2)/(RHOM*WDC*WDC*(1-FSILONV))
      B = Z/(C_1*RHO1*ADC)
      C = - H*G*(RHOA - RHOCHG)
      write(6,222) A,B,C
  222 FORMAT(5X,F8.3,8X,F8.3,8X,F8.3)
      MFDOT = (-B + SQRT(B**2 - 4*A*C))/(2*A)
C---      CALCULATE CHIMNEY TEMPERATURE
      CPA = 985.89 + 0.174*TAIN - 0.0007*TAIN**2 + 1E-6*TAIN**3
      R = (2*(WDC + BCH)*UL)/(MFDOTG*CPA)
      TOP1 =(ALPHAG/UL)*BHT
      TOP3 = (1 - EXP(-R*HCH))
      TOP4 =  TAIPIG - TATM - TOP1
      TCH = TATM + TOP1 +  TOP4*TOP3/(R*HCH)
C---      CALCULATE DRYING CHAMBER WALL TEMPERATURE
      TW  = TAIPIG - (TAIPIG - TATM)*UL/HI
C---      TEST FOR COVERGENCE OF MDOT, TCH, TW
      IF (((MFDOT-MFDOTG).GT.1.0E-3).OR.((TCH-TCHG).GT.1.)) THEN
      I = I +1
      MFDOTG=MFDOT
      TWG=TW
      TCHG=TCH
      GO TO 131
      END IF
        IF ((MFDOT-MFDOTG).LE.1.0E-3) THEN
        GO TO 15
      END IF
        END IF
   15   GA = 0.804*MFDOT/ADC
      WRITE(6,242)CT,KT,TCH,TW,MFDOT,GA
  242 FORMAT(F8.4,4X,F10.3,4X,F8.3,4X,F8.3,4X,F8.3,4X,F8.3)
C---CRITERIA FOR TERMINATING PROGRAM (Estimated maximum drying time)
      WRITE(*,*)'INPUT TTP (hrs):='
      READ (*,*) TTP
C---      COMPUTE STEP SIZE,NUMBER OF NODES AND DEPTH BETWEEN PRINTS
      DELZ = Z/NL
      NL1 = NL + 1
      DBTPR = NDIBO*DELZ
C---      COMPUTE OUTPUT DEPTHS FOR PRINTING
      D=.0
      PRT=.0
      TIME=.0
      ITERCT=0
      IEXIT=0
      JK=0
      NCOND=0
      KAB=0
      DR=.0
      ike=0
      TXWB=0
      DO 100, I=1,NL1,NDIBO
      JK = JK + 1
      DEEP(JK)=D
      D = D + DBTPR
  100 CONTINUE
      WRITE(*,*) 'INPUT TMN (K):='
      READ(*,*) TMN
      WRITE(*,*)'INPUT WMEND (decimal, wet basis):='
      READ (*,*) WMEND
C---      COMPUTE INLET RELATIVE HUMIDITY AND INITIALIZE ALL ARRAY POSITIONS RQD.
      WMCN=2.01
      AB=WMCN/(1+WMCN)
       write(6,400)AB
  400  FORMAT(F8.4)
      C36=-37357.912
      C37=-29.9857
```

```
      RO=8.315
      RHN=EXP((C36/(RO*TMN))*EXP(C37*AB))
      C25=-5.800220E3
      C26=-5.5162560
      C27=-4.8640239E-2
      C28=4.1764768E-5
      C29=-1.4452093E-8
      C30=6.5459673
      PVS=EXP((C25/TMN)+C26+C27*TMN+C28*TMN**2+C29*TMN**3+C30*LOG(TMN))
      PV = RHN*PVS
      HRN = (0.622*PV)/(PATM-PV)
      DO 2, I = 1,NL
      IP1    = I + 1
      WMC(I) = WMCN
      TM(I)  = TMN
      HR(IP1,1)= MIN(HRN1,HRN)
       TAIR(IP1,1)= TAIN
       RH(IP1) = RHN
     2 CONTINUE
       TAIR(1,1)=TAIN
       TAIR(1,2)=TAIN
       HR(1,1)=HRN1
       HR(1,2)=HRN1
       RH(1)=RHN
       TM(1)=(TAIN+TMN)/2.
C---      CALCULATE HEAT TRANSFER COEFFICIENTS AND EMC
       HV = 175.07*(GA**0.6906)
       HA = HV/DELZ
       C14 = 6.65707
       C15 =-12.6197
       C16 = 6.22394
       C17 =-0.0085
       C18 = 0.01055
       WME = (RHN*(C14+RHN*(C15+RHN*C16)))*EXP((RHN*(C17+
      $    RHN*(RHN*C18)))*TAIN)
       write(6,666) WME
   666 FORMAT(1F9.4)
       PRINT 211,(DEEP(I),I=1,JK)
       write(1,211),(DEEP(I),I=1,JK)
C---      BEGINNING COMPUTATION OF TIME INDEPENDENT CONSTANTS IN THE DEPTH LOOP
       TANC = TAIN - 273.15
       CPW = 1857+ 0.7918*TANC - 0.0064*TANC**2 + 0.0001*TANC**3
       CPL = 4209.3 - 1.778*TANC + 0.0291*TANC**2 - 0.0001*TANC**3
       A1  = 2.*GA*CPA
       B1  = GA*CPW
       C1  = HV*DELZ
       E1  = C1*AW/ADC
       A3  = RHOM*CPG
       B3  = RHOM*CPL
       LOS = 8*WDC+2*((B/COS(BTA))-DEPTH)+2*BDC+WDC+4*(HDC+DEPTH)
       MSCSF=LOS*MPULOS
       AOCV=2*0.5*(2*HDC+BDC*sin(BTA)/cos(BTA))*BDC+(HDC*WDC)
      $    +WDC*(HDC+DEPTH)
       MSCV =AOCV*MPUAOCV
       CMPRM = (MSCSF*SHCSF+MSCV*SHCV+MSDTRAY*SHDTRAY)
       E3  = CMPRM/ADC
       G1  = (HA/((KW/X) + HA))
       F1T = ALPHAG*BHT - HRWS*(TATM - 0.0552*(TATM**1.5))
       F1B = (KW/X) + HA
       F1  = F1T/F1B
C---      CALCULATE CURRENT TIME STEP, INCREMENT TIME AND COMPUTE
C---TIME DEPENDENT CONSTANTS
       DO 14 JN =1,2000
     4 DELT = 0.5*DELZ*(A3+B3*WMC(1))/(0.5*A1 + B1*HR(NL1,1))
       TIME = TIME+DELT
       tima = TIME/3600.
       D4  = RHOM*CPW*DELZ/DELT
       D2  = GA*DELT/DELZ
       D1  = HV*DELT*AW/ADC
       D3  = (ALPHAM*TAUG*DELT*BHT)/COS(BTA)
       F2  = (RHOM*DELZ)/(GA*DELT)
C---      LOOP TO ITERATE IN TIME
       WRITE(6,201) tima,WMC(1),WMC(NL),DELZ
   201 FORMAT(F10.4,6X,F6.3,5X,F6.3,5X,F7.3)
```

```
C—      BEGIN DEPTH LOOP
      DO 102, J=2,NL1
      JM=J-1
      QP=EXP(-(((2*JM*DELZ)/Z) - 2)*LOG(0.5))
      TMT=(TM(JM) + TAIR(JM,2))/2.
      WMT=WMC(JM)
C—      BYPASS TM EQUATION ON THE FIRST TIME STEP
      IF(ITERCT.EQ 0) THEN
      HFG = 2560000.
      GO TO 6
      END IF
      IF (ITERCT.GT.0) THEN
      PCL=221
      RCL=462.2
      TCL=647.3
      TBL=373.15
      HFG=RCL*TCL*TBL*LOG(PCL)*((TCL-TMT)**0.38)/((TCL-TBL)**1.38)
      WRITE (6,3000) HFG
3000  Format(F8.4)
      END IF
      AD = WMT/(1 + WMT)
      TM(JM) =(TM(JM)*(A3+B3*AD+E3-D1-D2*CPL*(HR(J,1)-HR(JM,1)))
     $+0.5*(TAIR(J,1)+TAIR(JM,1))*(D1+D2*(CPL+HFG)*(HR(J,1)-HR(JM,1)))
     $ +D3*QP+D3*VOLDCHM/WDC)/(A3+B3*AD + E3)
      GO TO 7
    6 TMT = (TAIR(JM,2)+2.*TAIR(JM,1)+TAIR(J,1))/4.
    7 HRT = ((HR(JM,1) + HR(J,1))/2. + HR(JM,2))/2.
      TT  = TMT
      C25 = -5.800220E3
      C26 = -5.5162560
      C27 = -4.8640239E-2
      C28 =  4.1764768E-5
      C29 = -1.4452093E-8
      C30 =  6.5459673
      PVS = EXP((C25/TT)+C26+C27*TT+C28*TT*TT+C29*TT**3+C30*LOG(TT))
      PV  = HRT*PATM/(0.622+HRT)
      RHT = PV/PVS
      write(6,3333)RHT,PV,PVS,HRT,TMT,TM(JM)
 3333 FORMAT(6F9.3)
C—      EVALUATING CURRENT MEAN MOISTURE CONTENT
      C14 = 6.65707
      C15 =-12.6197
      C16 = 6.22394
      C17 =-0.0085
      C18 = 0.01055
      WME =(RHT*(C14+RHT*(C15+RHT*C16)))*EXP((RHT*(C17
     $ + RHT*(RHT*C18)))*TAIR(JM,2))
      write(6,777)WME
  777 FORMAT(F9.4)
      if(WME-WMT)66,1,1
    1 ike=1
      TXMO=WME
      GO TO 5
   66 if(WMCN-WMT)3,44,44
    3 TXMO=WMT
      go to 5
   44 if (WMT.GT.WMEND) THEN
      TXMO=WMC(JM)
      end if
      if (WMT.LE.WMEND) THEN
      GO TO 13
      end if
    5 DELM=TXMO-WMEND
      if (ike-1)99,85,99
   85    KAB=KAB + 1
   99     XR = -2.*RHT + 1.2
      if (WMT.LT.0.4) then
     DR=((1.0E-23*PI**2)/(Z**2))*(-27400.-5.74*WMT+5.98*EXP(WMT)
    $    + 27500.*EXP(-1./TAIR(J,1)) + 2.23*XR)
      end if
      if ((WMT.GE.0.4).AND.(WMT.LT.0.7)) then
      DR=((1.0E-19*PI**2)/(Z**2))*(-27400.-5.74*WMT+5.98*EXP(WMT)
     $    + 27500.*EXP(-1./TAIR(J,1)) + 2.23*XR)
      end if
```

```
      if ((WMT.GE.0.7).AND.(WMT.LT.1.2)) then
      DR=((1.0E-14*PI**2)/(Z**2))*(-27400.-5.74*WMT+5.98*EXP(WMT)
     $    + 27500.*EXP(-1./TAIR(J,1)) + 2.23*XR)
      end if
      if (WMT.GE.1.2) then
      DR=((1.0E-12*PI**2)/(Z**2))*(-27400.-5.74*WMT+5.98*EXP(WMT)
     $    + 27500.*EXP(-1./TAIR(J,1)) + 2.23*XR)
      end if
      write(*,*) DR
      PUM = 0
      DO 434 N=1,100
       GM=(2*N -1)**2
       F(N)=EXP(-1.*GM *DR*TIME)
        PUM = PUM + F(N)
  434  CONTINUE
      WMC(JM) = WMT - (8./(PI**2))*DR*DELM*PUM*DELT
       WMT=WMC(JM)
       write (6,545) WMT,PUM
   545 FORMAT(2F9.4)
C---      COMPUTATION OF HUMIDITY RATIO (HR(J,2))
      HR(J,2)=HR(JM,2) - F2*(WMT-WMC(JM))
      HRT=(HR(JM,2)+HR(J,2))/2.
C---      COMPUTATION OF AIR TEMPERATURE (TAIR(J,2))
      TAIR(J,2)=(TAIR(JM,2)*(A1+B1*2.*HRT- C1+ D4*(WMT-WMC(JM))
     $ + E1*(G1-1))+2*TM(JM)*(C1-D4*(WMT-WMC(JM)))+2*E1*F1)/
     $(A1+B1*2.*HRT+C1+D4*(WMT-WMC(JM))+E1*(1-G1))
      TABS=TAIR(J,2)
C---      CALCULATE RH AND CHECK FOR CONDENSATION
      SS=TABS
      C25=-5.800220E3
      C26=-5.5162560
      C27=-4.8640239E-2
      C28=4.1764768E-5
      C29=-1.4452093E-8
      C30=6.5459673
      PVS=EXP((C25/SS)+C26+C27*SS+C28*SS*SS+C29*SS**3+C30*LOG(SS))
      PV   = (HR(J,2)*PATM)/(0.622 + HR(J,2))
      RH(J)= PV/PVS
      IF((RH(J)-RHTP).LT.0) THEN
      GO TO 9
      END IF
      IF ((RH(J)-RHTP).GE.0) THEN
      GO TO 8
      end if
    8 TXWB = TMT
      I= 0
 2111   IF(I.LT.50) THEN
      T1WBC = TXWB
      T1DB =TABS
      C25=-5.800220E3
      C26=-5.5162560
      C27=-4.8640239E-2
      C28=4.1764768E-5
      C29=-1.4452093E-8
      C30=6.5459673
      PWS1B=EXP((C25/T1WBC)+C26 +C27*T1WBC +C28*T1WBC**2 +
     $ C29*T1WBC**3+C30*LOG(T1WBC))
      W1STAR=(0.62198*PWS1B)/(PATM-PWS1B)
      T1WB=(2501*(HR(J,2)-W1STAR)+(TABS-273)*(1.805*HR(J,2)+1))
     $    /(1.-2.381*W1STAR + 4.186*HR(J,2)) + 273
      T1DBC=T1DB-273
      P1V=HR(J,2)*PATM/(0.62198+HR(J,2))
      A1LF = LOG(P1V/1000.)
      C31=6.54
      C32=14.526
      C33=0.7389
      C34=0.09486
      C35=0.4569
      T1DPC=(C31+C32*A1LF+C33*A1LF**2+C34*A1LF**3+
     $ C35*(P1V/1000.)**0.1984)
      IF(TXWB.GE.T1DBC) THEN
      TXWB=(T1DBC+T1DPC)/2.
      END IF
      IF(TXWB.LE.T1DPC) THEN
```

```
      TXWB=(T1DBC+T1DPC)2.
      END IF
      IF ((TXWB.GE.T1DPC).AND.(TXWB.LT.T1DBC)) THEN
      TXWB=(T1DPC+T1DBC)2.
      END IF
      IF(ABS(TXWB-T1WBC).GT.1.0E-1) THEN
      I = I+1
      T1WBC=TXWB
      GO TO 2111
      END IF
       IF (ABS(TXWB-T1WBC).LE.1.0E-1) THEN
       GO TO 162
       END IF
  162  TWBA = TXWB
      HS=HR(J,2)
      END IF
C---TA=WETBULB TEMPERATURE, HR=WET BULB HUM. RATIO
      TAIR(J,2)=TWBA
      PP=TWBA
      C25=-5.800220E3
      C26=-5.5162560
      C27=-4.8640239E-2
      C28=4.1764768E-5
      C29=-1.4452093E-8
      C30=6.5459673
      PV=RHTP*EXP((C25/PP)+C26+C27*PP+C28*PP*PP+C29*PP**3+C30*LOG(PP))
      HR(J,2)=0.62198*PV/(PATM-PV)
      RH(J)=RHTP
      NCOND=NCOND+1
    9 WMT=WMT+(HS-HR(J,2))*F2
      WRITE(6,333) WMT
  333 FORMAT(1F8.4)
      WMC(JM)=WMT
C---        END OF DEPTH LOOP
C  SHIFT ARRAYS AND COMPUTE AVERAGE MOISTURE CONTENT
  102 CONTINUE
      SUM = 0
      DO 103, M=2,NL1
      J = M
      TAIR(J,1) =TAIR(J,2)
      HR(J,1)=HR(J,2)
      SUM = SUM + WMC(J-1)
  103 CONTINUE
      WMAVE=SUM/NL
      PAN = 0
      DO 111, J=1,NL
      PAN = PAN + TAIR(J,2)
  111 CONTINUE
      TAMEAN = PAN/NL
      PUN = 0
      DO 112, J=2,NL1
      PUN = PUN + TM(JM)
  112 CONTINUE
      TMMEAN = PUN/NL
      ITERCT=ITERCT+1
      NODES=NL*ITERCT
      PNCOND=NCOND*100./NODES
      PKAB=KAB*100./NODES
C---        CHECK IF TIME TO END, MOISTURE CONTENT LOW ENOUGH, OR TIME
C---        TIME TO PRINT.  IF NONE GO TO START OF PROGRAM
    IF((time-TTP).LE.0) THEN
    GO TO 10
      END IF
       IF((time-TTP).GT.0) THEN
       GO TO 12
        END IF
 10 IF ((WMAVE-WMEND).LE.0) THEN
    GO TO 12
     END IF
      IF ((WMAVE-WMEND).GT.0)THEN
      GO TO 11
    END IF
 11 IF((time-PRT).LE.0) THEN
    GO TO 4
```

```
      END IF
      IF((time-PRT).GT.0) THEN
      go to 13
      END IF
C—        SET FLAG IF EXIT CONDITION IS MET
   12 IEXIT=1
      If (IEXIT-1)4,13,4
   13 PRT=PRT+TBTXPR
      ENERGY= BHT*(ADC + L*WDC)*time*3600
      WMCN=2.01
      WMCNWB=WMCN/(1+WMCN)
      WMAVEWB=WMAVE/(1+WMAVE)
      WATER =HFG*WT*(WMCNWB - WMAVEWB)/(1 - WMAVEWB)
      ETAD = (WATER/ENERGY)*100.
      HSSTAR=(HR2*(2501+1.805*(TAIN-273.15)-4.186*T2WB)
     $    +(TAIN-T2WB-273.15))/(2501-2.381*T2WB)
      write(*,*)HSSTAR
      HIN = HR(J,1)
      W_t=WT*(WMCN-WMAVE)/(1+WMCN)
      PICKUP_E= (W_t/(MFDOT*TIMA*3600*(HSSTAR-HIN)))*100.
      write(6, 212) time,PNCOND,PKAB,WMAVE,ENERGY,WATER,ETAD,PICKUP_E
      write(1,212)time,PNCOND,PKAB,WMAVE,ENERGY,WATER,ETAD,PICKUP_E
      WRITE(6,218)time,WMAVE,TAMEAN,TMMEAN,ETAD,PICKUP_E,ETACIN,TAIN,
     $         RH2
      write(1, 213), (TAIR(I,2),I=1,NL1,NDIBO)
      write(6, 213), (TAIR(I,2),I=1,NL1,NDIBO)
      write(1, 214), TM(1),(TM(I),I=NDIBO,NL,NDIBO)
      write(6, 214), TM(1),(TM(I),I=NDIBO,NL,NDIBO)
      write(1, 215), WMC(1),(WMC(I),I=NDIBO,NL,NDIBO)
      write(6, 215), WMC(1),(WMC(I),I=NDIBO,NL,NDIBO)
      write(1, 216), (RH(I),I=1,NL1,NDIBO)
      write(6, 216), (RH(I),I=1,NL1,NDIBO)
      write(1,217), (HR(I,2),I=1,NL1,NDIBO)
      write(6,217), (HR(I,2),I=1,NL1,NDIBO)
      WRITE(2,218) time,WMAVE,TAMEAN,TMMEAN,ETAD,PICKUP_E,ETACIN,
     $         TAIN,RH2
      IF ((WMAVE.LT.WMEND).OR.(time.GT.TTP)) THEN
      STOP
      ELSE
      WMC(1) = WMAVE
      GO to 14
      end if
   14 CONTINUE
*****************************FORMAT*****************************************
  211 FORMAT(11H DEPTH    6F8.2)
  212 FORMAT(F8.3,2X,F8.3,2X,F8.4,3X,F8.4,2X,F10.1,2X,F9.1,2X,F6.2,1X,
     $         F6.2)
  213 FORMAT(11H AIR TEMP  6F8.3)
  214 FORMAT(11H PROD TEMP 1F7.3,5F8.3)
  215 FORMAT(11H MC DB     1F7.3,5F8.3)
  216 FORMAT(11H REL HUM   6F8.3)
  217 FORMAT(11H ABS HUM   6F8.5)
  218 FORMAT(F8.3,1X,F8.3,1X,F8.3,1X,F8.3,1X,F8.3,1X,F8.5, 1X,F7.3,
     $      1X,F7.3,1X,F7.3   )
      END
*****************************************************************************
      SUBROUTINE SAH (TF,TA,W,AC,DEPTH,P,Q,TF1OIN,TF2OIN,RH2,BHT,HR2,
     $ m1,m2,m,v1sin,v2sin,etacin,rh1,T2WB)
      integer ndim
      parameter(ndim=2000)
      DOUBLE PRECISION TF,TA,TP,TB,TC,M,RH1,RHN,HR2,BHT,T2WB
      DOUBLE PRECISION M1,M2,TF1OIN,TF2OIN,V1SIN,V2SIN
      DOUBLE PRECISION V1S(ndim),V2S(ndim),TF1O(ndim),TF2O(ndim)
      DOUBLE PRECISION AONE,ATWO,CP1,CP2,CPM,RHO1,RHO2,S1,S2,W
      double precision ac,DEPTH,p,q,tf1in,tf2in,DELTAY,ETACIN,RH2
      external sychart,getfur
********OPEN (UNIT=3, STATUS= 'new',FILE='chL3.DAT')***************
        J=0
      DO 6, J=1,1
      WRITE (*,*) 'INPUT THE AMBIENT TEMPERATURE TA:='
      READ (*,*) TA
     CALL GETFUR (ndim,V1S,V2S, TF1O, TF2O,S1,S2,W,TF1IN, TF2IN,TA,
    $ V1SIN,V2SIN,AC,DEPTH,P,Q,DELTAY,ETACIN,TP,TB,TC,BHT,TF,RH2,
```

```
$ M1,M2,M,RH1,RHN)
 TF1OIN = TF1IN
 TF2OIN = TF2IN
 W = SQRT(AC/Q)
 S1 = DEPTH*P/(P+1)
 S2 = DEPTH/(P+1)
CPM = 0.0098*(TF1OIN + TF2OIN)/2 + 1003.8
RHO1 = -0.0038*TF1OIN + 2.318
WRITE(*,*)'RHO1:=',RHO1,'kg/m^3'
RHO2 = -0.0038*TF2OIN + 2.318
WRITE(*,*)'RHO2:=',RHO2,'kg/m^3'
CP1 = 0.0098*TF1OIN+ 1003.8
WRITE(*,*)'CP1:=',CP1,'J/kg K'
CP2 = 0.0098*TF2OIN + 1003.8
WRITE(*,*)'CP2:=',CP2,'J/kg K'
AONE = S1*W
   ATWO = S2*W
   M1 = RHO1*AONE*V1SIN
   WRITE(*,*)'M1:=',M1,'kg/s'
   M2 = RHO2*ATWO*V2SIN
   WRITE(*,*)'M2:=',M2,'kg/s'
   M  = M1 + M2
    WRITE (*,*)'M:=',M,'kg/s'
   TF=((M1*CP1*TF1OIN+M2*CP2*TF2OIN)/((M1+M2)*CPM))
C--- calling sychart now------hobina---
   RH2=0.0
   call sychart(tf, TA,RH2,RH1,RHN,HR2,T2WB)
    WRITE(*,*)'TF:=',TF,'K'
    write(6,*)'tf1 in=',tf1 in
   WRITE(1,50)tf,etacin,p,q,ac,deltay,depth,tf1 in,tf2in,v1sin,v2sin,
  $ m1,m2,rh2,rh,rh1,rhn
 50  FORMAT (17(F8.3))
  6  continue
   END
C**********************************************************************
   SUBROUTINE GETFUR(ndim,V1S,V2S,TF1O,TF2O,S1,S2,W,TF1IN,TF2IN,TA,
  $  V1SIN,V2SIN,AC,DEPTH,P,Q,DELTAY,ETACIN,TP,TB,TC,BHT,TF,RH2,
  $  M1,M2,M,RH1,RHN)
integer ndim
DOUBLE PRECISION L,DELTAY,ETACIN,SBARC,SBARP,BHT,X,CA,V1S,V2S
DOUBLE PRECISION PHI1,PHI2,PHI3,PHI4,MDOT1S,MDOT2S,Q,TA,Y
DOUBLE PRECISION FF1, FF2,K1,K2,TF1O,TF2O,W,S1,S2,MDOT1,MDOT2
double precision v1sin,v2sin,ac,DEPTH,p,tf1in,tf2in,TF,RH2
double precision FACT1, FACT2,TP,TB,TC,RHOA,RHOINC1,RHOINC2
double precision M1,M2,M,RH1,RHN,FACT
INTEGER NTX
DIMENSION TF1O(ndim),TF2O(ndim),V1S(ndim),MDOT2S(2000),ETAC(2000)
DIMENSION X(2000),QU(2000),V2S(2000),MDOT1S(2000),Y(500)
PARAMETER (K1=2.0,K2=0.20,BETA=0.1135)
PARAMETER (FACT=0.2)
CA = 0.0098*TA + 1003.8
 RHOA= -0.0038*TA + 2.318
WRITE (*,*) 'INPUT THE VALUE OF Q:='
READ (*,*) Q
WRITE (*,*) 'INPUT THE VALUE OF AC:='
READ (*,*) AC
WRITE (*,*) 'INPUT THE VALUE OF DELTAY:='
READ (*,*) DELTAY
WRITE (*,*) 'INPUT THE VALUE OF DEPTH:='
READ (*,*) DEPTH
 WRITE (*,*) 'INPUT THE VALUE OF P:='
 READ (*,*) P
 CALL RADTNA(SBARC,SBARP,BHT)
 CALL GETSIX(PHI1,PHI2,PHI3,PHI4,MDOT1,MDOT2,L,W,TF1IN,TF2IN,TA,
$DEPTH,AC,P,Q,DELTAY,v1sin,v2sin,etacin,tf,rh2,tp,tb,tc,BHT)
 TF1IN = TA
 TF2IN = TA
 Y0 = 0
 L = SQRT(Q*AC)
 W = SQRT(AC/Q)
 S1 = DEPTH*P/(P+1)
 S2 = DEPTH/(P+1)
 NTX = NINT(L/DELTAY)
 WRITE (*,*)'NTX:=',NTX
```

```
      WRITE (6,21)
      DO 18 I=1,NTX
            Y(I) = Y0 + DELTAY
            X(I)= AC/Y(I)
      TF1O(I) = (1/(2 -PHI1*DELTAY))*((PHI1*DELTAY +2)*TF1IN
     $       + 2*PHI2*DELTAY)
       TF2O(I) =(1/(2 - PHI3*DELTAY))*((PHI3*DELTAY +2)*TF2IN
     $       + 2*PHI4*DELTAY)
      DH1    = 2*W*S1/(W + S1)
      DH2    = 2*W*S2/(W + S2)
      RHOINC1 = (-0.0038*(TA + 6) + 2.3180)
      RHOINC2 = (-0.0038*(TA + 3.6) + 2.3180)
      FF1= 1./(4*LOG10(K1/(3.7*1000*DH1))**2)
      FF2= 1./(4*LOG10(K2/(3.7*1000*DH2))**2)
      If (AC.LE.2.7) THEN
       FACT1 = 1.22
       FACT2 = 1.31
       V1S(I)=SQRT((DH1*16.445*1.29143*RHOA*SIN(1.0*BETA)*(TF1O(I)-TA))
     $     /(FF1*RHOINC1*(1.8*TF1O(I) + 1.8*(7./13)*TA -460)))*FACT1
       V2S(I)=SQRT((DH2*16.445*1.29143*RHOA*SIN(1.0*BETA)*(TF2O(I)-TA))
     $     /(FF2*RHOINC2*(1.8*TF2O(I) +1.8*(7./13)*TA - 460)))*FACT2
       MDOT1S(I) = RHOINC1*S1*W*V1S(I)
       MDOT2S(I) = RHOINC2*S2*W*V2S(I)
       END IF
       IF (AC.GE.2.8) THEN
       FACT2=0.230
       V1S(I)=SQRT((DH1*16.445*1.29143*RHOA*SIN(1.0*BETA)*(TF1O(I)-TA))
     $/(FF1*RHOINC1*(1.8*TF1O(I) + 1.8*(7./13)*TA -460)))*FACT
       V2S(I)=SQRT((DH2*16.445*1.29143*RHOA*SIN(1.0*BETA)*(TF2O(I)-TA))
     $/(FF2*RHOINC2*(1.8*TF2O(I) +1.8*(7./13)*TA - 460)))*FACT2
       MDOT1S(I) = RHOINC1*S1*W*V1S(I)
       MDOT2S(I) = RHOINC2*S2*W*V2S(I)
       END IF
C***** CALCULATION OF THE EFFICIENCY OF THE AIR HEATER
       QU(I) = MDOT1S(I)*CA*(TF1O(I)-TA) + MDOT2S(I)*CA*(TF2O(I)-TA)
       ETAC(I) = (QU(I)/(BHT*Y(I)*X(I)))*100.
       TF1IN = TF1O(I)
       TF2IN = TF2O(I)
       Y0 = Y(I)
       WRITE(6,'(3(F7.3,4X),**4(**F7.3,4X))')Y(I),X(I),TF1O(I),
     $     TF2O(I),ETAC(I),V1S(I),V2S(I)
 21    FORMAT('LENGTH',6X,'WIDTH',4X,'TEMP(1)',4X,
     $   'TEMP(2)',5X,'EFFICIENCY',5X,'V1',9X,'V2')
 18    CONTINUE
       write(6,*)'tf1 in = ',tf1 in
       V1SIN = V1S(NTX)
       V2SIN = V2S(NTX)
       ETACIN = ETAC(NTX)
       END
C*************************************************************************
       SUBROUTINE RADTNA (SBARC,SBARP,BHT)
C     THIS SUBROUTINE PREDICTS  PROGRAM THE SOLAR  RADIATION INCIDENT ON A  SLOPED  SURFACE PER UNIT
C     TIME AS WELL AS  SOLAR RADIATION ABSORBED BY THE COVER AND THE ABSORBER PLATE
      DOUBLE PRECISION SIE,BNOT,TITA,TAUAFAB,TAUGS,TAUDS
      DOUBLE PRECISION ALFAC,PIE,GSC,D,APP,RBARPRM,BETA
      DOUBLE PRECISION SBARP,SBARC,RKTBAR,BNBAR,OMGASP,B
      DOUBLE PRECISION OMEGAS,MEGSPP,HDHBAR,RHOG,PHI,DELTA,ALFADS,A
      DOUBLE PRECISION HBARNT,BPP,N,SNBAR,ALFAN,TAUAFN
      DOUBLE PRECISION RNUM1,RNUM2, RNUM3,RNUM4,RNUM5,RECON
      DOUBLE PRECISION TERM1,TERM2, TERM3, TERM4,BHT,ALFAGS
      DOUBLE PRECISION RNUMA,RNUMB,RNUMC,RNUMD,RNUME,NDS
      PARAMETER (SIE = 0.96, APP=0.249,RHOG =0.2,BETA=0.1135,PHI=0.1135,
     $ BPP=0.447,BNOT = -0.1, PIE= 3.142,TAUAFN=0.854,TAUDS=0.74,
     $ ALFAC=0.12,TAUGS=0.74,TITA=1.0471,ALFAN=0.88,
     $ RECON =0.968, NDS=11.0,N=5.0,GSC=1367,SNBAR=290)
C       COMPUTE DECLINATION
      DELTA = 23.45 * SIN(2*PIE*(284. + SNBAR)/365.)*PIE/180.
C       COMPUTE SUNSET HOUR ANGLE ON HORIZONTAL AND TILTED SURFACES
      OMEGAS= ACOS(-TAN(PHI)*TAN(DELTA))
      MEGSPP= ACOS(-TAN(PHI- BETA)* TAN(DELTA))
       IF (OMEGAS .GT. MEGSPP) THEN
         OMGASP = MEGSPP
       ELSE
         OMGASP = OMEGAS
```

```
      END IF
C       CALCULATE A, B, D, BNBAR,RKTBAR
      A    = 0.409 + 0.5016*SIN(OMEGAS - 60.*PIE/180.)
      B    = 0.6609 - 0.4767*SIN(OMEGAS - 60.*PIE/180.)
      D    = SIN(OMEGAS) - OMEGAS*COS(OMEGAS)
      BNBAR = 2./15.*(OMEGAS*180./PIE)
      RKTBAR= APP + BPP*NTBNBAR
C       CALCULATE HBARNT
      TERM1 = 1 + 0.033*COS(2*PIE*SNBAR/365.)
      TERM2 = COS(PHI)*COS(DELTA)*SIN(OMEGAS)
      TERM3 = OMEGAS*SIN(PHI)*SIN(DELTA)
      TERM4 = 24.*3600.*GSC/PIE
      HBARNT = TERM4*TERM1*(TERM2 + TERM3)
      WRITE(*,*)'HBARNT:=',HBARNT,'J/M^2'
C       COMPUTE HDHBAR
      IF ((OMEGAS.LE.81.4).AND.((RKTBAR.GE.0.3)
     $       .AND.(RKTBAR.LE.0.8))) THEN
        HDHBAR=(1.391 - 3.560*RKTBAR + 4.189*RKTBAR**2
     $       - 2.137*RKTBAR**3)
      ELSE
        HDHBAR=(1.311 - 3.022*RKTBAR + 3.427*RKTBAR**2
     $       - 1.821*RKTBAR**3)
      END IF
C   CALCULATION OF ABSORPTANCE OF DIFFUSE AND GROUND-REFLECTED RADIATION
      ALFADS= (1. + 2.3045E-3*TITA - 1.990E-4*TITA**2
     $       + 5.324E-6*TITA**3 - 4.799E-8*TITA**4)*ALFAN
      ALFAGS= (1.+ 2.3045E-3*TITA - 1.990E-4*TITA**2
     $       + 5.324E-6*TITA**3 - 4.799E-8*TITA**4)*ALFAN
C   CALCULATION OF TRANSMITTANCE-ABSORPTANCE PRODUCT OF DIRECT RADIATION
      TAUAFAB= (1. + BNOT*(1/COS(TITA) - 1.))*TAUAFN
C       COMPUTE RBARPRM
      RNUM1 = COS(PHI - BETA)/(D*COS(PHI))
      RNUM2 = SIN(OMGASP) - OMGASP*COS(MEGSPP)
      RNUM3 = OMGASP + SIN(OMGASP)*COS(OMGASP)
     $     -(2.*COS(MEGSPP))
      RNUM4 = HDHBAR*(1. + COS(BETA))*0.5*1.01*TAUDS*ALFADS
      RNUM5 = RHOG*1.01*TAUGS*ALFAGS*0.5*(1. + COS(BETA))
      RBARPRM=RNUM1*((A-HDHBAR)*RNUM2+B*0.5*RNUM3)*TAUAFAB+RNUM4+ RNUM5
C       COMPUTE MONTHLY-AVERAGE ABSORBED RADIATION BY THE ABSORBER
      SBARP = RECON*SIE*RKTBAR*RBARPRM*HBARNT/(NDS*3600.)
C       COMPUTE MONTHLY-AVERAGE ABSORBED RADIATION BY THE COVER
      RNUMA = COS(PHI - BETA)/(D*COS(PHI))
      RNUMB = SIN(OMGASP) - OMGASP*COS(MEGSPP)
      RNUMC = OMGASP + SIN(OMGASP)*(COS(OMGASP) - 2.*COS(MEGSPP))
      RNUMD = HDHBAR*(1. + COS(BETA))*0.5
      RNUME = RHOG*0.5*(1. + COS(BETA))
      RBAR=RNUMA*((A-HDHBAR)*RNUMB + B*0.5*RNUMC) + RNUMD + RNUME
      SBARC = RECON*RBAR*RKTBAR*HBARNT*ALFAC/(NDS*3600.)
C       COMPUTE AVERAGE MONTHLY RADIATION INCIDENT ON THE AIR HEATER
       BHT =RECON*RBAR*RKTBAR*HBARNT/(NDS*3600)
      WRITE (6,91)
      WRITE(6,'(6(F8.5,4X))')DELTA,A,B,D,TAUAFAB,OMEGAS
 91   FORMAT(' ','DELTA',8X,'A',11X,'B',10X,'D',10X,'TAUAFAB'
     $      ,6X,'OMEGAS')
      WRITE(6,92)
      WRITE(6,'(7(F8.5,2X))')RNUM1,RNUM2,RNUM3,RNUM4,RNUM4,ALFADS,
     $   ALFAGS
 92   FORMAT(' ','RNUM1',5X,'RNUM2',4X,'RNUM3',5X,'RNUM4',6X,
     $  'RNUM5',4X,'ALFADS',5X,'ALFAGS')
      WRITE(6,93)
      WRITE(6,'(2(F8.4,2X)," "2(E12.4,2X))')TERM1,TERM2,TERM3,TERM4
 93   FORMAT(' ', 'TERM1',6X,'TERM2',7X,'TERM3',9X,'TERM4')
     WRITE(6,23)
     WRITE(6,'(2(F5.3,5X)," ",E12.6,"      ",2(F5.3,6X))')RBARPRM,
     $    HDHBAR,HBARNT,RBAR,RKTBAR
 23   FORMAT('RBARPRM',3X,'HDHBAR',9X,'HBARNT',10X,'RBAR'
     $      ,7X,'RKTBAR')
     WRITE (6,55)
     WRITE(6,'(3(F7.3,5X))')SBARC,SBARP,BHT
 55   FORMAT(' ','SBARC',6X,'SBARP',8X,'BHT')
      RETURN
     END
```

```
*****************************************************************
      SUBROUTINE GETSIX(PHI1,PHI2,PHI3,PHI4,MDOT1,MDOT2,L,W,TF1IN,TF2IN,
     $ TA,DEPTH,AC,P,Q,DELTAY,v1sm,v2sm,tf,rh2,etacin,tp,tb,tc,BHT)
C*** PROGRAM PREDICTS THE AIR FLOW-RATE AND TEMPERATURE AT OUTLET SECTION
*    OF THE COLLECTOR AS WELL THE PLATE, COVER AND BOTTOM PLATE
*    TEMPERATURES. PROGRAM  ALSO ESTIMATES THE HEAT TRANSFER COEFFICIENTS
      integer i
      DOUBLE PRECISION TF2O,TF1O,TF1IN,TF2IN,RHOINC1,RHOA,CA,V1,S1,S2
      DOUBLE PRECISION V2,MDOT1,MDOT2,AR1,AR2,UE1,UE2,UB,VW,KVISTA,H1,H2
      DOUBLE PRECISION H3,H4,KVIST1,KVIST2,XSTAR,HRCS,HRPB,HRPC,HW,XINS
      DOUBLE PRECISION KINS,TS,TC,TP,DELTAY,TF1,TF2,RA2,KB,XB,PHI4
      DOUBLE PRECISION W,L,BETA,TA,FSLONP,FSLONC,FSLONB,SIGMA,NU1,NU2
      DOUBLE PRECISION GAMMA1,GAMMA2,GAMMA3,LAMDA1,LAMDA2,E,A1,B1,C1
      DOUBLE PRECISION D1,E1,F1,A2,B2,D2,E2,F2,A3,B3,D3,PHI1,PHI2,PHI3
      DOUBLE PRECISION T1,T2,BPRMT1,BPRMT2,RA1,GEE1,PR1,PR2,KTA,KT1,KT2
      DOUBLE PRECISION TF1PRMO,TF2PRMO,RHOAPRM,FA,P,Q,GPS,FF1,SBARC
      DOUBLE PRECISION LPRM,HB,RHOINC2,FF2,SBARP,K1,K2,BHT,DEPTH,ac,FACT
      double precision FACT1,FACT2,v1sm,v2sm,etacin,rh2
      double precision TB
      PARAMETER (SIGMA = 5.67E-8, FSLONP = 0.96,
     $ HB=13,
     $ FSLONC = 0.94,FSLONB = 0.93,
     $ KINS = 0.17 , XINS = 0.02,VW=0.01,
     $ PR1=0.704,PR2=0.704,K2=0.20,
     # KB=0.12,XB=.012,G=9.81,BETA=0.1135,PHI=0.1135,K1=2.0,FACT=0.2)
      GPS=0.0
C****   GUESS VALUES OF ABSORBER PLATE, COVER AND BOTTOM PLATE TEMPERATURES
C****         AND MASS FLOW RATES****
      WRITE (*,*) 'INPUT INITIAL OR GUESSED VALUE OF TP:='
      READ (*,*) TP
      WRITE (*,*) 'INPUT INITIAL OR GUESSED VALUE OF TB:='
      READ (*,*) TB
      WRITE (*,*) 'INPUT INITIAL OR GUESSED VALUE OF TC:='
      READ (*,*) TC
      WRITE (*,*) 'INPUT INITIAL VALUE OF MDOT1:='
      READ (*,*) MDOT1
      WRITE (*,*) 'INPUT INITIAL VALUE OF MDOT2:='
      READ (*,*) MDOT2
      CA = 0.0098*TA + 1003.8
      RHOA = -0.0038*TA + 2.318
C****   EVALUATION OF THE BACK AND EDGE LOSS HEAT TRANSFER COEFFICIENTS ***
       I = 0
  101 IF (I.LT.100) THEN
      W = SQRT(AC/Q)
      L = SQRT(Q*AC)
      S1 = DEPTH*P/(P + 1)
      S2 =DEPTH/(P + 1)
      UE1   = 2*(((KINS/XINS)*S1)/W)
      UE2   = 2*(((KINS/XINS)*S2)/W)
      UB    = 1./(XB/KB + 1./HB)
C****   EVALUATION OF THE DEPTH ASPECT RATIOS ****
      AR1   = L/S1
      AR2   = L/S2
C****   EVALUATION OF WIND HEAT TRANSFER COEFFICIENT ****
      KTA = (0.0732*TA +  4.1672)/1000.
      KVISTA = (0.0942*TA +  2.3180)/1000000.
      RE    = VW*L/KVISTA
      HW    = (KTA/L)*(75. + 0.42*RE**0.6)
C****   EVALUATION OF FREE CONVECTION TRANSFER COEFFICIENTS ****
      CA = 0.0098*TA + 1003.8
      RHOA=-0.0038*TA + 2.318
      XSTAR = S1*W/(2*(S1 + W))
      T1    = (TP + TC)/2.
      T2    = (TP + TB)/2.
      BPRMT1 = 1/T1
      BPRMT2 = 1/T2
      KVIST2 = (0.0942*(TA + 3.6) + 2.3180)/1000000.
      KVIST1 = (0.0942*(TA + 6) + 2.3180)/1000000.
      RA1   = G*BPRMT1*(TP - TC)*S1**3.*PR1/KVIST1**2.
      GEE1  = 1708/(COS(PHI)*RA1)
      TERMF = 1. - (GEE1*SIN(1.8*BETA)**1.6)
       IF (GEE1.GE.1) THEN
         TERMG= 0
       ELSE
```

```
      TERMG = 1. - GEE1
     END IF
    TERMH = ((RA1*COS(BETA)/5830)**1./3 - 1)
    IF (TERMH.LE.0) THEN
     TERM = 0
    ELSE
     TERM = TERMH
    END IF
IF (AR1.LT.12) then
     H2 = 0.54*(RA1*COS(BETA))**0.25
    END IF
   IF (AR1.GT.12) THEN
    IF ((BETA .GT. 0).AND.( BETA.LE.60)) THEN
      KT1 = (0.0732*(TA + 11) + 4.1672)/1000.
      H2 = (4*KT1/S1)*((1+(1.44*TERMF*TERMG)+TERM))
     IF (H2.GT.20) THEN
      H2=20
     END IF
    END IF
   END IF
   RA2  = G*BPRMT2*(TP - TB)*(S2**3)*PR2/(KVIST2**2)
   GEE2  = 1708/(COS(PHI)*RA2)
   TERMI = 1 - GEE2*SIN(1.8*BETA)**(1./6)
   TERMK = (RA2*COS(BETA)/5830)**(1./3) - 1
   IF (AR2.GT. 12) THEN
    IF ((BETA.GT.0).AND. (BETA.LE.60)) THEN
      KT2 =(0.0732*(TA + 6) + 4.1672)/1000.
      H4 = (1*KT2/S2)*((1 + (1.44*TERMI*(ABS(TERMK) + TERMK)/2)
$       + (ABS(TERMK) + TERMK)/2))
     END IF
    END IF
   KT1 = (0.0732*(TA + 11) + 4.1672)/1000.
   GRT1  = (G*BPRMT1*(TP - TC)*L**3)/(KVIST1**2)
    H1 = (2.*KT1/L)*0.54*((GRT1*PR1*COS(BETA))**(1./3))
   KT2 =(0.0732*(TA + 6) + 4.1672)/1000.
   GRT2  = (G*BPRMT2*(TP - TB)*L**3)/(KVIST2**2)
    H3 = (1.*KT2/L)*0.135*((GRT2*PR2*COS(BETA))**(1./3))
    IF (AR2.LT.12) THEN
     H4 = 0.15*(RA1*COS(BETA))**0.25
     END IF
C****   EVALUATION OF RADIATION TRANSFER COEFFICIENTS ****
     TS   = 0.0552* TA**1.5
     HRPC  = SIGMA*(TP**2 + TC**2)*(TP + TC)/(1/FSLONP + 1/FSLONC -1)
     HRPB  = SIGMA*(TP**2 + TB**2)*(TP + TB)/(1/FSLONP + 1/FSLONB -1)
     HRCS  = SIGMA*FSLONC*(TC**2 + TS**2)*(TC + TS)
C**** ESTIMATION OF THE AIR TEMPERATURE AT THE OUTLET OF THE COLLECTOR ****
     CALL RADTNA (SBARC,SBARP,BHT)
     TF1IN = TA
     TF2IN = TA
     E    = HRCS + HW + H1 + HRPC
     FA    = UB + HRPB + H4
     A1    = H3 + H2 + HRPB - HRPB**2/FA + HRPC - HRPC**2/E
     B1    = H2 + HRPC*H1/E
     C1    = H3 + HRPB*H4/FA
     D1    = HRPB*UB/FA + HRPC*HW/E
     E1    = HRPC*HRCS/E
     F1    = HRPC/E
     A2    = W*(H2 + H1*HRPC/E)
     B2    = W*(H2 + H1 - H1**2/E + UE1*S1/W)
     D2    = W*(H1*HW/E + UE1*S1/W)
     E2    = W*(H1*HRCS/E)
     F2    = W*(H1/E)
     A3    = W*(H3 + H4*HRPB/FA)
     B3    = W*(H3 + H4 - H4**2/FA + UE2*S2/W)
     D3    = W*( H4*UB/FA + UE2*S2/W)
     GAMMA3 = D1*TA + E1*TS + F1*SBARC + SBARP
     GAMMA2 = (1/(MDOT2*CA))*((A3*D1/A1 + D3)*TA + A3*E1/A1*TS
$       + A3*F1/A1*SBARC + A3/A1*SBARP)
     GAMMA1 = (1/(MDOT1*CA))*((A2*D1/A1 + D2)*TA + (A2*E1/A1 + E2)*TS
$       +(A2*F1/A1 + F2)*SBARC + A2/A1*SBARP)
     LAMDA1 = (1/(MDOT1*CA))*(A2*B1/A1 - B2)
     LAMDA2 = (1/(MDOT2*CA))*( A3*B1/A1)
     NU1   = (1/(MDOT1*CA))* (A2*C1/A1)
     NU2   = (1/(MDOT2*CA))*(A3*C1/A1 - B3)
```

```
      PHI1  = LAMDA1 - NU1*B1/C1
      PHI2  = NU1*A1/C1*TP - NU1*GAMMA3/C1 + GAMMA1
      PHI3  = NU2 - LAMDA2*C1/B1
      PHI4  = LAMDA2*A1/B1*TP-LAMDA2*GAMMA3/B1+GAMMA2
      TF1O  = (1/(2 - PHI1*DELTAY))*((PHI1*DELTAY + 2)*TF1IN
     $      + 2*PHI2*DELTAY)
      TF2O  = (1/(2 - PHI3*DELTAY))*((PHI3*DELTAY + 2)*TF2IN
     $      + 2*PHI4*DELTAY)
C**** ESTIMATION OF THE COVER, THE ABSORBER PLATE AND BOTTOM PLATE
C     TEMPERATURES ****
      TP2  = TP
      TB2  = TB
      TC2  = TC
      TF1IN = TA
      TF2IN = TA
      TF1  = (TF1IN + TF1O)/2
      TF2  = (TF2IN + TF2O)/2
       IF (AC.LE.2.7) THEN
       CTP = 1.04
       CTB = 0.958
       CTC = 1.03
      TP   = (CTP/A1)*(B1*TF1 + C1*TF2 + GAMMA3)
      TC   = CTC/(HRCS + HW + H1 + HRPC )* (SBARC + HRPC*TP + H1*TF1
     $     + HW*TA + HRCS*TS)
      TB   = CTB/(UB + HRPB + H4) * ( UB*TA + HRPB*TP + H4*TF2)
      END IF
        IF (AC.GE.2.8) THEN
          CTP = 1.0
          CTB = 1.0
          CTC = 1.02
      TP   = (CTP/A1)*(B1*TF1 + C1*TF2 + GAMMA3)
      TC   = CTC/(HRCS + HW + H1 + HRPC )* (SBARC + HRPC*TP + H1*TF1
     $     + HW*TA + HRCS*TS)
      TB   = CTB/(UB + HRPB + H4) * ( UB*TA + HRPB*TP + H4*TF2)
      END IF
C**** TEST FOR CONVERGENCE OF TB, TP AND TC
      IF ((TP - TP2).GT.1.0E-3) THEN
       IF ((TB - TB2) .GT.1.0E-3) THEN
        IF ((TC - TC2) .GT.1.0E-3) THEN
         I = I + 1
         GO TO 101
        END IF
       END IF
      END IF
      IF (ABS(TP-TP2).LE.1.0E-3) THEN
        IF (ABS(TB - TB2).LE.1.0E-3) THEN
         IF (ABS(TC - TC2) .LE. 1.0E-3) THEN
         GO TO 108
         END IF
        END IF
      END IF
C**** CONVERSION OF METRIC UNITS TO IMPERIAL UNITS ****
 108 LPRM  = L*3.821
     TAPRM  = (9./5.*TA) - 460
     TF1PRMO= (9./5.*TF1O) - 460
     TF2PRMO= (9./5.*TF2O )- 460
     RHOAPRM= RHOA*1.96E-3
C**** EVALUATION OF AIR VELOCITY AND MASS FLOW RATE IN THE AIR-HEATER **
     TF1IN = TA
     TF2IN = TA
     MDOT1G = MDOT1
     MDOT2G = MDOT2
     DH1   = 2*W*S1/(W + S1)
     DH2   = 2*W*S2/(W + S2)
     RHOINC1 = (-0.0038*(TA + 6) + 2.3180)
     RHOINC2 = (-0.0038*(TA + 3.6) + 2.3180)
     FF1= 1./(4*LOG10(K1/(3.7*1000*DH1))**2)
     FF2= 1./(4*LOG10(K2/(3.7*1000*DH2))**2)
      If (AC.LE.2.7) THEN
     FACT1 = 1.22
     FACT2 = 1.31
     V1=SQRT((DH1*49.7*16.445*RHOAPRM*LPRM*SIN(BETA)*(TF1PRMO-TAPRM))
    $    /(FF1*L*RHOINC1*(TF1PRMO + 7./13*TAPRM ))) *FACT1
```

```
 V2=SQRT((DH2*49.7*16.445*RHOAPRM*LPRM*SIN(BETA)*(TF2PRMO-TAPRM))
$     /(FF2*L*RHOINC2*(TF2PRMO + 7./13*TAPRM)))*FACT2
 MDOT1 = RHOINC1*S1*W*V1
 MDOT2 = RHOINC2*S2*W*V2
  END IF
  IF (AC.GE.2.8) THEN
   FACT2=0.230
 V1=SQRT((DH1*49.7*16.445*2*RHOAPRM*LPRM*SIN(BETA)*(TF1PRMO-TAPRM))
$     /(FF1*L*RHOINC1*(TF1PRMO + 7./13*TAPRM ))) *FACT
 V2=SQRT((DH2*49.7*16.445*2*RHOAPRM*LPRM*SIN(BETA)*(TF2PRMO-TAPRM))
$     /(FF2*L*RHOINC2*(TF2PRMO + 7./13*TAPRM)))*FACT2
 MDOT1 = RHOINC1*S1*W*V1
 MDOT2 = RHOINC2*S2*W*V2
 END IF
  IF(ABS(MDOT1-MDOT1G).GT.1.0E-4) THEN
   IF (ABS(MDOT2-MDOT2G).GT.1.0E-4)THEN
    I =I+ 1
     GO TO 101
    END IF
   END IF
   IF (ABS(MDOT1-MDOT1G).LE.1.0E-4) THEN
    IF (ABS(MDOT2-MDOT2G).LE.1.0E-4) THEN
     IF (I.EQ.30) THEN
     GO TO 120
     END IF
    END IF
   END IF
  END IF
  WRITE (6,65)
  WRITE (6,'("",3(F8.3,1X)," "2(E12.4,1X)," " 2(F9.4,1X))')
 $   AR1,AR2,XSTAR,RA1,GEE1,TERM,TERMG
65  FORMAT(" ",'AR1',4X,'AR2',6X,'XSTAR',6X,'RA1',9X,'GEE1',9X,
 $     'TERM',8X,'TERMG')
  WRITE(6,75)
  WRITE(6,'("",F7.4," "3(E12.5,3X)," "F7.3)')TERMF,GRT1,
 $     GPS,GRT2,TS
75  FORMAT(" ",'TERMF',6X,'GRT1',11X,'GPS',14X,'GRT2',8X,'TS')
  WRITE(6,76)
  WRITE(6,'(" ",4(F7.3,3X)," "E10.4)')LPRM,TAPRM,TF1PRMO,
 $     TF2PRMO,RHOAPRM
76  FORMAT(" "'LPRM',6X,'TAPRM',6X,'TF1PRMO',2X,'TF2PRMO',
 $ 7X, 'RHOAPRM')
120 WRITE (6,27)
  WRITE(6,'("",8(F11.5,1X))')H1,H2,H3,H4,V1,V2,MDOT1,MDOT2
27  FORMAT(" "'H1',9X,'H2',6X,'H3',5X,'H4',6X,'V1',6X,'V2',6X,
 $     'MDOT1',3X,'MDOT2')
   WRITE(6,34)
   WRITE(6,'("",7(F7.3,1X))')HRPC,HRPB,HRCS,HW,UB,UE1,UE2
34  FORMAT (" "'HRPC',5X,'HRPB',4X,'HRCS',5X,'HW',6X,'UB',5X,
 $      'UE1',6X,'UE2')
   WRITE(6,44)
   WRITE (6,'("", 4(F11.5,3X))')PHI1,PHI2,PHI3,PHI4
44  FORMAT(" "'PHI1',5X,'PHI2',7X,'PHI3',3X,'PHI4')
   WRITE (6,54)
   WRITE(6,'(" " ,5(F7.3,3X))')TP,TB,TC,TF1O,TF2O
54  FORMAT (" " ,'TP',9X,'TB',8X,'TC',8X,'TF1O',6X,'TF2O')
  RETURN
  END
C    This sub-program estimates the psychrometric properties of the drying air at the inlet and outlet of the air-heater
  subroutine sychart(tf,TA,RH2,RH1,RHN,HR2,T2WB)
  double precision tf,TA,RH1,RHN,HR2
  DOUBLE PRECISION RH1, P1SV, P1V,H,A,B,C,D,V,F,G
  DOUBLE PRECISION T1DB, A1LF, T1DP, P,Q, R, S, Y, HR1, PATM
  DOUBLE PRECISION T1WB, FAKI,FOKI,W1STAR
  DOUBLE PRECISION A2LF,P2V, P2SV,T2DP, RH2, T2DB,T2WB
  DOUBLE PRECISION PWS1B,PWS2B,T1WBC,W2STAR,T1DPC,T2DPC
  DOUBLE PRECISION C8,C9,C10,C11,C12,C13,HFG1,HFG2
  DOUBLE PRECISION T1DBR,T2DBR,T1DBC,T2DBC
  PARAMETER(H=0.2210584739E8,A=-0.274055258361E5,
$ D=0.215321E-4, V=-0.462027E-8,F=0.241613E1,
$ G=0.121547E-2,PATM=1.0132E5,P=6.54,Q=14.526,
$ S=0.09486,Y=0.4569,R=0.7389,B=0.541894E2,
$ C = -0.451370E-1,C8=-5.8002206E3,C9=-5.516256,
$ C10=-4.8640239E-2,C11=4.1764768E-5,C12=-1.4452093E-8,
```

```
     $ C13=6.5459673)
C--- setting the passed valu of tf to t2db
      t2db=tf
      T1DB=TA
      WRITE (*,*) 'INPUT INITIAL VALUE OF T2WB='
      READ (*,*) T2WB
      WRITE (*,*) 'INPUT INITIAL VALUE OF T1WB:='
      READ (*,*) T1WB
       T1DBC = T1DB -273
        T2DBC = T2DB - 273
      WRITE (*,*) 'INPUT VALUE OF RH1:='
      READ (*,*) RH1
       T1DBR = T1DB*9/5
      FOKI = ((A+B*T1DBR+C*T1DBR**2+D*T1DBR**3+V*T1DBR**4)/
     $     (F*T1DBR-G*T1DBR**2))
      WRITE (*,*) 'FOKI:=',FOKI, 'F'
      FAKI = EXP(FOKI)
      PISV = H*FAKI
       WRITE (*,*) 'PISV:=',PISV,'N/m^2'
      PIV  = RH1*PISV
       WRITE (*,*) 'PIV', PIV, 'N/M^2'
      A1LF = LOG(PIV/1000)
      WRITE (*,*)'A1LF', A1LF,''
      T1DP = (P+Q*A1LF+R*A1LF**2+S*A1LF**3+Y*(PIV/1000)**0.1984)+273
       WRITE (*,*) 'T1DP:=', T1DP, 'K'
      HR1  = (0.6219*PIV)/(PATM-PIV)
       WRITE (*,*) 'HR1:=', HR1, 'kg_w/kg_a'
       T1DPC = T1DP - 273
C     ESTIMATION OF T1WBPRM
      I = 0
   12 IF (I.LT.50) THEN
     T1WBC=T1WB
     PWS1B=EXP(C8/(T1WBC+273) + C9+C10*(T1WBC+273)+
     $         C11*(T1WBC+273)**2+C12*(T1WBC+273)**3
     $      + C13*LOG(T1WBC+273))
     W1STAR = (0 62198*PWS1B)/(PATM - PWS1B)
     T1WB = (2501*(HR1-W1STAR)+(T1DB-273)*(1.805*HR1 + 1))
     $       /(1-2.381*W1STAR + 4.186*HR1)
      write(*,*) 't1wb',t1wb
      write(*,*)'-------'
      IF (T1WB GE.T1DBC) THEN
      T1WB = (T1DBC +T1DPC)/2
      END IF
      IF (T1WB.LE.T1DPC) THEN
       T1WB = (T1DBC+T1DPC)/2
      END IF
      IF ((T1WB.GE.T1DPC).AND.(T1WB.LT.T1DBC)) THEN
       T1WB=(T1DPC + T1DBC)/2
       END IF
     IF (ABS(T1WB-T1WBC).GT.4.0E-1) THEN
     I= I+1
     GO TO 12
    END IF
     END IF
    IF (ABS(T1WB-T1WBC).LE.4.0E-1) THEN
    GO TO 15
    END IF
 15  T1WBK = T1WB + 273
    WRITE (*,*) 'T1WBK:=',T1WBK,  'K'
   WRITE (*,*) 'T1DP:=',T1DP, 'K'
    WRITE (*,*) 'PWS1B:=',PWS1B,'N/m^2'
     IF ((T1WBK.GE.273).AND.(T1WBK.LT.339)) THEN
HFG1 =2502535.259 - 2385.764244*(T1WBK-338.72)
     END IF
     IF ((T1WBK.GE.339).AND.(T1WBK.LT.533)) THEN
HFG1 =SQRT(7.3291559780E12 - 1.5599596408E7*T1WBK**2)
 END IF
HR2  = HR1
 T2DBR = T2DB*9/5
P2V  = (PATM*HR2)/(HR2 + 0.6219)
 WRITE (*,*) 'P2V', P2V, 'N/M^2'
A2LF = LOG(P2V/1000)
 WRITE (*,*)'A2LF', A2LF,''
T2DP = (P+Q*A2LF+R*A2LF**2+S*A2LF**3+Y*(P2V/1000)**0.1984) + 273
```

```
      P2SV = H*EXP((A+B*T2DBR+C*T2DBR**2+D*T2DBR**3+V*T2DBR**4)/
     $     (F*T2DBR-G*T2DBR**2))
      RH2  = P2V/P2SV
      WRITE (*,*) 'RH2:=',RH2, 'decimals'
      RHN = RH2/RH1
      WRITE (*,*)'RHN:=',RHN,'decimals'
      T2DPC = T1DP - 273.15
C     Estimation of T2WBPRM
      J = 0
 24   IF (J.LT.10) THEN
      T2WBC=T2WB
      PWS2B=EXP(C8/(T2WBC+273) + C9+C10*(T2WBC+273)+
     $          C11*(T2WBC+273)**2+C12*(T2WBC+273)**3
     $      + C13*LOG(T2WBC+273))
      W2STAR = (0.62198*PWS2B)/(PATM - PWS2B)
      T2WB = (2501*(HR2-W2STAR)+(T2DB-273)*(1.805*HR2 + 1))
     $      /(1-2.381*W2STAR + 4.186*HR2)
       write(*,*) 't2wb',t2wb
      IF (T2WB.GE.T2DBC) THEN
      T2WB = (T2DBC +T2DPC)/2
       END IF
       IF (T2WB.LE. T2DPC) THEN
       T2WB = (T2DBC+T2DPC)/2
       END IF
       IF((T2WB.GE.T2DPC).AND.(T2WB.LT.T2DBC)) THEN
        T2WB = T2WB
        END IF
       write(*,*) 't2wb',t2wb
     IF (ABS(T2WB-T2WBC) GT.4.0E-1) THEN
     J= J+1
     GO TO 24
     END IF
      END IF
     IF (ABS(T2WB-T2WBC).LE.4.0E-1) THEN
     GO TO 36
     END IF
 36   T2WBK = T2WB +273
      WRITE (*,*) 'T2WBK:=',T2WBK,  'K'
      IF ((T2WBK.GE.273).AND.(T2WBK.LT.339)) THEN
     HFG2 =2502535.259 - 2385.764244*(T2WBK-338.72)
       END IF
      IF ((T2WBK.GE.339).AND.(T2WBK.LT.533)) THEN
     HFG2 =SQRT(7.3291559780E12 - 1.5599596408E7*T2WBK**2)
      END IF
      WRITE (*,*)'T2DP:=',T2DP,  'K'
      WRITE (*,*) 'PWS2B:=',PWS2B,  'N/M^2'
      WRITE (*,*)'HFG1:=',HFG1,    'J/kg'
      WRITE (*,*)'HFG2:=',HFG2,    'J/kg'
     END
```

Appendix B

LIST OF REFERENCES

ACHENBACH, P.R. and COLE, S.D. 1949. Performance of fourteen masonry chimneys under steady state conditions. *Trans. of* ASHVE, vol. 55, p.129-154.

AGRAWAL, Y.C. and SINGH, R.D. 1977. Thin layer drying studies for short grain rice. *ASAE Paper 77-3531. Am. Soc. Agric. Eng.*, St. Joseph, MI.

AKYURT, M. and SELCUK, M.K. 1973. A solar drier supplemented with auxiliary heating systems for continuous operation. *Solar Energy*, vol. 14, no. 3, p. 313-320.

ALAM, A. and SHOVE, G.C. 1973. Simulation of soybean drying. *Trans. am. Soc. agric. Engrs.*, vol. 16, no. 1, p.134-136.

ALANIS, E., SARAVIA, L., and ROVETTA, L. 1977. Measurement of rock pile heat transfer coefficients. *Solar Energy*, vol. 19, p.571-572.

AMOUZOU, K., GNIVINVI, M. and KERIM, B. 1986. Solar drying problems in Togo. In: *Proc. of a Workshop on Solar Drying in Africa* IDRC-255e, Senegal, Dakar, 21-24 July, 1986. (M.W. BASSEY, and O.G. SCHMIDT, eds.).

ANON, 1994. U.N. Statistical Yearbook 1994. (pub. 1996), 41st edition, United Nations, New York, p. 9.

ANON. 1962. *Wealth of India, Raw Materials.* vol. 6 (L-M), p.293-297. Coun. Sci. ind. Res., New Delhi. Quoted by Ingram and Humphries, 1972.

ARINZE, E.A., SCHOENAU, G. and BIGSBY, F.W. 1979 . Solar energy absorption properties of some agricultural products. *Paper No. 79-3071 of Joint Meeting of ASAE & CSAE*, Winnipeg, Monitoba.

ASHRAE !977. *Handbook and Product directory*:. *Fundamentals*: ASHRAE, Inc., Atlanta, USA.

ASHRAE 1993. *Fundamentals handbook*, ASHRAE Inc., Atlanta, USA

ASHRAE. 1989. *Fundamentals handbook* (SI edition). ASHRAE Inc., Atlanta, USA.

AYENSU, A. and ASIEDU BONDZIE. 1986. Solar drying with convective self-flow and energy storage. *Solar & Wind Technology*, vol. 3, no. 4, p.273-279.

BABBITT, J.D. 1949. Observations on the adsorption of water vapour by wheat. *Can. J. Res. Sec.* F. 27: 55-72.

BAKKER-ARKEMA, BROOK, R.C, and LEREW, L.E. 1978. Cereal grain drying. In *Advances in Science and Technology*, (Y. Pomeranz ed.), vol. 2. American Association of Cereal Chemists Incorporated, St. Paul, Minnesota, p. 1-90.

BAKKER-ARKEMA, F.W., BICKERT, W.G. and PATTERSON, R.J. 1967. Simultaneous Heat and Mass Transfer During the Cooling of a Deep Bed of Biological Products Under Varying Air Conditions. *J. agric. Engng. Res.*, vol 12, no. 4, p. 297-307.

BAKKER-ARKEMA, F.W., LEREW, L.E., DE BOER, S.F. and ROTH, M.G. 1974. Grain Dryer Simulation. *Farm Science:- Agricultural Experimental Station Research Report No. 224*, January 1974. Michigan State University, East Lansing.

BALA, B. K. 1983. Deep bed drying of malt. Unpubl. PhD Thesis, University of Newcastle Upon Tyne, England.

BALA, B.K. and WOODS, J.L. 1984. Simulation of Deep Bed Malt Drying. *J. agric. Engng. Res.*, vol. 30, p. 235-244.

BALA, B.K. and WOODS, J.L. 1994. Simulation of the Indirect Natural Convection Drying of Rough Rice. *Solar Energy*, vol. 53, no. 3, p. 259-266.

BALA, B.K. and ZIAUDDIN, A.T.M. 1990. Simulation of Solar Drying of Rough Rice. In: *Proceedings of Ist World Renewable Energy Congress* (A.A.M. Sayigh, ed.), 2, 938-942.

BARKER, J.J. 1965. Heat transfer in packed beds. *Ind. Engng. Chem.*, 57(4): 43-49.

BARRE, H.J. and HAMDY, M.Y. 1974. Optimal filling rates for in-storage drying. *Trans. ASAE*, vol. 17, no. 4, p.705-710.

BARRE, H.J., BAUGHMAN, G.R. and HAMDY, M.Y. 1971. Application of the logarithmic model to cross-flow bed grain drying. *ASAE*, vol. 14, p.1061-1064.

BASSEY, M.W. 1994. Using Heated Chimneys and Reduced Collector Air Gap Height to Improve the Performance of Indirect Passive Solar Dryers. *Solar Energy* 4, 2, 169-178.

BASSEY, M.W., WHITFIELD, M.J.C.C., and KOROMA, E.Y. 1986. Problems and solution for natural-convection solar crop drying. In: *Proc. of a Workshop on Solar Drying in Africa* IDRC-255e, Senegal, Dakar, 21-24 July, 1986. (M.W. BASSEY, and O.G. SCHMIDT, eds.).

BECKER, H.A. and SALLANS, H. R. 1956. A study of desorption isotherms of wheat at 25°C and 50°C. *Cereal Chem.*, vol. 33, no. 2, p. 79-91.

BLOOME, P. D. and SHOVE, G. C. 1971. Near Equilibrium Simulation of Shelled Corn Drying. *Transactions of the ASAE*, Vol. 14, No. 4, pp. 709-712.

BOINDI, P., CICALA, L. and FARINA, G. 1988. Performance Analysis of Air Heaters of Conventional Design. *Solar Energy* 41, 1, 101-107.

BOYCE, D.S. 1965. Grain moisture and temperature changes with position and time during through drying. *J. agric. Engng. Res.*, 10(4): 333-341.

BRAMHALL, G. 1979. Sorption diffusion in wood. *Wood Sci.* 12(1): 3-13.

BRANDEMUEHL, M.J. and BECKMAN, W.A. 1980. Transmission of diffuse radiation through CPC and flat plate collector glazing. *Solar Energy* 24(5): 511-513.

BRENNDORFER, B., KENNEDY, L., OSWIN BATEMAN, C.O., TRIM, D.S., MREMA, G.C. and WEREKO-BROBBY, C. 1987. *SOLAR DRYERS- their role in post-harvest processing.* London: Commonwealth Science Secretariat.

BROOKER, D.B., BAKKER-ARKEMA, F.W. and HALL, C.W. 1974. *Drying Cereal Grains.* Westport, Connecticut: AVI Publishing Co., Inc.

BROWN, W.G. and COLBORNE, W.G. 1956. Fundamentals of Chimney Performance. *Can. J. Tech.*, vol. 34, p.354-365.

BROWNE, D.A. 1962. Variation of bulk density of cereals with moisture content. *J. agric. Engng. Res.*, 7, 228-290.

BRUCE, J.M. 1978. Natural convection through openings and its application to cattle building ventilation. *J. agric. Engng. Res.*, 23, 151-167.

BUCHBERG, H., CATTON, I. and EDWARDS, D.K. 1974. Natural convection in enclosed spaces : review of applications to solar energy collection. *ASME Paper 74-WA/HT-12.*

BUNN, J.M., HENSON Jr., W.H. and WALTON, L.R. 1972. Drying equation for high moisture materials. *J. agric. Engng. Res.*, 17, 343-347.

CENGEL, Y.A. 1998. Heat transfer: a practical approach. McGraw-Hill Inc., Boston, USA.

CENKOWSKI, S., JAYAS, D.S. and PABIS, S. 1993 Deep-bed grain drying:- a review of particular theories. *Drying Technology*, 11(7), 1553-1581.

CHEEMA, L.S. 1978. Solar drying of cassava for alcohol production. ISES Congress, New Delhi, India, p. 1940-4.

CHHINNAN, M.S. 1984. Evaluation of selected mathematical models for describing thin-layer drying of in-shell pecans. *Trans. ASAE* 27, 610-619.

CHIANG, WIN-CHIN and PETERSEN, J.N. 1985. Thin-layer air drying of french fried potatoes. *Journal of Food Technology,* vol. 20, p.67-78.

CHINNAN, M.S. and YOUNG, J.H. 1977. A Study of diffusion equations describing moisture movement in peanut pods- I: comparison of vapour and liquid diffusion equations. *Trans. of ASAE* 20, 3, 539-546.

CHIRARATTANANON, S., CHINPORNCHAROENPONG, C. and CHIRARATTANANON, R. 1988. A steady-state model for the forced convection solar cabinet dryer. *Solar Energy*, vol. 41, no. 4, p.349-360.

CHIRIFE, J. 1971. Diffusional process in the drying of tapioca root. *Journal of Food Science* 36, 327-330.

CHIRIFE, J. and CACHERO, R.A. 1970. Through-circulation drying of tapioca root. *Journal of Food Science* 35, 364-368.

CHITTENDEN, D.H. and HUSTRULID, A. 1966. Determining drying constants for shelled corn. *Transactions of ASAE*, 9(1):52-55.

CHOI, Y and OKOS, M.R. 1986. Thermal properties of liquids foods-review. In: *Physical and Chemical properties of food.* (Edited by M.R. Okos), ASAE, pp 35-77.

CHUNG, D.S. and CONVERSE, H.H. 1971. Effect of moisture content on some physical properties of grains. *Trans. am. Soc. agric. Engrs.* 552-555.

CHUNG, D.S. and PFOST, H.B. 1967. Adsorption and desorption of water vapour by cereal grains and their products. Part I: Heat and free energy change of adsorption and desorption. *Trans. am. Soc. agric. Engrs.*, 10 (4), 549-551 and 555.

CHUNG, D.S. and PFOST, H.B. 1967. Adsorption and desorption of water vapour by cereal grains and their products. Part II: Development of the general isotherm equation. *Trans. am. Soc. agric. Engrs.*, 10 (4), 552-555.

CLARK, R.G. and LAMOND, W.J. 1968. Drying of wheat in 2ft beds. I. *J. agric. Engng. Res.*, vol. 13, no. 2, p. 141.

CLOSE, D.J. 1963. Solar Air Heaters for Low and Moderate Temperature Applications. *Solar Energy* 7, 3, 117-124.

COLBORNE, W.G. and MOFFATT, W.C. 1959. A Fundamental Analysis of Chimney Performance. *ASHRAE Journal*,1,3,55-60.

COLBOURN, A.P. 1933. A method of correlating forced convection heat transfer data and a comparison with fluid friction, *Inst. ch. Engrs.*, 29, 174-209.

COLLARES-PEREIRA, M and RABL, A. 1979. The average distribution of solar radiation - correlations between diffuse and hemispherical and between daily and hourly insolation values. *Solar Energy*, 22, 2, 155 - 164.

COOPER, P.I. (1969). The Absorption of Radiation in Solar Stills. *Solar Energy* 12, 3, 333-346.

CRANK, J. 1975. *The mathematics of diffusion*, 2nd Ed., Oxford University Press, Oxford.

DALY, B.B. 1992. *Woods Practical Guide to Fan Engineering.* 3rd edn. Ipswich, Suffolk: Woods of Colchester Limited, UK.

DANIELS, F. 1972. *Direct Use of the Sun's Energy.* (First Edition , Fourth Printing) New Haven and London, Yale University Press.

DAPAAH, S.K. 1991. *Evaluation of Post-production Systems for Cereals in Ghana.* Phase One Report Prepared for National Energy Board (now Ministry of Mines and Energy), Ghana, October, 1991.

DAY, D.L, and NELSON, G.L. 1965. Desorption isotherms for wheat. *Trans. am. Soc. agric. Engrs.*, vol. 8, no. (2), p.293-297.

DIAMANTE, L.M. and MUNRO, P.A. 1990. Water desorption isotherms of two varieties of sweet potato. *International of Food Science and Technology* 25, 140-147.

DIAMANTE, L.M. and MUNRO, P.A. 1991a. Mathematical modelling of the thin layer solar drying of sweet potato slices. *Solar Energy,* 2, 4, 271-276.

DIAMANTE, L.M. and MUNRO, P.A. 1991b. Mathematical modelling of hot Air drying of sweet potato slices. *Int. J. Food Science & Technology* 26, 99-109.

DIAMANTE, L.M. and MUNRO, P.A. 1993. Mathematical modelling of thin layer solar drying of sweet potato slices. *Solar Energy*, vol. 2, no. 4, p.271-276.

DIOUF, J. 1993. The right to food, Communication by the Director General of the F.A.O.

DOUGLAS, J.F.; GASIOREK, J.M.; SWAFFIELD, J.A. 1995. Fluid Mechanics, 3rd edition, Longman Scientific & Technical, Essex, England.

DOUGLAS, P.L., JONES, J.A.T, and MALLICK, S.K. 1994. Modelling and simulation of crossflow grain dryers. *Trans IChemE*, Vol. 72 Part I, 325-331.

DUFFIE, J.A. and BECKMAN, W.A 1991. *Solar engineering of thermal processes.* 2nd edition, John Wiley & Sons, Inc., New York, USA.

DUFFIE, J.A. and BECKMAN, W.A. 1974. *Solar energy thermal processes.* John Wiley & Sons, Inc., New York, U.S.A., pp. 76.

EKECHUKWU, O.C. 1987. Natural convection solar crop dryers, PhD thesis, Cranfield University, Bedford, England.

EKECHUKWU, O.V; NORTON, B. 1997. Design and measured performance of a solar chimney for solar-energy dryers, *Renewable Energy*, Vol. 10, No. 1, pp 81-90.

ELSAYED, M.M. 1990. Mathematical modelling of a thin layer solar kiln. *TRANS. ASME, J. Solar Energy Engng.* 12, 196-203.

ERBS, D.G., KLEIN, S.A. and DUFFIE, J.A. 1982. Estimation of the diffuse radiation fraction for hourly, daily and monthly-average global radiation. *Solar Energy*, 28, 4, 293-302.

EXELL, R.H.B. 1980. Basic Design Theory for a Simple Solar Rice Dryer. *Renewable Energy Review Journal* 1, 2, 1-14.

EZEKWE, C.I. 1981. Crop drying with solar air heaters in tropical Nigeria. *ISES*, Solar World Forum, Brighton, UK, p. 997-1005.

EZEKWE, C.I. 1993. Introduction to solar drying. Paper submitted at the second training workshop on solar drying technologies for agriculture and industry, 24-27 November 1993, Nsukka-Nigeria.

FLOOD, C.A., SABBAH, M.A., MECKER, D. and PEART, R.M. 1972. Simulation of natural air corn-drying system. *Trans. ASAE*, vol. 15, p. 156-159, & 162.

FORSON, F.K. 1993. Design and evaluation of a natural convection solar crop dryer. Unpubl. M.Sc. Thesis, University of Science and Technology, Ghana.

FORSON, F.K., NAZHA, M.A.A. and AKUFFO, F.O. 1996. Natural convection solar crop dryers of commercial scale in Ghana: design, construction and performance. *Ambient Energy*, vol. 17, no. 3, p. 123-130.

FOSTER, G.H. and PEART, R.M. 1976. Solar grain drying. U.S. Dep. Agr., Agr. Inform. Bull. 401.

FRASER, B.M. and MUIR, W.E. 1980. Energy consumption predicted for drying grain with ambient and solar-heated air in Canada. *J. agric. Engng. Res.* 25, 325-331.

FRUS, J.D. 1968. Stirring devices research. *Amer. Soc. Agr. Eng.* Paper MC-68-402.

FURNAS, C.C. 1930. Heat Transfer from a Gas Stream to a Bed of Broken Solids. *Trans. of American Institute of Chemical Engineers*, 24, 142-193.

GALLAHER, G.L. 1951. A method of determining the latent heat of agricultural crops. *Agricultural Engineering* 32, 1, 34&38.

GAMSON, B.W., THODOS, G. and HOUGEN, O.A. 1943. Heat, mass and momentum transfer in the flow of gases through granular solids. *Trans. American Institute of Chemical Engineers*, 39, 1-35.

GARBA, M.M., MAISHANU, A.T. and SAMBO, A.S. 1990. Comparative Studies of Some Passive Solar Dryers. In *Proceedings of 1st World Renewable Energy Congress* (A.A.M Sayigh, ed.), 2, 927-931.

GARG, H.P. and SHARMA, SANJAY. 1990. Mathematical modelling and experimental evaluation of a natural convection solar dryer. In *Proceedings of 1st World Renewable Energy Congress* Reading .U.K. (Sayigh, A.A.M ed.), 2, 904-908.

GLENN, T.L. 1978. Dynamic analyses of grain drying system. Ph. D. Thesis. The Ohio State University. Univ. Microfilms No. 79-15-977, Ann Arbor, MI.

HAGHIGHI, K and SEGERLIND, L.J. 1988. Modelling simultaneous heat and mass transfer in an isotropic sphere: A finite element approach. *Trans. ASAE,* vol. 31, no. 2, p.629-637.

HAGHIGHI, K., IRUDAYARAJ, J., STROSHINE, R.L. and SOKHANSANJ, S., 1990. Grain kernel drying simulation using the finite element method. *Trans. ASAE*, vol. 33, no. 6, p.1957-1965.

HALL, C.W. 1980. *Drying and storage of agricultural crops*. Connecticut, Westport: AVI Publishing Company, Inc.

HALL, C.W. and RODGRIGUEZ-ARIAS 1958. Application of Newton's equation to moisture removal from shelled corn at 40- 140° F. *J. agric. Engng. Res.*, 3, 275-280.

HALL, D.W. 1975. *Manual handling and storage of food grains in tropical and sub-tropical areas.*, F.A.O. Development Paper No. 90.

HAMDY, M.Y. and BARRE, H.J. 1970. Analysis and hybrid simulation of deep-bed drying of grain *Trans. ASAE* 13,6, 752-757.

HARVEY, W.O'N., HEADLEY, O. St.C. and OSUJI, P.O. 1985. Simple solar crop dryers for rural areas. In: *Proceedings of the Ninth Biennial Congress of the ISES* (E. Bilgen. and K.G.T. Hollands, eds.),Montreal, Canada 2, 1082-1086, 1986.

HEARN, E.J. 1997. *Mechanics of Materials 2.* 3rd edn., Butterworth Heinmann, Oxford, Chapter 6.

HENDERSON, S. M. and PABIS, S. 1961. Grain drying theory I: -temperature effect on drying coefficient. *J. agric. Engng. Res.*, 6, 169-174.

HENDERSON, S.M. 1952. A basic concept of equilibrium moisture. *Agric. Engng.*, 29-32.

HENDERSON, S.M. and PABIS, S. 1962. Grain drying theory IV: the effect of airflow rate on the drying index. *J. agric. Engng. Res.*, 7, 85-89.

HENDERSON, S.M. and PERRY, R.L. 1976. *Agricultural Process Engineering* (3rd edit.). Westport, Connecticut: AVI Publishing Co,, Inc.

HOLLANDS, K.G.T., UNNY, T.E., RAITHBY, G.D. and KONICEK, L. 1976. Free cnvective heat transfer across inclined air layers. *TRANS. ASME, Journal of Heat Transfer*, 98, 189-193.

HOUGEN, O.A., McCAULEY, H.J., and MARSHALL, W.R. 1940. Limitations of diffusion equation in drying. *AIChE Transactions* 36(2):183-209.

List of references.

HOWE, E.D. 1980. Principles of drying and evaporating. *Sun World* 4, 6, 182-185.

HUKILL, W.V. 1947. Basic principles in drying corn and grain sorghum. *Agricultural Engineering* 28, 8, 335-338 & 340.

HUKILL, W.V. 1954. Grain drying. AACC Monograph II. Storage of Cereal Grains. Am. Assoc. Cereal Chemists, St. Paul, Minn. (Cited by Bakker-Arkema *et. al.* 1974.)

HUKILL, W.V. and SCHMIDT, J.L. 1960. Drying rate of fully exposed grain kernels. *Transactions of ASAE* 3(2): 71-77 & 80.

HUSAIN, ASHFAQ, CHEN, C.S., CLAYTON, J.T. and WHITNEY, L.F. 1972. Mathematical simulation of mass and heat transfer in high moisture foods. *Trans. of the ASAE*, 15, pp.732-736.

HUSTRULID, A. 1963. Comparative drying rates of naturally moist, re-moistened and frozen wheat. *Trans. ASAE*, 6: 304-308.

HUSTRULID, A. and FLIKKE, A.M. 1959. Theoretical drying curve for shelled corn. *Trans. ASAE* 3, 112-114.

HUTCHINSON, D. and OTTEN, L. 1983. Thin-layer air drying of soybeans and white beans. *J. Fd Technol.* 18, 507-522.

IBRAHAM, M.N. and HANSEN, R.W. 1984. Natural convection solar grain drier, *ASAE Paper No. 84-3010.*

IGBEKA, J.C. 1982. Simulation of moisture movement during drying a starchy food product-cassava *J. Fd Technol.* 17, 27-36.

IGBEKA, J.C.,BLAISDELL, J.L., HERUM, F.L. and HAMDY, M.Y. 1976. Moisture Diffusivity of Cassava and White Potato. *Trans. ASAE* Paper No. 76-3039, St Joseph Michigan.

IGLESIAS, H.A. and CHIRIFE, J. 1982. *Hanbook of food isotherms.* Academic Press, New York.

ILOEJE, O.C., EKECHUKWU, O.V. and EZEIKE, G.O.I. 1993. Design, construction and test run of a two-tonne capacity soler rice dryer with rice-husk-fired auxialliary heater. Paper submitted at the Second training workshop on solar drying technologies for agriculture and industry, 24-27 November 1993, Nsukka-Nigeria.

IMRE, L. (1997). Solar dryers. In: *Industrial drying of foods* (Baker, C.G.J. ed.), First edition, Blackie Academic and Professional, London. chapter 10.

INCROPERA, F.P. and DeWITT, D.P. 1996. Fundamentals of heat and Mass transfer, 4th edition, John Wiley and Sons Inc., New York.

INGRAM, G.W. 1976. Deep Bed Drier Simulation with Intra-particle Moisture Diffusion. *J. agric. Engng. Res.* 21, 263-272.

INGRAM, J.S. and HUMPHRIES, J.R.O. 1972. Cassava Storage. *Tropical Science*, 14,(2), pp. 131-148.

ISLAM, M.N. and FLINK, J.M. 1982. Dehydration of Potato. *J. Fd Technol.* 17, 373-385.

ISLAM, M.N. and JINDAL, V.K. 1981. Agricultural mechanisation in Asia, Africa and Latin America. 37-41.

JACKSON, E.A. and AKUFFO, F.O. 1992. Correlation Between Monthly Average Global Iradiation and Relative Duration of Sunshine at Kumasi. *Energy Conversion and Management*, 33, 1, 13-22.

JANJAI, S., ESPER, A. and MUHLBAUER, W. 1994. A procedure for determining the optimum collector area for a solar paddy drying system. *Renewable Energy* 4, 4, 409-416.

JARARAMAN, K.S., DAS GUPTA, D.K and BABU RAO, N. 1992. Solar drying of vegetables. In: Drying of Solids (A.S. Mujumdar, ed.). Oxford IBH, New Delhi, p. 405-432.

JAYAS, D.S, CENTOWSKI, S and PABIS, S. 1991 Review of Thin-Layer Drying and wetting Equations. *Drying Technology*, 9(3), 551-588.

JINDAL, V.K. and GUNASEKARAN, S. 1982. Estimating Air Flow and Drying Rate due to Natural Convection in Solar Rice Dryers. *Renewable Energy Review Journal* 4, 2, 1-9.

JOHNSON, H.K. and DALE, A.C. 1954. Heat required to vaporise moisture. *Agricultural Engineering*, Vol. 33, No. 10, pp. 705-709, 714.

KARCZMARCZYK, S. 1990. Determination of water diffusion coefficient in grain of wheat. M.Sc. thesis (unpubl.), Warsaw Agricultural University, Poland. Cited by Jayas. *et. al.*, 1991.

KAREL, M., FENNEMA, O.R. and LUND, D.B. 1975. *Physical principles of food preservation*. vol. 4 part 2, Marcel Dekker, New York.

KAZARIAN, E.A. and HALL, C.W. 1965. Thermal Properties of Grain. *Trans. ASAE* 8, 1, 33-37, 48.

KEENER, H.M., MEYER, G.E., SABBAH, M.A. and CURRY, R.B. 1978. Simulation of solar grain drying. *Agric. Engng., Series 102.* Ohio Agricultural Research Development Centre, Wooster, Ohio, USA.

KEEY, R.B. 1972. Drying: principles and practice. Pergamon Press, Oxford, England.

KEEY, R.B. 1978. *Introduction to Industrial Drying Operations*. Pergamon Press, Oxford.,Chapter 1, pp. 6

KERKHOF, P.J.A.M. 1994. The role of theoretical and mathematical modelling in scale-up. *Drying Technology*, 12(1&2), 1-46.

KERN, J. and HARRIS, I. 1975. On the Optimum Tilt of a Solar Collector. *Solar Energy*, 17, 2, 97-102.

KIRANOUDIS, C.T., MAROULIS, Z.B. and MARINOS-KOURIS, D. 1993. Mass transfer model building in drying, 11(6): 1251-1270.

KIRANOUDIS, C.T., MAROULIS, Z.B., and MARINOS-KOURIS, D. 1992. Drying Kinetics of onion and green pepper. *Drying Technology*, 10(4): 995-1011.

KLEIN, S.A. 1979. Calculation of the Monthly-Average Transmittance-Absorptance Product. *Solar Energy* 23, 6, 547-551.

KLEIN, S.A. and THEILACKER, J.C. 1981. An algorithm for calculating monthly-average radiation on inclined surfaces. *Trans. ASME, J. Solar Energy Engng.* 103, 29-33.

KUMAR, A. and SODHA, M.S. 1986. Computer siumulation models for solar drying processes. In: Reviews of renewable energy resources (M.S. Sodha, Mathur, S.S. and M.A. Malik, eds.), vol. 3, p.269-344: New Delhi, Wiley Eastern Ltd.

LAWS, N. and PARRY, J.L. 1983. Mathematical modelling of heat and mass transfer in agricultural grain drying. *Proc. R. Soc. Lon.*, A385, 169-187.

LEWIS, W.K., 1921. The Rate of Drying of Solid Materials. *Industrial and Engineering Chemistry* 13, 5, 427-432.

LI, H and MOREY, R.V. 1984. Thin-layer drying of yellow dent corn. *Trans. ASAE*, 27:581-585.

LILEY, P.E. and GAMBILL, W.R. 1973. Pysical and chemical data. In *Chemical Engineers' Handbook*, 5th edition (Perry, R.H and Chilton, C.H. eds.) McGraw-Hill Book Company, Section 3.

LIU, B.Y.H. and JORDAN, R.C. 1977. Availability of solar energy for flat-plate solar heat collector. In *Application of Solar Energy for Heating and Cooling of Buildings*, ASHRAE, New York. (Cited by Duffie and Beckman, 1991).

LOF, G.O.G. and HAWLEY, R.W. 1948. Unsteady-State Heat Transfer Between Air and Loose Solids. *Industrial and Engineering Chemistry* 40, 1061-1070.

LOF, G.O.G., 1962. Recent Investigations in the Use of Solar Energy for the Drying of Solids. *Solar Energy*, 6, 4, 122-128.

LUIKOV, A.V. 1966. *Heat and Mass Transfer in Capillary-Porous Bodies*, Pergamon Press, London.

List of references.

M'EWEN, EWEN and O'CALLAGHAN, J.R. 1954. Through Drying of Deep Beds of Wheat Grain. *The Engineer* 198, 817-819.

MACEDO, I.C. and ALTEMANI, C.A.C. 1978. Experimental Evaluation of Natural Convection Solar Air Heaters. *Solar Energy* 20, 5, 367-369.

MARINOS-KOURIS, D and MAROULIS, Z.B. 1995. Transport properties in the drying of solids. In: *Handbook of Industrial Drying* Volume1 (Arun S. Mujumdar ed.), 2nd edition, Marcel Dekker, Inc. New YorK , pp 113-160.

MATOUK, A.M. 1976. Heat and moisture movements during low temperature drying and storage of maize grain. PhD Thesis, University of Newcastle upon Tyne, England.

McADAMS, W.H. 1954. *Heat Transmission* (3rd edit.). New York: McGraw-Hill Book Company, Inc.

McLEAN, K.A. 1980. *Drying and storage of combinable crops*, Farm Press Ltd., Ipswich, Suffolk, UK.

MISRA, M.K. and BROOKER, D.B. 1980. Thin-Layer Drying and Rewetting Equations for Shelled Yellow Corn. *Trans ASAE* 23, 1254-1260.

MISRA, R.N and Young, J.H. 1980. Numerical Solution of Simultaneous Mixture Diffusion and Shrinkage During Soybean Drying. *Trans ASAE*, Vol 23, pp. 1277-1282.

MISRA, R.N. and YOUNG. J.H. 1978. Finite element analysis of simultaneous moisture diffusion and shrinkage of soybeans during drying, ASAE Paper No. 78-3056, ASAE, St. Joseph, MI.

MISRA, R.N. and YOUNG. J.H. 1979. The finite element approach for solution of transient heat transfer in sphere, Trans. of the ASAE, 22(4):944-949.

MOHAMAD, A.A. 1997. High efficiency solar air heater. *Solar Energy*, 60, 2, 71-76.

MOREY, R.V., CLOUD, H.A., GUSTAFSON, R.J. and PETERSON, D.W. 1979. Evaluation of the Feasibility of Solar Energy Grain Drying. *Trans. of the ASAE* 22, 2, 409-417.

MOREY, R.V., KEENER, H.M., THOMPSON, T.L., WHITE, G.M. and BAKKER-ARKEMA, F.W. 1978. The Present Status of Grain Drying Simulation. *ASAE Technical Paper No. 78-3009*, St. Joseph, Michigan.

MORITA, T and SINGH, R.P. 1979. Physical and thermal properties of short grain rough rice. *Trans. am. Soc. agric. Engrs.*, 630-636.

MUJUMDAR, A.S 1991. Drying Technologies of the Future, *Drying Technology*, 9, 2, pp 325-347.

MUJUMDAR, A.S. 1995. *Hanbook of Industrial Drying*, Volume 1, 2nd edn., Marcel Dekker, Inc., New York, 1995.

MUJUMDAR, A.S. and MENON, A.S. 1995. Drying of solids: Principles, Classification and Selection of Dryers. In: *Handbook of Industrial Drying* Volume1 (Arun S. Mujumdar ed.), 2nd edition, Marcel Dekker, Inc. New YorK , pp 1-40.

NELLIST, M.E. 1974. The drying of ryegrass seeds in deep layers. Ph.D. Thesis, University of Newcastle upon Tyne.

NELLIST, M.E. 1976. Exposed layer drying of ryegrass seeds. *J. agric. Engng. Res.* vol. 21, p.49-66.

NEWMANN, A.B. 1931. The drying of Porous Solids: Diffusion and Surface Emission Equations. *Trans. of American Institute of Chemical Engineers* 27, 203-220.

NORTON, B. 1992. *Solar Energy Thermal Technology.* Berlin: Springer-Verlag, London.

O'CALLAGHAN, J.R. 1954. Drying of wheat grain: Effects of air condition on through drying. M.Sc. Thesis, university of Durham.

O'CALLAGHAN, J.R., MENZIES,D.J. and BAILEY, P.H. 1971. Digital Simulation of Agricultural Drier Performance. *J. agric. Engng. Res.* 16, 3, 223-244.

OKOS, M.R. (Ed.). 1986. *Physical and Chemical Properties of Food.* St. Joseph Michigan: ASAE.

ONG, K.S. 1982. Results of Investigations into Forced and Natural Convection Solar Air Heater and Crop Dryers. *Reg. J. Energy Heat Mass Transfer* 4, 1, 29-45.

ONG, K.S. 1995a. Thermal Performance of Solar Air Heaters: Mathematical Model and Solution Procedure. *Solar Energy* 55, 2, 93-109.

ONG, K.S., 1995b. Thermal Performance of Solar Air Heaters: Experimental Correlation. *Solar Energy* 55, 3, 209-220.

OoTHUIZEN, P.H. 1986. A numerical model of a natural-convection solar grain dryer: development and validation. In: *Proc. of a Workshop on Solar Drying in Africa* IDRC-255e, Senegal, Dakar, 21-24 July, 1986. (M.W. BASSEY, and O.G. SCHMIDT, eds.).

OTHIENO, H. 1987. Natural Convection Solar Crop Dryers in Kenya- Theory and Practical Application. CSC Technical Publication Series No. 24 (CSC(87) ENP-20).

OTHMER, D.F. 1940. Correlating Vapour Pressure and Latent Heat Data. *Industrial and Chemical Engineering* 32, 16, 841-856.

OVERHULTS, D.G., WHITE, H.E., HAMILTON, H.E., and ROSS, I.J. 1973. Drying soybeans with heated air. Trans. ASAE, Vol. 16, p.112-113.

PABIS, S. 1982. Theory of convective drying of agricultural crops (Pol.),. PERiL, Warszawa. Cited by Jayas *et. al.*, 1991.

PABIS, S., and HENDERSON, S.M. 1961. Grain drying theory II: A critical analysis of the drying curve for shelled maize. *J. agric. Engng. Res.*, vol. 6, no. 4, p. 272-277.

PAGE, G.E. 1949. *Factors influencing the maximum rate of air drying shelled corn in thin layers*. M.S. Thesis. Mechanical Engineering Department, Purdue University, Lafayette, IN.

PAKOWSKI, Z and MUJUMDAR, A.S. 1995. Basic process calculations in drying, In: *Handbook of Industrial Drying* Volume1 (Arun S. Mujumdar ed.), 2nd edition, Marcel Dekker, Inc. New YorK , pp 71-112.

PARKER, B.F. 1980. Design Equations for Solar Air Heaters. *Trans. ASAE* 23, 1494-1499 & 1504.

PARKER, B.F. 1981. Derivation of Efficiency and Loss factors for Solar Air Heaters. *Solar Energy* 26, 1, 27-32.

PARRY, J.L. 1985. Mathematical modelling and computer simulation of heat and mass transfer in agricultural grain drying: A Review. *J. agric. Engng.Res.* Vol. 32, pp. 1-29.

PATIL, B.G. and WARD, G.T. 1989. Simulation of Solar Air Drying of Rape Seed. *Solar Energy* 43, 5, 305-320.

PAWAR, R.S. TAKWALE, M.G., and BHIDE, V.G. 1994. Evaluation of the Performance of the Solar Air Heater. *Energy Convers. Mgmt.* 35, 8, 699-708.

PETERSON, W.H. 1973. Solar collectors for agriculrural use. Paper presentred at Grain drying and management workshop, Champaign, USA.

PIERCE, R.O. and THOMPSON, T.L. 1979. Solar Grain Drying in the North Central Region - Simulation Results. *Trans. of the ASAE* 22, 1, 178-187.

PIXTON, S.W. and HOWE, R.W. 1983. The Suitability of Various Linear Transformations to Represent the Sigmoid Relationship of Humidity and Moisture Content. *J. Stored Prod. Res.* 19, 1, 1-18.

POPLE, J. 1979. BSSM Strain measurement reference book. British Society for Strain Measurement, Quayside, Newcastle-upon-Tyne, England.

PORTER, H.F, McCORMICK, P.Y., LUCAS, R.L and WELLS, D.F. 1973. Gas-Solid Systems In *Chemical Engineers' Handbook*, 5th edition (Perry, R.H and Chilton, C.H. eds.) McGraw-Hill Book Company, Section 20.

PUIGALLI, J.R., and LARA, M.A., 1985. Fodder drying in barns with the aid of ventilated greenhouses. In: *Proceedings of ISES Congress, INTERSOL 85*, Montreal, Canada, 1985, p. 1043-1047.

RATTI, C. and MUJUMDAR, A.S. 1995. Simulation of Packed Bed Drying of Foodstuffs with Airflow Reversal. *Journal of Food Engineering*, 26, 3, 259-271.
RATTI, C. and MUJUMDAR, A.S. 1997. Solar drying of foods: modelling and numerical simulation. *Solar Energy*, 60, 3/4, 151-157.

REID, R.C., PRAUNSNITZ, J.M. and POLING, B.E. 1987. *The Properties of Gases and Liquids*, 4th Ed., McGraw-Hill Book Company, New York,chapter 11 pp577-631(diffusion), Chapter 7pp205-240(latent heat of vaporisation)

ROA, G. (1974). Natural drying of cassava. PhD thesis, Michigan State University, USA.

ROA, G. and MACEDO, I.C. 1976. Grain Drying in Stationary Bins with Solar Heated Air. *Solar Energy*, Vol. 18, No. , pp. 445-449.

RODRIGUEZ-ARIAS, J.H. 1956. Moisture equilibria of shelled corn. Unpubl. Ph.D. Thesis, Michigan State University. Cited by Bakker-Arkema et. al., 1974.

ROMAN, G.N., ROTSTEIN, E., and URBICAIN, M.J. 1979. Kinetics of water desorption from apples J. Food Sci. 44:193-197.

ROSS, I.J. and WHITE, G.M. 1972. Thin layer drying characteristics of white corn. *Trans ASAE* 15, 175-176 & 179.

SABBAH, M.A., KEENER, H.M. and MEYER, G.E. 1979. Simulation of solar drying of shelled corn using the logarithmic model. *Trans. ASAE*, vol. 22, no. 3, 637-643.

SABBAH, M.A., MEYER, G.E., KEENER, H.M., and ROLLER, W.L. 1976. Reversed-air drying for fixed bed of soybean seed. Am. Soc. Agr. Emg. Paper 76-3023.

SARKER, N.N., KUNZE, O.R, and STROUBOULIS, T. 1994. Finite element simulation of rough rice drying. *Drying Technology*, 12(4), 761-775.

SCHUMANN, T.E.W. 1929. Heat Transfer: A Liquid Flowing Through a Porous Prism. *J. Franklin Inst.* 208, 405-416.

SELCUK, M.K. 1977. Solar Air Heaters and Their Applications. *in* Sayigh, A.A. (Ed.) *Solar Energy Engineering* , New York: Academic Press. 155-182.

SELCUK, M.K., ERSAY, O. and AKYURT, M. 1974. Development, Theoretical and Performance Evaluation of Shelf Type Solar Dryers. *Solar Energy* 16, 2, 81-88.

SHARAF-ELDEEN, M.Y., HAMDY, M.Y., KEENER, H.M. and BLAISDELL, J.L. 1979a. Mathematical Description of Drying Fully Exposed Grains. ASAE Technical Paper No. 79-3034, St. Joseph, Michigan.

SHARAF-ELDEEN, Y.I., BLAISDELL, J.L. and HAMDY, M.Y. 1980. A modeo for ear corn drying. *TRANSACTIONS of the ASAE*, Vol. 23, No. 5, p. 1261-1265, 1271.

SHARAF-ELDEEN, Y.I., HAMDY, M.Y. and BLAISDELL, J.L. 1979b. Falling rate drying of fully exposed biological materials. A review of mathematical models. ASAE paper No. 79-6522, ASAE, St. Joseph, MI 49085.
SHARP, J.R. (1982) A Review of Low Temperature Drying Simulation Models. *J. agric. Engng. Res.* 27, 169-190.

SHERWOOD, T.K. (1929) The Drying of Solids I *Ind. and Eng. Chem.* 21,10, 976-980.

SHERWOOD, T.K., (1936). Air Drying of Solids. *Trans. Amer. Inst. Chem. Engrs.* 12, 150-168.

SHEWEN, E.C., SULLIVAN, H.F. HOLLANDS, K.G.T. and BALAKRISHNAN, A.R. (1978). A heat storage subsystem for solar energy. Report STOR-6, Waterloo Research Institute, University of Waterloo. Cited in Duffie and Beckman, 1991.

SIEBEL, J.E. (1892). Specific heat of various products. *Ice and Refrigeration*, vol. 2, p. 256-257.

SIMMONDS, W.H.C., WARD, G.T. and McEWEN, EWEN (1953a). The drying of wheatgrain Part I: Through-drying of deep beds. *Trans. Instn. Chem. Engrs.* 31, 3, 265-279.

SIMMONDS, W.H.C., WARD, G.T. and McEWEN, EWEN (1953b). The drying of wheatgrain Part II: Through-drying of deep beds. *Trans. Instn. Chem. Engrs.* 31, 3, 279-288.

SINJERI, LJ and KULISIC, P. 1994. Solar Radiation on Variously Oriented Collectors in Croatia. *Renewable Energy* 4, 3, 235-240.

SMITH, S.E. 1947. The sorption of water vapour by high polymers. *J. am. chem. Soc.*, 69, 646-651.

SODHA, M.S., BANSAL, N.K., KUMAR, K., BANSAL, P.K. and MALIK, M.A.S. 1987. *Solar crop drying*, Vol. 1 CRC Press Inc. Florida, USA.

SODHA, M.S., MATHUR, S.S., and MALIK, M.A. 1986. Computer simulation models for solar drying processes. Reviews of Renewable Energy Resources,

SOKHANSANJ, S and JAYAS, D.S. 1995. Drying of foofstuffs. In: *Handbook of Industrial Drying* Volume1 (Arun S. Mujumdar ed.), 2nd edition, Marcel Dekker, Inc. New YorK , pp 589-626.

SOKHANSANJ, S. and GUSTAFSON, R.J. 1980. Prediction of heat and mass transfer within a grain kernel. A finite application, p.229-232. In: Mujumdar, A.S (ed.), *Proceedings of the 2nd International Symposium, Drying '80.*

SPENCER, H.B. 1969. A Mathematical Simulation of Grain Drying. *J. agric. Engng. Res.* 14, 3, 226-235.

SPENCER, H.B. 1972. A Revised Model of the Wheat Drying Process. *J. agric. Engng. Res.* 17, 189-194.

STEFFE, J.F. and SINGH, R.P. 1982. Diffusion Coefficients for Predicting Rice Drying Behaviour. *J. agric. Engng. Res.* 27, 489-493.

STEINFELD, A. and SEGAL, I. 1986. A Simulation Model for Solar Thin-Layer Drying Process. *Drying Technology* 4, 4, 535-554.

STROHMAN, R.D. and YOERGER, R.R. 1967. A new equilibrium moisture content equation. *Trans. am. Soc. agric. Engrs.*, 10(5), 675-677.

SUAREZ, C., VIOLLAZ, P. and CHIRIFE, J. 1980. Diffusional Analysisof air Drying of Grain Sorghum. *Journal of. Food Technology* 15, 523-531.

SWINBANK, W.C. 1963. Long-wave Radiation from Clear Skies. *Quart. J. R. Met. Soc.* 89, 339-348.

SYARIEF, A.M., GUSTAFSON, R.J., and MOREY, R.V. 1987. Moisture diffusion coeficient s for yellow-dent corn components. *Trans. ASAE*, Vol., 30, p. 522-528.

SYARIEF, A.M., MOREY, R.V. and GUSTASON, R.J. (1984). Thin-Layer Drying of Sunflower Seed. *Trans ASAE* 27, 195-200.

TABOR, H. 1958. Radiation, Convection and Conduction Coefficients in Solar Collectors. *Bull. Res. Council Israel* Vol. 6C, pp. 158-176

TAYLOR, K.J. and WEIR, A.D. 1985. Simulation of a solar timber drier. *Solar Energy*, vol. 34, no. 3, p.249-255.

TETER, C.N. and CITELLY, F. 1970. Biongenieria. Mimeo. Instituto Colombiano Agropecuario, Universidad Nacional, Tibaitata, Colombia. Cited by Roa, 1974.

THOMPSON, T.L. 1967. *Predicted Performances and Optimal Designs of Convection Grain Dryers*, PhD Thesis, Purdue University, Lafayette Ind., USA,

THOMPSON, T.L. 1972. Temporary Storage of High-Moisture Shelled Corn Using Continuous Aeration. *Trans. ASAE* 15, 2, 333-337.

THOMPSON, T.L. and PEART, R.M. 1968. Useful search techniques to save research time. *Trans. of ASAE* 2, 4, 461-467.

THOMPSON, T.L., PEART, B.M. and FOSTER, G.H. 1968. Mathematical Simulation of Corn Drying - A New Model. *Trans. of the ASAE* 11, 3, 582-586.

TRIM, D.S.; BRENNDORFER, B; KAMAU, A.N. 1984. A new parchment drying system for co-operative factories I: system design and operating principles, *Kenya Coffee*, 49, 577, 128-136.

TROEGER, J.M., and HUKILL, W.V. 1971. Mathematical description of the drying rate of fully exposed corn. Trans. ASAE, vol. 11, p.582-586.

TURNER, I.W. and PIERCE, P. 1995. A comparison of the drying simulation codes TRANSPORE and WOOD'D which are used for the modelling of two-dimensional wood processes. *Drying Technology*, 13(3), 695-735.

VACCAREZZA, L.M., LOMBARDI, J.L. and CHIRIFE, J. 1974. Kinetics of moisture movement during air drying of sugar beet root. *Journal of Food Science* 9, 317-327.

VAN ARSDEL, W.B. 1947. Approximate diffusion calculation for the falling-rate phase of drying. *Chem. Eng. Progr.*, vol. 43, 13-24.

VAN BRAKEL, J. 1980. Mass transfer in convective drying. In: Mujumdar, A.S. (ed.). Advances in drying, Vol. 1, Hemisphere Publishing Corp., New York.

VAN REST, D.J. and ISACCS, G.W. 1968. Exposed layer drying rates of grain. *Trans. am. Soc. Engrs.*, 11 (2) 236-239.

VEMUGANTI, G.R., and PFOST, H.B. 1980. Pysical properties related to drying of 20 food grains. *ASAE Paper No. 80-3539.*

VERMA, L.R., BUCKLIN, R.A., ENDAN, J.B. and WRATTEN, F.T. 1985. Effects of Drying Air Parameters on Rice Drying Models. *Trans. of the ASAE* 28, 296-301.

WAANANEN, K.M., LITCHFIELD, J.B. and OKOS, M.R. 1993. Classification of Drying Models for Porous Solids. *Drying Technology*, 11(1), 1-40.

WALKER, L.P. 1977. *Optimization of rice dryers.* Ph.D. Thesis, Mich. State Uni. Uni. Mocrifilms, Ann Arbor, Mich.

WALLAPAPAN, K. 1986. Thermal properties of porous foods. In: *Physical and chemical properties of food* (Edited by M.R. Okos), St. Joseph Michigan, ASAE, pp. 78-119.

WANG, J.K. and HALL, C.W. 1961. Moisture movement in microscopic materials and mathematical analysis. *Trans. of the ASAE*, 42, pp. 33-36.

WANG, C.Y. and SINGH, R.P. 1978. A single layer drying equation for rough rice. *ASAE Paper 78-3001. Am. Soc. Agric. Eng.*, St. Joseph, MI.

WARREN, A. 1994. Energy: Doing More With Less. *Energy World Yearbook*, 50-51.

WATMUFF, J.H., CHARTERS, W.W.S. and PROCTOR, D. 1977. Solar and Wind Induced External Coefficients of Solar Collectors. *COMPLES Bull.* 2, 56.

WATSON, E.L. and BHARGAVA, V.K. 1974. Thin layer drying studies on wheat. *Can. Agric. Eng.*, Vol. 16, no. 1, p. 18-22.

WESTERMAN, P.W., WHITE, G.M. and ROSS, I.J. 1973. Relative humidity effect on high temperature drying of shelled corn. *Trans. am. Soc. agric. Engrs.*, 1136 1139 of ASAE

WHILLIER, A. 1967. Design factors affecting solar collectors. *Low temperature engineering applications of solar energy, ASHRAE !967.*

WHILLIER, AUSTIN 1963. Plastic Covers for Solar Collectors. *Solar Energy* 7, 3, 148-151.

WHILLIER, AUSTIN 1964. Performance of Black-Painted Solar Air Heaters of Conventional Design. *Solar Energy* 8, 1, 31-37.

WHITAKKER'S ALMANAC 1997. An almanack for the year 1997, J. Whitaker & Sons Ltd., London.

WHITE, G.M., BRIDGES, T.C., LOEWER, O.J., and ROSS, I.J., 1981. Thin layer drying model for soybeans. Trans. am. Soc. agric. Engrs., 1643-1646.

WHITE, G.M., ROSS, I.J. and PONELEIT, C.G. 1981. Fully-Exposed Drying of Popcorn. *Trans ASAE* 24, 466-468 & 475.

WHITE, G.M., ROSS, I.J. and WESTERMAN, P.W. 1973. Drying Rate and Quality of White Shelled Corn as influenced by Dew Point Temperature. *Trans. ASAE* 16, 118-120.

WIJEYSUNDERA, N.E., Ah Lee Lee and Tjoe, L.E. 1982. Thermal Performance Study of Two-Pass Solar Air Heaters. *Solar Energy* 28, 5, 363-370.

WILEMAN, R.H. 1941. Shrinkage of artificially dried seed corn. *Agric. Engng.*, July, 256.

WILKE, C.R. and HOUGEN, O.A. 1945. Mass transfer in flow of gases through granular solids extended to low modified Reynolds numbers. *Trans. AIChE*, vol. 41, p.445-451.

WONG, H.Y, 1977. *Handbook of Essential Formulae and Data on Heat Transfer for Engineers*. New York: Lonman Inc.

WRATTEN, F.T., POLE, W.D., CHESNESS, J.L., BAL, S., and RAMARAO, V. 1969. Pysical and thermal properties of rough rice. *Trans. am. Soc. agric. Engrs.*, 12 (6), 801-803.

XIONG, X., NARSIMHAN, G. and OKOS, M.R. 1992. Effect of Composition and Pore Structure on Binding Energy and Effective Diffusity of Moisture in Porous Food., *Journal of Food Engineering*, vol. 15, no. 3, p.187-208.

YOUNG, J.H. and WHITAKER, T.B. 1971a. Evaluation of the diffusion equation for describing thin-layer drying of peanuts in the hull. *Trans. of the ASAE*, vol. 14, no. 2,

ZAHED, A.H. and ELSAYED, M.M. 1989. Mathematical Modelling of a Solar Kiln. *Solar & Wind Technology*, vol. 6, no. 1, p.19-27.

List of references.

ZAHED, A.H. and ELSAYED, M.M. 1994. Transient Performance of a Natural Ventilation Solar Kiln. *Renewable Energy,* vol. 4, no. 2, p.189-198.
ZAMAN, A. (1986). *Low cost solar food drying technology for Bangladesh.* Department of Farm Power and Machinery, Bangladesh Agricultural University, Mymensingh. Cited by Bala and Ziauddin, 1990.

ZAMAN, M.A. and BALA, B.K. 1989. Thin Layer Solar Drying of Rough Rice. *Solar Energy,* vol. 42, no. 2, p.167-171.

ZAMBRANO, W. and ALVARADO, S. 1984. Design, Construction and Testing of a chimney that reduces dangerous temperatures in a radiative convective solar dryer. *Solar Energy*, vol. 32, no. 5, p. 581-584.

ZAREMBA, A. 1977. Method of calculation of average temperatures and moisture contents in a deep bed of wheat during convective drying, Ph.D. thesis (unpubl.), University of Krakow, Poland. Cited by Jayas *et. al.*, 1991.